NI 5/31 Recon

SQT

ADVANCED ENERGY PROGRAMS
MULTI-HUNDRED WATT PROGRAM

Document No. GESP-7134
GEMS-430

MULTI-HUNDRED WATT RADIOISOTOPE THERMOELECTRIC GENERATOR PROGRAM

1976-1977 Annual Report/Final Report

for the

Voyager Program

Contract No. EX-76-C-16-3066

(NASA-CR-158184) MULTI-HUNDRED WATT RADIOISOTOPE THERMOELECTRIC GENERATOR PROGRAM Final Annual Report, 1976-1977 (General Electric Co.) 460 p

N79-74676

Unclas
00/73 35526

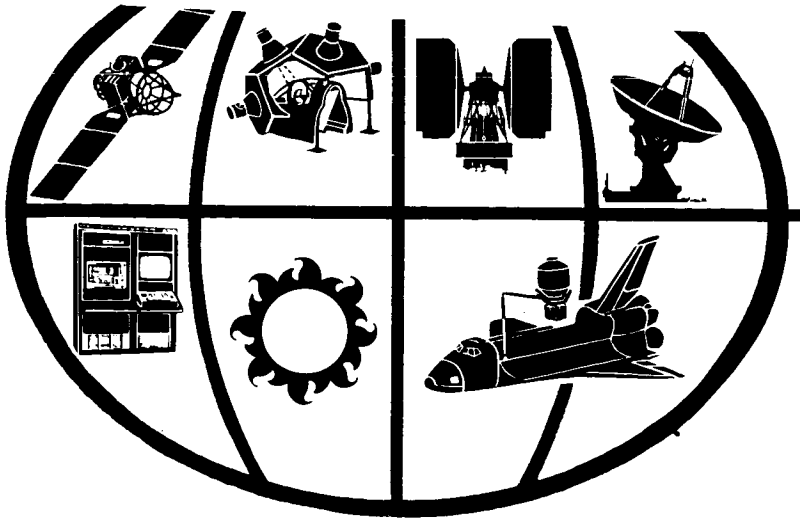

space division

ADVANCED ENERGY PROGRAMS
SPACE DIVISION
MULTI-HUNDRED WATT RTG PROGRAM
KING OF PRUSSIA PARK
P.O. Box 8661 · Philadelphia, Penna. 19101

GENERAL ELECTRIC

MULTI-HUNDRED WATT RADIOISOTOPE THERMOELECTRIC GENERATOR PROGRAM

CONTRACT NO. EX-76-C-16-3066

1976-1977 ANNUAL REPORT/FINAL REPORT

FOR THE

VOYAGER PROGRAM

PREPARED FOR

U.S. DEPARTMENT OF ENERGY
GERMANTOWN, MD.

BY

NUCLEAR PROGRAMS

SPACE DIVISION

P. O. Box 8661 • Philadelphia, Penna. 19101

GENERAL ELECTRIC

LIST OF ORGANIZATIONS

AFETR	Air Force-Eastern Test Range (USAF-DOD)
AFWL	Air Force Weapons Laboratory (USAF-DOD)
ALO or AL	Albuquerque Operations Office (ERDA)
ANL	Argonne National Laboratory (ERDA)
APL or APL/JHU	Applied Physics Laboratory Johns Hopkins University
ARC	Ames Research Center (NASA)
BMI-CL	Battelle Memorial Institute - Columbus Laboratories
DAO	Dayton Area Office (ERDA)
DBER	Division of Biological and Environmental Research (ERDA)
EPA	Environmental Protection Agency
ERDA (USERDA)	U.S. Energy Research and Development Administration
GD/C	General Dynamics/Convair
GE	General Electric
GE-AEP	General Electric-Advanced Energy Programs
GE-NP	General Electric-Nuclear Programs
GE-SD	General Electric-Space Division
GE-VF	General Electric-Valley Forge
INSRP	Interagency Nuclear Safety Review Panel (DOD-ERDA-NASA)
JPL	Jet Propulsion Laboratory of The California Institute of Technology (NASA)
KSC	Kennedy Space Center (NASA)
LaRC	Langley Research Center (NASA)
LASL	Los Alamos Scientific Laboratory - University of California (ERDA)
LeRC	Lewis Research Center (NASA)
ML/MRC	Mound Laboratory/Monsanto Research Corp. (ERDA)
NASA	National Aeronautics and Space Administration
NRA (ERDA/NRA)	Division of Nuclear Research and Applications (ERDA)
NUS	Nuclear Utilities Services

LIST OF ORGANIZATIONS (Cont'd)

ORNL	Oak Ridge National Laboratory (ERDA)
RCA	Radio Corporation of America
SFO	San Francisco Operations Office (ERDA)
SL	Sandia Laboratories/Sandia Corp. (ERDA)
SRP	Savannah River Plane (ERDA)

LIST OF ABBREVIATIONS

CG	Center of Gravity
CSC	Converter Shipping Container
DVM	Digital Volt Meter
EPC	Environmental Protection Container
ETG	Electrically-Heated Thermoelectric Generator
FSA	Fuel Sphere Assembly
FSAR	Final Safety Analysis Report
GIS	Graphite Impact Shell
GMV	Gas Management Valve
GSC	Gas Service Cart
GSE	Ground Support Equipment
HSA (see IHS)	Heat Source Assembly
IHS	Isotope Heat Source
IIP	Instantaneous Impact Point
LES (LES 8/9)	Lincoln Experimental Satellites Numbers 8 and 9
MHW	Multi Hundred Watt
MJS (MJS '77)	Mariner-Jupiter/Saturn* 1977 Mission
PICS	Post Impact Containment Shell
PISA	Post Impact Shell Assembly
PM	Propulsion Module
PRD	Pressure Relief Device
PSC	Power Supply Console
PTU	Portable Test Unit
RHU	Radioisotope Heater Units
ROC	Read Out Console
RTD	Resistance Temperature Device
RTG	Radioisotope Thermoelectric Generator
RTG-SC	Radioisotope Thermoelectric Generator - Shipping Container

*Renamed: Voyager

SC	Shipping Container
S/C	Spacecraft
SPC	Storage Protection Container
T/E	Thermoelectric
T/P	Thermopile
T/V	Thermal/Vacuum
USAR	Updated Safety Analysis Report

TABLE OF CONTENTS

Section		Page
1	INTRODUCTION AND SUMMARY	1-1
	1.1 Introduction	1-1
	1.2 Summary	1-1
2	SAFETY	2-1
	2.1 Safety Analysis and Reporting	2-1
	2.1.1 Updated Safety Analysis Report	2-1
	2.1.2 Fuel Safety Analysis Report	2-3
	2.1.3 Re-entry Subpanel Meeting	2-11
	2.1.4 FSAs Review	2-21
	2.2 Safety Testing	2-22
	2.3 Operational Safety	2-30
	2.3.1 MJS Ground Safety Analysis Report (GSAR)	2-30
	2.3.2 Radiological Protection Program	2-30
	2.3.3 MJS Safety Analysis Report for Packaging	2-30
	2.3.4 MJS Operations Analysis	2-31
	2.3.5 Building 300 Long Life Laboratory Facility Modification	2-31
3	RTG SYSTEMS	3-1
	3.1 Interface Environments and Performance Requirements Definition	3-1
	3.2 Design Requirements and Surveillance	3-1
	3.3 System Analysis	3-2
	3.3.1 Design Differences	3-2
	3.3.2 Temperature Distributions	3-2
4	PRODUCT ASSURANCE	4-1
	4.1 Reliability	4-1
	4.1.1 Reliability Program Plan	4-1
	4.1.2 Prediction of EOM Power	4-1
	4.1.3 Review of Qualification Test Program	4-1
	4.2 Quality Assurance	4-1
	4.3 Configuration Management	4-2

TABLE OF CONTENTS (Cont)

Section		Page
5	ISOTOPE HEAT SOURCE	5-1
5.1	The Fuel Sphere Assembly - FSA	5-3
5.1.1	The Isotopic Fuel - $^{238}PuO_2$	5-3
5.1.1.1	Development and Fabrication	5-4
5.1.1.2	Fuel Form and Basic Requirements	5-4
5.1.1.3	Fuel Characterization	5-4
5.1.1.4	Determination of Fines Production From MHW MJS Fuel Spheres	5-14
5.1.1.5	Potential Interactions of PuO_2 Fuel to Product CO	5-16
5.1.2	Post Impact Shell Assembly - PISA - Development, Fabrication and Testing	5-17
5.1.2.1	Development and Fabrication	5-18
5.1.2.2	PISA Venting	5-22
5.1.3	Graphite Impact Shell - GIS	5-28
5.1.3.1	Impact Behavior of the GIS	5-28
5.1.3.2	Vibration Behavior of the GIS	5-28
5.1.4	Fuel Sphere Assembly - FSA	5-29
5.1.4.1	Compatibility Tests	5-31
5.1.4.2	Impact Testing of Individual FSAs	5-32
5.1.4.3	Impact Behavior of Iridium	5-50
5.2	The MJS Isotope Heat Source Assembly, IHS	5-54
5.2.1	The MHW-MJS IHS	5-54
5.2.1.1	Differences Between the LES and the MJS IHS	5-54
5.2.1.2	Significant Events Involving the MHS-IHSs	5-55
5.2.2	History of the Qualification Heat Source - Q-2 IHS	5-55
5.2.2.1	Background	5-55
5.2.2.2	Assembly of the Q-2 IHS	5-56
5.2.2.3	Radioactive Contamination Levels in the Q-2 IHS	5-56
5.2.2.4	Non Radioactive Contamination of the Q-2 IHS Middle 8-Pack	5-57
5.2.2.5	Fracture of the Q-2 IHS End Caps	5-58
5.2.2.6	Testing of the Q-2R IHS	5-76
5.2.2.7	Disassembly of the Q-2R IHS	5-76
5.2.3	Loss of Preload in MHS-IHSs	5-84
5.2.3.1	Background	5-84
5.2.3.2	Design Changes	5-86
5.2.3.3	F-9 Disassembly and Rebuild	5-86

TABLE OF CONTENTS (Cont)

Section		Page
	5.3 Isotope Heat Source Analyses and Testing	5-88
	5.3.1 Interface Conductance Tests - POCO AXF-5Q versus Pyrocarb 406	5-88
	5.3.1.1 Interface Conductance Problem	5-88
	5.3.1.2 Test Description	5-88
	5.3.1.3 Results	5-89
	5.3.2 Stress Analyses of the IHS End Caps	5-90
	5.3.2.1 History	5-90
	5.3.2.2 Stress Analyses Assumptions	5-93
	5.3.2.3 Analytical Results	5-94
	5.3.2.4 Conclusions	5-97
	5.3.2.5 Stress Analyses on the MJS-MHW-IHS Support	5-98
	5.3.3 Effect of Pad Explosion on MJS-RTG	5-100
	5.3.3.1 Analytical Assumptions	5-100
	5.3.3.2 Analytical Results	5-101
	5.3.3.3 Conclusions	5-110
	5.3.3.4 References	5-110
	5.3.4 Reentry Analyses	5-111
	5.3.5 Analysis of the Q-2R Heat Source Failure	5-115
	5.3.6 Tests on Aft Tie Bolt Head	5-122
	5.3.7 Analysis of the F-6 and F-7 Heat Source Failure	5-123
	5.3.8 Vibration Testing of the MHW-MJS Explosion Test IHS	5-126
	5.3.9 Static Load Test of the IHS Internal Preload	5-127
	5.3.10 Possible Longitudinal Offset of the Center of Gravity in the IHSs F-6 and F-7	5-129
	5.3.11 Thermal Stress Analysis - Steep Angle - End-On	5-133
	5.3.11.1 HSA Thermal Stress Analysis Techniques	5-134
	5.3.11.2 HSA Thermal Stress Analysis	5-137
	5.3.12 Reentry Analysis of Aeroshell Center Section	5-138
	5.3.12.1 Evaluation of the Margin of Safety	5-138
	5.3.12.2 Additional Analyses on Safety Margins	5-141
6	HEAT SOURCE FABRICATION	6-1
	6.1 Rework of Q-2 IHS and F-9 IHS	6-1
	6.1.1 Rebuilding and Disassembly of Q-2 IHS	6-1
	6.1.2 Rework of Flight Unit F-9	6-1

TABLE OF CONTENTS (Cont)

Section		Page
7	CONVERTER DEVELOPMENT	7-1
	7.1 Materials	7-1
	7.1.1 Materials Testing and Development	7-1
	7.1.1.1 Cold End Strap Plating	7-1
	7.1.1.2 Cold End Bond Braze Anomaly	7-1
	7.1.1.3 RTV 566 Potting Development	7-13
	7.2 Design Analyses	7-19
	7.2.1 Q-2 and F-7 Shunt Resistance Anomaly Investigations	7-19
	7.2.1.1 Introduction	7-19
	7.2.1.2 Summary	7-19
	7.2.1.3 Test Data Review and Analyses of Q-2	7-21
	7.2.1.4 Test Data Review and Analyses of F-7	7-38
	7.2.1.5 Summary of Q-2 and F-7 Test Data Review and Analysis	7-40
	7.2.2 Unicouple Vibration Test	7-42
	7.2.2.1 History	7-42
	7.2.2.2 RCA Tests	7-42
	7.2.2.3 General Electric Tests	7-46
	7.2.3 Conclusions	7-50
	7.3 Design Testing	7-50
	7.4 RTG Performance Analyses	7-52
	7.4.1 Module Testing	7-52
	7.4.1.1 Dopant Precipitation Effects	7-52
	7.4.1.2 Thermal Insulation Conductance Changes	7-61
	7.4.1.3 Electrical Insulation Degradation	7-67
	7.4.1.4 Effects of Carbon Monoxide	7-78
	7.4.2 Performance Predictions	7-95
	7.4.2.1 Launch Pad Power	7-95
	7.4.2.2 Beginning of Mission Power	7-111
	7.4.2.3 Predicted Mission Performance	7-115
8	CONVERTER FABRICATION	8-1
9	CONVERTER DESIGN ANALYSIS, FABRICATION AND TESTING AT RCA	9-1

TABLE OF CONTENTS (Cont)

Section		Page
10	ACCEPTANCE TESTING	10-1
	10.1 ETG Acceptance Testing	10-1
	10.1.1 Q-1A ETG-MJS Cold Test Unit	10-1
	10.1.2 Q-2 ETG-MJS Qualification Unit	10-1
	10.1.3 E-5 ETG	10-3
	10.1.4 F-6 ETG-MJS Flight Unit (1)	10-5
	10.1.5 F-7 ETG-MHW-MJS Flight Unit Spare (1)	10-5
	10.1.6 F-8 ETG-MHW-MJS Flight Unit (1)	10-6
	10.1.7 F-9 ETG-MHW-MJS Flight Unit (1)	10-7
	10.1.8 F-10 ETG-MHW-MJS Flight Unit (2)	10-8
	10.1.9 F-11 ETG-MHW-MJS Flight Unit (1)	10-8
	10.1.10 F-12 ETG-MHW-MJS Flight Unit (1)	10-9
	10.2 RTG Acceptance Testing	10-11
	10.2.1 Q-2 RTG-MHW-MJS Qualification Unit	10-11
	10.2.2 F-6 RTG-MHW-MJS Flight Unit	10-14
	10.2.3 F-7 RTG-MHW-MJS Flight Unit	10-19
	10.2.4 F-8 RTG-MHW-MJS Flight Unit	10-25
	10.2.5 F-9 RTG-MHW-MJS Flight Unit	10-30
	10.2.6 F-10 RTG-MHW-MJS Flight Unit	10-43
	10.2.7 F-11 RTG-MHW-MJS Flight Unit	10-47
	10.2.8 F-12 RTG-MHW-MJS Flight Unit	10-51
	10.2.9 RTG Acceptance Testing Performance Summaries	10-56
11	QUALIFICATION TESTING - Q-2 RTG	11-1
	11.1 RTG Qualification Testing	11-1
	11.2 Q-2 RTG Dynamic Testing	11-1
	11.3 Q-2 RTG Thermal-Vacuum Testing	11-14
	11.4 Q-2 RTG Post Qualification Operations	11-18

LIST OF ILLUSTRATIONS

Figure		Page
2-1	POCO AXF 5Q Strength vs. Temperature	2-14
2-2	Statistics of Failure, AXF-5Q	2-16
2-3	Assembled Hardware for MHW-MJS Explosion Test	2-27
3-1	MJS-IHS Vacuum Operational Temperatures (^{o}F)	3-4
5-1	Cutaway View - MHW-MJS-IHS	5-2
5-2	MHW Fuel Sphere Assembly (FSA); Post Impact Shell Assembly (PISA) in Graphite Impact Shett (GIS)	5-3
5-3	LASL FSA Compatibility Configuration	5-10
5-4	Saturation Concentration of Helium in Solid PuO_2	5-11
5-5	Helium Generation vs. Time for Various MHW Components	5-12
5-6	LASL Test Configuration for CO/PuO_2 Reactions	5-20
5-7	PICS Components	5-21
5-8	Post-Impact Sphere Assembly	5-22
5-9	MHW PISA Vent Designs	5-23
5-9A	PuO_2 Release versus Time with 48 Vents	5-26
5-10	Graphite Impact Shell Configuration	5-29
5-11	Fuel Sphere Assembly Exploded View	5-30
5-12	Fuel Sphere Assembly (FSA) Assembly Sequence	5-30
5-13	FSA MHT-99	5-36
5-14	FSA MHT-100	5-37
5-15	FSA MHT-101	5-39
5-16	FSA MHT-102	5-40
5-17	FSA MHT-103	5-41
5-18	FSA MHT-104	5-43
5-19	FSA MHT-105	5-44
5-20	FSA MHT-106	5-45
5-21	Fracture Strain vs. Number of Grains/Thickness for Biaxial Punch Tests Comparing Previous Data for 45 m/s Impact Velocity to Two Tests at ~ 89 m/s	5-51
5-22	Q-2 IHS Forward End Cap	5-59
5-23	Average Tensile vs. Average Density - MJS and LES	5-65
5-24	POCO End Cap Test Specimens	5-66
5-25	Typical Size and Location of Verification Test Specimens	5-67
5-26	MJS RTG Vibration Test	5-79
5-27	Q-2R IHS	5-80
5-28	Undamaged IHS	5-85
5-29	Effect of Contact Pressure on POCO AXF-5Q/Pyrocarb 406 Interface Thermal Contact Coefficient	5-92

Figure		Page
5-30	Effect of Test Temperature on POCO AXF-5Q/Pyrocarb 406 Interface Thermal Contact Coefficient	5-92
5-31	Q-2 Aft End Cap	5-93
5-32	Forward End Cap,Case I Loading	5-94
5-33	Case IIA Loading, No Radial Restraint	5-95
5-34	Case IIA Loading, Restraint in Radial Direction	5-96
5-35	Case III Loading CTE Variation	5-98
5-36	Heat Source Support	5-99
5-37	Face Loading	5-103
5-38	Unit Solution for Half Latch Truss Assembly	5-105
5-39	Spacecraft Configuration Pre-Injection Configuration	5-112
5-40	Case 4 Altitude and Velocity History	5-112
5-41	Case 4 Heating Rates	5-113
5-42	Case 4 Temperature History	5-113
5-43	Case 4 Stagnation Point Surface Recession	5-114
5-44	Case 4 PICS Temperature History	5-114
5-45	MJS RTG Vibration Test	5-119
5-46	Heat Source Response	5-120
5-47	RTG Case Response	5-120
5-48	Strain Gage Signal Wave	5-121
5-49	MHW-MJS F-6 IHS Sketch of Internal Loss of Pre Load (from Radiograph)	5-124
5-50	MHW-MJS F-7 IHS Sketch of Internal Loss of Pre Load (from Radiograph)	5-125
5-51	Test Configuration	5-128
5-52	Forward End Cap Loaded in Compression Through Pre Load Nut	5-128
5-53	Undamaged IHS	5-130
5-54	F-6 IHS	5-131
5-55	F-7 IHS	5-132
5-56	MJS End Cap and Aeroshell	5-134
5-57	Finite Element Model with Isotherms in Increments of 400°F (Case 1)	5-135
5-58	Finite Element Model with Isotherms in Increments of 400°F (Case 2)	5-135
5-59	Finite Element Model with Isotherms in Increments of 400°F (Case 3)	5-136
5-60	Finite Element Model with Isotherms in Increments of 400°F (Case 4)	5-136
5-61	MJS End Cap Steep Angle JPL Case 2 Stress vs Time From 400,000 Feet	5-139
5-62	MJS End Cap Steep Angle JPL Case 2 Stress vs Time From 400,000 Feet	5-139

Figure		Page
5-63	Hoop Stress and Temperature vs. Wall Thickness	5-142
5-64	Statistics of Failure, AXF-5Q	5-143
7-1	MHW Radioisotope Thermoelectric Generator	7-0
7.1-1	Unicouple Pre Acceptance Thermal Cycle	7-11
7.1-2	Unicouple Post Vibration Thermal Cycle	7-11
7.2-1	Thermal Transient During Axis Change	7-33
7.2-2	Converter Circuit	7-36
7.2-3	Unicouple Test Results	7-43
7.2-4	Sinusoidal Vibration of Unicouple 1, Acceptance Level	7-46
7.2-5	Sinusoidal Vibration of Unicouple 3, Five g Input	7-47
7.2-6	Response Double Amplitude of Two Unicouples to Random Excitation	7-48
7.2-7	Sinusoidal Vibration D-5A Module, 5 g Input	7-48
7.2-8	Sinusoidal Vibration D-5A Module, 1/2 Acceptance Level	7-49
7.2-9	Sinusoidal Vibration D-5A Module, Acceptance Level	7-49
7.4-1	Module 18D Old and New T/E Data	7-53
7.4-2	Module 18D Comparison of Measured to Theoretical Performance	7-55
7.4-3	Module 18E Comparison of Measured to Theoretical Performance	7-56
7.4-4	Module 18G Comparison of Measured to Theoretical Performance	7-57
7.4-5	Module 18H Comparison of Measured to Theoretical Performance	7-58
7.4-6	SN-3 1035°C New Data, DR Factor	7-59
7.4-7	SN-3 1035°C New Data, DR Factor	7-60
7.4-8	SN-6 1035°C New Data, DR Factor	7-62
7.4-9	SN-2 1085°C New Data, DR Factor	7-63
7.4-10	SN-5 1085°C New Data, DR Factor	7-64
7.4-11	SN-1 1135°C New Data, DR Factor	7-65
7.4-12	SN-4A 1135°C New Data, DR Factor	7-66
7.4-13	T/E Leg Conductivity Changes Taken into Account	7-68
7.4-14	Insulation Thermal Conductance Rates	7-69
7.4-15	Insulation Thermal Conductance Changes	7-69
7.4-16	18-Couple Modules Resistance to Foil	7-70
7.4-17	Modules 18D, E, G and DC-13 Uncoated Couples	7-71
7.4-18	Modules Operated at 1000°C Hot Junction Design Temperatures	7-73
7.4-19	18-Couple Modules, Resistance to Foil	7-74
7.4-20	Mass Loss Per Couple as a Function of Time	7-76
7.4-21	Silicon Loss Per Unicouple Which Contributes to Shunt Resistance and Insulation Degradation as a Function of Hot Junction Temperature	7-77

Figure		Page
7.4-22	Hot and Cold Junction Temperature vs Time	7-80
7.4-23	DC-9, Couple 7, SiC Formation on Hot Shoe (22X)	7-83
7.4-24	Weight Loss Rate of Si_3N_4 Coated Hot Shoes in Vacuum	7-84
7.4-25	CO Pressure in RTG as a Function of Time and Calculated for Coated Couples	7-87
7.4-26	Weight Loss Rate of Si_3N_4 Coated SiMo Hot Shoes Operating in 1×10^{-4} Torr CO (JPL Data)	7-88
7.4-27	Mass Loss Rate as a Function of CO Pressure and Temperature	7-91
7.4-28	Mass Loss Rate as a Function of CO Pressure and Temperature	7-92
7.4-29	Coating Lifetime for Hot Shoes Operating in Vacuum	7-92
7.4-30	Critical Mass Loss as a Function of CO Pressure	7-93
7.4-31	Coating Life as a Function of Temperature and CO Pressure	7-94
7.4-32	Cumulative Mass Loss Per Couple as a Function of Time Using Average Hot Junction Temperature	7-96
7.4-33	Cumulative Mass Loss Per Couple as a Function of Time Using Average Hot Junction Temperature	7-97
7.4-34	T/E Leg Temperature Profiles	7-100
7.4-35	F-6 Xenon Power	7-100
7.4-36	F-7 Xenon Power	7-101
7.4-37	F-8 Xenon Power	7-101
7.4-38	F-9 Xenon Power	7-102
7.4-39	F-10 Xenon Power	7-102
7.4-40	F-11 Xenon Power	7-103
7.4-41	F-12 Xenon Power	7-103
7.4-42	F-6 RTG Expected Power with Xenon Gas Fill	7-104
7.4-43	F-7 RTG Expected Power with Xenon Gas Fill	7-105
7.4-44	F-8 RTG Expected Power with Xenon Gas Fill	7-105
7.4-45	F-9 RTG Expected Power with Xenon Gas Fill	7-106
7.4-46	F-10 RTG Expected Power with Xenon Gas Fill	7-106
7.4-47	F-11 RTG Expected Power with Xenon Gas Fill	7-107
7.4-48	F-12 RTG Expected Power with Xenon Gas Fill	7-107
7.4-49	Launch Transient Power	7-110
7.4-50	Power Loss as a Function of Equivalent Vacuum Aging Hours	7-114
7.4-51	LES 8 & 9 Flight Power Ratio Measured vs Predicted	7-116
7.4-52	Leg Conductivity Change	7-117
7.4-53	Leg Conductivity Change	7-118
7.4-54	LES 8 & 9 Flight Power Ratio Measured vs Predicted	7-118
7.4-55	F-6 Predicted Performance Power at RTG Connector	7-119
7.4-56	F-7 Predicted Performance Power at RTG Connector	7-120
7.4-57	F-8 Predicted Performance Power at RTG Connector	7-120
7.4-58	F-9 Predicted Performance Power at RTG Connector	7-121
7.4-59	F-10 Predicted Performance Power at RTG Connector	7-121

Figure		Page
7.4-60	F-11 Predicted Performance Power at RTG Connector	7-122
7.4-61	F-12 Predicted Performance Power at RTG Connector	7-122
10-1	MHW-MJS System Test Schedule 1976	10-2
10-2	Heat Source Loading vs Time	10-57
11-1	MJS RTG Qualification Test Program	11-1
11-2	MJS RTG Vibration Test	11-6
11-3	Q-2R IHS Before and After Qualification Vibration Tests	11-23

LIST OF TABLES

Table		Page
2-1	MHW-MJS USAR Review Meeting Agenda	2-2
2-2	Action Items from INSRP Meeting for the USAR	2-4
2-3	Summary of MJS 77 Mission Potential Fuel Release Events	2-10
2-4	Maximum Center of Gravity Offset for Damaged and Undamaged IHS	2-17
2-5	Topical Agenda for MHW-MJS 77 FSAR Review	2-22
3-1	MJS Steady State IHS/RTG Temperatures	3-3
5-1	MHW Fuel Characteristics	5-6
5-2	Fuel Characterization - 1	5-7
5-3	Fuel Characterization - 2	5-8
5-4	MHW Fuel Sphere Assembly Compatibility Test at LASL	5-9
5-5	$^{238}PuO_2$ Fines(*) Found in FSAs Subjected to Various Environments	5-15
5-6	Reduction of PuO_2 by CO Calculated vs. Observed Values	5-18
5-7	Calculated Reduction of PuO_2 by CO-PuO_2 at 1237°C (1600°K)	5-19
5-7A	Calculated Release of PuO_2 (g) from MHW-FSA with Two 0.005" Dia. Vents	5-25
5-8	Total Plutonium Content of MHW GISs	5-27
5-9	FSA Test Summaries - Impacted at GE-SD Valley Forge Bldg 8	5-35
5-10	LASL Fueled MHW Impact Test Summary	5-47
5-11	FSA Test Summaries - Impacted at LASL	5-49
5-12	Summary of FSA Impact Results Including Intensity Ratios from Anger Electron Spectrocopy	5-53
5-13	Radiological Contamination Data Q-2 IHS	5-57
5-14	Gas Analyses Results MHW-IHS	5-60
5-14A	Q-2 End Cap Failure Sequence	5-63
5-15	Summary of Acceptance and Verification Test Results - POCO Graphite Plates (Averaged Values)	5-68
5-16	Assignments of POCO Graphite in MJS IHS	5-73
5-17	MJS Plate Data (Acceptance Test Data)	5-74
5-18	Transverse Tensile Strength Data	5-75
5-19	Shock and Vibration, Acceptance Test	5-77
5-20	Shock and Vibration, Qualification Test	5-77
5-21	Shock and Vibration, Qualification Test	5-78
5-22	POCO AXF 5Q/Pyrocarb 406 Interface Conductance Test Results	5-91
5-23	Explosive Overpressure on RTG	5-102
5-24	Impulsive Loading on RTGs	5-104
5-25	Truss Loads for One Percent Yield (CBM)	5-104
5-26	Explosion Overpressure on Spacecraft	5-105
5-27	Impulsive Loading on Spacecraft	5-106
5-28	Spacecraft and RTG Velocities at Noted Yield	5-106

LIST OF TABLES (Cont'd)

Table		Page
5-29	RTG Allowable Loads Compared to Explosive Overpressure Loads	5-107
5-30	Centaur Projectile Velocity	5-107
5-31	Projectile Momentum	5-108
5-32	RTG Explosive Overpressures	5-108
5-33	Spacecraft Explosive Overpressures	5-109
5-34	Impulsive Loading on RTG and Spacecraft	5-109
5-35	Velocities at Noted Yield	5-110
5-36	Aeroshell Temperature Matrix (at 103 sec) Z Axis ~ Degrees	5-116
5-37	Sleeve Temperature Matrix (at 83 sec)	5-116
5-38	Shock and Vibration, Acceptance Test	5-117
5-39	Shock and Vibration, Qualification Test	5-117
5-40	Shock and Vibration, Qualification Test	5-118
5-41	Load Acting on Aft Tray Tie Bolt Head	5-122
5-42	Loads Acting on Aft Tray Tie Bolt Head	5-126
5-43	Maximum Center of Gravity Offset for Damaged and Undamaged IHSs	5-133
5-44	Stagnation Pressure, Altitude and Time	5-137
5-45	Margin of Safety Based on MJS Billet Data	5-140
5-46	Thermal and Air Load Results	5-141
6-1	Use of IHSs in MJS RTGs	6-2
7.1-1	RTG Component and Material Summary	7-2
7.1-2	Sodium Cyanide Treated Unicouples	7-12
7.1-3	"Same Day" Treated Unicouples with High ΔR_T and/or High ΔP_{CS} in Converters	7-14
7.2-1	Q-2 Vibration Test Data	7-24
7.2-2	Comparison of Measured Power Change with Predicted Power Change Based on Converter Open Circuit Voltage Measurements	7-30
7.2-3	Vibration Sequence	7-42
7.2-4	Comparison of Response of Wrapped and Bare Unicouples to Sinusoidal Acceleration	7-45
7.4-1	Extrapolated Resistance to Foil at Four Years Uncoated Couples	7-72
7.4-2	Module Characteristics	7-82
7.4-3	Quanity of Reacted CO	7-83
7.4-4	Mass Loss Rates from Hot Shoe, gm/cm^2 hr	7-85
7.4-5	Calculated CO Generation Rate in an RTG at 1035°C from 18 Couple Module Tests	7-85
7.4-6	Calculated Initial CO Pressure at 1035°C Hot Shoe	7-86
7.4-7	Percentage of Critical Mass Loss as a Function of CO Pressure and Time	7-98

LIST OF TABLES (Cont'd)

Table		Page
7.4-8	Calculated Xenon Power at Start of Storage	7-98
7.4-9	Average Hot and Cold Junction Temperature for Various Environments	7-99
7.4-10	Calculated Effective Age for Start of Storage Hours	7-103
7.4-11	Power at Electrical Performance Checks (F-10, F-11, F-12) Voyager II	7-108
7.4-12	Power at Launch (F-10, F-11, F-12) Voyager II	7-108
7.4-13	Power at Electrical Performance Checks (F-6, F-8, F-9) Voyager I	7-109
7.4-14	Power at Launch (F-6, F-8, F-9) Voyager I	7-109
7.4-15	Power Drop During Launch	7-111
7.4-16	Predicted Power Six Hours After Launch	7-111
7.4-17	Voyager RTGs-Thermal Vacuum Power at the End of Acceptance Testing	7-112
7.4-18	Storage Time from Thermal Vacuum Test to Launch and Fuel Loading at Launch	7-113
7.4-20	Calculated BOM Power Range	7-115
7.4-21	RTG Power Output Predictions (30 Volt Operation)	7-123
7.4-22	Projected Margin Over Design Requirements	7-123
7.4-23	Summary of Projected Performance	7-124
10-1	F-6 Performance Summary	10-59
10-2	F-7 Performance Summary	10-61
10-3	F-8 Performance Summary	10-63
10-4	F-9 Performance Summary	10-65
10-5	F-10 Performance Summary	10-67
10-6	F-11 Performance Summary	10-69
10-7	F-12 Performance Summary	10-71
10-8	Comparison of LAS Performance	10-73
10-9	Comparison of Post Vibration Vacuum Performance	10-74
11-1	Q-2/RTG Shock and Vibration - Acceptance Levels	11-3
11-2	Q-2/RTG Shock and Vibration - Qualification Levels	11-4
11-3	Q-2/RTG Shock and Vibration - Qualification Levels	11-5

SECTION 1

INTRODUCTION AND SUMMARY

1.1 INTRODUCTION

This report describes the work performed by the General Electric Company, for the United States Energy Research and Development Administration - Division of Nuclear Research and Application, on the Multi-Hundred Watt Radioisotope Thermoelectric Generator, for the NASA Mariner (now Voyager) Jupiter-Saturn (MJS) Program, under Contract Number E(49-15)-3066. The period covered by this report extends from 1 January 1976 through 30 June 1977. Much of the basic design of the MHW-LES was used for MJS. Consequently, reference is made in this report to the preceding reports on MHW-LES, as well as to the previous annual report for MHW-MJS. These reports and the periods covered are:

- GESP-7071 (1970-71)
- GESP-7097 (1972)
- GESP-7107 (1973)
- GESP-7122 (1974)
- GESP-7123 (1975) for LES
- GESP-7127 (1975) for MJS

During the reporting period, 1976-1977, development, fabrication and testing of the MHW-MJS RTGs were completed. The seven flight qualified units, six for flight and one spare, were delivered to KSC during May and June 1977. The two Voyager launches are scheduled for 20 August and 1 September 1977.

1.2 SUMMARY

The significant events and activities occurring on the MHW-MJS Program are summarized in the brief notes of the paragraphs following; details are provided in the subsequent sections of this report.

- An analysis was performed to determine the effects on the RTG of explosions and projectiles arising from a catastrophic accident to the launch vehicle.

- GE-NP was directed by ERDA to delete the proposed projectile test (MS-2) from the safety test program. This left only the explosion test (MS-1) remaining in the program. A test plan covering the explosion test was prepared and submitted to ERDA.

- A meeting of Safety Panel Coordinators was held 19 May 1976 to review NASA and USAF objections to the MHW-MJS Explosion Test Plan and to consider alternatives. A number of changes to the test plan resulted from the meeting.

- The MHW-MJS Explosion Test was conducted 6 October 1976 at Sandia Laboratories with somewhat less severe results than were predicted. An MHW converter with a dummy loaded heat source and two simulated RTGs were stacked vertically for the test.

- Modifications to the Building 300 thermal vacuum test area were approved by ERDA-ALO Operational Safety. A performance test was carried out on the system.

- Revision A to the MJS-GSAR for GE-VF, GEMS-422, was published on 29 March 1976.

- An addendum to the RTG-SC SARP, GEMS-408, was approved by ERDA and issued.

- The MJS Operations Analysis Group met at MRC on 21 January 1976 and at GE-VF on 21 January 1976 to review the MHW-MJS heat source operations at each facility. A document covering operations at ML, GE, JPL, and KSC was coordinated, edited and issued by Sandia.

- Initial plans were formulated for the JPL-supported magnetic-testing of F-8 and F-9 to be done at GE.

- An assessment was made of the radiation dosage to personnel anticipated in the direct handling of the RTGs (F-8, F-9, F-10, F-11, and F-12) for determination of their magnetic characteristics. A new Standing Instruction (SI) was issued to cover these operations in Building 800 and Building 300. An amendment to the GSAR for this activity was prepared and approved by ERDA/ALO-OSD. Actual exposures incurred were lower than originally projected.

- Magnetic characteristic determinations were made at GE-SD for RTGs F-8 through F-12; RTGs F-6 and F-7 were measured at KSC in June 1977. All units satisfied the specification requirements.

- The Updated Safety Analysis Report was completed and published on schedule, in June 1976.

- The review of the MHW-MJS Updated Safety Analysis Report was held at General Electric Company, Valley Forge on 14, 15 and 16 September 1976. The meeting was attended by representatives from 27 different agencies and contractors. A result of the meeting was a list of nineteen action items as additional input for the Final Safety Analysis Report (FSAR).

- Interface conduction tests between the ablation sleeve and aeroshell materials demonstrated that the values assumed for reentry calculations were acceptably close.

- The Final Safety Analysis Report (FSAR) for the MHW-MJS 77 Mission was completed and published in February 1977.

- A meeting of the Interagency Nuclear Safety Panel (INSRP) was held at General Electric Co., Valley Forge Space Center on 23 February 1977 to review the reentry analyses for the FSAR.

- The Final Safety Analysis Report (FSAR) for the MJS 77 Mission was reviewed in a meeting of the Interagency Nuclear Safety Review Panel (INSRP) at Kennedy Space Center, Florida on 29-31 March 1977.

- The four top-level RTG specifications were approved by ERDA, and these specifications, as revised, were then issued in April 1976.

- Outstanding differences between GE specifications and JPL interface specifications were discussed in a meeting at JPL on 21 April 1976 and basic understanding was reached on the more salient points.

- The forward end cap, in the MJS qualification unit Q-2, was found to be cracked when the unit was removed from the EPC at GE-SD in January 1976. The unit was returned to ML-MRC and was rebuilt as Q-2R IHS.

- With strong ERDA/NRA assistance, a vigorous investigation of the possible causes of the Q-2 end cap failures was instituted which involved Sandia Labs, ML-MRC, OR/Y-12 and POCO, Inc. in addition to GE-SSL and GE-SD-NP. It was determined that the POCO material contained excessive metallic impurities as carbides which reacted with water absorbed by the IHS middle 8-pack following a leak in the 8-pack storage container at ML-MRC. The reaction caused swelling of the end caps into interference with the aeroshell and consequent fracture.

- At a meeting of the Q-2 End Cap Anomaly Task Force, on 5 August 1976, all outstanding questions of the Task Force were resolved and the conditions placed on acceptance of heat sources Q-2R, F-6, F-7, F-8 and F-9 were subsequently removed.

- A test program to verify the survivability of all POCO flight hardware was pursued to the end of the program. Three end cap plates, meeting the acceptance specifications, were eliminated from flight use by the results of the verification tests.

- During the shock and vibration testing of the Q-2 RTG at the original qualification levels, later recognized as in excess of necessary requirements, low electrical resistance developed between the T/P and the foil insulation. These remained after the end of testing.

- A similar low resistance developed in the F-7 RTG, also during shock and vibration testing. This low resistance disappeared during resistance checks made after test and did not reappear.

- Extensive analyses, based on the electrical data, were made to locate the low resistance shunts in the Q-2-RTG.

- The Q-2 RTG was disassembled down to the thermopile level to determine the cause(s) of the low resistances and to verify their locations.

- The disassembly confirmed that abrasion of varglass insulation on the degaussing loop permitted intermittent contact with the foil insulation.

- Additional mechanisms for forming low resistance paths between the T/P and the foil insulation were particles of foil, fragmented during the high level qualification shock and vibration, lodged in the astroquartz connector wrap between the electrical connectors and the heat shunts. Two shorts from this mechanism were found after disassembly.

- Analyses of the Q-2 RTG vibration exposure indicated that the internal failure probably occurred during the 25 Hz sine 30-second dwell, a condition not expected to occur in any credible mission environment.

- Damage suffered by the Q-2 RTG during vibration testing led to a 12 June 1976 interface meeting at JPL which resulted in changes to the acceptance test vibration requirements of the RTG Product Specification.

- The Environmental and Test Requirements Specification was also revised to reflect the new vibration test levels.

- The reduced shock and vibration testing levels, agreed upon by JPL and GE as being more nearly representative of the MJS mission environments, were used on F-8 through F-12 RTGs with no recurrence of the problem.

- After vibration testing of the Q2 RTG at the original (excessive) qualification levels, it was determined that the preload on the Q-2R IHS was lost.

- Radiography of the Q-2R IHS at ML-MRC showed extensive damage to the internal structures of the IHS.

- Partial disassembly of the Q-2R IHS was done at ML-MRC in June 1976 but was stopped because of Pu contamination levels considered excessive for the ML-MRC IHS assembly cell.

- Radiographic examination of the F-6 and F-7 RTGs showed that both F-6 and F-7 IHS had lost preload by crushing of the aft spring assembly tie bolt head.

- Subsequent examination of radiographs, taken routinely at ML-MRC of the IHSs before shipment to GE, showed that the tie bolt heads in the aft spring assemblies of F-6 and F-9 were crushed and that in F-7 was probably damaged.

- Test of the explosion test dummy RTG showed that no additional damage to an IHS with a borken aft tie bolt head would occur during the shock and vibration expected in the launch phase of the MJS mission. This supported the decision to use the F-6 and F-7 IHSs for flight.

- The aft spring assembly tie bolt was redesigned to replace the bolt head with a POCO nut instead of the integral Pyrocarb-508 bolt head.

- Test of the redesigned aft spring assembly, as an individual part under static load and as part of a dummy RTG under vibration, demonstrated the survivability of the new design.

- A report, "MHW-MJS Program Summary Report, Loss of IHS Preload Problem", covering analyses and tests resulting in IHS redesign was issued, October 1976.

- The new design was used in the IHSs: F-10, F-11, F-12 and the rebuilt F-9, designated F-9R.

- The F-9 heat source was reworked to replace the tie bolts with the newly designed tie bolts in accordance with agreements reached at the 13 September 1976 meeting at GE. The F-9 is now designated F-9R and was used in the F-12 RTG.

- Complete disassembly of the Q-2R IHS was effected by BNI-CL, in its West Jefferson hot cells. No fracture of the fuel sphere containment (PSIA) was found. The damage to the aeroshell and ablation sleeve, designed for reentry protection was negligible. The damage was confined principally to internal, non-critical components.

- Disassembly of the Q-2R heat source was completed at Battelle-Columbus. A final report on the Q-2R disassembly was published by Battelle, on 14 March 1977 (BMI-X-678).

- Analyses were made of the F-6 and F-7 IHSs, to establish the maximum CG offset and to evaluate the possible effects of this offset on the reentry behavior. The effects were found to be trival. A document reporting this work, "Loss of IHS Preload Problem", was issued in September 1976.

- Revision A to the MJS Failure Mode Effects and Criticality Analysis (FMECA) was prepared and work was completed on a final reliability assessment report.

- The MJS FMECA report was completed.

- Testing on the 4-couple and 18-couple converter modules were completed at RCA by January 1977.

- These modules provided kinetic data, as a function of time/temperature, for the major degradation modes of the MJS converters.

- By the time the 18-couple module tests were ended, the exposure times had reached:

  - Approximately 30,000 hours for the modules without Si_3N_4 coating on the T/E elements, at 1035°C, 1085°C and 1135°C.

  - Approximately 23,000 hours for the module, with Si_3N_4 coating, at 1035°C and 1085°C.

  - Approximately 1800 hours for the modules, with Si_3N_4 coating, at 1035°C and 1085°C.

- Using updated thermoelectric materials properties data from JPL, the data from the module tests were adjusted and factored into the performance analyses.

- The performance analyses included the effects of:

  - Dopant precipitation.

  - Thermal insulation degradation.

  - Electrical insulation degradation.

  - CO.

- Using the cumulative effects of all degradation modes, aging before launch, and decay of the radioisotope fuel, the projected power margin over the required power was determined to be > 5 watts during all phases of the mission, for all flight units.

- An investigation of the cause of exterior residue on the F-9 RTG following the thermal vacuum test was satisfactorily concluded and reported in November 1976.

- An investigation of the spalling of the emissive coating on RTG F-11 was concluded and reported in April 1977.

- All fuel sphere fabrication was completed by ML-MRC in April 1976; welding into the Ir PICSs and assembly as FSAs was completed in November 1976.

- Final IHS assembly, rebuilding of the F-9 IHS as F-9R IHS, was completed in early January 1977.

- Tests of the FSA flight design He vent filter at LASL showed no permanent plugging after more than 23,000 hours at approximately 1330°C and no observable damage to the integrity of the PISA. Two MHW FSAs continued on test at LASL through 30 June 1977.

- Combustion analysis of the GISs removed from LASL test FSAs and from eight other FSAs, taken from Q-2R IHS after its disassembly, demonstrated the ability of the PISA vent filter to prevent significant losses of Pu from the PISA.

- Eight FSA impact tests were performed at GE-SD, with ThO_2 fuel-simulant, for verification of the Ir PICS fabrication.

- Four FSA impact tests were performed at LASL, with production line $^{238}PuO_2$ fuel spheres and flight quality hardware, in support of establishing realistic source terms for the safety analyses.

- LASL compatibility tests of the PuO_2 + Ir + C, materials constituting the FSA, carried out to more than 20,000 hours at 1330°C, established that no interaction occurs under MJS operational conditions.

- LASL continued to investigate the characteristics and behavior of the PuO_2 fuel, primarily in support of safety analyses.

- Approximately 120 ANs, 60 ECNs, and 400 NCRs were processed during 1976-77.

- QA surveillance of RCA, Speedring, and others continued through final hardware deliveries.

- Seven flight-qualified RTGs, six for flight plus one spare, were delivered to KSC in May and June 1977.

SECTION 2

SAFETY

2.1 SAFETY ANALYSIS AND REPORTING

2.1.1 UPDATED SAFETY ANALYSIS REPORT

The Updated Safety Analysis Report (USAR) for the MHW/MJS-77 mission was completed and published (Document No. 76SDS4241, General Electric Company) toward the end of June 1976. The results of the fourth and final re-entry breakup analysis case (powered re-entry) were received from JPL during mid-May, but the analysis of the RTG response after release from the spacecraft could not be completed in time to be included in the USAR. This analysis was subsequently presented in the final report (FSAR).

The review of the MHW/MJS Updated Safety Analysis Report was held at General Electric - Valley Forge on September 14, 15, 16, 1976. This meeting was convened by the Interagency Nuclear Safety Review Panel and was attended by approximately 60 persons representing 27 various agencies and contractors. The meeting agenda is presented in Table 2-1.

An area receiving considerable attention in the review was the analysis of the spacecraft and RTG re-entry following a launch vehicle malfunction and mission abort. Of special concern were the potential ramifications associated with use of the two flight heat sources having experienced failure of the tie-bolts internal to the heat source during acceptance testing (see Section 5 for details of the subsequent investigation and design modification).

The re-entry analysis presented in the review indicated that the RTGs/IHSs would possibly be in an end-on attitude during a portion of re-entry, and this could occur near or during the peak heating portion of the trajectory, especially for the superorbital, steep angle re-entry. For the USAR, the analysis addressed only the side-on stable attitude of the IHS once it was released because of the predominant stability in this orientation. Analyses conducted subsequently for a situation in which the IHS was assumed to remain end-on throughout the re-entry resulted in failure of the IHS end cap. As a result of these factors, the Re-entry Subpanel considered that more detailed re-entry analysis should be performed, especially

TABLE 2-1. MHW/MJS USAR REVIEW MEETING AGENDA

Tuesday, September 14, 1976	
I. Introduction	Panel Co-Chairman
II. Program Summary	
RTG Program Status	NRA/ERDA
MJS Program Status and Spacecraft Description	JPL
Launch Vehicle Safety Study Summary	LeRC/NASA, GD/C
Spacecraft Re-entry Breakup Analysis	JPL
RTG System Description and USAR Summary	GE
Hardware Acceptance Test Summary (Q2R/F6/F7/F8)	GE
RHU System Description and Safety Summary	ML/MRC
III. INSRP Subpanel and Special Reports	
Heat Source/RTG Ground Transportation and Handling	ALO
Cape Safety Activity Summary	KSC/NASA
Range Safety Display System	AFETR
MJS Safety Test Summary	LASL
Source Term Analysis	LASL
Project Vulcan Status	LASL, AFWL
Re-entry Subpanel Report	LaRC/NASA
Independent Risk Analysis	NUS
Biomedical Subpanel Report	DBER/ERDA
Wednesday, September 15, 1976	
I. Question and Answer/Discussion Session	
II. Co-Chairmen Summary	
Thursday, September 16, 1976	
I. Action Item Review	
II. Recommendation Paper	

for the Final Safety Analysis Report (FSAR). Consequently, the INSRP Coordinators sent a list of recommended action items to the ERDA NRA Director and to the JPL MJS Project Manager as additional input for the FSAR. Included in this list were items pertaining to other areas of the safety review, but many were associated with the concerns in the re-entry area. A list of the action items is presented in Table 2-2.

2.1.2 FINAL SAFETY ANALYSIS REPORT

For the preparation of the Final Safety Analysis Report (FSAR), the decision was made to restructure the phase breakdown of the mission and the accompanying launch vehicle accident probabilities to correspond as closely as possible with those given in the Convair Phase II report (Report No. CASD/LVP 76-994, "MJS '77 Safety Study. Phase II Range Safety Equipment, Launch Pad Hazards, Launch Vehicle Failure Probabilities, and Re-Entry Environment." General Dynamics Convair Division, 5 April 1976). Modifications to the Convair mission breakdown were made only to the extent necessary either to update or to correct discrepancies in the probabilities given. This approach was taken to facilitate comparison of the Accident Model Document probabilities and associated event sequences with those in the Convair report in order to avoid the confusion and differences which arose in the INSRP review of the Updated Safety Analysis Report (USAR). This prompted Action Item No. 11 (see Table 2-2) resulting from the USAR review in September. This item, to resolve the differences in failure probabilities, particularly for the superorbital re-entry case, was completed prior to the end of the USAR review by the committee made up of GE, GD/C, NUS, and AFWL.

A concerted analytical effort was undertaken to address the remaining action items (Items No. 2, 3, 6, 7, 8, 9, 10, 12, 13, and 14) given to General Electric /Nuclear Programs as a result of the USAR review. This effort was concentrated mainly in the area of the re-entry analysis, especially as related to the superorbital, steep-angle re-entry breakup case. Included in this analysis were the effects of using an IHS having a broken tie bolt in the bottom 8-pack of FSAs, such that the center-of-gravity location in the IHS could shift. The re-entry evaluation also included an analysis of the situation in which an RTG, after being released from the 3-stack on the MJS spacecraft, is arbitrarily assumed to attain and to

TABLE 2-2. ACTION ITEMS FROM INSRP MEETING FOR THE USAR

1. (LASL, APL, GE) A plan for FSA ablation and impact tests will be prepared by Bronisz and Hagan with GE assistance by October 15, 1976, for review by the panel and project.

2. (GE) Determine the residual source term to the atmosphere if the aeroshell fails on re-entry. This activity should include an analysis of the re-entry behavior of released FSAs, the footprint, source term, and radiological risk.

3. (GE, Panel) The biomedical subpanel recommends that the source term analysis show composition, quantity and quality of release for each RTG. Partition of vapor, particulates and isopleths at impact should be done without regard to probability. The range of isopleths should be from maximum per km^2 (e.g., "ground zero") down to low levels (suggest lung burdens of 0.3, 1.6, 5, 16 and "max" nanocuries).

   For highest probability cases, it is also requested that the effect of environmental modifiers be included in the analysis. Environmental fate of total source term (including other radionuclides) should be addressed.

4. (JPL) Determine if available energy on spacecraft could be made available to extend earth orbit in the event that mission objectives cannot be met. Define maximum attainable orbital lifetime.

5. (Project) Complete disassembly and analysis of Q-2R.

6. (GE) Determine the maximum CG offset for a normally preloaded IHS system.

7. (GE) Evaluate structural response of aeroshell during transition from end-on motion due to CG offset for a normally preloaded and a damaged IHS.

8. (GE) Conduct a break-up analysis of an end-on entry of a single RTG configuration, define the subsequent release condition of the IHS and conduct an end-on thermal stress analysis of the IHS.

9. (GE) Assess the motion and responses of all flight RTGs before the IHS is released and the IHSs after release. (Case II)

10. (GE) Determine under what conditions and at what time during reentry are the "g" loads at a level which would cause failure of the tie bolt head in the original design (F8, F10).

11. (GE, GDC, NUS, AFWL) Resolve apparent differences in failure probability numbers presented during this review, particularly for the superorbital reentry case.

12. (GE) Three risk assessments should be included in the FSAR: (1) utilizing F-6 as one of the flight units, (2) utilizing three RTGs with proper preload within the heat sources and (3) as an appendix, utilizing F-7 and F-6 as two of the flight units on one spacecraft.

TABLE 2-2. ACTION ITEMS FROM INSRP MEETING FOR THE USAR (continued)

13.	(GE) The FSAR should include rationale used by GE for RTG failures (e.g.,) (1) What constitutes aeroshell failures, (2) what constitutes IHS release from the converter.
14.	(GE) Review consistency of data in the USAR for source term presentation in the FSAR. Present source term in consistent manner with proper combinatorial analyses techniques for multiple units.
15.	(GE) Provide analyses or tests to define consequences of high velocity fragment impact with RTG/IHS on launch pad.
16.	(GE) Determine if a fireball environment on the launch pad can ignite the TE 364 motor.
17.	(Project) The Project should present a combined summary risk assessment to the panel for the RTGs and RHUs.
18.	(Panel) Panel should prepare special instructions for the Range Safety Officer procedures if required for safety considerations. At this time, the panel has no special requirements.
19.	(Panel) The reentry subpanel will review and comment on the analyses that have been carrier out to identify deficiencies in an attempt to improve analytical approaches for new systems.

maintain an end-on attitude throughout the remainder of the re-entry including release of the IHS, with the IHS then being assumed also to maintain an end-on attitude.

The other main portion of the action items pertained to the treatment of the source terms for those situations that could potentially release fuel. For the FSAR, the presentation of the source terms was expanded to show the composition, quantity, and quality of release for each IHS involved and as related to the several plutonium isotopes present in the fuel along with selected daughter radionuclides. In addition, the source terms were presented as a function of time from launch until a period of 100 years, this range reflecting a portion of the range of orbital lifetimes that could occur following a launch vehicle malfunction in orbit and prior to re-entry and impact of the IHSs. The range of isopleths for dispersed material following impact or other release mechanism was referenced to lung burdens of the ^{238}Pu isotope of 0.3, 1.5, 5, and 16 nanocuries. For elevated releases (due to thermal buoyancy

from solid propellant fires), the maximum lung burden was also determined. In the presentation of the population exposures, the numbers of people affected and the associated lung burdens were presented first without regard to probabilities, next with probabilities associated with the largest numbers of exposures, and finally with numbers of exposures averaged over meteorological and demographic conditions. The risk analysis also addressed the situation in which the aeroshell of the IHS was assumed to fail (i.e., as related to a stabilized end-on attitude re-entry, arbitrarily assumed to exist) with the resultant source terms arising from individual FSAs impacting on the Earth's surface.

One item that was not addressed in the FSAR was Action Item 16, pertaining to the effects of a launch pad fireball environment on the TE-M-364-4 solid propellant motor of the MJS spacecraft propulsion module (PM). The manufacturer of this motor, Thiokol Corporation, was contacted and questioned about the ignition potential of the propellant in the fireball. Thiokol stated definitely that the propellant could be ignited through the nozzle. On the other hand, the shaped destruct charge used on the PM would also be ignited by the fireball most probably before the TE-M-364-4 was ignited. The propulsive capability of the PM would consequently be nullified by the destruct charge, as it would be in activation of the Command Shutdown and Destruct System - CSDS.

The remaining item on the list (for GE), Action Item No. 15, pertained to analyses or tests to define the consequences of high velocity projectile impact with the RTG/IHS on the launch pad. This item had been previously addressed and presented in the USAR. There was no other action taken in this area since the analysis that had been performed, although simplified, was deemed to be all that could be done in a practical manner.

The Final Safety Analysis Report for the MHW-MJS-77 mission was completed and published in two documents as follows:

Document No. 77SDS4206 "Final Safety Analysis Report for the MJS-77 Mission.
Volume I: Reference Design Document
Volume II: Accident Model Document:
General Electric/Space Division, January 1977.

Document No. GESP-7129 (Confidential-Defense Information)
"Final Safety Analysis Report for the MJS-77 Mission.
Volume III. Nuclear Risk Analysis Document (U)." General Electric/Space Division, January 1977.

These documents presented the analyses and test results used to finalize the evaluation of the nuclear safety potential and associated risks for the MHW-RTG as employed in the MJS-77 mission. This final evaluation expanded and completed the work published in the Updated Safety Analysis Report. The FSAR addressed also the action items established by the Interagency Nuclear Safety Review Panel (INSRP) at the USAR review held in September, 1976.

For purposes of the FSAR, the reference mission was divided into four distinct phases for the safety analysis. These phases covered all mission related operations beginning with mating of the spacecraft with RTGs to the launch vehicle on pad and ending with the successful attainment of the hyperbolic Earth escape trajectory during the second burn (including the shutdown) of the Centaur. Since an incorrect burn of the propulsion module (TE-M-364-4) of the spacecraft would not result in atmospheric re-entry (following a successful second burn of Centaur), escape of the MJS' 77 from the Earth's gravity would be effected, and the RTGs would no longer present a potential hazard to the population. Definition of the phases follows:

1. Phase 0 - Prelaunch. Mating of MJS-77 spacecraft to launch vehicle at T-13 days to ignition for launch at T-0.
2. Phase 1 - Launch Area. Ignition at T-0 until the instantaneous impact point (IIP) clears the Cape Canaveral land mass at T + 22 sec.
3. Phase 2 - Ascent. From T + 22 sec until park orbit injection (IIP Vanish point) at T + 572 sec during Centaur first burn.
4. Phase 3 - Orbit. From T + 572 sec until escape from the Earth's gravitational pull occurs at 4440 seconds. This period contains the completion of the first Centaur burn (MECO-1), the park orbit coast period, and the start of the second Centaur burn (MES-2).

Generally, the phases as defined, are equivalent to those given in the General Dynamics-Convair Phase II Report (CASD/LVP 76-004) with the exception that the final phase in that report was omitted since the spacecraft would have escaped from the Earth, and malfunctions that could occur would not result in conditions that would return the RTGs to Earth.

An evaluation of the potential malfunctions and accidents that could occur during the MJS'77 mission and their consequences with respect to the effect on the MHW RTGs was completed in the AMD, Volume II of the FSAR. For purposes of the evaluation, the mission was divided into four phases as defined in the previous section. Each of the phases was evaluated for the events that could present potentially severe environments to the RTGs, and the response of the heat sources was analyzed through the sequence of events following the initiating accident and until either they no longer posed a hazard or they had returned to impact on Earth, followed by a prolonged residence time prior to appreciable decay of the radioactive fuel. As a result of this evaluation, several situations were identified that presented conditions severe enough to breach some of the FSAs, allowing relatively small quantities of the radioactive material to escape. These situations included the following:

1. Impact of the spacecraft in a side-on attitude (with or without the Centaur) with RTGs impacting first onto the concrete launch pad. In this case, impact of the spacecraft propulsion module on top of the RTGs is the breaching mechanism.
2. Impact of the spacecraft with the Centaur onto the concrete launch pad in an end-on attitude (nose first) such that the stack of RTGs impact end-on.
3. Impact of the spacecraft in a side-on attitude (with or without the Centaur) onto sand or earth with RTGs impacting first. Impact of the spacecraft on top of the RTGs breaches some of the FSAs, at the same time driving them into the sand or earth.
4. Impact of the free heat source on a rigid surface such as granite following a re-entry from orbit or in a ballistic return.
5. In combination with 1 and 2., some of the breached spheres can come into contact with a piece of burning solid propellant (resulting from breakup of the solid rocket motors), and the radioactive material released from the spheres becomes vaporized and boosted to elevated release heights due to the thermally buoyant gaseous cloud generated in the deflagration of the UTP-3001.

A breakdown of the accident probability by mission phase was as follows:

Mission Phase	Accident Probability
0 - Prelaunch	0.0043
1 - Launch Area	0.00071
2 - Ascent	0.036
3 - Orbit	0.018
Total	0.060

These were the absolute accident probabilities for each phase and for the total mission through escape from the Earth's gravity. The probabilities were based on a combination of FMEA data adjusted for historical launch data for the Centaur and Titan and adjusted to the predicted reliability for Centaur as projected to the date of launch. Given these values, the overall mission probability of failure (through escape) is seen to be 6.0 percent.

For any appreciable quantity of fuel to escape from the heat source, the iridium post-impact containment shell, PICS, around the fuel sphere must be breached and the other components damaged to the extent that the fuel has free access to the atmosphere or other medium. Table 2-3 presents a summary of the MJS '77 potential accidents by mission phase that were identified as leading to fuel release. The range of source terms for these releases is 2.2 to 20.3 mCi for respirable material and 0.37 to 3.0 Ci of total material for those accidents not involving contact of the breached FSAs with pieces of burning solid propellant. For accidents involving contact with the burning UTP-3001, the fuel quantities involved vary from 0.18 Ci to 3.0 Ci (the latter with probabilities no larger than 9.0×10^{-21}) of vaporized material at effective release heights or cloud heights varying from 105 to 3970 meters (no correspondence between quantity of release and effective release heights).

TABLE 2-3. SUMMARY OF MJS '77 MISSION POTENTIAL FUEL RELEASE EVENTS

Mission Phase	Initial Accident	Mechanism Causing Fuel Release	Location Affected	Mission Probability of Fuel Release
0 - Prelaunch	none	none	none	none
1 - Launch Area	A. Explosion and fire in Centaur	1. Spacecraft impacts on concrete launch pad side-on with RTGs hitting first	Launch Pad	
		a. No contact with burning UTP-3001		5.0×10^{-5}
		b. Contact with burning UTP-3001		5.0×10^{-7}
		2. Spacecraft impacts on sand near launch pad side-on with RTGs hitting first	Launch Complex	8.3×10^{-5}
	B. Tumbling vehicle-guidance/control	1. Centaur/SC impacts on concrete launch pad nose first	Launch Pad	
		a. No contact with burning UTP-3001		9.5×10^{-6}
		b. Contact with burning UTP-300p		1.6×10^{-7}
		2. Centaur/SC impacts on concrete launch pad side-on with RTGs hitting first	Launch Pad	
		a. No contact with burning UTP-3001		1.3×10^{-5}
		b. Contact with burning UTP-3001		2.1×10^{-7}
		3. Centaur/SC impacts on sand near launch pad side-on with RTGs hitting first	Launch Complex	2.2×10^{-7}
2 - Ascent	Spacecraft ballistic re-entry due to launch vehicle malfunction	IHS impacts on rock following re-entry	Ground Track	
		a. High velocity impact		2.2×10^{-7}
		b. Low velocity impact		5.1×10^{-7}
3 - Orbit	Launch vehicle malfunction resulting in prompt re-entry or orbit decay			
	1. Multiple skip re-entry	IHS impacts on rock following re-entry	28° N to 28° S	
		a. High velocity impact		6.3×10^{-10}
		b. Low velocity impact		1.5×10^{-9}
	2. All other re-entries	IHS impacts on rock following re-entry	28° N to 28° S	
		a. High velocity impact		1.5×10^{-5}
		b. Low velocity impact		3.5×10^{-5}

2.1.3 RE-ENTRY SUBPANEL MEETING

A meeting of the INSRP Re-Entry Subpanel was held at GE-Nuclear Programs in February, 1977. The purpose of the meeting was to review the detailed re-entry analyses completed by GE for the FSAR. The following list of topics were covered in the presentations:

- Motion response of all flight RTGs before IHS release and of the IHSs after release (Action Item No. 9).
- Breakup analysis of end-on re-entry of a single RTG (Action Item No. 8).
- Maximum CG offset for damaged and undamaged IHSs (Action Item No. 6).
- Structural response of the IHS during transition from end-on to side-on motion for damaged and undamaged IHSs (Action Items No. 7 and No. 10).
- Maximum stresses for the JPL Case II trajectory (Action Item No. 9).
- Failure criteria for release of IHSs and for aeroshell structural failure (Action Item No. 13).
- FSA re-entry response and footprint (Action Item No. 2).

The notations in parentheses after each item are the action items from the USAR review (see Table 2-2) which these topics addressed. A summary of the results and conclusions from the analyses for these action items is included in the following paragraphs.

Failure Criteria - IHS Release and Structural Failure (Action Item No. 13)

RTG End-on Re-entry - IHS release is taken to occur when the titanium spider melts.

RTG Side-on Re-entry - IHS release is taken to occur when complete burn through occurs along the length of the converter shell over an arc of 30^{o} from the stagnation line in a circumferential direction.

Aeroshell Structural Failure - the POCO AXF-5Q aeroshell is taken to fail when the calculated elastic stress exceeds the material allowable.

Case II Maximum Stress (Action Item No. 9)

This re-entry breakup case is the steep angle, superorbital velocity case having initial conditions of,

Velocity:	36,000 fps
Re-entry Angle:	-46°
Configuration:	MJS S/C in Cruise Mode
Attitude:	Trimmed

The analysis presented in the meeting and also in the FSAR for this case addressed only the side-on stable orientation of the Heat Source after its release from the converter. Preliminary motion analyses conducted earlier in the program had indicated that this was the orientation to be expected both in the supersonic and subsonic flow regimes. Subsequent analyses for the FSAR, to be discussed in later paragraphs, indicated that the possibility for an end-on stable mode of the heat source as influenced by the motion and breakup conditions was essentially nonexistent. However, results of analyses are presented in later paragraphs, to indicate the expected response of the RTG and IHS, assuming arbitrarily that a stable end-on attitude is acquired and maintained throughout the major portion of the re-entry; this is in response to Action Item No. 8.

Analyses conducted earlier for the USAR had shown that the highest stressed area occurred in the center section of the aeroshell. For this reason, only the center section was chosen for the more detailed analyses to be presented in the FSAR. This analysis used the SAP IV computer program which performed a three dimensional analysis with combined thermal and aerodynamic stresses. The resulting maximum principal stresses are shown below and are compared with the stresses reported at the USAR review in September, 1976.

AEROSHELL COMBINED STRESSES

METHOD	HOOP (psi)	AXIAL (psi)
Plane Stress	6186	5836
(Corrected for 3D stress field) plus aero loads - USAR	6949	5100*

*Aerodynamic stress not included

In order to determine whether or not the 3D stress values (SAP IV) shown above resulted in aeroshell failure, the following procedure was followed to arrive at the material allowable strength. First, the statistical distribution of strength for the individual test specimens from the AXF-5Q billets accepted for flight use was determined. This resulted in the following values:

POCO AXF-5Q BILLET TEST DATA*

	ROOM TEMP.	3000° F
Mean Tensile Strength	8288 psi	10,484 psi
Standard Deviation	714 psia	677 psi

*Values shown differ slightly from those given in the FSAR since the BS-33 billet (shown in Table E-5 of the FSAR) was subsequently replaced by billet BS-34 due to the re-build of the F-9 IHS.

Based on these statistics, the 95% failure probability occurs at a value of 9150 psi ultimate at 3000° F. This value was adjusted for the approximate re-entry back face (inside surface of aeroshell) temperature of 2100° F for the Case II re-entry by the use of the design allowable curve shown on Figure 2-1. (The design allowable curve had been derived during the initial phase of the MHW-MJS program on the basis of the minimum aeroshell billet strength data from the LES 8/9 program.) The adjusted ultimate tensile allowable is then:

$$F_u \text{(tensile)} = 9150 \times \frac{7200}{8100} = 8133 \text{ psi}$$

Finally, an adjustment was made to the above value, which was based on uniaxial tension allowable data, by considering the effects of a biaxial tension stress field according to the method recommended by the Re-entry Subpanel in the USAR review. This method was based on the paper by Batdorf and Crose ("A Statistical Theory for the Fracture of Brittle Structures Subjected to Non-Uniform Polyaxial Stresses.") No report number available.

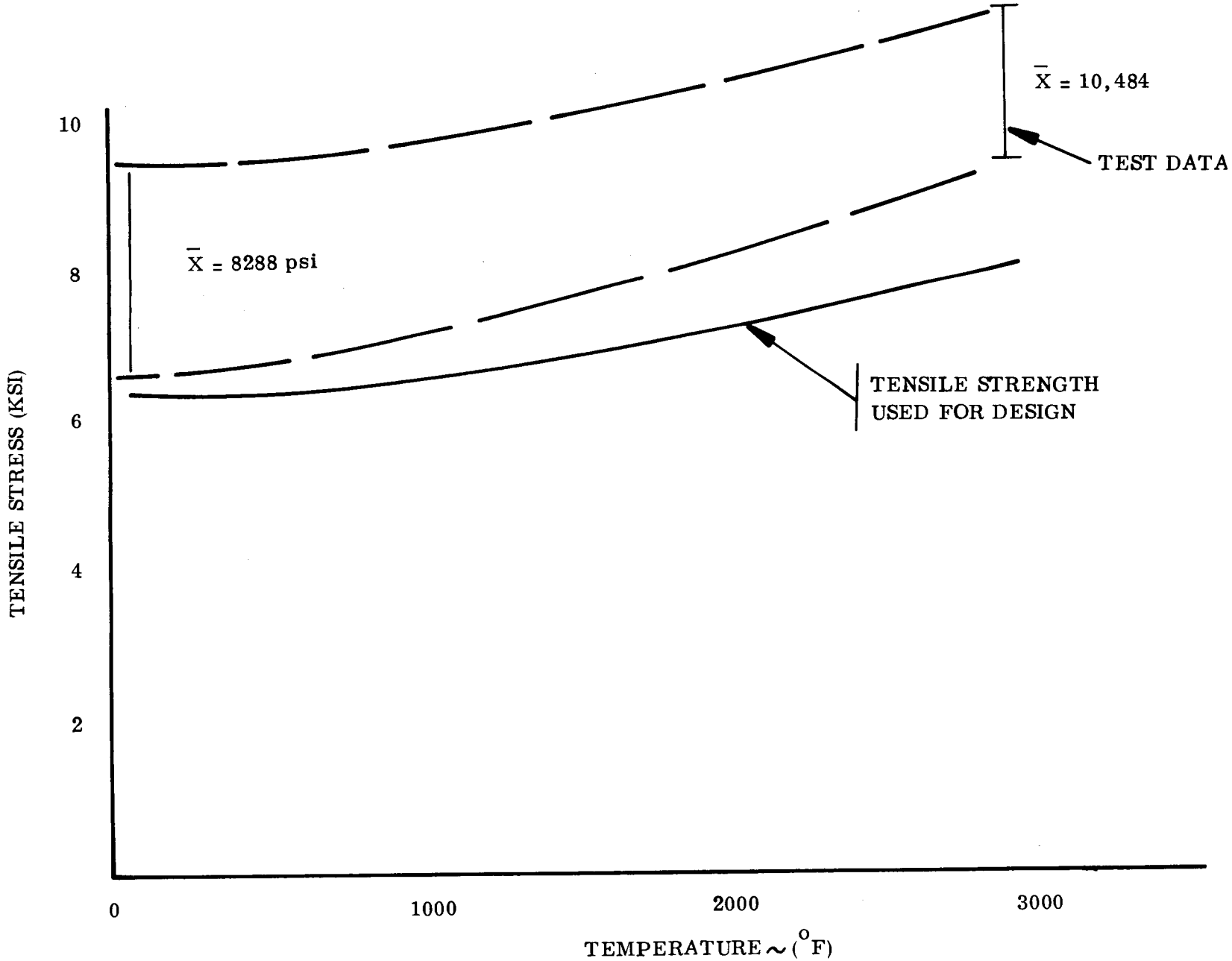

Figure 2-1. POCO AXF 5Q Strength Vs. Temperature

Figure 2-2 was taken from that paper with the statistics for the MJS-MHW billets added as indicated. At the 95% failure probability, the adjusted ultimate allowable for the biaxial stress field is:

$$F_u \text{ (tensile)} = 8133 \times \frac{5100}{5750} = 7214 \text{ psi}$$

The resulting minimum margin of safety is:

$$MS = \frac{7214}{6186} - 1 = + 0.166$$

as compared with the design allowable value (from Figure 2-1) of

$$MS = \frac{7250}{6186} - 1 = + 0.172$$

A comparison of the values for the minimum margin of safety reported to date are as follows:

AEROSHELL MINIMUM MARGIN OF SAFETY
(CASE II RE-ENTRY)

PLACE REPORTED	TYPE OF ANALYSIS	MS
USAR	Plane Stress - ORTHOSAFE + Aero Loads - SABOR-G	+ 0.20
INSRP (USAR review)	Plane Stress (Corrected for 3D stress field) + Aero Loads	+ 0.15
FSAR	3D Thermal + Aero Loads - SAP IV	+ 0.17

NOTE: For interest, the following observation is made. Referring to Figure 2-2, the no-failure value of stress at 3000° F for the uniaxial billet data is seen to be around 8400 psi. Correcting this for 2100° F and for the corresponding biaxial or volumetric effect, the material allowable is found to be:

$$F_u \text{ (Tensile)} = 8400 \times \frac{7200}{8100} \times \frac{4800}{5200} = 6890 \text{ psi}$$

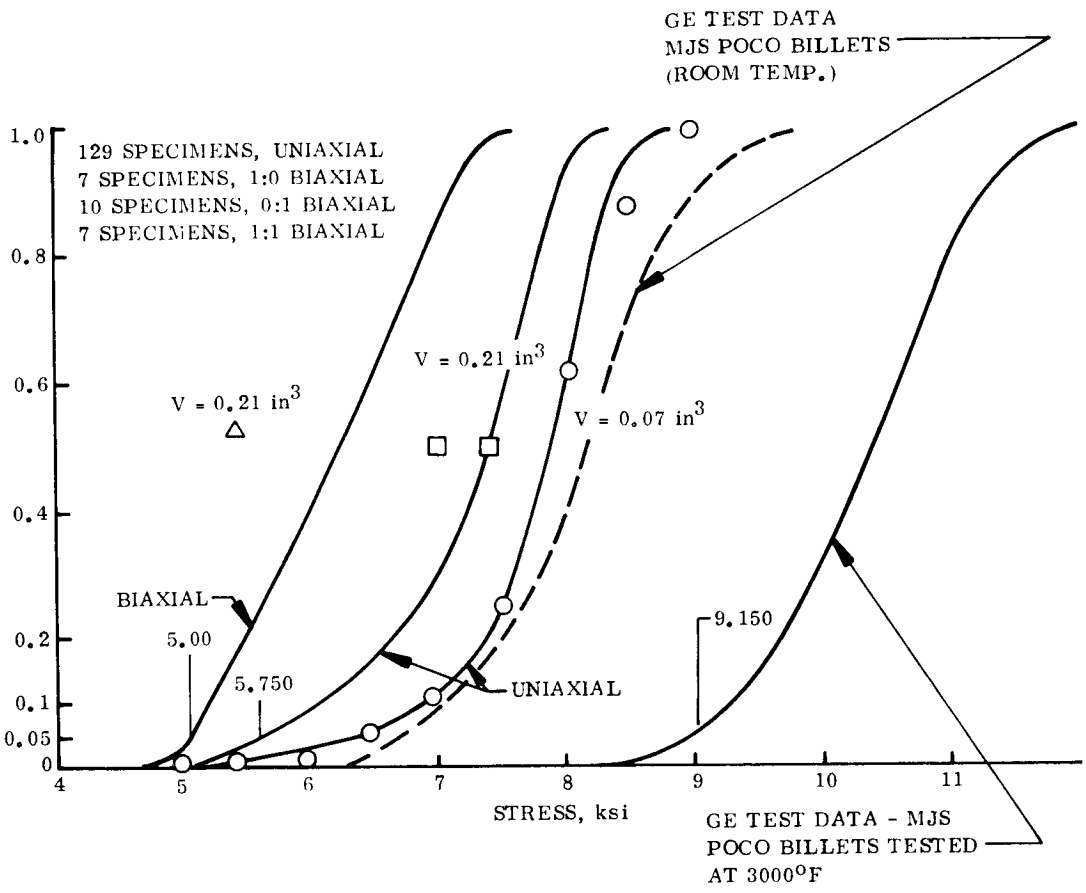

Figure 2-2. Statistics of Failure, AXF-5Q

with the corresponding margin of safety

$$MS = \frac{6890}{6186} - 1 = +0.114$$

Maximum CG Offset - Normal and Discrepant IHSs (Action Item No. 6)

To determine the maximum center of gravity offset for the two discrepant IHSs and for three normal IHSs, the following assumptions were made.

1. Initially, the fuel spheres and the iridium shell were assumed to be located at the geometric center of each Fuel Sphere Assembly (FSA). To determine the maximum center of gravity offset, each fuel sphere and iridium shell was then assumed moved to the extreme longitudinal position resting against the inner surface of the Graphite Impact Shell (GIS).
2. For a discrepant IHS, the total weight of the internal components was assumed to shift the entire distance from its unfailed position so that the lower spring assembly rested on the boss of the aft end cap.

3. To account for the tolerance build up in the assembled IHS components, several different heights of nuts for the forward tie bolt were provided. Quality Control records showed that each assembled IHS used the same nut height. For this reason the total height of the assembled IHS components were assumed the same for each IHS.

The results of the CG analysis are shown in Table 2-4. These values are the maximums that could possibly occur. Spring back of the aft spring assembly and compliance pads and relocation of the FSAs would reduce the amount of the offset.

TABLE 2-4. MAXIMUM CENTER OF GRAVITY OFFSET FOR DAMAGED AND UNDAMAGED IHS

IHS No.	Nominal[1] CG Location	Maximum CG Offset Due to Fuel and Iridium Shell	Maximum[2] CG Offset Due to Failed Tie Bolt Head	Total Limits of CG Offset	
				Fwd	Aft
6	-0.032	± 0.022	+ 0.172	-0.054	+ 0.162
7	-0.042	± 0.022	+ 0.159	-0.064	+ 0.139
8	-0.041	± 0.023	-----	-0.064	+ 0.018
9	-0.022	± 0.022	-----	-0.044	0.0
10	-0.031	±0.023	-----	-0.054	-0.008

[1] Center of Gravity referred to geometric center of the IHS. Postive signs indicates that the CG location is toward the aft end cap.

[2] Tie bolt head failed on F6 and F7 IHS only.

Motion and Response of all Flight RTGs/IHSs (Action Item No. 9)

This portion of the study involved a detailed investigation of the motion and breakup of the Case II re-entry as influenced by the release from the MJS spacecraft and included the following:

- RTG 3-stack motion
- RTG motion
- RTG breakup
- HSA motion
  - During RTG breakup
  - During free flight

The results of these analyses indicate the following:

- RTGs will all break up at about 208 kft ± 10 kft regardless of their early motion behavior.
- RTGs have a strong tendency to seek a broadside attitude and are negligibly affected by CG offsets.
- RTGs have greater tendency toward side burn-through than end dome burn-through due to fin heating augmentation.
- Rapid HSA tumbling motion results from RTG breakup (~1000 deg/sec pitch rate)
  - Large subsequent aerodynamic loading occurs (~270 Gs normal, 48 Gs axial)
  - Essentially broadside orientation (with oscillations) occurs at peak heating and peak aerodynamic loading.
- Normal (mass-symmetric) IHS cannot trim end-on
- Discrepant (tie bolt failure) IHS can trim end-on only if all following conditions are met:
  - Axial CG offset is maximum predicted (0.160 inch), and
  - RTG end dome burns through before side burns through, and
  - RTG is itself nearly end-on (± 4 degrees) with attendant low tumble rates
- Likelihood of discrepant IHS/RTG end burn-through is remote due to location on spacecraft (F-6 heat source to be in middle RTG in the 3-stack) and to be shielded from the flow until stack breakup.

Therefore, the following conditions were taken to occur for purposes of the FSAR evaluation:

- IHS is predicted to attain a broadside attitude for all RTG side and end dome burn throughs.
- No IHS aeroshell failure will occur as a result of the Case II (or any other) re-entry.

Structural Response of all IHSs During Transition from End-on to Side-on Motion

For this analysis, the maximum axial acceleration of 48 Gs determined in the motion analysis previously discussed, was used along with the maximum possible free play of 0.31 inch for the internal components (for a discrepant IHS). The maximum stress was found to occur at the lock ring groove in the end cap with a value of 1984 psi; the corresponding margin of safety is 3.6 based on the plate strength data for the flight end cap material. Based on this analysis, the conclusion was drawn that the IHSs having broken tie bolt nuts would not experience failure of the end cap. Furthermore, while those IHSs without the redesigned tie bolt nut might suffer failure of this nut, the resulting loads would not be as severe as those calculated above, and the IHSs would not fail in the end caps. For those IHSs with the redesigned tie bolt nut, no failure would occur. The new design was static tested to approximately 4000 pounds without failure. The maximum expected load (without tie bolt head failure) is 1344 pounds resulting in a margin of safety of approximately 2.0. The above analysis is conservative since it neglects the frictional forces induced by the lateral components of load.

Structural Analysis of End-on RTG (Action Item No. 8)

This analysis investigated the Case II type of re-entry in which it was arbitrarily assumed that an individual RTG acquired and maintained an end-on attitude until the IHS was released, after which the IHS maintained an end-on attitude. As a starting point, based on the JPL Case II breakup results, the RTG was assumed to be end-on when it (actually, the 3-stack of RTGs) turned end-on into the flow after failure of the folding strut. With the folding strut failing at 4.3 seconds, approximately another second was required for the stack to turn into

the flow, making the end-on attitude occur at 5.3 seconds for purposes of the analysis. The RTG was then taken to be exactly end-on to the flow. The results of the analyses are as follows:

- IHS release occurs @ 190 kft
- Initial failure of IHS aeroshell end cap occurs at the base of the lock ring groove resulting in the complete cap being unrestrained by the cylinder. This occurs at 9.75 seconds. After failure, the cap is still capable of supporting load.
- Secondary failure of the end cap occurs at 10.4 seconds or at an altitude of approximately 130 kft, resulting in radial cracking which is assumed to cause complete radial separation of the cap.

While either of the predicted end cap failures could result in complete fracture of the cap, most probably the air loading would tend to prevent removal of the cap from the cylinder and thus prevent release of the FSAs. If stabilized end-on re-entry of the IHS were to take place, the IHS would eventually restabilize broadside in the subsonic regime at around 38 kft altitude. While the axial 'g' loading is small at the point where the IHS turns broadside, the ability of the fractured end cap to restrain the FSAs was considered negligible, and it was assumed that the FSAs would be released at that altitude during the subsonic flight.

FSA Re-entry Response and Footprint (Action Item No. 2)

Since the analyses for a number of the action items were being done concurrently, the FSA analysis being one of those, it was assumed conservatively that the FSAs were released at 120 kft, the approximate altitude of the first failure of the end cap. The FSA was then taken to be stable, with no spin, throughout the remainder of the re-entry, and surface roughness of the GIS was assumed to be sufficient to effect boundary layer transition for augmented heating. The following results were obtained:

- Maximum ablation = 0.22 inch
  (total GIS thickness is 0.46 inch)
- Impact temperatures:

  stag point : 1840°F
  45° away from stag point: 1600°F

To estimate the possible dispersion and resulting footprint of the FSAs, three trajectory deviation sources were assumed present:

- differences in ballistic coefficients of one FSA relative to another
- deflections caused by FSAs hitting/rolling against each other in the act of being released
- effect of FSA lift forces

The resulting footprint based on an assumed 10% difference in ballistic coefficient, an estimated incremental roll off velocity of 40 fps, and assuming a lift coefficient of 0.01 as being representative was found to extend 7640 feet down range and 5300 feet cross range.

Action Item No. 2 also requested that the source terms and radiological risk be determined for the situation in which the aeroshell fails in a forced end-on re-entry of the RTG and IHS. These analyses were completed and presented in the FSAR, but they were not reviewed in the Re-entry Subpanel meeting.

2.1.4 FSAR REVIEW

The Final Safety Analysis Report (FSAR) for the MJS '77 Mission was reviewed in a meeting of the Interagency Nuclear Safety Review Panel (INSRP) held at the NASA Kennedy Space Center (KSC), Florida, on March 29-31, 1977. The following agencies, companies, and other groups were represented:

NASA	ERDA	DOD
JPL	NRA	Hq AFSC
MSFC	ALO	AFISC/SNS
HQ	SFO	AFISC/IGD
KSC	DAO	OATSD
Ames	LASL	AFETR
LeRC	ORNL	AFWL
LaRC	ANL	Aerospace Corp.
General Dynamics/Convair	ML/MRC	Teledyne - Isotopes
	NUS	USAF Surgeon General Office
	APL/JHU	
	U. of Cal.-Davis	
	Battelle-Columbus	
	GE	EPA

Table 2-5 lists the topics covered in the meetings. As requested previously by ERDA/NRA, General Electric presented only summaries of the studies conducted to address the action items assigned to them at the USAR meeting. (The results of these studies and action items were summarized in the MHW-MJS Bimonthly Progress Report for January-February 1977.) They did not review the FSAR as part of the presentation. The INSRP had been requested to be prepared to comment on the information in the FSAR, and time was allotted for questions on the contents of the document.

TABLE 2-5. TOPICAL AGENDA FOR MHW-MJS 77 FSAR REVIEW

Program Summary	
RTG Program Update and Hardware Status	ERDA/NRA
MJS Program Status	JPL
Launch Vehicle Safety Update	LeRC
Spacecraft Flight Safety Contingency	JPL
Action Items Summary and FSAR Questions	GE
RHU Documentation Questions	MRC
Supporting Activities and Subpanel Reports	
Cape Ground Handling	ALO
Cape Safety Activity Summary	KSC
Range Safety Requirements and Status	ETR
MJS/IHS and RHU Safety Tests Summary	LASL
Source Term Analysis-IHSs and RHUs	LASL
Re-entry Subpanel Report	LaRC
Project Vulcan Results	LASL/AFWL
Environmental Test Results	LASL
Safeguards - Loss of Nuclear Material	LASL
Biomedical Subpanel Report	ERDA/BER
Independent Risk Analysis	NUS/AFWL

2.2 SAFETY TESTING

A meeting was held at GE in January between the ERDA/NRA Program Office and the GE/NP Program Office to discuss the safety test program for MHW-MJS. At that meeting, ERDA indicated that the safety community had generally agreed that projectiles would not be a potential source of damage to the MHW heat sources. Consequently, GE/NP was directed to

delete the proposed projectile test (MS-2) from the test program. This action resulted in only the expolsion test being left in the program.

Additional recommendations made by ERDA/NRA for the explosion test included increasing the size (mass) of the test specimen to a full heat source and adding weight to simulate that of the other two RTGs. The purpose of this was to duplicate the inertia of the system as closely as possible, so that the resulting momentum and motion of the heat source and FSA's would be more representative of the actual situation. Concern was expressed that unrealistic momentum of the FSAs could result in secondary damage effects that would be more severe than the primary effects of the blast, similar to that occurring in the explosion test (S-1) for LES 8/9. Since the MJS explosion environment was potentially more severe than that for LES 8/9, it was felt that the damage to the FSAs resulting from the test should be as realistic as reasonably possible. This would preclude the evaluation of the potentially ensuing solid propellant fire environment from predicting overly pessimistic results. Toward this end and directed to this concern, GE/NP indicated that there were piece parts (outer shell, end enclosures and end caps) available that could be used to build up a converter simulator for use in the test for an even closer simulation of the expected damage, or protection, resulting to the FSAs. This refinement to the test conditions was subsquently to be incorporated into the test plan.

After the meeting previously discussed, a test plan was written to include the recommended changes to the explosion test. In effect, this plan (GESP-7125, dated 24 February 76) replaced the safety test program plan (GESP-7114-R2, October 1975) previously submitted. The provisions of the GESP-7125 plan included the following:

1. The test specimen heat source would have a full-size aeroshell with two trays (8-packs) of FSAs. The third tray would be mass-simulated only.
2. The heat source specimen would be encased in a simulated converter having an actual beryllium outer case and at least one beryllium end dome plus end enclosures. The remaining parts (without unicouples) would be simulated.

3. There would be mass simulation of the other two RTGs attached to the rear of the simulated converter.
4. The simulated three-stack of RTGs would be mounted on simulated struts as on the MJS spacecraft.
5. The explosion would be effected by the use of HE in an open field arrangement with the test specimen positioned directly above in order to duplicate the upward motion and subsequent fallback of the RTGs.

The purpose of the test would be to determine the overall effects of the converter and heat source components in protecting the FSAs, and the GISs capability of maintaining their integrity for protection of the PISAs in a pad abort blast environment. The purpose was not to determine the capability of the PISAs to withstand the blast environment effects, because the test would be run at ambient temperature which precludes the use of iridium PISAs. (It was not practicable to preheat the converter and heat source to the required operating temperatures for a hot test of the PISAs.)

Objections to the MHW/MJS Heat Source/Converter Explosion Test Plan, GESP-7125, were received from NASA and the USAF during March 1976. In response to these objections, ERDA scheduled a meeting of the Safety Panel Coordinators at GE in April to review the objections and to consider alternatives. The meeting was subsequently delayed until May to allow completion of the GE explosion and projectile analysis, which had been delayed due to conflicting requirements for analysis of the Q-2 end cap anomaly. (See Section 5.0)

The explosion analysis was completed (refer to Section 5), and the INSRP meeting was held to review the proposed test plan. A summary of the comments and conclusions of that meeting follows:

- An explosion yield of 10 percent as proposed was considered to be overly conservative; a yield around 3 percent was believed to be more representative and the most probable for pad abort situations.
- An area of great concern was related to the possibility of an abort environment sequence that would result in free PISAs (i.e., FSA with GIS removed), since subsequent contact with burning blocks of solid propellant would result in breaching of the PICS and release of fuel. Therefore, the basic question was whether or not the GISs would remain intact following the explosion.

- Based on the explosion analysis previously discussed, the GISs would be expected to survive for yields up to 10%. In addition, the FSAs have been shown to survive impacts associated with pad abort conditions.
- If the analytical model was representative of the RTG response in the pad abort environment, the resulting consequences did not appear to be radiologically significant. Thus, the objectives and value of the test were in question.
- The conclusion was reached that a single high yield test would not be likely to improve the current knowledge of the FSA survivability over the spectrum of abort explosions. Neither could the cost of the test and hardware be justified on this basis. On the other hand, a lower yield test (around 3 percent) could add confidence in the ability to predict the damage analytically over a wide range of explosion conditions. The 3 percent level would be representative of the most probable environment, and the test specimen could be made in a simpler and less costly manner in order to achieve the test objectives.

As a result of the meeting and subsequent test planning, the following test provisions evolved:

- 3% equivalent yield explosion
- use of available test hardware for realistic RTG simulation down to the graphite impact shells.
- use of mass and configuration simulation for the other two RTGs
- test RTG to be preheated to the temperature of the beryllium converter case for launch conditions
- latching truss and RTG interstitial mounting brackets (part of JPL spacecraft design)

The target date for completion of the test was set for the end of September, 1976, and arrangements were made with Sandia Laboratories to have the test conducted at their facilities.

The hardware for the test was collected, fabricated, and assembled as required. The decision was reached between ERDA and GE to use a flight type converter for the test. This converter consisted of the Q-2 thermopile and a flight type beryllium shell that had previously been rejected because of a hairline crack running longitudinally from the forward stiffening ring for a length of approximately six inches. Because of the location (end away from intial shock wave encounter), orientation, and limited extent of this crack, the opinion was that it

would not affect the results of the test. As an additional precaution, the ends of the crack were drilled with small holes to prevent propagation of the crack during the test. (Note: the condition of this crack did not change as a result of the test.) Because of being cracked early in manufacture, this case had not been drilled for the unicouple screw penetrations The decision was made to drill only one hole at the top and one hole at the bottom of every other column since this would be adequate to hold the thermopile in position. The remaining hardware for the full RTG test specimen consisted of the following:

Converter

- Engineering end enclosures
- Q-2 mounting brackets
- Q-2 heat source supports
- Beryllium end domes
  (1 prime, 1 repaired)
- Engineering preload screws and bushings

Heat Source

- 24 steel ball bearings (PISA simulation)
- 8 prime impact shells (GIS)
- 16 engineering impact shells (GIS)
- Q-2 aeroshell cylinder
- 2 prime (reject) end caps
- 1 thin wall (0.100) in) ablation sleeve
- 1 set internal graphite parts (Q-2)

Other

- 2 dummy RTGs (steel pipe with simulated stiffening rings and flat capped ends)
- 1 simulated latching truss assembly
- 2 flight type interstitials (JPL supplied)

A photograph of the assembled test specimen with truss and mounting plate is shown in Figure 2-3. The full-up RTG was instrumented with chromel-alumel thermocouples to be able to monitor the temperature of the beryllium case while it was being preheated. The decision had been made to preheat the RTG outer case to the temperature that would exist

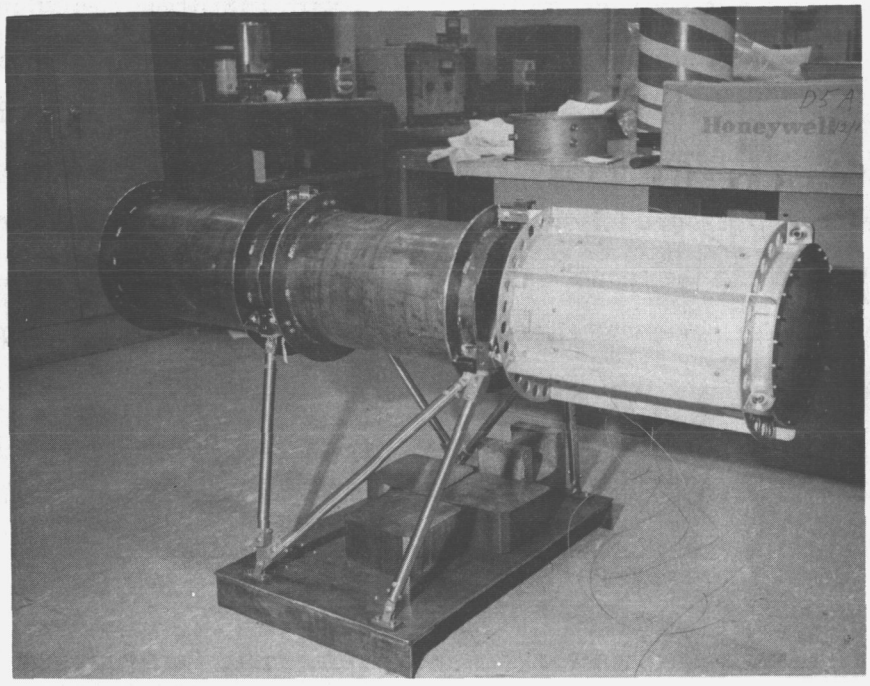

Figure 2-3. Assembled Hardware for MHW-MJS Explosion Test

under launch conditions (around 350°F or 177°C) as requested by the INSRP at the test plan review meeting in May.

The test was conducted on on October 6, 1976. This delay beyond the target date was necessitated by a conflict with another test program at Sandia and because of the necessity to perform additional calibration explosions and checkout of the test procedure before committing the single available test specimen. The test was conducted in a 10-foot diameter, vertically mounted shock tunnel. This tunnel was imbedded in soil to a depth of about four-fifths of its length (20 feet) with its bottom end closed by a metal plate. The mounting plate shown in Figure 2-3 was welded to a heavy angle iron structure on the wall of the tunnel near the top edge. The stack of three RTGs was mounted in the vertical orientation as would exist on the launch vehicle and spacecraft, with the full-up RTG facing down (nearest the explosive charge). Eighteen pounds of C-5 explosive was used in seven (7) blocks spaced over the bottom of the tunnel.

The explosion resulted in tearing the upper struts of the latching truss loose from the mounting plate. All three RTGs were still held together by the interstitials and were still hanging onto the bottom two struts (ones nearest the full-up RTG with IHS) from its mounting ring; several pieces were imbedded in the end foil packet. A large piece of the converter shell in the area of the aft stiffening ring and end dome had been torn out and was missing. The thermopile could be observed in this area, but it was still essentially intact. Probably, the characteristic negative pressure following the primary shock overpressure resulted in pulling the RTG stack back into the tunnel causing the lower struts to bend around the bottom edge of the mounting plate (as observed after the test). Either the shock of stopping the motion of the stack or possibly the impact of the end of the full-up RTG with the tunnel wall, was believed to have caused the failure of the converter case. This type of failure, especially localized as it occurred, was not predicted to result from the explosion. Generally, the results of the explosion test were somewhat less severe than had been predicted in the analysis.

The RTG test specimen used in the test was received from Sandia Laboratories for inspection and disassembly at GE. Disassembly of the RTG was subsequently accomplished starting at the more intact end (forward end) of the RTG. This was done because the RTG was removed from the shipping container with this end upward. To preclude shaking up the internals any more than necessary, the decision was made to disassemble starting at the forward end (end away from the blast). The following results were found:

Converter

- Forward end dome undamaged
- End closures and fittings undamaged - preload screws still intact
- Forward heat source support (graphite) completely broken up along with zirconium bearing disc.
- Many hot shoes broken off and parts of unicouple legs broken off.
- Parts of edge of aft heat source support (graphite) were chipped and broken off - otherwise it was intact.
- Aft end dome, except for most of mounting flange, removed by blast.

Heat Source

- Forward end cap broken completely in circumferential as well as in radial directions (numerous locations).
- Forward and aft end crush-up (laminated spring assemblies) undamaged.
- Top 8-pack undamaged. Tie bolt still intact. Slight rotation of FSA's seen - may be due either to shipping or test.
- Middle 8-pack undamaged. Tie bolt intact.
- Tie bolt broken in bottom 8-pack. No other damage.
- No apparent damage to FSAs.
- Aft end cap broken radially in several pieces and partially circumferentially.
- Both end cap snap rings intact.
- Aeroshell cylinder cracked in near circular segment at forward end (i.e. crack started at forward edge, progressed about 1/3 of length of cylinder, turned and came out at forward edge roughly 150^{o} from other edge of crack). This localized damage is believed to have occurred as a result of test unit being pulled backed into tunnel by blast wave rarefaction and suddenly stopped.
- Ablation sleeve cracked from top to bottom in one longitudinal crack, with smaller crack, with smaller crack propagating from large crack about 1/3 from bottom and running to bottom edge.

The test data for the explosion parameters as received from Sandia indicated the following at the test RTG location:

Peak static overpressure	=	120 psi
Peak stagnation overpressure	=	380 psi
Peak reflected overpressure	=	650 psi
Static impulse	=	0.42 psi-sec

On the basis of the overpressures shown above, the explosive yield was on the order of 4%. The detailed test report was included in Appendix D of the Accident Model Document (Volume II) of the FSAR.

2.3 OPERATIONAL SAFETY

2.3.1 MJS GROUND SAFETY ANALYSIS REPORT (GSAR)

Revision A to Document No. GEMS 422, "Safety Analysis Report of MHW Isotope Heat Source Operations at GE Valley Forge Space Center for MHW-RTG MJS Program" (the MJS GSAR for GE Operations) was published on 29 March 1976 and incorporated changes suggested by comments from ERDA/ALO Operational Safety, ERDA/NRA and Sandia, relative to the original document which was approved on 31 October 1976 via TWX from J. Lombardo to E. Williams.

At the MJS interface meeting on 21 April 1976, the agreement was reached that the submission of GEMS-422 constituted satisfaction of contract requirements calling for the preparation of a single integrated ground safety analysis report (refer to Task 2.2 of Appendix A to the Statement of Work).

2.3.2 RADIOLOGICAL PROTECTION PROGRAM

The MHW Radiological Protection Program document was revised and submitted to ERDA/ALO Operational Safety for approval (GEMS 409, Rev. C1, February 1976).

2.3.3 MJS SAFETY ANALYSIS REPORT FOR PACKAGING

An addendum to the Safety Analysis Report for Packaging (SARP) Multi-Hundred Watt Radioisotope Thermoelectric Generator (MHW-RTG) Shipping Container, GEMS 408, was submitted to ERDA/ALO for review and approval on 11 March 1976. The addendum concluded that the design changes incorporated in the MJS Isotope Heat Source, RTG Converter, and RTG Shipping Container did not invalidate the conclusions of the LES 8/9 RTG Shipping Container SARP. In support of this conclusion, GEMS-423, "Containment Capability of the MHW Isotope Heat Source", and GE drawings of the RTG Shipping Container, MJS Retrofit (47E303339) and Shipping Cask Assembly, MHW-RTG, MJS (47J303322) were enclosed with the addendum. Acceptance of the conclusion was provided by ERDA/ALO in a letter from J. Roeder to F. Witt dated 2 April 1976. Certificate of Compliance USA/9502/BLF remained in effect for the MJS Program.

Because of a magnetics test being added for the MHW-MJS RTG later in the program, the possible consequences of an accident to the RTG during the magnetics testing were reviewed, and an addendum to the MHW-MJS was prepared. This addendum also included an estimate of the radiation exposure of personnel performing the test, based on the walk-thru data. Approval of the draft addendum was obtained from ERDA-ALO-OSD before the magnetics test was performed.

2.3.4 MJS OPERATIONAL ANALYSIS

The MJS Operations Analysis (OA) Task Group met both at Mound Laboratory and at GE-VFSC in January 1976 to review the MHW-MJS heat source operations at each facility. The review was conducted by means of operations flow charts which described the sequence of events at each facility. Operations Analysis Sheets were prepared for each event on flow charts in accordance with a standard format provided by ERDA. As a consequence of some confusion on the completion of the forms, guidelines were prepared to define the information required in each block of the Operations Analysis Sheets.

Revised GE flow charts and OA sheets were forwarded to Sandia and supplemented with additional text and illustrations. This material was subsequently incorporated in the first issue of the MHW-MJS OA Report by Sandia, on 28 April 1976.

2.3.5 BUILDING 300 LONG LIFE LABORATORY FACILITY MODIFICATION

The HEPA filtered ventilation system modification to the Building 300 MHW thermal vacuum test area was approved by ERDA/ALO Operational Safety. In addition to ventilating the test area, the HEPA filtered system provided an exhaust for the chamber roughing and turbo-molecular pumps and for the Gas Service Cart to prevent the release of radon and its daughter products to the work area.

After installation of the system, a performance test indicated that the HEPA filtered system produced a negative 0.105 inches of H_2O pressure differential with respect to the outside of the building. A particulate survey was made across the filter and seal which indicated that the filtration efficiency was at least 99.9959 percent.

SECTION 3

RTG SYSTEMS

3.1 INTERFACE ENVIRONMENTS AND PERFORMANCE REQUIREMENTS DEFINITION

The previous document in this series, (GESP-7127/GEMS-428, MHW RTG Program, 1975 Annual Report for MJS) discussed the interface environments and performance requirements definition. A major change in the launch vehicle shock and vibration environments and performance requirements resulted from:

- A more realistic evaluation of the launch vehicle shock and vibration, based on test data with the vehicle structures.
- The outcome of the Q2R/RTG testing, at the original qualification levels, which produced some non-catastrophic damage to both the Q-2R/IHS and Q-2 converter.

The shock and vibration levels for acceptance were reduced to those used for LES.

3.2 DESIGN REQUIREMENTS AND SURVEILLANCE

Design requirements for the RTG, ETG, IHS and GSE were translated into five top-level GE specifications:

SS47A14617	Systems Specification, MHW Radioisotope Thermoelectric Generator for the Mariner Jupiter Saturn Spacecraft
NS-0020-05-03	Environmental Criteria and Test Requirements for the MJS Multi-Hundred Watt Program
CP47A14619	Product Specification for the MHW-RTG, MJS
CP47A14618	Product Specification for the MHW-ETGs, MJS
CP47A14616	Product Specification for the MHW Isotope Heat Source - MJS

All of the customer and User comments and questions were resolved and changes through ANs were accepted by the Customer, constituting by mutual agreement, final specification approval. Design surveillance and evaluation were intended to assure adequacy of test planning and analyses and thus to provide the necessary and sufficient data for verification of compliance

with design requirements, when the end items were accepted for delivery. Standing Instructions, SIs, for all testing and handling operations were prepared, reviewed, and approved, (by ERDA Project and Safety) prior to the start of operations at GE-SD.

3.3 SYSTEM ANALYSIS

3.3.1 DESIGN DIFFERENCES

The MJS RTGs are similar in design and function to the RTGs previously furnished for the LES 8/9 program. The significant differences which affect the RTGs furnished for these two programs are shown below:

1. The forward ring of the converter case has been reinforced for the increased loading predicted for the MJS mission.
2. The iridium cannister has been deleted. While this modification requires additional ground handling equipment, the reduction in RTG cost and weight is significant.
3. The heat source has been redesigned to eliminate the threaded attachment between the end caps and the aeroshell.
4. The PMD has been eliminated
5. The PRD mounting has been changed, eliminating tubing from the case cavity to the PRD.

3.3.2 TEMPERATURE DISTRIBUTIONS

Table 3-1 summarizes converter and IHS temperatures under a variety of conditions that were encountered during assembly, test and operation. All temperatures listed are steady-state averages for the condition described. The RTG case temperature is the average of the three fin RTD readings. Since the MJS IHS has no clad, the RTG gas fill is assumed to fill the cavities within the IHS as well, except for the fuel-to-PICS gap. This region was assumed to be filled with helium at all times, including vacuum operation. For heat transfer purposes, this assumption is valid if the helium pressure within the PISA is on the order of 0.1 psia or greater. Assuming the RTG gas fill in this gap would increase fuel temperatures roughly $50^{o}F$.

TABLE 3-1. MJS STEADY STATE IHS/RTG TEMPERATURES

CONDITION	RTG[1] VOLTAGE	IHS/RTG GAS FILL	IHS/RTG SINK TEMPERATURE	RTG CASE TEMPERATURE	RTG HOT SHOE TEMPERATURE	IHS SURFACE TEMPERATURE	PICS TEMPERATURE	FUEL[2] SURFACE TEMPERATURE	FUEL CENTERLINE TEMPERATURE
IHS in EPC in SPC	---	Helium	900°F	-----	------	1040°F	1550°F	1630°F	1795°F
IHS in LAS	---	Argon	70°F	-----	------	700°F	1525°F	1605°F	1770°F
RTG in LAS	O/C	Argon	70°F	400°F	1615°F	1670°F	2080°F	2135°F	2325°F
	30V	Argon	70°F	390°F	1515°F	1570°F	2020°F	2075°F	2265°F
	S/C	Argon	70°F	400°F	1400°F	1455°F	1930°F	1990°F	2175°F
RTG in RTG-SC	O/C	Argon	140°F	465°F	1680°F	1725°F	2125°F	2175°F	2370°F
	30V	Argon	140°F	455°F	1580°F	1630°F	2055°F	2110°F	2300°F
	S/C	Argon	140°F	465°F	1465°F	1515°F	1975°F	2030°F	2220°F
RTG in Air	O/C	Argon	70°F	360°F	1570°F	1625°F	2050°F	2100°F	2295°F
	30V	Argon	70°F	350°F	1470°F	1525°F	1980°F	2040°F	2225°F
	S/C	Argon	70°F	360°F	1355°F	1410°F	1900°F	1960°F	2145°F
RTG in Air	O/C	Xenon	70°F	360°F	1830°F	1875°F	2290°F	2330°F	2535°F
	30V	Xenon	70°F	345°F	1625°F	1680°F	2165°F	2215°F	2410°F
	S/C	Xenon	70°F	360°F	1505°F	1560°F	2075°F	2130°F	2320°F
Vacuum Operation	30V	Vacuum	100°F	505°F	1895°F	1930°F	2370°F	2410°F	2615°F
	S/C	Vacuum	100°F	520°F	1790°F	1825°F	2295°F	2340°F	2540°F

[1]OPEN CIRCUIT, 30 VOLTS, SHORT CIRCUIT.

[2]ASSUMES >.01 PSIA HELIUM RETAINED WITHIN PISA.

Figure 3-1 shows the IHS temperature distribution during 30-volt vacuum operation of the RTG.

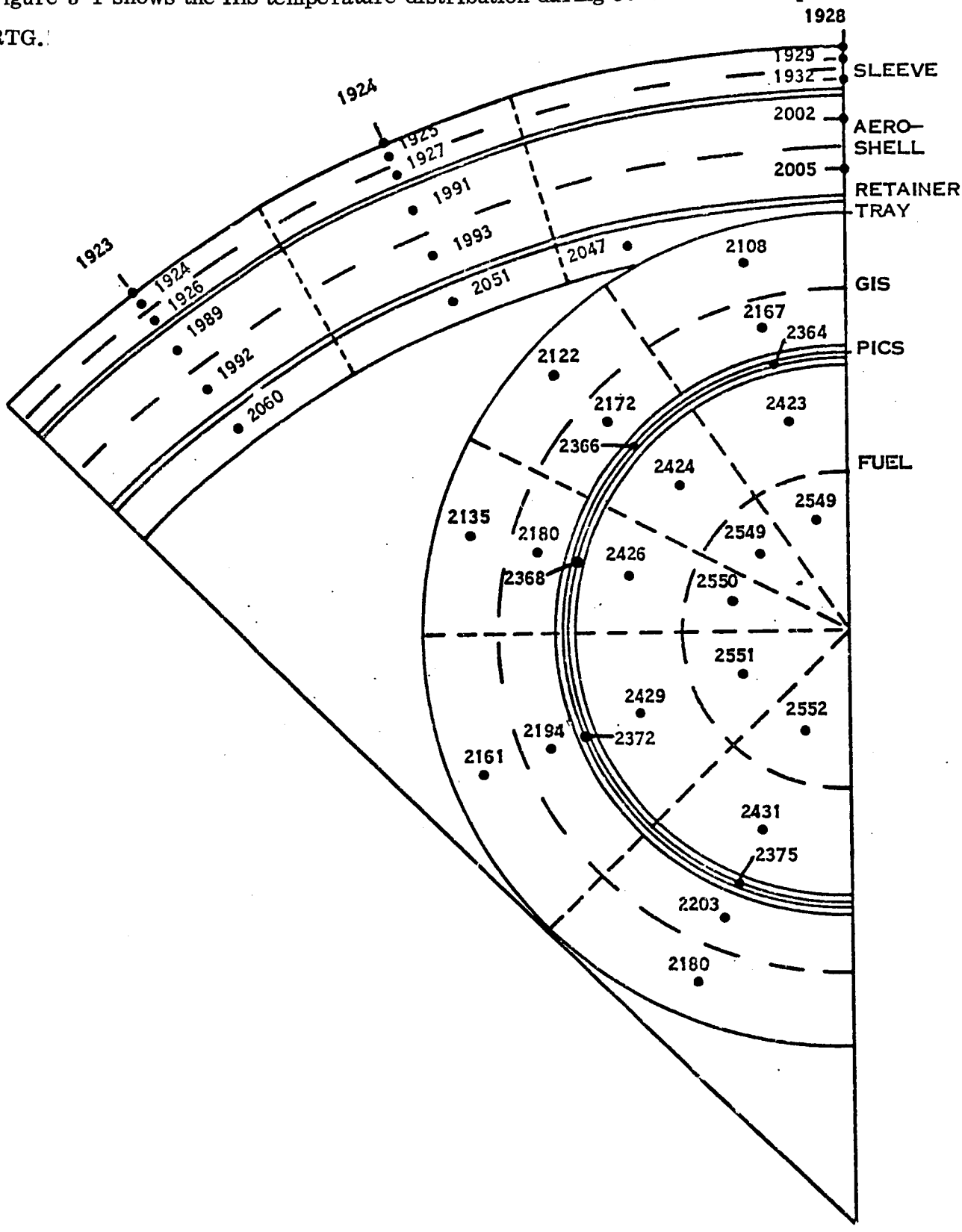

Figure 3-1. MJS IHS Vacuum Operational Temperatures (° F)

SECTION 4

PRODUCT ASSURANCE

4.1 RELIABILITY

4.1.1 RELIABILITY PROGRAM PLAN

The Reliability Program Plan GESP-7109, as approved by US ERDA-NRA, was implemented throughout the MHW-MJS program activities. This implementation used the experience gained during the MHW-LES program, with strong emphasis on the hardware differences between the LES and MJS configurations.

4.1.2 PREDICTION OF EOM POWER

The EOM power predictions, accounting for all identified degradation modes, are discussed in detail in Section 7, Subsection 7.4. These projections included all data from test modules on test at RCA and JPL and, from April 1976 onwards, also included the actual performance data telemetered from the four MHW-LES units operating in the Lincoln Experimental Satellites (LES) on station in synchronous orbit.

4.1.3 REVIEW OF QUALIFICATION TEST PROGRAM

Reliability Engineering reviewed the results of the Q-2 RTG Qualification Tests and the flight acceptance tests (FA) on flight units F-6 through F-12 RTGs. Although the mechanical qualification testing of Q-2/RTG was subsequently determined to be overly severe, it was concluded that adequate design margins for flight application had been established and that single point failures were improbable. The successful mechanical acceptance tests on flight units F6 and F7, also performed at unrealistically high levels, provided additional support for these conclusions. The mechanical acceptance tests of the flight RTGs: F8 through F12 supplied further confirmation of the ability of the MJS RTG design to meet the mission requirements without significant failures.

4.2 QUALITY ASSURANCE

Quality Assurance efforts were highlighted by:

1. Continued support for fabrication, assembly, test, and shipment of the qualification unit Q-2 and for the MJS flight-qualified RTGs: F-6 through F-12.

2. Performance of internal GE-QA audits and support for ERDA/Sandia Quality Audits at GE and RCA.

3. Support for the disassembly and detailed inspection of the Q-2 converter, after qualification testing at GE. (See also Sections 5 and 7)

4. Implementation of the MJS Quality Assurance Plan, approved by ERDA/NRA, for assistance in inspection activities and ETG/RTG testing.

5. Maintaining surveillance of vendors especially:

   a. Speedring for the converter Be case.

   b. Hitco, for the GIS, IHS internal structures and the Pyrocarb 406 ablation sleeve.

   c. POCO for the aeroshell cylinders and end caps.

6. Support of the Program Office/Engineering investigation of the Q-2/IHS end cap failures (see Section 5).

7. Maintenance of the monthly reporting of the Nonconformance Reports (NR) status.

8. Implementation of the GEMS-420 Test Policy Document.

4.3 CONFIGURATION MANAGEMENT

The objectives established in the Configuration Management Plan, GESP 7063, have been complied with since the start of the MJS Program. Document format and content for drawings and associated lists meet the requirements of MIL-D-1000. The format and content for System and End Item Specifications peculiar to MJS were per agreement between ERDA and GE, using MIL-STD-490 as a guide. All drawings, associated lists and specifications required to define MJS End Items were issued. The System, Environmental and End Item Specifications requiring approval of ERDA per Technical Direction 74 M-1 were submitted to ERDA and approved. All documents supplying configuration identification, at GE and RCA, were under configuration control. In addition, the documents for flight-associated hardware for the ETG/IHS/RTG, the RTG Shipping Container,

and the Storage Protection Container were under configuration control. Those drawings and documents covering components and assemblies involving interfaces between GE and the Fueling Agency, ERDA's Mound Laboratory, and between GE and the User, NASA/JPL, were also under configuration control.

Configuration Identification Lists for End Items were issued.

SECTION 5

ISOTOPE HEAT SOURCE

This section reviews significant information concerning the design, development, fabrication, testing and use of the MHW-MJS Isotope Heat Source (IHS). See Figure 5-1 for the configuration and principal components of the MJS-IHS. The Annual Reports for the MHW-LES 8/9 Programs give extensive discussions for the rationale of the basic IHS design. These are:

- GESP-7071 (1970-1971)
- GESP-7097 (1972)
- GESP-7107 (1973)
- GESP-7122 (1974)
- GESP-7123 (1975)

The changes to the IHS design for the MHW-MJS Program are discussed in:

- GESP-7127 (1975)

Functional and safety considerations have been the principal determinants of the design and development efforts. The present review considers:

- The source of heat for the RTG, a fuel module called the fuel sphere assembly - FSA (see Figure 5-2) consisting of the:
  - Isotope fuel - $^{238}PuO_2$
  - Post Impact Containment Shell - PICS
  - Graphite Impact Shell - GIS

and

- The IHS structure which provides:
  - The physical/mechanical/thermal interface with the RTG.
  - Protection of the radioactive fuel in the event of a reentry.

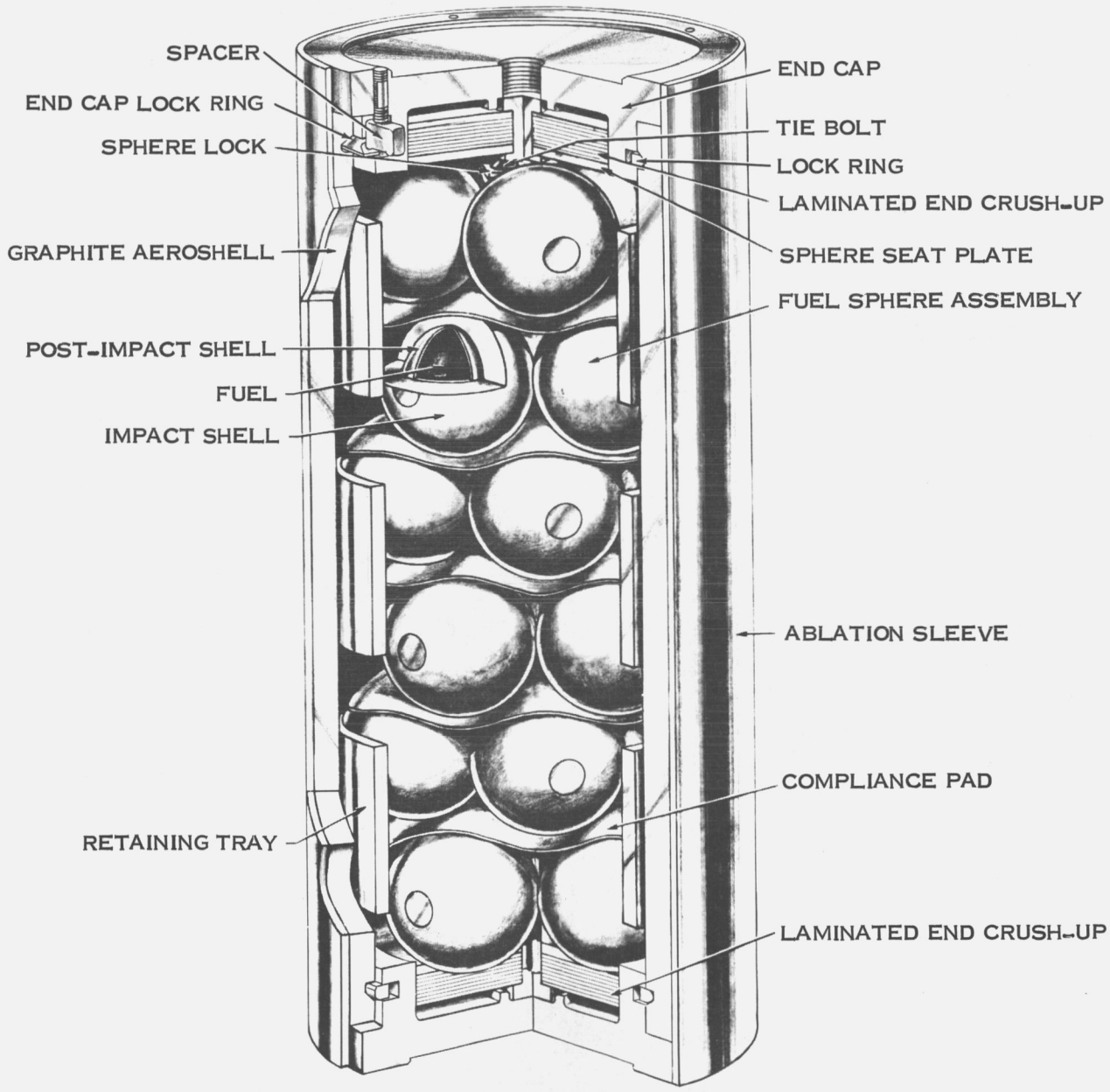

Figure 5-1 . Cutaway View - MHW-MJS-IHS

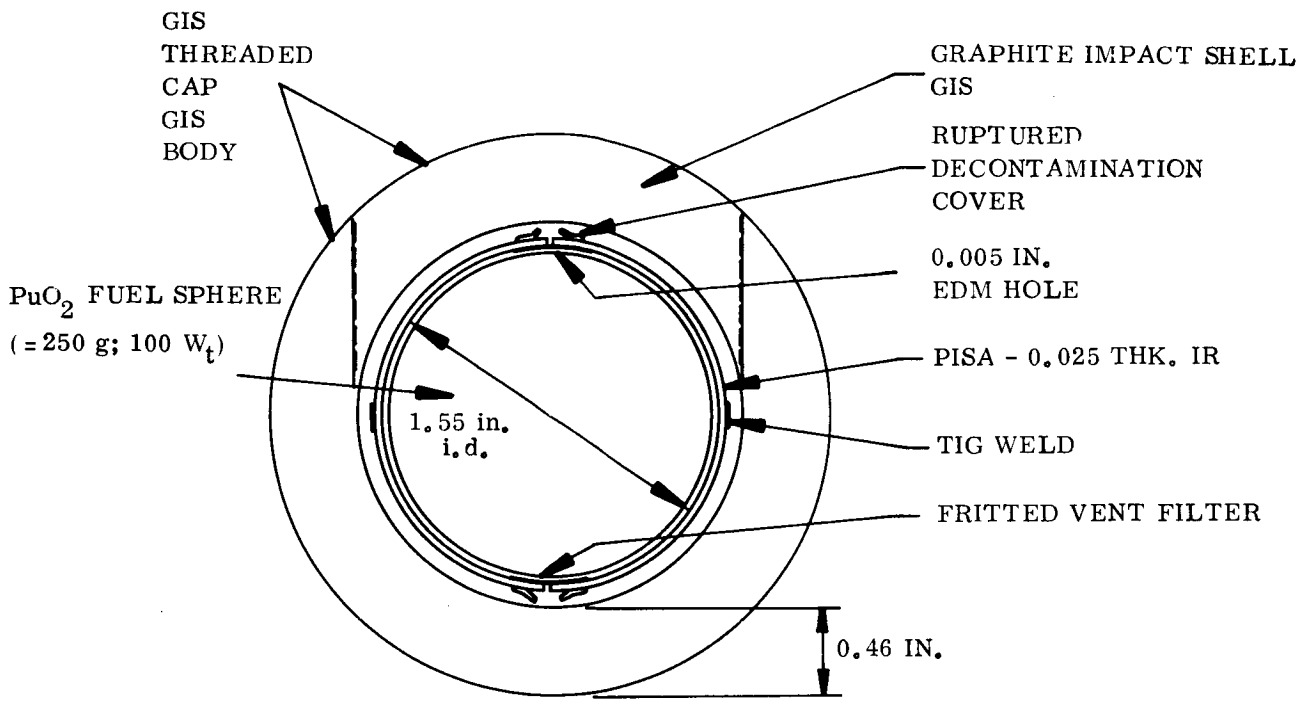

Figure 5-2. MHW Fuel Sphere Assembly (FSA); Post Impact Shell Assembly (PISA) in Graphite Impact Shell (GIS).

5.1 THE FUEL SPHERE ASSEMBLY - FSA

Figures 5-1 and 5-2 show the FSA and its use in the IHS. Work on the three principal components of the FSA during this reporting period is given in the succeeding paragraphs:

5.1.1 The Isotopic Fuel

5.1.2 The PICS

5.1.3 The GIS

5.1.4 FSA Performance Testing and Analyses

5.1.1 THE ISOTOPIC FUEL - $^{238}PuO_2$

Thermal energy for the MHW-RTG is produced by the radioactive alpha decay of the isotope, ^{238}Pu.

5.1.1.1 Development and Fabrication

Fabrication of the radioisotope fuel, $^{238}PuO_2$, into fuel spheres for the MHW-RTG MJS Program is the responsibility of the Fueling Agency (FA), which is the ERDA Mound Laboratory (operated by Monsanto Research Corp.) (ML/MRC). Raw material, as $^{238}PuO_2$ powder, is supplied by the ERDA Savannah River Plant (operated by E.I. DuPont de Nemours Co., Inc.) (SRP). Research and development on isotopic fuels for various applications, including MHW-RTG, is the responsibility of the Fuel Development Laboratory (FDL) which is the ERDA Los Alamos Scientific Laboratory (University of California). Liaison is maintained on a continuing basis with ML/MRC, SRP and LASL to acquaint these organizations with program status and fuel-related problems and to keep GE current on changes, developments and program status of these groups.

5.1.1.2 Fuel Form and Basic Requirements

The ^{238}Pu isotope fuel is used in a stable chemical form, the dioxide, PuO_2, and in the physical form of spheres, with diameters of 1.465 ± 0.015 inches. These chemical and physical forms are adequate to satisfy the basic operational and safety requirements of the MHW system.

The MHW-RTG fuel form is required to provide thermal energy of 2400 Watts, at a heat source surface temperature of around 1050°C. This produces a fuel/PICS interface temperature of around 1300°C with vacuum in the IHS. The fuel form must be fabricable to the desired physical shape and size must be stable during and after encapsulation in all of the expected operational and credible accident conditions to which it may be exposed.

5.1.1.3 Fuel Characterization

Fuel form characterization and compatibility test program was carried out during the period January 1976 through June 1977 under US ERDA-NRA direction at Los Alamos Scientific

Laboratory (LASL), and Mound Laboratory (ML/MRC). These programs were designed to establish or verify high temperature properties and behavior of the IHS materials.

The basic properties of the fuel form affect its behavior/response to a variety of thermal, physical, chemical, and mechanical conditions. These are separated somewhat arbitrarilly as shown in Table 5-1 . Specific tests associated with these categories are summarized as to status and results in Tables 5-2 and 5-3. In briefly reviewing the results here, the properties and behavior/response are considered as they influence functions and not necessarily in the discrete categories listed.

All of the fuel spheres for the IHS, F-6 through F-12 were fabricated by ML/MRC by the end of April 1976. Thus the fabrication development work at LASL during 1976-1977 did not directly affect the production of fuel spheres for MHW-MJS. The characterization of $^{238}PuO_2$, however, does provide significant data on the anticipated behavior of the fuel spheres in operational and accident conditions. In addition, LASL performed impact tests of typical ML/MRC FSAs and analyzed the results. LASL also examined 8 of the spheres taken from the Q-2R/IHS forward 8-pack. Data from these tests and analyses were incorporated into the final safety analysis report.

Most of the fuel characterization and compatibility test programs were completed during 1974-75 (see GESP-7122). A small number of compatibility tests involving the FSAs in the test configuration shown in Figure 5-3 continue at LASL (See Table 5-4 for the test conditions). The discussion presented here touches on the following area in which experimental and analytical work was done during 1976-77 LASL, ML/MRC, and GE-SD:

- Determination of basic mechanical properties at temperature (LASL)
- Correlation of processing parameters with mechanical properties (LASL)
- Determination of fines formed by impact and other tests of FSAs. (LASL)
- Interaction with CO (LASL)

TABLE 5-1. MHW FUEL CHARACTERISTICS

Properties	Behavior/Response

• Density
• Mechanical
  • Compressive
  • 4 Point Bend
  • Youngs Modulus
  • Poisson's Ratio
• Conductivity
• Specific Heat
• Melting Point
  • Pure Fuel
  • PPO + Ir + C
• Thermal Expansion
• Emittance
• Solubility
• Vapor Pressure
• Radiation
• Sinterability
	• Vibration
	  • FSA
	  • HSA
	• Impact
	  • Pellets
	  • Hot Bare Spheres
	  • FSA
	  • HSA
	• Oxidation/Reduction
	• Helium Retention/Radiation Damage
	  • Pellets
	  • Large Samples
	  • Spheres
	• Pu Release
	  • Vapor
	  • Alpha Knock-on
	  • Particulates
	• Ablation/Vaporization
	• Compatibility
	• Temperature Ramping

5.1.1.3.1 Determination of Basic Mechanical Properties

The behavior of $^{238}PuO_2$ at high temperatures ($\geqslant$1000C) was investigated by LASL in tests to determine mechanical properties. Data from some of the early impact tests suggested that PuO_2, like its congener, UO_2, had some plasticity. Work during the previous reporting period indicated that the behavior of $^{238}PuO_2$ in compression resulted in completely brittle fracture up to temperatures of around 1200° C. At that time, LASL considered the possibility that the accumulation of He in the crystal structure might have been responsible for the brittle behavior. To verify this, LASL tested pellets which had large differences in lifetime, from a few days to as much as 2 years. The results of these tests were ambiguous because other

TABLE 5-2. FUEL CHARACTERIZATION - 1

1.0 Fuel Properties (Status - as of 30 June 1977)

Category	Status	Results, Comments
1.1 Density	Complete For MJS	Flight quality spheres from ML/MRC production: variable density, 82% TD nominal average; 15% surface-to-center, 90% to 75% LASL (and SRP) made homogeneous within ± 5% TD
1.2 Mechanical • Compressive • 4-point Bend • Young's Modulus • Poisson's Ratio	Complete For MJS Continuing Continuing Continuing Continuing	Room temp data on LASL and ML/MRC material completed; high temp. data in process; $^{238}PuO_2$ unlike UO_2 shows no plasticity up to 1400°C; at 1500°C, 'normal' ceramic plastic behavior is observed; differences between $^{238}PuO_2$ and $^{239}PuO_2$ appear related to O/Pu ratio; O/^{239}Pu = 1.90 shows markedly greater plasticity than O/Pu = 2.000 studies continuing MJS flight fuel spheres were all O/Pu = 2.000 ± 0.005
1.3 Thermal Conductivity	Partial data	Complete to 1350°C; high temperature data, to 2200°C, waiting on installation and checkout of apparatus; data needed but no work is planned
1.4 Specific Heat	Complete	Data avail. from studies on Pu fuels: $^{239}PuO_2$ assumed same as $^{238}PuO_2$
1.5 Melting Point • Pure Fuel • Fuel + Ir + Carbon	Complete Complete	Data on production fuel shows effects of impurities Needed to determine synergistic MP depression, no enhanced reaction below Ir + C eutectic at 2200°C. (data by LASL)
1.6 Thermal Expansion	Partial data	Complete to 1400°C; verifies previous work; requires high temperature apparatus; data required but no work is now planned
1.7 Emittance	Partial data Cancelled	LASL reported data through 1400°C to 2000°C later; no work planned
1.8 Solubility	Continuing	Solubility in fresh and salt water continuing under study; encapsulated sphere test (MHFT-13) in sea water; no Pu release observed during over one year; post-test examination showed attack on Ir from inside probably from radiolytic decomposition of sea water
1.9 Vapor Pressure	Available	Data are for "Pure" $^{239}PuO_2$; data checks on production material are required. Ca, Si, Al, Fe oxides in vents
1.10 Radiation	Complete For MJS	Neutron counts and gamma measurements made on all flight units showed all FSAs and IHSs = 6 x 10^3 neutrons per second per gram of ^{238}Pu
1.11 Sinterability	Complete For MJS	See LASL reports for fuel development studies; = 20,000 hours data show some densification from as-pressed and He bubbles at grain junctions

TABLE 5-3. FUEL CHARACTERIZATION - 2

2.0 Fuel Behavior/Response (Status - as of 30 June 1977

Category	Status	Results/Comments
2.1 Vibration		
• FSA at MRC/ML	Complete for MJS	MHFT-11: Hi-level vib'd; broke; fines = 0.6% wt. All SVT & SVT vib'd @ LES levels; fuel fines range: 0.004 to 0.04% WT. Q-2R/IHS MJS qual. vib'd
• HSA at GE		fuel fines flight FSAs = 0.19% wt.
2.2 Impact		
• Pellets at LASL	Partial	Low temperature pellet impact data; need high temperature data
• Hot bare spheres	Complete	Two spheres dropped at 1000°C; broken in large pieces
• FSA at LASL	Complete MJS	15 impacts with ORNL-ML Ir PISAs; 3 pass; 12 failures
• IHS at Sandia	Complete	Full-scale IHS (24-pack) with ThO_2 fuel simulant impacted; all ORNL-ML/MRC Ir PISAs cracked (9 TOT) 3 badly damaged
2.3 Aging Effects		
2.3.1 He Retention/Release		
• Small pellets at LASL	Complete	Data available indicate no problem at 1300°C for small pieces
• Large samples at LASL	In process	Quantitative retention data at 900, 1150, 1250, 1370 and 1450°C obtained
• Stored spheres at LASL	Complete	No significant damage; affects mechanical strength; see 2.3.2
2.3.2 Radiation Damage + He Ingrowth	In process	Change in mechanical properties and microstructure may result from He bubble concentration along grain boundaries; new specimens being made; tests with $^{239}PuO_2$ are underway
2.4 Oxidation at LASL & ML	Complete for MJS	Reduction and reoxidation showed small dimensional changes, apparent reduction of fuel identified as an artifact
2.5 Pu Release		
• Vapor	Complete for MJS	Vapor transport of PuO_2 cal'd for Knudsen flow; need additional calc's at pressure reached in FSAs with intermittent venting
• Alpha Knock-on	Calculated	
• Particulates	Continuing	LASL makes fines measurements on all impacted and vibrated FSAs
2.6 Ablation/Vaporization	Cancelled	Facilities problems in the use of live fuel
2.7 Compatibility at LASL	Complete for MJS	No interaction with MJS system materials: PuO_2 + Ir + C after ≥ 23000 hours at ≥ 1330°C
at DWDL	Test complete	No effect on tensile properties of Ir
2.8 Thermal Response		
• Reentry Thermal Ramp	Complete	Included in the SSST
• Asymmetrical Thermal Ramp	Complete	Sphere cracked but remained integral; LASL & MRC/ML spheres run
• Summetrical Ramp to Operational - 1450°C	Complete	LASL spheres checked after 1 year showed no damage or change when heated to 1450°C @ MRC/ML: 1 sphere after 6 mos. storage at 1250°C OK

TABLE 5-4. MHW FUEL SPHERE ASSEMBLY COMPATIBILITY TESTS AT LASL

Specimen, Number	MHW Operational Mode - Gas in Ir/Fuel Gap	Helium Vent Hole Diameter - Inch	Exposure Temperature Degrees Celstus		Test Start Date	Exposure Time Hours		Status As of 30 June 1977
			O.D. GIS Measured	Ir/Fuel Calculated		Planned	Actual	
MHFT-1	Vacuum	0.0008	1340	1440	Aug. 1972	2150	2150	Exposure complete; data reported
MHFT-15	Vacuum	0.0015	1340	1440	25 May 1973	3300	7395	Exposure complete; data reported
MHFT-19	Vacuum	0.005	1340	1440	18 May 1973	1480	1105	Exposure complete; data reported
MHFT-20	Vacuum	0.005	1340	1440	May 1973	8760	18293	In storage; not yet examined
MHFT-22	Vacuum	0.005	1340	1440	15 Jun 1973	3300	3300	Exposure complete; data reported
MHFT-14	Helium	0.0008	1180	1250	May 1973	2150	1248	Exposure complete; data reported
MHFT-18	Helium	0.005	1180	1250	21 May 1973	1460	1365	Exposure complete; data reported
MHFT-21	Helium	0.005	1180	1250	1 Jun 1973	8760	4500	Exposure complete; data reported
MHFT-10	Helium	0.0008	1018	1150	Mar 1973	4380	1244	Exposure complete; data reported
MHFT-16	Helium	0.0015	1018	1150	6 Jun 1973	3300	17339	In storage; not yet examined
MHFT-17	Helium	0.005	1018	1150	7 May 1973	3300	17713	In storage; not yet examined
MHFT-23	Helium	0.005	1018	1150	Test not begun	---	---	Transferred to environmental test
MHFT-37	Vacuum	0.005	1210	1335	24 Feb 1974	3000	23818	Exposure complete; data not reported
MHFT-42	Vacuum	0.005	1210	1335	21 Feb 1974	3000	5440	Exposure complete; data reported
MHF-30	Vacuum	0.005	1210	1335	Nov 1974	3300	22226	Test continuing; vent(s) open
MHFT-44	Helium	0.005	1180	1250	3 Jun 1974	1500	22545	Test continuing; vent(s) open

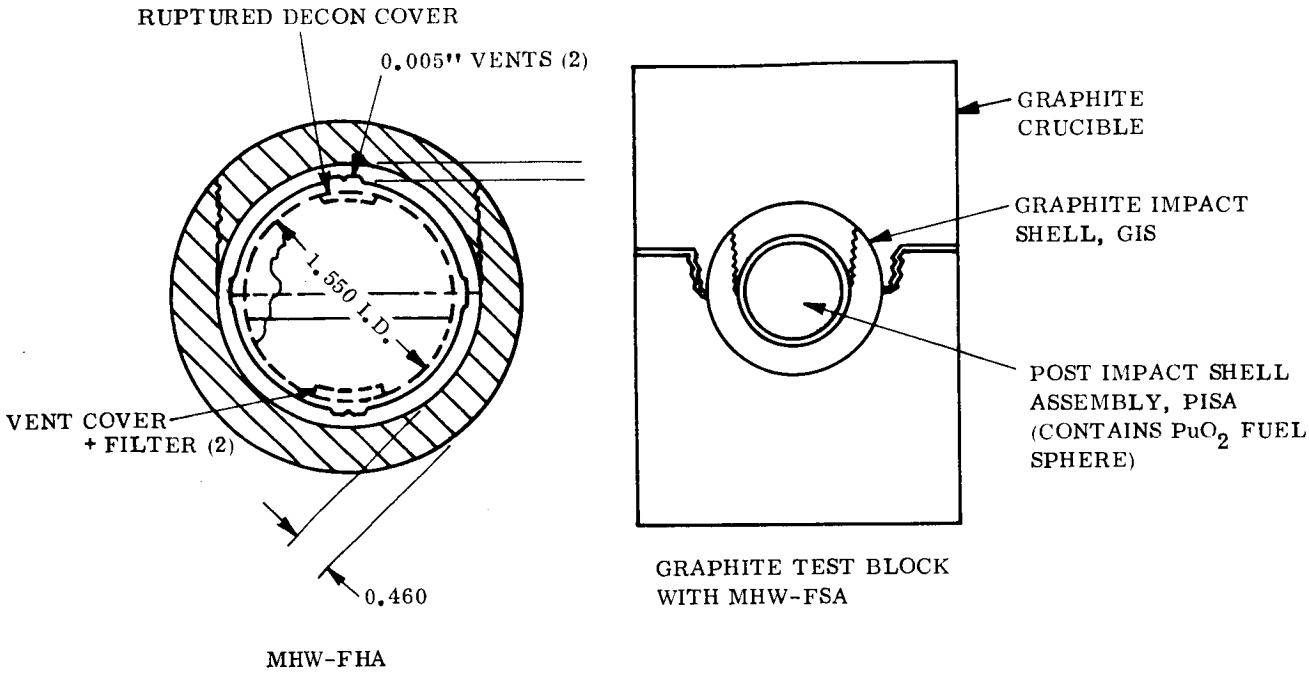

Figure 5-3. LASL FSA Compatibility Configuration

factors such as differences in fabrication may have affected the behavior. During the current reporting period, LASL fabricated and tested a number of specimens using substantially identical fabrication parameters and including finished pieces made from the isotope ^{239}Pu. This was done to provide a material which was ostensibely identical as a ceramic to the $^{238}PuO_2$ specimens. There were some differences in chemistry, the $^{239}PuO_2$ material generally having less than 300 ppm of total extraneous impurities. Since the half lives of the two plutonium isotopes differ by a factor of 270, it was anticipated that the pieces fabricated from the $^{239}PuO_2$ would not accumulate a significant amount of helium within the crystal structure of the specimen prior to testing. The saturation concentration of He in solid PuO_2, in terms of cubic centimeters of He at 760 torr and 0° C, is strongly temperature dependent as shown by Figure 5-4. At temperatures of 900° C, one gram of PuO_2, nominally 90% TD, will retain ~0.5 SCC of He. Figure 5-5 shows the cumulative generation of He for various components of the MHW-IHS. To reach an inventory of 0.5 SCC requires approximately one year. For one gram of $^{238}PuO_2$, however, the same concentration would not be reached in less than ~ 270 years. The results of these tests again were ambigious. The possible effects

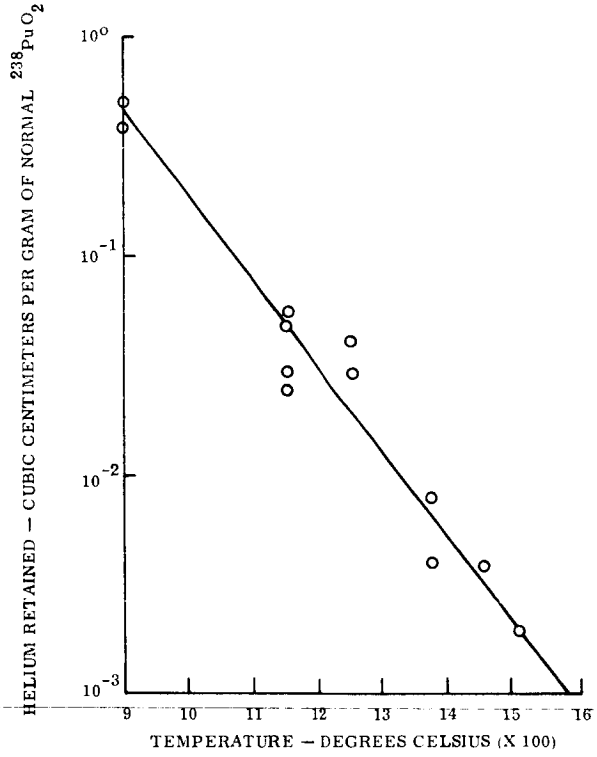

Figure 5-4. Saturation Concentration of Helium in Solid PuO_2 (From LASL Data)

helium could not be entirely ruled out as a factor contributing to the brittle facture of $^{238}PuO_2$. However, an additional area of possible significance in the behavior of $^{238}PuO_2$, was discovered when pellets of $^{239}PuO_2$ were impacted without a final sintering in the argon-oxygen-16 atmosphere normally used by LASL to remove carbon from the finished specimens. As pressed, the material is substoichiometric, with a O/Pu ratio of ~ 1.90. Compressive strength tests on the $^{239}PuO_2$ pellets were made at temperatures ranging from 25°C - 1200°C. Brittle facture occurred at room temperature but at all other temperatures, including 800° C, there was significant plastic deformation of the material. Thus, the behavior of the substoichiometric $^{239}PuO_2$ as well its strength more nearly parallels that of UO_2 than it did the behavior of the $^{238}PuO_2$ specimens. LASL inferred from this behavior that some reduction in the O/Pu ratio below the stoichiometric value of 2.00, may enhance plastic deformation processes in plutonium oxide. The most recent experimental data indicate that the substoichiometric materials, $PuO_{(2-x)}$ does exhibit significant plasticity in compression even though there may be internal microcracking of the materials prior to tests. It should be noted that there

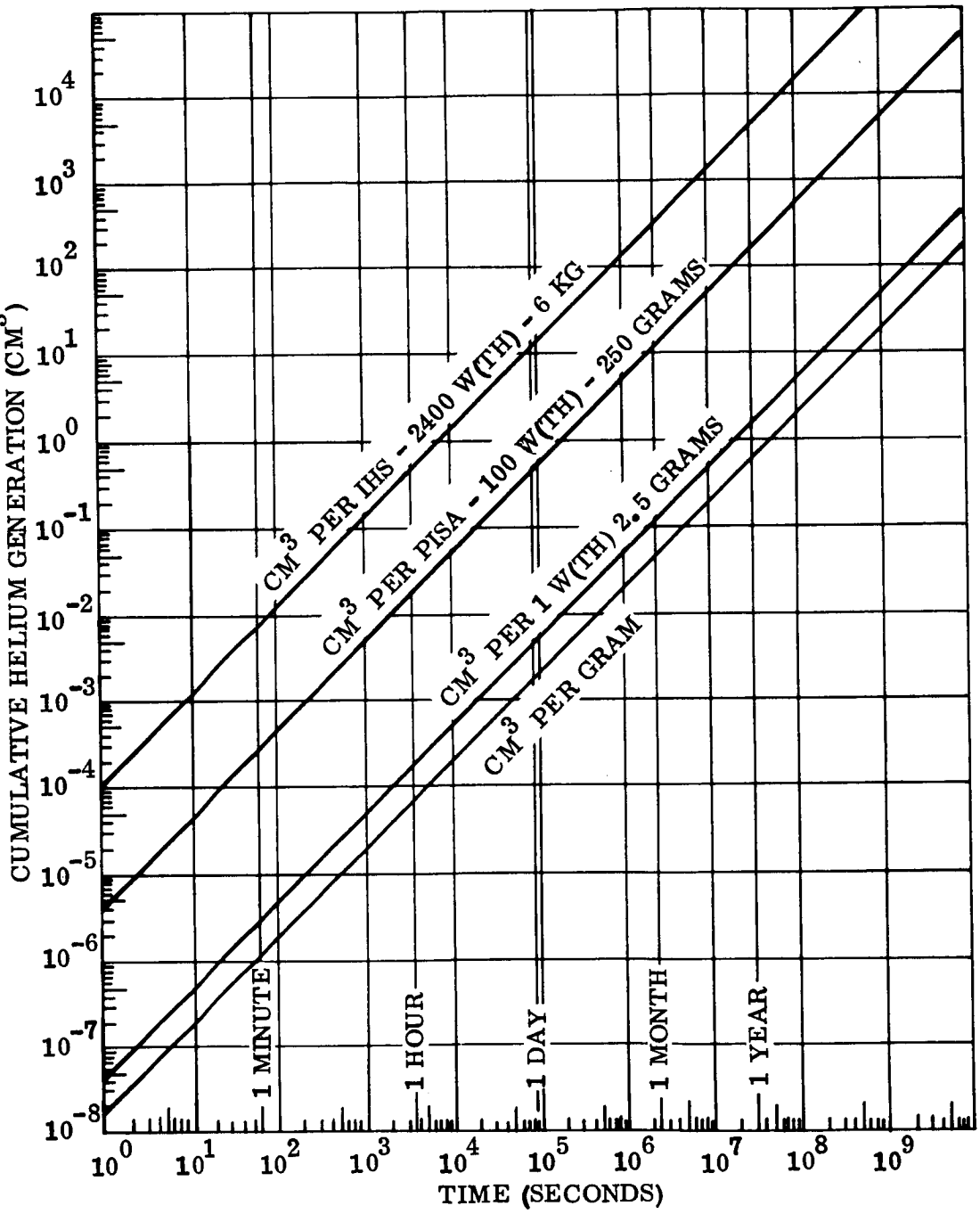

Figure 5-5. Helium Generation vs. Time for Various MHW Components

is a significant difficulty in attempting to maintain specimens of $^{238}PuO_2$ below the stoichiometric composition. This arises from the fact that even relatively small pellets have appreciable selfheating which permits oxidation of the specimens after fabrication, to near stoichiometric composition, even when they are maintained in controlled atmospheres having less than 200 ppm of oxygen. The $^{239}PuO_2$ specimens do not exhibit significant self-heating and consequently oxidize from their as-pressed condition much more slowly than specimens of $^{238}PuO_2$. In the continuing studies, LASL now plans to work with fuel pellets in which the O/Pu ratio can be very carefully controlled by oxidation or reduction in a small furnace. Another line of investigation includes the addition to the sesquioxides of yttrium and lanthanum, to stabilize the $PuO_{(2-x)}$ at a fixed value of x. The use of these metal oxides as additives has shown promise in the stabilization of uranium oxide O/M ratios. At the end of this reporting period, work in this area was continuing at LASL. As noted below in the discussion of the behavior of fuel spheres during impacts, the absence of plasticity in the $^{238}PuO_2$ fuel has caused failure of the iridium containment when tears occurred over hard, jagged segments of the fractured fuel. Details of these investigations are given in the LASL monthly reports and in topical reports covering the subject.

5.1.1.3.2 Fuel Fabrication Development

As noted in para. 5.1.3, the recent LASL fuel fabrication developments have not been reflected in the production fuel spheres for MHW MJS. The behavior of fuel specimens made by LASL advanced techniques, when subjected to mechanical properties test, is different from the behavior of fuel made by the ML/MRC production technique. Fuel made by the advanced LASL processes is basically homogeneous, with uniform grain size and porosity distribution. The ultimate strength of these materials in compression is roughly twice that of specimens made by the production fuel processes. The MHW MJS production fuel spheres are characterized by variations in density, from center to poles and to the equatorial lands, of as much as 15 percent, reflecting both the heterogeneous distribution of porosity and non-uniform grain size. Impact tests of FSAs made with fuel spheres fabricated by the LASL process show lower fines production and less tendency to produce the sharp jagged fractures against which the iridium PICS may tear. This difference in behavior indicates that the fracture of production spheres in a hard, brittle mode is not random or atypical but is characteristic of fuel

made by the current production processes for all of the MHW MJS fuel spheres. These results validate the decision in the safety analysis to assume failures of the FSAs permitting fines formation and potential fuel release through the fractured or torn PICS in the event of impact after reentry.

5.1.1.4 Determination of Fines Production from MHW MJS Fuel Spheres

The MHW MJS fuel spheres show extensive internal cracking when examined radiographically after hot pressing, cooldown, and carbon cleanup, Subsequent to assembly of the fuel spheres into the PICS, a number of the fuel spheres undergo fracture, leaving the sphere no longer integral. The fractured spheres generally consist of from two to six fairly large segments. The fractured surfaces of these sphere segments produce small particles by abrasion of mating surfaces. Particles of fuel in the range of ≤ 10 micrometers diameter are of concern if introduced into the biosphere by accidental rupture of the PICS. The principal source of concern is that particles in the range of ≤ 4 micrometers are considered to be respirable by man. Throughout the MHW program, LASL has examined the fuel removed from FSAs vibrated and/or impacted, to measure the size and quantity of the small particles produced, with special attention to the fractions below 10 micrometers and 4 micrometers. Fines production on impact is discussed in Section 2 of this report, as fines generation is related to the evaluation of source terms for the safety analysis. (see also GE Report 77SDS4206-FSAR for MJS and GEMS-419-FSAR for LES 8/9, Section 5).

The production of fines, by vibration processes alone, became a concern during this reporting period because of the anomalies found in the Q-2R/IHS, the MJS qualification unit, and in the F-6 and F-7 IHSs, which are flight units. The weight fraction of fines produced in a number of impact and vibration environments is given in Table 5-5. The quantity of fines found in MHFT-11, a special test sphere and in MHF-64 and -164, FSAs removed from the Q-2R IHS are 16 to 50 times larger than from FSAs MHF-27, -28, and -29, removed from the Q-1 IHS, the LES qualification unit. Moreover, the fines found in MHFT-11, and MHF-64 and -164, are 4 to 13 times higher than the fines produced by simulated launch vibration, followed by impact tests simulating impact at terminal velocity after reentry. Details of the anomaly found in Q-2R and F-6 and F-7 IHSs are given in para. 5.2.3. MHFT-11, as a single FSA was

TABLE 5-5. $^{238}PuO_2$ FINES(*) FOUND IN FSAs SUBJECTED TO VARIOUS ENVIRONMENTS

FSA No.	Weight Fraction	Fines Measured By-Org	Environment(s)
MHFT-11	6.0 (-3)	LASL	ML/MRC Preliminary vib.
MHF-28	1.1 (-5)	ML/MRC	Q-1 LES
MHF-29	4.0 (-6)	ML/MRC	Q-1 Qual
MHF-27	1.2 (-4)	LASL	Q-1 Vibration
MHFT-28	1.2 (-5)	LASL	SST Vibration only
MHFT-41	3.3 (-5)	LASL	SVT-vib and impact
MHFT-45	1.9 (-4)	LASL	SVT-vib and impact
MHFT-49	4.76 (-4)	LASL	SVT-vib and impact
MHF-64	1.7 (-3)	LASL	Q2R Original MJS
MHF-164	1.9 (-3)	LASL	Q2R Qual Vibration

* ≤ 4 micrometers average diameter

subjected to high levels of vibration, greater in terms of energy input, than would ever occur even under worst-case conditions in a flight unit. This test was conducted in 1972, before the expected vibration regime for either LES or MJS had been defined. MHF-64 and -164 were removed from the forward 8-pack of Q-2R/IHS, after disassembly of this unit at BMI-CL; See para. 5.2.2.7. The Q-2R/IHS was also subjected to vibration levels as a qualification unit which later were found to be much more severe than those actually anticipated for the MJS launch and other mission vibration environments. The concern regarding F-6 and F-7 FSAs, stems from the fact that these units were subjected to acceptance levels of vibration testing which also were found, subsequently, to be excessive. A concern, therefore, arose that these units, which were designated as flight units, might have produced quantities of fines significantly larger than those generated in some impact modes and, consequently, might require a reassessment of the source term, potentially ascribable to these two units.

The results of the fines determination permit the inference that any fines generated in the vibration testing of F-6 and F-7 IHS are probably of the same order as anticipated and will not not significantly exceed the levels found in the FSAs removed from the Q-1 IHS which had been subjected to the LES qualification levels.

5.1.1.5 Potential Interactions of PuO_2 Fuel to Produce CO

The problem of CO production in the MHW IHS was discussed at length in the previous Annual Reports referenced in the introduction to this section. During 1976, LASL reviewed the potential interactions between the $^{238}PuO_2$ and the carbon/graphite in the IHS. It was concluded that oxygen release and consequent fuel reduction did not appear as probable sources of CO generation, in the storage conditions, but that some exchange between the ^{16}O of the fuel and the normal O of the contained CO, could occur. These discussions were contained in LASL report, LA-6396-MS, and are in substantial agreement with the referenced discussion presented in the MHW Annual Reports.

In reviewing the possible interactions between the fuel and the carbon material in the IHS, LASL indicated that there were uncertainties regarding the possibility of interactions through the medium of the CO gas in the IHS. The IHS may contain some CO from;

- incomplete outgassing of the carbon/graphite components
- CO produced by reactions of the IHS carbon/graphite with O_2 or H_2O picked up from the very low contamination in the production line box atmospheres
- release of O_2 from the fuel at operational temperatures and its consequent reaction with the carbon/graphite components.

A possible mechanism for cyclic interactions between residual CO and the fuel was presented: see LASL report LA-6534 pages 8-10. The postulated interactions are:

- $CO + PuO_2 \longrightarrow CO_2 + PuO_{(2-x)}$ (1)
- $CO_2 + C \longrightarrow 2CO$ (2)

It has been shown by LASL experiments that flowing CO in contact with solid carbon can produce some reduction of the PuO_2. Tables 5-6 and 5-7 show the conditions of the experiments and the degree of reduction after exposures for a number of times and temperatures. A LASL report, LA-6534, using these data and thermodynamic calculations, presents the extent of possible fuel reduction,at the conditions of temperature and pressure, under which it is possible thermodynamically for the reactions to proceed. In addition, LASL has initiated an experiment to determine the extent to which the interaction shown in equations (1) and (2) will proceed for various initial partial pressures of CO and FSA temperatures. A sketch of the physical set up for this experiment is shown in Figure 5-6. Results from this experiment are given in the LASL monthly reports.

During the period 1976-77, a number of long term FSA tests were completed and the fuel was examined. At moderate temperatures, $PuO_{(2-x)}$ is a mixture of PuO_2 plus a second phase, alpha-Pu_2O_3. This second phase becomes more abundent as the O/Pu ratio approaches 1.61. The appearance of this second phase in metallographic examination is distinctive and is readily apparent, if present. In none of the fuel sphere specimens examined metallographically by LASL, was there evidence of the second phase, alpha-Pu_2O_3. The specimens involved are noted in Table 5-6. With the conditions of exposure and the total accumulated exposure time. From these results, it appears reasonable to conclude that no significant reduction of PuO_2 occurs under either the LES or MJS operational conditions, as simulated in the LASL tests. Although the thermodynamics indicate the possibility of the cyclic $CO/CO_2/CO$ reaction proceeding, conclusive evidence must wait on the outcome of the LASL experiments referred to previously.

5.1.2 POST IMPACT SHELL ASSEMBLY-PISA-DEVELOPMENT, FABRICATION AND TESTING

The PISA consists of the fuel sphere in a vented iridium sphere, the post impact containment shell, PICS, which is the primary containment for the fuel; see Figures 5-7 and 5-8.

TABLE 5-6. REDUCTION OF PuO_2 BY CO CALCULATED VS OBSERVED VALUES

Temperature (°C)		P_{CO} (atm)	Calculated		Observed[a]	
PuO_2	Graphite		O/Pu	Weight[b] Loss (g)	O/Pu	Weight Loss (g)
927	927	0.08	1.999	0.001	1.994	0.003
		0.80	2.000	0.000	1.997	0.002
1027	927	0.08	1.989	0.006	1.979	0.011
		0.80	1.999	0.001	1.995	0.003
1127	927	0.08	1.953	0.025	1.960	0.021
		0.80	1.992	0.004	1.979	0.011
1227	1027	0.08	1.879	0.063	1.851	0.078
		0.80	1.947	0.028	1.952	0.025
1327	1027	0.08	1.852	0.078	1.867	0.069
		0.80	1.920	0.042	1.910	0.047
1427	927	0.08	1.870	0.068	1.878	0.064
	1027	0.08	1.832	0.088	1.846	0.081
	1127	0.80	1.868	0.069	1.868	0.069
1527	1127	0.08	1.755	0.128	1.770	0.121
	1127	0.80	1.823	0.093	1.840	0.084

[a] Equilibrium (10-yr) values obtained from least-squares fit of reduction vs time.

[b] Based on average size pellet (8.850 gms $PuO_{2.00}$).

5.1.2.1 Development and Fabrication

The history of the PICS development and fabrication is described in the annual reports referred to in the introductory paragraphs of this section. Currently, the basic iridium sheet, for the fabrication of the iridium hollow hemispheres, is produced by Oak Ridge National Laboratory (ORNL) from raw iridium powder. These discs are formed and finished by ML/MRC as Ir hemispheres. The vent filter structure is fabricated by GE-SD and is welded into place by ML/MRC. Details of these production efforts are given in the reports of the responsible organizations.

TABLE 5-7. CALCULATED REDUCTION OF PuO_2 BY CO - PuO_2 AT 1237°C (1600°K)

Graphite Temperature (°C)	Equilibrium Stoichiometry (O/Pu) CO Pressure (atm)			
	0.008	0.08	0.8	8.0
827	1.87	1.93	1.99	2.00
927	1.82	1.89	1.95	1.99
1027	1.78	1.85	1.92	1.98
1127	1.73	1.82	1.89	1.95
1227	1.65	1.78	1.86	1.93
1327	1.50 + l	1.76	1.83	1.90
1427	1.50 + l	1.72	1.81	1.88
1527	1.50 + l	1.66	1.79	1.86

5.1.2.1.1 Ir Sheet

The Ir sheet produced by ORNL contains about ≤400 ppm of the platinum metals as impurities, the exact amounts varying from batch to batch. Based on experimental performance results, the alloy now used for PICSs is Ir and 0.3% W. Other impurities are limited by specification to ~100 ppm total. The performance of the ORNL - ML/MRC PICS on terminal velocity impacts, with ThO_2 fuel simulant, at GE-SD and, with $^{238}PuO_2$ production fuel, at LASL is discussed in a subsequent paragraph, and in previous reports in this series (see Introduction). Persistent failures of the ORNL-ML/MRC PICSs led to the introduction of an alloy modification containing ~50 to 100 ppm of Th in the bulk material, but yielding concentrations of 2-5% at the grain boundaries. This material has greatly improved impact performance.

5.1.2.1.2 Ir Hemispheres

The hollow Ir hemispheres are produced by ML/MRC using the ORNL Ir blanks. The Ir blanks are sealed between Ta waster sheets, heated, and formed while hot. The Ta is dissolved in acid and the hemispheres are processed to incorporate the vent holes, vent filter assemblies, vent hole covers (to permit decontamination), and weld shields.

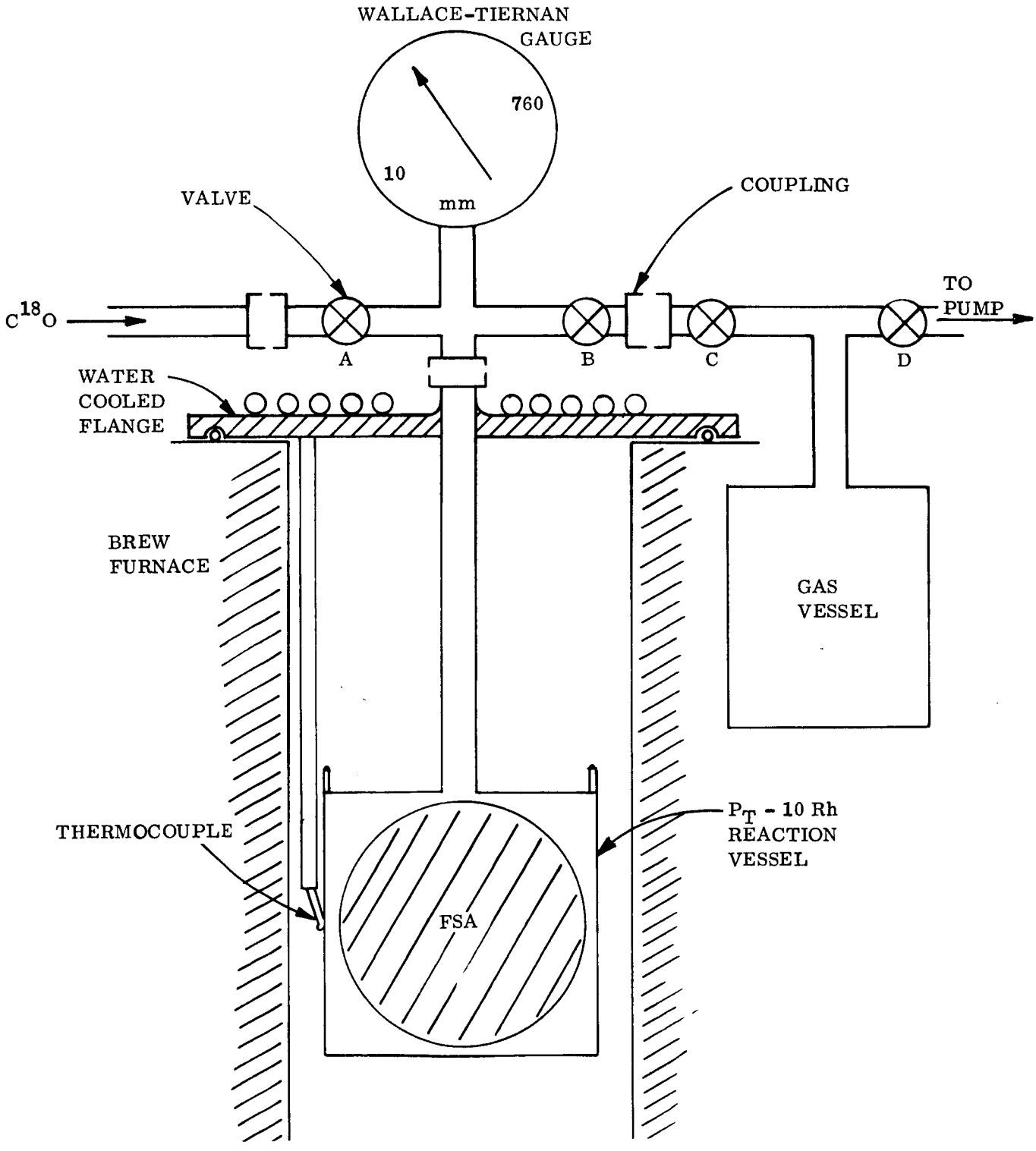

Figure 5-6. LASL Test Configuration for CO/PuO_2 Reactions

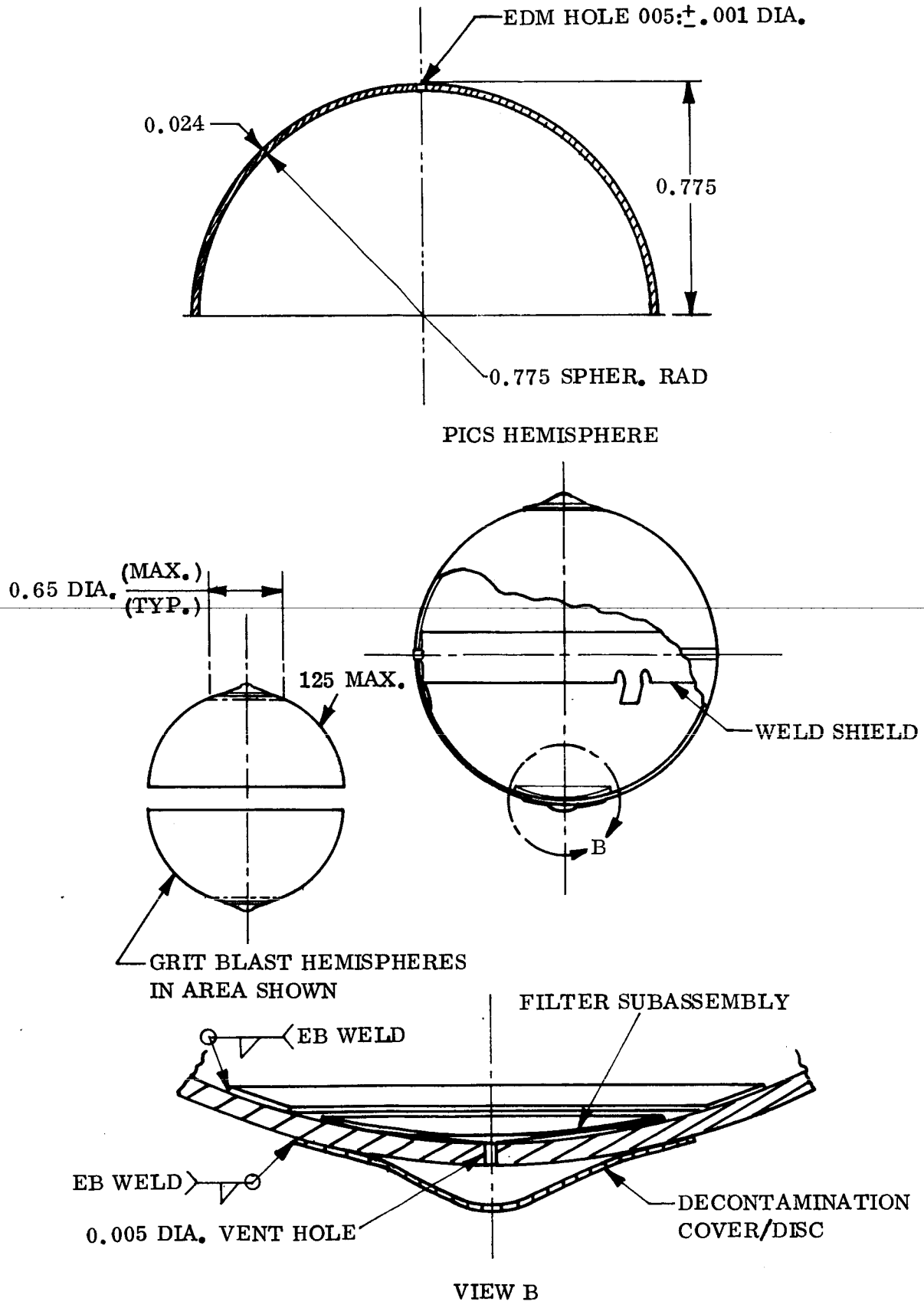

Figure 5-7. PICS Components

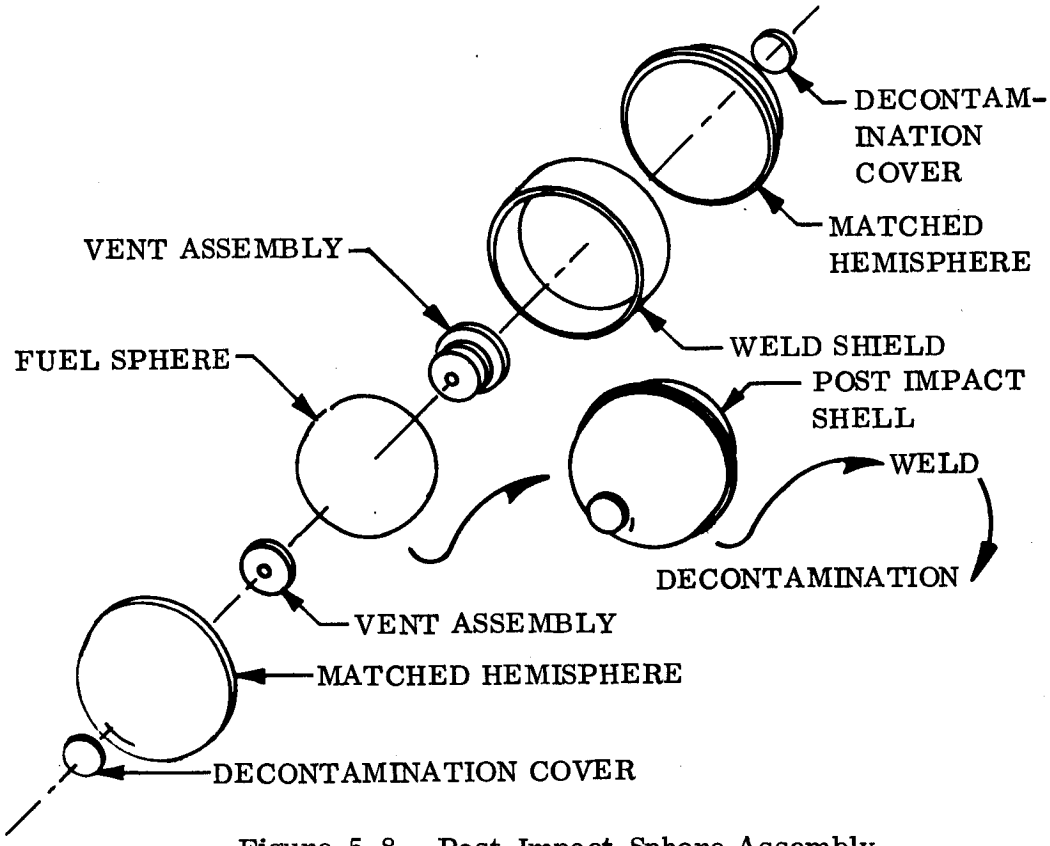

Figure 5-8. Post-Impact Sphere Assembly

5.1.2.1.3 Post Impact Shell Assembly - PISA

When the fuel sphere is assembled into the PICS, the assembly is sealed with a circumferential weld at the equator. After decontamination, both vent covers (decontamination covers) are ruptured to permit He to be released (see Figure 5-8).

5.1.2.2 PISA Venting

5.1.2.2.1 He Release

Previous Annual Reports for the LES and MJS Programs have reviewed the problems of venting the He generated by the alpha-decay of ^{238}Pu. See Figures 5-4 and 5-5 for the saturation concentrations of He with temperature and the production of He by the MHW-IHS

fuel. The intermittent plugging of the vent filters was observed by LASL on a number of specimens. Pre-flight and flight vent filter designs are shown on Figure 5-9.

Testing of the vent structure of the PISA flight design continued at LASL with fueled FSAs operating at temperatures simulating the operational conditions: for LES 8/9, on MHFT-44, in helium; and for MJS, on MHFT-37 and MHF-30, in vacuum.

a. MHFT-37 was operated in vacuum at an effective fuel/Ir PICS interface temperature of approximately 1335° C. This unit was removed from test at the end of January 1977 after having been exposed for 23,818 hours. Analyses and descriptions of this specimen have not yet been reported by LASL.

b. MHFT-44 is operated in helium with the fuel/Ir PICS interface temperature at approximately 1220° C. This unit was placed on test in June 1974 and is checked once a month for He release, since continuous monitoring is precluded by the He furnace atmosphere, which is maintained at approximately 0.1 atmosphere. When the unit was monitored in May 1977, the helium venting was found to be equal to the generation rate. At the end of May 1977, the unit had accumulated 21,928 hours of exposure.

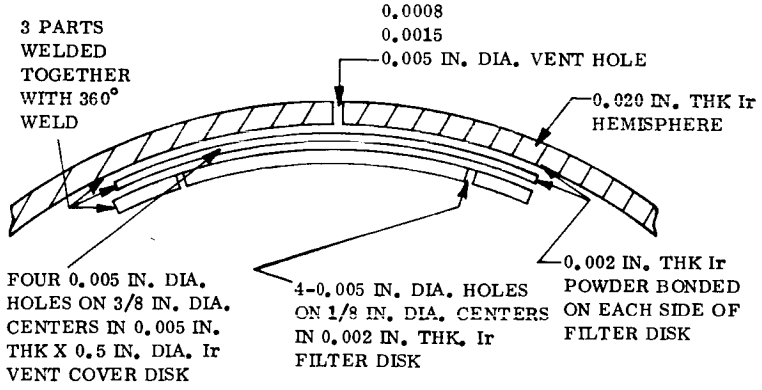

PRE-FLIGHT VENT DESIGN

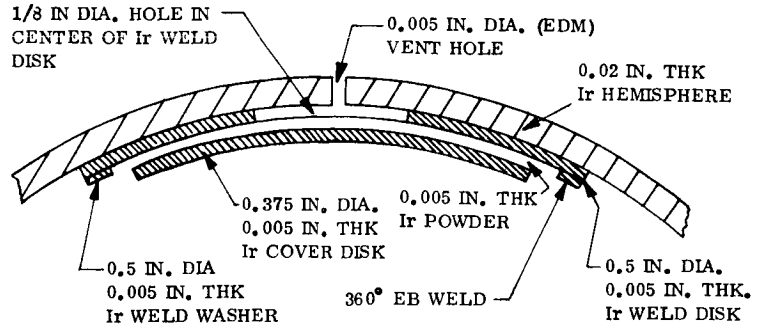

FLIGHT VENT DESIGN

Figure 5-9. MHW PISA Vent Designs

c. MHF-30, one of the FSAs removed from the Q-1 IHS, is exposed in vacuum, with the fuel/Ir PICS interface temperature at approximately 1335° C. The release of He from this unit was not measured during the last 4 months due to equipment problems. At the end of May, this unit had been on test for a total of 21,511 hours.

The vent filter assemblies, in MHFT-37 and -44, are representative of the flight design filter made during development fabrication. In MHF-30, the vent filter is representative of the production runs.

He release from MHF-30 has been continuous at approximately the generation rate, except for a brief period in June 1976. The MJS flight units are expected to respond similarly. Intermittent release of the He generated has not yet been shown to produce any demonstrable adverse effects on the PISA.

5.1.2.2.2 Pu Contamination Release from the PISA

The potential release of Pu-bearing materials from the intact PISA has been reviewed in previous reports of this series: GESP-7097, 4-79 thru 4-87, GESP-7122, PP 5-26 thru 5-29; GESP-7127, PP 5-12 thru 5-20, and GEMS-423 PP 3-5 thru 3-25.

The effusion of ^{238}Pu-bearing materials is dependent on temperature, as reflected in the partial pressures, and on the effective vent size (see Table 5-6). The maximum release of ^{238}Pu materials through the vents has been calculated, disregarding the resistance of the vent filter (see Table 5-7A and Figure 5-9A). The intermittent plugging (see paragraph 5.1.2.2.3) of the vent filters, may further inhibit the actual release. These data suggest that the substantially larger quantities of Pu found by the LASL combustion analyses of the GIS are not produced by effusion of ^{238}Pu-bearing materials through the PISA vents but arise from the residues on the external surfaces of the:

- PISA, which are not removed by the decontamination process,
- GIS, which are not decontaminable.

TABLE 5-7A. CALCULATED RELEASE OF PuO_2 (g) FROM MHW-FSA WITH TWO 0.005" DIA. VENTS

Conditions	Storage		Test		Operation		Reentry	
Temperature	835°C (1530°F)		1140°C (2080°F)		1327°C (2420°F)		1500°C (2732°F)	
Source	FSA	IHS[1]	FSA	IHS	FSA	IHS	FSA	IHS
Grams-Second^{-1}	1.1 (-20)	2.7 (-19)	1.7 (-15)	4.1 (-14)	2.6 (-14)	6.3 (-13)	1.5 (-12)	3.6 (-11)
Grams - Year^{-1}	3.5 (-13)	8.5 (-12)	5.4 (-8)	1.3 (-6)	8.3 (-7)	2.0 (-5)	5.0 (-5)	1.2 (-3)
Curies - Second^{-1}	1.3 (-19)	3.2 (-18)	2.0 (-14)	4.9 (-13)	3.3 (-13)	7.8 (-12)	1.8 (-11)	4.4 (-10)
Curies - Year^{-1}	4.2 (-12)	1.0 (-10)	6.4 (-7)	1.5 (-5)	1.0 (-5)	2.5 (-4)	5.8 (-4)	1.4 (-2)

(1) IHS contains 24 FSAs

It has been demonstrated by ML/MRC that the surface of the PISA, after as many as four decontamination washes, could still release significant amounts of ^{238}Pu bearing materials, See GESP-7127 PP 5-12 thru 5-16 for a discussion of the behavior of the test PISA, MHD-26. However, there is no satisfactory method currently available to apportion the amount of contamination released through the PISA vents and from a PISA surface contaminated to an indeterminable level. A good estimate of the total Pu present, outside the PISA after testing, can be obtained by combustion analyses of the GISs, removed from various test FSAs. LASL has determined the Pu content of these GISs as shown in Table 5-8.

5.1.2.2.3 Vent Plugging

Sufficient evidence has accumulated, with metallographic examination and microprobe analysis of the vent filters, to establish that the material closing the porosities is a mixture of Ca and Si oxides with admixtures of Al and Fe oxides. PuO_2 is also found in the filters. Work at Battelle Memorial Institute - Columbus Laboratory (BMI-CL), is proceeding in an effort to define the mechanisms of intermittent filter operation more completely. BMI-CL has also produced a new filter design which is on test at LASL in MHFT-60-LB.

The fact that the glassy constituents found in the filters appear to derive primarily from impurities in the PuO_2 fuel, led to consideration of the need to effect a more complete removal of the offending impurities during fuel feed processing. Although the Savannah River Plant

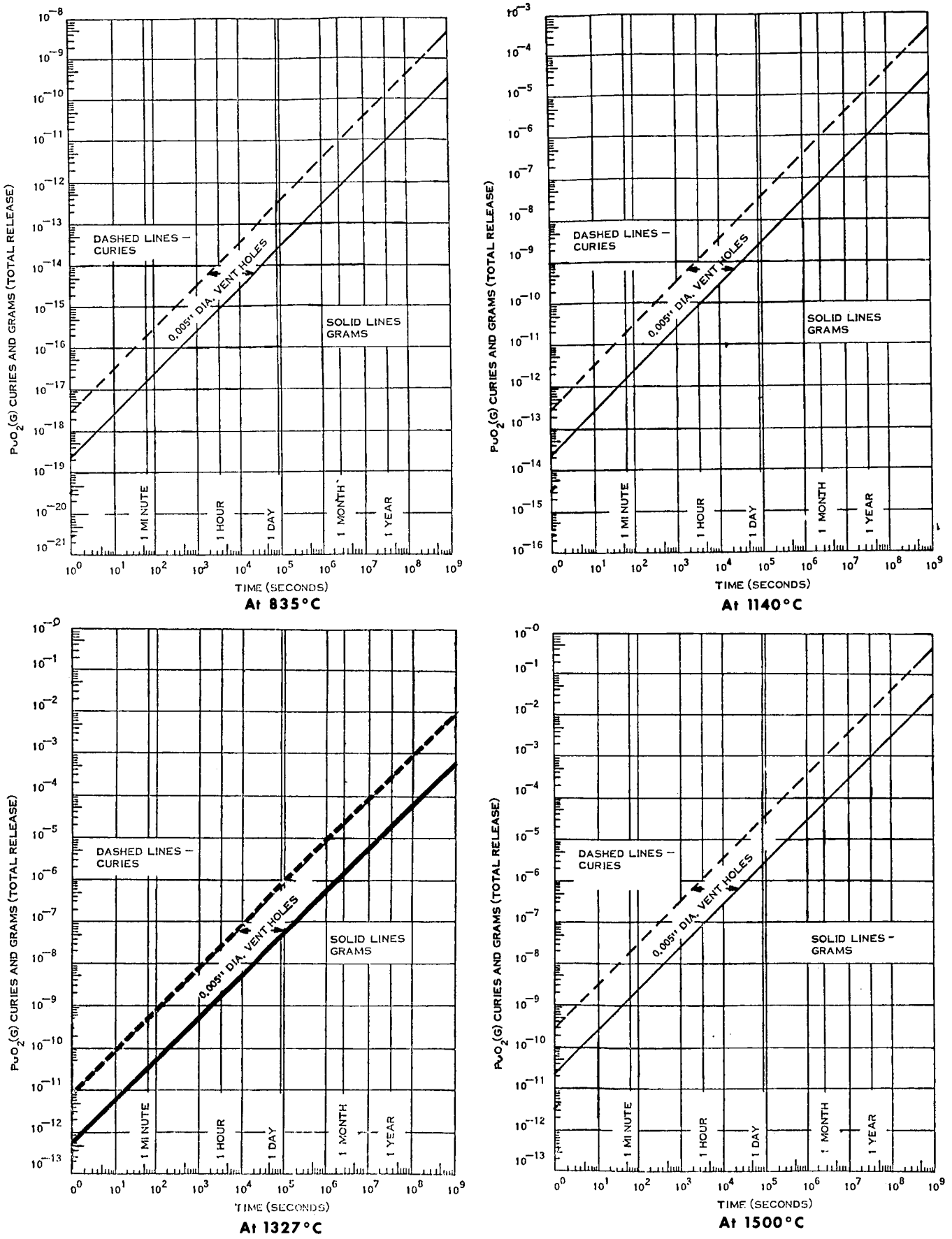

Figure 5-9A. PuO_2 Release versus Time with 48 Vents

TABLE 5-8. TOTAL PLUTONIUM CONTENT ON MHW GISs

SAMPLE NO.	EXPOSURE CONDITIONS			FILTER DESIGN	TOTAL Pu μg
	TIME, h	TEMP. °C	ATMOSPHERE		
MHFT-15	7395	1450	vacuum	pre-flight	19
MHFT-16	17339	1150	helium	pre-flight	1.8
MHFT-17	17713	1150	helium	pre-flight	2.6
MHFT-18	1332	1250	helium	pre-flight	17
MHFT-19	1100	1450	vacuum	pre-flight	56
MHFT-20	18293	1450	vacuum	pre-flight	305
MHFT-21	4500	1250	helium	pre-flight	8
MHFT-22	3400	1450	vacuum	pre-flight	625
MHFT-39 (1,2)	2009	1335	vacuum	flight	720 (3)
MHFT-40 (1,2)	2009	1335	vacuum	flight	15 (3)
MHFT-41 (1)	2009	1335	vacuum	flight	8
MHFT-42	5440	1335	vacuum	flight	1600
MHFT-45 (1,2)	720	1335	vacuum	flight	460
MHFT-47 (1,2)	720	1335	vacuum	flight	18700 (3)
MHFT-48 (1,2)	720	1335	vacuum	flight	14700 (3)
MHFT-49 (1,2)	720	1335	vacuum	flight	160 (3)
MHFT-54 (2,5)	720	1335	vacuum	flight	51 (3)
MHF-27	200	1220	Q-1 heat source, He	flight	38
MHF-29	200	1220	Q-1 heat source, He	flight	0.05 (4)
MHF-15 (7)	200	1220	Q-1/IHS-He	pre-flight	2180.0 (6)
	200	1310	Q2R/IHS vac		
MHF-21 (7)	200	1220	Q-1/IHS-He	pre-flight	9.0
	200	1310	Q2R/IHS-vac		
MHF-64	200	1310	Q2R/IHS-vac	flight	125.0
MHF-161	200	1310	Q2R/IHS-vac	flight	37.0
MHF-162	200	1310	Q2R/IHS-vac	flight	22.0
MHF-164	200	1310	Q2R/IHS-vac	flight	225.0
MHF-165	200	1310	Q2R/IHS-vac	flight	21.0
MHF-166	200	1310	Q2R/IHS-vac	flight	24.0

(1) SVT sample
(2) Impacted
(3) Measured after PISA fracture on impact
(4) Measurement at ML/MRC; all others by LASL
(5) ORNL Type WG Iridium
(6) PICS damaged by saw in removing GIS; probably leaked contamination
(7) These units were used both in Q-1/IHS (LFS/qual) and in Q-2R/IHS (NJS/Qual).

(SRP) production has shown considerable variability in the amount of Ca, Si, Al, and Fe-Ni-Cr, tightening of operational controls resulted in a more consistent product. To effect a reduction of the impurity levels by factors of 5 to 10 would require an investment in process equipment and process management estimated at several millions of dollars. Because the intermittent filter operation has not yet been shown to produce any demonstrable adverse effects on the system behavior, the additional effort to purify the fuel does not appear to be warranted.

5.1.3 GRAPHITE IMPACT SHELL- GIS

The GIS (see Figure 5-10) consists of a hollow sphere of Thornel 50 graphite yarn, impregnated with an organic resin, randomly wound over a graphite mandrel, and carbonized at 2100°C. A threaded cap permits the PISA to be placed inside the GIS. The function of the GIS is to prevent rupture of the PISA in the event of post reentry impact. During the current reporting period, no significant problems have been identified in the design, the fabrication, or the performance of the GISs for MJS.

5.1.3.1 Impact Behavior of the GIS

The GIS deforms and crushes on impacts, effectively absorbing $\geq$ 90% of the impact energy. LASL has investigated and reported on the behavior of impact shells made from other materials as part of the development of advanced heat sources. To date, the FSA impact tests discussed in paragraph 5.1.4, show the GIS to be adequate protection under any of the credible MJS accident conditions.

5.1.3.2 Vibration Behavior of the GIS

The Q-2R/IHS was subjected to shock and vibration levels much in excess of any credible mission exposure. When the Q-2R/IHS was disassembled, the condition of the GISs was carefully observed:

a. One of the GISs from the bottom row of the middle 8-pack had opened; this appeared to be due to the loss of threads on the body of the GIS. The PISA from this unit appeared to be undamaged and showed contamination by wipe of its surface of around 4000 dpm indicating that no significant release of ^{238}Pu had occurred.

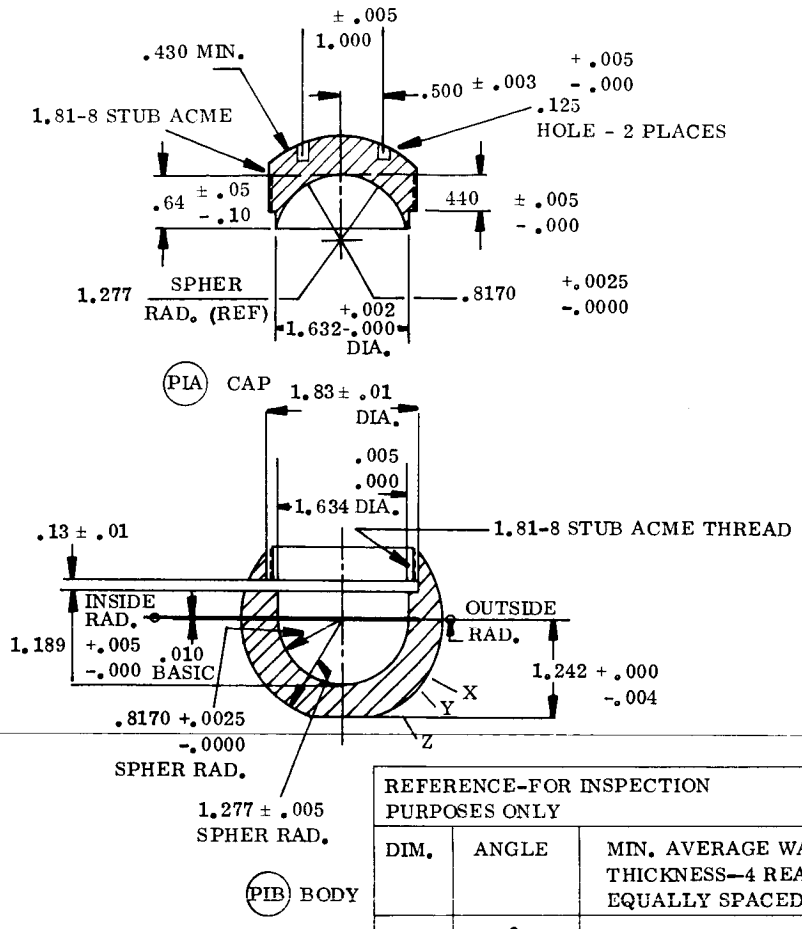

REFERENCE-FOR INSPECTION PURPOSES ONLY		
DIM.	ANGLE	MIN. AVERAGE WALL THICKNESS—4 READINGS EQUALLY SPACED
X	60°	.4555 (REF)
Y	45°	.4565 (REF)
Z	30°	.4570 (REF)

Figure 5-10. Graphite Impact Shell Configuration

b. The GISs on all of the FSAs, removed from the top 8-pack and sent to LASL for assay, showed little if any mechanical damage. The plutonium content of these GISs was determined by LASL as noted in paragraph 5.1.2.2.2 and shown in Table 5-8.

c. The GISs in the middle and lower 8-packs were abraded by the vibration to which the unit was exposed. The degree of abrasion varied from slight breaks in the surface layer to a sufficient removal of material to make the sphere appear out of round on two or three FSAs. The bottom layer of FSAs in the bottom 8-pack, which were completely free of restraint, appeared to have sustained no damage as far as the GISs were concerned.

5.1.4 FUEL SPHERE ASSEMBLY - FSA

The Fuel Sphere Assembly, FSA, consists of the fueled PISA assembled into the GIS (Figures 5-11 and 5-12).

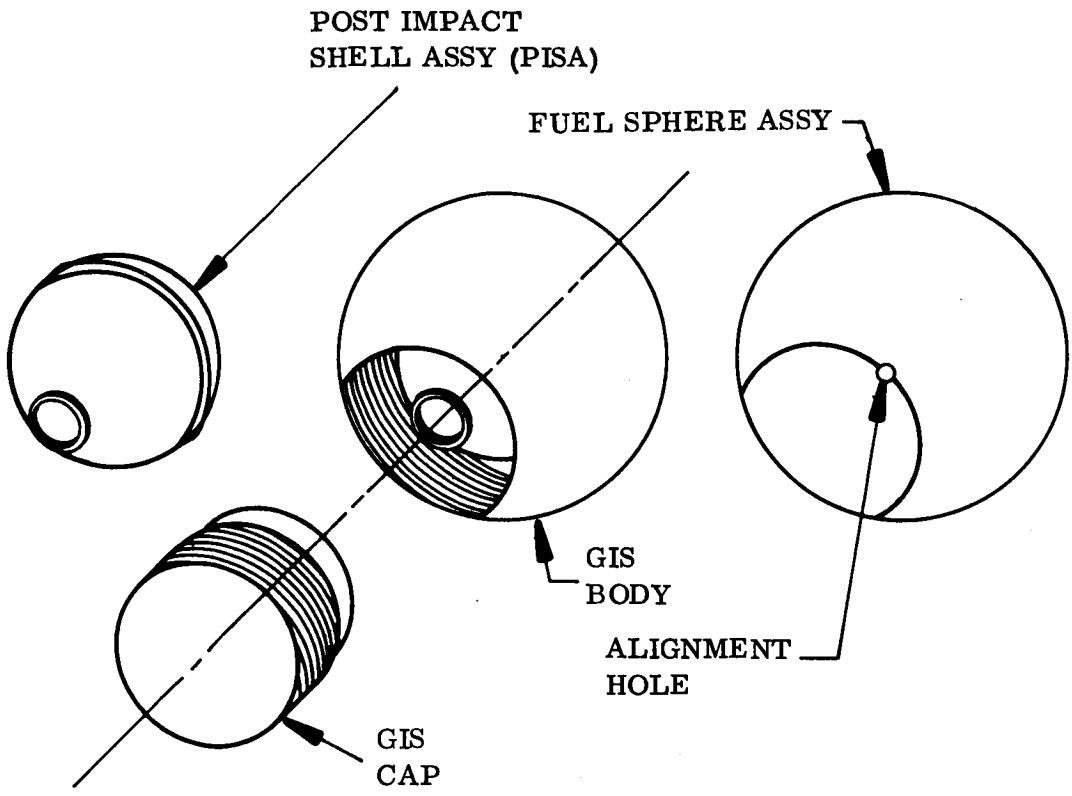

Figure 5-11. Fuel Sphere Assembly Exploded View

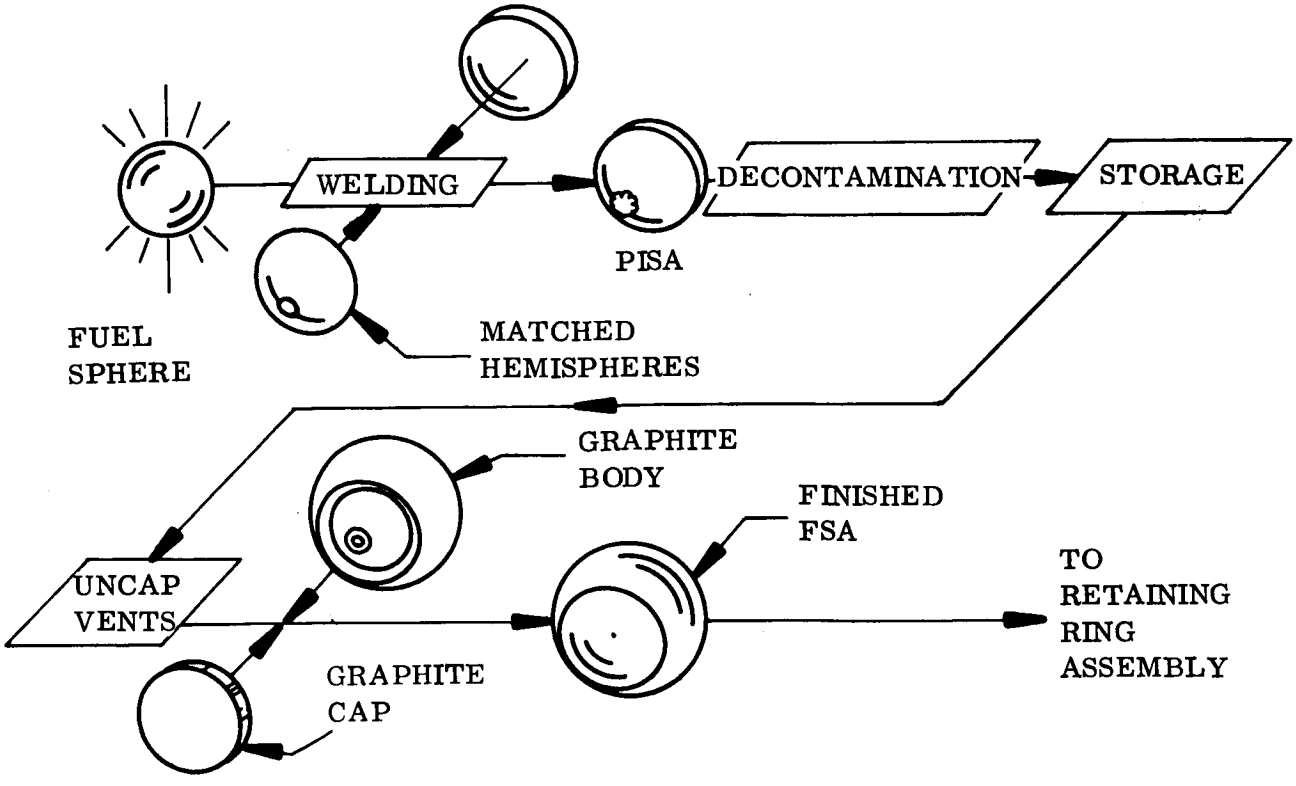

Figure 5-12. Fuel Sphere Assembly (FSA) Assembly Sequence

5.1.4.1 Compatibility Tests

A total of 15 FSAs containing the normal fuel loading of ~252 grams of $^{238}PuO_2$ (80% ^{238}Pu) have been tested at LASL, at times, temperature, and atmospheres, simulating various aspects of the LES and MJS mission conditions, from handling and storage through flight. Table 5-4 summarizes test exposure conditions. Figure 5-3 shows the test specimen configuration.

Details of the LASL compatibility tests on FSAs are given in the LASL monthly reports. No Ir/PuO_2 interactions have been observed in any of the test specimens examined to date. This examination includes not only the tests specifically designed for the determination of compatibility, but also the incidental examination of the iridium from FSAs impacted under the various safety test series, subsequent to their exposure to various thermal environments, including high temperature reentry simulation.

The FSA compatibility tests have completed their exposure with the exceptions of MHFT-44 and MHF-30. During the current reporting period, 1 January 76 thru 30 June 77 MHFT-16, -17, -20, and -37 were removed from test; see Table 5-4 for the total exposure time for each sepcimen. Of these specimens only MHFT-37 has not been examined.

MHF-64 and MHF-164, removed from the top 8-pack of the Q-2R/IHS, were also dissected at LASL. The fines produced by the fuel were determined (see Table 5-8) and the iridium was examined. At least one vent in each of these units was operable. The metallographic examination of the vent structures showed the usual infiltration of glassy material identified as a mixture of silicon-aluminium-calcium with some plutonium and iron. No interaction was observed between the iridium and the PuO_2 fuel. These results all confirm the mutual stability and compatibility of the FSA materials:

- PuO_2 - fuel
- Iridium - PICS
- Graphite - GIS

under all the operational and most of the credible accident conditions anticipated for the MJS applications.

5.1.4.2 Impact Testing of Individual FSAs

The results of impact testing performed during previous years for the MHW program are covered in the reports referenced in the introduction to this section.

Two types of FSA impact have been conducted for the MHW programs:

- impacts at GE-SD using thoria, ThO_2, as a simulant for the isotopic fuel
- impacts at LASL using the standard loading of the plutonia, $^{238}PuO_2$, isotopic fuel.

The paragraphs following discuss the conditions and the results of the impact testing program.

5.1.4.2.1 Impact Testing at GE-SD

Two types of impact testing have been carried out in the GE impact test facility in Building 8 of theValley Forge Space Center.

- One group of tests was designed to determine the impact response of the various components of the FSA. These tests included evaluations of the GIS, the iridium PICS, and the thoria fuel-simulant. These tests were primarily developmental in character.
- The second group of tests was designated as verification tests of the Ir PICS, as produced and fabricated into the PISA at ML/MRC, in accordance with specifications. Two spheres were produced for verification testing in each run of flight qualified fuel PISAs.

The preconditions for these tests and the tests conditions themselves have varied only slightly during the impact testing program. Unless explicitly indicated otherwise, the impact tests at GE-SD used the Ir PICS subsequent to an initial one hour thermal soak at 1500°C in vacuum, to remove the oxides of iridium. This was followed by a soak of 18 hours at 1500°C in vacuum; both thermal vacuum exposures were carried out prior to the assembly of the unit with the thoria fuel-simulant sphere. There was, therefore, no other material involved in this thermal soak pre-conditioning to produce interactions with the Ir of the PICS. Subsequent to the thermal pre-conditioning, the PICS was assembled with the thoria fuel-simulant sphere and

the normal welding operation was performed. The spheres used in the verification test program were designed to provide examples of the ML/MRC fabrication and welding techniques. It should be emphasized that the verification test spheres were not welded on the same equipment as the production line fueled flight spheres. The equipment used for welding the fuel-simulant loaded spheres duplicated as nearly as possible the equipment used in the ML/MRC hot cells in the "F" production line. After assembly of the thoria sphere into the PISA, no further heat treatment was used. The simulant PISA was then assembled into a flight qualified GIS selected at random from other similar flight units. In the GE-SD impact facility, the simulant FSA was heated in argon to a temperature of 1370° C (2500° F). This preimpact heating usually required less than one hour of exposure in the argon-blanketed furnace. Thus, the assembled PISA was never exposed to the GIS material for more than one hour, at high temperature. Approximately 30 minutes of this period was at the nominal impact temperature to insure that the FSA had reached thermal equilibrium.

Impact tests were conducted at GE-SD in the Building 8, Impact Test Facility (Coppa Gun). These tests were designed to simulate the impact of FSAs, on a flat granite surface, at velocities at least ten percent above the calculated maximum terminal velocity, following a reentry abort, ~275 fps. To this was added an additional velocity increment to ~295 fps making the impact of the ThO_2 simulant weighing ~ 210 grams, of equal energy with the 250 gram PuO_2 fuel at ~275 fps. The FSA temperatures at impact were achieved by the pretest heating described in the preceding paragraph. The impact facility is instrumented to measure impact velocities by:

- Pressure calibration
- Probes in the gun
- Fastax visible light photography

In addition, three high speed X-ray cameras record the actual impact and rebound from the granite block.

5.1.4.2.1.1 GE FSA Impact Test Results. During 1976 through June 1977, eight simulant-loaded impact tests of FSAs were performed in the GE facility:

FSA No.	Date of Test	Type Ir
MHT-99	14 Mar 76	WGD
MHT-100	15 Mar 76	WGD
MHT-101	4 Apr 76	WGD
MHT-102	14 Apr 76	WGD
MHT-103	5 Aug 76	HD
MHT-104	10 Aug 76	HD
MHT-105	5 Oct 76	HD
MHT-106	7 Oct 76	HD

The results of these test are discussed in the paragraphs following and pertinent data are summarized in Table 5-9.

5.1.4.2.1.1.1 MHT-99 and MHT-100. Two FSAs, using the ORNL-ML/MRC WGD-doped iridium PICS, with ThO_2 fuel simulant, were impacted in the GE-SD test facility during March 1976, (see Figures 5-13 and 5-14). The test results are summaried in Table 5-9. These specimens recieved the usual thermal exposure of one hour at 1500^{o}C for cleanup, followed by the 18-hour soak at 1500^{o}C, prior to closure welding. As is usual with simulant-filled specimens, these units recieved no subsequent heat treatment beyond the heat-up to the impact temperature of 1370^{o}C (2500^{o}F). Both specimens survived the impact without detectable failures of any kind. No cracks were found either by visual examination at 70X or by Zyglo inspection. No evidence of fingerprinting was found.

TABLE 5-9. FSA TEST SUMMARIES - IMPACTED AT GE-SD-VF BLDG. 8

Date and Test Number	Impact Specimen Data			Impact Conditions				Results
	Graphite Impact Shell No. Density = ρ - g-cm^{-3} Thickenss = t_c - inch Type	Iridium Containment: No. Thickness Heat treament + date Other, Welced by:	Sphere Material Fuel: PuO_2 Simulant: ThO_2 No. ; Dia. ; % TD; Heat treat. ; other	Specimen weight total - grams	Velocity - fps	Energy - ft-lbs	Temperature - ^{o}C (^{o}F)	Pass/Fail Height/Diameter Strain % = D_1-D_o/D_o Impact Angle - degrees from zero degrees
14 Mar. 76 MHT-99	934376-1 ρ = 1.21 t_c = 0.46	WGD 267-2 WGD 266-3 H/T 19 hours @ 1500°C prior to butt weld @ ML/MRC	ThO_2 #722-1 NO H/T with Ir		304		1370 (2500)	Passed: H/D = 1.211/ 1.718 S = 7.1% Rotation = 0° No cracks; no finger-print
15 Mar. 76 MHT-100	934377-2 ρ = 1.21 t_c = 0.46	WGD 279-4 WGD 279-3 H/T 19 hours @ 1500°C prior to butt weld @ ML/MRC	ThO_2, #719-1 NO H/T with Ir		297.4		1370 (2500)	Passed: H/D = 1.127/ 1.775 S = 10.6% Rotation = 0° No cracks; no finger prints
4 Apr. 1976 MHT-101	931363-1 ρ = 1.20 t_c = 0.46 T-50	WGD-290-4 & WGD-290-2; 0.022", H/T 18 hours @ 1500°C prior to butt weld @ ML/MRC	ThO_2; #915; 1.460 76% TD; NO H/T with Ir		295		1370 (2500)	Passed: H/D = 1.218"/ 1.725" S(%) = 7.5 GIS rotation = 5°
14 Apr. 1976 MHT-102	931636-2 ρ = 1.20 t_c = 0.46 T-50	HD-408-4 & HD-408-1; 0.022"; H/T 18 hours @ 1500°C prior to butt weld @ ML/MRC	ThO_2; #916; 1.46 76% TD; not H/T with Ir		297		1370 (2500)	Passed: H/D = 1.154"/ 1.734" S(%) = 8.2 GIS rotation = 5°
5 Aug. 1976 MHT-103	934368-1 ρ = 1.20 t_c = 0.46	HD-412-2; HD-412-1 0.025"; H/T @ 1500°C 19 hours before butt weld at ML/MRC	ThO_2; #917 76% TD; not H/T with Ir		300		1370 (2500)	Fail: H/D = 1.145/1.744 S (%) = 8.6 GIS Rotation = 40° Weld ruptured in maximum stress zone, extended to impact face (2.5 cm long X 0.1 cm wide); no failure in parent metal
10 Aug. 1976 MHT-104	934368-2 ρ = 1.20 t_c = 0.46	HD-424-4; HD-424-3 0.025"; HT @ 1500°C 19 hours before butt weld at ML/MRC	ThO_2; #918 76% TD; not HT with Ir		305		1370 (2500)	Fail: H/D = N/A S (%) = 9.2 (?) GIS rotation ≤ 5° Severe 'fingerprint' secondary impact 90° from primary impact; weld rupture in maximum stress zone; fingerprint punched out; maybe by secondary impact
5 Oct 76 MHT-105	935125-1 ρ = 1.20 t_c = 0.46	HD-442-2; HD-443-2 0.025"; H/T @ 1500°C 19 hours before butt weld at ML/MRC	ThO_2; #922 76% TD; not H/T with Ir		302		1370 (2500)	Fail: H/D = 1.145/1.751 S (%) = 9.3 GIS rotation ~5° two breaches perpendicular to and crossing weld bead; ~ 0.752 x 0.004 w, penetrating wall
7 Oct 76 MHT-106	935125-2 ρ = 1.20 t_c = 0.46	HD-445-3; HD-445-2 0.025"; H/T @ 1500°C 19 hours before butt weld at ML/MRC	ThO_2; #923 76% TD; not H/T with Ir		300		1370 (2500)	Pass (?): 1.167/1.744 S (%) = 8.9 GIS rotation: ~3° 70X examination shows shallow cracking in the area of high stress region; do not penetrate wall

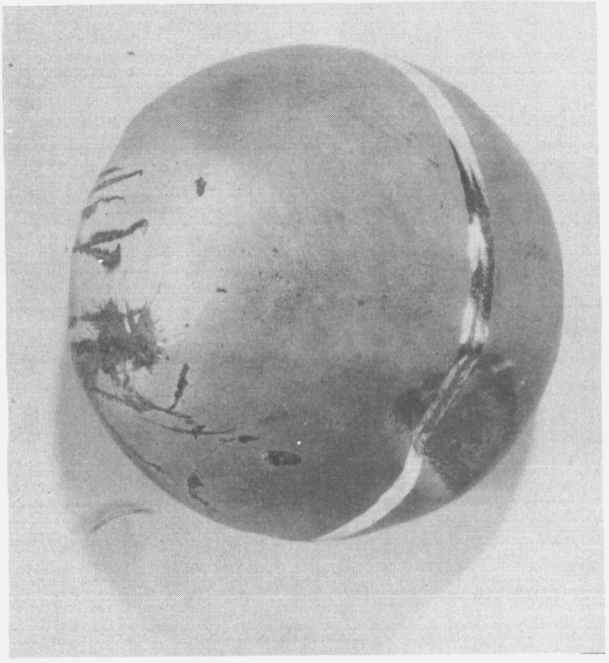

MHT 99 TOP VIEW

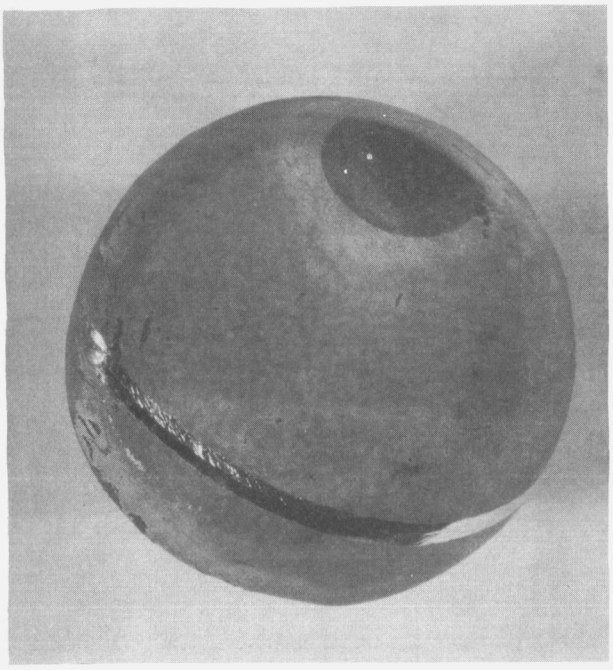

MHT 99 IMPACT FACE

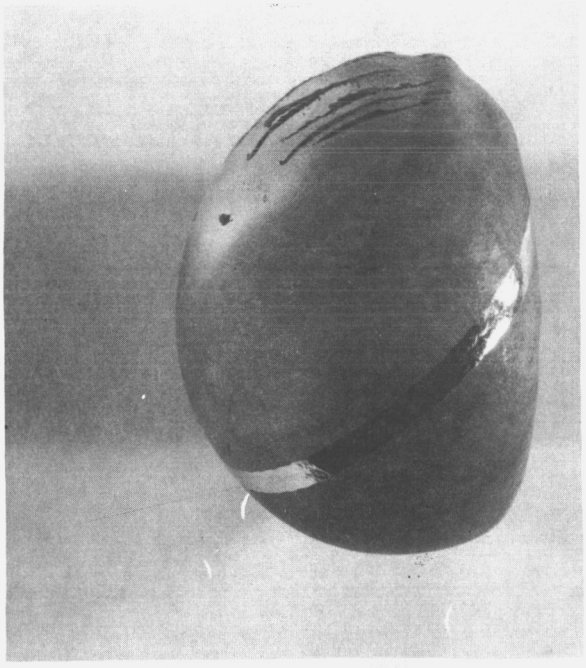

MHT 99 SIDE VIEW

Figure 5-13. FSA MHT-99

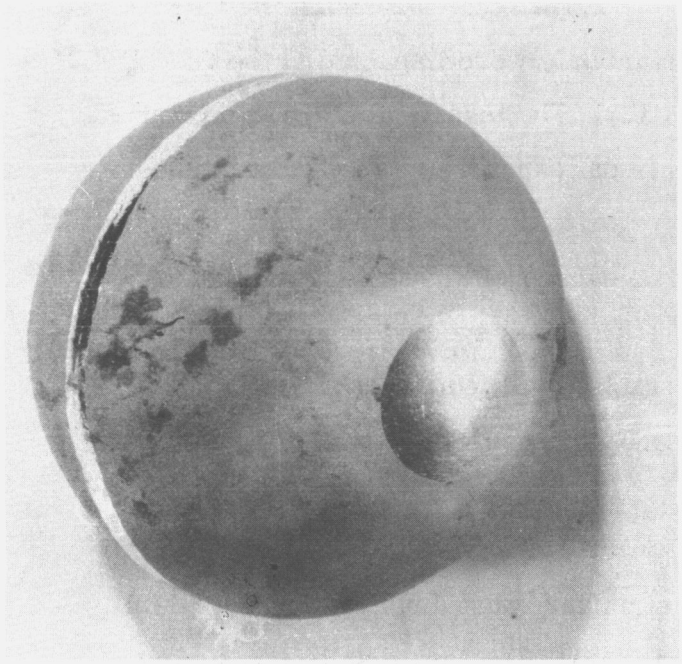

MHT 100 TOP VIEW

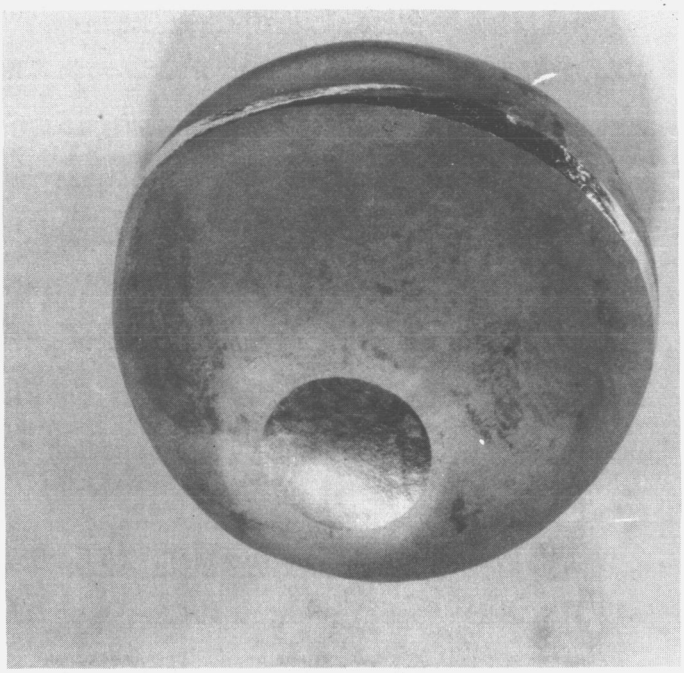

MHT 100 IMPACT FACE

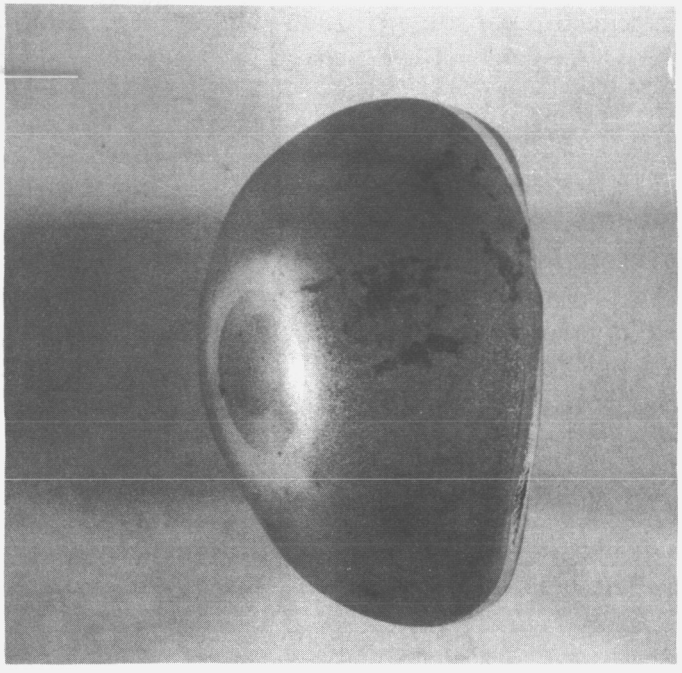

MHT 100 SIDE VIEW

Figure 5-14. FSA MHT-100

5.1.4.2.1.1.2 MHT-101 and MHT-102. Two FSAs, MHT-101 and -102, using the ORNL-ML/MRC WGD-doped iridium PICS, with ThO_2 fuel simulant, were impacted in the GE-SD test facility during April 1976 (see Figure 5-15 and 5-16). The test results are summarized in Table 5-9. These specimens received the usual thermal exposure of one hour at 1500°C for cleanup, followed by the 18-hour soak at 1500°c, prior to closure welding. As is usual with simulant-filled specimens, these units received no subsequent heat treatment beyond the heat-up to the impact temperature of 1370°C (2500°F). Both specimens survived the impacts without detectable failures of any kind. No cracks were found either by visual examination at 70X or by Zyglo inspection. No evidence of fingerprinting was found.

5.1.4.2.1.1.3 MHT-103 and MHT-104. Two FSAs, MHT-103 and 104, using the ORNL-ML/MRC HD (doped) iridium PICSs, with ThO_2 fuel simulant, were impacted in the GE-SD test facility during August 1976 (see Figures 5-17 and 5-18). The test results are summarized in Table 5-9. These specimens received the usual thermal exposure of one hour at 1500°C for cleanup,followed by the 18-hour soak at 1500°C,prior to closure welding. As is usual with simulant-filled specimens, these units received no subsequent heat treatment beyond the heat-up to the impact temperature of 1370°C (2500°F). Both specimens failed in impact:

1. MHT-103 ruptured in the weld exposing the ThO_2. This is the first weld failure on impact observed since the first tests on ORNL-ML/MRC Ir in 1973. No cracks or other failures were observed at any other point in this specimen.

2. MHT-104 exhibited severe fingerprinting on the primary impact surface. A secondary impact ~ 90° from the initial impact, apparently forced the fingerprint to rupture catastrophically, dumping most of the ThO_2 fuel simulant. The weld ruptured in the maximum stress region and extended into the impact face (see 1. above).

The Ir from both specimens has been sent to ML/MRC for further examination.

5.1.4.2.1.1.4 MHT-105 and MHT-106. Two FSAs, MHT-105 and MHT-106, using the ORNL-ML/MRC HD (doped) iridium PICS with ThO_2 fuel simulant, were impacted at the GE-SD impact test facility, during October 1976 (see Figures 5-19 and 5-20). These specimens

MHT 101 TOP VIEW

MHT 101 BOTTOM VIEW

MHT 101 SIDE VIEW

Figure 5-15. FSA MHT-101

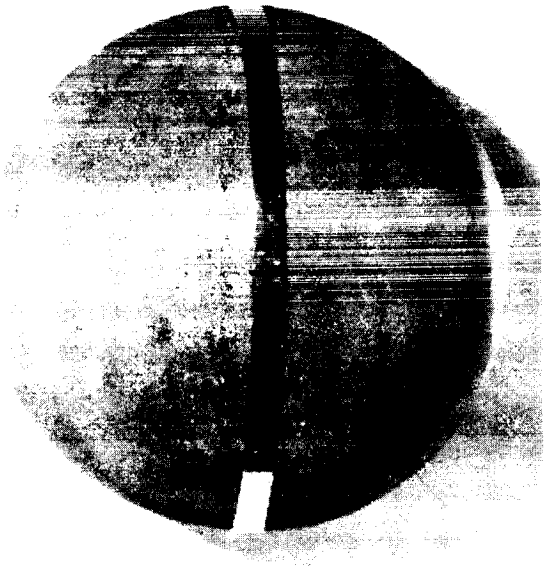

MHW 102 TOP VIEW

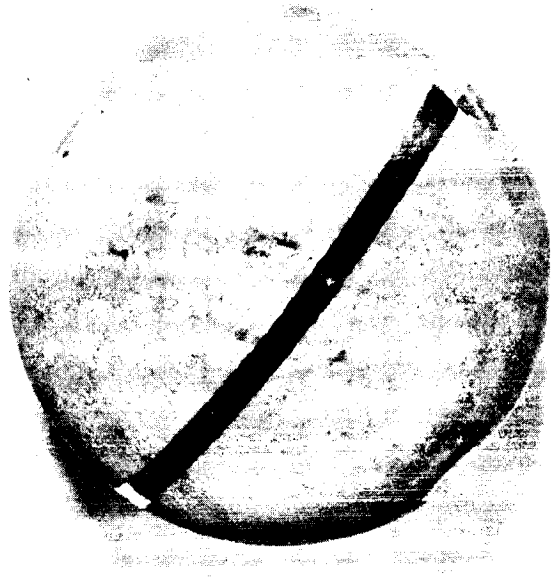

MHT 102 BOTTOM VIEW

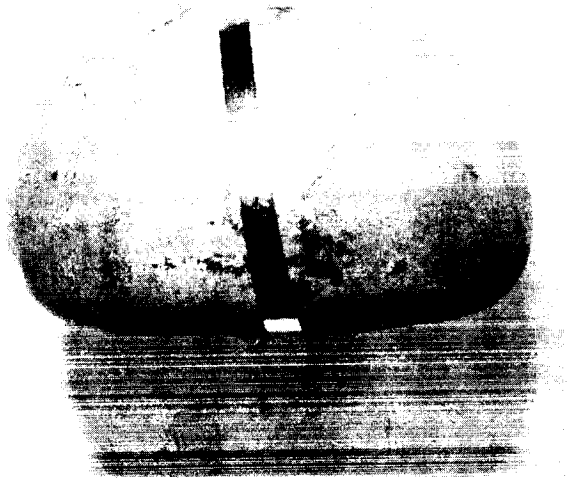

MHT 102 SIDE VIEW

Figure 5-16. FSA MHT-102

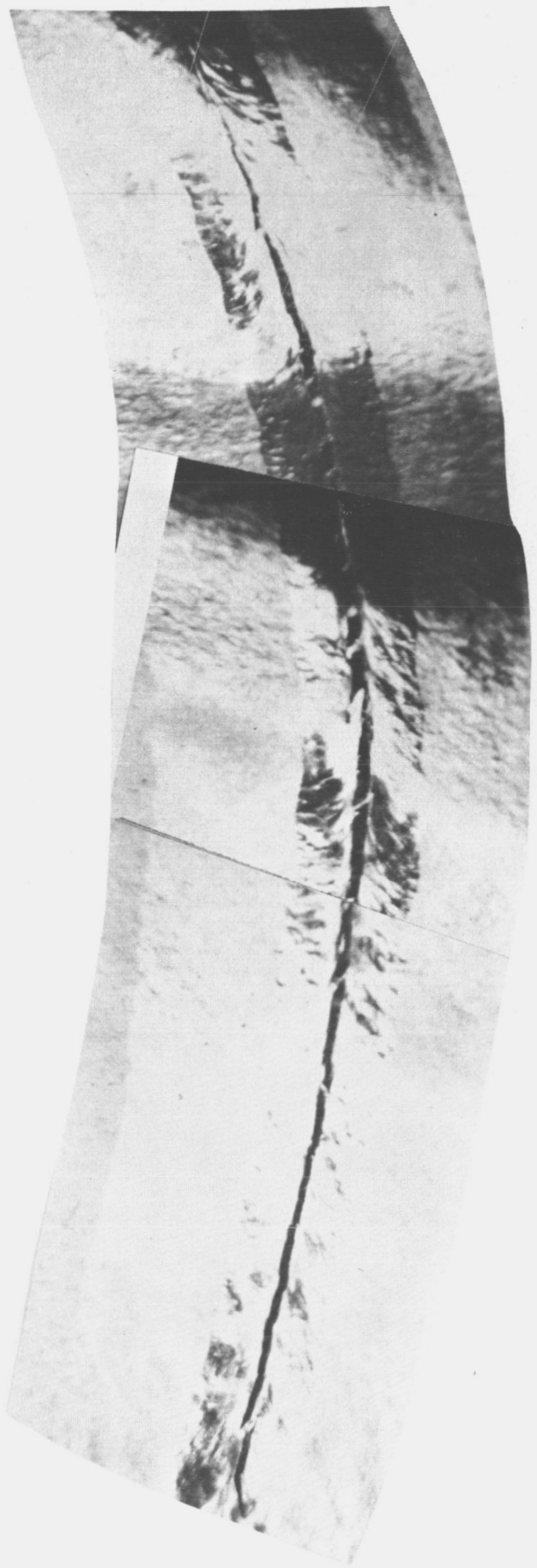

MHT 103 ENLARGED VIEW OF WELD
RUPTUER 70X

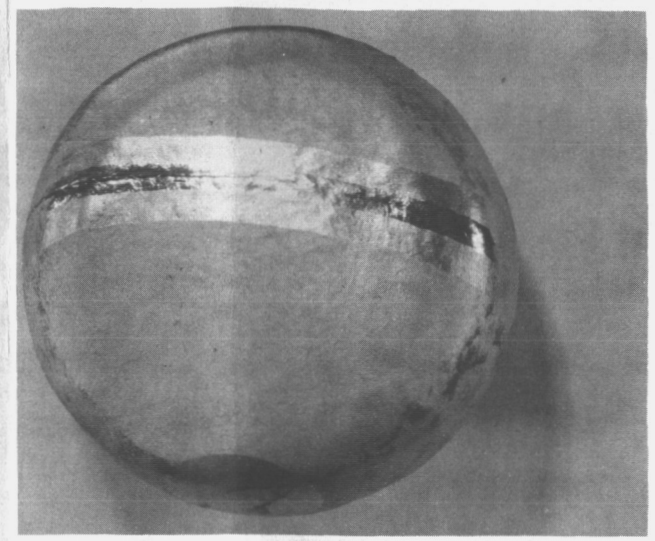

MHT 103 BOTTOM VIEW

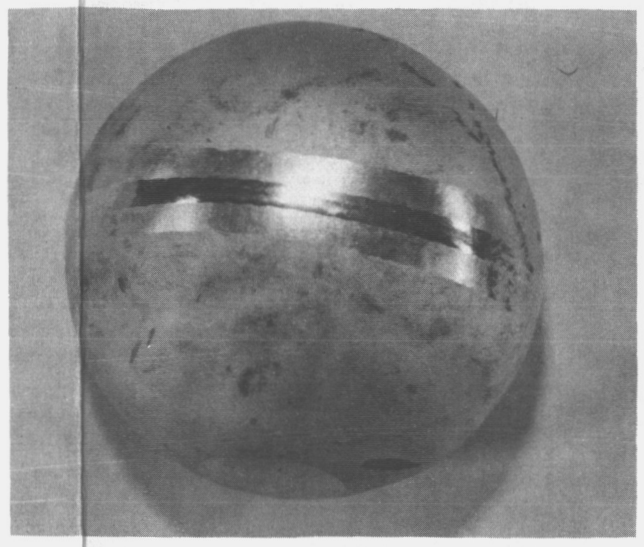

MHT 103 TOP VIEW

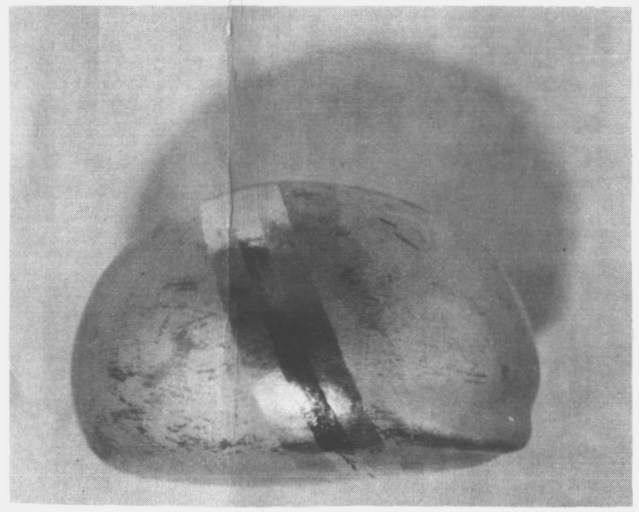

MHT 103 SIDE VIEW

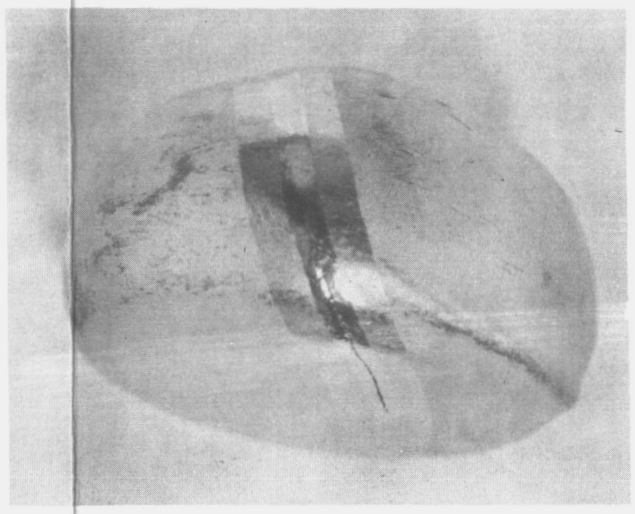

MHT 103 SIDE VIEW SHOWING WELD
RUPTURE

Figure 5-17. FSA MHT-103

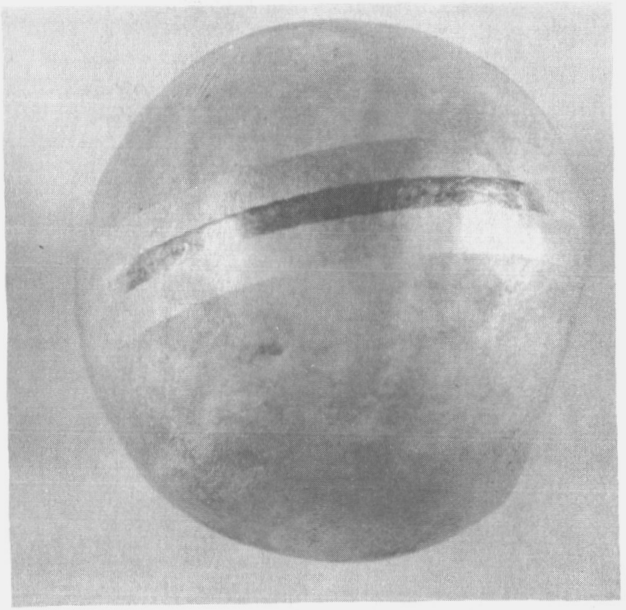

MHW 104 TOP VIEW

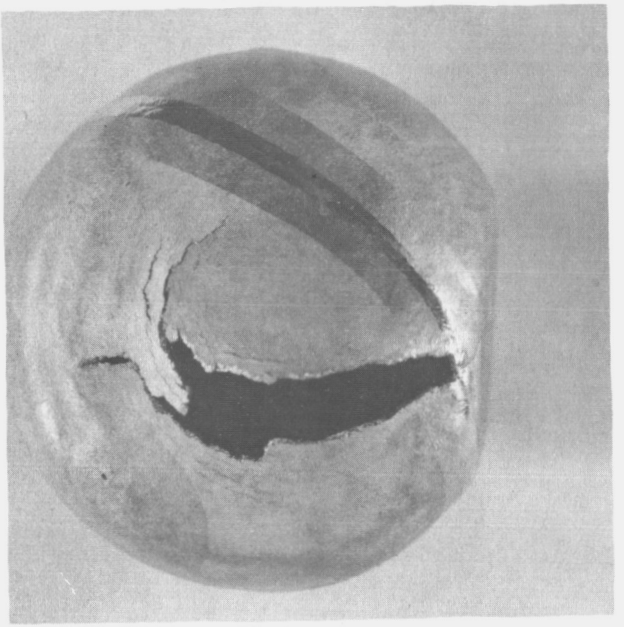

MHT 104 BOTTOM VIEW

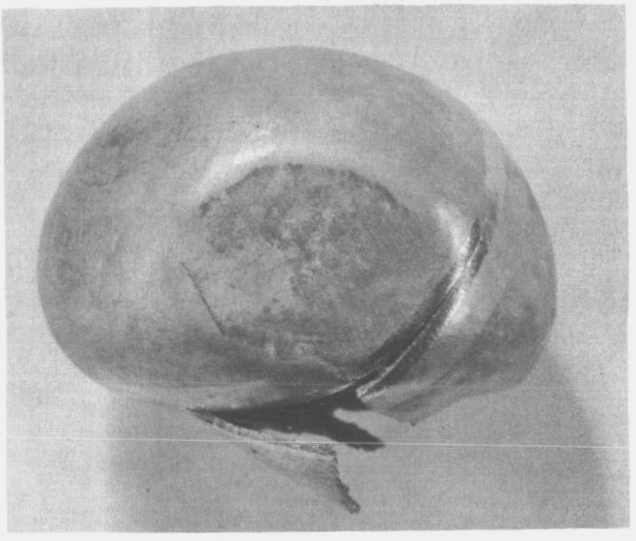

MHT 104 SIDE VIEW NO. 1

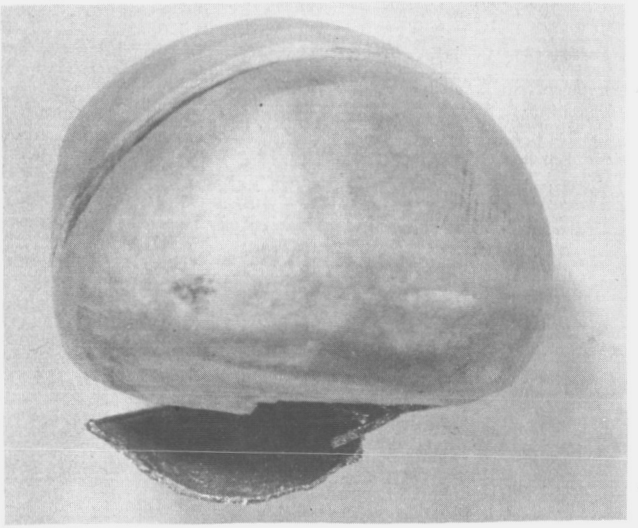

MHW 104 SIDE VIEW NO. 2

Figure 5-18. FSA MHT-104

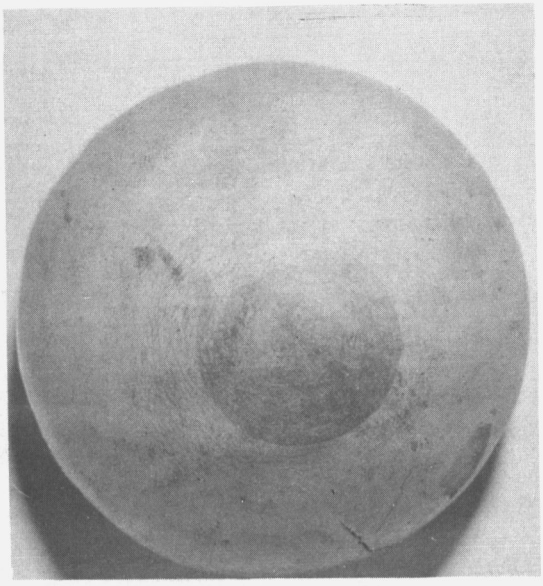

MHT 105 TOP VIEW

MHT 105 BOTTOM VIEW

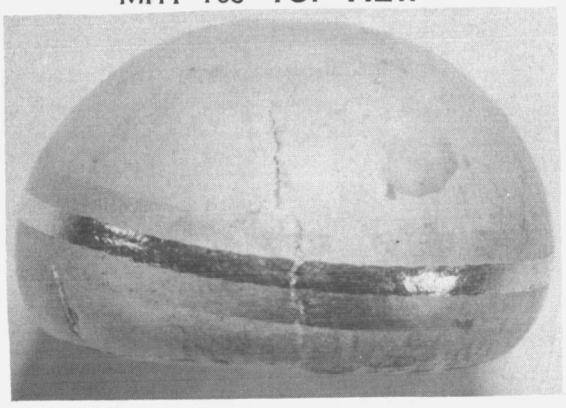

MHT 105 SIDE VIEW
BREACH NO. 1

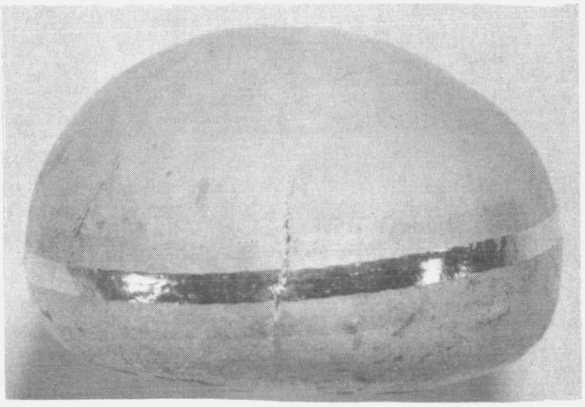

MHW 105 SIDE VIEW
BREACH NO. 2

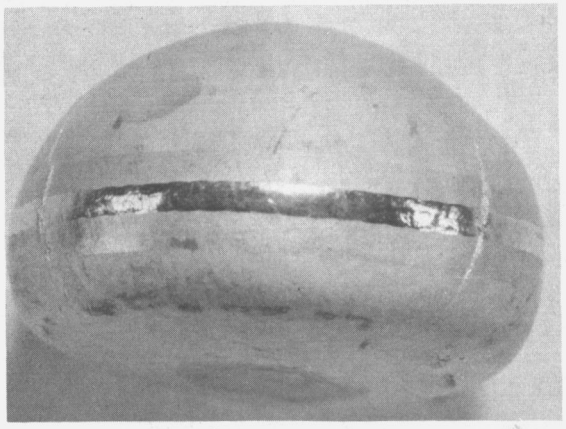

MHT 105 SIDE VIEW
BREACH NO. 2 & NO. 1

MHW 105 GIS REMAINS

Figure 5-19. FSA MHT-105

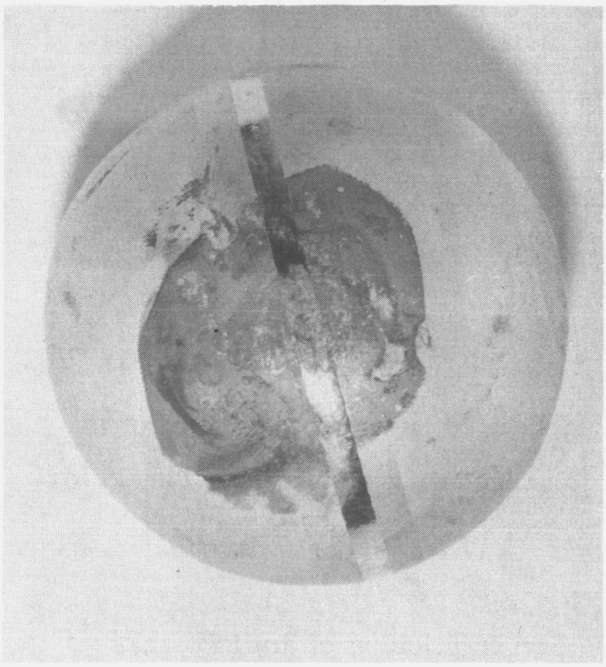

MHT 106 TOP VIEW

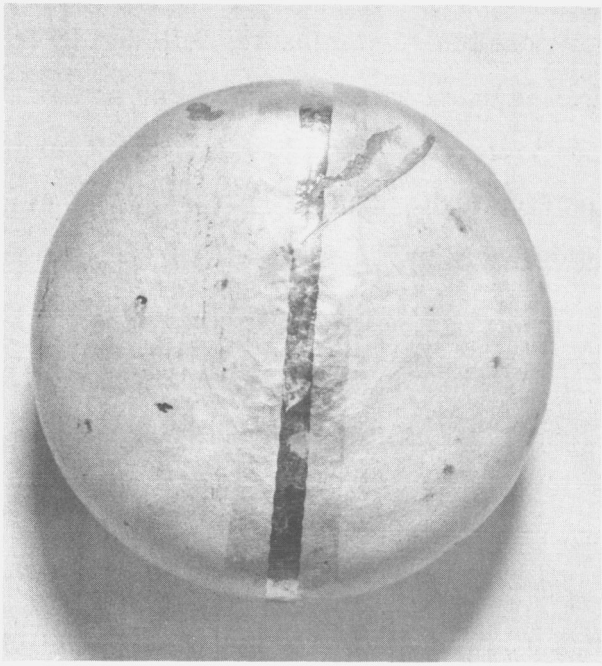

MHT 106 BOTTOM VIEW

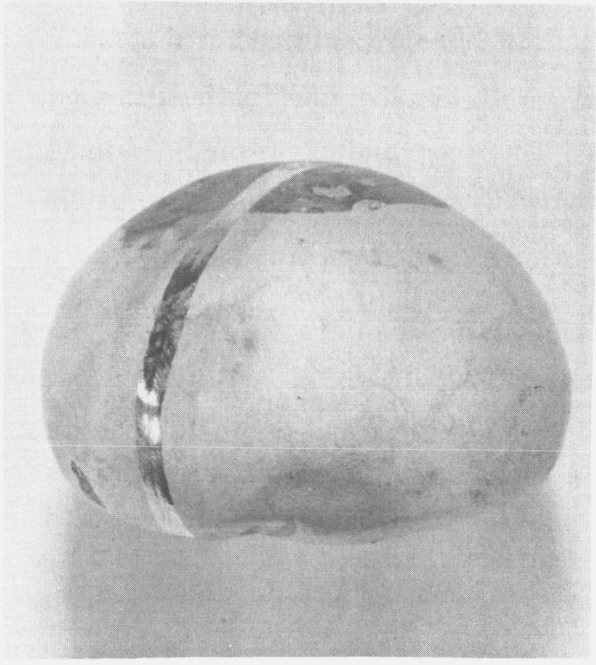

MHT 106 SIDE VIEW

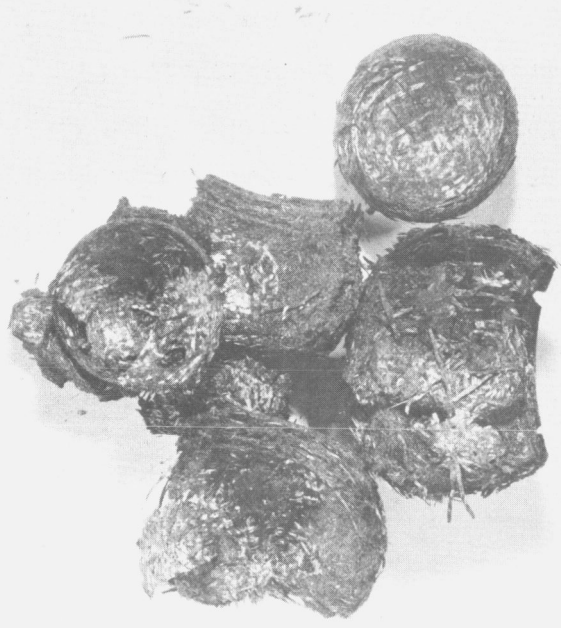

MHT 106 GIS REMAINS

Figure 5-20. FSA MHT-106

received the usual thermal exposure of one hour at 1500°C for cleanup of the iridium oxide and other possible contaminants, followed by the 18 hour soak at 1500°C, prior to closure welding, as is usual with simulant filled specimens; these units received no subsequent heat treatment beyond the heat up to the impact temperature of 1370°C (2500°F). One specimen, MHT-105 failed; the other MHT-106 showed small cracks which did not penetrate the PICs wall (see Table 5-9).

5.1.4.2.2 Impact Testing at LASL

Impact testing of FSAs, containing the standard MHW fuel sphere have been carried out in LASL's Impact Test Facility primarily to provide data for estimating the "Source Term" for the safety analyses (see Section 2).

5.1.4.2.2.1 Preconditioning and Test Conditions. The preconditioning of the FSAs has varied only slightly throughout the impact testing. Unless explicitly noted otherwise, the LASL impact tests used the Ir PICS after a one hour thermal scouring at 1500°C in vacuum, to remove volatile oxides of iridium. The fuel sphere was then welded in place and the PISA was aged thermally for 18 hours at 1500°C, at ML/MRC. The pre-impact exposure time for the FSA at LASL has varied from under one hour to over 2000 hours, at predicted operational temperatures. After completing this aging expsoure at LASL, the thermal regimes immediately prior to the impact have been varied to include a reentry thermal excursion, 5 minutes at ~ 1650°C, and impact at various temperature from 1100°C to 1550°C. A summary of the LASL impact testing is given in Table 5-10, taken from LA-6977-PR, September 1977. Complete data for these tests are contained in the LASL monthly reports.

5.1.4.2.2.2 LASL FSA Impact Test Results. During 1976-77 LASL impacted four FSAs yielding data relevant for the MHW MJS safety analyses.

FSA No.	Impact Date	Type Ir
MHFT-54	20 Feb 76	WG
MHFT-55	22 Jul 76	HD
MHFT-56	23 Jul 76	HD
MHFT-57	10 Mar 77	HD

TABLE 5-10. LASL FUELED MHW IMPACT TEST SUMMARY

Sample No.	Velocity [fps(m/s)]	Temp (°C)	GIS Orientation	Post-impact Dimensions Height [in.(mm)]	Post-impact Dimensions Diam [in.(mm)]	Hoop Strain	Failure Type Hoop	Failure Type Fingerprint	Failure Type Fuel	Iridium Lot
MHFT-2	274 (83.5)	1374	180°	1.22 (30.99)	1.69/1.72 (42.93/43.69)	0.065		No failure		4A, 4A
MHFT-3	276 (84.1)	1365	180°	1.05 (26.67)	1.78/1.85 (45.21/46.99)	0.134	x	--	--	5, 5
MHFT-4	279 (85.6)	1375	180°	1.14 (28.96)	1.71/1.75 (43.43/44.45)	0.081	x	x	--	5, 4A
MHFT-12	286 (87.2)	R, 1480[a]	180°	1.19 (30.23)	1.74 (44.20/)	0.088	x	--	--	15B, 13
MHFT-26	247 (75.3)	R, 1550	70°	1.12 (28.45)	1.83/1.85 (46.48/46.99)	0.147	--	x	--	51, 50
MHFT-27	249 (75.9)	R, 1550	180°	1.46 (37.08)	1.66/1.68 (42.16/42.67)	0.043	--	--	x	--
MHFT-29	253 (77.1)	1093	180°	1.18 (29.97)	1.67/1.72 (42.42/43.69)	0.059	x	x	x	51, 51
MHFT-30	250 (76.2)	R, 1550	180°	1.21 (30.73)	1.65/1.68 (41.91/42.67)	0.045	--	x	--	51, 52
MHFT-31	243 (74.1)	R, 1550	180°	1.23 (31.24)	1.64/1.69 (41.66/42.93)	0.039	x	--	x	44, 44
MHFT-32	285 (86.9)	1370	180°	1.18 (29.97)	1.70/1.74 (43.18/44.20)	0.075		No failure		EI-III
MHFT-33	282 (86.0)	1370	180°	1.14 (28.96)	1.69/1.72 (42.93/43.69)	0.066		No failure		EI-III
MHFT-34	284 (86.6)	1375	180°	1.17 (29.72)	1.66/1.72 (42.16/43.69)	0.056		No failure		NC
MHFT-35	281 (85.7)	1375	180°	1.15 (29.21)	1.68/1.73 (42.67/43.94)	0.066	--	x	x	NC
MHFT-36	280 (85.3)	1375	135°	1.17 (29.72)	1.69/1.73 (42.93/43.94)	0.069	--	x	x	NC
MHFT-39	284 (86.6)	R, 1100	180°	1.23 (31.24)	1.67/1.72 (42.42/43.69)	0.061	x	--	x	NC, n
MHFT-40	224 (68.3)	R, 1440	180°	1.25 (31.75)	1.64/1.68 (41.66/42.67)	0.038	--	--	x	NC, n
MHFT-45	279 (85.0)	R, 1440	180°	1.13 (28.70)	1.70/1.77 (43.18/44.96)	0.083	--	x	x	EI-III
MHFT-47	281 (85.7)	R, 1440	180°	1.16 (29.46)	1.66/1.73 (42.16/43.94)	0.073	--	--	x	WE
MHFT-48	285 (86.9)	R, 1440	~ 45°	1.13 (28.70)	1.80/1.83 (45.72/46.48)	0.133	x	x	--	WE
MHFT-49	286 (87.2)	R, 1100	180°	1.24 (31.50)	1.65/1.71 (41.91/43.43)	0.051	x	x	x	WE
MHFT-50	281 (85.7)	R, 1440	~ 80°	1.20 (30.48)	1.76/1.81 (44.70/45.97	0.116	--	x	x	EI-III
MHFT-54	280 (85.3)	R, 1440	180°	1.15 (29.21)	1.74/1.78 (44.20/45.21)	0.100	x	--	x	WG
MHFT-55	285 (86.9)	R, 1440	180°	1.16 (29.46)	1.72/1.77 (43.69/44.96)	0.091	--	--	x	HD
MHFT-56	284 (86.6)	R, 1440	180°	1.18 (29.97)	1.68/1.73 (42.67/43.94)	0.066	x	x	--	HD
MHFT-57	283 (86.3)	R, 1400	180°	1.15 (29.21)	1.73/1.76 (43.94/44.70)	0.091	--	x (?)	--	HD
MHFT-58	281 (85.7)	R, 1440	180°	1.20 (30.48)	1.73/1.73 (43.94/43.94)	0.081		No failure		HD
MHFT-59	283 (86.3)	R, 1440	180°	1.25 (31.75)	1.68/1.69 (42.67/42.93)	0.050		No failure		HD
MHFT-60	282 (86.0)	R, 1440	180°	1.08 (27.43)	1.69/1.73 (42.93/43.94)	0.0675	x	x	--	HD

[a] R = reentry.

5.1.4.2.2.2.1 MHFT-54. A single, live-fueled FSA, identified as MHFT-54, was impacted in the LASL test facility during February 1976. The test results are summarized in Table 5-11. This specimen received the usual thermal exposure of 1 hour at 1500°C, for clean up of the iridium prior to assembly. There was no further additional heat treatment of this specimen prior to its exposure under the simulated MHW MJS operational conditions. At LASL, the exposure time for this specimen was approximately 30 days, prior to impact. The specimen was given a thermal ramp to simulate a reentry thermal pulse and the impact temperature was estimated to be approximately 1400°C. The failures by cracking were not catastrophic.

5.1.4.2.2.2.2 MHFT-55 and MHFT-56. Two FSAs, MHFT-55 and MHFT-56, using the ORNL-ML/MRC HD (doped) iridium PICSs, with live $^{238}PuO_2$ fuel, were impacted in the LASL test facility during July 1976. The test results are summarized in Table 5-11. These specimens received the usual thermal exposure of one hour at 1500°C for removal of iridium oxides, only. Subsequently, these specimens were exposed at LASL for ~ 720 hours (30 days), at 1350°C, nominal Ir/fuel interface temperature. After this soak, they were raised to the reentry temperature of 1650°C, allowed to cool, and impacted at ~ 1440°C.

LASL has examined the Ir from these specimens: MHFT-55 and -56. Both FSAs were defueled. The fuel spheres had deformed plastically. After defueling, the four vents were closed to the helium bubble test, although at least one vent of each FSA had been open prior to the reentry thermal pulse and impact. Metallography showed that the plugging was a combination of three effects: residual iridium in the vent ports, apprently from the drilling operation, deposition of a metallic crust at the vent ports (analyses of similar materials indicated that the crusts were essentially alloys of W and Pu), and deposition of nonmetallic material throughout the vent frits.

With the exception of the push-through in MHFT-55, penetration of neither PICS was confirmed in the metallographic sections examined. These included tensile cracks in the maximum diameter, tensile cracks in heat-affected zones of weld assemblies, and fingerprint cracks.

TABLE 5-11. FSA TEST SUMMARIES - IMPACTED AT LASL

Date and Test Number	Impact Speciment Data: Graphite Impact Shell No. Density = ρ - g-cm^{-3} Thickenss = t_c - inch Type	Impact Speciment Data: Iridium Containment: No. Thickness Heat treatment + date Other; Welded by:	Impact Speciment Data: Sphere Material: Fuel: PuO_2 Simulant: ThO_2 No. ; Dia. ; % TD; Heat treat. ; other	Impact Conditions: Specimen weight total - grams	Impact Conditions: Velocity - fps	Impact Conditions: Energy - ft-lbs	Impact Conditions: Temperature - ^{o}C (^{o}F)	Results/Comments: Pass/Fail Height/Diameter Strain % - D_1-D_o/D_o Impact Angle - degrees from zero degrees
MHFT-54 20 Feb. 76	922470-2 ρ = 1.20 t_c = 0.46	WG-226-1 WG-226-2 H/T 1 hour only @ 1500^{o}C prior to butt weld at ML/MRC + 756 hours @ 1335^{o}C at LASL + reentry 5 min. @ 1850^{o}C	PuO_2 PPS-261 NO H/T except exposure 756 hours @ 1335^{o}C + reentry 5 min @ 1850^{o}C	456.0	279.6		1440^{o}C	Failed: H/D = 1.3/1.76 S = 10% Rotation = 0^{o} Four small ruptures: Fuel push thru on backface, crack at vent on impact face, two in area of maximum stress; fuel deformed plasticly
22 Jul 76 MHFT-55	ρ = 1.20 t_c = 0.46	HD-404-2; HD-404-1 0.025" H/T 1 hour @ 1500^{o}C butt weld by ML + 720 hours @ 1335^{o}C @ LASL	PuO_2: PPS 305 H/T with PICS broken in 3 pieces before impact	455.8	284.9		1440 (2625)	Failed (?) HD = 1.17/1.78 S (%) = 11 Rotation: = 0^{o} One crack penetrated PICS: Fuel exposed;other cracks did not expose fuel.
23 Jul 76 MHFT-56	ρ = 1.20 t_c = 0.46	HD-406-4; HD-406-1 0.025" H/T 1 hour @ 1500^{o}C butt weld by ML + 720 hours @ 1335^{o}C @ LASL	PuO_2: PPS 306 H/T with PICS broken in 2 pieces before impact	454.6	284.2		1440 (2625)	Passed (?) H/D = S (%) = 7 Rotation: = 0^{o} Fingerprint cracks on impact face cracks near vents, however no penetration seen in metallography
10 Mar 77 MHFT-57	934387-1 ρ = 1.20 t_c = 0.46	HD-410-4 HD-411-1 H/T 1 hour @ 1500^{o}C before butt weld by ML/MRC + 4045 hours @ 1335^{o}C at LASL + 5 min reentry @1680^{o}C	PuO_2 PPS 332 H/T with PICS, broken prior to impact	4557	283		1400 (2552)	Pass (?) H/D = 1.15/1.76 S % = 9.1 GIS rotation: $\pm$ 0^{o} Fingerprint pattern on impact face; no hoop strain cracks observed. Penetration of wall by cracks is doubtful.

Grain growth appeared to have taken place in the iridium to the extent that MHFT-56 had 2 to 5 grains across the wall, opposed to the 20 to 25 expected. MHFT-55 had equally large grains, near the inside of the shell, but appeared to have irregular remnants of the original structure near the outside, giving it a greater grain count across the wall, varying from 3 to 12.

Hardness of the iridium were not different from those of previously examined containment shells.

5.1.4.2.2.2.3 MHFT-57. A single, live-fueled FSA, identified as MHFT-57, was impacted in the LASL test facility during March 1977. The test resuts are summarized in Table 5-11. This specimen received the usual thermal exposure of 1 hour at 1500°C, for clean up of the iridium prior to assembly. There was no further additional heat treatment of this specimen prior to its exposure under the simulated MHW MJS operational conditions. At LASL, the exposure time for this specimen was approximately 170 days, 4095 hours, prior to impact. The specimen was given a thermal ramp to simulate a reentry thermal pulse and the impact temperature was estimated to be approximately 1400°C. The failures by cracking were not catastrophic.

5.1.4.3 Impact Behavior of Iridium

5.1.4.3.1 Change to Thorium-Doped Ir

The change to thorium-doped iridium made by ORNL, and fabricated into hemispheres by ML/MRC, occured in the later part of the MHW-MJS program. LASL has conducted a series of biaxial strain rate tests on both undoped and Th-doped materials. Figure 5-21 shows the behavior of the materials in specimen tests. Note that the letter 'D' appearing in the material designation indicates the 'doped' iridium.

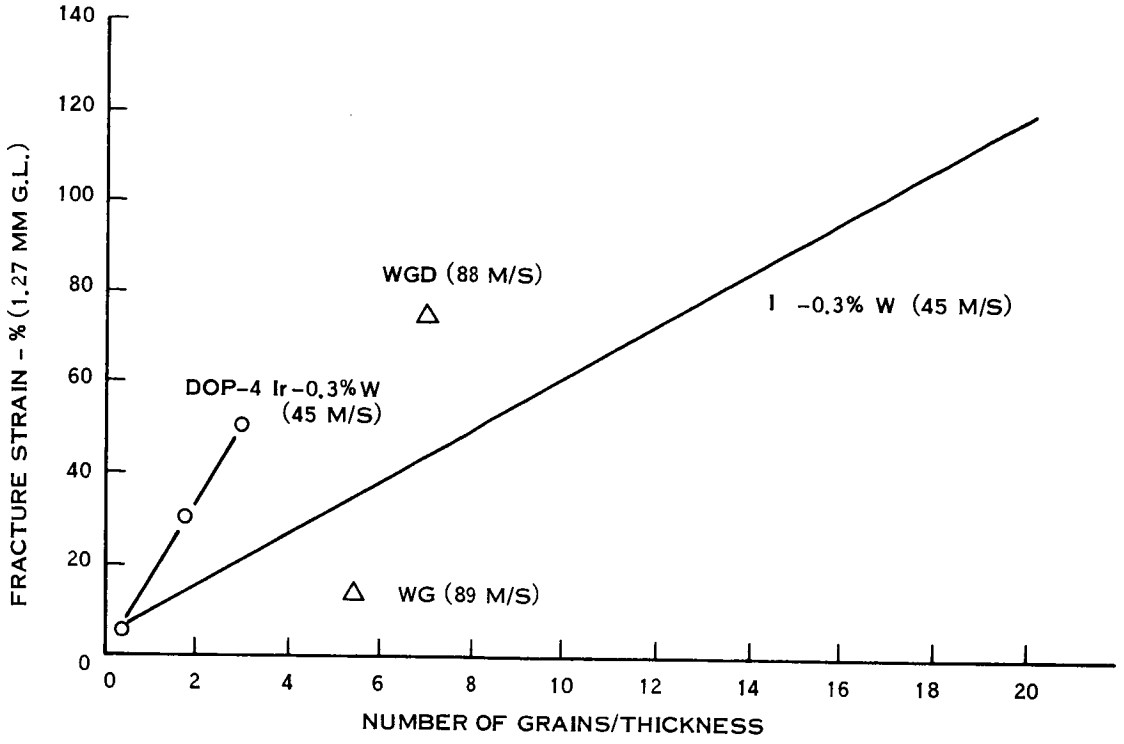

Figure 5-21. Fracture Strain vs. Number of Grains/Thickness for Biaxial Punch Tests Comparing Previous Data for 45 m/s Indirect Velcoity to Two Tests at ~89 m/s (from LASL CMB-2284)

5.1.4.3.2 Behavioral Differences of Doped and Undoped Ir

A series of successful impacts with ThO_2 simulant at GE-SD with doped Ir indicated an apparent improvement in behavior correlated with the presence of Th in the Ir.

LASL reported the results of continuing studies of the MJS iridium used in the simulant and live fuel impacts. The DOP-4 iridium specimens numbered MHT-90, -91, -92 were examined using Auger electron spectroscopy. The surfaces of the grains, examined after a fresh break under controlled conditions in vacuum, showed the presence of 3-5 percent Th on the grain surfaces. No significant segregation of this material was detected. In this examination no phosphorous was found in the grain boundaries. This was noted because most of the previous experiments had detected phosphorus in the simulant impacts. The source of the phosphorous is still unknown but a test of originally clean WE type iridium exposed to a Graphite Impact Shell (GIS) showed no pickup from the graphite.

The total deformation in the PICS, as determined by the diametral and height strains, varied considerably. These deformations depend primarily upon the angle of impact rather than the type of iridium. All fractures in the WG iridium PICS were intergranular. The grain structures of all the iridium PICS were quite uniform, unlike the fueled PICS tested in the LASL SST and SVT impact series. The number of grains across the PICS thickness varied from 6 to 9 for the WG series and 11 to 14 for the WGD series. The smallest grain size in the WG series (9 grains/thickness for MHT-97) was achieved with a 1 h heat treatment of 1500°C instead of the 18 h received by all other PICS. The grain structures in the doped Ir series were also very uniform.

The results of Auger Electron Spectroscopy (AES) analysis of the grain boundary chemistry of this impact series have been reported. The WG series contained 5 to 9% P on the grain boundaries whereas the doped series contained 2 to 4% P and 3 to 5% Th (see Table 5-12).

To summarize, the doped iridium PICS contained less P in the grain boundaries, more Th, and were smaller grained than WG PICS. It is beleived that all of these factors result in better impact resistance and help to explain why the WG PICS failed and the doped PICS survived the FSA simulant impacts.

5.1.4.3.3 Effects of Impurities in Ir

The iridium from MHT-103 and 104 and from MHFT-55 and 56 was examined by LASL to determine if any significant correlation could be established between the behavior of these materials and the impurity content found by various analytical techniques. The results of these analyses were inconclusive,in that in some cases phosohorous has been observed on the inside of the PICS,uniformly distributed through the PICS wall,and in some cases only on the outside of the PICS. Some differences were also noted in the distribution of thoria across the PICS wall. No satisfactory correlation was made of the impurity content versus the iridium behavior. The one significant point that remains unchanged is that the presence of thoria in the grain boundaries at levels of 2-10% does signficiantly enhance the capability of iridium to withstand high velocity impact. The effect,if any, of phosphorous on this behavior is not demonstratable. Phosphorous was not found in the Ir blanks as fabricated by ORNL.

TABLE 5-12. SUMMARY OF FSA IMPACTED RESULTS INCLUDING INTENSITY RATIOS FROM AUGER ELECTRON SPECTROSCOPY

Specimen	Type of Ir	Type of Specimen	Heat Treatment	Impact Results	Diametral Strain	Grain Size # Grains/ Thickness	Intensity Ratios			
							Th_{65}/Ir_{229}	P_{120}/Ir_{229}	C_{270}/Ir_{229}	O_{510}/Ir_{229}
MHT-58	WC	Simulant FSA	Th at 1600°C + 18h at 1500°C with ThO_2	Failed	6.8	4.5	0	1.20	0	0
MHT-60	WC			Failed	6.8	4.5	0	0.17	0.04	1.5
MHT-93	WG		19h at 1500°C	Failed	6.9	6-7	0	0.97	0	0
MHT-94	WG			Failed	Could not measure	7	0	0.94	0.41	0.35
MHT-95	WG			Failed	13.9	8	0	0.74	0	0.08
MHT-97	WG		1h at 1500°C	Failed	14.8	9	0	0.73	0	0.09
MHT-45	EI-III		1h at 1500°C + 18h at 1500°C with ThO_2	Passed	6.8	6	0.25	0.36	0	0
MHT-90	DOP-4		19h at 1500°C	Passed	10.2	10-12	0.75	0.04	0.10	0
MHT-91	DOP-4			Passed	9.7	10-12	0.74	0	0.11	0.19
MHT-92	DOP-4			Passed	11.1	10-12	0.71	0	0	0
MHT-99	WGD			Passed	7.1	12	0.78	0.25	0.11	0.19
MHT-100	WGD			Passed	10.6	11	0.81	0.19	0.17	0.42
MHT-101	WGD			Passed	7.5	14	0.74	0.22	0.07	0.10
MHT-102	HD			Passed	8.2	14	0.76	0.47	0.08	0
MHFT-40	WC	Fueled FSA	2000h - 1214°C* with PuO_2	Failed	3.8	1-2	0	0	0	0.28
MHFT-47	WE		720h - 1214°C with PuO_2	Failed	7.3	1-3	0	0	0	0.20
MHFT-55	HD		777h - 1214°C with PuO_2	Failed	9.1	4.5	0.32	0.03	0.10	0.60
MHFT-55	HD			Fracture but no breech	6.5	2.5	0.26	0.11	0.25	0.5

5.1.4.3.4 Sources of Impurities in Ir

There has been some concern with respect to the possible pickup of phosphorous from either the thoria simulant or from the GIS. LASL investigated this possibility by exposing samples of iridium with known thoria and phosphorous content both to typical thoria simulant spheres and to typical GIS material. No determinable contamination found in the simulant FSAs came from either the thoria simulant or the GIS. The LASL data showed little likelihood of any pickup of phosphorous into the iridium from either the thoria simulant material or from the typical GIS material. (The detailed results of these tests are presented in the LASL monthly reports.) Because of some questions regarding the previous LASL tests, on the depletion of thorium from the grain boundaries, four additional tests were performed. These tests showed conclusively, that phorphorous was not picked up from either the GIS or the thoria simulant. The tests also demonstrated that depletion of thorium from the grain boundaries, when the iridium is in contact with ThO_2 (thoria), does not occur after an exposure for 72 hours at 1500°C. These tests confirmed the results of the previous LASL experiments.

5.2 THE MJS ISOTOPE HEAT SOURCE ASSEMBLY, IHS

5.2.1 THE MHW-MJS-IHS

5.2.1.1 Differences Between the LES and the MJS IHS

The differences between the MHW-LES-IHS and the MHW-MJS-IHS designs were discussed in GEMS 428 (Ref. 1, p. 5-93). The MJS IHS System differs from the LES 8/9 configuration in the following areas:

- The iridium clad has been eliminated.
- A separate IHS gas management system is not used, thus eliminating the PMD/PRD.
- The aeroshell to end cap joints have been changed from threaded graphite joints to a locking ring arrangement.
- The laminated end crush-up spring assemblies have been reduced in diameter to fit within the re-designed end caps.
- The ablation sleeve material has been changed to Pyrocarb 406, tabs have been added to secure the sleeve to the aeroshell and the thickness has been increased to 0.13".

- The IHS and converter case share a common environment, thus the slight helium pressure maintained within the LES IHS by the flow characteristics of the PMD, to enhance thermal exchange, has been eliminated.
- IHS handling is effected by use of a threaded bore in the forward end cap, which replaces the lifting lugs previously used on the LES 8/9 outer clad.
- To provide compatibility with the Storage Protection Container (SPC), a metal shroud was designed by ML/MRC. This Environmental Protection Container (EPC) contains a gas management valve, and essentially provides protection previously afforded by the iridium clad on the LES 8/9 system during the loading of the IHS into the SPC.

A cut-away view of the Heat Source is shown on Figure 5-1.

5.2.1.2 Significant Events Involving the MJS IHSs

Seven flight IHSs, F-6/IHS through F-12/IHS, were fabricated, integrated with converters, tested, stored at ML/MRC, and shipped to KSC during 1976-77. A single qualification unit Q-2/IHS was fabricated, rebuilt as Q-2R/IHS tested and finally disassembled during this same period.

Some of the significant events involving these IHSs are discussed in succeeding paragraphs and include:

- History of the Q-2 and Q-2R/IHS
- Loss of preload problems
- Consequences of loss of preload
- Rebuilding of F-9/IHS

5.2.2 HISTORY OF THE QUALIFICATION HEAT SOURCE - Q-2 IHS

5.2.2.1 Background

The Q-1/IHS used for the qualification tests of the Q-1 RTG on the LES program was disassembled at ML/MRC (see Ref. 1). The middle and bottom (aft) 8-packs were placed in storage; the top (forward) 8-pack was disassembled. Four FSAs of the flight design and two FSAs

of the preflight design were removed from the top 8-pack for analyses. The Q-1/IHS Ir outer clad and the aeroshell with its end caps was sent to GE-SD for examination, analyses and evaluation. Substantially no radioactive contamination was found on these components.

The Q-2/IHS was assembled in August of 1975. Three major anomalies occurred to this IHS which are breifly discussed in the succeeding paragraphs:

- Non-radioactive contamination of the middle 8-pack.
- Fracture of the aeroshell end caps.
- Destructive effects of the original MJS qualification vibration levels.

The Q-2R IHS was disassembled in February 1977 and its FSAs and internal structures were examined.

5.2.2.2 Assembly of the Q-2 IHS

The emissivity sleeve, aeroshell and end caps were redesigned for MHW-MJS (see Ref. 1, GEMS-428 pp. 5-31 thru 5-93). These new components were baked-out prior to use in the Q-2 IHS. The assembly of the Q-2 IHS was performed by ML/MRC in early August 1975. In addition to the new reentry hardware, the Q-2 IHS included the middle and bottom (aft) 8-packs from Q-1 IHS which contained 16 FSAs whose PISAs used the preflight vent filter design (see Figure 5-1). The top eight pack was rebuilt completely. New graphite/carbon parts included: the tie bolt, sphere lock, compliance pads and retaining rings. The FSAs included two units MHF-5 and MHF-21, removed from the Q-1 IHS, and six new FSAs from the LM/MRC production line: MHF-64, -161, -162, -164, -165, and -166. A new aft spring assembly was used for the bottom (aft) eight-pack.

5.2.2.3 Radioactive Contamination Levels in the Q-2 IHS

The levels of radioactive contamination, determined by wipe on the FSAs of the Q-2 IHS as assembled in August 1975 are given in Table 5-13.

TABLE 5-13. RADIOLOGICAL CONTAMINATION DATA Q-2 IHS

	FSA Number MHF	Source of Ir	^{238}Pu Activity DPM	
Top 8-Pack (made new)	21 (old)	EI-2	10	
	64 (new)	HNL	8	Tray - New
	15 (old)	EI-2	10	
	161 (new)	HNL	24	
	162 (new)	HNL	12	
	165 (new)	HNL	22	
	166 (new)	HNL	10	
	164 (new)	HNL	24	120
Middle 8-Pack (from Q-1/ IHS)	22 (old)	EI-2	6	
	5 (old)	EI-2	8	
	17 (old)	EI-3	8	
	9 (old)	EI-2	2	Tray - 0 DPM
	4 (old)	EI-2	16	
	16 (old)	EI-2	14	
	11 (old)	EI-2	4	
	23 (old)	EI-2	0	58
Bottom 8-Pack (all FSA's from Q-1/ IHS)	26 (old)	EI-3	12	
	24 (old)	EI-2	12	
	18 (old)	EI-3	0	Tray - 2 DPM
	8 (old)	EI-2	10	
	3 (old)	EI-2	6	
	10 (old)	EI-2	12	
	12 (old)	EI-2	2	
	7 (old)	EI-2	10	54
				232

5.2.2.4 Non-Radioactive Contamination of the Q-2 IHS Middle 8-Pack

As noted in Para. 5.2.2.1, the middle and bottom 8-packs were placed in stainless steel containers, sealed, and placed in an agitated water bath to maintain low temperatures during storage. The two 8-packs were kept in storage for ~10 months prior to assembly into the Q-2/IHS. When the middle 8-pack was removed from its storage can, a reddish deposit was observed on the outside surface of the retaining ring. Subsequent investigation showed that the stainless steel storage container had been attacked and penetrated at the waterline prob - ably by chloride and dichromate in the cooling water. An unknown amount of water had

leaked into the interior of the container. The quantity of water was sufficient to produce additional attack on the bottom of the container. A detailed discussion of the history, analyses, and conclusions is given in Ref. 3. The contaminated middle 8-pack was already assembled into the Q-2/IHS by the time the contamination problem was identified. The risk of using Q-2/IHS was recognized, but it was decided that schedule and funding considerations precluded disassembly and rebuilding of the IHS. It was recommended that Q-2/IHS be disassembled after the system qualification tests at GE-SD.

One factor, which was not considered at the time, was the presence of water vapor in the contaminated graphite/carbon parts. When the gas sample from Q-2/IHS was analyzed, it was found to contain ~0.1% H_2 and ~0.07% of H_2O, the highest values found in any of the IHS gas analyses. Its presence was readily explained by the H_2O contamination of the middle 8-pack, but the consequences were unexpected.

5.2.2.5 Fracture of the Q-2/IHS End Caps

The Q-2/IHS was assembled at ML/MRC on 6 August 1975 and was shipped to GE-SD in early November 1975. Prior to shipment from ML/MRC, samples of the gas in the EPC were taken on four occasions. The results of these gas analyses are shown in Table 5-14. The Q-2/IHS was stored at GE-SD and on 15 January 1976, the SPC/EPC/IHS was placed in the LAS loadlock.

On 16 January 1976, the lid of the EPC was removed in the LAS loadlock. Visually observable cracks were found in the forward end cap of the Q-2/IHS. It was immediately recognized that a major problem existed and the unit was prepared for shipment back to Mound Laboratory, see Figure 5-22.

5.2.2.5.1 Statement of Q-2/IHS Problem

The discovery of cracks in the Q-2/IHS forward end cap presented at least 3 major questions:

- What caused the Q-2 forward end cap to fail?
- Was the design of the MJS-IHS adequate?

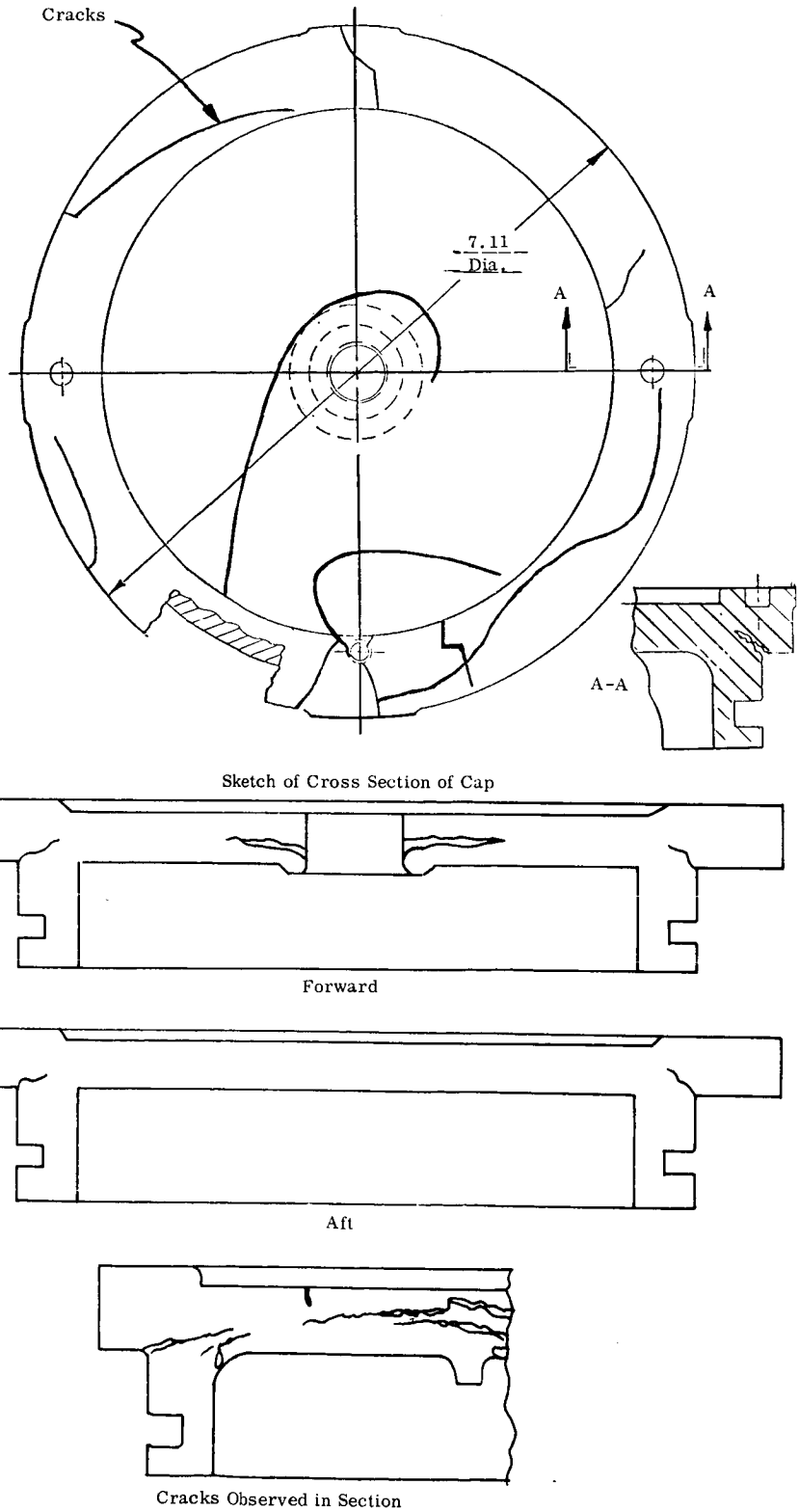

Figure 5-22. Q-2 IHS Forward End Cap
(as seen 16 January 1976)

TABLE 5-14. GAS ANALYSES RESULTS MHW- IHS

CONSTITUENT	VOLUME PERCENT CO	CO_2	H_2	H_2O	N_2	O_2	Ar	He	SAMPLING DATE	ANALYSIS BY:
Q-2/IHS										
Sample No. 1	3.89	5.15	0.85	0.07	0.03	0.01	0.20	89.73	13 Aug. '75	ML/MRC
(a) 1	3.48	0.24	0.76	0.04	0.04	--	--	95.45	13 Aug. '75	ML/MRC
2	3.74	1.73	0.22	0.01	0.10	0.01	0.03	94.18	26 Aug. '75	ML/MRC
(a) 2	0.87	0.15	0.16	0.01	0.16	0.03	0.01	98.62	26 Aug. '75	ML/MRC
3	1.21	0.54	0.10	0.01	0.14	0.02	0.07	97.92	8 Sept. '75	ML/MRC
(a) 3	0.16	0.03	0.08	0.01	0.02	--	--	99.72	8 Sept. '75	ML/MRC
4	0.69	0.28	0.08	0.00	0.26	0.05	0.20	98.47	1 Oct. '75	ML/MRC
(a) 4	0.09	0.01	0.06	0.01	0.05	0.00	--	99.79	1 Oct. '75	ML/MRC
Q-2R/IHS 1	0.10	0.00	0.04	0.00	0.05	0.00	T	99.81	16 Feb. '76	ML/MRC
(a) 1	T	0.00	0.03	0.00	0.03	0.00	0.00	99.93	16 Feb. '76	ML/MRC
F-6 IHS										
Sample No. 1	12.16	10.69	0.10	trace	0.0	0.0	0.0	77.05	21 Nov. '75	ML/MRC
(a) 1	0.93	0.28	0.15	0.0	trace	trace	0.01	98.62	21 Nov. '75	ML/MRC
2	0.61	0.31	0.04	trace	0.6	trace	0.0	98.98	3 Dec. '75	ML/MRC
(a) 2	0.07	0.03	0.03	trace	0.4	trace	0.0	99.87	3 Dec. '75	ML/MRC
3	0.39	0.17	0.04	trace	0.4	0.0	0.0	99.38	17 Dec. '75	ML/MRC
(a) 3	0.03	0.02	0.03	0.0	0.6	trace	0.0	99.86	17 Dec. '75	ML/MRC
4	0.36	0.14	0.03	0.0	0.5	0.0	0.0	99.43	21 Jan. '76	ML/MRC
F-7/IHS										
Sample No. 1	13.26	10.46	0.10	0.0	0.00	T	0.0	76.18	5 Feb. '76	ML/MRC
(a) 1	0.70	0.21	0.16	0.0	0.04	0.0	0.0	98.89	5 Feb. '76	ML/MRC
2	0.52	0.23	0.04	0.0	0.30	0.08	0.0	98.84	23 Feb. '76	ML/MRC
(a) 2	0.21	0.06	0.08	T	0.12	0.04	T	99.57	23 Feb. '76	ML/MRC
F-8/IHS										
Sample No. 1	1.06	0.88	0.06	<0.01	0.22	0.0	0.0	97.79	7 Apr. '76	ML/MRC
(a) 1	0.43	0.17	0.10	<0.01	0.15	0.02	0.0	99.14	7 Apr. '76	ML/MRC

(a) = Backfill with pure He
(1) Q-2/IHS remade as Q-2R/IHS with new aeroshell and end caps

CONSTITUENT	VOLUME PERCENT CO	CO_2	H_2	H_2O	N_2	O_2	Ar	He	SAMPLING DATE	ANALYSIS BY:
F-9/IHS										
Sample No. 1	7.71	12.18	0.06	<0.01	0.0	0.01	0.0	80.25	7 Jun. '76	ML/MRC
(a) 1	0.60	0.24	0.07	<0.01	0.0	0.0	0.0	99.10	7 Jun. '76	ML/MRC
2	5.43	4.80	0.02	<0.01	0.16	0.03	T	89.56	21 Jun. '76	ML/MRC
(a) 2	1.71	0.43	0.04	0.0	0.16	0.0	0.0	97.67	21 Jun. '76	ML/MRC
3	0.00	0.00	0.01	0.02	0.03	0.01	0.42	99.49	7 Oct. '76	ML/MRC
(a) 3	0.04	0.01	T	0.01	0.04	0.02	0.04	99.89	7 Oct. '76	ML/MRC
4	0.00	0.00	0.02	0.00	0.02	T	0.00	99.91	8 Dec. '76	
(a) 4	0.00	0.00	0.02	T	0.01	0.00	0.00	99.96	8 Dec. '76	
F-10/IHS										
Sample No. 1	13.22	10.43	0.09	trace	0.09	0.00	0.00	76.17	5 Aug. 1976	ML/MRC
(a) 1	0.67	0.10	0.10	0.00	0.03	0.00	0.00	99.11	5 Aug. 1976	ML/MRC
1	18.0	16.0	0.10	n/r	<0.2	<0.1	<0.1	>66.0	5 Aug. 1976	LASL
(a) 1	0.8	0.1	<0.1	n/r	<0.1	<0.1	<0.1	>99.0	5 Aug. 1976	LASL
F-11/IHS										
Sample No. 1	13.57	12.62	0.14	0.02	0.16	0.02	0.07	73.42	28 Sep. '76	ML/MRC
1	1.92	0.49	0.20	0.00	0.34	0.02	T	97.05	28 Sep. '76	ML/MRC
F-1R/IHS 1	0.00	0.00	0.03	0.00	0.20	T	0.02	99.75	12 Oct. '76	ML/MRC
(a) 1	0.03	0.00	0.02	0.00	0.05	T	0.00	99.90	12 Oct. '76	
F-12/IHS 1	15.72	12.98	0.09	T	0.00	T	0.00	71.22	7 Dec. '76	ML/MRC
(a) 1	4.32	1.01	0.13	0.00	0.02	T	0.00	94.53	7 Dec. '76	ML/MRC
F-9R/IHS 1	0.87	0.21	0.03	0.00	0.05	0.00	0.00	98.83	19 Jan. '77	ML/MRC
(a) 1	0.09	0.01	0.01	0.00	0.60	0.12	T	99.29	19 Jan. '77	ML/MRC

- Was the existing graphite flight hardware, already assembled and in stock, adequate to meet the MJS mission requirement?

5.2.2.5.2 Investigation of the Q-2 End Cap Anomaly

The investigation of the Q-2/IHS problem was carried out under a plan developed by a Task Force set up by US ERDA/NRA.

5.2.2.5.3 Extent of Q-2/IHS Damage

Disassembly of the Q-2/IHS was done at ML/MRC. The visible cracks in the forward end cap did not appear to be worsened by shipment. The cracks were random, having no clearly defined locus of initiation and ending. A crack at the root of the aft end cap lip was not found until the part was examined at GE-SD, under magnification.

5.2.2.5.4 Possible Causes of Cracking

The possible causes of cracking considered included:

- Lack of preload
- Excessive preload
- Thermal expansion interferences
- Excessive loads in handling
- Deviant handling of materials
- Contamination of the IHS
- EPC pressures
- Stresses induced by machining
- Deviations in assembly
- Defective material in the end caps

5.2.2.5.5 Conditions Affecting Q-2/IHS End Caps

Conditions potentially affecting Q-2/IHS end caps included:

a. The Q-2 IHS middle 8-pack was contaiminated during storage. Analyses by ML/MRC of material taken from the forward end cap surface indicated no significant contamination by the metallic impurities found on the 8-pack assembly. (GE PIR-5727, 28 January 1976)

b. The water vapor absorbed/chemisorbed on the middle 8-pack was not entirely driven off by self-heating before assembly. The initial gas analysis of the Q-2/IHS showed this unit to have the highest levels of H_2 and H_2O of any of the IHSs processed at ML/MRC (see Table 5-14).

c. The final bakeout procedure for the MHW-MJS carbon/graphite materials was not completed until after the assembly of the Q-2/IHS. The aeroshell was baked out, without the bakeout jig used for the flight units, and with the forward end cap out of the cylinder. No difficulties were found in fit-up or final assembly, indicating that no interfering distortion had occurred. (GE-PIR 5728, 29 January 1976).

d. A careful study of the drawing tolerances and actual hardware used for the Q-2/IHS EPC showed that no significant misalignment or hangup of the internal support pads occurred in the handling of the unit.

e. ML/MRC reported that there were no accidentally-induced mechanical shock loads to the IHS and the EPC during assembly and transfer operations to the SPC.

f. Damage by thermal shock to the end caps due to cold gases used for backfill in the gas sampling operations was determined by analysis and experiment to be improbable.

5.2.2.5.6 Interactions Potentially Affecting Q-2/IHS End Caps

Analyses of the interactions among the IHS, the EPC and the SPC showed that the effective preloads used were adequate, if somewhat low. The instrumentation used in shipping showed the maximum shock load was 4 g; this is far less than the qualification test load of 50 g. This review of the thermal and mechanical interactions of the units used for the Q-2/IHS showed that none of the actually existing conditions could have fractured POCO graphite having normal specified properties; the inference was made that the Q-2 POCO end cap material was deficient.

5.2.2.5.7 Review of POCO, Inc. Data

The review of POCO Inc. data included:

a. Some of the data relating to the Q-2/IHS POCO graphite end cap material were reviewed and discussed at a meeting with representatives of POCO Inc. at GE-SD on 13 February 1976 (GE-PIR-5758, 24 February 1976). The end caps used for Q-2/IHS were both taken from a plate designated B-268. This plate was the only one of twelve pieces, made in one run for GE-SD, which was not discarded for failure to meet internal POCO standards. Even this plate had defects identified in the ultrasonic inspection, which were so extensive that one half of the piece was scrapped by POCO. The B-268 plate was bought to the requirements of the LES Program Specification, NS-0060-02-63, which at the time of order, did not require tensile testing. The specimens finally taken from this plate were tested in October 1975. The Q-2/IHS was assemlbed at ML/MRC on 6 August 1975. The room temperature tensile strength was ~ 25% below the specified limit of 8500 psi; one of the high-temperature specimens failed at ~ 1100 psi in the specimen grip area, with the failure clearly initiated by large carbon inclusions.

b. All of the existing data on other POCO material used for aeroshell end caps were reviewed. Those parts accepted for flight hardware, in all cases, met or exceeded the specification requirements of NS-0060-02-89 and showed very close uniformity among the test specimens measured for density, tensile strength, and ultrasonic velocity. This indicated homogeneous, fine-grained, POCO graphite, typical of the AXF-5Q type. Rejected materials, conversely, showed considerable variation of density and tensile properties as well as failure to meet the specification requirements (see Figure 5-23).

5.2.2.5.8 Experimental Analyses on POCO Materials

Experimental analyses and testing were performed on the Q-2/IHS end cap materials and other POCO material. The organizations cooperating in this effort included:

- OR/Y-12
- ML/MRC
- Sandia Laboratories
- POCO, Inc.
- Southern Research Institute
- GE-SD

5.2.2.5.9 Results of the Task Force Investigation

The third Report of the Task Force investigating the Q-2 anomaly was published on 16 April 1976 (Ref. 4). The results of the investigation showed:

- The POCO end cap material had low tensile strength with inclusions, pervasive microcracks, the other microstructural features anomalous for POCO AXF-5Q graphite.
- High levels (>2300 ppm) of metallic impurities, including Fe, V, and Ca, were present in the end caps as carbieds, but converted to oxycarbides/oxides/hydrated oxides when exposed to water vapor at the IHS storage temperatures. The difference in the densities of the carbides and the conversion products, produced swelling of the material (see Table 5-14A).
- High levels of water vapor were present in the Q-2/IHS (demonstrated by the gas analyses) coming from the inadvertently contaminated middle 8-pack (see Table 5-14).
- Swelling of the end caps into interference with the restraint of the aeroshell cylinder resulted in catastrophic fracture of the forward end cap and less extensive fracture of the aft end cap; permanent growth of material from the aft end cap was proven to exceed 0.42 percent by experiments at OR/Y-12, (see Report Y/DA-6793, June 1976).

TABLE 5-14A. Q-2 END CAP FAILURE SEQUENCE

Activity/Operation/Status	Material Response
Mix of POCO starting materials: carbon, binder; impurities in B-268 = 2000 ppm Na, Ca, Fe, V, etc.	Dispersion of carbon particles in binder; Na and Ca probably in binder.
Graphitization @ 2500°C	Formation of graphite + some loss of volatile metals and formation of metal carbides.
Handling, machining, and storage in normal atmosphere: Air + Water Vapor	Graphite chemisorbs O_2 and H_2O; some reaction with metal carbides to form oxycarbides/oxides; potential microcracking
Bakeout of graphite before assembly 24 hours @1500°C.	Chemisorbed oxygen and water vapor removed to low levels; some reversion of oxycrabides/oxides to carbides; potential for additional microcracking.
Exposure to oxygen and water vapor desorbed at 500°C from Q-2 middle 8-pack accidentally contaminated during storage; exposure time about 5 months.	Metal carbides react to form oxycarbides/oxides with increase in volume; end caps try to grow but are constrained by aeroshell; end caps crack.

- analyses were performed on the thermal and mechanical interactions among the IHS, the EPC, and the SPC for the design and as-built tolerances and for the actual conditions of use in the Q-2/IHS assembly, shipping, and handling. These analyses showed that none of the known conditions existing at any point could have exerted stresses large enough to fracture POCO end caps having the normal specified POCO AXF-5Q graphite properties.
- a testing program was initiated to verify that all of the POCO material accepted for use as flight hardware for MHW-MJS will adequately meet the mission requirements. Results from this testing program were reported as they became available. Specimens for this testing program were taken from the tag ends of the POCO plates from which the end caps were machined (see Figures 5-23 and 5-24). This location permitted an evaluation of material which was immediately adjacent to the material from which the end cap was fabricated.

5.2.2.5.10 Results of the Verification Testing Program

The fracture of the aeroshell end caps in the Q-2/IHS raised the question of the acceptability of the end caps already used in the F-6, F-7, and F-8 IHSs. The acceptability for flight of the remaining end cap materials was also in question, and the verification program was begun. The verification test program used specimens taken from the tag ends of the graphite plates from which the end caps were cut. The location of the specimens was as shown in Figure 5-24 and the approximate sizes of the specimens were as shown in Figure 5-25. The verification tests included a repetition of the acceptance tests for:

- tensile strength
- density
- modulus
- sonic velocity
- chemical impurity content and composition
- total ash content
- flaws, both internal and external

All the POCO graphite end cap material, accepted for the MJS flight IHSs to date, satisfied all the specification requirements as shown by the acceptance tests; see Table 5-15. The

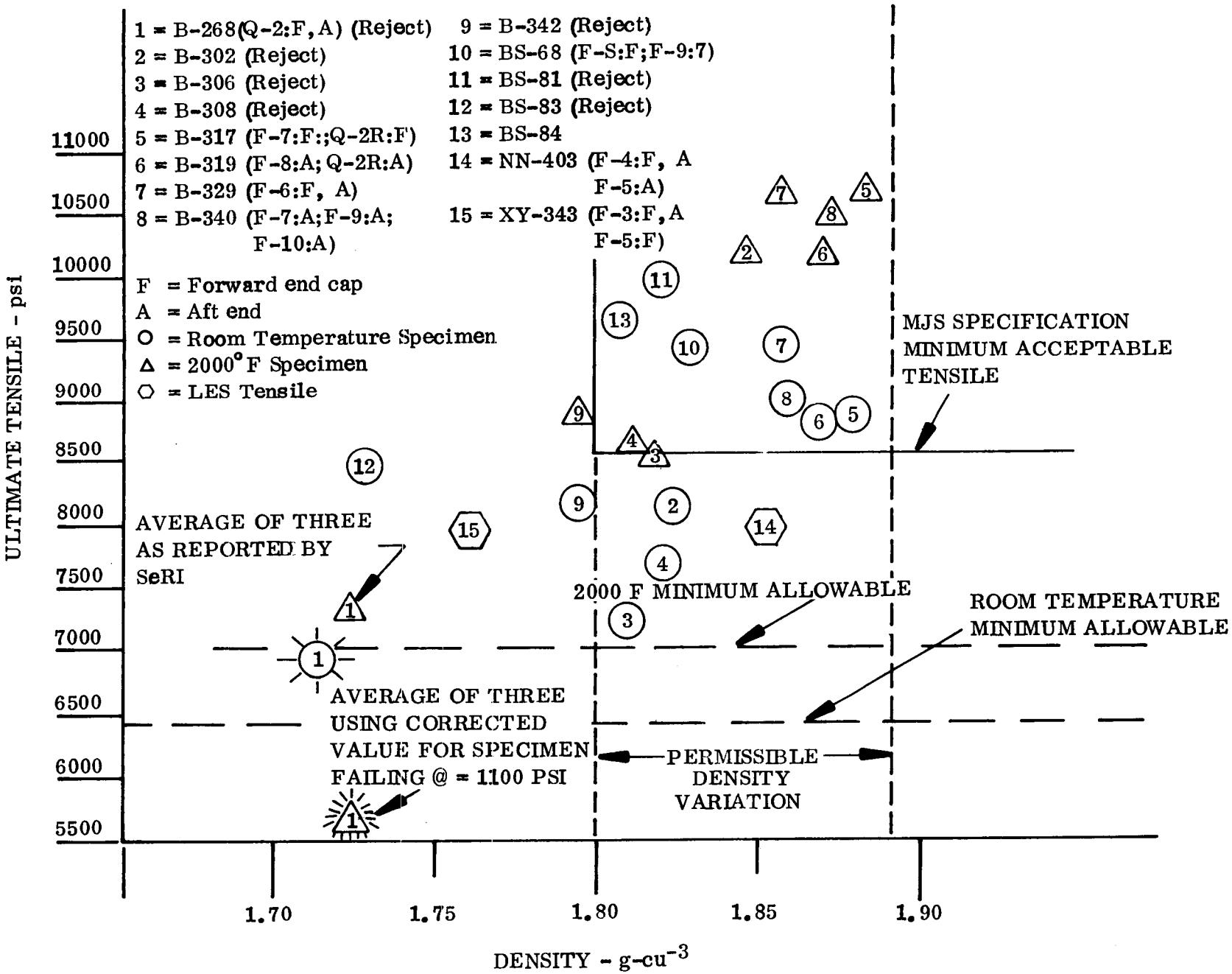

Figure 5-23. Average Tensile versus Average Density - MJS and LES

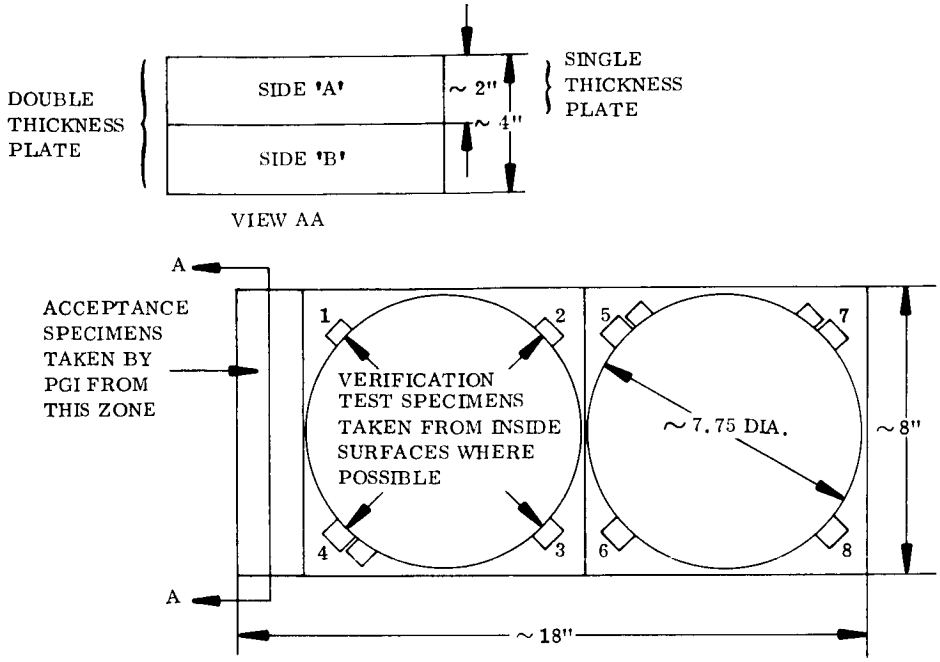

(1) Original dimensions of POCO plate for end caps; plate thickness may be either ~ 2" or ~ 4" and yield 2 or 4 caps.

(2) Not all tag ends are available for every plate; double thickness plates are designated side 'A' and side 'B'.

Figure 5-24. POCO End Cap Test Specimens

specimens for the acceptance tests were taken from the edges of the POCO plates as fabricated and usually from one end only. The data acquired from these specimens were considered representative of the end cap material,on the implicit assumption that the plate material was homogeneous.

The verification testing program produced confirmatory data for the tensile strength, density, chemical impurity, total ash content, and sonic velocity. In addition, data were obtained showing the abundance and distribution of high density particles, the microstructural characteristics, and the extent of permanent dimensional changes occurring when the material was exposed at temperatures simulating those experienced during reentry. Verification test specimens were taken from tag ends of plate material at four points as close as possible to the edges of the blanks from which the end caps were machined. These specimens thus permitted the determination of the degree to which the plates were homogeneous in physical, chemical and mechanical characteristics (see Figures 5-23 and 5-24).

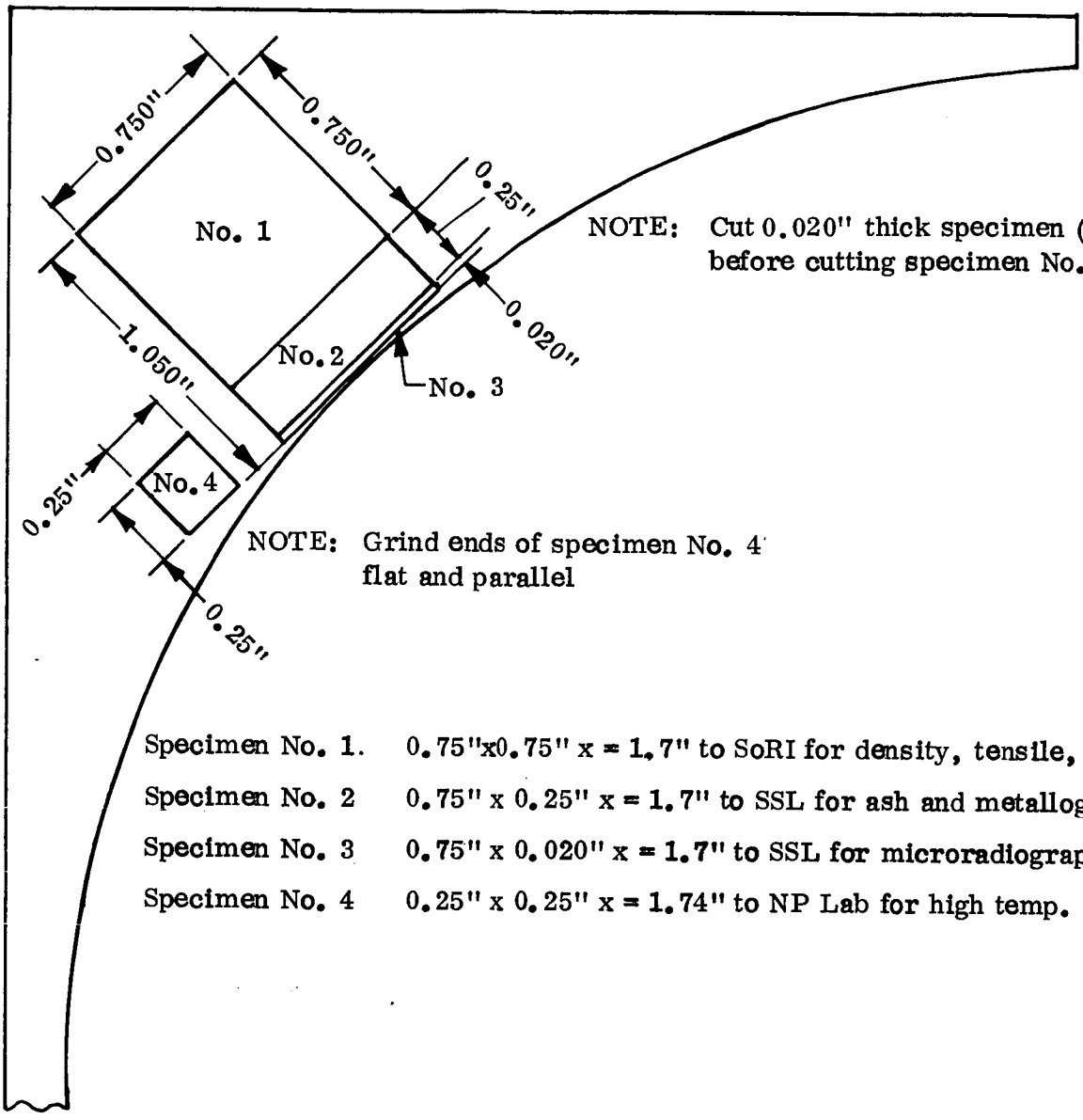

Figure 5-25. Typical Size and Location of Verification Test Specimens

TABLE 5-15. SUMMARY OF ACCEPTANCE AND VERIFICATION TEST RESULTS - POCO GRAPHITE PLATES (AVERAGED VALUES)

POCO Plate Number:		B-317		B-319		B-329		B-340		BS-68	
Application:		FWD. End Caps Only: F-7, Q-2R		Aft End Caps Only: F-8, Q-2R		Fwd. End Cap: F-6 Aft End Cap: F-6		Aft End Caps Only: F-7, F-9 (3), and F-11		Fwd. End Caps Only: F-8 and F-9 (3)	
Type of Test:		Acceptance	Verification	Acceptance	Verification	Acceptance	Verification	Acceptance	Verification	Acceptance	Verification
Characteristic Tested:	Specification Limits										
Tensile Strength - psi @ 20°C (70°F)	≥ 8,500 (min.)	8,770	8,700 (1)	8,730	8,840 (1)	9,310	9,160 (1)	8,830	8,970 (1)	9,360	9,100 (1)
Chemical Impurities - ppa	≤ 1,000 (max.)	=200	=200	≦200	≦200	≦200	≦200	≦200	≦200	≦200	≦700
SH Content -ppa	≤1,000 (max.)	192	225	186	≤350	179	≤400	180	≤400	≤200	≤1800 (2)
Defects Internal and External - dia. inches	0.020	OK	n/a	OK	n/a	OK	n/a	OK	n/a	OK	n/a
Dense Particles - volume fraction	Not req'd	n/a	$<1 = 10^{-6}$	n/a	$<1 \times 10^{-5}$	n/a	$<1 \times 10^{-5}$	n/a	$<1 \times 10^{-5}$	n/a	$<2 \times 10^{-2}$
Permanent Growth at = 1850 C - percent	Not req'd	n/a	<0.01	n/a	≤0.01	n/a	≤0.01	n/a	≤0.01	n/a	≤0.017
Density - Average grams - 3	1.80 - 1.89	1.885	1.881	1.872	1.867	1.830	1.868	1.826	1.834	1.834	1.786

(1) Sub-size, transverse tensile specimen @ 70 F
(2) See PIR-5811 for discussion
(3) In original F-9/IHS; for F-9R/IHS see D066(A) and DK104(F)

TABLE 5-15. SUMMARY OF ACCEPTANCE AND VERIFICATION TEST RESULTS - POCO GRAPHITE PLATES (AVERAGED VALUES) (Cont)

POCO Plate Number:		B-317		B-319		B-329		B-340		BS-68	
Application:		Fwd. End Caps Only: F-7, Q-2R		Aft End Caps Only: F-8, Q-2R		Fwd. End Cap: F-6 Aft End Cap: F-6		Aft End Caps Only: F-7, F-9 (3), and F-1		Fwd. End Caps Only: F-8 and F-9(3)	
Type of Test:		Acceptance	Verification	Acceptance	Verification	Acceptance	Verification	Acceptance	Verification	Acceptance	Verification
Characteristic Tested:	Specification Limits										
Tensile Strength - psi @ 20°F (70°F)	≥ 8,500 (min)	8,770	8,700(1)	8,730	8,840(1)	9,310	9,161(1)	8,830	8,970(1)	9,360	9,100(1)
Chemical Impurities - ppm	≥1,000 (max)	=200	=200	≦200	≦200	≦200	≦200	≦200	≦200	≦200	≦700
Ash Content - ppm	≤1,000 (max)	192	225	186	≦350	179	≦400	180	≦400	≦200	≦1800(2)
Defects: internal and External - dia. inches	0.020	OK	n/a	OK	n/a	OK	n/a	OK	n/a	OK	n/a
Dense Particles - volume fraction	Not req'd	n/a	$< 1 \times 10^{-6}$	n/a	$<1 \times 10^{-5}$	n/a	$< 1 \times 10^{-5}$	n/a	$<1 \times 10^{-5}$	n/a	$<2 \times 10^{-2}$
Permanent Growth at = 1850 C - percent	Not req'd	n/a	≤0.01	n/a	≤0.01	n/a	≤0.01	n/a	≤0.01	n/a	≤0.017
Density - Average grams-cm^{-3}	1.80 - 1.89	1.885	1.881	1.872	1.867	1.857	1.830	1.868	1.826	1.834	1.786

(1) Sub-size, transverse tensile specimen @ 70 F

(2) See PIR-5811 for discussion

(3) In original F-9/IHS; for F-9R/IHS see D066(A) and DK104(F)

TABLE 5-15. SUMMARY OF ACCEPTANCE AND VERIFICATION TEST RESULTS - POCO GRAPHITE PLATES (AVERAGED VALUES) (Cont)

POCO Plate Number:		BS-73		BS-74		BS-76		BS-84	
Application:		Fwd End Cap: F-11		Fwd End Cap: F-12		Aft End Cap: F-12		Fwd. End Cap: F-10 Aft End Cap: F-10	
Type of Test:		Acceptance	Verification	Acceptance	Verification	Acceptance	Verification	Acceptance	Verification
Characteristic Tested:	Specification Limits								
Tensile Strength - psi @20°F (70°F)	≥ 8,500 (min)	9,300	9,370 (1)	9,490	9,530	9,150	8,290	9,550	9,400
Chemical Impurities - ppm	≤ 1,000 (max)	≤ 262	≤ 300	≤263	≤300	≤ 275	≤ 350	170	120
Ash Content - ppm	≤ 1,000 (max)	≤ 200	≤ 350	≤240	≤400	≤ 450	≤ 550	361	406
Defects: Internal and External - dia. inches	0.020	OK	n/a	OK	n/a	OK	n/a	OK	n/a
Dense Particles - volume fraction	Not in spec. 'Std' POCO = 1×10^{-4}	n/a	1×10^{-4}	n/a	$\leq 1 \times 10^{-4}$	n/a	$\leq 1 \times 10^{-4}$	n/a	1×10^{-5}
Permanent Growth at = 1850°C - percent	Not in spec. 'Std' POCO = ~ 0.02	n/a	≤ 0.02	n/a	≤ 0.014	n/a	≤ 0.009	n/a	0.007
Density - Average grams - cm^{-3}	1.80 - 1.89	1.846	1.811	1.845	1.825	1.82	1.760	1.818	1.800

(1) Sub-size, transverse tensile specimen @ 70°F
(2) See PIR-5811 for discussion

TABLE 5-15. SUMMARY OF ACCEPTANCE AND VERIFICATION TEST RESULTS - POCO GRAPHITE PLATES)AVERAGED VALUES (Cont)

POCO Plate Number:		DO 66		DK 104					
Application:		Aft End Cap: F-9R		Fwd. End Cap: F-9R					
Type of Test:		Acceptance	Verification	Acceptance	Verification	Acceptance	Verification	Acceptance	Verification
Characteristic Tested:	Specification Limits								
Tensile Strength - psi @20°C (70°F)	≥ 9,500 (min)	9,890	10,320	9,430	9,700				
Chemical Strength - ppm	≤1,000 (max)	≤ 300	≤ 350	≤ 300	≤ 450				
Ash Content - ppm	≤1,000 (max)	< 550	< 700	< 825	< 900				
Defects: Internal and External - dia. inches	0.020	OK	n/a	OK	n/a				
Dense Particles - volume fraction	Not in spec. 'Std" POCO = 1×10^{-4}	n/a	$\leq 1 \times 10^{-4}$	n/a	$\leq 1 \times 10^{-4}$				
Permanent Growth at = 1850°C percent	Not in spec. 'Std' POCO = ~ 0.02	n/a	≤0.02	n/a	≤ 0.018				
Density - Average grams-cm^{-3}	1.80 - 1.89	1.81	1.811	1.81	1.810				

(1) Sub-size, transverse tensile specimen @ 70°F
(2) See PIR-5811 for discussion

5.2.2.5.11 Data from the Verification Test Program

Verification test data were obtained for POCO plate material used to make the end caps for all the MJS-IHS flight units and for the Q-2R/IHS. The end cap plate materials and the MJS-IHS units in which they were used are shown in Table 5-16. A summary of the verification test data, showing average values, as compared to the average values for comparable parameters, found in the acceptance tests, is given in Table 5-15. The tensile strength and density data from all of the acceptance tests agreed well with all the data acquired in the verification tests. Similarly, the chemical purity data from both sets of tests show generally good agreement. The one exception, POCO plate BS-68, showed relatively low ash content and chemical impurity content in the acceptance tests but was found to have substantially higher levels in the verification tests. These chemical impurity levels were still within the accepted maximum permitted.

5.2.2.5.12 Statistical Analyses of Tensile Strength and Density Data

The tensile strength and density data for the POCO graphite materials used in the end caps from both the acceptance and verification tests have been subjected to statistical analyses. These analyses show that all the accepted end caps materials are members of a well-defined group with narrow limits. The data for these analyses are shown respectively for the acceptance and verification tests in Tables 5-17 and 5-18. Forty-one specimens are included in the analyses. It is a point of interest that the material from POCO plate B-268 which was used to make the end caps, which failed in the Q-2/IHS, falls outside the statistical tolerance limits.

TABLE 5-16. ASSIGNMENT OF POCO GRAPHITE IN MJS IHS

Heat Source Number	POCO Graphite Plate Number	
	3326 FWD	3327 AFT
F-6	B-329	B-329
F-7	B-317 A3	B-340 A
F-8	BS-68 A	B-319 A2
F-9	BS-68 B	B-340 B
F-10	BS-84	BS-84
F-11	BS-73	B-340 C
F-12	BS-74	BS-76
Q-2	B-268	B-268
Q-2R	B-317 A1	B-319 A3
F-9R	DK-104	DO-66

POCO Graphite Plate Number	Heat Source Use	
	3326 FWD	3327 AFT
B-268	Q-2	Q-2
B-317 A1, A3	F-7, Q-2R	n/a
B-319 A2, A3	n/a	F-8, Q-2R
B-329 A, B	F-6	F-6
B-340 A, B, C	n/a	F-7, F-9, F-11
BS-68 A, B	F-8, F-9	n/a
J-444 'STD'	n/a	n/a
BS-84	F-10	F-10
BS-73	F-11	n/a
BS-74	F-12	n/a
BS-76	n/a	F-12
DO-66	n/a	F-9R
DK-104	F-9R	n/a

TABLE 5-17. MJS PLATE DATA (ACCEPTANCE TEST DATA)

	ρ AT RT	UTS @ RT	E x 10^{-6} @ RT	ρ AT 2000°	UTS @ 2000°	E x 10^{-6} @ 2000°
	1.86	9080	1.99	1.851	10300	2.22
B329	1.86	9240	1.83	1.858	10500	2.24
	1.855	9600	1.91	1.86	10900	2.14
	1.871	8560	1.81	1.874	10400	2.27
B340	1.846	8380	2.05	1.873	10500	2.54
	1.871	9540	1.92	1.876	10300	2.30
	1.883	9020	1.82	1.888	10900	2.19
B317	1.883	8680	2.03	1.883	10300	2.33
	1.884	8600	1.96	1.887	10600	2.29
	1.873	8820	1.94	1.864	9940	2.19
B319	1.88	8440	2.02	1.878	10400	2.35
	1.87	8920	1.88	1.87	9960	2.14
	1.835	9560	2.05	1.84	10360	2.35
BS68	1.825	9280	1.95	1.83	10120	2.27
	1.839	9240	1.93	1.833	10480	1.97
	1.809	9040	1.92	1.831	10480	1.90
BS84	1.800	9520	2.03	1.821	10760	2.30
	1.819	10080	1.90	1.83	10680	2.67
	1.812	10000	1.89	1.84	11440	2.13
BS81	1.814	9460	2.01	1.824	11000	2.37
	1.824	10000	2.26	1.828	11280	2.63
X	1.848	9146	1.96	1.85	10552	2.27
S	0.0281	552	0.101	0.0229	389	0.185
(.95, .90)	1.784	7884	1.73	1.798	9662	1.85
Tol. Limits	1.912	10407	2.19	1.902	11441	2.69
(.95, .95)	1.77	7642	1.69	1.788	9492	1.77
Tol. Limits	1.92	10649	2.24	1.912	11611	2.77
Correlation Coefficient	0.655		0.254	0.328		0.202

TABLE 5-18. TRANSVERSE TENSILE STRENGTH DATA

	ρ AT RT	UTS AT RT
B317	1.893	9040
	1.882	8640
	1.896	9000
	1.876	7940
	1.897	9020
	1.879	9100
	1.858	8600
	1.865	8260
B319	1.852	8880
	1.882	9180
	1.866	8160
	1.886	8820
	1.867	8820
	1.832	9260
	1.867	8740
B329	1.815	9100
	1.836	8900
	1.821	8600
	1.835	9100
	1.841	9520
	1.830	9520
	1.832	9400

	ρ AT RT	UTS AT RT
B340	1.773	7830
	1.846	9440
	1.842	9160
	1.773	8420
	1.835	9060
	1.844	8800
	1.775	8480
	1.854	9420
BS 68	1.836	9120
	1.768	8480
	1.840	9260
	1.849	9600
	1.858	9520
	1.868	9440
	1.803	9680
	1.800	8920
	1.749	8600
	1.794	9000
	1.802	9320

X S	1.84 .0377	8956 449
(.95, .90) Tol. Limits	1.763 1.917	8035 9877
(.95, .95) Tol. Limits	1.748 1.932	7858 10054
Correlation Coefficient	0.1766	

5.2.2.6 Testing of the Q-2R/IHS

The Q-2R/IHS was assembled into the Q-2 RTG and subjected to operational checks and to the levels of vibration and shock specified in the original JPL requirements for qualification. The level and duration of these S&V environments are shown in Tables 5-19 through 5-21 and Figure 5-26. The Q-2 RTG was also subjected to the qualification levels for performance in vacuum and with various gases filling the RTG case. (See Section 7 for performance data on this unit.)

5.2.2.7 Disassembly of the Q-2R IHS

5.2.2.7.1 Background

The Q-2R IHS was removed from the Q-2 RTG, in the LAS, in Building 800 of the GE-SD, on 21 May 1976. To effect this removal, the graphite plug in the forward end cap was removed and the IHS handling tool was threaded into place. After the Q-2R IHS was placed in the EPC, the graphite plug was replaced in the forward end cap. When this plug was threaded into position, the plug failed to bottom-out against the top of the forward graphite spring assembly in the IHS. The plug was again removed. The distance between the top surface of the end cap to the point where a scale made contact, was measured and was found to be approximately 1.3 inches. The correct dimension between the top surface of the forward end cap and the top of the forward spring assembly is approximately 0.5 inches. The internal structure of the Q-2R IHS had changed and it was concluded that the preload maintained by the graphite spring, in the correct stacking of the internal parts, had been lost. It was decided that the Q-2R IHS assembly into the EPC/SPC should be completed and that the unit would then be shipped to Mound Laboratory. Figure 5-27 shows the relative positions which exist in a normal assembly and the dimensions found in the Q-2R IHS.

5.2.2.7.2 Radiography at ML/MRC

When the Q-2R IHS was received at ML/MRC it was radiographed while still within the EPC/SPC structures. The radiographs showed beyond question that the internal structure of the Q-2R IHS had altered as follows:

TABLE 5-19. SHOCK AND VIBRATION, ACCEPTANCE TEST

Mounted on end opposite uniballs (inverted).

X-AXIS		
1/2 g (O-P) Sine Survey	2 Oct/Min	20-2000 HZ
1/2 Level Accept. Sine	2 Oct/Min	5-2000 HZ
Full Level Accept. Sine	7 Oct/Min Log.	5-2000-5 HZ
1/3 Level Accept. Random (EQ)	≦ 20 Sec.	
Full Level Accept. Random	1.0 Min	
Z-AXIS		
1/2g (O-P) Sine Survey	2 Oct/Min	20-2000 HZ
1/2 Level Accept. Sine	2 Oct/Min	5-2000 HZ
Full Level Accept. Sine	6 Oct/Min Log.	5-2000-5 HZ
1/3 Level Accept. Random (EQ)	≦ 20 Sec.	
Full Level Accept. Random	1.0 Min	
Y-AXIS		
1/2g (O-P) Sine Survey	2 Oct/Min	20-2000 HZ
1/2 Level Accept. Sine	2 Oct/Min	5-2000 HZ
Full Level Accept. Sine	6 Oct/Min	5-2000-5HZ
1/3 Level Accept. Random (EQ)	≦ 20 Sec.	
Full Level Accept. Random	1.0 Min	

TABLE 5-20. SHOCK AND VIBRATION, QUALIFICATION TEST

Mounted on end opposite uniballs (inverted).

Y-AXIS		
Full Level Qual. Sine	2 Oct/Min	5-2000 HZ
1/3 Level Accept. Random (EQ)	≦ 20 Sec.	
Full Level Qual. Random	1.5 Min	
12g (O-P) Sine	30 Sec Dwell @ 25 HZ	
Z-AXIS		
1/2g (O-P) Sine Survey	2 Oct/Min	20-2000 HZ
Full Level Qual. Sine	2 Oct/Min	5-2000 HZ
1/3 Level Accept. Random (EQ)	≦ 20 Sec.	
Full Level Qual. Random		
X- AXIS		
1/2g)O-P) Sine Survey	2 Oct/Min	20-2000 HZ
Full Level Qual. Sine	2 Oct/Min	5-2000 HZ
1/3 Level Accept. Random (EQ)	≦ 20 Sec.	
Full Level Qual. Random	1.5 Min	

TABLE 5-21. SHOCK AND VIBRATION, QUALIFICATION TEST

Mounted on uniballs (upright).

X-AXIS		
1/2g (O-P) Sine Survey	2 Oct/Min	20-2000 HZ
1/2 Level Accept. Sine	2 Oct/Min	2000-5 HZ
Full Level Qual. Sine	2 Oct/Min	2000-5 HZ
1/3 Level Accept. Random (EQ)	≦ 20 Sec.	
Full Level Qual. Random	1.5 Min.	
Qual. Shock	3 Shocks	
Z-AXIS		
1/2g (O-P) Sine Survey	2 Oct/MIN	20-2000 HZ
1/2 Level Accept. Sine	2 Oct/Min	2000-5 HZ
Full Level Qual. Sine	2 Oct/Min	2000-5 HZ
1/3 Level Accept. Random (EQ)	≦ 20 Sec.	
Full Level Qual. Random	1.5 Min.	
Qual. Shock	3 Shocks	
Y-AXIS		
1/2g (O-P) Sine Survey	2 Oct/Min	20-2000 HZ
1/2 Level Accept. Sine	2 Oct/Min	2000-5 HZ
Full Level Qual. Sine	2 Oct/Min	2000-5 HZ
1/3 Level Accept. Random (EQ)	≦ 20 Sec.	
Full Level Qual. Random	1.5 Min	
Qual. Shock	3 Shocks	
1/2g (O-P) Sine Survey	2 Oct/Min	20-2000 HZ

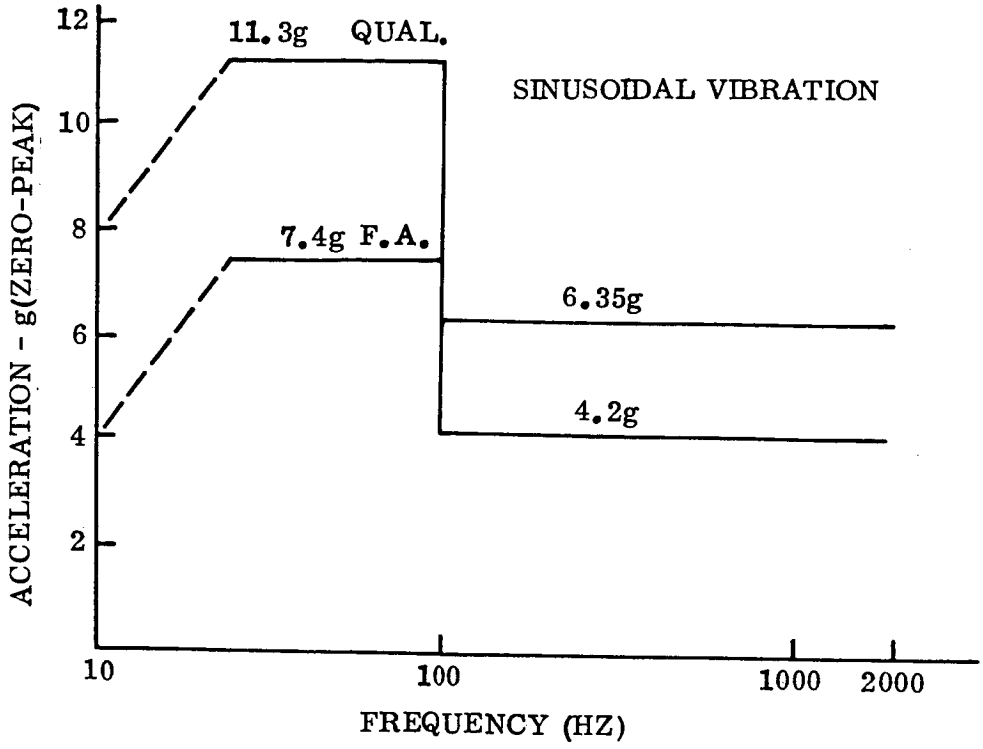

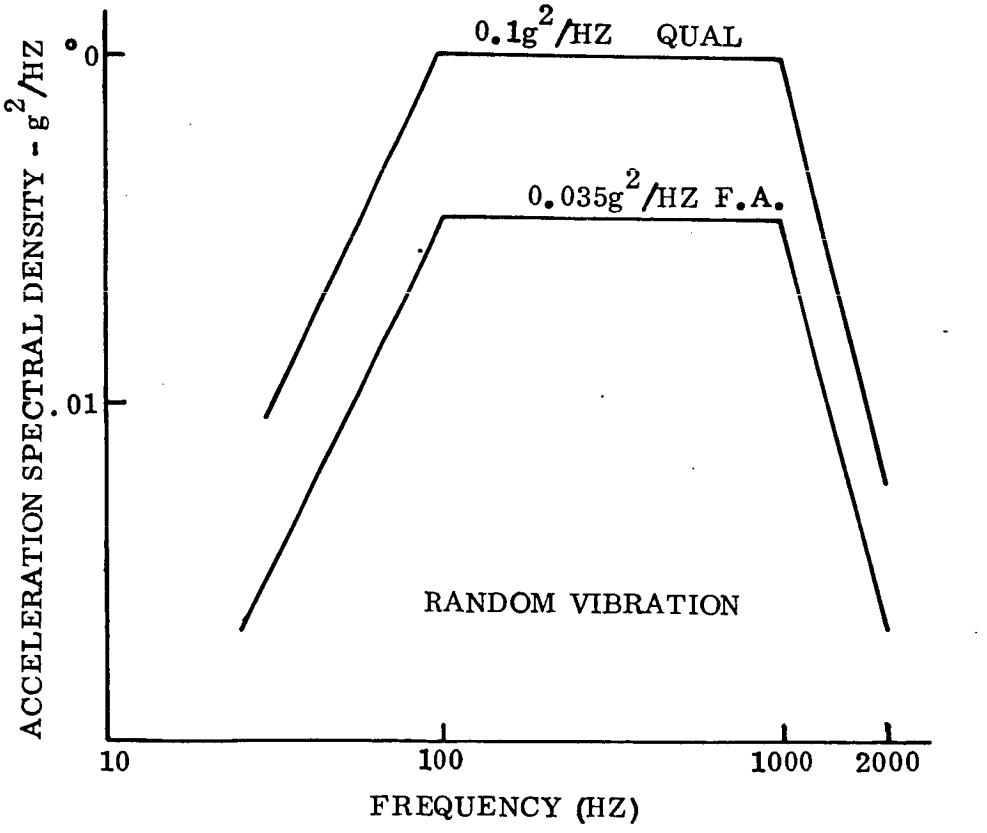

Figure 5-26. MJS RTG Vibration Test

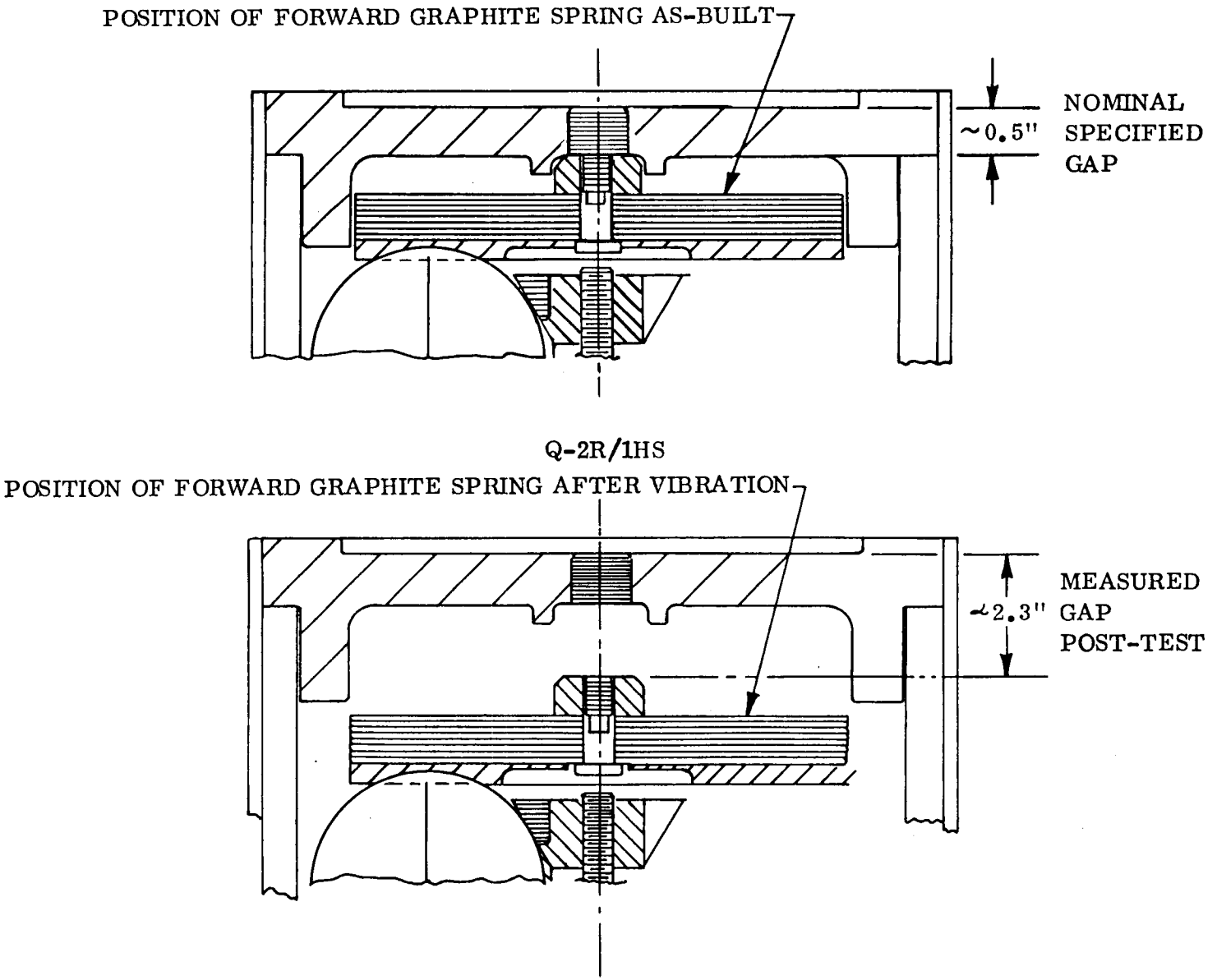

Figure 5-27. Q-2R IHS

1. The bolt head of the aft spring assembly was not visible; the bottom 8-pack had come apart

2. The bottom 8-pack retaining ring had moved upward and some of the spheres were against the aeroshell

3. All of the tie-bolts in all of the 8-packs were broken

4. The sphere lock nut in the middle 8-pack was rotated approximately 90° from its normal position

5. The top spring assembly was moved down from the normal position and was cocked at an angle.

5.2.2.7.3 Contamination in the Q-2R/IHS

When the Q-2R/IHS was removed from the Q-2/RTG at GE-SD, plutonium contamination was found on the surface of the forward end support which was in contact with the top surface of the Q-2R/IHS forward end cap. The readings were very low, approximately 300 dpm. A small amount of graphite dust,adhering to the bottom surface of the threaded plug,removed from the Q-2R/IHS forward end cap,was deposited on one of the trays within the LAS. The activity level found in this dust was determined to be approximately 1000 dpm and by pulse height analysis and half-life estimation was determined to be ^{238}Pu.

Because of the possible presence of internal plutonium-238 contamination, it was decided to proceed with great care in the disassembly of the Q-2R/IHS. The disassembly cell in the ML/MRC F-line is the same cell used for assembly of the IHSs. It was imperative that this cell not be contaminated. Consequently, at a meeting involving ERDA, ML/MRC and GE-SD-NP participants on 10 June 1976, it was decided to proceed with the disassembly of the Q-2R/IHS, but to determine, at each step, the levels of contamination. It was also decided that if the internal smearable contamination exceeded 2,000 dpm, disassembly would be stopped and the unit would be placed in storage.

5.2.2.7.4 Description of Disassembly Process

ML/MRC and GE-SD-NP cooperated in planning the disassembly of the Q-2R/MRC. The SPC was checked for contamination in the cover gas; no evidence of contamination was found. The

cover gas in the EPC was also checked for contamination and no contamination was found. Disassembly of the Q-2R/IHS was begun in handling cell F-605 at ML/MRC on 14 June 1976. When the cover of the EPC was removed, wipe checks were made on its internal surfaces and subsequently on the top surface of the Q-2R/IHS forward end cap. Only negligible levels of contamination, less than 20 dpm, were found on the external surface. It was thus decided that disassembly should proceed. Several attempts, by various means, were made to effect normal removal of the forward end cap. It was found that such removal was not possible and the decision was made to use a core drill to remove most of the central portion of the forward end cap, in such a way as not to damage the aeroshell cylinder. On the morning of 15 June 1976 the forward end cap was cut through and removed. Wipes taken on the bottom surface of the end cap indicated levels of less than 1000 dpm. The nut on the forward spring assembly was found to be delaminated and the forward spring assembly was removed. A wipe was taken on the upper surface of the FSAs on the top 8-pack. The contamination level was found to be approximately 5988 dpm, well in excess of the 2000 dpm limit. In accordance with the agreements made at the meeting of 10 June 1976, the disassembly was halted and the heat source was packed with graphite felt and closed up in the EPC. The EPC was then placed in the SPC and removed from box F-605 pending a decision by ERDA on the final disposition of the Q-2R/IHS. Examination of the forward graphite spring assembly after its removal from the heat source showed, by direct counting, plutonium contamination producing in excess of 75000 dpm.

5.2.2.7.5 Disposition of the Q-2R/IHS

The contamination levels found in the Q-2R/IHS precluded further disassembly in the Mound F605 assembly box. At the USAR meeting at GE-SD in September 1976, the INSRP developed an Action Item, requesting complete disassembly of the Q-2R/IHS. This was needed to permit evaluation of the effects of the internal damage on the magnitude of the potential source terms from the F-6 and F-7 IHSs which were designated as flight units. It was known from radiography that the F-6 and F-7 units were damaged, to the extent that the aft sphere seat plate spring assembly bolt head was broken, and that the internal preload was lost. (See Paragraph 5.2.3 below for further discussion of the loss of preload in F-6 and F-7.)

5.2.2.7.6 Final Disassembly of the Q-2R/IHS

In November 1976, under ERDA direction, arrangements were initiated between ML/MRC and Battelle Memorial Institute-Columbus Laboratories, BMI-CL, to complete the disassembly of the Q-2R/IHS. Final arrangements were concluded in December 1976, and preparations for disassembly were made by BMI-CL to perform the task at the West Jefferson Nuclear Facility in one of the hot cells.

A report has been prepared by BMI-CL giving full details and providing photographic views of the dissassembly as it took place (Report, BMI-X-678).

Briefly, the findings, made during the examination of the Q-2R/IHS as it was disassembled, follow:

1. Only one of the GISs had opened; this appeared to be due to the loss of threads on the body of the GIS. The PISA from this unit appeared to be undamaged and showed contamination by wipe of its surface of around 4000 dpm indicating that no significant release of ^{238}Pu had occurred.

2. The GISs on all of the FSAs, removed from the top 8-pack and sent to LASL for assay, showed little if any mechanical damage. The plutonium content of these GISs was determined by LASL as noted in Paragraph 5.1.2.2.2 and shown in Table 5-7A.

3. The PISAs removed from the FSAs of the top 8-pack were also examined and were found to have sustained no significant damage. The vents of all 8 units were found to be operative with the estimated flow rate as given in Table 5-14.

4. The fines produced during the vibration environments to which the Q-2R was subjected were determined by LASL on two of the 'new' units in the forward 8-pack. The fines fraction, less than 4 microns, was approximately 0.0019 for MHF-164 and 0.0017 for MHF-64. These fines were significantly less than those found in MHFT-11 subsequent to its vibration tests at Mound:

   0.006 (MHFT-11) versus 0.0019 (MHF-164)

5. The GISs in the middle and lower 8-packs were abraded by the vibration to which the unit was exposed. The degree of abrasion varied from slight breaks in the surface layer, to a sufficient removal of material to make the sphere appear out-of-round, on two or three FSAs. The bottom layer of FSAs in the bottom 8-pack, which was completely free of restraint, appeared to have sustained no damage as far as the GISs were concerned.

6. No examination has been made of the PISAs in the middle and bottom 8-packs, now at ML/MRC. No evaluation has been made of the Pu content of these GISs.

7. Damage to miscellaneous parts in the 8-pack assembly was severe: the bolts in all cases were found to be broken,with the threads significantly abraded; the sphere lock on the upper 8-pack had delaminated. The compliance pads between layers of FSAs were almost completely abraded away. No observable damage to the retainer rings was found.

8. With all of the debris removed from the interior of the IHS, no damage was observed, at BMI-CL,on the interior of the aeroshell or the interior surface of the bottom end cap. The graphite parts were repackaged in the EPC and shipped to ML/MRC for further examination.

9. When the aeroshell was examined at ML/MRC it was found that there had been no significant damage. In the areas where the retainer rings had moved under vibration, abrasion had removed wall material to depths ranging from 0.001 to 0.003 inch. The locking ring in the aft end cap was jammed by debris which prevented it from moving when the locking screw was removed. This necessitated removal of the aft end cap by breaking the cap at the lip below the lock ring. It is probable that the same condition, debris in the lock ring, prevented normal removal of the forward end cap.

A discussion of the Q-2R/IHS disassembly was presented at the MJS FSAR by ML/MRC, BMI-CL, LASL and GE-SD-NP.

5.2.3 LOSS OF PRELOAD IN MJS-IHSs

5.2.3.1 Background

In July 1976, radiography of the F-6 and F-7 RTGs at ML/MRC showed clear evidence that the internal preload had been lost because the head of the bolt in the aft sphere support plate spring assembly had been damaged. Initially, it was thought that this damage had resulted from the acceptance level shock and vibration testing on the F-6 and F-7 RTGs. The experience with the Q-2R/IHS discussed in Paragraph 5.2.2.7 plus radiography of this unit after its return to ML/MRC, had shown loss of internal preload and similar damage.

During August 1976, it was decided to review the radiographs routinely made by ML/MRC after assembly of the IHSs into the SPC but prior to their shipment to GE-SD, Figure 5-28 shows the IHS configuration with the deflection of the aft end support spring for eight (8) MHW IHSs, as measured from the radiographic plates.

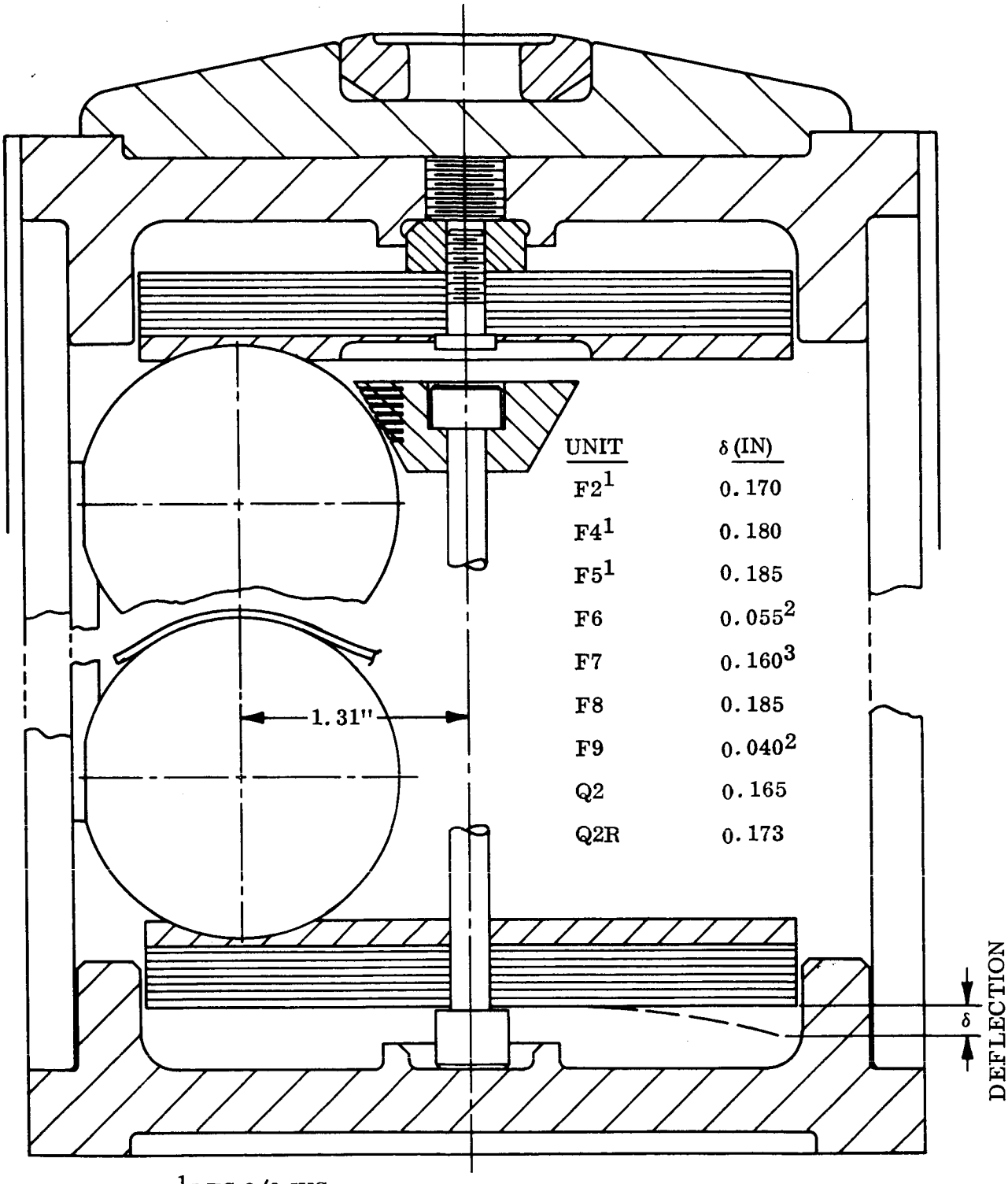

[1]LES 8/9 IHS.

[2]TIE BOLT HEAD FAILED (F9 WAS REBUILT)

[3]TIE BOLT HEAD 'BROOMED' BUT DID NOT FAIL COMPLETELY

Figure 5-28. Undamaged IHS

It was clear,immediately,that the aft sphere support spring assembly bolt head in F-6 and F-9 IHSs, had failed during assembly at ML/MRC and before shipment to GE-SD-VF. F-7 had apparently sustained some damage to the bolt head but failure was not complete until after testing.

5.2.3.2 Design Changes

Schedule constraints did not permit time for disassembly of the F-6 and F-7 RTGs and rebuilding of their respective IHSs. It was, however, possible to make changes to the aft spring assembly and to incorporate these changes into the F-10, F-11, and F-12 IHSs. The schedule was shuffled to permit the rebuilding of the F-9/IHS which had been received but not yet tested by GE-SD.

The tie bolt in the aft spring assembly like all the tie bolts in the MHW IHSs, was made by Pyrocarb 508. (The initial design of the IHS had used POCO for tie bolts and for nuts where needed. This was changed because there was some concern that the hard POCO might damage the GISs on impact.) Pyrocarb 508 is a woven, impregnated, and laminated carbon/graphite composite. Fabrication of a tie bolt from this material required the bolt be cut so that the laminations ran parallel with the axis of the bolt. Excessive pressure could and did deform the bolt head, resulting in complete collapse as in Q-2R, F-6 and F-9, or 'brooming' as in F-7.

Consequently, it was decided to make the tie bolt head out of POCO and to increase its diameter to approximately the same size as that used in the forward spring assembly. This design change was made effective for F-10, F-11 and F-12 IHSs and F-9/IHS was rebuilt to incorporate the change.

5.2.3.3 F-9 Disassembly and Rebuild

The radiographs of the F-9/IHS made at ML/MRC before shipment to GE-SD, were carefully examined after the discovery of the preload loss in Q-2, F-6, and F-7 IHSs. It was found that the bolt head in the bottom 8-pack assembly had flattened during assembly. It was decided to rebuild the F-9/IHS,before testing at GE-SD,and to replace the defective bolt,with the new design assembly,in which the bolt head is replaced with a POCO nut.

5.2.3.3.1 Disassembly

Disassembly of F-9/IHS was begun on 4 January 1977 and was accomplished without incident. The forward end cap was easily removed using the normal procedure (see Para. 5.2.2.7.4 regarding difficulties encountered with removal of both end caps from Q-2R/IHS).

The three 8-packs were removed readily. The bottom 8-pack was disassembled and the new retaining bolt was used to reassemble the 8-pack. No evidence of Pu contamination exceeding the as-built levels, was found by wipe samples.

5.2.3.3.2 Water Leak in the Assembly Cell

At this time, a plastic water line to the chill block ruptured,spraying water directly on the bottom 8-pack. Water accumulated in the bottom of the assembly cell before the water supply could be cut off. The atmosphere in the assembly cell was thus saturated with water vapor.

5.2.3.3.3 Remedial Action

It had been anticipated that difficulties in disassembly of F-9 could have damaged the aeroshell and some of the internal parts. A complete set of flight qualified carbon/graphite parts, except for the GISs of the FSA, had been prepared for possible use in the reassembly. To remove the absorbed water vapor from the 8-packs, these sub-assemblies were baked-out under vacuum using their self-heating to reach the desired temperature. After the assembly cell was cleaned and the cell atmosphere restored to the specified levels, the F-9 IHS was rebuilt using the stand-by hardware and the baked-out 8-packs. The reassembled unit was designated F-9R.

5.2.3.3.4 Further History of F-9R/IHS

The gas samples taken from the F-9R in storage, were analyzed, with the results as shown in Table 5-14. These data indicate that the removal of CO-forming contaminants had been satisfactory.

The F-9R/IRS was used as the heat source for the F-12/RTG. Processing, assembly, and testing of the F-12/RTG with the F-9R/IHS was accomplished without incident at GE-SD.

5.3 ISOTOPE HEAT SOURCE ANALYSES AND TESTING

Analyses and testing of the IHS and its components, explicitly to resolve potential problems and to establish margins in the safety area are discussed in Section 2. Other analyses and testing to verify design, to predict performance, and to elucidate anomalies, are presented here. Data from some of these tests were also used in support of the safety analyses.

5.3.1 INTERFACE CONDUCTANCE TESTS - POCO AXF-5Q VERSUS PYROCARB 406

5.3.1.1 Interface Conductance Problem

The purpose of the Pyrocarb 406 ablation sleeve,on the MJS IHS,is to protect the POCO AXF5Q aeroshell from excessive thermal stress,during steep angle, superorbital reentry. Heat flow to the aeroshell is determined by the thermal resistance of both the sleeve material and the sleeve/aeroshell interface. No data were previously available on the interface contact coefficient for the materials of interest. For analysis purposes, GE has assumed an order of magnitude interface conductance of 1000 Btu/hr-ft^2-^{o}F. Due to the lack of data, analyses conducted by the Applied Physics Laboratory have been based on the very conservative assumption of infinite interface conductance, resulting in significantly higher thermal stresses. To resolve this conflict and improve the analysis in general, a series of tests were initiated to measure the interface conductance between the sleeve and aeroshell materials.

5.3.1.2 Test Description

The tests were conducted by Dynatech R/D Company. Three Pyrocarb 406 specimens were tested. One had smooth, as-machined surfaces,and two had grooved surfaces, similar to the grooved I.D. of the ablation sleeve. The test matrix consisted of three mean temperatures (50, 550, 1150^{o}C) and three contact pressures (50, 100, 150 psi).

The Comparative Cut-Bar Method was chosen as the test method. The sample was placed between two POCO Graphite AXF-5Q reference standards of known thermal conductivity, with thermocouple instrumentation at the interfaces. The composite stack was placed between the plates of an upper heater, an auxiliary heater and a lower heat sink. A

reproducible load was applied to the top of the complete system with a hydraulic ram. A guard tube with three-mode temperature control was placed around the system and the interspace and surroundings filled with an insulating powder; the stack was then covered with a bell jar and evacuated with a diffusion pump to 10^{-3} torr. By means of adjustments to the power in the various heaters and of the heat sink temperature, a steady temperature distribution was maintained in the system and undue radial loss prevented by maintaining the guard tube temperature gradient similar to that of the test stack. The temperature difference across the sample was maintained at approximately 20 deg K. At equilibrium conditions the temperatures at various points in the system were evaluated from the thermocouple readings.

The thermal conductance was calculated from

$$C_s = \frac{1}{2\,\Delta T_s} \left(\frac{\lambda 1\ \Delta T_1}{\Delta\ \lambda_1} + \frac{\lambda 2\ \Delta T_2}{\Delta\ \lambda_2} \right)$$

where

C_s = thermal conductance of sample

ΔT_s = temperature difference across sample obtained from temperature difference between bottom of top reference and top of bottom reference

$\lambda 1$ and 2 = thermal conductivities of references at temperature

ΔT_1 and 2 = temperature difference between thermocouple probes placed in holes in references

$\Delta_{\chi 1}$ and 2 = distance between thermocouple probes in reference

5.3.1.3 Results

The conductance C_s determined by Dynatech is the total conductance across two interfaces and the Pyrocarb 406 sample itself. The parameter needed for the reentry analysis is the interface contact conductance h_c for one interface excluding radiation. Linearizing the radiation term, h_c was calculated from the test results by:

$$h_c = \frac{2}{\frac{1}{C_s} - \frac{\Delta X_s}{\lambda_s}} - 4\left(\frac{1}{\frac{2}{\epsilon} - 1}\right) \sigma T_m^3$$

where X_s = Pyrocarb 406 sample thickness $\approx 0.0072'$ (0.086")

λ_s = Pyrocarb 406 conductivity ≈ 7 Btu/hr-ft-^oF

ϵ = Graphite emissivity = 0.8

σ = Stefan-Boltzman constant = 0.17×10^{-8} Btu/hr-ft^2-$^oR^4$

T_m = Mean test temperature - ^oF

Since the radiation term is relatively small at the test conditions, the use of one mean temperature instead of individual surface temperature does not introduce significant error.

The resulting values of C_s and h_c are listed in Table 5-22, and h_c is plotted versus contact pressure in Figure 5-29 and mean temperature in Figure 5-30. The results show that the grooving of the sleeve I.D. significantly reduces the interface conductance. The readings for the two grooved samples showed very good agreement. The assumed value in the GE analyses to date of $h_c = 1000$ Btu/hr-ft^2-^oF is the proper order of magnitude, falling between the smooth and grooved surface values.

5.3.2 STRESS ANALYSES OF THE IHS END CAPS

5.3.2.1 History

The Q-2/IHS was assembled at Mound Laboratories and delivered to General Electric. During shipping, the IHS is inside the EPC (Environmental Protection Container) which, in turn, is placed in the SPC (Storage Protection Container). Subsequent to delivery of the IHS, the EPC was opened and the forward end cap was found to be cracked. The unit was returned to Mound, and after disassembly, the aft end cap was also found to be cracked.

TABLE 5-22. POCO AXF5Q/PYROCARB 406 INTERFACE CONDUCTANCE TEST RESULTS

Sample	T_m °C	P_c psi	C_s W/m^2-°K	C_s Btu/hr-ft^2-°F	h_c Btu/hr-ft^2-°F
Smooth	50	50	1850	325	1010
		100	2200	387	1340
		150	2430	428	1600
	550	50	2210	389	1280
		100	2610	460	1720
		150	2970	523	2240
	1150	50	2120	373	1120
		100	2610	460	1630
		150	3150	555	2430
Grooved #1	50	50	1440	254	695
		100	1700	299	880
		150	1880	331	1020
	550	50	1380	243	629
		100	1650	291	807
		150	1700	299	843
	1150	50	1470	259	606
		100	1650	291	738
		150	1700	299	773
Grooved #2	50	50	1420	250	682
		100	1740	306	910
		150	1810	319	966
	550	100	1650	291	807
	1150	100	1600	282	703

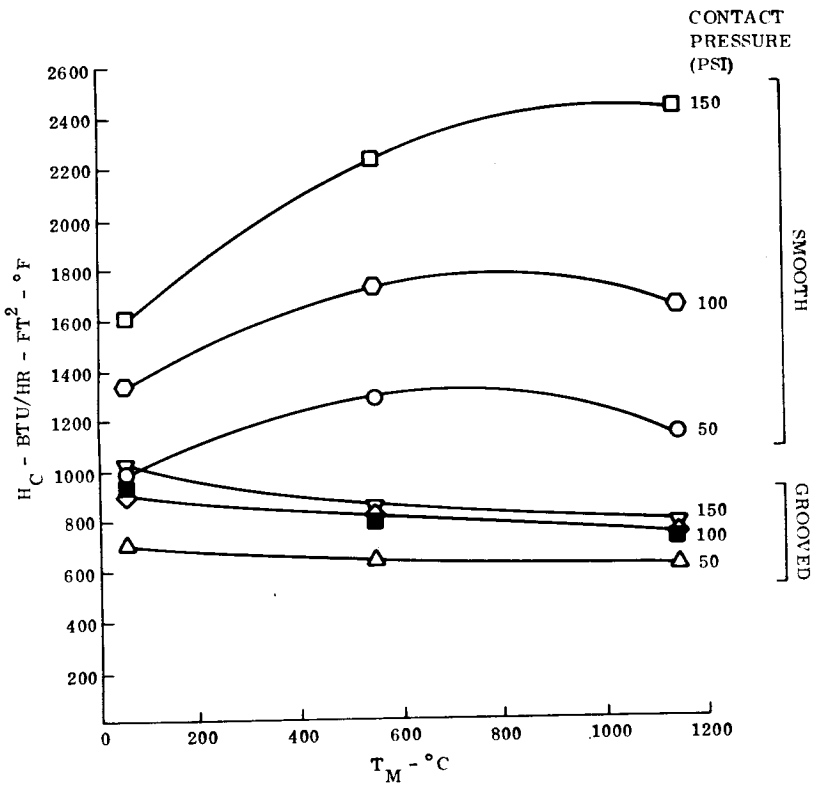

Figure 5-29. Effect of Contact Pressure on POCO AXF 5Q/Pyrocarb 406 Interface Thermal Contact Coefficient

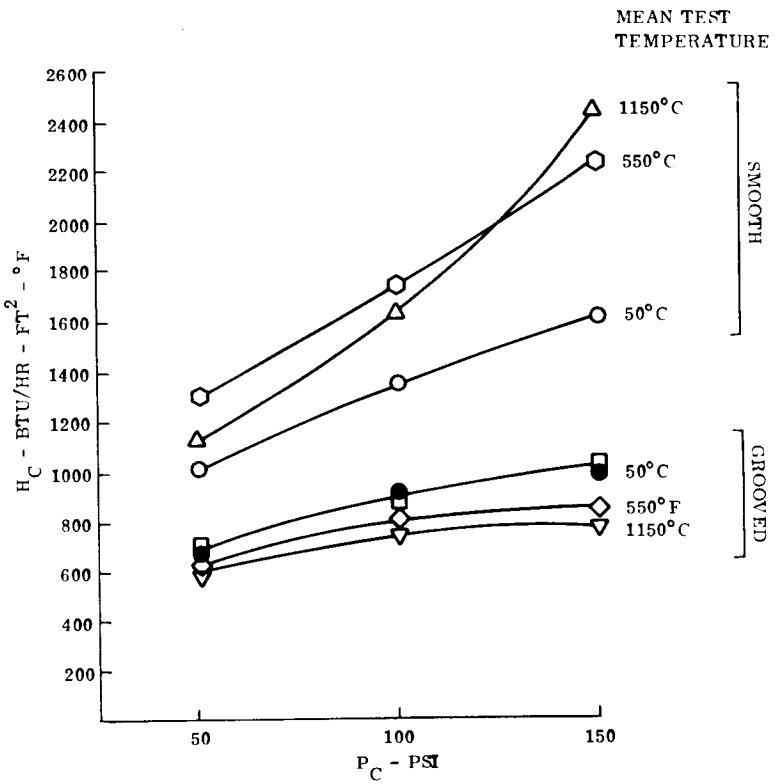

Figure 5-30. Effect of Test Temperature on POCO AXF 5Q/Pyrocarb 406 Interface Thermal Contact Coefficient

The cracks in the aft end cap were located in the radius as shown on Figure 5-31.

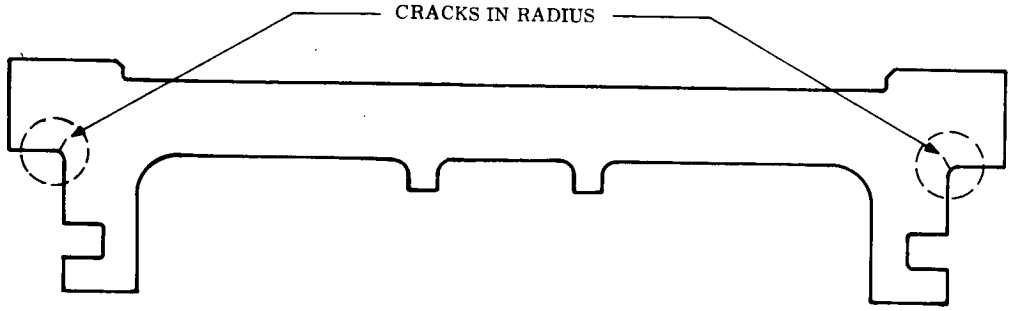

Figure 5-31. Q-2 Aft End Cap

The Q-2/IHS end caps were fabricated from plate B268, supplied by POCO Graphite and conforming to their AXF-5Q formulation. Plate B268 was accepted to the requirements of GE Specification NS 0060-02-89. Except for the low tensile properties (6300 psi in lieu of the specification value of 8500 psi), this material supposedly met the acceptance criteria. (See para. 5.2.2.5)

5.3.2.2 Stress Analyses Assumptions

Prior to installing the cover on the EPC, the IHS has an internal preload of approximately 800 pounds applied. This load condition was identified as Case I.

After the EPC cover is installed, the SPC applies an external load to the EPC and IHS end cap. The magnitude of this load was intended to be on the order of 1200 pounds. Prior to running this case, it was decided to static test a rejected end cap (fabricated from plate B306) to see if the cracks in the radius of the Q-2 aft end cap could be reproduced by static loading. The static test was conducted with inspections performed after each increment of load.

When the total applied load reached 4000 pounds without failure, the test was discontinued. Case IIa was run to determine the stress in the radius with the 4000 pounds applied. Case IIb was performed with the 4000-pound load applied and assuming a reaction at the aeroshell.

Preliminary reports on the material investigation indicated a varying density through the thickness of the end cap. If this varying density was indicative of partially-graphitized material, then the CTE (coefficient of thermal expansion) could vary by as much as a factor of two over the thickness of the end cap. Case III was performed assuming that the CTE did vary by a factor of two.

5.3.2.3 Analytical Results

Each case was analyzed using the BIG-2D computer program. One-half of the end cap was modeled. The model is composed of 269 model points and 222 elements.

Figure 5-32 shows the loading on the forward end cap and the restraint at the lock ring. The results of this analysis show that the maximum stress in the cap (approximately 2100 psi) occurs in the root of the groove for the lock ring. The strsses in the radius, where the crack was discovered on the Q-2 aft end cap, were low (approximately 200 psi) and in compression. The calculated deflections show, as expected, that the gap between the end cap and aeroshell increases with the application of the internal load.

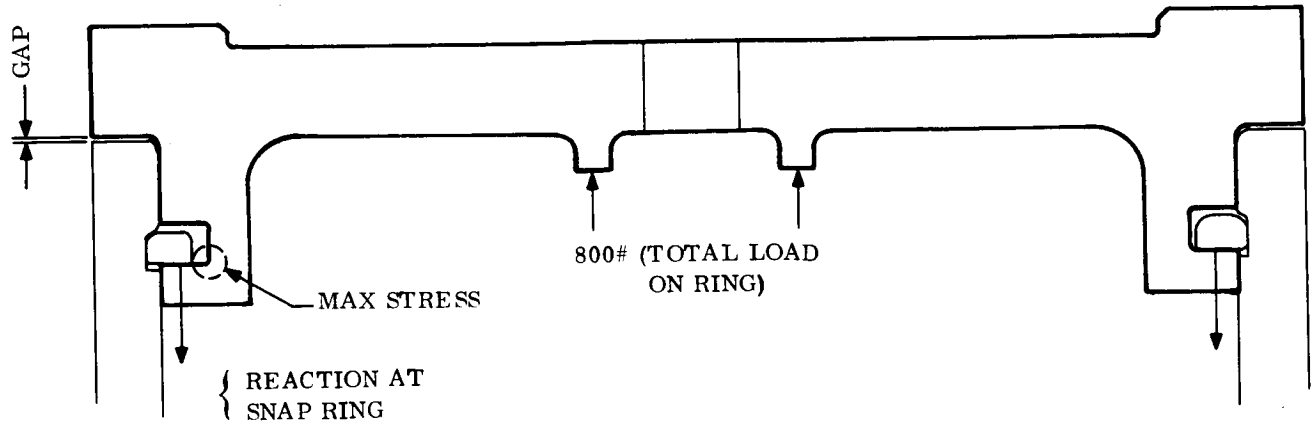

Figure 5-32. Forward End Cap Case I Loading

Figure 5-33 shows the load applied to the cap for the Case IIa analysis. In this figure the external load of 4000 pounds is shown as a triangular distributed load. The actual analysis was conducted with the load introduced at 12 concentric nodal circles simulating the load distribution shown.

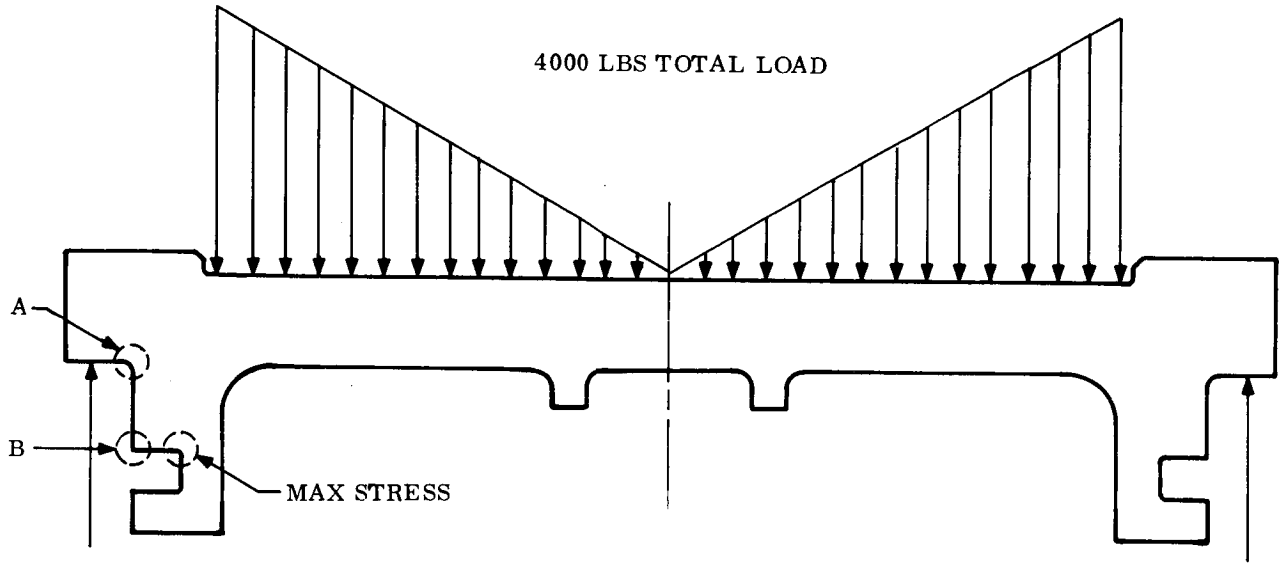

Figure 5-33. Case IIA Loading, No Radial Restraint

The results of this analysis show that the maximum stress again occurs at the root of the lock ring groove (see Figure 5-33). The magnitude of this stress is approximately 3670 psi. The maximum stress in the radius (see "A" Figure 5-33) is approximately 2330 psi. Calculated deflections show that "B" (see Figure 5-33) is the point which under the 4000-pound load deflects to minimize the clearance between the end cap and the aeroshell. The calculated deflection of this point in the radial direction is approximately 4.5 mils. The minimum radial clearance between the end cap and aeroshell is 5 mils. Based on this analysis, it is concluded that the stresses in the radius for the 4000-pound applied load are not sufficiently high to cause cracking in the radius and that the end cap does not deflect to cause an interference with the aeroshell.

Figure 5-34 shows the loads applied to the cap for the Case IIb load condition. As shown,

the loading is similar to Case IIa, except that the radial deflection is not allowed. This simulates an "out of tolerance" condition where the aeroshell provides radial support. This condition is conservative in that the radial deflection is constrained to be zero.

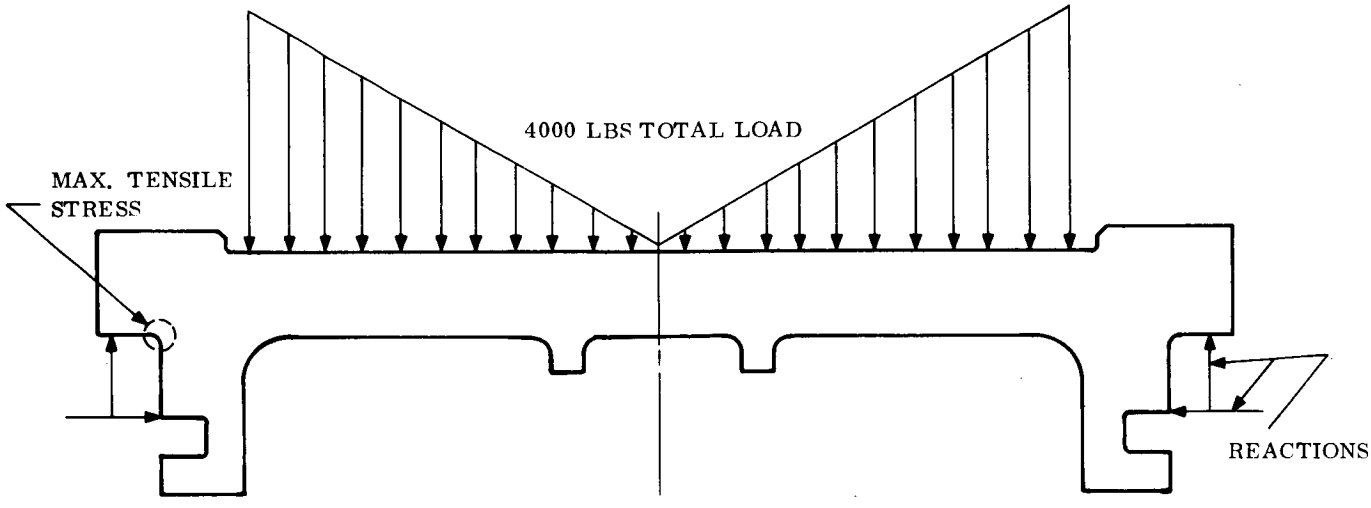

Figure 5-34. Case IIA Loading, Restraint in Radial Direction

The results for this condition show the maximum tensile stress, approximately 3000 psi, occurs in the radius.

Figure 5-35 shows the assumed variation in CTE used in the analysis. The shaded area represents that portion of the cap which was assumed to have a CTE one-half the value for the remainder of the end cap. The thickness of the area of reduced CTE was approximately one-eighth inch near the center of the end cap and was as much as one-half inch near the edge. These thicknesses were selected to accommodate the nodal spacing of the existing finite element model.

To perform this analysis it was assumed that the plate was initially stress-free at the graphitization temperature of 2500^{o}C (4532^{o}F). The stresses in the end cap were calculated with the temperature reduced to zero and the CTE variation as noted above.

The results of this analysis show that tensile stresses exceeding the ultimate tensile strength of the end cap material occur at many places. Selecting 7000 psi as the minimum surface stress that will probably cause cracking, it was found that stresses of this magnitude exist on the outer face, at the radius and at the root of the lock ring groove. Figure 5-35 shows these areas.

5.3.2.4 Conclusions

Based on the results of these analyses, the following conclusions were drawn:

1. The 800-pound internal preload did not cause stresses in the end cap which would induce cracking similar to the cracks found in the Q-2 end cap.

2. The externally-applied load on the end cap was probably less than 1200 pounds. Since the analysis performed using a total load of 4000 pounds did not cause stresses of sufficient magnitude to cause cracking of the end cap, it was assumed that the externally-applied load did not cause the cracks found on the Q-2 end cap.

3. Since the analysis showed that the cap does not deflect sufficiently to bear on the aeroshell with a 4000-pound load, it was concluded that the externally-applied load did not cause the cap to interfere with the aeroshell.

4. Should the cap (or aeroshell) have been out of tolerance to such an extent that the radial deflection of the cap was prevented, the calculated stress in the end cap with a 4000-pound load applied is still not sufficient to predict cracking.

5. The arbitrary case which assumed a two-to-one variation in the CTE did not show stresses of sufficiently high magnitude to predict cracking. However, with the assumptions made, the cap should have failed at the lowest temperature to which it was exposed. Any increase in temperature (such as occurs in the SPC) should reduce the stresses.

6. In summary, it was concluded that no loading condition defined is sufficient to predict the cracks found in the Q-2 end cap, if the POCO was homogeneous. (See Paragraph 5.2.2.5.)

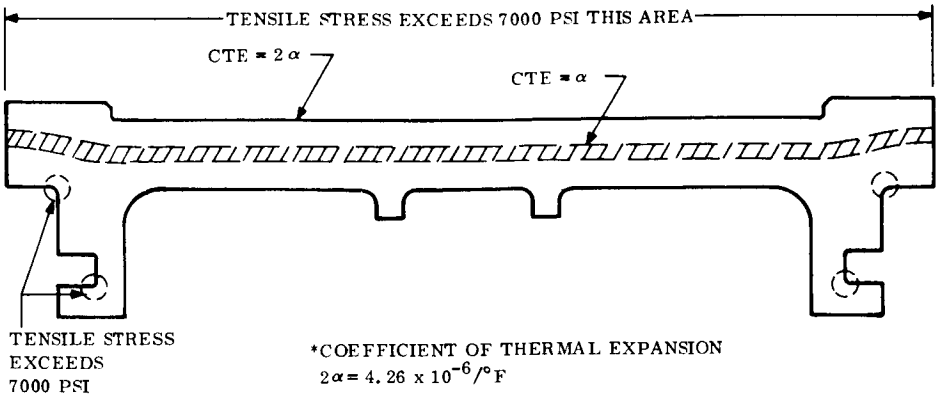

Figure 5-35. Case III Loading CTE Variation

5.3.2.5 Stress Analyses on the MJS MHW-IHS Support

In the MHW-MJS RTG, the IHS is mounted in place using two POCO AXF-5Q graphite disks which interface between the converter and the IHS.

The heat source support fits into the recess in the IHS end cap. The function of the heat source support is to transfer the load from the zirconia disk to the IHS. The design load on the heat source support is 3600 pounds. This load is derived by assuming a 50g dynamic response superimposed on the static preload.

Conservatively, it is assumed that one-half of the load is beamed out along each web and that the remaining load is resisted as a uniform load. Figure 5-36 shows the configuration of the heat source support and indicates this load distribution. Based on this load distribution, the maximum moment (381 ip) occurs at section AA. The calculated moment of inertia is 0.033 in.^{4}. The resulting bending stresses are:

$$f_c = \frac{MC}{I} = \frac{381 \times 0.55}{0.033} = 6350 \text{ psi}$$

$$f_t = \frac{MC}{I} = \frac{381 \times 0.29}{0.033} = 3410 \text{ psi}$$

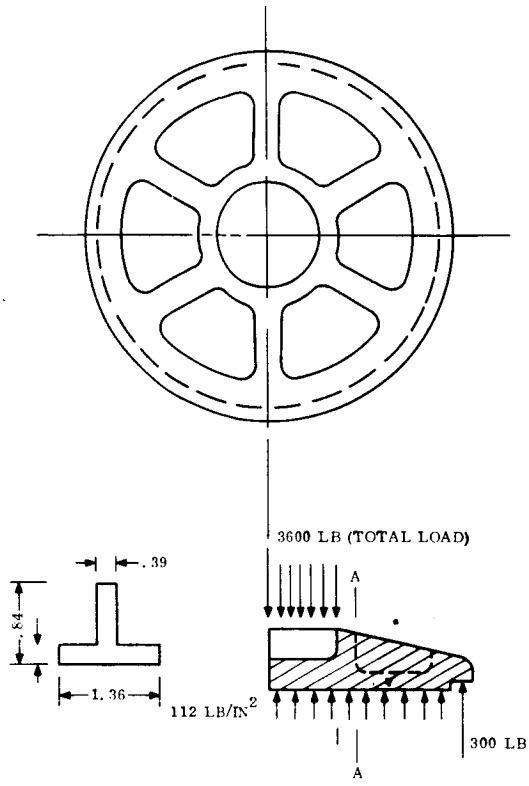

Figure 5-36. Heat Source Support

The resulting margin of safety based on a tensile strength of 8500 psi is:

$$MS = \frac{8500}{3410} - 1 = 1.49$$

Subsequent investigation has shown that the heat source support is more critical in shear. The shear strength is estimated as shown below:

$$F_{tu} = C\ E$$

$$G = \frac{E}{2\ (1 + \mu)}$$

$$F_{su} = C\ E$$

$$\frac{F_{su}}{F_{tu}} = \frac{G}{E} = \frac{1}{2\ (1 + \mu)} \qquad \text{Assume } \mu = 0.3$$

$$F_{su} = \frac{F_{tu}}{2\ (1.3)} = 38\%\ F_{tu}$$

where

F_{tu} = Tensile strength

F_{su} = Shear strength

E = Tensile modulus

G = Shear modulus

C = Strain

μ = Poisson's ratio (0.3)

Using the load distribution shown in Figure 5-34, the maximum shear stress (f_s) is found to be 1970 psi. Based on the assumed shear allowable (0.38 F_{tu}), the resulting margin of safety is shown below:

$$MS = \frac{0.38\ F_{tu}}{f_s} - 1$$

$$MS = \frac{0.38 \times 8500}{1970} - 1 = 0.64$$

Based on the results of this analysis, it is concluded that the heat source support should sustain 5900 pounds (1.64 x 3600) prior to failure in shear.

5.3.3 EFFECT OF PAD EXPLOSION ON MJS-RTG

5.3.3.1 Analytical Assumptions

The effect of two explosive environments on the RTGs were considered. One environment, Confinement by Missile (CBM), represents an explosion of the Centaur stage with the vehicle vertical. The second environment, Confinement by Ground System (CBGS), represents an explosion of the Centaur stage after the vehicle has tipped over and is in close proximity to the ground. Previous studies have shown that the maximum overpressures on

the spacecraft and RTGs are caused by the explosion of the Centaur stage of the launch vehicle. Therefore, this analysis considered only the exposure to the environment caused by the explosion of the Centaur stage.

5.3.3.2 Analytical Results

5.3.3.2.1 CBM Case

The analysis was performed using the explosive overpressure and projectile velocities presented in Reference 5.3.3-1. Using these data and assuming that the two ends of the RTG stack are 22 and 28 feet from the center of the explosion, the data shown in Table 5-23 were derived for the CBM case.

Using the data from Table 5-23, time-pressure diagrams were constructed. Figure 5-37 shows typical diagrams constructed by the method suggested in Reference 5.3.3-2. As shown, the front face (nearest to the explosion) feels the reflected pressure which peaks at time zero. This pressure decays as the pulse spreads over the face and spills over the sides. The time (t_1) for this decay is one-half the smallest dimension of the face cross-section (in the case of the RTGs: a radius), divided by the blast wave velocity (S/UX). When the time equals 3 t_1, the blast has decayed to the stagnation pressure (P_{stag}). The pressure decay then proceeds to zero at time equal to t_d (blast duration).

The loads on the rear face do not start to rise until the blast wave has travelled the length of the structure. The time to attain peak value is three times the smallest dimension of the rear face divided by the sonic velocity in undisturbed air. The peak value of the pressure is the stagnation pressure, minus the drag pressure, multiplied by a drag coefficient.

The total area under these two curves multiplied by the cross-sectional area of the face gives the impulse applied to that face.

Table 5-24 shows the net impulse on the RTGs calculated using this method for each of the noted yields.

TABLE 5-23. EXPLOSIVE OVERPRESSURE ON RTG

	Yield							
	1%		3%		5%		10%	
	Base	Top	Base	Top	Base	Top	Base	Top
Static (psi)	51	31	98	63	144	88	232	142
Stagnation Overpressure (psi)	99	52	271	138	440	231	840	425
Reflected Over-pressure (psi)	198	108	490	265	800	416	1480	780
Drag Overpressure (psi/cd)	40	28	70	47	97	63	150	97
Blast Duration (Msec)	6.2	8.5	5.3	7.8	5.7	7.5	4.8	6.7

The truss supporting the RTG must be capable of sustaining a static load equivalent to the response load of the truss. Assuming that the truss responds as a single degree of freedom system, it is found that the equivalent static load is 60,200 pounds. Figure 5-38 shows the truss geometry and a unit solution for the applied load. Table 5-25 shows the truss loads and stresses compared to the calculated allowable loads.

As seen from Table 5-25, the truss will fail for 1 percent yield. It is assumed that the truss will fail for all higher yields. At approximately the same time the blast wave reaches the RTGs, the spacecraft is also impacted. Table 5-25 shows the blast overpressures on the spacecraft for the CBM case. These values were also derived from data obtained from Reference 5.3.3-1.

From the data of Table 5-26 and using the same method as was used for the RTGs, the total impulse on the spacecraft was calculated. Since the spacecraft is longer than the RTGs and the projected areas of each end are different, the impulse to each end of the spacecraft was calculated separately. Table 5-27 shows the impulse for each end of the spacecraft as a function of the expected yield.

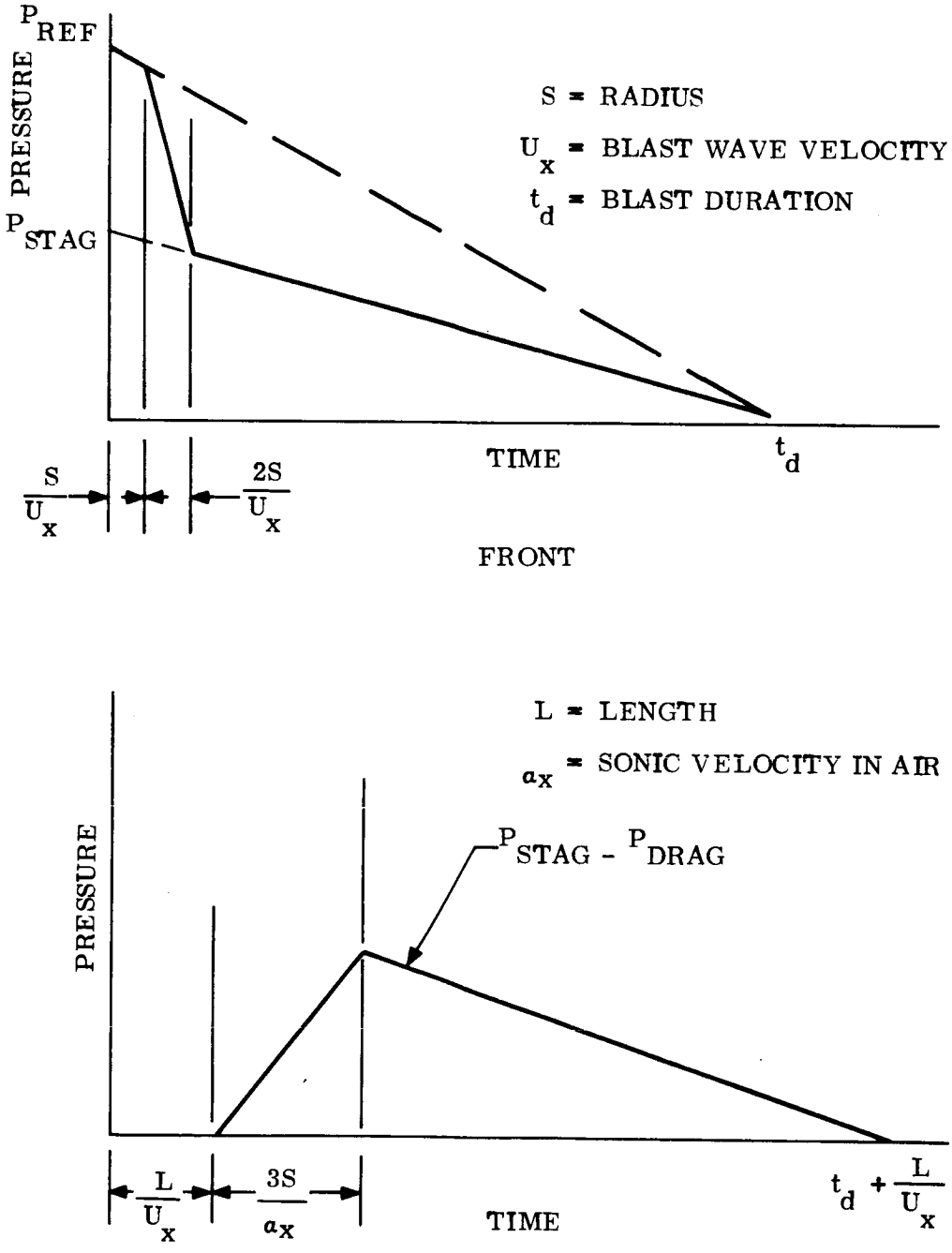

Figure 5-37. Face Loading

TABLE 5-24. IMPULSIVE LOADING ON RTGS

Yield	Impulse (lb/sec)
10%	60.2
3%	85.6
5%	168.3
10%	252.1

TABLE 5-25. TRUSS LOADS FOR 1 PERCENT YIELD (CBM)

Member	Load (lbs)	f Stress (psi)	Fa^1 Allowable Stress (psi)	MS^2
$V_o V_1$	-5,227	-35,700	-60,000	0.68
$L_u L_1$	52,280	+357,000 n	118,000	-0.67
$L_u V_1$	-61,700	-422,000	-45,000	-0.89

1 Allowable stresses are based on net tension or column buckling. Estimated allowable ultimate tensile stress for 1/8 hard 304 Cres it 118,000 psi.

2 Margin of Safety (MS)

$$MS = \frac{Fa}{f} - 1$$

Using the data from Tables 5-24 and 5-27, the velocities of the RTGs and the spacecraft were calculated. Since the truss supporting the RTGs fails, the RTGs are assumed free of the spacecraft. The purpose of calculating the velocities is to assess the possibility of damage to the RTG by secondary impacts with the spacecraft after the explosion. Table 5-28 gives the velocities.

Based on these calculated velocities, it is concluded that the possibility of damage due to secondary impacts is slight. Since the maximum difference in velocity is on the order of 10 FPS, the time for an impact to occur is small. The paths of the RTG and spacecraft are nearly parallel so that any collision could only occur at a small angle.

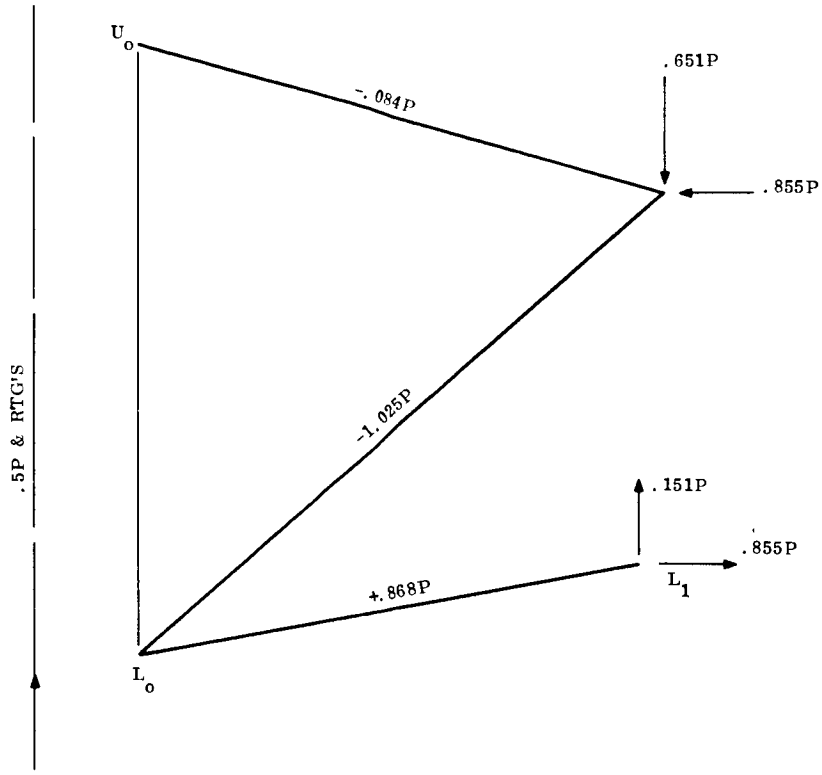

Figure 5-38. Unit Solution for Half Latch Truss Assembly

TABLE 5-26. EXPLOSIVE OVERPRESSURE ON SPACECRAFT

	Yield							
	1%		3%		5%		10%	
	Base	Top	Base	Top	Base	Top	Base	Top
Static (psi)	60*	25	120	53	175	73	290	115
Stagnation Over-Pressure (psi)	115	40	360	102	560	175	1050	315
Reflected Over-pressure (psi)	255	84	640	200	1020	340	1920	600
Drag Pressure (psi/cd)	46	26	85	42	115	54	175	79
Blast Velocity (ft/sec)	2400	1800	3200	2270	2800	2600	4750	3150
Blast Duration (Msec)	5.4	9.0	4.9	8.8	4.5	8.4	4.1	7.6

TABLE 5-27. IMPULSIVE LOADING ON SPACECRAFT

Yield (%)	Impulse	
	Base (lb/sec)	Top* (lb/sec)
1	1074	-728
3	3580	-1202
5	6247	-2213
10	10516	-3821

*Negative sign indicates the impulse at the top is in the opposite direction to that at the base.

TABLE 5-28. SPACECRAFT AND RTG VELOCITIES AT NOTED YIELD

	1% (FPS)	3% (FPS)	5% (FPS)	10% (FPS)
RTG	9.1	14.7	28.0	40.3
Spacecraft	2.6	18.0	30.5	50.8

To determine the effect of the explosive overpressure on the RTGs, the loads created by the explosion have been compared to the allowable strength of the RTG. This comparison is shown in Table 5-29 for each of the four yields. As shown, the aft dome is predicted to fail for each of the four yields noted. The RTG case is predicted to not collapse for any of the four yields. For yields of 5 percent or greater, the axial compression exceeds the case allowable. However, this does not necessarily indicate a rupture or fragmentation of the case. For the purpose of this analysis it is assumed that the case is severely deformed but not ruptured to the degree that the IHS would be free. As seen from the table, yields in excess of 3 percent will cause the lug bolts to shear. This results in at least one of the RTGs being separated from the other two. Again, this failure will not cause a free IHS.

In addition to the critical loading shown in Table 5-29, the shattering of the spider fitting has been investigated. Analyzing the spider fitting as a single degree of freedom system, it was found that an impulse of 44 lb-sec will cause failure. Assuming that the aft dome shatters and that the impulse is transmitted directly to the spider, it was found that a yield of 10 percent causes failure of the spider. It is assumed that failure of the spider results in a free IHS.

TABLE 5-29. RTG ALLOWABLE LOADS COMPARED TO EXPLOSIVE OVERPRESSURE LOADS

	Allowable	Load at Yield Noted			
		1%	3%	5%	10%
RTG Dome (Collapse Pressure)	107 psi	198 psi	440 psi	800 psi	1480 psi
RTG Case (Collapse Pressure)	223 psi	48 psi	92 psi	135 psi	217 psi
RTG Case (Axial Compression)	102,000 #	60,200 #	86,500	168,000	252,000
Lug Bolt (Double Shear)	50,000	40,100	57,700	112,200	168,000

Table 5-30 shows the weight and velocity of typical Centaur components accelerated by the explosion. Because the velocity of the projectile is large, it is assumed that the projectiles reach the RTG before it has moved.

TABLE 5-30. CENTAUR PROJECTILE VELOCITY

Projectile	WT (LBS)	Velocity at Noted Yield			
		1% (FPS)	3% (FPS)	5% (FPS)	10% (FPS)
TLM	37.1	52	145	220	380
RMU	19.5	52	145	220	380
SED	25	42	112	172	300
INST	9.8	93	245	365	610
SKIN	.286	1310	2250	2850	3700

Table 5-31 shows the momentum (impulse) of the projectiles. Projectiles above and to the right of the heavy dotted line have sufficient momentum to cause failure of the spider and result in a free IHS.

TABLE 5-31. PROJECTILE MOMENTUM

Projectile Mass $\frac{\text{lbs-sec}^2}{\text{ft}}$	Momentum at Noted Yield			
	1% lbs-sec	3% lbs-sec	5% lbs-sec	10% lbs-sec
TLM 1.15	59.9	167.1	253.5	437.8
RMU 0.61	31.5	87.8	133.2	230.1
SEU 0.78	32.6	87.0	133.5	232.9
INST 0.30	28.3	74.6	111.1	185.7
SKIN 0.009	11.6	20.0	25.3	32.9

5.3.3.2.2 CBGS Case

A similar analysis was performed for the CBGS explosive overpressures. Table 5-32 whos the blast loading parameters on the RTG. Corresponding blast loading parameters on the spacecraft are shown in Table 5-33. The resulting impulse on the RTGs and the spacecraft are shown in Table 5-34 for each of four noted yields.

TABLE 5-32. RTG EXPLOSIVE OVERPRESSURES

	Yield							
	5%		10%		15%		20%	
	Base	Top	Base	Top	Base	Top	Base	Top
Reflected Pres. Pressure (psi)	1130	600	2080	1100	3000	1580	3800	2050
Stagnation Pressure (psi)	640	320	1200	620	1700	910	2180	1180
Static Over-Pressure (psi)	190	115	310	185	430	245	510	305
Drag Pressure (psi/cd)	125	80	197	122	268	160	315	192
Blast Wave Velocity (FPS)	3850	3100	5000	3800	5100	4400	6500	4800
Blast Duration (MSEC)	5.6	7.8	5.6	7.8	5.6	7.8	5.6	7.8

TABLE 5-33. SPACECRAFT EXPLOSIVE OVERPRESSURES

	Yield							
	5%		10%		15%		20%	
	Base	Top	Base	Top	Base	Top	Base	Top
Reflected Pres. Pressure (psi)	1440	460	2700	850	3900	1190	4950	1560
Stagnation Pressure (psi)	820	235	1560	430	2200	680	2700	900
Static Over-Pressure (psi)	230	94	380	150	530	197	640	295
Drag Pressure (psi/cd)	148	66	240	100	340	128	390	159
Blast Wave Velocity (FPS)	4500	2900	5600	3500	6600	4000	7000	4400
Blast Duration	5.4	9.0	5.4	9.0	5.4	9.0	5.4	9.0

TABLE 5-34. IMPULSIVE LOADING ON RTG AND SPACECRAFT

	Impulse at Noted Yield			
	5% (lb-sec)	10% (lb-sec)	15% (lb-sec)	20% (lb-sec)
RTG	225.6	360.9	492.5	535.5
Spacecraft				
Base	9774.9	19298	23547	28741
Top	-3275.5	-6298	-10406	-13934

The impulse to the RTGs causes the truss to fail for each of the noted yields. From the impulsive loading, the RTG and spacecraft velocities were calculated. These velocities are shown in Table 5-35.

TABLE 5-35. VELOCITIES AT NOTED YIELD

	Velocity at Yield			
	5% FPS	10% FPS	15% FPS	20% FPS
RTG	35.9	56.8	74.4	80.9
Spacecraft	49.4	98.9	100	117.2

Examination of the applied loads compared with the load-carrying capacity of the RTG shows:

1. For all yields in excess of 5 percent the impulsive loading on the spider causes failure resulting in a free IHS.

2. Axial load is of sufficient magnitude to cause lug bolts to shear and buckling of the RTG case for all yields.

3. External collapse pressure exceeds RTG load-carrying capacity for yields of 10 percent or greater.

5.3.3.3 Conclusions

Based on this analysis, it was found that the truss structure supporting the RTGs would fail resulting in the RTGs being separated from the spacecraft. While significant structural damage was predicted for all explosion yields considered, it was found that:

1. Overpressure from a CMB yield of 10 percent or greater could result in a free IHS.

2. Overpressure from a CBGS yield of 5 percent or greater could result in a free IHS.

3. Projectile impacts resulting from a 10 percent CBM yield can cause sufficient structural damage to allow a free IHS.

5.3.3.4 References

5.3.3-1. Multi-hundred Watt Radioisotope Thermoelectric Generator Program, Bi-Monthly Progress Report - 1 May to 30 June 1974.

5.3.3-2. Explosive Shocks in Air: G. F. Kinney: Macmillan Company.

5.3.4 REENTRY ANALYSES

An analysis of the JPL case 4, powered reentry, was performed. Case 4 is a shallow angle powered reentry of the Centaur vehicle with motor burning; TE-364-4 solid motor and spacecraft in the pre-injection configuration. (See Figure 5-39.) The initial conditions at 400,000 feet are V_e = 27kfps, φ_e = -5, and 0^o angle of attack. It should be noted that orientation of the RTGs to the flow is end-on. During the early part of the reentry, the RTG stack is shielded by the antenna. But, as the antenna melts, the end of the array is exposed to the flow. JPL's analysis of the RTG response showed the hottest segment of the dome to melt at about 66 secs. and individual RTG release at 68 secs. However, radiation was not included in the dome melt calculation. The response was recalculated using JPL's heating rates and including radiation. At RTG release, the maximum dome temperature was about 2000^oF, below the melt temperature of 2340^oF. Even if the dome should melt, the IHS would not be exposed to the flow until the end enclosure mounting brackets melted. It was concluded that the IHS would not be exposed to the flow while the RTGs were still attached to the spacecraft. The RTG release conditions were:68 secs, 244kft, 30110 ft/sec (inertial) and -4.06^o (inertial). RTG breakup was calculated to occur at 78 secs. The release conditions for the IHS were:223kft, 27,920 fps relative velocity and -4.06^o relative path angle. The initial IHS temperatures were assumed to be operational. Material properties and other assumptions were the same as in the previous three cases.

The DYNMAS, ABTON, and THTDA computer codes were used to obtain the trajectory, heating rate and temperature response, respectively: Figures 5-40 through 5-42. The stagnation point temperature histories for the sleeve and aeroshell are presented in Figure 5-42. Figure 5-43 shows the stagnation point recession history for the sleeve which does not burn through. The PICS temperature histories are presented in Figure 5-44. Nodes 103, 128, 148 and 198 from the "Keystone" thermal model are plotted. Node 103 represents the maximum PICS temperature during reentry and Nodes 128, 148 and 198 are approximately equal to the average temperatures of the front, side and rear PICS respectively. The highest temperature experienced by the PICS is 1427^oC (2600^oF), well below the 2215^oC (4020^oF) C/Ir eutectic. At impact, the average PICS temperatures are in the 1316^o-1427^oC (2400^oF - 2600^oF) range.

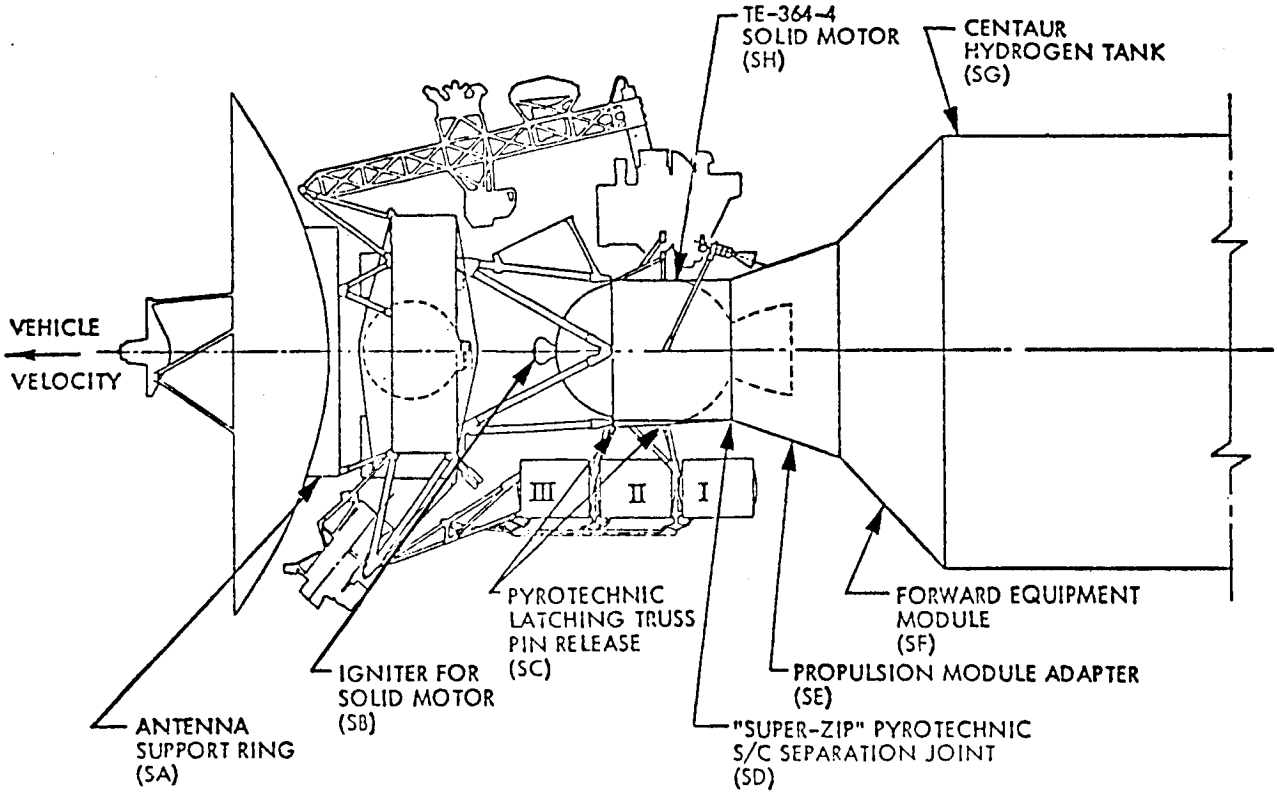

Figure 5-39. Spacecraft Configuration Pre-Injection Configuration

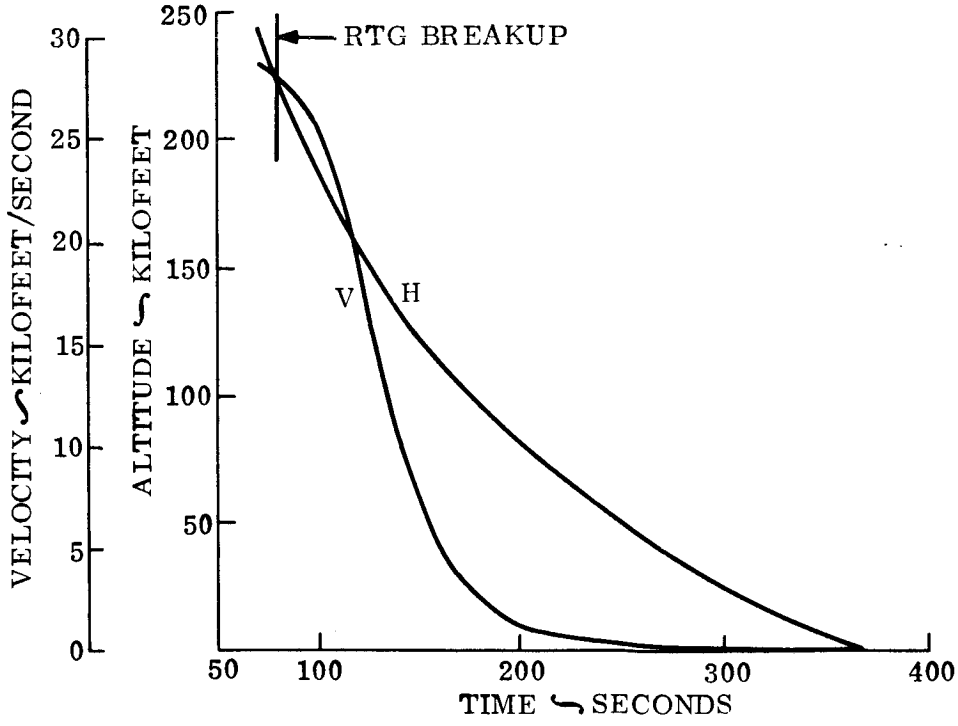

Figure 5-40. Case 4 Altitude and Velocity History

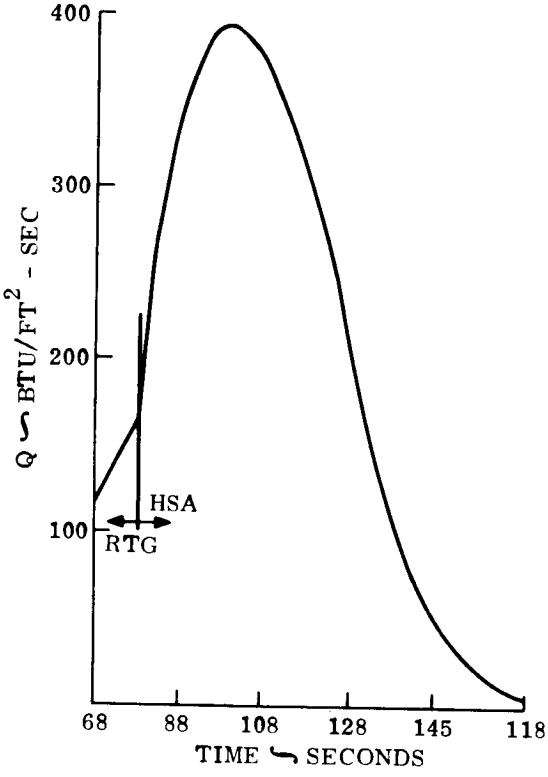

Figure 5-41. Case 4 Heating Rates

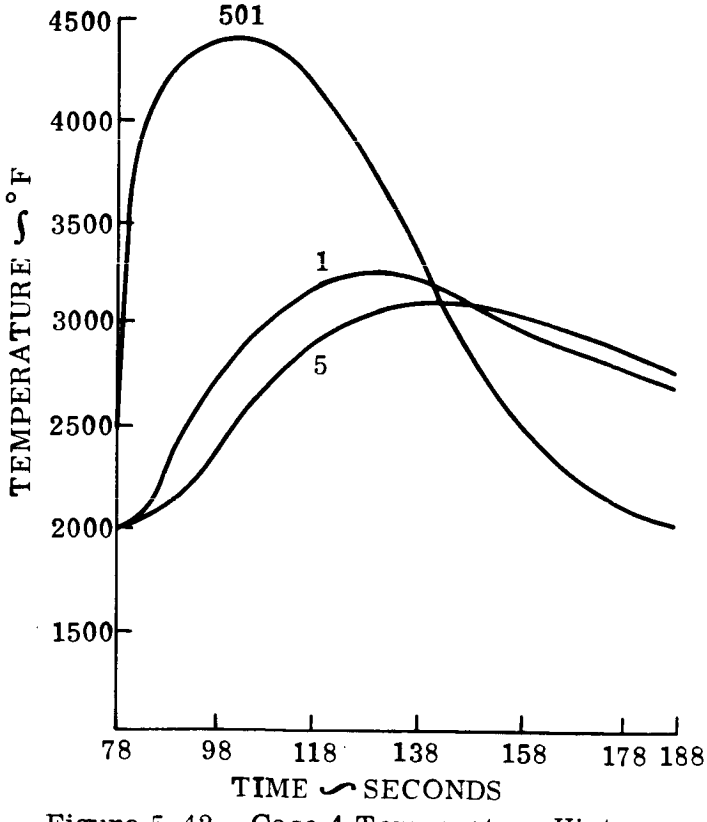

Figure 5-42. Case 4 Temperature History

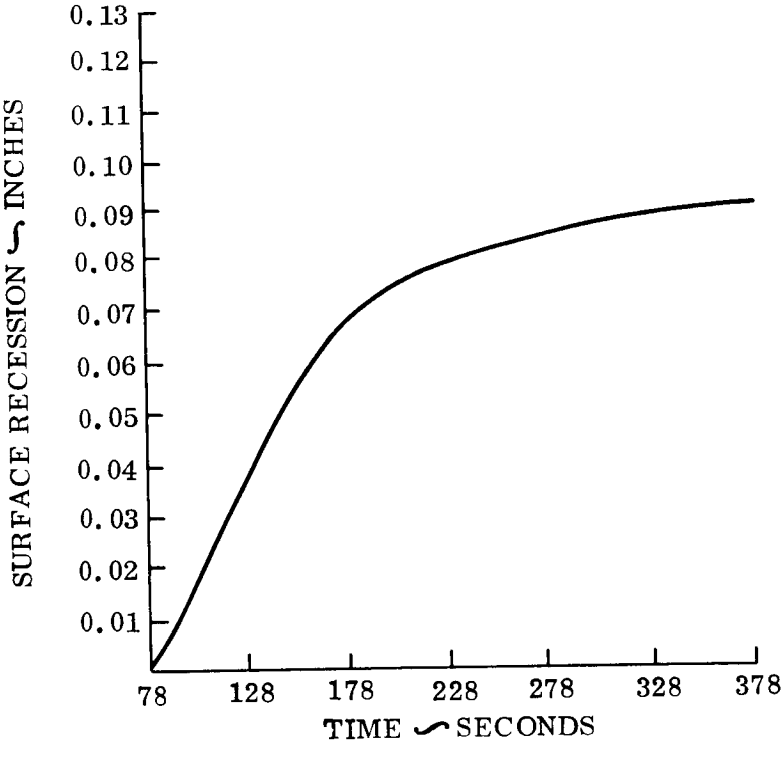

Figure 5-43. Case 4 Stagnation Points Surface Recession

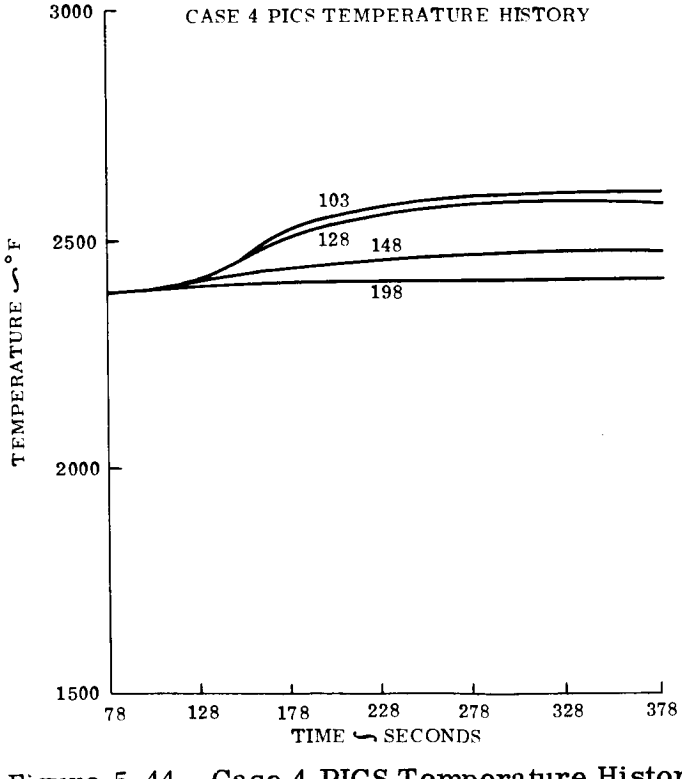

Figure 5-44. Case 4 PICS Temperature History

The aeroshell thermal stress analysis was conducted at the time of maximum radial temperature gradient, 103 seconds. The complete temperature map from the thermal model is shown in Table 5-36. Air loads for Case 4 are quite small and were neglected. The margin of safety for the aeroshell is 6.65. The ablation sleeve thermal stress analysis was also determined at the time of maximum radial gradient, which was 83 seconds. The temperature matrix is also shown in Table 5-37. The margin of safety was calculated to be 3.38. Since Case 4 is a low stress profile, the sleeve margin is not critical. Analyses conducted on the LES 8/9 program showed that an unsleeved aeroshell can survive shallow angle reentries.

5.3.5 ANALYSIS OF THE Q-2R HEAT SOURCE FAILURE

An investigation was conducted to determine the cause of the Q-2R/IHS internal damage. The damage had been discovered when during disassembly of the Q-2 RTG, in preparation for sending the Q-2R/IHS to Mound Laboratory for post-qualification evaluation, it was determined that the plug in the forward aeroshell end cap bottomed out below the normal seating position. Subsequent radiographic examination at Mound Laboratory revealed that the internal preload had been lost, the tie bolts were broken and the aft retainer tray had been displaced (see also Para. 5.2.2.7).

The Q-2R/RTG had been subjected to the shock and vibration test sequence shown in Tables 5-38 through 5-40. The vibration input levels are shown in Figure 5-45. The Q-2 RTG instrumentation included externally mounted accelerometers to measure the responses of the RTG case and internally mounted strain gages to measure the responses of the heat source.

Examination of the strain gage data revealed an unexpected change in the response of the heat source during the Y axis (longitudinal) qualification level sinusoidal sweep with the RTG mounted in the inverted position. Figure 5-46 shows the response of the heat source for three levels of input; 1/2 FA level, FA level and TA level. With increased input levels a resonant condition appeared to develop in the 40 Hz to 60 Hz region. At the TA level the response increased with frequency up to 44 Hz and then dropped suddenly indicating a non-linearity or a structural change which could be attributed to the internal preload being

TABLE 5-36. AEROSHELL TEMPERATURE MATRIX (AT 103 SECONDS) Z AXIS ~DEGREES

X Axis	0.0	21.0	42.5	66.4	90.0	118.6	151.5	180.0
3.28	2538	2711	2581	2289	2069	1987	1968	1978
3.41	2644	2777	2631	2321	2081	1986	1965	1973
3.535	2777	2882	2711	2366	2096	1984	1961	1968
3.595	2854	2952	2764	2395	2105	1983	1958	1965
$M.S. = \frac{8300}{1085} - 1 = 6.65$								

TABLE 5-37. SLEEVE TEMPERATURE MATRIX (AT 83 SECONDS)

X Axis	0.0	21.0	42.5	66.4	90.0	118.6	151.5	180.0
3.6125	3447	3327	3056	2575	2147	1903	1859	1850
3.6775	3755	3615	3277	2692	2182	1895	1854	1835
3.71	4035	3875	3477	2800	2216	1890	1833	1822
$M.S. = \frac{13200}{3013} - 1 = 3.38$								

TABLE 5-38. SHOCK AND VIBRATION

A C C E P T A N C E T E S T

Mounted on end opposite uniballs (inverted).

X-AXIS		
1/2 g (O-P) Sine Survey	2 Oct/Min	20-2000 HZ
1/2 Level Accept. Sine	2 Oct/Min	5-2000 HZ
Full Level Accept. Sine	7 Oct/Min Log.	5-2000-5 HZ
1/3 Level Accept. Random (EQ)	≦ 20 Sec.	
Full Level Accept. Random	1.0 Min	
Z-AXIS		
1/2g (O-P) Sine Survey	2 Oct/Min	20-2000 HZ
1/2 Level Accept. Sine	2 Oct/Min	5-2000 HZ
Full Level Accept. Sine	6 Oct/Min Log.	5-2000-5 HZ
1/3 Level Accept. Random (EQ)	≦ 20 Sec.	
Full Level Accept. Random	1.0 Min	
Y-AXIS		
1/2g (O-P) Sine Survey	2 Oct/Min	20-2000 HZ
1/2 Level Accept. Sine	2 Oct/Min	5-2000 HZ
Full Level Accept. Sine	6 Oct/Min	5-2000-5HZ
1/3 Level Accept. Random (EQ)	≦ 20 Sec.	
Full Level Accept. Random	1.0 Min	

TABLE 5-39. SHOCK AND VIBRATION

Q U A L I F I C A T I O N T E S T

Mounted on end opposite uniballs (inverted).

Y-AXIS		
Full Level Qual. Sine	2 Oct/Min	5-2000 HZ
1/3 Level Accept. Random (EQ)	≦ 20 Sec.	
Full Level Qual. Random	1.5 Min	
12g (O-P) Sine	30 Sec Dwell @ 25 HZ	
Z-AXIS		
1/2g (O-P) Sine Survey	2 Oct/Min	20-2000 HZ
Full Level Qual. Sine	2 Oct/Min	5-2000 HZ
1/3 Level Accept. Random (EQ)	≦ 20 Sec.	
Full Level Qual. Random		
X- AXIS		
1/2g)O-P) Sine Survey	2 Oct/Min	20-2000 HZ
Full Level Qual. Sine	2 Oct/Min	5-2000 HZ
1/3 Level Accept. Random (EQ)	≦ 20 Sec.	
Full Level Qual. Random	1.5 Min	

TABLE 5-40. SHOCK AND VIBRATION

Q U A L I F I C A T I O N T E S T

Mounted on uniballs (upright).

X-AXIS		
1/2g (O-P) Sine Survey	2 Oct/Min	20-2000 HZ
1/2 Level Accept. Sine	2 Oct/Min	2000-5 HZ
Full Level Qual. Sine	2 Oct/Min	2000-5 HZ
1/3 Level Accept. Random (EQ)	≦ 20 Sec.	
Full Level Qual. Random	1.5 Min.	
Qual. Shock	3 Shocks	
Z-AXIS		
1/2g (O-P) Sine Survey	2 Oct/MIN	20-2000 HZ
1/2 Level Accept. Sine	2 Oct/Min	2000-5 HZ
Full Level Qual. Sine	2 Oct/Min	2000-5 HZ
1/3 Level Accept. Random (EQ)	≦ 20 Sec.	
Full Level Qual. Random	1.5 Min.	
Qual. Shock	3 Shocks	
Y-AXIS		
1/2g (O-P) Sine Survey	2 Oct/Min	20-2000 HZ
1/2 Level Accept. Sine	2 Oct/Min	2000-5 HZ
Full Level Qual. Sine	2 Oct/Min	2000-5 HZ
1/3 Level Accept. Random (EQ)	≦ 20 Sec.	
Full Level Qual. Random	1.5 Min	
Qual. Shock	3 Shocks	
1/2g (O-P) Sine Survey	2 Oct/Min	20-2000 HZ

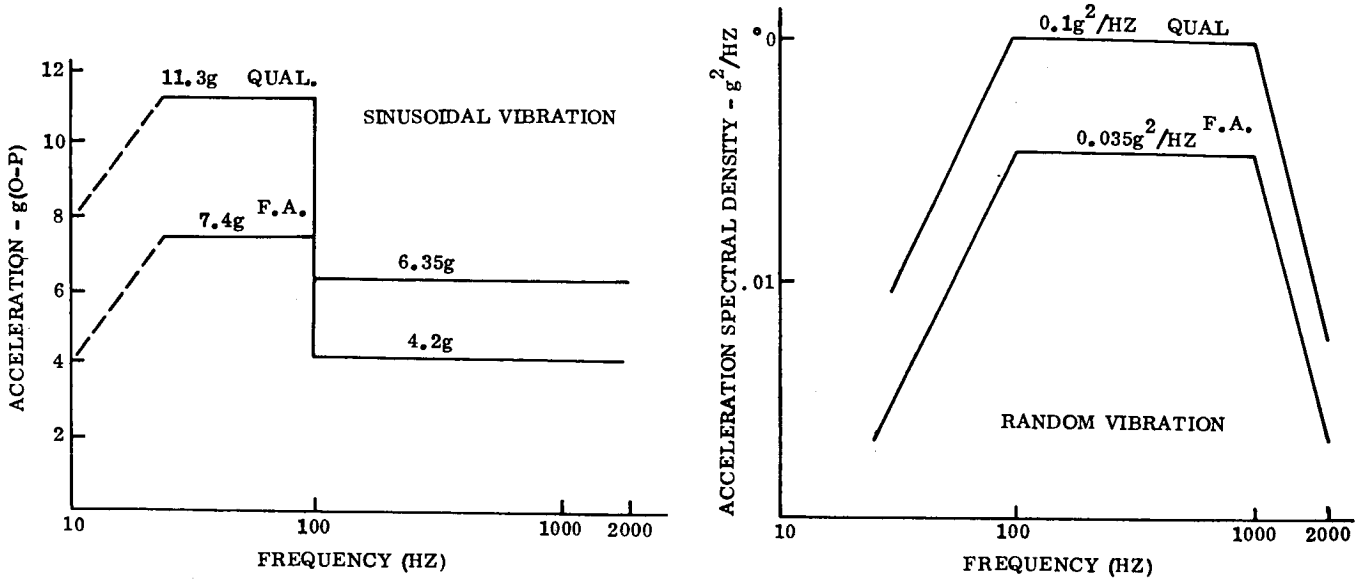

Figure 5-45. MJS RTG Vibration Test

exceeded, resulting in internal impacting, break away of the internal elements due to overcoming internal static friction, or structural damage leading to de-tuning of the resonance. Figure 5-47 shows the responses of the RTG case for the same test conditions, at the same time. No feedback of the heat source response into the case is indicated in the 40 Hz to 60 Hz region. An examination of the strain gage signal wave forms did not indicate any detectable structural change.

Examination of the strain gage data for the 12g Z-P (Zero-to-Peak) sinusoidal dwell revealed a major change in dynamic response of the heat source occurred during the dwell. Figure 5-48 shows the strain gage signal wave forms at the beginning of the dwell, 3/4 of the way through the dwell and at the end of the dwell. The initial wave form is primarily a 25 Hz sinusoidal wave with a minor amount of high frequency superimposed. Shortly after initiation of the dwell, the wave form began to degrade with the 25 Hz component reducing in level while a major increase in high frequency response, probably due to internal hammering, began to develop.

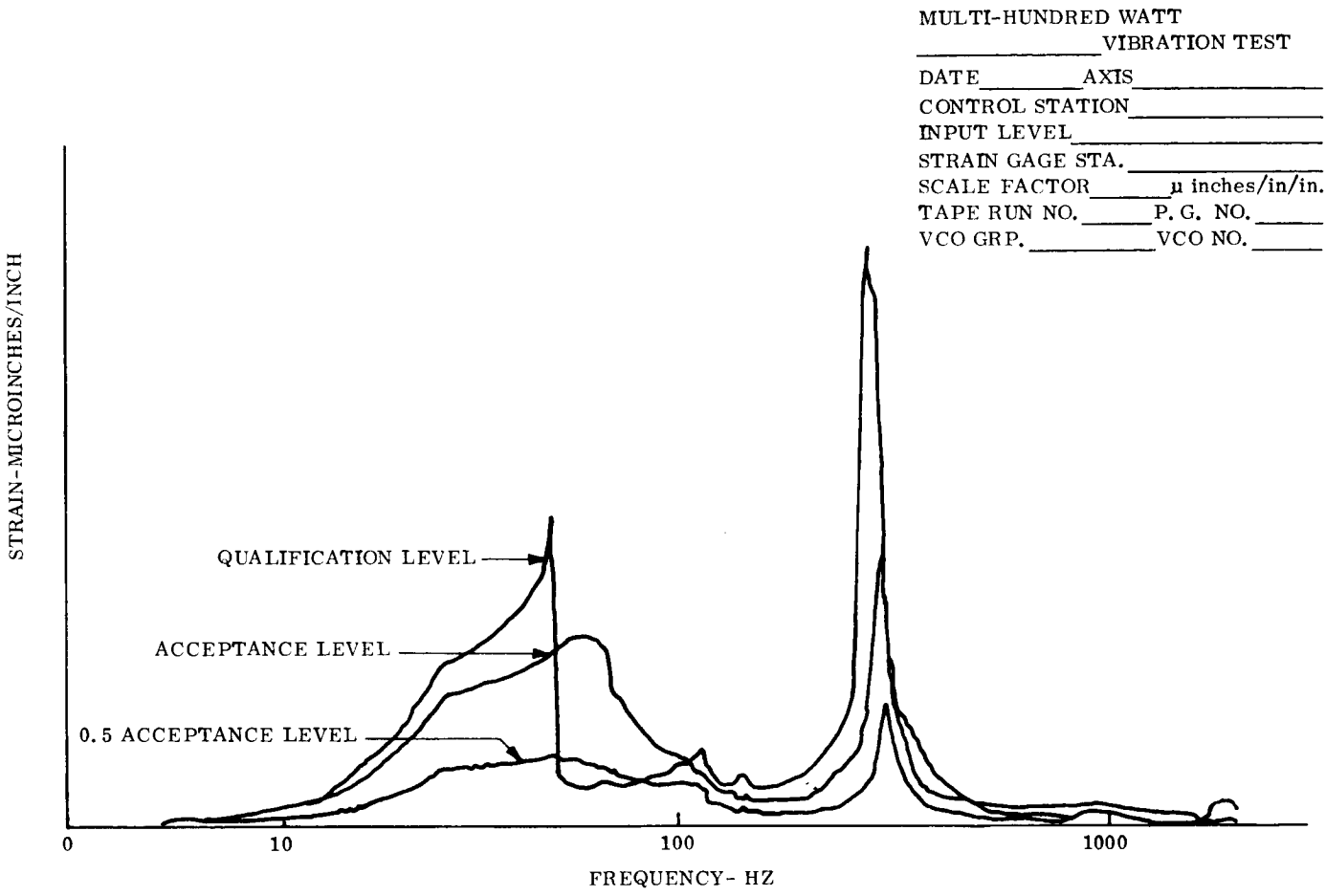

Figure 5-46. Heat Source Response

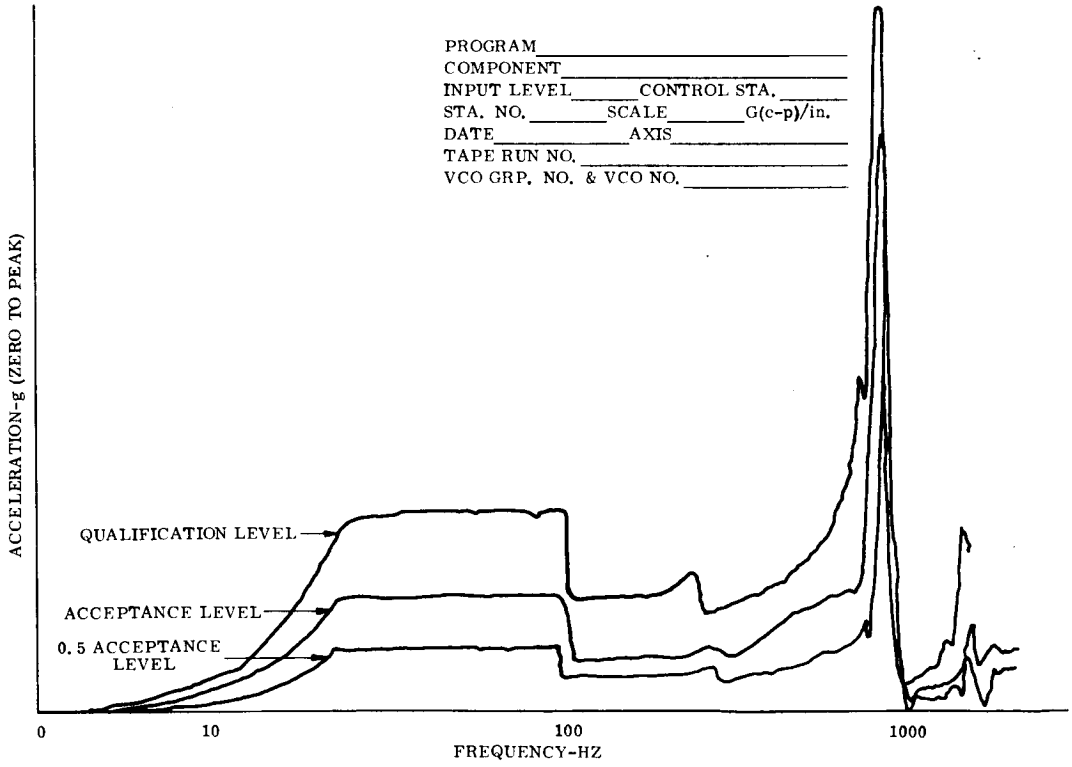

Figure 5-47. RTG Case Response

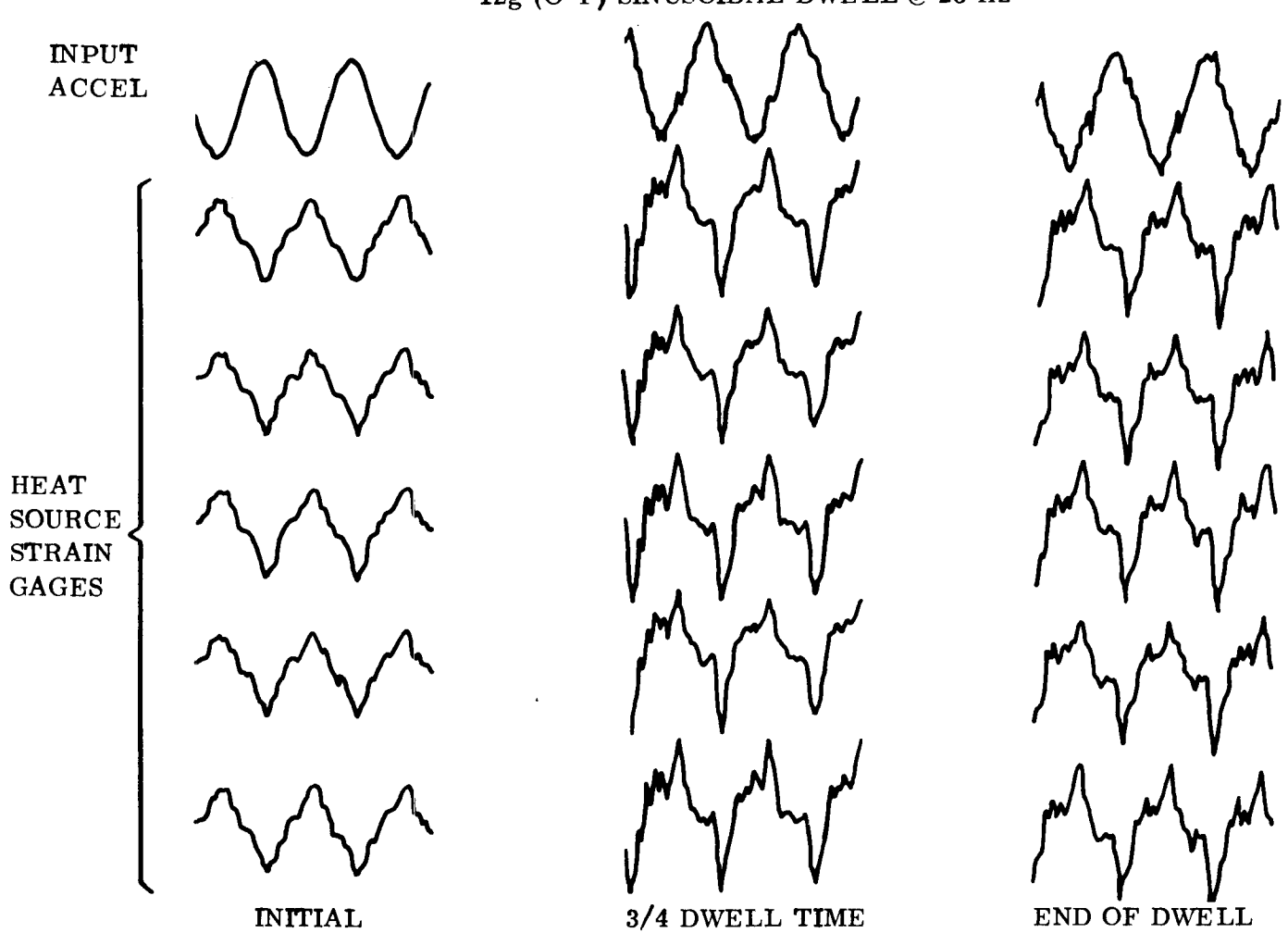

Figure 5-48. Strain Gage Signal Wave

Based on examination of these data, it is possible that some initial damage occurred during the Y axis qualification level sinusoidal sweep with the RTG mounted in the inverted position. However, the major damage developed during the sinusoidal dwell.

5.3.6 TESTS ON AFT TIE BOLT HEAD

As noted in Para. 5.2.2.7, the loss of internal preload in the Q-2R/IHS occurred due to failure of the aft retainer tray tie bolt head. This bolt was machined from Pyrocarb 508 with the laminations oriented in the longitudinal direction. Compression tests performed subsequent to failure of the Q-2R/IHS resulted in the following compression failure loads:

1. Test 1. Loaded against steel washer 810(a) pounds
2. Test 2. Loaded aginst laminated spring 1060(b) pounds
   a. In this test the head was rigidly supported. Failure occurred due to interlaminar shear.
   b. In this test the resilience of the spring assembly simulated the joint. Visual examinations revealed cracks parallel to laminations at 860 pounds. Lack of load capability did not occur until 1060 pounds had been applied.

An estimate was made of the peak dynamic loads acting on the tie bolt head based on the strain gage response which occurred at 44 Hz during the Y axis qualification level sinusoidal sweep. This load was combined with the internal preload to determine the peak load acting on the tie bolt head. Table 5-41 shows the results.

TABLE 5-41. LOAD ACTING ON AFT TRAY TIE BOLT HEAD

	Minimum	Maximum	Best Estimate
Preload	270 lb.	670 lb.	500 lb. *
Dynamic Load	323 lb.	323 lb.	323 lb.
Total Load	593 lb.	993 lb.	823 lb.

* Based on measured preload for F-10

Based on Table 5-41 and the load capability indicated by the static load tests, the following conclusions were arrived at:

1. Impacting due to the dynamic load exceeding the preload could have occurred if the installed preload was near the minimum limit. However, based on later measurements of installed preload, it is unlikely that the preload was low.

2. The load capability of the bolt head could have been exceeded without reaching the level required to cause impacting for a nominal strength bolt head if the preload was near the best estimate level.

5.3.7 ANALYSIS OF THE F-6 AND F-7 HEAT SOURCE FAILURE

As a result of finding that the tie bolt head of the Q-2R heat source had failed, a decision was made to radiograph the F-6 and F-7 heat source which had been subjected to the FA vibration test. These radiographs showed that the preload in both heat sources had been lost due to failure of the lower tray tie bolt heads as shown in Figure 5-49 and 5-50.

The F-6 and F-7 RTGs were not instrumented for measurement of the dynamic response of the heat sources. However, it was assumed that the responses were identical to those of the Q-2 heat source during flight acceptance testing.

The peak heat source response for the crucial mode occurred in the 44 to 47 Hz range during sinusoidal vibration along the longitudinal axis.

Based on the responses of the Q-2R heat source, the peak loads acting on the tie bolt head were calculated and the results are shown in Table 5-42.

Comparison of the dunamic loading with the range of preloads shown in Table 5-42 indicates that sufficient preload should have been present to prevent separation and impacting of the internal elements.

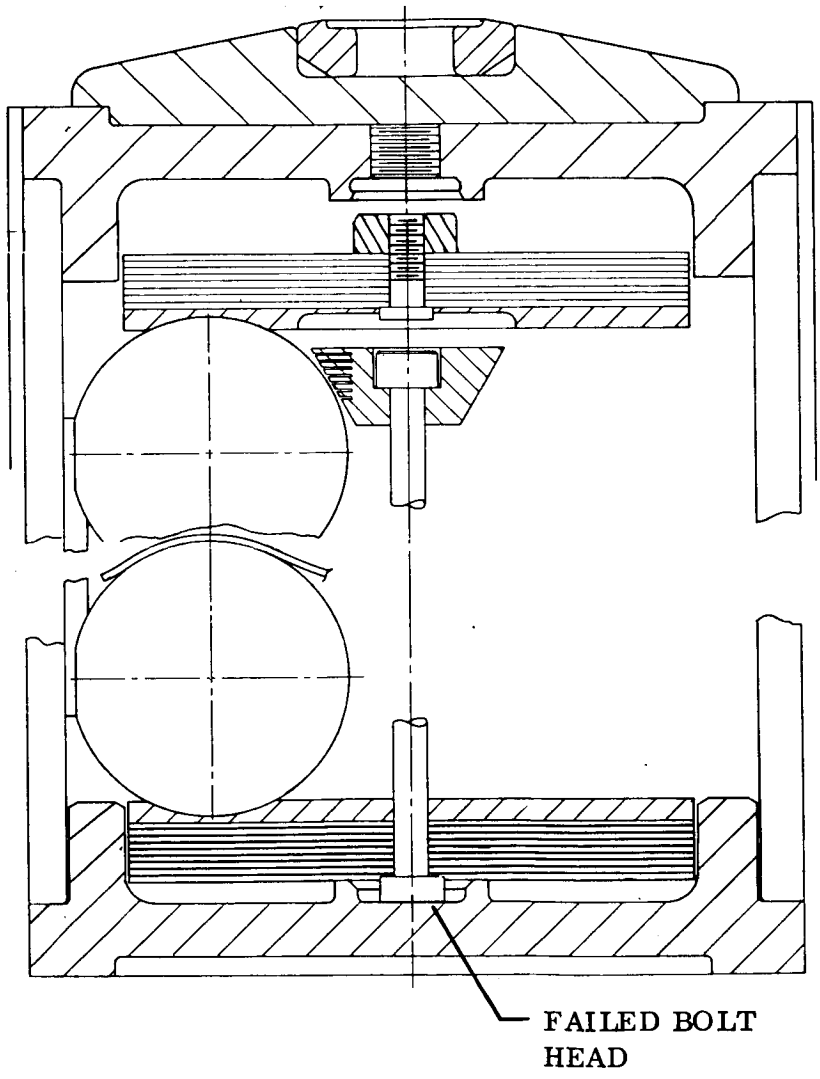

Figure 5-49. MHW-MJS F-6/IHS Sketch of Internal Loss of Pre Load (From Radiograph)

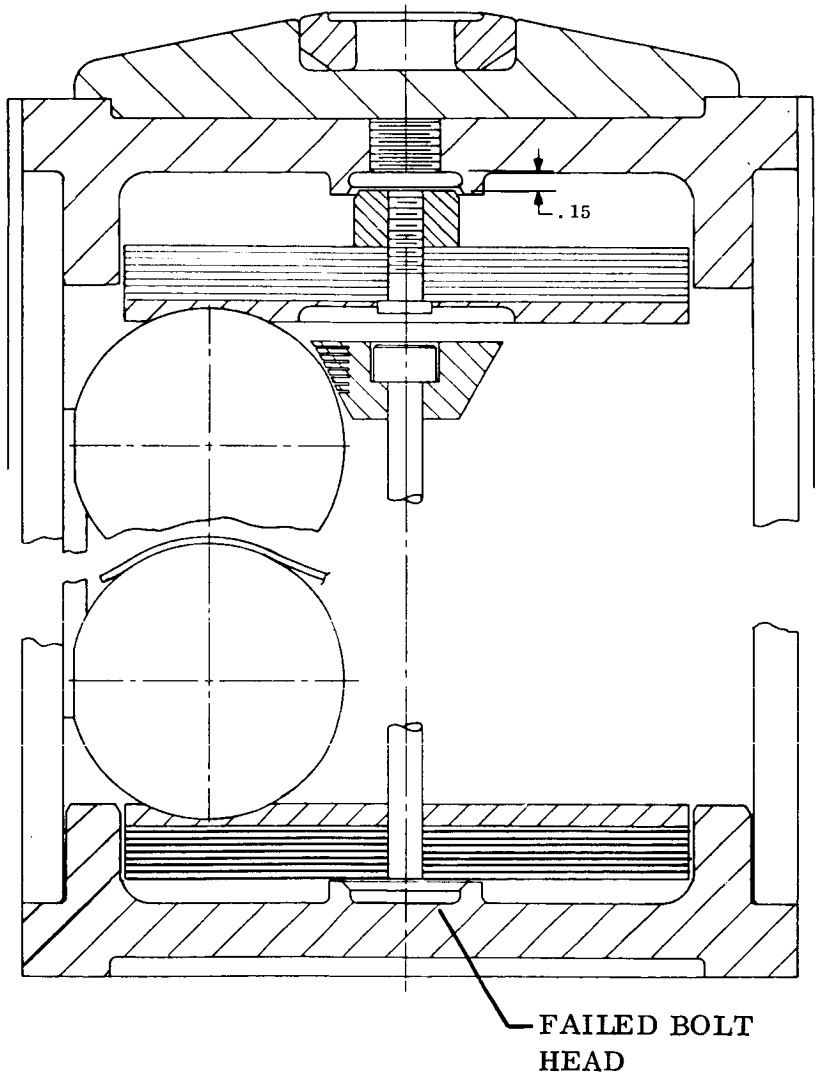

Figure 5-50. MHW-MJS F-7/IHS Sketch of Internal Loss of Pre Load (From Radiograph)

TABLE 5-42. LOADS ACTING ON AFT TRAY TIE BOLT HEAD

	Minimum	Maximum	F-6/ F-7 (Estimated)
Preload	270 lb.	670 lb.	500 lb.
Dynamic Load	236 lb.	236 lb.	236 lb.
Total Load	506 lb.	906 lb.	736 lb.

Based on the measured load capability, the tie bolt heads of F-6 and F-7 should not have failed during the flight acceptance test if the preload of F-10 was representative of the assembled preload of F-6 and F-7. However, a combination of high assembly loads and minimum strength of the tie bolt head have resulted in the failures found on F-6 and F-7 after vibration.

Examination of radiographs of the F-9 heat source as assembled and before test, revealed a damaged aft tray tie bolt head. As a result, the as-assembled radiographs (before shipment to GE) of the F-6 and F-7 heat sources were reexamined. The reexamination revealed that the F-6 tie bolt head have been damaged before vibration testing. It was concluded that the F-7 heat source failed as a result of vibration testing coupled with low bolt strength and high assembly preload.

5.3.8 VIBRATION TESTING OF THE MHW-MJS EXPLOSION TEST IHS

The test,for the evaluation of the effect on the IHS, due to the loss of preload caused by the failure of the aft crush up assembly bolt head, was performed as planned and a detailed description of the results was provided in the GE PIR # 1E40-MJS-5913. The test subjected the dummy IHS to the same acceptance test levels as those used for F-6 and F-7 IHS. Prior to assembling the 8-packs into the explosion test dummy, the FSAs were marked clearly to show their position relative to their retainer rings and to each other. The unit was photographed as each successive layer of spheres was assembled first into 8-packs and then into the dummy IHS aeroshell. The bottom aft 8-pack in the dummy unit was assembled initially using the standard Pyrocarb 508 bolt having the Pyrocarb bolt head which had failed in F-6, F-7 and F-9.

When the explosion test dummy IHS was examined after the vibration test, the bolt head was found to have broken, as expected, and individual FSAs were found to have moved within their retainer trays. No structural damage was suffered by the GISs in this test and likewise no structural damage was sustained by the aeroshell, the aeroshell end caps, the locking rings and the ablation sleeve. It was concluded from the results of this test that these same conditions would apply in the F-6 and F-7 IHSs which were subjected to the same shock and bibration inputs. None of the conditions found as a result of the tests would effect the operational performance of the F-6 and F-7 IHSs.

The tests also showed that no additional damage would occur to the internal structure of the F-6 and F-7 IHSs as a result of this exposure to the MJS launch environment, since these are now known to be significantly less severe than those to which the test unit and the F-6 and F-7 IHSs were subjected.

5.3.9 STATIC LOAD TEST OF THE IHS INTERNAL PRELOAD

This test was performed to verify the compression load capability of the IHS forward end cap when loaded through the redesigned preload bolt nut. The new design used POCO Polycrystalline graphite in place of the composite, Pyrocarb 508.

The test configuration (see Figure 5-51) consisted of the cap uniformly supported with the load applied to the nut. For the first series of tests the plug was installed in the cap. The load was applied by a hydraulic cylinder with the load calculated by reading the pressure and converting to load in pounds. Figure 5-52 shows the load versus deflection measurements taken during the first and second loading. In the first loading cycle the reflection was taken as zero when the ram of the cylinder appeared to be in contact with the nut. The load was increased in increments until the limit of the cylinder was reached (4938 pounds). The load was reduced to a pressure equivalent to 238 pounds and a deflection of 19 mils recorded. This was taken as the zero point for the second application of load. The load was again applied in increments to 4938 pounds and the deflection measured. The load was reduced to 238 pounds and the deflection returned to zero. The curve for the second loading was plotted with an initial deflection of 19 mils to compare with the first loading. Both load deflection curves are similar at higher loading.

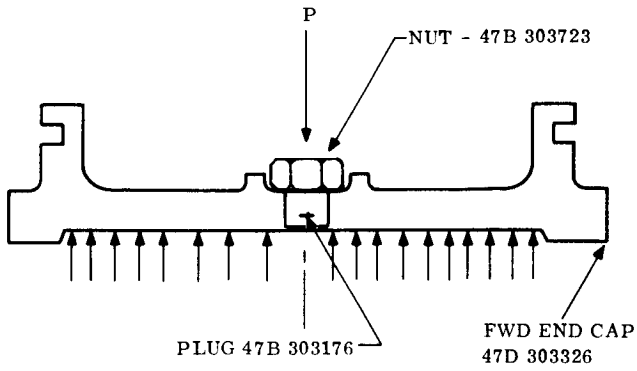

Figure 5-51. Test Configuration

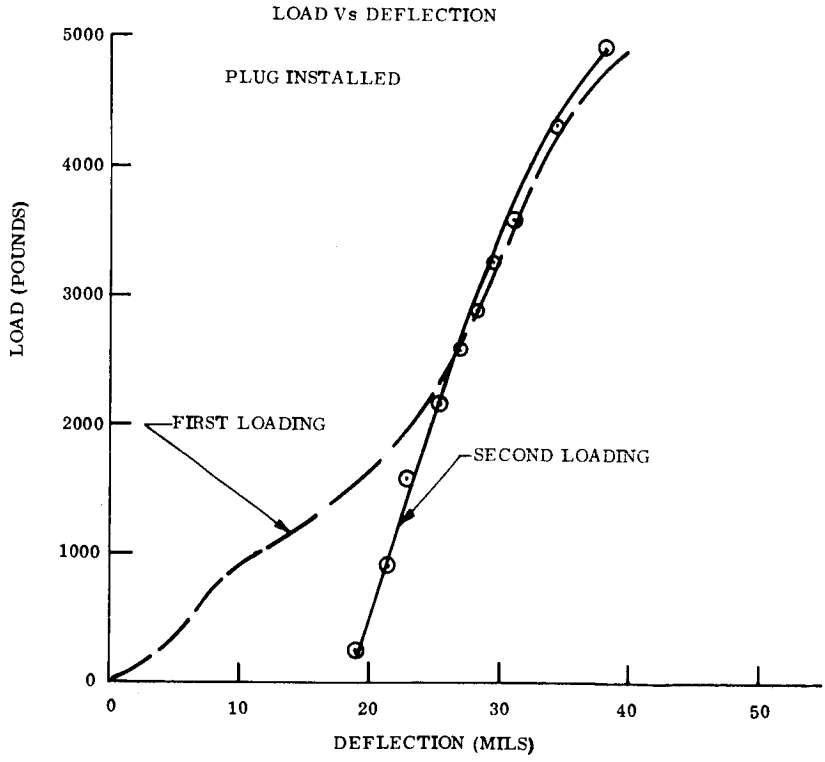

Figure 5-52. Forward End Cap Loaded in Compression Through Pre Load Nut

After loading this configuration twice to 4938 pounds without failure, the parts were examined visually for evidence of damage. No damage was found.

Based on the results of these tests, it was concluded that the assembly could withstand a load of 4938 pounds without failure.

5.3.10 POSSIBLE LONGITUDINAL OFFSET OF THE CENTER OF GRAVITY IN THE IHSs F-6 AND F-7

The IHSs in RTGs F-6 and F-7 were damaged due to the failure of the Aft Spring Assembly tie bolt head. The failure of this bolt head resulted in the loss of internal IHS preload and a maximum free play of 0.31 inch in the IHS internal components. The maximum offset in the center of gravity of the two damaged and three undamaged Isotope Heat Sources (IHS) was calculated.

The results of this study were based on the following assumptions:

1. Initially, the fuel spheres and the iridium shell were assumed to be located at the geometric center of each Fuel Sphere Assembly (FSA). To determine the maximum center of gravity offset, each fuel sphere and iridium shell was then assumed moved to the extreme longitudinal position resting against the inner surface of the Graphite Impact Shell (GIS).

2. For a damaged IHS, the total weight of the internal components was assumed to shift the entire distance from its unfailed position, so that the aft spring assembly rests on the boss of the aft end cap.

3. To account for the tolerance build up in the assembled IHS components, several different heights of nuts for the forward tie bolt were provided. Quality Control records showed that each assembled IHS used the same nut height. For this reason the total height of the assembled IHS components was assumed the same for each IHS.

After assembly of each IHS at Mound Laboratories, radiographic inspection was performed. From these x-ray photographs the deflection of the aft spring assembly was measured. Figure 5-53 shows an undamaged IHS and indicates the deflection measured on each heat source.

Figures 5-54 and 5-55 show the internal configuration of the F-6 and F-7 IHS with the aft tie bolt head failed. For each of these IHSs, it was assumed that the entire weight of the internal components were shifted aft by 0.31 inch.

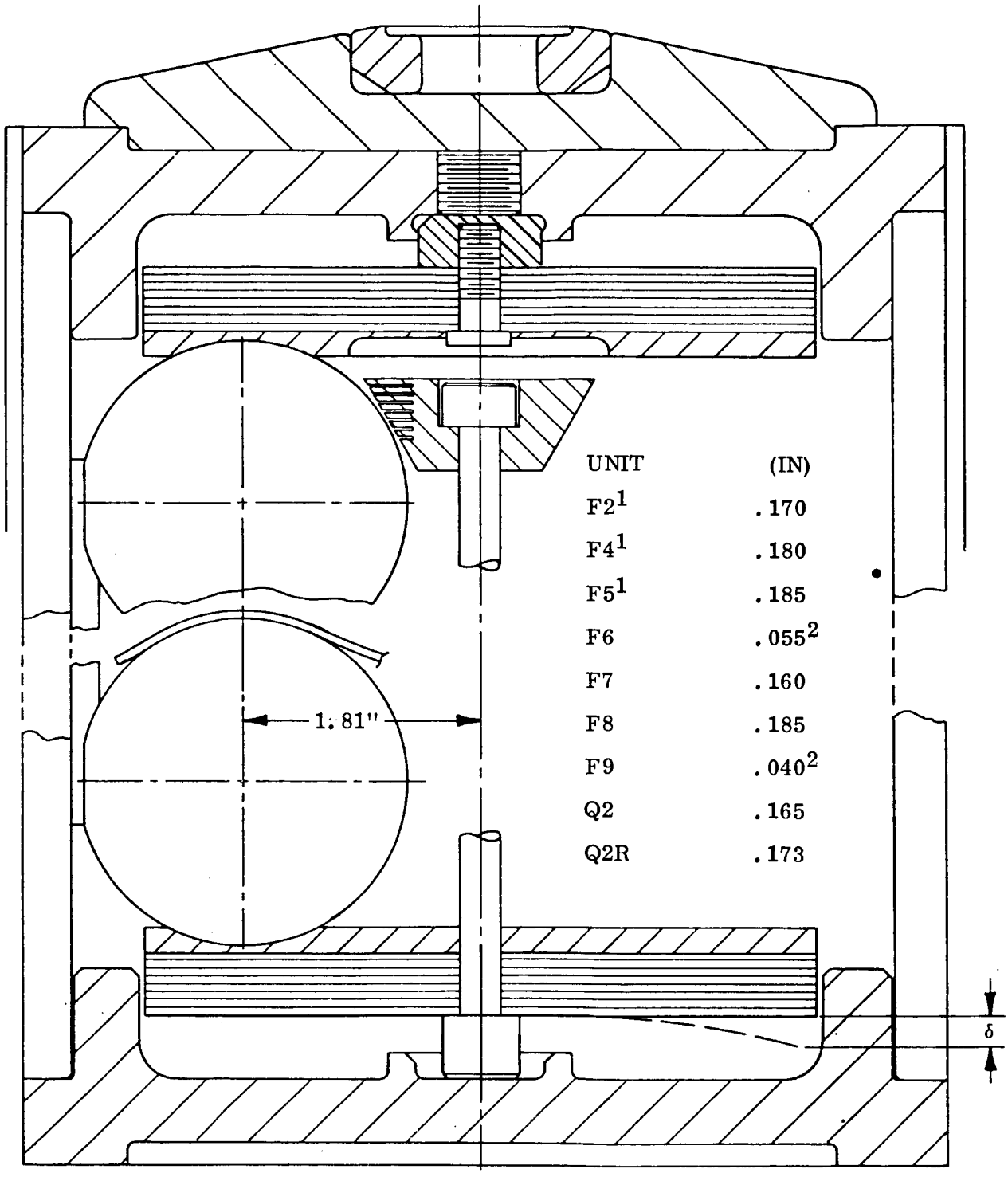

[1]LES 8/9 IHS.

[2]TIE BOLT HEAD FAILED (F9 TO BE REBUILT).

Figure 5-53. Undamaged IHS

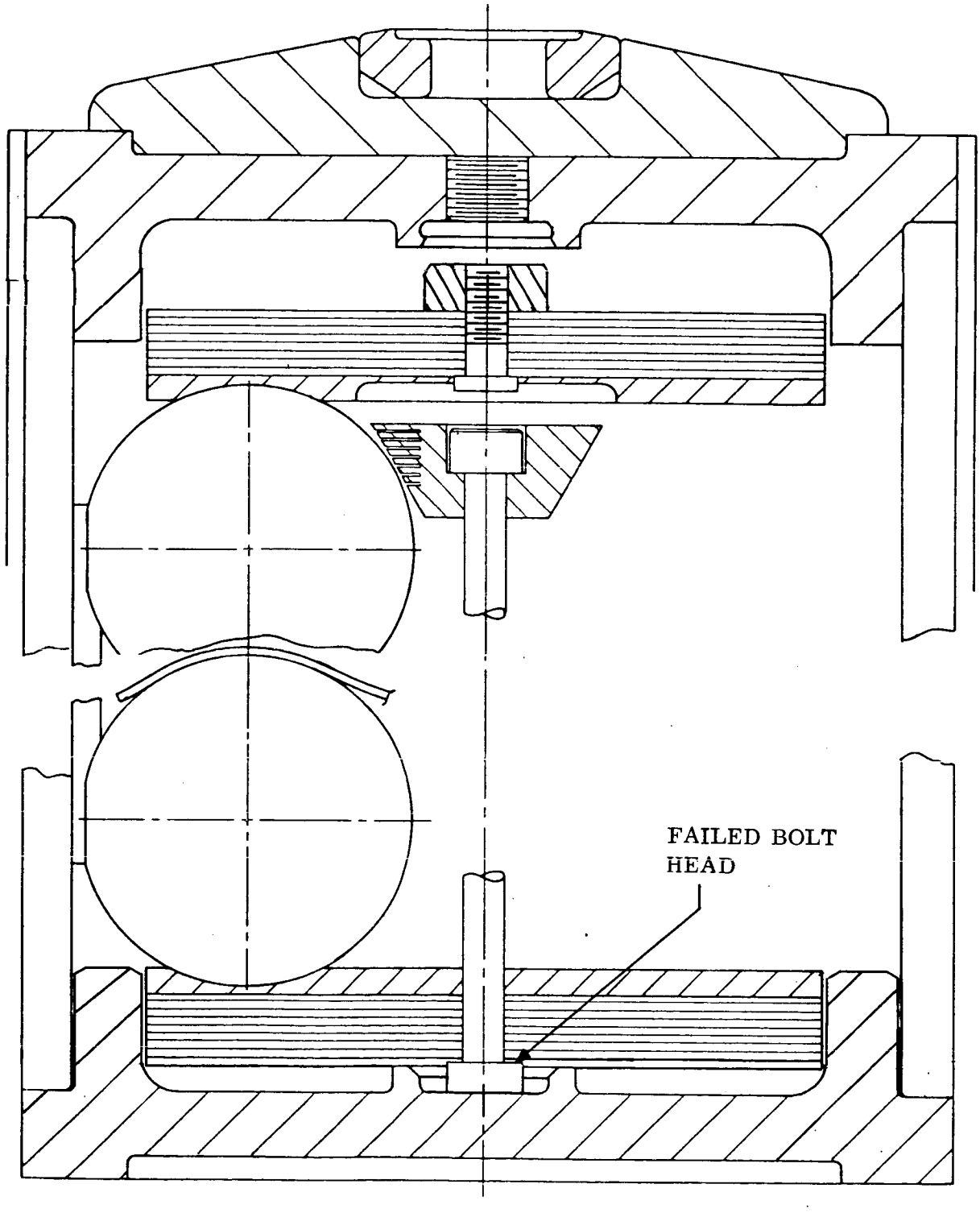

Figure 5-54. F-6 IHS

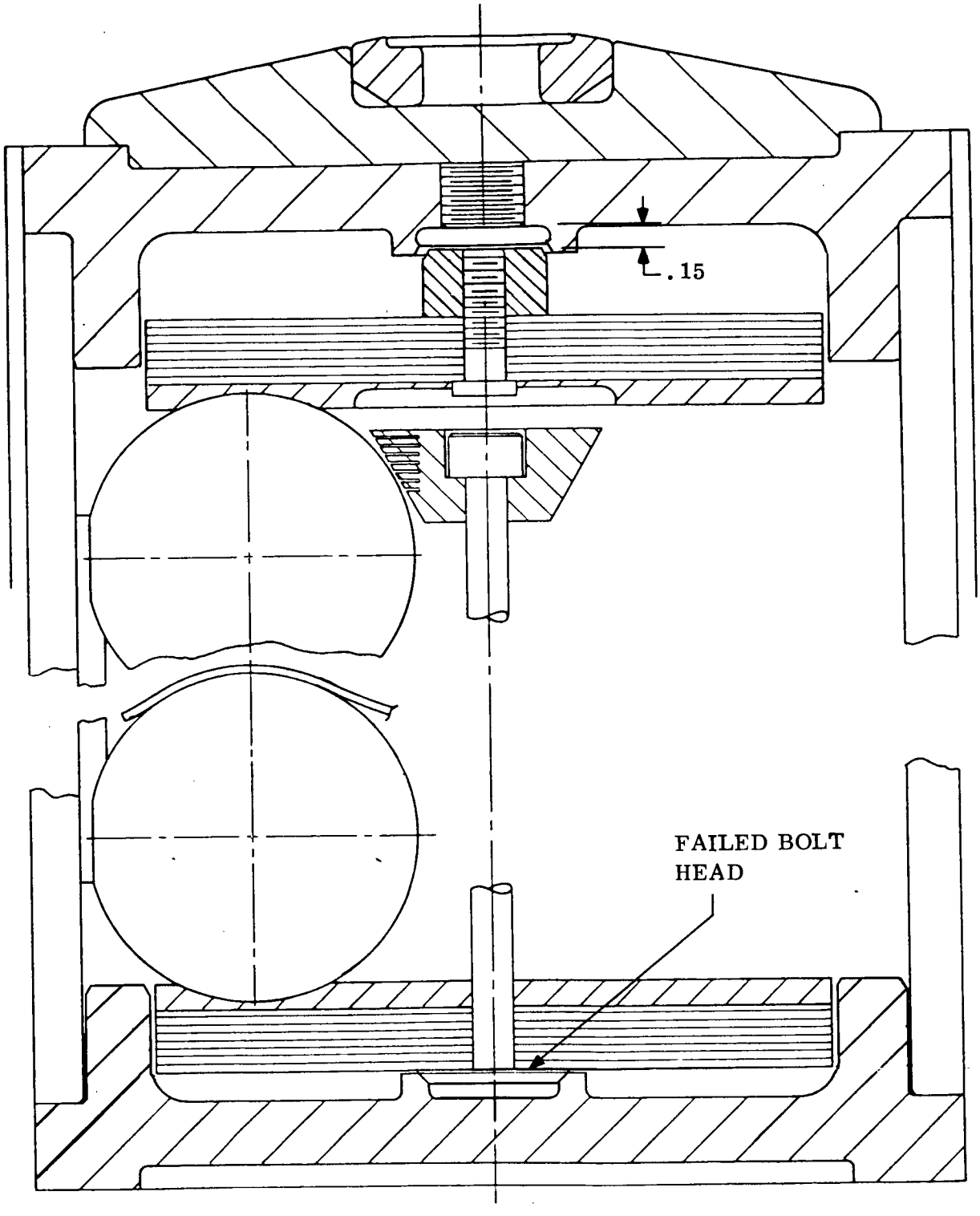

Figure 5-55. F-7 IHS

Table 5-43 shows the nominal center of gravity location referred to the geometric center of each of the noted IHSs and the maximum offset of the center of gravity caused by the extreme movement of the fuel spheres and iridium shells. In addition, Table 5-43 shows the maximum possible offset in the center of gravity of the F-6 and F-7 IHSs which could result due to the longitudinal movement caused by the aft tie bolt head failure. Combining the offset due to the bolt head failure with the maximum offset due to fuel sphere and iridium shell motion the maximum possible c.g. offset of the F-6 and F-7 was determined.

TABLE 5-43. MAXIMUM CENTER OF GRAVITY OFFSET FOR DAMAGE AND UNDAMAGED IHS'S

IHS No.	Nominal[1] CG Location	Maximum CG Offset Due to Fuel and Iridium Shell	Maximum CG Offset Due to Failed Tie Bolt Head	Total Limits of CG Offset	
				Fwd	Aft
F-6[2]	-0.032	± 0.022	+ 0.172	- 0.054	+ 0.162
F-7[2]	-0.042	± 0.022	+ 0.159	- 0.064	+ 0.139
F-8	-0.041	± 0.023	-------	- 0.064	- 0.018
F-9	-0.022	± 0.022	-------	- 0.044	0.0
F-10	-0.031	± 0.023	-------	- 0.054	- 0.008

[1]Center of Gravity referred to geometric center of the IHS. Positive sign indicates that the CG location is toward the aft end cap.

[2]Tie bolt head failed on F-6 and F-7 IHS.

It should be noted that the values shown in Table 5-43 for the CG offset are the maximum which could occur. The calculations and assumptions neglect spring back of the aft spring assembly and of the compliance pad. Also neglected was the relocation of the FSA which would reduce the amount of the CG offset.

5.3.11 THERMAL STRESS ANALYSIS - STEEP ANGLE - END-ON

A stress analysis of the HSA end cap was prepared, to estimate the time at which the end cap would fail during an end on reentry, with the JPL Case II steep angle trajectory.

5.3.11.1 HSA Thermal Stress Analysis Techniques

The stress analysis was performed using a General Electric finite element computer program called BIG2D. In this case, a two dimensional, axisymmetric analysis was performed to determine the stresses induced by thermal and aerodynamic loads.

The finite element model developed for these analysis includes the end cap and a four inch long segment of the aeroshell. Figure 5-56 shows the geometry of this model and indicates the conditions of restraint and the applied loads. The model has 401 nodal points and 328 elements. The air load was applied as annular loads at 23 nodal points on the cap. The temperature at each node was calculated and used as program input. Figures 5-57 through 5-60 show the finite element model with isotherms for each of the four cases analyzed. Table 5-44 shows the stagnation pressure, altitude, and time (measured from 400,000 feet) for these cases.

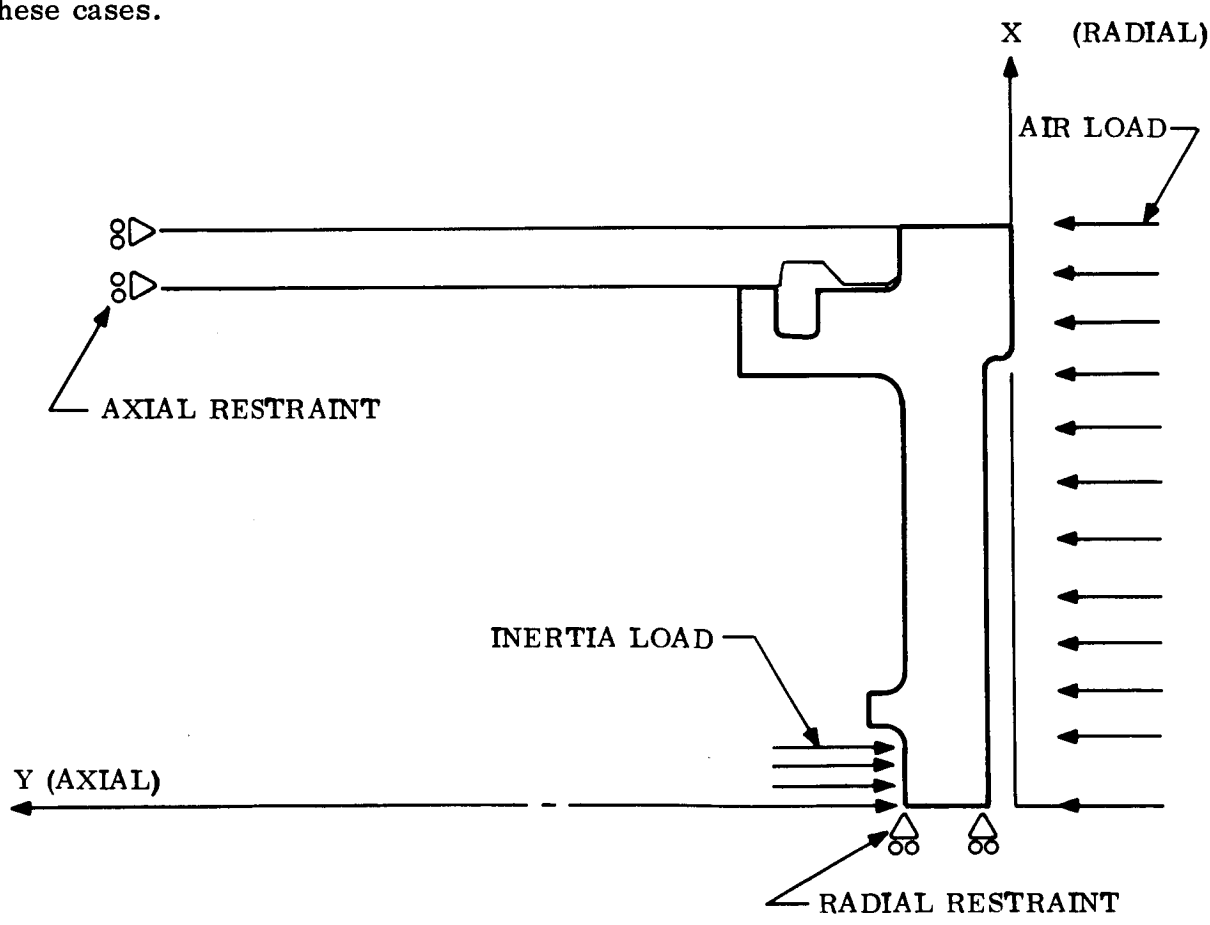

Figure 5-56. MJS End Cap and Aeroshell

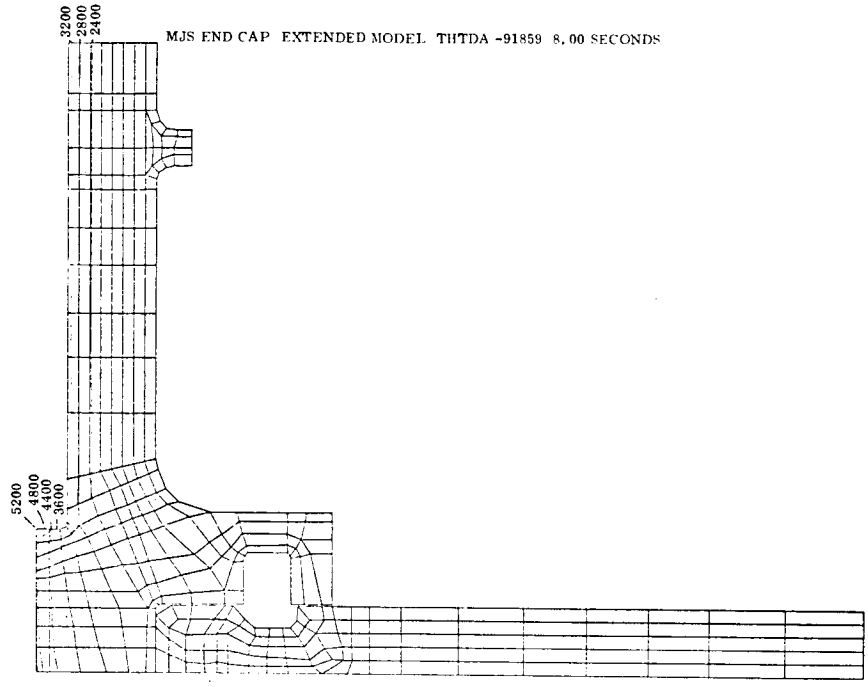

Figure 5-57. Finite Element Model With Isotherms in Increments of 400°F (Case 1)

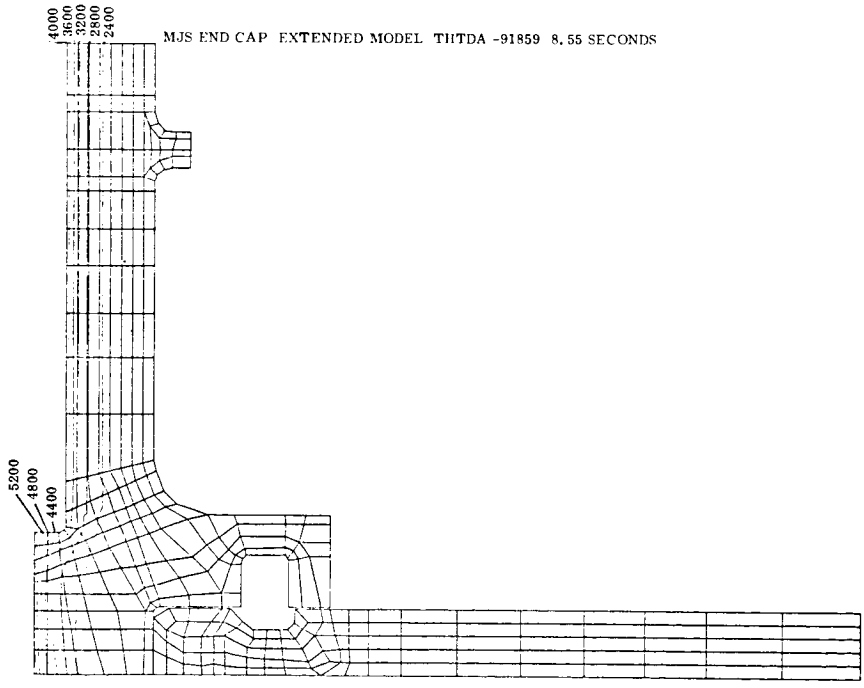

Figure 5-58. Finite Element Model With Isotherms in Increments of 400°F (Case 2)

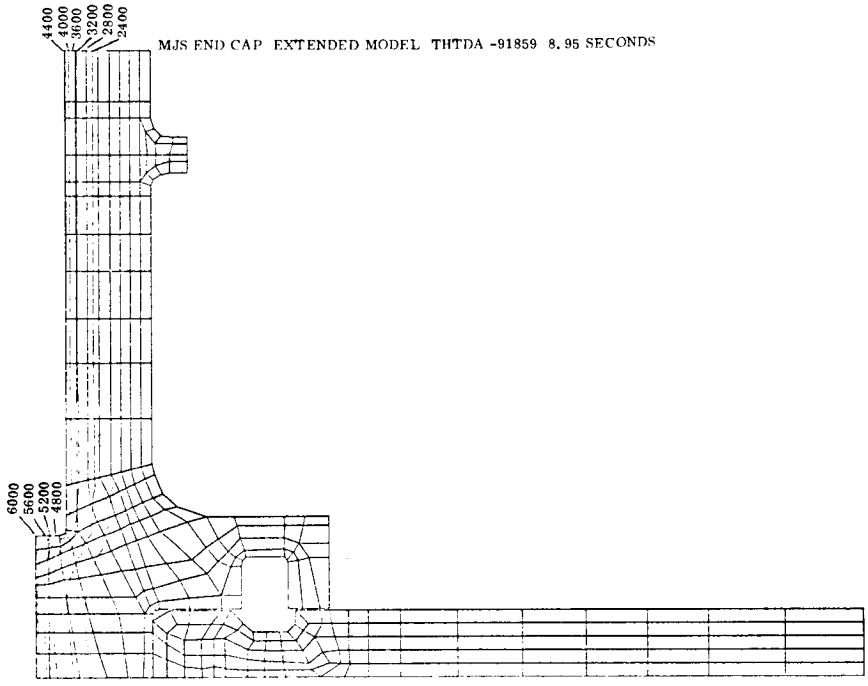

Figure 5-59. Finite Element Model With Isotherms in Increments of 400°F (Case 3)

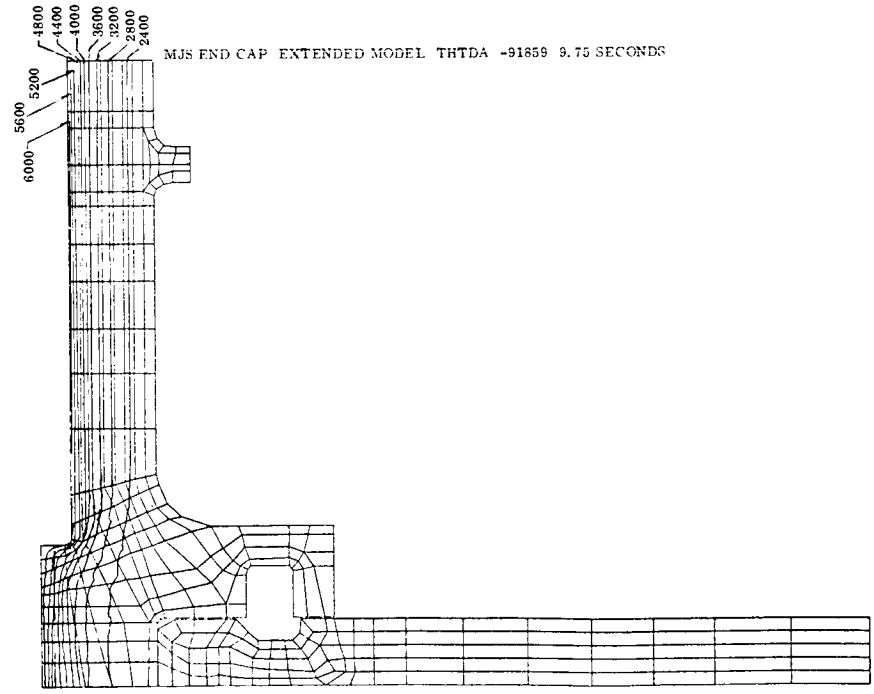

Figure 5-60. Finite Element Model With Isotherms in Increments of 400°F (Case 4)

TABLE 5-44. STAGNATION, ALTITUDE AND TIME

Case	Time (Seconds)	Altitude (feet)	Stagnation Pressure (lbs/ft^2)
I	8.0	192,800	822
II	8.55	179,000	1350
III	8.95	168,700	2000
IV	9.75	148,200	4250

The following assumptions were used in these analyses to predict the time at which the cap would fail:

1. The allowable tensile strength, at temperature, for the graphite end cap is 8500 psi.
2. Failure occurs when the maximum principal stress exceeds 8500 psi.
3. Inertial forces cause the aeroshell to bear directly on the end cap. In this configuration the clearance between the lock ring and the aeroshell is approximately 20 mils.

5.3.11.2 HSA Thermal Stress Analysis

The stress analyses were performed using the techniques and assumptions described in the previous section. The analytical results are the calculated stresses at the center of each element and the radial and axial displacement of each node.

Figure 5-61 identifies the local area in the cap which is subjected to the highest tensile stress. The finite element solution calculates the stresses only at the center of the element. To obtain the maximum tensile stress, the stresses at the element centers were plotted across the critical section and extrapolated to the free edge. As shown from the figure, the calculated axial tensile stress exceeds the allowable tensile stress at a time of 9.75 seconds. Consistent with the assumptions, this constitutes failure. The predicted mode of failure is the fracture of the material at the base of the lock ring groove resulting in a complete separation of cap along line AA (see Figure 5-61).

After the initial failure the cap is still capable of sustaining load. Figure 5-62 shows the predicted area of the secondary failure. This failure results in a radial crack that is assumed to cause complete radial separation of the cap. This secondary failure occurs at approximately 10.4 seconds.

While either of these predicted failures could result in a complete fracture of the cap, it is difficult to postulate a failure sequence which will result in a probable release of the fuel spheres.

5.3.12 REENTRY ANALYSIS OF AEROSHELL CENTER SECTION

The critical condition for the aeroshell side-on reentry analysis is the JPL Case 2 at 12.9 seconds. The critical stress occurs at the inside surface of the center section in the hoop direction. Based on a conservative analysis, the magnitude of the combination of thermal and airload stresses was calculated as σ Hoop = 6949 psi. The margin of safety for POCO Graphite AXF-5Q at T = 2100°F was evaluated to be: MS = 0.15 using the specification allowable of 8000 psi. When based on minimum test properties of the MJS billet material this margin of safety was reevaluated to be MS = 0.10 based on stress and MS = 0.15 based on strain; see PIR-MJS-5946. Subsequent analysis performed with a three-dimension program of the SAP IV finite element computer program yielded about the same thermal hoop stress while the stress due to airloads was reduced. The combined hoop stress reduced to σ = 6186 psi and the margin of safety was evaluated to MS = 0.17 using an allowable for a 95 percent probability of F_U = 7214 psi derived from the MJS billet test data and adjusted for the effects of the biaxial stress field as discussed below.

5.3.12.1 Evaluation of the Margin of Safety

The maximum combined stress for the center section was found in the hoop direction to be σ Hoop = 6949 psi at an operating temperature of 2100°F at the inside surface.

This stress is compared with the specification value of POCO AXF-5Q at 2100°F of F_U = 8000 psi. The margin of safety is then:

$$MS = \frac{8000}{6949} - 1 = +0.15$$

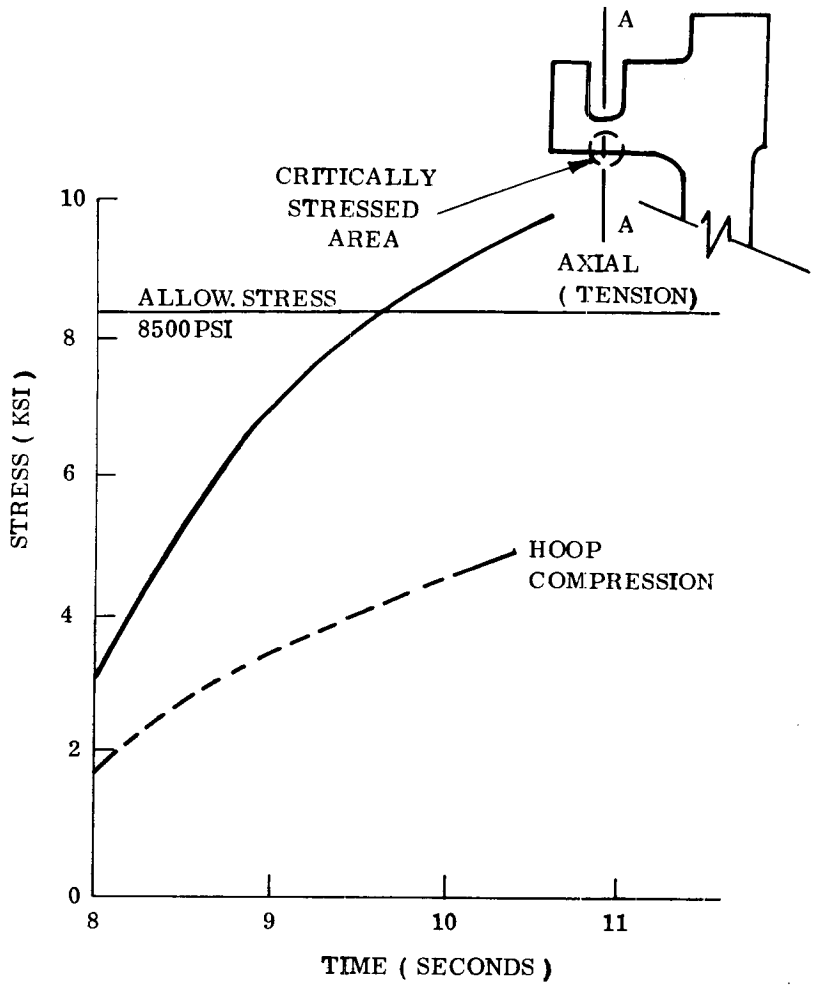

Figure 5-61. MJS End Cap Steep Angle JPL Case 2 Stress vs. Time from 400,000 Feet

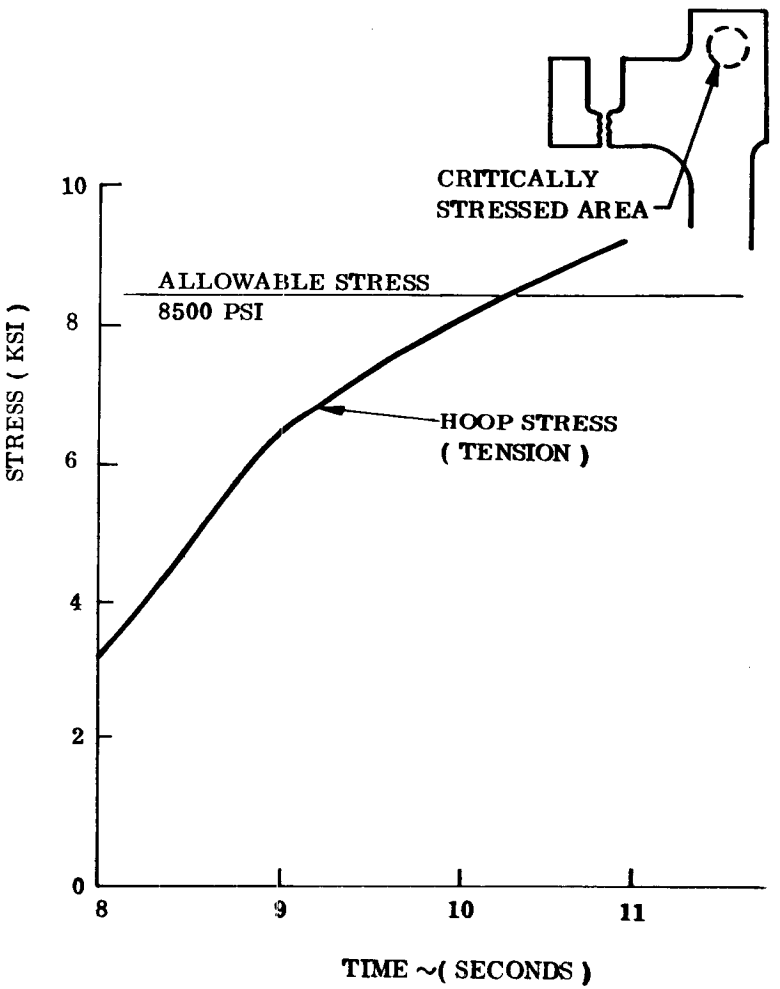

Figure 5-62. MJS End Cap Steep Angle JPL Case 2 Stress vs. Time from 400,000 Feet

To adjust this margin of safety for the individual test data from the MJS flight billets, a margin of safety on stress and strain was computed. The hoop stress calculated using specification properties was adjusted with the individual E-Module and a margin of safety for each test specimen calculated. The values are shown in Table 5-45 for stress and strain. The lowest margin of safety obtained is for billet BS-33 used in F9/IHS.

MS = 0.10 for stress

MS = 0.37 for strain

TABLE 5-45. MARGIN OF SAFETY BASED ON MJS BILLET DATA

Billet No.	Flight Unit	Specimen	F_{ULT}	Margin of Safety	
				Stress	Strain
JJ-685	F-6	2-A	11400	0.48	2.42
		5-A	10600	0.25	1.64
		7-B	11200	0.29	1.77
		10-A	10900	0.32	1.53
XX-100	F-7	2-A	10000	0.16	.73
		5-A	10900	0.24	1.09
		7-B	10200	0.15	.81
00-400	F-8	2-A	10900	0.33	1.78
		5-A	10200	0.16	.90
		11-A	10900	0.17	.96
BS-33	F-9	T-A	9640	0.21	.78
		T-5	8980	0.10	.37
		T-6	9940	0.20	.85
BS-37	F-10	T-4	9840	.22	.73
		T-5	10800	.32	1.42
		T-6	10100	.24	.98
BS-32*	F-11		10440		
			10114		
			10214		
BS-36*	F-12		9400		
			9340		
			9840		

*Note: The stress-strain curves for these two billets were not available, but the ultimate stress values indicate that the M.S. will be higher than the lowest one shown for F-9.

5.3.12.2 Additional Analyses on Safety Margins

To verify the results of the previous analysis, a three-dimensional analysis was performed using the SAP IV computer program with four elements across the wall thickness. The thermal and airload conditions were run separately and yielded the results as shown in Table 5-46. The margins of safety shown are based on a biaxial ultimate stress allowable for a 95 percent probability derived in the next paragraph. The stress distribution for the hoop stress, a condition where the thermal stress and the stress due to airloads are additive, and the temperature distribution across the wall at the stagnation line are shown in Figure 5-63.

Final stresses and margins of safety for the aeroshell center section at I.D. are shown below.

TABLE 5-46. THERMAL AND AIRLOAD RESULTS

Condition	Hoop Stress (psi)	Axial Stress (psi)
Thermal	+ 4747.0	+ 6052.0
Airload	+ 1439.0	- 216.0
Combined Stress	6186.0	5838.0
Allowable	7214.0	7214.0
Margin of Safety	0.17	0.24

The ultimate allowable of POCO AXF-5Q billets material for a biaxial tension stress field can be evaluated as follows.

Uniaxial tension tests at 3000^{o}F were performed with test specimen of the POCO AXF-5Q billets of the flight units F-6 - F-12. These results were checked for normalcy by using the Kolmogorov-Smirnov statistical method. The "F" test and students "t" checks were used to derive the means of the test series.

The following data was obtained:

Statistical means	$\bar{X}$ = 10422 psi
Standard derivation	S = 728 psi

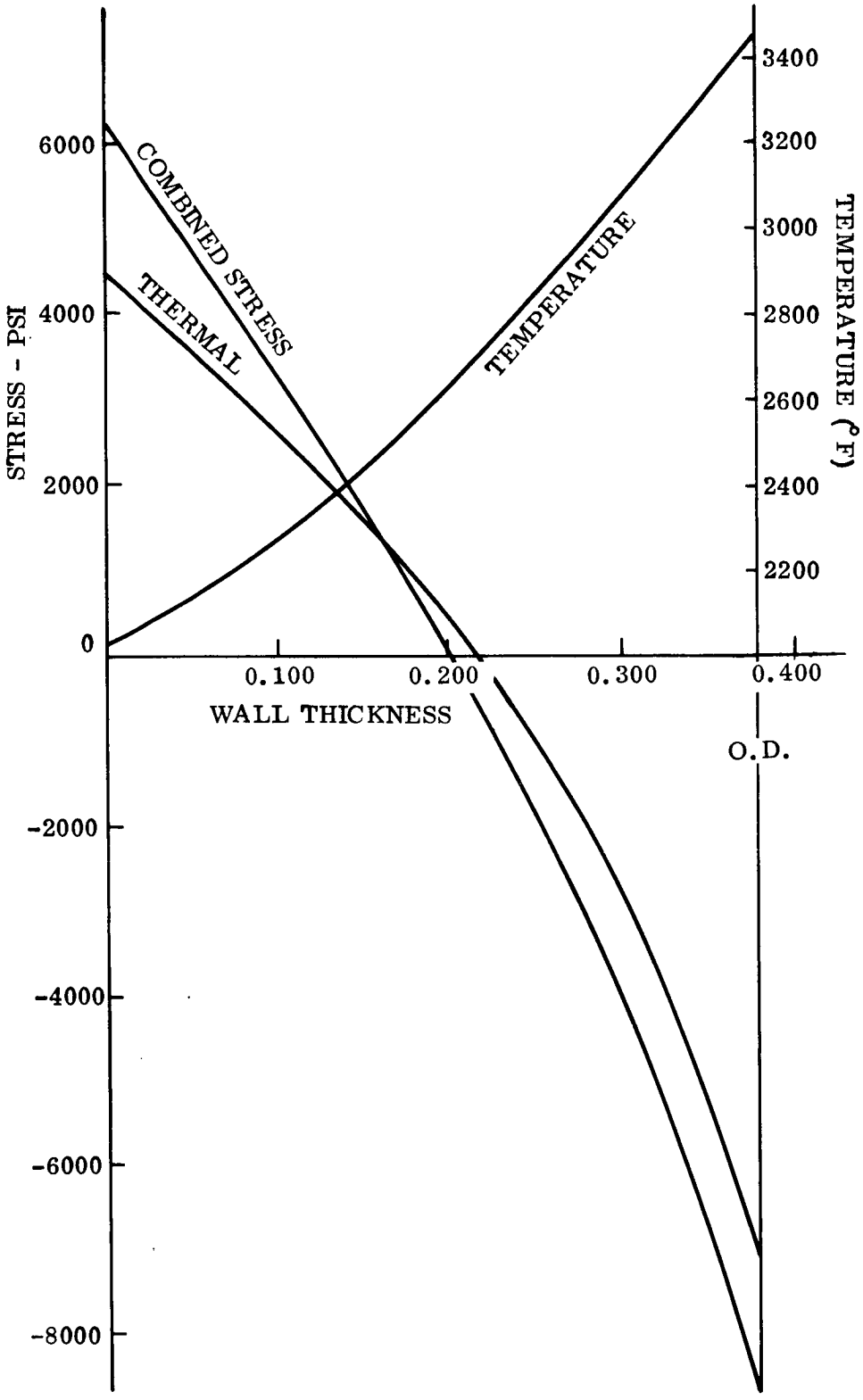

Figure 5-63. Hoop Stress and Temperature vs. Wall Thickness

The distribution curve was then added to the statistics of failure plot of Figure 5-64. For a 95% probability an ultimate stress of F_U = 9150 psi can be obtained from this plot. This value has to be adjusted for the operating temperature of 2100°F by using Figure E21 of USAR, Page E-32 which shows the ultimate stress as a function of temperature. This curve gives a value of F_U = 8100 psi at 3000°F and F_U = 7200 psi at 2100°F. The adjusted ultimate tension allowable is then:

$$F_U = 9150 \frac{7200}{8100} = 8133 \text{ psi}$$

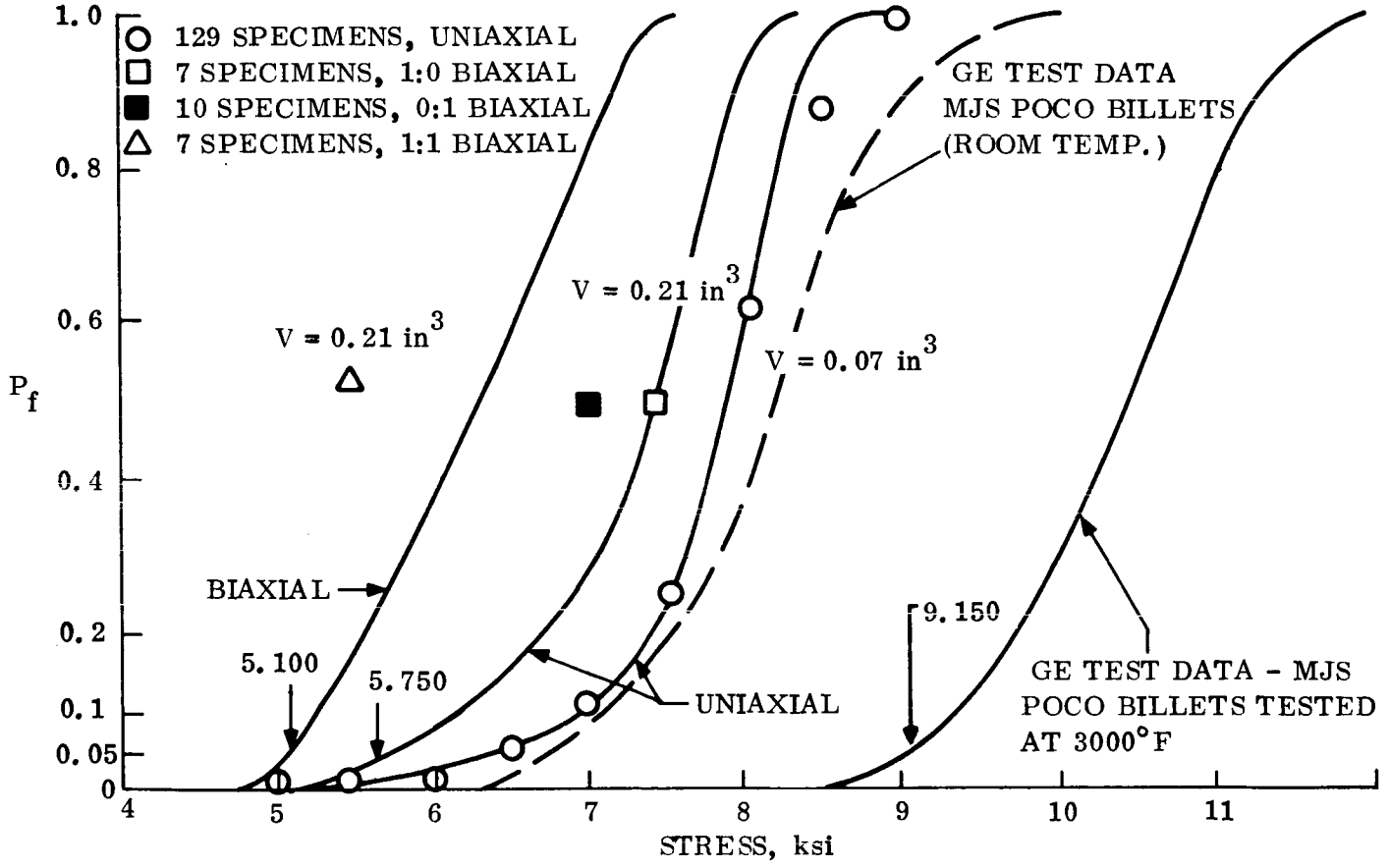

Figure 5-64. Statistics of Failure, AXF-5Q

A further adjustment of the uniaxial tension allowable can be made by considering the effects of a biaxial tension stress field. From Figure 4 the statistics of failure curve for POCO AXF-5Q, a value of F_U = 5750 psi can be picked for uniaxial tension and a value of F_U = 5100 psi can be taken for the biaxial stress for a 95% probability. The adjusted ultimate allowable for a biaxial stress field is then:

$$F_U = 8133 \frac{5100}{5750} = 7214 \text{ psi}$$

Additional analyses performed in response to Action Items from the USAR, are reviewed in Section 2 and details are presented in the FSAR (74SDS4602 Appendix E) and in the classified volume.

SECTION 6

HEAT SOURCE FABRICATION

All heat sources for the MJS Program were fabricated by ML/MRC and delivered to GE-NP-SD by mid January 1977.

6.1 REWORK OF Q-2/IHS AND F-9/IHS

6.1.1 REBUILDING AND DISASSEMBLY OF Q-2/IHS

The Q-2/IHS was completed on 6 August 1975. As noted in Section 5, Para. 5.2.2.4, the Q-2/IHS forward end cap was found to be fractured when the EPC for this unit was opened in the LAS on 16 January 1976. The unit was shipped to ML/MRC and was rebuilt, as Q-2R/IHS, using all new materials except for the FSAs. After qualification testing, it was found that the preload was lost. Disassembly of the unit was attemated at ML/MRC in June 1976 but internal contamination was too high to complete the work. A complete disassembly of Q-2R/IHS was carried out in February 1977 at the BML/CL hot laboratory. See Section 5, Para. 5.2.2.4 for details.

6.1.2 REWORK OF FLIGHT UNIT F-9

Section 5, Para. 5.2.2.7 details the loss-of-preload problem found in F-6, F-7, and F-9. F-6 and F-7 had been assembled in their respective RTGs, before the preload loss was discovered. Schedule constraints imposed by ML/MRC work-load prevented rework of F-6 and F-7 IHSs. By assembling the F-10/IHS in the F-9 converter, sufficient time was gained to permit rework of F-9 to incorporate the design fix. The MJS flight RTGs used the IHSs listed in Table 6-1.

TABLE 6-1. USE OF IHSs IN MJS RTGs

IHS No.	RTG No.
Q-2R	Q-2
F-6	F-6
F-7	F-7 (became spare)
F-8	F-8
F-9 (Reworked)	
F-10	F-9
F-11	F-10
F-12	F-11
F-9R	F-12

SECTION 7
CONVERTER DEVELOPMENT

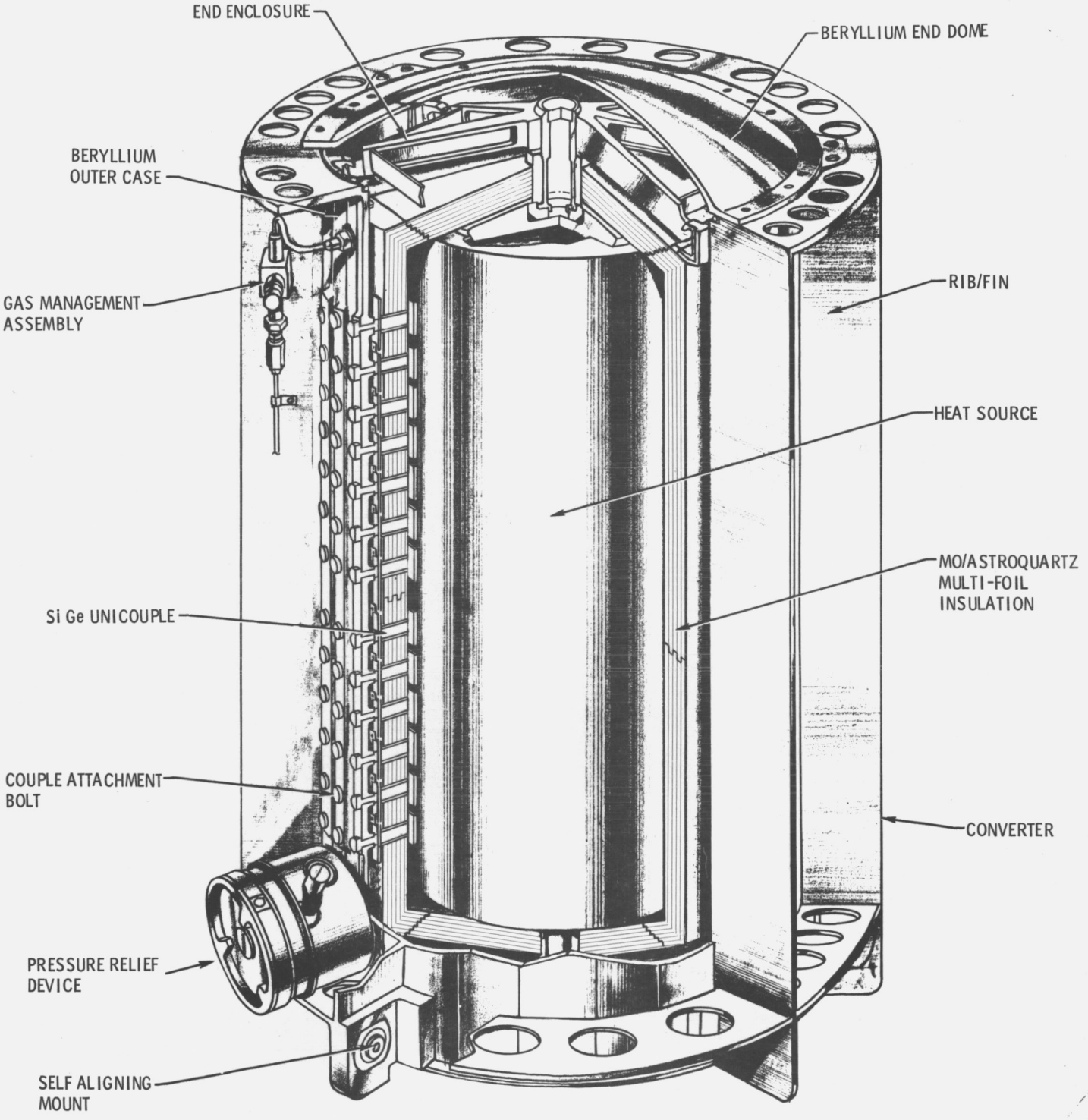

Figure 7-1. MHW Radioisotope Thermoelectric Generator

SECTION 7

CONVERTER DEVELOPMENT
(SEE FIGURE 7-1)

7.1 MATERIALS

The MJS RTG components are identified by part number and materials in Table 7.1-1.

7.1.1 MATERIALS TESTING AND DEVELOPMENT

7.1.1.1 Cold End Strap Plating

RCA experienced problems with the quality of the brazed joint between the electrical strap and the tungsten pad. Small fissures had opened up in the strap plating while bending the straps. A series of room temperature vibration tests was conducted to help verify the integrity of this lot of unicouples, some of which were included in the F-7 converter assembly. As a final verification test, a 14-couple module was assembled using unicouples having the most severe braze separations and subjected to room temperature FA vibration testing. No detectable damage was incurred.

The module was placed in a furnace and the thermal cycles shown in Figures 7.1-1 and 7.1-2 were initiated. Upon completion of the thermal cycles, the module was subjected to FA vibration along the longitudinal (Y) axis at temperature while being monitored for changes in electrical characteristics. The module was then disassembled and inspected for damage. Successful completion of this test series verified the integrity of the F-7 unicouples.

7.1.1.2 Cold End Bond Braze Anomaly

At RCA, there was some incidence of a Cold Shoe Bond Anomaly. The anomaly occurred after unicouple assembly braze at the cold-shoe-to-segment-bond. This bond was made at second bond assembly but was affected by unicouple assembly braze. The bond developed a crack on about two percent of the product. The cause of the unicouple cracking problem was determined and the affected unicouples were sufficiently characterized to permit recommended disposition and actions to be taken.

TABLE 7.1-1. RTG COMPONENT AND MATERIAL SUMMARY

PART NO.	COMPONENT	MATERIAL	MATERIAL FORM	MATERIAL SPECIFICATION	FINISH	FINISH FORM	FINISH SPECIFICATION
47D301619 P1	DOME, AFT	BERYLLIUM	HOT PRESSED BLOCK	NS 0060-07-08	THERMAL COATING	SPRAYED & SINTERED	RP5230-201
47D302382 P2	DOME, FWD	"	"	"	"	"	"
47J303354 P10	OUTER SHELL	"	"	"	"	"	"
47C301616 P2	SCREW, SEALING - T/E	TITANIUM 6 AL-4V	ROD	MIL-T-9047	-	-	-
47C301631 P2	NUTPLATE - T/E	"	"	"	-	-	-
47C302658 P2 or P3	MTG. BKTS., AFT	TITANIUM 6-2-4-2	PLATE	AMS 4976	AL_2O_3	SPRAYED	ON DWG
47C302659 P2 or P3	MTG. BKTS., FWD	"	"	"	"	"	"
47D302660 P1	END ENCLOSURE, AFT	"	"	"	RADIFRAX RC 356	SPRAYED	NS 0060-05-03
47D302661 P1	END ENCLOSURE, FWD	"	"	"	"	"	"
47B302662 P6	BUSHING - EE, FWD	"	"	"	-	-	-

TABLE 7.1-1. RTG COMPONENT AND MATERIAL SUMMARY (CONT)

PART NO.	COMPONENT	MATERIAL	MATERIAL FORM	MATERIAL SPECIFICATION	FINISH	FINISH FORM	FINISH SPECIFICATION
47B301685 P2	RETAINER - PRELOAD SCR.	INCONEL X-750	BAR	AMS 5667	SILVER	PLATING .0003 THK.	AMS 2410
47B302024 P1	SPRING - END ENCL.	"	SHEET/BAR	AMS 5542 AMS 5668	-	-	-
47B302253 P2	ADAPTER - P.O. RECP.	"	BAR	AMS 5667 AMS 5668	NICKEL	PLATING .0002 THK	MIL-C-26074
47C302322 P7 & P8	PRELOAD SCREW	"	"	AMS 5667 AMS 5668	SILVER	PLATING 10,000°A THK	NS-0060-05-22
47B302562 P1	SCREW, DOME	"	"	AMS 5667	SILVER	PLATING .003 THK	AMS 2410
47B302563 P1	SCREW, MTG. BKTS.	"	"	"	"	"	"
47C302638 P_	'C' SEAL	"	SHEET	AMS 5542 AMS 5562 AMS 5598	"	PLATING .001 THK	NS 0060-05-21
47B303062 P1	WASHER - P.O. RECP	"	"	AMS 5542	-	-	-
47B303615 P1	SCREW - END ENCL.	"	BAR	AMS 5667	-	-	-
47C302815 P2	HANDLE - GMV	SST-304	BAR	QQ-5-763, CONDA	MOLY. DISULFIDE	COATING	171A4566, TYI
47B303345 P1	ADAPTER - GMV	"	"	"	-	-	-
47B303346 P1	FEED THRU - GMV	"	"	"	-	-	-
47B303347 P1	FITTING - GMV	"	"	MIL-F-18280	-	-	-

TABLE 7.1-1. RTG COMPONENT AND MATERIAL SUMMARY (CONT)

PART NO.	COMPONENT	MATERIAL	MATERIAL FORM	MATERIAL SPECIFICATION	FINISH	FINISH FORM	FINISH SPECIFICATION
47C303348 P1	TUBING - GMV	SST-304	TUBE	MIL-T-8504	-	-	-
47B303369 P1	NUT - PRD	SST-	BAR	FF-N-836	SILVER	PLATING 10,000°A	NS 0060-05-22
47C303453 P1	DIAPHRAGM - PRD	SST-304	SHEET	QQ-S-766, COND A	-	-	-
47B303456 P2	SCREW - PRD	SST-300 SERIES	BAR	-	MOLY DISULFIDE	COATING	171A4566, TYI
47C303463 P1	LANCE - PRD	SST-440C	BAR	QQ-S-763	-	-	-
47C303511 P1	PENETRATION - PRD	SST-304	BAR/PLATE	QQ-S-763, COND A QQ-S-766, COND A	-	-	-
MS16634 -	BOWED E RING - PRD	SST-	SHEET	MIL-R-21248	-	-	-
MS20613 C	RIVET - END ENCL.	SST-300 SERIES	BAR	FED-STD-66	-	-	-
MS 20995C	LOCKWIRE	SST-304	WIRE	QQ-W-423	-	-	-
MS 21209	HELI-COIL INSERT	SST-	WIRE	MIL-1-8846	-	-	-
MS 24673	SCREW - GMV	SST-	BAR	FED-STD-86	-	-	-
MS 124651	HELI-COIL INSERT	SST-	WIRE	AMS 7245	-	-	-
MS 17143X	PIN SPRING	SST-	SHEET	AMS 5506	-	-	-
NAS 620C	WASHER - GMV	SST-300 SERIES	SHEET	QQ-S-766, COND A	-	-	-
NAS 1291C	NUT	SST-A286	BAR	AMS 5525 AMS 5535 AMS 5537	SILVER	PLATING .0002 THK	AMS 2410

TABLE 7.1-1. RTG COMPONENT AND MATERIAL SUMMARY (CONT)

PART NO.	COMPONENT	MATERIAL	MATERIAL FORM	MATERIAL SPECIFICATION	FINISH	FINISH FORM	FINISH SPECIFICATION
47B301686 P2	WAFER - H.S. SHPT	IRIDIUM	SHEET	NS 0060-01-02 TY1CL1	-	-	-
47B303025 P2	RETENTION WASHER - H.S.S.	"	"	NS 0060-01-11 CL1TY3	-	-	-
47B303425 P1	BARRIER, PRELOAD SCR.	"	"	"	-	-	-
47B302208 P4	BARRIER, H.S. SUPT	TUNGSTEN	SHEET	AMS 7898	-	-	-
47B302721 P1	STRIP, NAMEPLATE	AL ALY-6061-T6	SHEET	QQ-A-250/1	ANOD12E	-	MIL-A-8625TYII
47C303543 P1	PLATE, FRD	AL. ALY 2D24-T351 2D24-T4	SHEET BAR	QQ-A-250/4 QQ-A-225/6	"	-	"
47B302252 P2	TERM. LUG-P.O. RECP	COPPER	SHEET	QQ-C-576	SILVER	PLATING .0001 THK	QQ-S-365 TYIGRB
47B303477 P1 & P2	WIRE - P.O. RECP	COPPER	WIRE	ASTM-B8-64, CLC	-	-	-
47D303494 P—	WIRE - INSTRU CABLE	COPPER	WIRE	-	NICKEL CLAD	-	-
47B303174 P1	CONTACT - INSTRU. CABLE	NICKEL	ROD	ASTM-B160,GRA	-	-	-
MS20995N	LOCKWIRE	MONEL	WIRE	QQ-W-390	-	-	-

TABLE 7.1-1. RTG COMPONENT AND MATERIAL SUMMARY (CONT)

PART NO.	COMPONENT	MATERIAL	MATERIAL FORM	MATERIAL SPECIFICATION	FINISH	FINISH FORM	FINISH SPECIFICATION
47C301528 P3	BEARING						
	BALL	SST-440C	BAR	AMS5630	-	-	-
	RACE & NUT	INCONEL X-750	BAR	AMS5667 AMS5668	-	-	-
47C302247 P2	RECP., ELEC.-P.O.						
	NUT	INCONEL X-750	BAR	AMS5667 AMS5668	SILVER	PLATING .0003 THK	AMS2410
	SHELL	"	"	"	-	-	-
	PINS	"	WIRE	AMS 5698	RHODIUM	PLATING	MIL-R-46085 TY1 CL2
47C302506 P1	VALVE - GMS						
	STEM	SST-316L	-	-	-	-	-
	STEM INSERT	" 17-4PH	-	-	-	-	-
	BELLOWS	" 321	-	-	-	-	-
	RETAINING RING	" 15-7 Mo	-	-	-	-	-
	RING	" 316	-	-	-	-	-
	SPRING	" 17-7PH	-	-	-	-	-
	BODY	" 316L	-	-	-	-	-
	PIN	" 420	-	-	-	-	-
	OTHER	" 316	-	-	-	-	-

TABLE 7.1-1. RTG COMPONENT AND MATERIAL SUMMARY (CONT)

PART NO.	COMPONENT	MATERIAL	MATERIAL FORM	MATERIAL SPECIFICATION	FINISH	FINISH FORM	FINISH SPECIFICATION
47D303435 P1	RTD - INSTRU CABLE						
	SHELL	SST-304	-	-	-	-	-
	SENSOR HOUSING	" -300 SERIES	-	-	-	-	-
	SOCKET	INCONEL X750	-	-	-	-	-
	INSULATION	Mg D	-	-	-	-	-
	SHEATH	PLATING UM-10% RODIUM	-	-	-	-	-
47D303452 P1	BELLOWS - PRD						
	BELLOWS	SST-AM350	SHEET	AMS 5548	-	-	-
	END PLATE	SST-300 SERIES	SHEET	-	-	-	-
	FITTINGS	SST-300 SERIES	PLATE	-	-	-	-
	SPRING GUIDES	AL ALY2024	SHEET		NICKEL	PLATING	-
	SPRING	INCONEL X750	WIRE	AMS 5698	-	-	-
47C302706 P1	BEARING DISK - H.S. SUPT	ZIRCONIUM OXIDE	SINTERED	NS 0060-01-05	-	-	-
47B302861 P1 & P2	PLUG - THERMOPILE	ALUMINA OXIDE	SINTERED	99.8% PURE	-	-	-

TABLE 7.1-1. RTG COMPONENT AND MATERIAL SUMMARY (CONT)

PART NO.	COMPONENT	MATERIAL	MATERIAL FORM	MATERIAL SPECIFICATION	FINISH	FINISH FORM	FINISH SPECIFICATION
171A8241TY1	PAINT - GMV	HI-TEMP REFRACTORY	-	171A8241	-	-	-
HPOO-18-1PF5-PB2	CONN.-INSTRU CABLE						
(GULTON IND.)	SHELL	SST-300 SERIES	-	-	RHODIUM	PLATING	-
	PINS	INCONEL X750	-	-	NICKEL	PLATING	-
322798 (AMP INC)	TERMINAL-INSTRU CABLE	COPPER	-				
S1600TY.H (VARGLAS)	SLEEVING-INSTRU CABLE	-	-	-	-	-	-
171A4175	COMPOUND-INSTRU CABLE	SILICONE RTV 566	-	171A4175	-	-	-
B20F9	BRAZE ALLOY-INSTRU CABLE	SILVER/ COPPER	-	B20F9	-	-	-
IHS & SUPPORT	FUEL	$^{238}PuO_2$	CERAMIC COM-PACT SPHERES				
	POST IMPACT SHELL	IRIDIUM					
	GRAPHITE IMPACT SHELL	T-50	COMPOSITE				
	AEROSHELL & H.S. SUPT.	POCO AXF-5Q					
	ABLATION SLEEVE	PYRO-CARB 406	COMPOSITE				
	IHS INTERNAL GRAPHITE	PYRO-CARB 508	COMPOSITE				

TABLE 7.1-1. RTG COMPONENT AND MATERIAL SUMMARY (CONT)

PART NO.	COMPONENT	MATERIAL	MATERIAL FORM	MATERIAL SPECIFICATION	FINISH	FINISH FORM	FINISH SPECIFICATION
47C302247P5	THERMOPILE ASSY.						
RCA ASSY. & PART DWG.	INSULATION	ASTROQUARTZ	CLOTH	M9A (RCA)	-	-	-
	THERMOPILE	"	"	"			
	INSULATION	MOLYBDENUM	FOIL	M8A1 (RCA)	-	-	-
	END CAPS	"	"	"	-	-	-
	INNER	MOLYBDENUM	SHEET	M8C1 (RCA)			
	FRAME	MOLYBDENUM	"	"	-	-	-
	MISCELLANEOUS INSULATION	ASTROQUARTZ MICROQUARTZ	YARN FIBROUS	M9D1 (RCA) M9A1 (RCA)	-	-	-
	THERMOELECTRICS	SILICON GERMANIUM 63.5 A/O & 78 A/O and SILICON MOLYBDENUM 85 W/O	HOT PRESSED	M28A (RCA)	-	-	-
	HOT SHOE SPACER	ALUMINA Al_2O_3	FIRED SHEET	NS0060-01-06 (GE)	-	-	-
	ELECTRICAL STRAPS	COPPER	STRIP	M1A1 (RCA)	NICKEL	PLATING .0002 THK	

TABLE 7.1-1. RTG COMPONENT AND MATERIAL SUMMARY (CONT)

PART NO.	COMPONENT	MATERIAL	MATERIAL FORM	MATERIAL SPECIFICATION	FINISH	FINISH FORM	FINISH SPECIFICATION
COLD STACK							
HEAT SHUNT	AMZ1RC	SHEET	M1B1				
PRESSURE PAD	SST 303	SHEET	M5A2				
COMPENSATOR	Mo	SHEET	M8B1				
ELECTRICAL INSULATOR	Al_2O_3		M4C2				
ELECTRICAL CONDUCTOR	Cu		M1A1				
COMPENSATOR	W		M2A1				
PEDESTAL	Cu		M1A1				
COLD SHOE	W		M2A1				
BRAZE SHIMS	NICUSIL						
" "	CUSIL						
" "	INCUSIL						
COLD STACK PLATING -	NI	.0005 THK					
RIVETS - INNER FRAME	MOLYBDENUM	BAR	M8E3				
RIVETS - ELEC STRAPS	COPPER COATED CARBON STEEL	POP RIVET	VENDOR SUPPLIED				

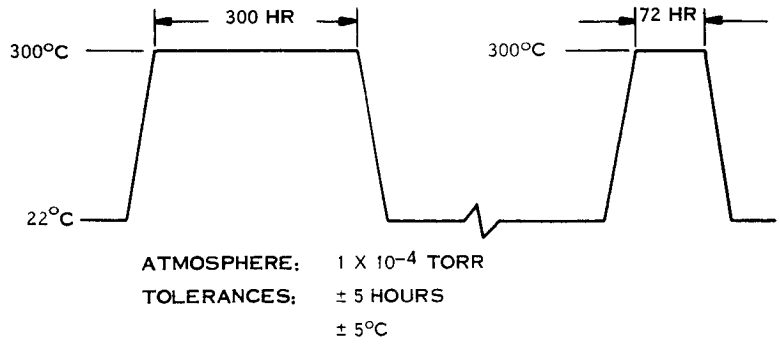

Figure 7.1-1. Unicouple Pre Acceptance Thermal Cycle

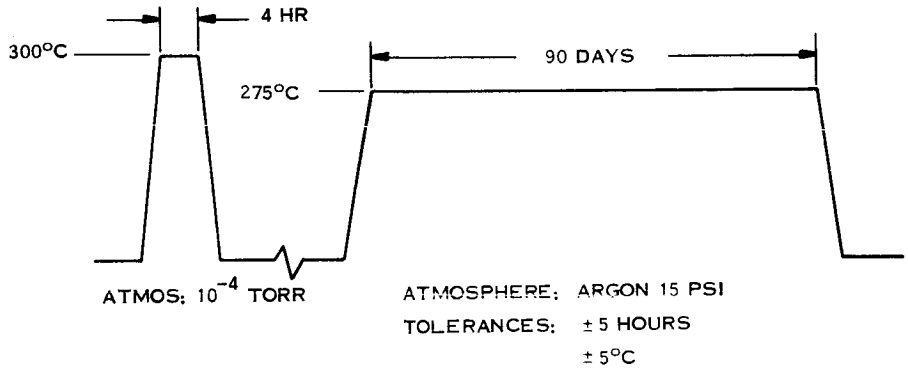

Figure 7.1-2. Unicouple Post Vibration Thermal Cycle

7.1.1.2.1 Cause

The unicouples which exhibited cracking in the cold shoe bonds, predominately 'P' side, were isolated to a distinct group of the unicouple population. These unicouples had been subjected to the optional sodium cyanide cleaning treatment, which was used to remove surface oxides from the pedestals on the couple pre-assemblies prior to unicouple brazing; the treatment also included an ultrasonic wash of 50/50 acetone/methanol solution after rinses in water. The unicouples in question were also hydrogen brazed in the unicouple bonding operation on the same day that they received the sodium cyanide treatment. The unicouples of this population that had micropores in the cold shoe bond zone or had microcracks in the same region, that may have been induced by the ultrasonic treatment, entrapped liquids from the cleaning operation. By subjecting these to hydrogen brazing on the same day as they were chemically cleaned, sufficient time was not available to naturally dry out or evaporate the entrapped liquids. The hydrogen brazing induced a thermal stress condition where the silicon germanium, basically a brittle crystalline solid, fails by a form of stress corrosion cracking in the unicouples with the entrapped liquids.

7.1.1.2.2 Characterization

In the most obvious cases, the failures manifested themselves as electrical rejects - high change in total electrical resistance (ΔR_T) from 2nd Bond to unicouple or unacceptable total unicouple resistance (R_T), or unacceptable cold shoe bond resistance, (P_{cs} or N_{cs}), or as visual rejects by 30X or Zyglo examination. The established inspection procedures were capable of picking such failures out of the production line. (Zyglo was not an in-line inspection step, but was used to confirm the presence of cold shoe bond cracks for electrically rejected unicouples, which did not show a crack at 30X examination).

Statistical analyses of electrical inspection data and cold beam deflection tests were conducted using unicouples from the "same day cleaned and brazed" population as well as unicouples from different production periods for control and comparison purposes. What was revealed is that there existed a group of unicouples from the "same day" production that constitute a second population with lower strength. This group was characterized by a ΔR_T of 0.4 milliohms or greater, and/or a ΔP_{cs} of 0.06 milliohms or greater, and an average ($\bar{x}$) strength (beam deflection) of 6.6 pounds.

A review of the data showed that unicouples that received sodium cyanide treatment and which exhibited the cold shoe bond anomaly were unicouples washed and brazed the same day. No cold shoe bond anomaly occurred when there were one or more days between the was and braze operation. Table 7.1-2 shows the data.

TABLE 7.1-2. SODIUM CYANIDE TREATED UNICOUPLES

		Number with Cold Shoe Bond Anomaly
Number NaCn Treated and brazed same day	264	13
Number NaCn treated and brazed one or more days later.	211	0

Drawing a correlation between the observed electrical characteristics and strength values of this group prompted a delineation of all unicouples, in converters already fabricated or in-process, that possessed the same electrical values. Table 7.1-3 shows that there are three such unicouples in F-8, three in F-9, and eight in F-10. An assessment was made of the probability that those unicouples or any one of them may be from the population with lower strength ($\bar{x}$ of 6.6 pounds).

7.1.1.2.3 Recommendation and Actions Taken

Inasmuch as the F-10 thermopile assembly was in the base wrap stage (on 6/4/76) and replacement acceptable unicouples were available, it was recommended by NR to GE MRB to replace the eight unicouples in question. This was done on 6/5/76 by GE MRB approval.

It was further recommended that Converter F-9 be disassembled and its three questionable unicouples be replaced. In view of schedule considerations, this course of action was not approved.

Because of the very low probabilities of low strength associated with the unicouples in question in Converter F-8 and in consideration of its present status (processed and tested), it was recommended that no action be taken with regard to that unit.

An additional test (beam deflection) of two of the unicouples removed from F-10 to gain characterization of low ΔR_T, high ΔP_{cs} product was performed to assess the ability of the questionable unicouples in Converter F-8 to withstand the expected launch environment. Values of 18.0 and 18.2 lbs. strength were measured for those unicouples which provides additional assurance of the suitability of the F-8 unicouples in question.

7.1.1.3 RTV 566 Potting Development

7.1.1.3.1 Introduction

A potting development program was devised to resolve the problem of cracked potting in

TABLE 7.1-3. "SAME DAY" TREATED UNICOUPLES WITH HIGH ΔR_T AND/OR HIGH ΔP_{cs} IN CONVERTERS

F8	ΔR_T	ΔP_{cs}	Converter Position	
			Circum.	Axial
027	0.3	0.06	22	13
034	0.2	0.06	7	4
035	0.2	0.06	5	7
F9				
821	0.2	0.06	11	12
819	0.6	0.15	8	6
843	0.5	0.11	18	4
F10				
1106	0.3	0.06	18	2
1102	0.3	0.08	24	6
1097	0.1	0.08	16	6
1096	0.2	0.06	5	1
1060	0.3	0.06	3	6
1040	0.2	0.06	8	8
1030	0.2	0.06	19	9
1003	0.4	0.06	9	3

the 47D303494G1 MJS Instrumentation Cable on the Q2 unit. The program as originally designed consisted of five series of tests, Series Nos. A through E, defined in the November-December 1975 report. The following paragraphs cover the implementation of the program and the conclusions drawn therefrom.

7.1.1.3.2 Development Program Implementation

The program as originally conceived was modified for the following reasons:

1. To incorporate the results of the bakeout of the E-5 cable into the test program.
2. To factor in the input from the RTV manufacturer that the RTV used in the Q-2 and E-5 cables were from the same lot although the lots had different MA numbers.

In Test Series "D", the test samples were placed in a furnace already pre-heated to $200^{o}F$ instead of being heated at a rate of $40^{o}F$/hour. Also, the final inspection was done by radiograph in addition to the visual inspection.

In Test Series "E", Header 9 was cured per Series "D" cure procedure rather than by the method originally described.

7.1.1.3.3 Results of the Test Program

Conclusions based on the results of the test program, were as follows:

1. The basic problem was that the potting material could not withstand a high temperature differential (referenced to the temperature of setting).
2. Series D cure procedure would be adequate for the rework operation of the E-5 cable.
3. Further testing would be done to:
   a. Demonstrate improved margin over that existing
   b. Simplify the manufacturing procedure regarding cooldown time and humidity conditions during the operation

7.1.1.3.4 Rework Procedure

The following potting rework procedure was generated and followed in reworking the E-5 RTD cable:

1. Perform post-pot electrical measurements per standard procedure.
2. Remove cracked potting in connector and header to the depth of the crack but not to exceed the following dimensions:

   Connector: 0.25" maximum depth from top edge of potting boot

   Header: 0.15" maximum depth from top edge of potting boot
3. Reprime walls of potting boot -- do not prime nor roughen the surface of the remaining potting -- minimize amount of primer used so as not to prime the existing potting.
4. Mix potting using 5 drops of catalyst per 100 grams of potting material. Mixing to be performed in an environment whose relative humidity is 50 percent minimum.
5. The potting boots shall be filled with potting material to ~1/32 below the edge of the potting boot.
6. After potting, insert cable into oven that has been preheated to $200 \pm 10^{o}F$. (no humidity control required).
7. Hold at $200^{o}F$ for a minimum of 6 hours.
8. Cool down to ambient temperature at a rate $<40^{o}F$/hour.
9. Visually inspect the reworked potting for cracking.
10. Heat cable from ambient temperature to $325 \pm 25^{o}F$ at a rate $\cong 40^{o}F$/hour.
11. Hold at $325^{o}F$ for a minimum of 8 hours.
12. Cool down to ambient temperature at rate $<40^{o}F$/hour.
13. Perform visual inspections, post pot measurements, etc. per standard procedures.

7.1.1.3.5 New Tests

The following additional RTV potting tests were instituted to accomplish the following:

1. Improve the margin of the potted product relative to the operating temperature
2. Improve the potting process to facilitate manufacturing.

A minimum of 5 header specimens (includes 1 spare) and 2 connector specimens were required. The header specimens would have the 0.093 diameter potting hole. Test specimens definition is provided in PIR 5690, Revision "A".

Two test series were performed. Test Series F was structured to facilitate manufacturing. Test Series G was structured to improve the operating temperature of the potting as well as facilitate manufacturing. The following test procedures were followed:

Test Series F

Test Specimens: 2 Header types
1 Connector type
1 Puck (residual)

Procedures:

1. Prime specimens per standard procedures.
2. Using the 100 $\mu\ell$ microsyringe, add 0.07 to 0.1 grams of catalyst per 100 grams of potting material. Mixing to be performed in ambient humidity conditions.
3. Fill test specimens to ~ 1/32 to 1/16" below edge of potting boot.
4. After potting, insert specimens and puck into oven that has been pre-heated to 200 $\pm$ 5°F. (No humidity control).
5. Hold at 200°F for 6 hours minimum.
6. After 6 hours at 200°F, raise oven temperature to 325 $\pm$ 25°F at a rate $\approx$ 40°F/hour.
7. Hold at 325°F for a minimum of 8 hours.
8. Cool down to ambient temperature at rate $<$ 40°F/hour.

9. Visually inspect specimens for RTV cracking and measure hardness of puck.

10. To verify product, perform the following:

    a. Heat specimens and puck to 425 $\pm$ 5°F at a rate $\sim$ 50°F/hour in a vacuum $< 1 \times 10^{-4}$ Torr.

    b. Hold at 425°F for a minimum of 20 hours.

    c. Cool to ambient at rate < 50°F/hour.

    d. Inspect specimens and measure hardness of puck.

Test Series G

Test Specimens: 2 Header type
1 Connector type
1 Puck (residual)

Procedure: The same procedure will be followed as defined in Test Series F except:

Step 4 - After potting insert specimens and puck into oven that has been pre-heated to $225 \pm {}^{10}_{0}$ °F.

Step 10a - Heat specimens to $450 \pm {}^{10}_{0}$ °F at a rate $\sim$ 50°F/hour in a vacuum $< 1 \times 10^{-4}$ Torr.

Steps b, c, and d - Same as Test Series F.

Based upon the successful rework of the E-5 RTD cable, it was concluded that Q2 RTD cable could be reworked successfully. This rework was done in accordance with the same rework potting procedure.

7.1.1.3.6 Test Results

The test program was conducted, and the conclusions reached were as follows:

1. An improved margin of the potted product relative to the operating temperature was not obtained.

2. The test series to provide a more efficient procedure for Manufacturing was inconclusive due to an inadvertent evacuation of the temperature chamber (all tests were to be conducted at ambient pressure).

Based on results of the total test program and the successful rework of cables E5 and Q2 utilizing the Series D cure procedure, however, it was recommended that Instrumentation Cable Assembly Drawing, 47D303494, be revised by AN.

7.2 DESIGN ANALYSES

Work on the converter design was effectively completed in January 1976. The design development prior to that time is described in Section 7 of the previous LES and MJS annual reports, see Section 1.

7.2.1 Q2 AND F7 SHUNT RESISTANCE ANOMALY INVESTIGATIONS

7.2.1.1 Introduction

During vibration testing of the Q-2 and F-7 RTGs, electrical isolation between the thermopile and case and/or foil was lost. Measured resistance between thermopile and case on Q-2 was approximately 2 ohms, whereas it should have been greater than 30 kohms. A similar measurement on F-7 showed less than 70 ohms.

To establish the cause(s) of the short(s), a series of diagnostic evaluations was implemented to confirm that the short was located within the RTG. The diagnostic evaluations provided an insight as to the location of the short(s) within the RTG, but were not able to establish the cause(s) of the short(s). To answer this specific question, a decision was made to disassemble the Q-2 RTG after the completion of RTG qualification testing down to thermopile level, if necessary, to establish the specific cause(s) of the shorts encountered during the vibration testing of the two units.

7.2.1.2 Summary

The evaluations of the indicated shorts in both the F-7 and Q-2 RTGs were conducted using documented procedures mutally agreed upon by all the functional organizations (e.g., Engineering, Quality Assurance, and Systems Test) and the Program Office.

For both units, the initial diagnostic activities were directed toward eliminating the GSE, cables, and dynamic test instrumentation as the source of the anomalous resistance readings.

Once it was verified that the short was internal to the RTG, the magnitude of the resistance between thermopile and case was determined and its approximate location within the thermopile was established, based on the common-mode voltage. The short(s) in the Q-2 RTG remained throughout the diagnostic evaluation; the F-7 short, however, disappeared during the diagnostic evaluation.

Decisions were made to complete the qualification test program for Q-2 and to complete the F-7 RTG acceptance test cycle. The Q-2 short(s) became intermittent throughout the remainder of the qualification test program; the F-7 short did not recur.

The results of the diagnostic evaluations conducted on both Q-2 and F-7 RTGs were unable to answer the primary question, namely: What is the cause of the shorts? Therefore, a decision was made to disassemble the Q-2 RTG, down to the thermopile level if necessary, to establish the specific cause of the short(s) encountered during vibration testing and attempt to determine the flight worthiness of the F-7 RTG on the basis of the Q-2 data.

The Q-2 disassembly was performed in two phases; in the LAS and in the Clean Room in Building B.

While the RTG was in the LAS, resistance readings were taken at various locations within the thermopile. In addition, an optical evaluation, using borescopes, was performed in an attempt to detect any visible particles that may have been entrapped between the thermopile and case. The borescope analysis provided no definitive information.

The teardown of the Q-2 converter was initiated by RCA personnel in Building B. The examination and electrical testing of the thermopile, after removal of the outer case revealed the following:

1. Four different shorting paths were found. Three were foil particles; one in row 10 couple 10, another in row 17 couple 9, and one in row 14 couple 4. The particles were found in the vicinity of the Al_2O_3 insulator under the astroquartz wrap; the shorting mechanism being the bridging of this insulator, thereby shorting the T/P to the case. In addition, the degaussing loop insulation was worn away at one position at the foil corner between rows 2 and 3.

2. Several other foil particles were found in the wrap but were not in position to cause shorts.

3. Many foil particles and pieces of insulation were found on the bottom end dome and foil end cap.

4. The joint between the foil end caps and cylinder was badly damaged.

Examination of the test data showed:

1. There was no net resulting permanent power loss due to the shorts after testing was completed.

2. At no time did two low-resistance shorts (of the order of a few ohms) occur for any length of time; two hard shorts would have caused power losses of 3 to 12 watts, which were not observed.

3. While power fluctuations were observed through comparison of performance data before, during, and after vibration testing, these power changes are primarily caused by changes in the thermal state of the converter. An analysis of the effects of a single short within one RTG on the spacecraft power system showed no harmful effects. Shorts occurring simultaneously in more than one RTG, if low enough resistance, could cause a loss in power.

7.2.1.3 Test Data Review and Analyses of Q-2

7.2.1.3.1 Vacuum Performance - Q2

- LAS Initial Performance
- Building 300 Thermal Vacuum Post Vibration Test
- LAS Final Performance

The initial LAS power was measured at 155.8 watts at the voltage taps. Corrected for the cable loss (R = 0.083 ohms), the power at 30 volts at the connector was 158.1 watts. The resistance from T/P (thermopile) to case was 54.1 k ohms. During post-vibration thermal vacuum testing in Building 300, the measured power stabilized at 148.2 watts, corrected to 150.0W (0.070 ohm cable resistance). The thermopile resistance to case was 6.2 k ohms, indicating that

the isolation between the foil and case was lost during vibration. (Measurements during vibration showed the resistance between foil and case was 0.2 to 0.45 ohms.)

The power loss of 8 watts was due to an internal RTG pressure of ~ 400 μ. The power loss is in agreement with measurements made on the Q1A converter with He which was ~ 8.5 watts loss for 400 μ of He. Subsequent testing in Building 800 (LAS), with the dome off, yielded 155.5 watts corrected for cable losses. The power was 2.6 watts lower than the previous LAS corrected power.

Fuel decay over the two-month time interval was 3 watts. This would result in a 0.3 watt electrical power drop. The other identifiable mechanism is the effect of dopant precipitation. The total difference in time between the first and second LAS tests is 1343 hours. However, the age time for vacuum operation is considerably less because of changes in dopant solubility effects between low temperature argon operation and higher temperature vacuum operation. The actual vacuum time between tests was 138 hours. Taking these factors into consideration, the effective age time was estimated to be 530 hours. The predicted power drop is then 0.9 watts.

The expected changes in open-circuit voltage (E_{oc}) and internal resistance (R_I) as a function of time are summarized below:

	Measured	Predicted
ΔE_{oc}	0.12 volts	0.6 volts
ΔR_I	103m Ω	140m Ω

While the internal resistance agreement is fair, the open-circuit voltage change is much too low. This is the type of result that would be expected if the thermal losses in the converter have increased.

The resistance to case in the 2nd LAS test was 219 ohms. This is the particle short in row 10 as indicated by the voltage to case measurement, V_{oc}, of 10.6 volts. Consequently, there is no power loss due to shorts since a single short drains no power. It is concluded from the

vacuum performance data that the unaccounted for power is due to additional heat losses and not due to electrical shorts.

7.2.1.3.2 Vibration Testing - Q-2

The Q-2 converter was subjected to approximately 50 individual vibration tests. Table 7.2-1 summarizes converter performance before and after each of these tests.

During the vibration testing, there were power output fluctuations, mostly caused by changes in the thermal conditions. The ambient air temperature varied from 68°F to 98°F, and the outer case temperature ranged from 171°C (340°F) to 195°C (383°F). Since an abrupt case temperature change of 2°C can cause a power output change of 0.9 watts, interpretation of some specific test points is difficult. Along with the changes caused by ambient temperature and air flow patterns, the vibration itself (particularly at large displacements) can change the internal heat flow and shift the hot junction temperature. Vibration can cause increased heat flow within the foil package by causing some convective heat transfer. In addition, convective currents can carry heat from the IHS directly out the foil joints, to varying degrees, based on the state of the joints and motion induced by a particular vibration. Also, transient changes in the IHS internal heat transfer characteristics can cause changes in the hot junction temperature.

Thermal changes causing fluctuations in the temperature drop across the thermopile will be reflected in changes in converter open circuit voltage (E_{oc}). It is possible to calculate the expected power output change for a measured change in E_{oc}. This has been done and the predicted changes are in good agreement with the measured changes as shown in Table 7.2-2.

A discussion follows for those tests; the results of which are particularly significant.

X-Axis Vibration (Test 3)

After the full level sine vibration, there was loss of isolation between the foil and case, and a 0.8 watt power loss, accompanied by an open circuit voltage drop of 100 millivolts, was measured. Since foil-to-case isolation was lost, (later measurements showed the resistance from foil to case to be 0.2 to 0.45 ohms), the power loss is probably due to thermal effects, the mechanism being helium release from the IHS.

TABLE 7.2-1. Q-2 VIBRATION TEST DATA

	Date & Time 4/8/76	Axis	Test		P watts	ΔP watts	R_I ohms	ΔR_I mΩ	E_{oc} volts	ΔE_{oc} mv	volts	volts	R_{case}	RTD °C	Ambient Temp. °F
(1)	(0825)	X	1/2 g Sine	PRE	76.3		4.505(1)		41.31		15.4		2.3M	171	74
	(0855)		Sweep	POST	76.2	-0.1	4.520	+ 15	41.26	- 50	15.6		2.4M	171	74
(2)	(0945)		1/2 Level	PRE	76.4		4.520		41.33	+ 70	14.5		2.6M	171	74
	(1025)		(3.3g) Sine	POST	76.5	+0.1	4.517	- 3	41.33	0	13.8		2.7M	171	74
(3)	(1125)		Full Level	PRE	76.5		4.513		41.31	- 20	13.9		2.7M	171	74
	(1150)		Sine	POST	75.7	-0.8	4.517	+ 4	41.21	-100	17.4		711K	171	74
(4)	(1430)		Random	PRE	75.4		4.515		41.18	- 30	21.7		522K	172	76
	(1500)		Equalization 1/3 Level	POST	75.5	+0.1	4.528	+ 13	41.23	+ 50	23.2		509K	173	78
(5)	(1515)		Full Level Random	POST	72.3	-2.3	4.749	+219	41.27	+ 40	23.0		559K	172	77
(6)	(2200)	Z	1/2g Sine	PRE	76.0		4.529		41.29		22.4		518K	171	76
	(2220)		Sweep	POST	76.0	0	4.527	- 2	41.29	0	22.3		524K	171	76
(7)	(2245)		1/2 Level	PRE	75.8		4.529		41.26	- 30	21.3		541K	171	75
	(2315)		Sine	POST	75.4	-0.4	4.545	+ 16	41.24	- 20	22.6		513K	172	75
(8)	(2400)		Full Level	PRE	75.4		4.529		41.21	- 30	22.4		538K	172	75
	4/9/76 (0030)		Sine	POST	75.0	-0.4	4.578	+ 49	41.25	+ 40	22.2		541K	171	75
(9)	(0200)		Random	PRE	75.7		4.523		41.23	- 20	22.1		536K	171	73
			Equalization 1/3 Level	POST	75.7	0	4.523	0	41.23	0	22.0		544K	171	73
(10)	(0240		Full Level Random	POST	73.6	-2.1	4.656	+133	41.24	+ 10	21.5		571K	171	73

(1) Value not stable (low)

(2) Value not stable (high)

TABLE 7.2-1. Q-2 VIBRATION TEST DATA (CONT)

Note: Before Y Axis Testing, Replaced
JPL & 3500 Cable with 2428 Cable

	Date & Time 4/12/76	Axis	Test		P watts	ΔP watts	R_I ohms	ΔR_I mΩ	ΔE_{oc} volts	ΔE_{oc} mv	V_{oc} volts	ΔV volts	R_{case}	RTD °C	Ambient Temp. °F
(11)	(1100)	Y	1/2g Sine	PRE	76.0		4.547		41.34		22.4			172	68
	(1115)	ACCEPT.	Sweep	POST	75.7	-0.3	4.551	+ 4	41.31	- 30	23.6		348K	173	69
(12)	(1330)		1/2 Level	PRE	75.7	0	4.554		41.31		22.1		371K	173	71
	(1350)		Sine	POST	75.4	-0.3	4.553	- 1	41.26	- 50	23.0		366K	174	73
(13)	(1440)		Full Level	PRE	75.4	0	4.555		41.27		22.8		358K	175	72
	(1515)		Sine	POST	75.5	+0.1	4.565	+ 10	41.31	+ 40	22.9		365K	175	73
(14)	(1600)		Random 1/3	PRE	75.4	-0.1	4.562		41.30		22.5		359K	175	74
	(1630)		Level	POST	75.6	+0.2	4.571	+ 9	41.32	+ 20	22.4		377K	175	74
(15)	(1700)		Full Level	POST	75.6	0	4.565	- 6	41.32	+ 20	22.4		396K	179	74
	4/13/76														
(16)	(1000)		Full Level	PRE	75.7	+0.1	4.552		41.32		22.5		384K	174	74
	(1045)		Sine	POST	75.5	-0.2	4.555	+ 3	41.30	- 20	22.9		38.5K	175	75
		QUAL.													
(17)	(1400)		Random	PRE	75.4		4.582		41.33		22.4		340K	179	78
	(1415)		Equalization	POST	75.5	+0.1	4.577	- 5	41.36	+ 30	23.4		355K	179	79
(18)	(1500)		Full Level Random	POST	75.5	0	4.581	+ 4	41.36	0	18.1		479	179	80
		QUAL(11.1g)													
(19)	(1542)		30 Second Sine	POST	75.3	-0.2	4.573	- 8	41.31	- 50	21.3		453K	180	81
	(1600)		Dwell, 25 Hz	POST	72.8	-2.5	4.559	- 14	40.89	-420	21.3		453K	179	82
	(1800)		12g (o-P)	POST	75.7	+3.9	4.589	+ 30	41.43	+540	22.7		369K	181	83
	(1900)			POST	76.1	+0.4	4.592	+ 3	41.49	+ 60	22.3		374K	181	
	(2000)			POST	76.1	0	4.596	+ 4	41.51	+ 20	22.4		363K		

TABLE 7.2-1. Q-2 VIBRATION TEST DATA (CONT)

	Date & Time 4/14/76	Axis	Test		P watts	ΔP watts	R_I ohms	ΔR_I mΩ	E_{oc} volts	ΔE_{oc} mv	V_{oc} volts	ΔV volts	R_{case}	RTD °C	Ambient Temp °F
(20)	(0500)	Z-AXIS	1/2 g sine	PRE	76.4		4.555		41.42		23.2		370K	175	77
	(0520)	QUAL	Sweep	POST	77.6	+1.2	4.554	- 1	41.60	+180			330K	171	77
(21)	(1415)		Full Level	PRE	76.2	-1.4	4.557		41.40	-200	22.1		399K	176	83
	(1455)		Sine	POST	74.0	-2.2	4.552	- 5	41.06	-340	22.9		407K	178	84
(22)	(1730)		Random	PRE	76.0	+2.0	3.455		41.40	+340	Not Taken		Not Taken	180	88
	(1742)		Equalization	POST	76.0	0	3.473	+ 8	41.43	+ 30	22.6		394	181	88
(23)	(1814)		Full Level	PRE	75.8	-0.2	4.580		41.42		Not Taken			182	88
	(1817)		Random	POST	75.8	0	4.578	- 2	41.41	- 10	21.7		452K	181	88
	(2130)		Removed 2428 Cable -- Replaced with JPL and 3500 Cable.												
	4/15/76	X-AXIS													
(24)	(0100)	QUAL	1/2g Sine	PRE	76.9		4.596		41.61		23.4		350K	181	84
	(0130)		Sweep	POST	77.0	+0.1	4.602	+ 6	41.65	+ 40	23.6		364K	181	83
(25)	(0230)		Full Level	PRE	77.0	0	4.595	- 7	41.62	- 30	Not Taken		Not Taken	180	82
	(0240)		Sine	POST	75.8	-1.2	4.600	+ 5	41.44	-180	22.9		354K	179	81
(26)	(0330)		Random	PRE	74.1	-1.7	4.570	- 30	41.11	-330	21.9		361K	178	82
	(0345)		Equalization	POST	74.5	+0.4	4.565	- 5	41.16	+ 50	23.5		369K	178	81
(27)	(0400)		Full Level	PRE	75.0	+0.5	4.572	+ 7	41.25	+ 90	23.5		403K	177	81
	*(0420)		Random	POST	67.4	-7.6	5.092	+520	41.25	0	23.5		470K	182	81
	(0500)			POST	73.8	+6.4	4.732	-360	41.46	+210	22.5		392K	182	
	(0700)			POST	75.0	+1.2	4.717	- 15	41.61	+150	21.9		437K	180	
	(1300)		JPL & 3500 Cable Removed and Replaced with 2428 Cable												

* Camera lamps in during runs

TABLE 7.2-1. Q-2 VIBRATION TEST DATA (CONT)

	Date & Time 4/16/76	Axis	Test		P watts	ΔP watts	R_I ohms	ΔR_I mΩ	E_{oc} volts	ΔE_{oc} mv	V_{oc} volts	ΔV volts	R_{case}	RTD °C	Ambient Temp. °F
(28)	(0800)	UPRIGHT POSITION X-AXIS QUAL LEVEL	1/2 g Sine Sweep	PRE	76.3		4.620		41.57		22.5		359K	184	83
				POST	76.3	0	4.612	- 8	41.55	- 20	23.6		358K	184	85
(29)	(1000)		1/2 Level Sine	PRE	76.2	-0.1	4.616	+ 4	41.56	+ 10	22.6		354K	185	85
	(1045)			POST	76.4	+0.2	4.632	+16	41.63	+ 70	23.4		361K	185	86
(30)	(1300)		Full Level Sine	PRE	76.6	+0.2	4.625	- 7	41.64	+ 10	22.8		298K	187	89
	(1400)			POST	78.2	+1.6	4.637	+12	41.93	+290	22.7		329K	187	90
	(1500)			POST	75.3	-2.8	4.629	- 8	41.45	-380	22.3		368K	187	90
	(1700)			POST	76.0	+0.7	4.639	+10	41.59	+140	22.5		347K	189	92
	(1900)			POST	76.7	+0.7	4.638	- 1	41.68	+ 90	22.6		348K	187	92
	4/19/76														
(31)	(0900)		Random Equalization	PRE	76.2	-0.5	4.664		41.69		22.4		341K	188	87
	(0922)			POST	76.2	0	4.660	- 4	41.69	0	20.91		SHORT	188	87
	(1000)			POST	76.95	+0.75	4.656	- 4	41.81	+120	20.91		↓	187	87
	(1500)			POST	76.3	-0.65	4.663	+ 7	41.72	- 90	22.3		350K	190	96
(32)	(1600)		Repeat Random Equalization	PRE	76.0	-0.3	4.659	- 4	41.66	- 60	20.0		406K	193	98
				POST	76.1	+0.1	4.671	+12	41.70	+ 40	21.1		374K	191	98
(33)	(1700)		Full Level Random	PRE	75.9	-0.2	4.672	+ 1	41.68	- 20	22.3		338K	194	98
	(1715)			POST	76.0	+0.1	4.667	- 5	41.69	+ 10	20.9		SHORT	195	98
	(1800)			POST	76.6	+0.6	4.673	+ 6	41.83	+140	20.9		↓	194	98
	(1900)			POST	79.1	+2.5	4.692	+19	42.27	+440	20.9			194	97
	(2000)			POST	78.8	-0.3	4.669	-23	42.28	- 10	20.9		↓	187	96
	(1950)		Measured Resistance Between Foil and Case = 0.45 Ω												
	4/20/76														
(34)	(1500)		Determined Magnitude of Short TR-1E45-0392: = ~ 2 ohms.												
	4/21/76														
(34)	(1700)		SHOCK 1/4 Level 1/2 Level Full Level	PRE	77.3(1)		4.622		41.80(1)		18.9		516K	179	70
	(1800)			POST	76.6	-0.7	4.615	-17	41.67	-130	20.9		SHORT	181	72
	(1900)			POST	77.3	+0.7	4.620	+ 5	41.77	+100	17.8		583K	178	71
	(1940)			POST	77.5	+0.2	4.622	+ 2	41.79	+ 20	17.0		620K	175	70
	(2130)	↓	Remeasured Measured Foil to Case Resistance = 0.2 ohms with T/P to Case = 600K												

(1) TR 0392 not Stable -- RTG had been on Open Circuit; Previous Stable Point 76.7W

TABLE 7.2-1. Q-2 VIBRATION TEST DATA (CONT)

	Date & Time 4/22/76	Axis	Test		P watts	ΔP watts	R_I ohms	ΔR_I mΩ	E_{oc} volts	ΔE_{oc} mv	V_{oc} volts	ΔV volts	R_{case}	RTD °C	Ambient Temp. °F
(35)	(0100)	UPRIGHT POSITION Z-AXIS QUAL	1/2 Sine	PRE	77.2		4.612		41.68		15.6		641K	173	68
	(0115)		Sweep	POST	77.0	-0.2	4.611	- 0	41.65	- 30	15.2		682K	174	68
(36)	(0200)		1/2 Level	PRE	76.5	-0.5	4.618	+ 7	41.58	- 70	15.4		660K	175	72
	(0235)		Sine	POST	75.7	-0.8	4.610	- 8	41.43	-150	15.3		687K	173	73
(37)	(0500)		Full Level	PRE	75.7	0	4.609		41.46	+ 30	15.3		627K	175	70
	(0515)		Sine	POST	79.3	+3.6	4.604	- 5	42.00	+540	20.9		SHORT	173	70
	(0600)			POST	75.8	-3.5	4.589	-15	41.39	-610	20.9			172	70
			RTG GAS SAMPLE												
(38)	(0700)		Random	PRE	75.5	-0.3	4.605	+16	41.39	0	20.9			174	72
	(0710)		Equalization	POST	76.0	+0.5	4.607	+ 2	41.47	+ 80	20.9			172	68
(39)	(0730)		Full Level	PRE	76.4	+0.4	4.594	-13	41.51	+ 40	20.9			173	72
	(0809)		Random	POST	76.6	+0.2	4.616	+22	41.60	+ 90	15.6		667K	175	72
(40)	(1400)		SHOCK	PRE	77.0	+0.4	4.622		41.70	+100	21.7		433K	175	70
	(1413)		1/4 Level	POST	76.4	-0.6	4.621	- 1	41.61	- 90	15.16		SHORT	177	73
(41)	(1440)		1/2 Level	PRE	77.3	+0.9	4.620		41.74	+130	15.16			174	71
	(1451)			POST	76.5	-0.8	4.615	- 5	41.60	-140	15.16			178	72
(42)	(1511)		Full Level	PRE	77.0	+0.5	4.616		41.68	+ 80	15.15			175	70
	(1528)			POST	76.7	-0.3	4.626	+10	41.66	- 20	17.85		606K	173	71

TABLE 7.2-1. Q-2 VIBRATION TEST DATA (CONT)

	Date & Time 4/23/76	Axis	Test		P watts	ΔP watts	R_I ohms	ΔR_I mΩ	E_{oc} volts	ΔE_{oc} mv	V_{oc} volts	V volts	R_{case}	RTD °C	Ambient Time °C
(43)	(0100)	QUAL	1/2g Sine	PRE	77.0		4.630		41.68		15.1		593K	178	71
	(0120)		Sweep	POST	78.0	+1.0	4.646	+16	41.86	+180	14.8		607K	175	69
(44)	(0230)		1/2 Level	PRE	76.0	-2.0	4.646	0	41.59	-270	14.8		605K	180	72
	(0250)		Sine	POST	76.8	+0.8	4.631	-15	41.69	+100	15.1		657K	173	67
(45)	(0350)		Full Level	PRE	76.5	-1.2	4.628	- 3	41.48	-210	14.5		620K	178	70
	(0425)		Sine	POST	78.4	+2.8	4.626	- 2	41.94	+460	15.1		SHORT	176	68
(46)	(1030)		Random	PRE	76.06	-2.3	4.648	+22	41.65		15.2			182	73
	(1045)		Equalization	POST	76.09	+0.03	4.661	+13	41.69	+ 40	15.2			183	75
(47)	(1120)		Full Level	PRE	76.7	+0.6	4.656	- 5	41.78	+ 90	15.2			183	76
	(1130)		Random	POST	76.4	-0.3	4.686	+30	41.82	+ 40	15.2			184	77
			SHOCK												
(48)	(1300)		1/4 Level	PRE	77.0		4.663	-23	41.86	+ 40	15.2			186	79
	(1321)			POST	76.85	-0.15	4.668	+ 5	41.84	- 20	15.2			186	80
(49)	(1400)		Full Level	PRE	77.06		4.663	- 5	41.87	+ 30	15.2			187	81
	(1435)			POST	77.0	-0.06	4.661	- 2	41.87	0	14.9		700K	187	82
(50)	(1500)		Sine Survey	PRE	77.0		4.671	+10	41.87	0	16.2		589K	187	82
	(1535)			POST	76.8	-0.2	4.677	+ 6	41.87	0	15.2		624K	188	82
	(1800)		6-Hour	START	77.3	+0.5	4.679	+ 2	41.94	+ 70	14.7		581K	188	84
	(2400)		Pressure Decay Test	END	77.4	+0.1	4.679	0	41.91	- 30	14.4		615K	185	82

TABLE 7.2-2. COMPARISON OF MEASURED POWER CHANGE WITH PREDICTED POWER CHANGE BASED ON CONVERTER OPEN CIRCUIT VOLTAGE MEASUREMENTS

ΔP = measured power change

ΔP_c = calculated power change

Test		ΔP	ΔE_{oc} (mv)	ΔP_C	Comments
3	Post Full Level Sine (X)	-0.8	-100	-0.65	Foil to Case Isolation Lost R_C = 700K RTD Constant
19	Post 30 Sec., 25 Hz (Y) Sine Dwell	-2.5	-420	-2.6	R_C = 450K RTD down 1°C
21	Post Full Level Sine (Y)	-2.2	-340	-2.1	R_C = 407K RTD up 2°C
25	Post Full Sine (X)	-1.2	-180	-1.1	R_C = 354K RTD down 1°C
30	Post Full Sine (X)	+1.6	+290	+1.8	R_C = 298K RTD constant
31	40 Minutes after the Post Random equalization Reading	+0.75	+120	+0.75	Hard Short Appeared 40 Minutes after Test. RTD down 1°C
34	Post 1/4 Level Shock (Y)	-0.7	-130	-0.8	Hard Short Returned RTD up 2°C
	Post 1/2 Level Shock (Z)	+0.7	+100	+0.6	Hard Short Gone RTD down 3°C
36	Post 1/2 Level Sine (Z)	-0.8	-150	-0.9	
37	Post Full Level Sine (Z)	+3.6	+540	+3.4	Hard Short Reappeared RTD down 2°C
	45 Minutes Later	-3.5	-610	-3.8	Hard Short Still Present RTD down 1°C
40	Post 1/4 Level Shock (Z)	-0.6	- 90	-0.6	Short Reappeared RTD up 2°C
41	Post 1/2 Level Shock (Z)	-0.8	-140	-0.9	Short Still Present
43	Post 1/2g Sine (Y)	+1.0	+180	+1.1	No Short RTD down 3°C

After the full level random vibration, there was a 2.3 watt power drop accompanied by a 219m ohms increase in internal resistance attributed to JPL cable resistance change.

Z-Axis Vibration (Test 10)

The 2.1 watt power drop after full random vibration is again due to the cable problem; the internal resistance rose 133m ohms.

Y-Axis Vibration (Test 19)

Post sine dwell showed no change but the next set of data, taken 20 minutes later, showed power down by 2.5 watts accompanied by a 420 mv decrease in E_{oc}. The resistance to case was 453 K and the power loss and E_{oc} are consistent with a change in $\sim$ 6°C in thermopile ΔT.

Z-Axis Vibration (Test 21)

A post sine power drop of 2.2 watts was measured. The resistance to case was 407 K and open circuit voltage was down 340 mv consistent with a ΔT drop of 5°C.

X-Axis Vibration (25)

Post full sine power was down by 1.2 watts. E_{oc} was down by 180 mv and the power loss was consistent with 2.5°C temperature drop.

X-Axis Vibration (Test 27)

Post full random resulted in a power drop of 7.6 watts accompanied by rise in internal resistance of 520 m ohms and an RTD temperature rise of 5°C. Log books show that camera lights were on the case to take PRD pictures. Power recovered 4 hours later.

Upright Position (Test 30)

Post full level sine showed power rise of 1.6 watts accompanied by an increase in open circuit voltage of 290 mv. This is definite indication of thermal changes inside the converter. The RTDs indicated no temperature change and the resistance to case was 329K ohms. The 78.2 watts level reached can only be attained under transient conditions. A heat flow surge, possibly due to a decrease in the thermal resistance inside the heat source due to gaps closing could account for a heat surge. The power dropped by 2.9 watts at the next reading

one hour later; this is a typical phenomenon for thermal transients. For example, a known thermal transient was experienced during an axis change on 4/13/76 as shown in Figure 7.2-1. When the RTG was lifted from the shaker table, there was a case temperature rise and a drop in power open circuit voltage. This was followed by a rise in power beyond the steady state value when the RTG was repositioned on the shaker table. The indicated RTD change was 4^{o}C as the power changed -1.2 and +2.6 watts.

X-Axis (Test 31)

During the post random equalization, the hard short first appeared. There was no loss in power. The short was a single point short, since there is no power loss, and later measurements show the value to be 2 to 3 ohms from T/P to case. Short location was calculated to be in row 17, 18 from V_{oc} = 20.9 measurement. The short disappeared before any more vibrations were performed.

X-Axis (Test 33)

During post full random, the short reappeared at the same location with no power loss. The hard short remained for 20 hours until measurements were made to determine its magnitude by varying the standard 10K down to lower levels. The magnitude was determined to be ~20 ohms. The short disappeared when the measuring resistor was lowered to ~20 ohms. At this value, the current through the short was 1 amp, indicating that the contact point was burned away.

X-Axis (Test 34-1)

During post 1/4 level shock the short reappeared at the same location, and V_{oc}, 20.9 volts. A 0.7 watt power drop and E_{oc} drop of 130 mv and an RTD rise of 2^{o}C indicate a thermal effect. The short disappeared before the next shock.

Z-Axis (Test 37)

During post full level sine the power rose to 79.3 watts with a 520 mv rise in E_{oc} and the hard short came back. Normal power was 76 to 77 watts. This was another thermal transient, since power dropped down 45 minutes later to the pre-vibration level. The short was still in the same location, and V_{oc} = 20.9 volts.

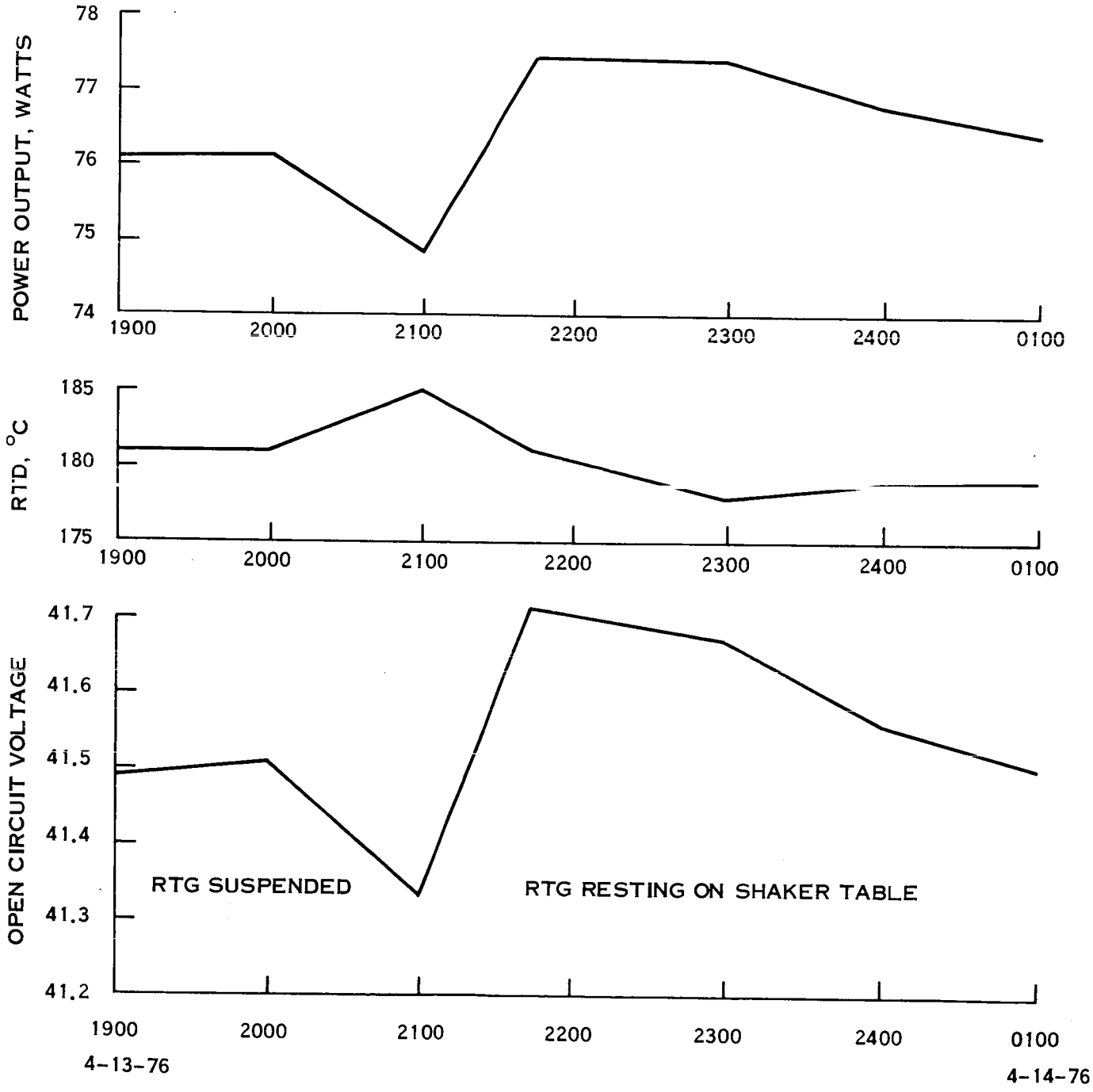

Figure 7.2-1. Thermal Transient During Axis Change

Z-Axis (Test 38)

During random equalization the short was present before and after the test at the same location, and V_{oc} = 20.9 volts.

Z-Axis (Test 39)

The short disappeared after the Full Level Random.

Z-Axis (Test 40)

During post 1/4 level shock the hard short appeared with V_{oc} = 15.2 volts. Power drop was 0.6W from the pre-shock value. RTDs were up 2°C and E_{oc} was down 90 mv. Location of short was from near the top of row 13, 14 if it was a single point short. (After disassembly a foil particle was found in couple 4 of this row.)

Z-Axis (Test 41)

During 1/2 level shock the short was at the same location with V_{oc} = 15.2 volts before and after. Power was down 0.8W, E_{oc} was down 140 mv, and RTDs up 4°C, indicating a thermal effect.

Z-Axis (Test 42)

During post full level the short was gone.

Y-Axis (Test 45)

During post full level sine the power rose to 78.4 watts and the short came back in at V_{oc} = 15.1 volts, therefore it was still in row 13, 14. Power rise due to another thermal transient was induced by the full level sine. This was the third large power rise and each was after a full level sine.

The short remained at V_{oc} = 15.2 through tests 46, 47 and 48. It disappeared after the Y-axis full level shock. The resistance to case was 700 k ohms. The final power output point was 77.4 watts with a resistance to case of 615 k ohms at an RTD temperature of 185°C.

7.2.1.3.3 Q-2 Disassembly in Building B

A summary of results from the disassembly follows:

1. Multiple foil particle shorts were found from T/P to heat shunt (case) (3 or 4).
2. The degaussing loop was shorted at one location
3. The locations of the shorts correlate with the locations indicated at various times during vibration testing and with electrical measurements made in the LAS (with the heat source removed) before transfer to Building B.
4. The electrical connector wrap was found to be variable in tightness in some rows, forming a receptive tunnel for particle entry.
5. The thermopile internal resistance of each row was very uniform, indicating no structural damage to couples.

7.2.1.3.4 Calculation of Short Location From V_{oc} and Correlation with Cold Resistance Measurements in the LAS and Building B Disassembly

Figure 7.2-2 shows the converter circuit. For uniformly-distributed resistance between the thermopile and foil/case, the voltage to case (V_{oc}) will measure 1/2 the converter output voltage (V_L) i.e., when measuring from the (+) side of the converter the V_{oc} will be $+0.5\ V_L$, the absolute sum being equal to the total, V_L. The resistance path to the foil is through the astroquartz insulation, typically 300 k ohms to 500 k ohms at argon temperatures; the resistance to case is across the 20 mil $A\ell_2O_3$, typically 2 megohms at argon temperatures. At assembly there is a high resistance between the foil and case. During vibration, this is usually lost and the resistance from thermopile to foil then measures the same as thermopile to case, and foil and case are at the same potential.

Individual couple resistances to foil are of the order 312 x 500 k ohms $\cong$ 160 megohms and individual T/P to case are $\sim$600M ohms. The V_{oc} or null point when resistances are high is merely an indication of the uniformity of individual paths.

When the resistance of one path drops considerably below the others, there is a shift in V_{oc} to a value indicative of the location of the short. The fraction of the distance into the pile from the (+) end is:

$$F = \frac{V_{oc}}{V_L}$$

where V_L is the converter line voltage at the point where V_{oc} is measured.

(A) $V_{oc} = 20.9$ Volts

The first hard short that appeared showed $V_{oc} = +20.9$ volts. The converter voltage at the RTG voltage taps was 29.7 volts and there was a 0.45 volt line loss to the point where the V_{oc} tap was located. The fraction of the distance in from the plus end of the T/P is then

$$F = \frac{20.9}{29.7 - 0.45} = 0.714$$

Since there are 156 couple pairs in series (13 in each row and 12 double rows), the short location was then established as being near (156 x 0.714 = 111.2) couple 8 from the top of row 17, 18. During disassembly, a foil particle was found under the wrap near the $A\ell_2O_3$

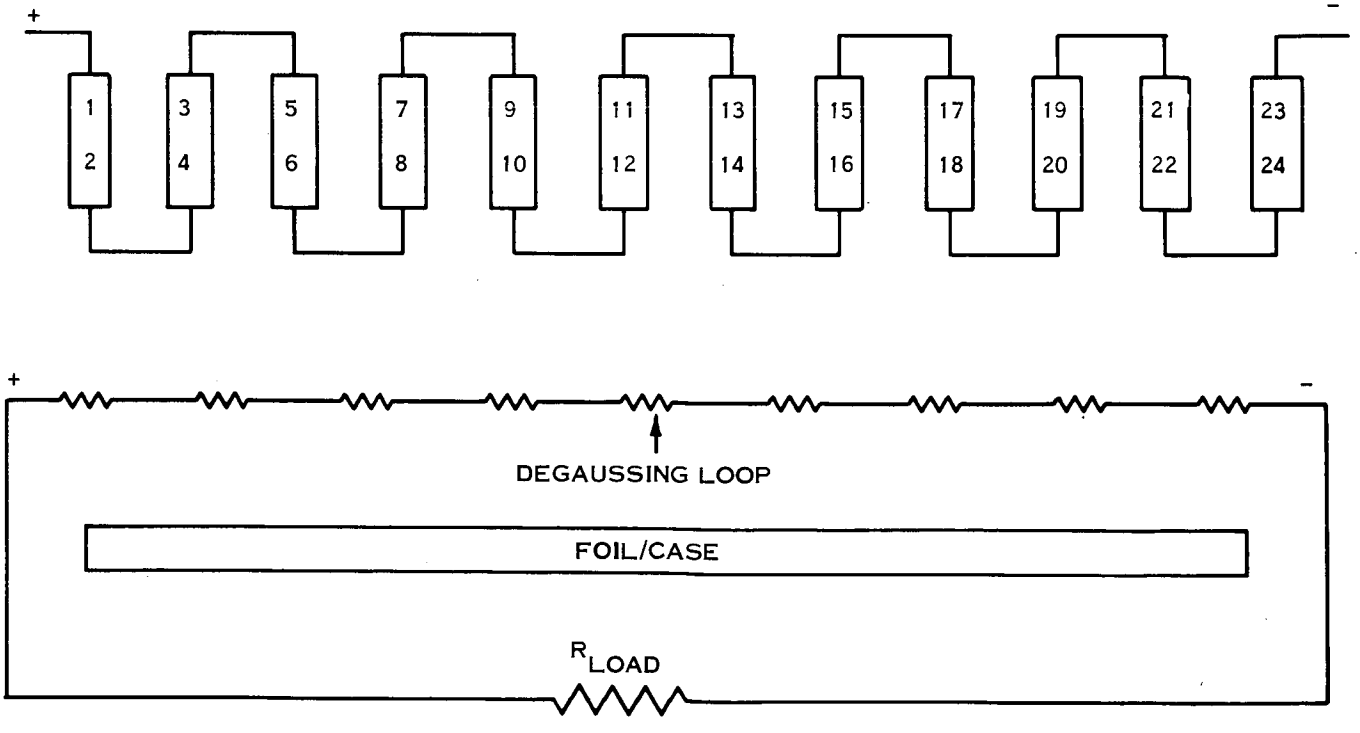

Figure 7.2-2. Converter Circuit

insulator in row 17, 18 couple 9, forward end. The particle was lost in trying to remove it. Later a particle was found in couple 8 but this may have been the same particle found in couple 9.

(B) V_{oc} = 15.2 Volts

Late in the vibration testing, V_{oc} shifted to +15.2 volts in the hard short condition. The fraction of the distance in from the (+) end of the pile is:

$$F = \frac{15.2}{(29.7 - 0.45)} = 0.52$$

The number of couples in from the (+) end is:

(0.52) (156) = 81 or between couple 3 and 4 of row 13, 14.

During disassembly, a foil particle was found under the wrap near the $A\ell_2O_3$ insulator on the forward side of couple 4.

(C) V_{oc} = 11.1 Volts

In Building 800, with the short measured at 250 ohms, V_{oc} was 11.1 volts with argon fill. In Building 800, the line resistance from the point where the RTG voltage is measured to where the V_{oc} was measured was 0.430 ohms compared to 0.180 ohms in Building 400. The line drop was then 1.1 volts. The fraction of the distance in from the (+) end was then

$$F = \frac{11.1}{29.7 - 1.1} = 0.388$$

The number of couples in from the (+) end is

(0.388) (156) = 61 or between couple 9 and 10 or row 9, 10.

During disassembly, a foil particle was found under the wrap bridging the Al_2O_3 insulaton on the forward end of couple 10. This was the hard short that remained during converter cooldown to room temperature as evidenced by the constant ratio of $\frac{V_{co}}{V_L}$ during cooldown.

At room temperature, careful electrical measurements were made and it was determined that a short was in couple 10 (calculated magnitude 1.5 to 2.0 ohms), but in addition, the measurements showed that the degaussing loop was hard-shorted to the foil. This hard short to the degaussing loop may have developed during cooldown due to differential contraction of the loop and foil basket. At no time during the testing was a V_{oc} seen that would correspond to the degaussing loop by itself being shorted. The value would be:

Degussing Loop, V_{oc}

$$\frac{85}{156} \times (29.7 - 0.45) = 16 \text{ volts}$$

The short in row 9, 10 and the degaussing loop short would shift the V_{oc} to between 11 and 16 volts, and the 15.2 volt value at the end of testing could have been this combination. However, since a particle was found at the 15.2 volt point, it is concluded that the degaussing loop short during testing was probably only intermittent or of a high value since no power loss was seen. Intermittent degaussing loop shorts, as well as intermittent multiple particle shorts would cause negative current and voltage spikes.

7.2.1.4 Test Data Review and Analyses of F-7

7.2.1.4.1 Vibration Testing - F-7

During the Y-axis full acceptance level sinusoidal run, there were load voltage and current transients of approximately 1 volt and 0.1 amp, respectively, indicated at the 75 Hz point in the sweep down from 2000 to 5 Hz. The post-run data scan showed a decrease in output power of 0.6 watts and decrease in open-circuit voltage of 0.08 volts. Circuit internal resistance was normal. In addition, a major change was seen in shunt resistance between circuit and case. Having been 400K ohms prior to the vibration input, the shunt resistance indicated some very low value after the run. The common-mode voltage between thermopile and case showed

a change from a pre-run 23.6 volts to 9.3 volts post-run. The voltage after the 10k ohm resistor in the ROC was switched in parallel to the thermopile-to-case circuit showed no change, indicating that shunt resistance was something much smaller than 10k ohms.

Vibration operations were suspended and a trouble-shooting mode was instituted to ascertain the reality of the anomalous condition. As had been done on Q-2, a decade box was interconnected into the ROC measuring circuit to allow smaller values of parallel resistance than 10k ohms to be used. With a 654 ohm parallel resistance, a shunt resistance value of 72 ohms was calculated. The actual value of shunt resistance was probably very low. A smaller than 650 ohm parallel resistor would have allowed a more accurate calculation of shunt resistance, but the increased current flow would have most probably caused the low shunt resistance to return to its former high value, as had occurred during the trouble-shooting on Q-2. It was desirable at this time to maintain the low value on F-7 for the next stage of trouble-shooting.

To eliminate the ROC and associated power-out cable string as a contribution to the low shunt resistance, the RTG was open-circuited and that equipment was removed from the RTG. As had been done on Q-2, a breadboard resistive load was applied to the RTG and adjusted for a 30 volt load. Shunt resistance measurements were then performed using the decade box as the parallel resistor between circuit and case. It was immediately evident that the shunt resistance had returned to a high value, since the common-mode voltage had changed from approximately 9 volts to the original 21 volts. Measurement/calculation was completed using the breadboard, and shunt resistance indicated 300k ohms. This test was performed as a means of isolating the ROC and power-out cable string as the reason for anomalous shunt resistance and it would have been advantageous if the short was still present with the breadboard load.

When the same test had been performed on Q-2, the low shunt resistance value had still been in evidence with the breadboard load. The F-7 RTG was again interconnected with the ROC and shunt resistance measurements using the ROC yielded the same 300k ohms as the breadboard test, verifying that case-to-circuit isolation had returned.

7.2.1.4.2 Discussion of F-7 Results

The disassembly of the power cable was always performed with the RTG in the open circuit mode to prevent possible arcing. When the RTG was placed in open-circuit, the hot side temperature stabilized at ~60°C higher than the 30 volt load condition. This temperature increase caused movement between the outer shell, foil and the thermoelectric circuit. It was established on other RTGs that electrical shorts had disappeared by introducing the RTG to different loads and environments. These conditions caused the RTG hot and cold side temperatures to change significantly. It was believed the temperature change on F-7 caused the short to disappear.

Based on the common-mode voltage between the thermopile and the outer shell of 9.3 volts, the short would most likely lie about the center of axial T/C rows 7 and 8. Even though the cable was removed to attempt to isolate the short, it was believed the short lies within the RTG. Based on Q-2 inspection, it was also believed to be caused by a metallic particle between the circuit and foil/case.

7.2.1.5 Summary of Q-2 and F-7 Test Data Review and Analysis

Test data and review and analysis summary of Q-2 and F-7 units are as follows:

1. The Q-2 and F-7 converter vibration test data indicated the internal shorts developed during the vibration testing.

2. The vibration test data showed there was no net resulting permanent power loss due to the shorts after testing was completed.

3. The test data showed that at no time did two low resistance shorts (of the order of a few ohms) occur for any length of time since two hard shorts would have caused power losses of 3 to 12 watts (based on Q-2 short locations) which were not observed.

4. Simultaneous low resistance shorts, if they occured, were only momentary.

5. During the Q-2 vibration testing, power fluctuations were seen when pre- and post-vibration test data were compared. These power changes were primarily caused by changes in the thermal state of the converter. The ambient temperature ranged from 68°F to 98°F, the outer case temperature ranged from 171°C (340°F) to 195°C (383°F) and the vibration levels themselves appear to have caused changes in the internal heat flow, resulting in changes in the hot junction temperature and ΔT across the thermopile.

These measured power changes were closely correlated with power changes expected for a measured open circuit voltage change which is directly proportional to the temperature difference between the hot and cold junction temperature.

6. Examination of the Q-2 thermopile after the outer case removal uncovered four shorting paths. Three foil particles were found, one in row 10 couple 10, another in row 17 couple 9, and one in row 14 couple 4. The particles were found in the vicinity of The Al_2O_3 insulator, the shorting mechanism being the bridging of this insulator, thereby shorting the T/P to the case. In addition, the degaussing loop insulation was worn away at one position at the foil corner between rows 2 and 3. The location of these paths can be related to the voltage to case measurements made during testing. The particle short in row 17 by itself would cause a voltage to case (V_{OC}) of ~21 volts as observed in the vibration testing with the first appearance of the hard short (~ 2 ohms). The particle in row 13, by itself, would cause a V_{OC} of ~15.2 volts as observed later in the vibration testing. The degaussing loop short, by itself, would cause a V_{OC} of ~16 volts which was not observed. The particle in row 10, by itself, would cause a V_{OC} of ~ 11 volts, not observed during vibration, but observed in Building 300 and Building 800. This does not mean that the degaussing loop did act as a shorting path during vibration. If the particle in row 10 had relatively high resistance, about three times larger than the degaussing loop short, this would shift the V_{OC} down from 16 volts which could be the 15.2 volt point observed. However, since a particle was found at the 15.2 volt location, it appeared likely that during the testing the degaussing loop caused only momentary shorts.

   At the termination of testing in Building 800, the short in row 10 was the lowest resistance (~ 200 ohms), the others being absent or much greater in value (based on the voltage to case, V_{OC}, of 11 volts).

7. The nature of metal particle shorts was such that the major portion of the resistance was in the contact area. The passage of current through the contact points caused localized heating and could cause burnout of the contact points. When measurements were made to determine the magnitude of the short during vibration testing, the short disappeared when a 20 ohm resistor was placed across the T/P and outer case. At a V_{OC} of 21 volts, this corresponded to a 1 amp current flow through the shorting particle. Consequently, the nature of the short was such that if large shorting currents were drawn (two low resistance shorts were required), then the shorts would probably disappear, particularly under zero g conditions where there was no force holding the particles against the surface.

8. The physical examination of Q-2 showed foil particles as well as pieces of astroquartz insulation on both the end dome and bottom foil stack. These observations and the battered and curled condition of the foil joints and the worn-through insulation on the degaussing loop, lead to the conclusion that the large displacement caused by the sine vibrations particularly, the 30-second dwell at 25 Hz, were the causes of most of the damage.

7.2.2 UNICOUPLE VIBRATION TEST

7.2.2.1 History

RCA experienced problems with the quality of the diffusion-bonded joint between the 63 percent silicon leg segment and the tungsten pedestal. After the problem was identified, RCA instituted a quality control screening to identify all faulty unicouples. To assure that the screening did identify all faulty parts, RCA selected 10 accepted unicouples from two manufacturing lots for dynamic testing. During the vibration test one unicouple failed at 6.6 G_{rms} random vibration after 1.5 minutes in the Y axis. Since the RTG acceptance random vibration level is 6.6 G_{rms} for one minute in each of three axes, this failure cast doubt on the adequacy of the unicouples to survive acceptance testing.

7.2.2.2 RCA Tests

For the random vibration test the ten unicouples were mounted in five pairs. To simulate the weight of the thermopile, a nut (weight 0.015 pounds) was fixed to the free end of each unicouple. Table 7.2-3 shows the test sequence.

TABLE 7.2-3. VIBRATION SEQUENCE

Level	Overall G_{rms}	Axis*
Acceptance	6.6	X, Y
Qual	9.9	X, Y
1.5 Qual	15.0	X, Y
2 Qual	20.0	X, Y
2.5 Qual	25.0	X, Y
3.0 Qual	30.0	X, Y

*Y axis corresponds to RTG Y axis.
X axis is the other lateral (i.e., produces bending in the legs) axis of the unicouple.

The acceptance level in the X axis was completed. During the Y axis acceptance level vibration one unicouple failed. Figure 7.2-3 shows a time history of this vibration test with the failures of this and subsequent unicouples noted. Only the first unicouple (N850) failure occurred at the diffusion bond between the 63 percent silicon leg segment and the tungsten pedestal. All other failures occurred in the copper heat shunt.

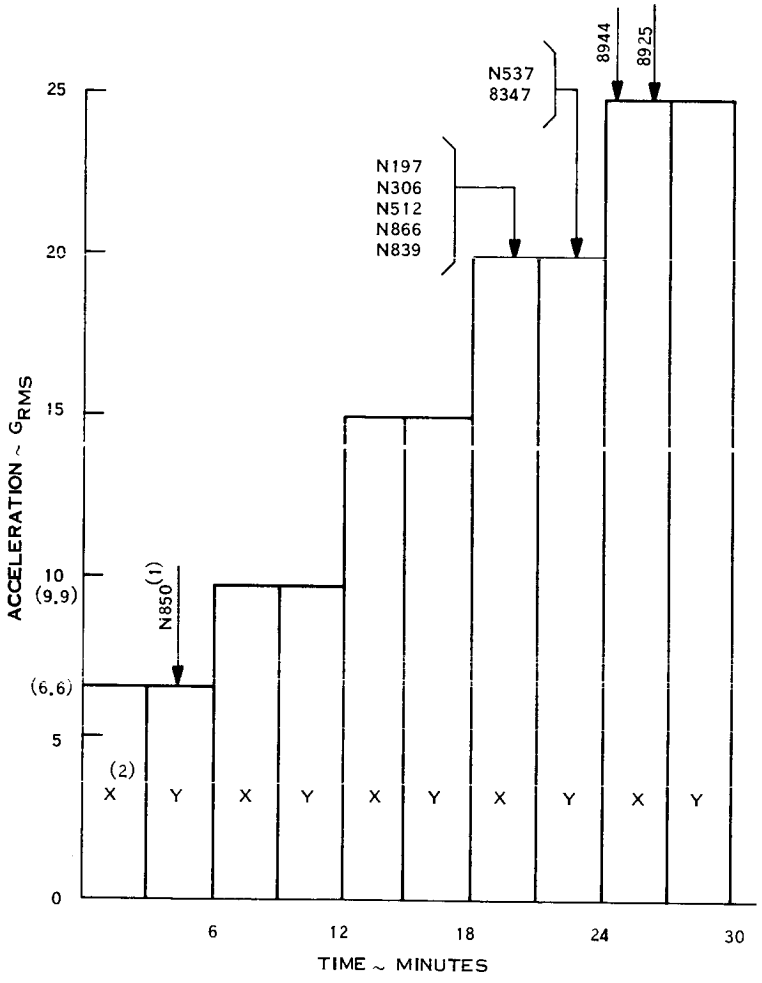

(1) DENOTES FAIL OF UNICOUPLE
(2) DENOTES VIBRATION AXIS

Figure 7.2-3. Unicouple Test Results

Since these tests were performed with bare unicouples, it was suspected that the lack of damping could have resulted in an overtest.

To evaluate the effect of damping due to the microquartz stuffing, the astroquartz yarn wrap and the alumina wafer, the response of two unicouples was compared. The one unicouple was tested bare, the other unicouple was prepared with the microquartz stuffing between the legs, the astroquartz yarn wrapped around the legs and the alumina wafer under the hot shoe. The former configuration was identified as bare and the latter configuration as wrapped.

Each unicouple was instrumented with a miniature accelerometer (ENDVECO #2226) attached to the hot shoe of each unicouple using a bonded aluminum block. The total weight of the block and accelerometer was approximately 0.015 pounds. The total weight of foil insulation and inner moly frame is 9.04 pounds or 0.029 pounds (9.04/312) per unicouple. Since the natural frequency of a cantilever beam with a uniform load of $W\ell$ is approximately equal to that of a cantilever beam with a load of $W\ell/2$ at the free end, this is an acceptable approximation.

These two unicouples were rigidly attached to the shaker head and subjected to a 1 g sinusoidal sweep (2 oct/min. from 20 Hz to 2000 Hz) in the Y axis. The conductor straps were not connected. The measured acceleration response indicated that the wrapped unicouple had the highest peak response. However, it was believed that the damping afforded by the accelerometer leads may have overshadowed the inherent damping of the unicouples. The results of this test and subsequent tests performed at RCA are shown in Table 7.2-4.

The next test was conducted with the accelerometer leads disconnected. A thirty-power microscope was used to monitor the displacement of the hot shoes at the resonant frequency for two different acceleration levels. The results of these tests showed that the response of a wrapped unicouple was approximately 20 percent less than a bare unicouple.

To more closely simulate the RTG configuration, two conductor straps, one from each of two unicouples, were fastened together with a screw and a nut. The remaining two conductor straps were left free. A sine sweep was performed with the accelerometer leads

TABLE 7.2-4. COMPARISON OF RESPONSE OF WRAPPED AND BARE UNICOUPLES TO SINUSOIDAL ACCELERATION

Test Conditions	Unicouple	Response At Noted Input		Resonant Frequency (Hz)
		1 g	2 g	
Straps Not Joined	9526[1]	35.6[3] g	-----	771
Accelerometer Leads Attached	9529[2]	25.9[3]	-----	771
Straps Not Joined	9526[1]	4 Div.[4]	5 Div.[4]	814
Accelerometer Leads Not Attached	9529[2]	5 Div.[4]	6 Div.[4]	835
Straps Joined	9526[1]	2 Div.[4]	3 Div.[4]	840
Accelerometer Leads Not Attached	9529[2]	4 Div.[4]	5 Div.[4]	871

Notes:

1. Unicouple 9526 wrapped.
2. Unicouple 9529 bare.
3. Acceleration response measured with accelerometer during sinusoidal sweep.
4. Displacement response measured with 30X microscope during resonance dwell. One division = 1 mil (approximately)

attached to identify the resonant frequencies. With the accelerometer leads disconnected, the peak displacements, for two different acceleration levels, were read with the thirty-power microscope. The results of this test indicate that the response of the wrapped unicouple is approximately one-half that of the bare unicouple.

7.2.2.3 General Electric Tests

While the tests performed at RCA indicated that the failure at 6.6 g_{rms} random vibration was not representative of the performance of a unicouple in an RTG, it was felt that further tests were required to demonstrate that the 6.6 g_{rms} was actually a severe over-test. A four-couple fixture was used to test each of two bare unicouples. Since the tests at RCA indicated that the accelerometer leads damped the unicouple system to mask the results, it was decided to use an optron to measure displacements.

The first series of tests was performed on two bare unicouples, each of which was tested separately in the four-couple fixture. Figures 7.2-4 and 7.2-5 show the response of the bare unicouple to sinusoidal vibration. As shown, the response and resonant frequency are comparable to that obtained at RCA for a bare unicouple.

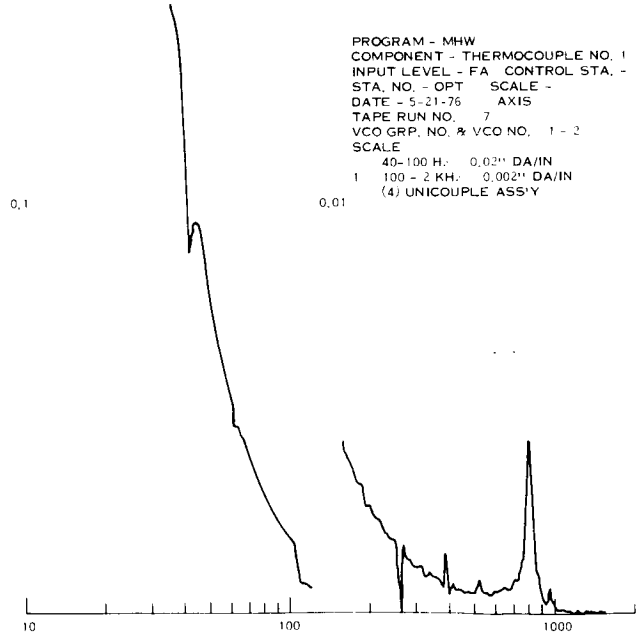

Figure 7.2-4. Sinusoidal Vibration of Unicouple 1, Acceptance Level

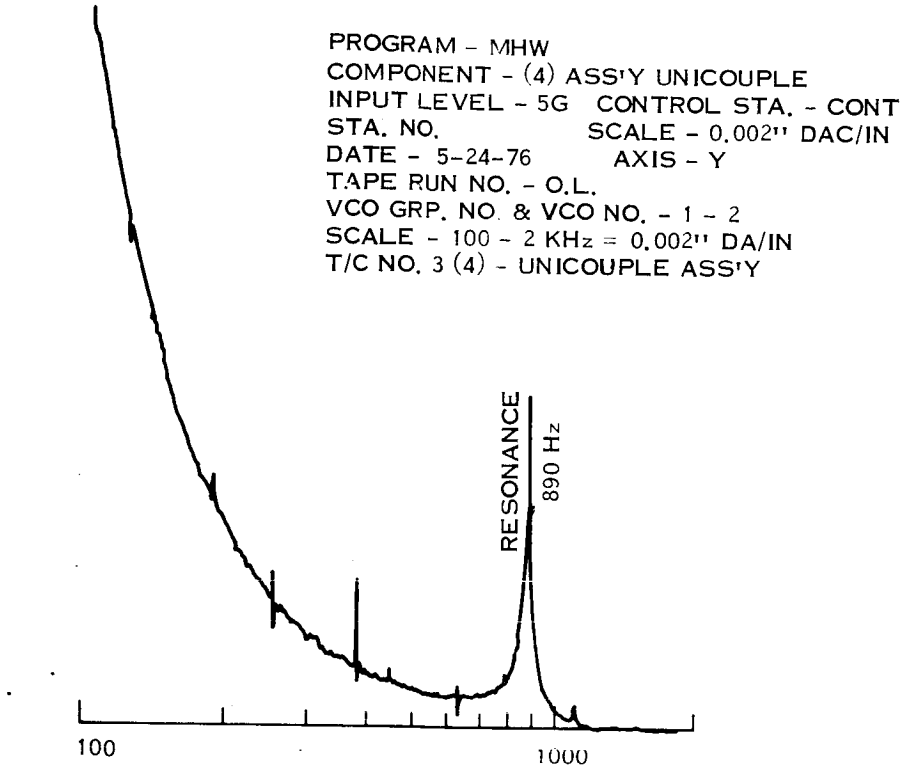

Figure 7.2-5. Sinusoidal Vibration of Unicouple 3, Five g Input

In this same fixture, each of the two unicouples was subjected to random vibration and the displacements were measured. Figure 7.2-6 shows a plot of these response displacements as a function of the input random vibration. As shown, the response is not linear with increased vibration levels. With a three-fold increase in input vibration (from 6.6 to 20 g_{rms}), the increase in response is about 40 percent.

The second series of tests was performed on the D5A module, which consisted of 14 unicouples configured to simulate closely the installed configuration in the RTG. Figures 7.2-7 through 7.2-9 show the response of two different unicouples due to sinusoidal vibration. Comparison of Figures 7.2-9 and 7.2-4 show the difference in response of the bare unicouple with that expected from a unicouple installed in the RTG. Since the vibration input and the response scale were identical, the effect of damping may be estimated by comparison of the peak responses from each curve. As shown, the response of a unicouple installed in the D5A module (and thus in the RTG) was expected to be less than 10 percent of the response of a bare unicouple.

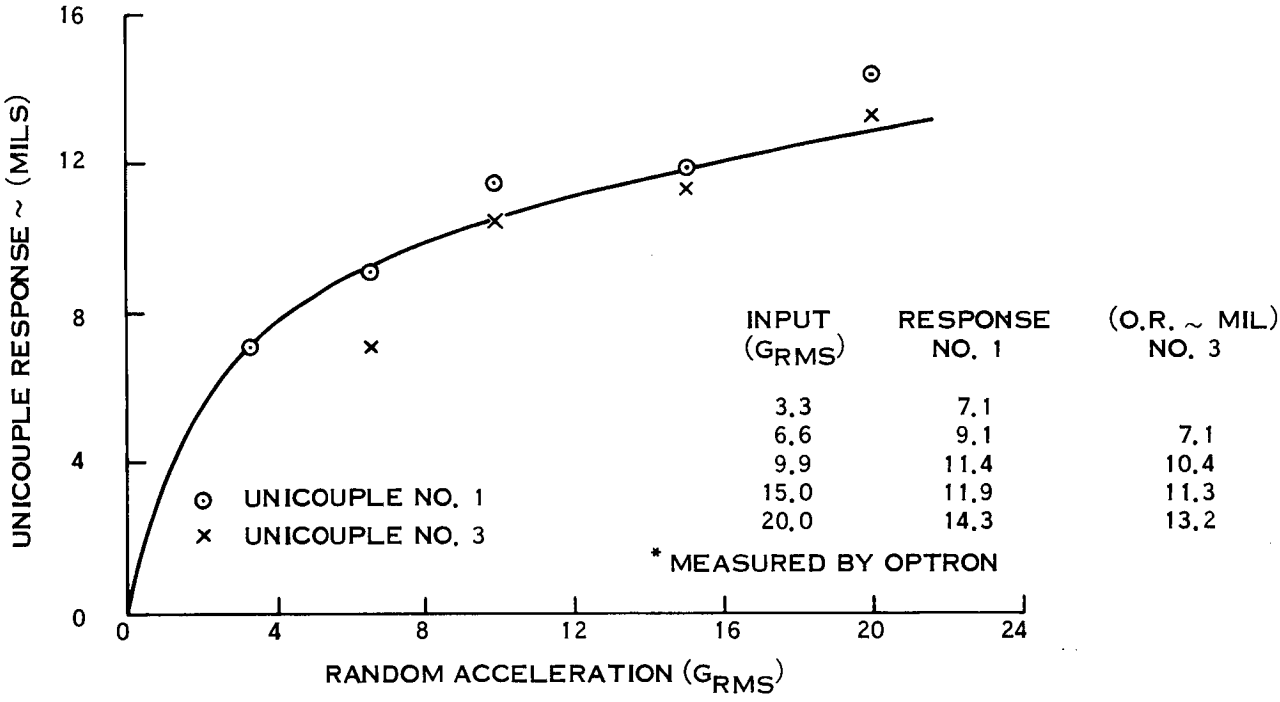

Figure 7.2-6. Response Double Amplitude of Two Unicouples to Random Excitation

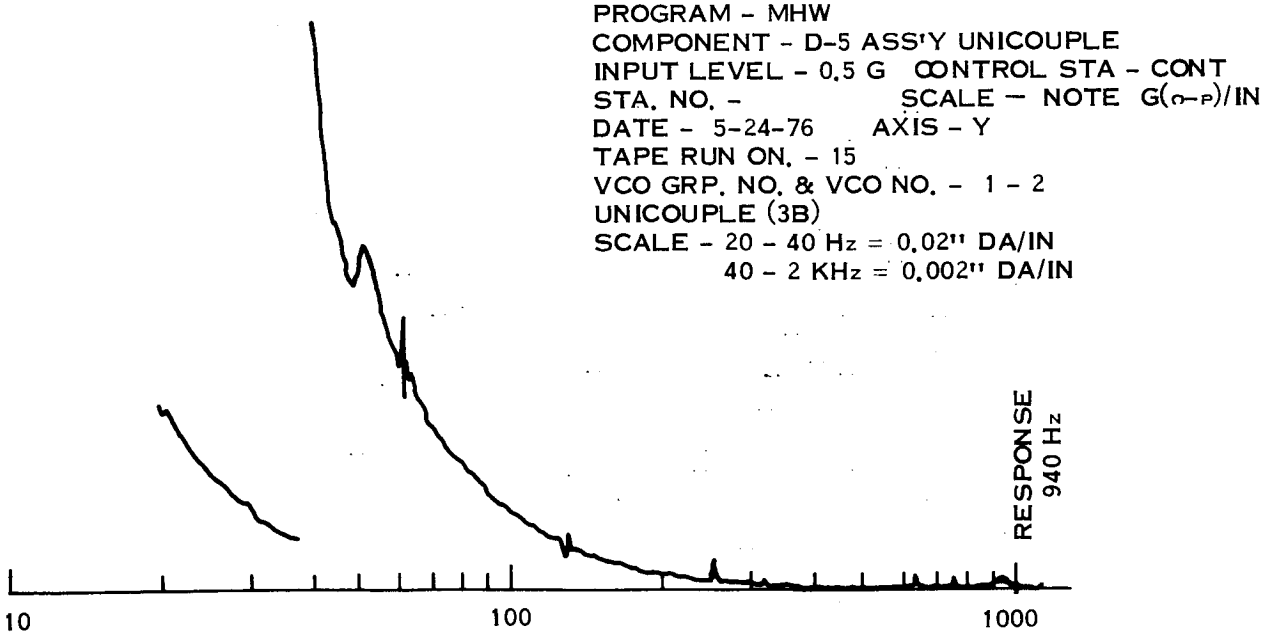

Figure 7.2-7. Sinusoidal Vibration D-5A Module, 5 g Input

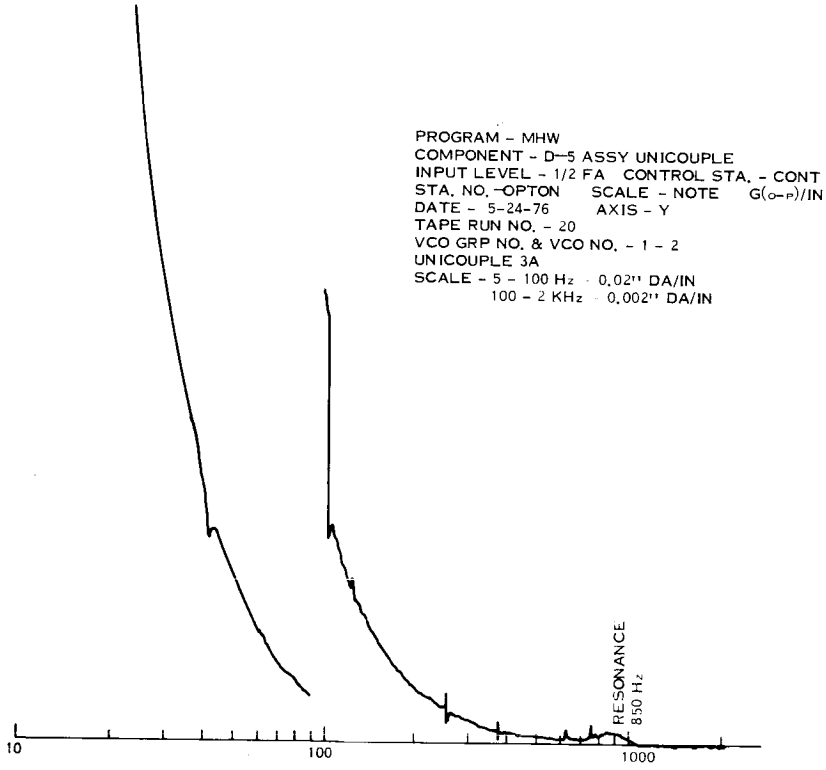

Figure 7.2-8. Sinusoidal Vibration D-5A Module, 1/2 Acceptance Level

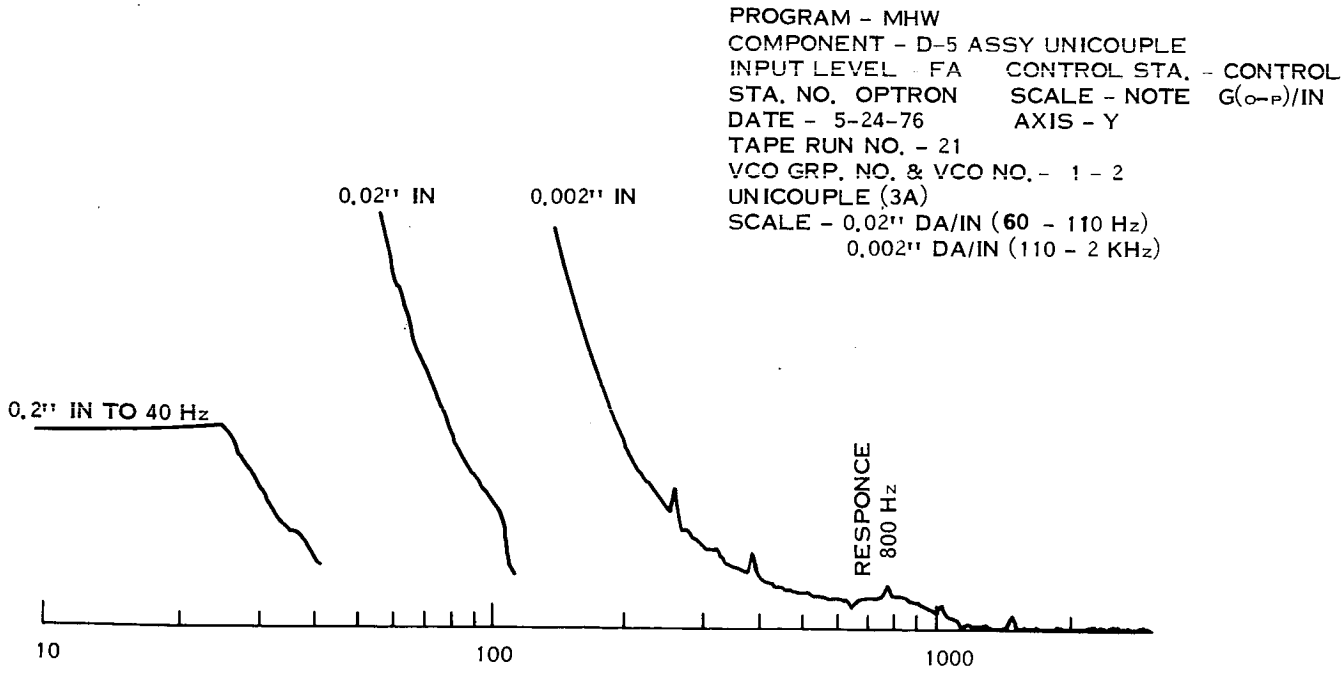

Figure 7.2-9. Sinusoidal Vibration D-5A Module, Acceptance Level

After the sinusoidal tests were completed, the 14 unicouples installed in the D5A module were sequentially exposed to random vibration of 3.3 g_{rms} and 6.6 g_{rms}. During these tests it was found that the measurement system was not sufficiently sensitive to adequately determine the displacement of the unicouples during random vibration. It was estimated that the threshold of sensitivity was approximately 2.8 mils.

7.2.3 CONCLUSIONS

Based on the described tests, it is concluded that:

1. Displacement response of bare unicouples to the 20 g_{rms} random vibration was about 40 percent greater than the response of bare unicouples to 6.6 g_{rms} random vibration.

2. Displacement response of bare unicouples to sinusoidal vibration was about 10 times greater than the response of unicouples to sinusoidal vibration when installed in the D5A module.

3. Comparison of displacement response of bare unicouples and D5A installed unicouples to random vibration was not possible with any degree of certainty because the sensitivity of the measurement system was not sufficiently accurate to discern motion less than about 2.8 mils. However, even assuming that the unicouple displacement response in the D5A was 2.8 mils, it would still be about one-third of the displacement response of a bare unicouple.

4. The tests, performed at RCA, of the bare unicouple to the 6.6 g_{rms} random vibration spectrum represents a severe overtest compared to that expected for unicouples installed in the RTG during acceptance testing.

7.3 DESIGN TESTING

Testing of components to define their magnetic characteristics were carried out as described in the MJS Annual Report for 1975 GESP-7127 (GEMS-428). Magnetic signature determinations on the as-built RTGs were planned for performance at the NASA Goddard facilities, but various problems of scheduling and handling of the fueled units resulted in a change of plans. Decisions to carry out the magnetic signature determination at GE-SD were reached in May 1976. Subsequent to the shipment of F-6 and F-7 RTG to ML/MRC, arrangements to perform the magnetic field characterization tests were made using equipment supplied

by JPL. Testing was begun with the F-8 and F-9 RTGs in Building 800 and continued afterward in Building 300, on F-10, F-11, and F-12 RTGs. The test equipments were set up and the fueled RTGs were handled by GE-SD personnel. All data acquisition, reduction and analyses were carried out by JPL and NASA Goddard personnel.

Magnetic characterization of the F-6 and F-7 RTGs was obtained by JPL as part of the activities at KSC during June 1977. The results of these tests are given in the JPL reports.

7.4 RTG PERFORMANCE ANALYSES

7.4.1 MODULE TESTING

Four-couple and 18-couple modules have been tested for times up to 30,000 hours to provide a data base for the prediction of full-scale converter performance for space missions of four to five years. All module testing was terminated by January 1977.

These modules provided kinetic data as a function of temperature for the four major degradation modes of the MHW converter; namely, (1) dopant precipitation effects, (2) thermal insulation conductance degradation, (3) electrical insulation degradation, and (4) effects of CO.

7.4.1.1 Dopant Precipitation Effects

Updated T/E property data was received from JPL in September 1976. This update was the result of measurements and analyses done by Raag of Syncal Corp. The new data were incorporated into the module data reduction computer program. Figure 7.4-1 shows the results for 180 (1035^{0}C uncoated couples) using the old and new T/E data, for the ratios of the measured to theoretical power, internal resistance and open circuit voltage. The theoretical values are calculated from the measured hot and cold junction temperatures to eliminate the effect of insulation conductance changes and leg conductance changes on power and open circuit voltage, so that only changes due to dopant precipitation (and bond resistances) can be correlated. An effective T/E age of 100 hours was used for the couples at the start of testing.

If the test data agree perfectly with the theoretical, the plot would show a horizontal line at a ratio of 1.0. A resistivity multiplier of 1.075 and a Seebeck multiplier of 0.969 were applied to the T/E property data over the entire time range for the old T/E data. These multipliers were determined from the measured internal resistance and open circuit voltage of the full scale TBC-4 converter at 1500 hours of age time. For the new T/E data, the Seebeck multiplier is 0.977 and the resistivity multiplier is 1.056.

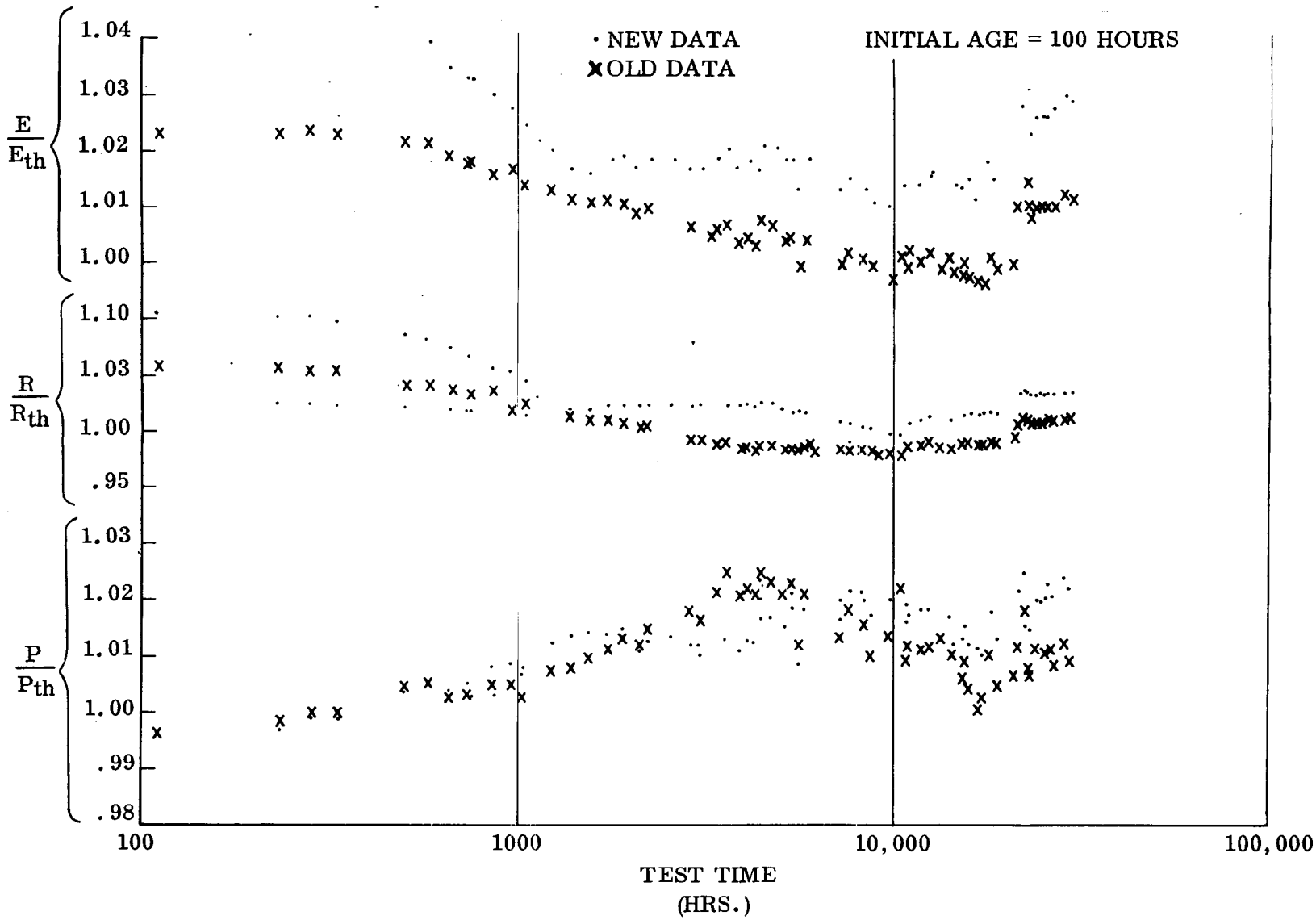

Figure 7.4-1. Module 18D Old and New T/E Data

What is of primary concern is not the absolute level but rather the slope of the curves. A positive slope indicates less degradation predicted. Use of the new data shows the slope of the power ratio to be positive, indicating slightly less degradation than predicted from the dopant precipitation model. The old data gave a slightly negative slope in the 6,000 to 23,000 hour time interval indicating, 1 percent more degradation than predicted in this interval.

Figure 7.4-2 shows the 18D data for previous age times of 100 and 800 hours, using the new data. It is seen that a better fit to the data is achieved by using an 800 hour effective age time at the start of testing. It is seen that out to 30,000 hours of test time the slope is flat within ± 1 percent. The remaining module plots have a previous age time of 100 hours.

Figure 7.4-3 and 7.4-4 shows the measured-to-theoretical ratios for the other two modules (without the Si_3N_4 coating) operating at 1035°C. Module 18E shows the same spread in power ratio as 18D, i.e., ± 1 percent.

Module 18G, Figure 7.4-4, shows the same general trend as the other two modules when allowance is made for the step changes in indicated temperature level at 4,200 hours and 28,800 hours.

Figure 7.4-5 shows the performance of module 18H operated at a 985°C hot shoe temperature for 30,000 hours.

Figures 7.4-6 to 7.4-12 show the performance of the 18 couple modules having the Si_3N_4 coating. Figure 7.4-6 shows module SN-3, operated at 1035°C with a previous age time of 100 hours. The power trend is upward again, indicating less degradation due to dopant precipitation effects than predicted. Figure 7.4-7 shows the trends for a previous age time of 100 and 800 hours. As in 18D, better agreement is found with the 800 hour previous age time for the first few thousand hours of testing. It is also noted in comparison with 18D (Figure 7.4-2), that the coated module is continuing to show an upward power ratio trend out to 20,000 hours, which means slightly less degradation than predicted.

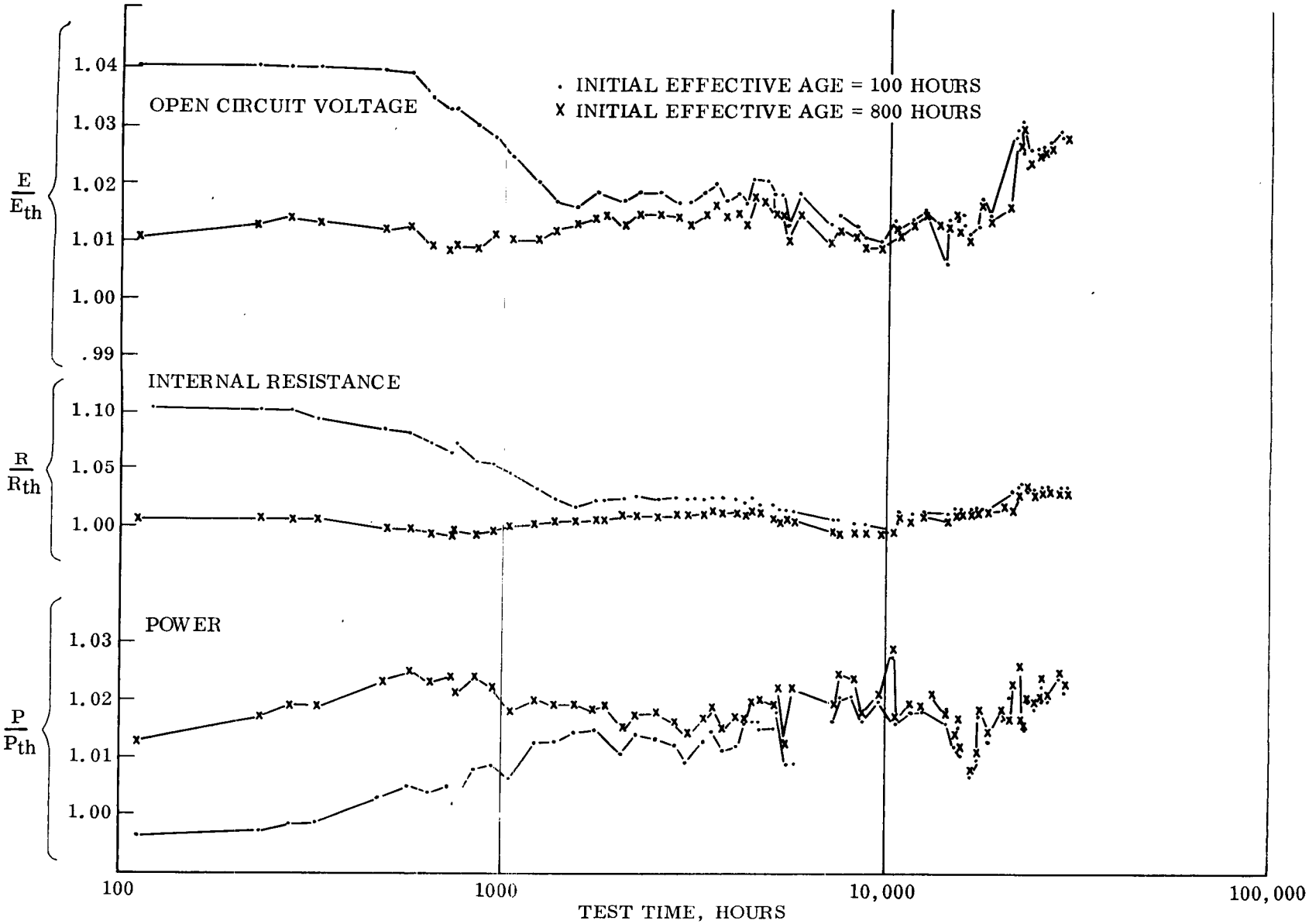

Figure 7.4-2. Module 18D Comparison of Measured to Theoretical Performance

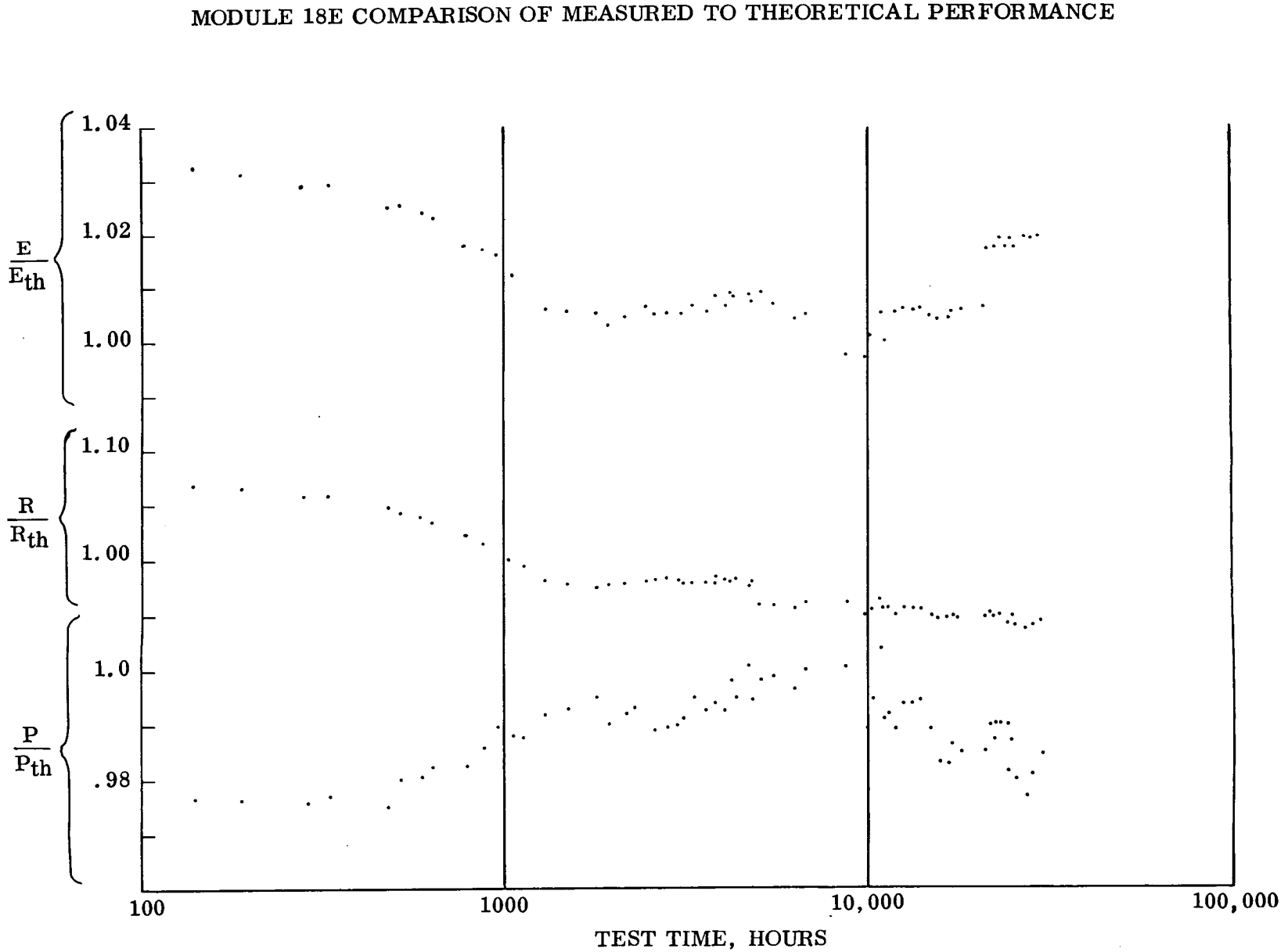

Figure 7.4-3. Module 18E Comparison of Measured to Theoretical Performance

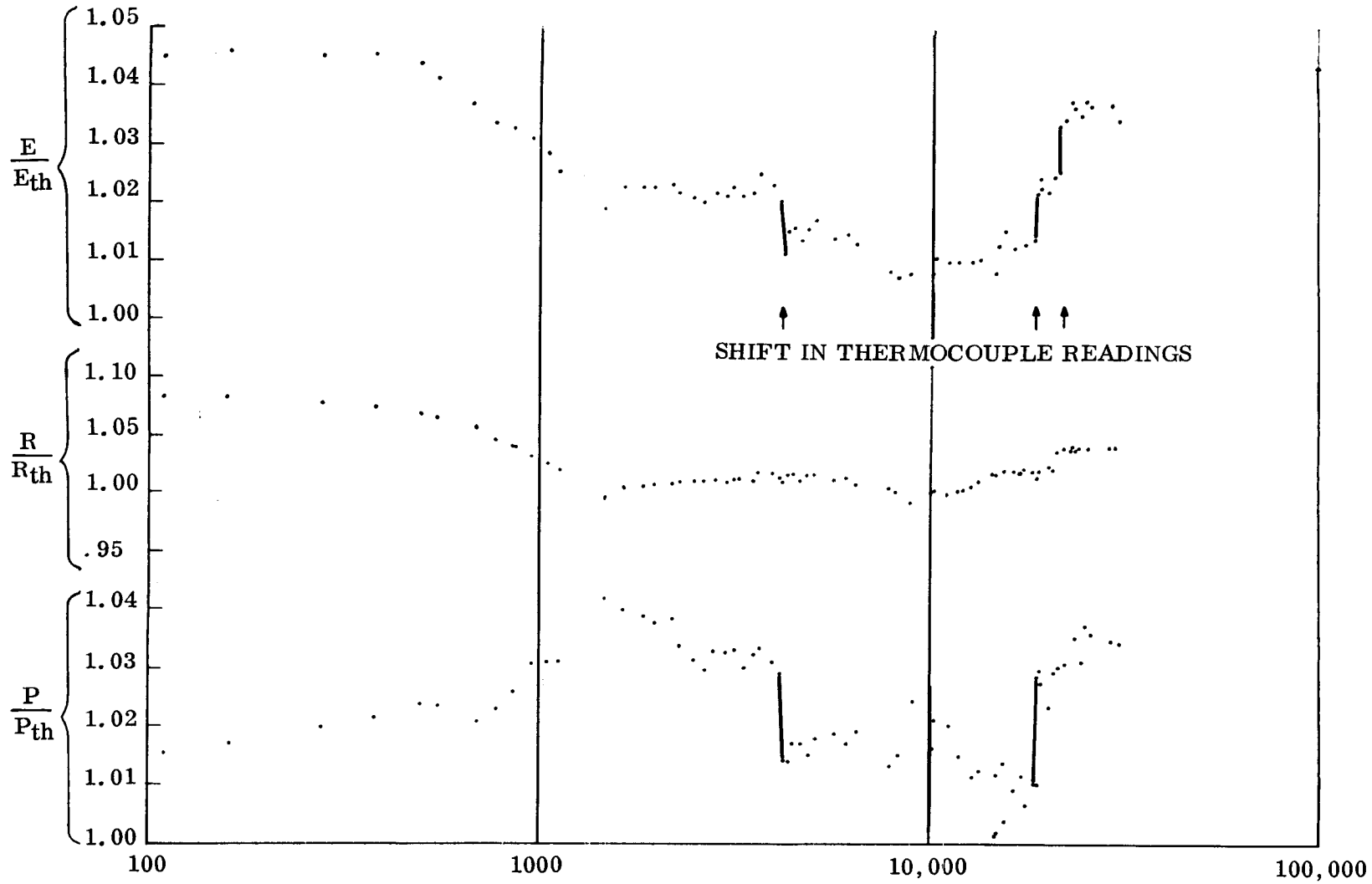

Figure 7.4-4. Module 18G Comparison of Measured to Theoretical Performance

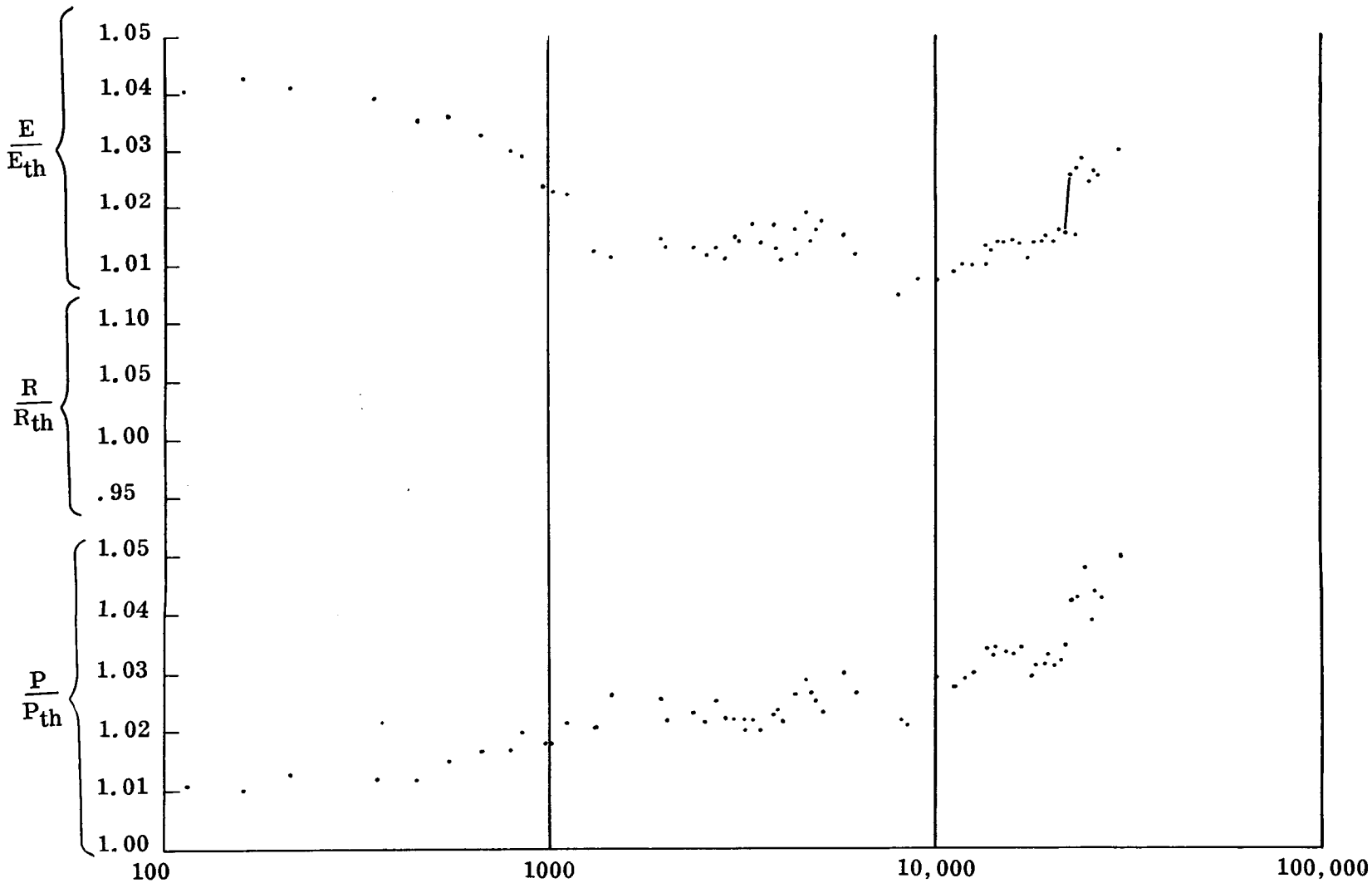

Figure 7.4-5. Module 18H Comparison of Measured to Theoretical Performance

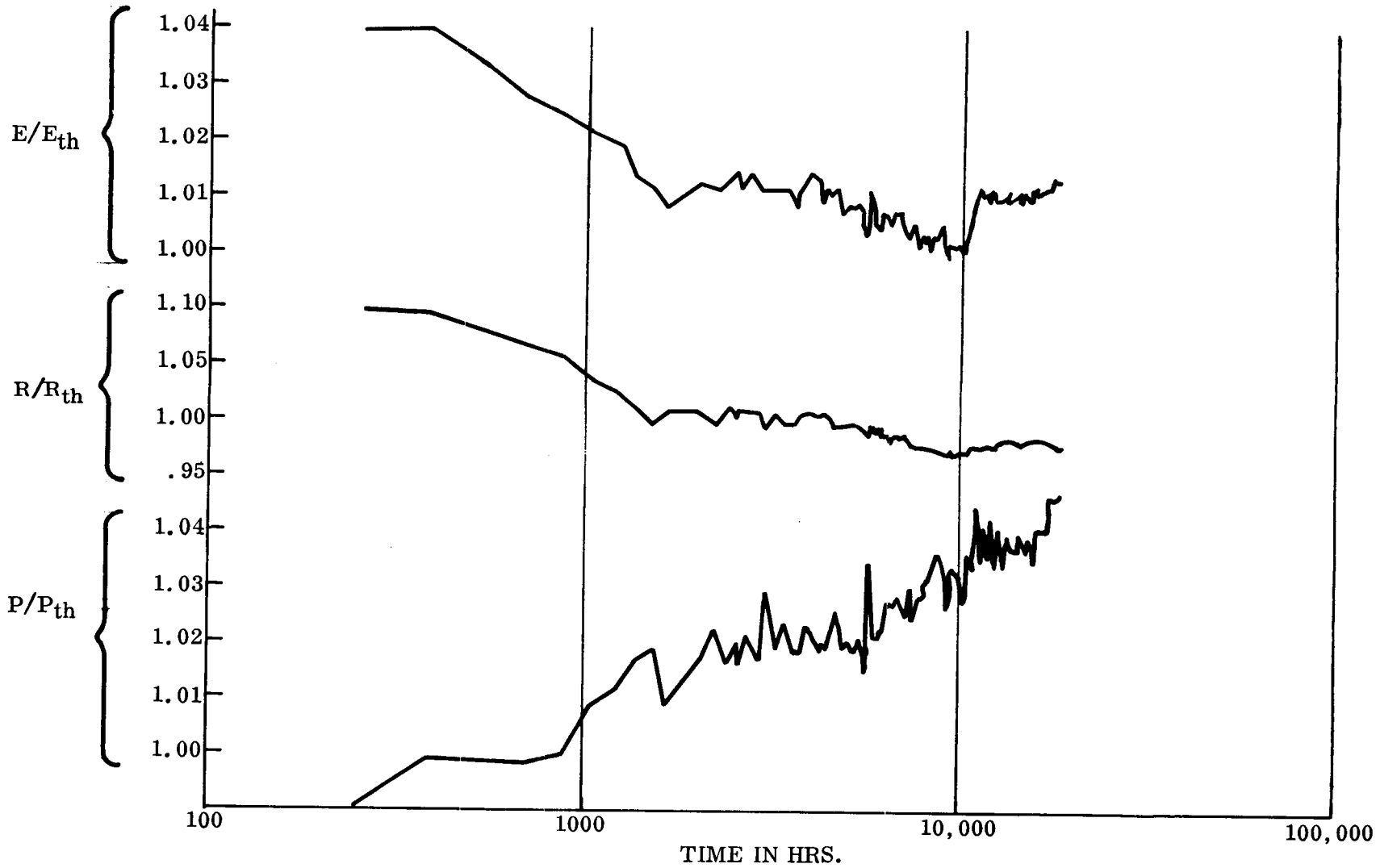

Figure 7.4-6. SN-3 1035°C New Data, DR Factor

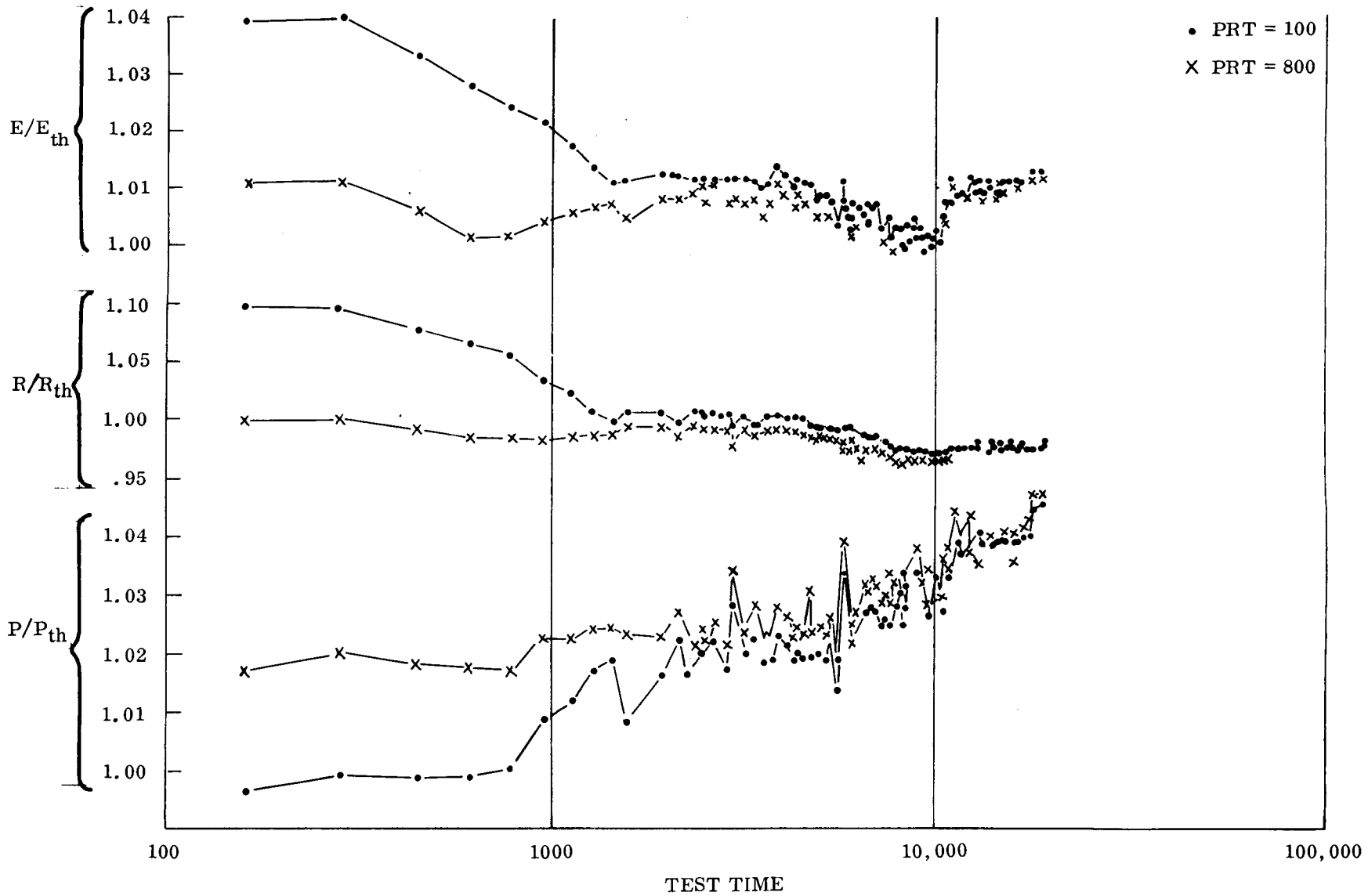

Figure 7.4-7. SN-3 1035°C New Data, DR Factors

Figure 7.4-8 shows the performance of the other 1035°C Si_3N_4 module, SN-6, with a previous age time of 100 hours. It is showing the same type of trend as SN-3.

Figures 7.4-9 and 7.4-10 show the performance of the two modules operated at 1085°C. Again, the power ratio trend is upward and appears to be leveling out at 10,000 hours indicating sublimation effects.

Figures 7.4-11 and 7.4-12 show the performance of the two Si_3N_4 modules operating at 1135°C, SN-1 and SN-4A. The power ratio and resistance trends clearly shows the effects of sublimation beyond 10,000 hours for SN-1.

It is concluded from these 18-couple module test trends that, at the design operating temperature of 1035°C, the power loss due to dopant precipitation effects will be slightly less ($\sim$ 1 percent) than predicted using the updated T/E data.

7.4.1.2 Thermal Insulation Conductance Changes

The sublimation and reaction products, namely Si, Ge and SiO generated at the hot zones of the T/E couple, migrate to the cold regions of the RTG and condense there. These condensates increase the thermal conductance of the SiO_2 wrap around the T/E legs, and increase the emissivity of the molybdenum foils. The result is a reduction in hot junction temperature and a loss of some output power.

From the 18-couple module data, the heat flow through the insulation system is calculated by subtracting the calculated heat flow through the T/E legs and heater leads from the total measured heat input. The conductance is this net heat flow divided by the measured temperature drop from hot junction to cold junction.

Previously, the insulation thermal conductance was determined by taking into account the change in leg thermal conductivity due to temperature. The present data reduction also incorporates the change in leg conductivity as a function of time, due to the initial inhomogenity of the SiGe alloy.

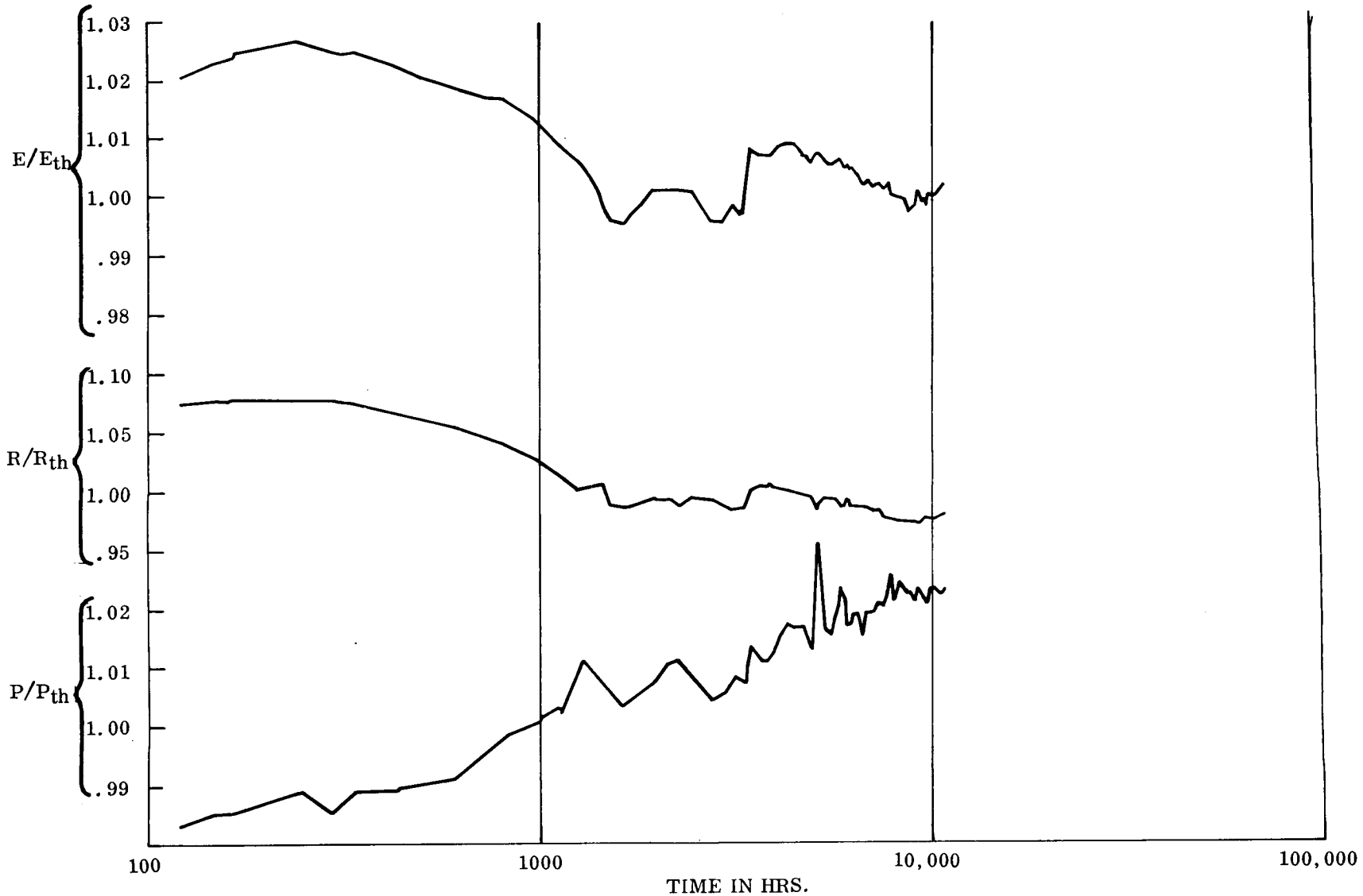

Figure 7.4-8. SN-6 1035°C New Data, DR Factor

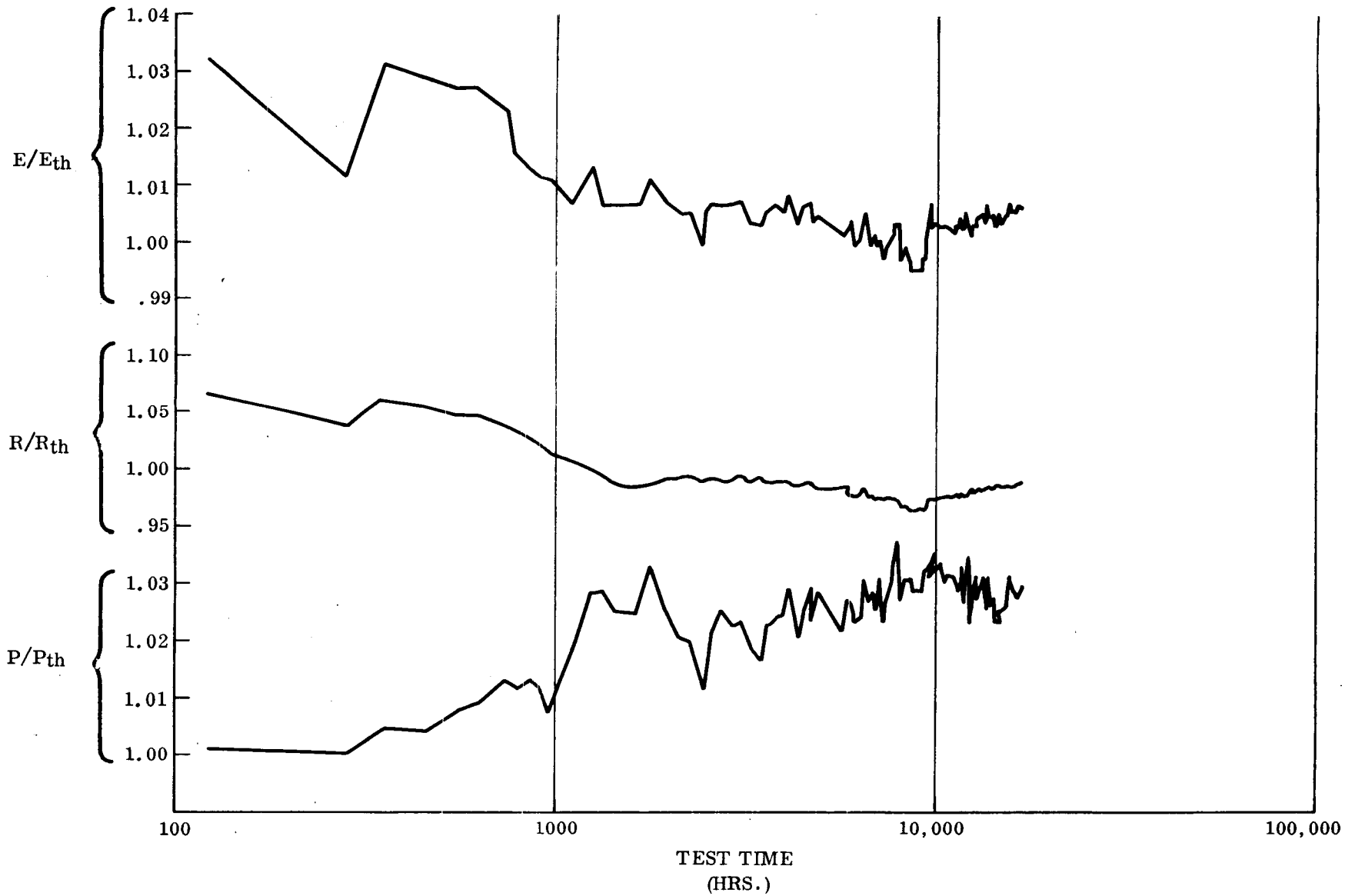

Figure 7.4-9. SN-2 1085°C New Data, DR Factors

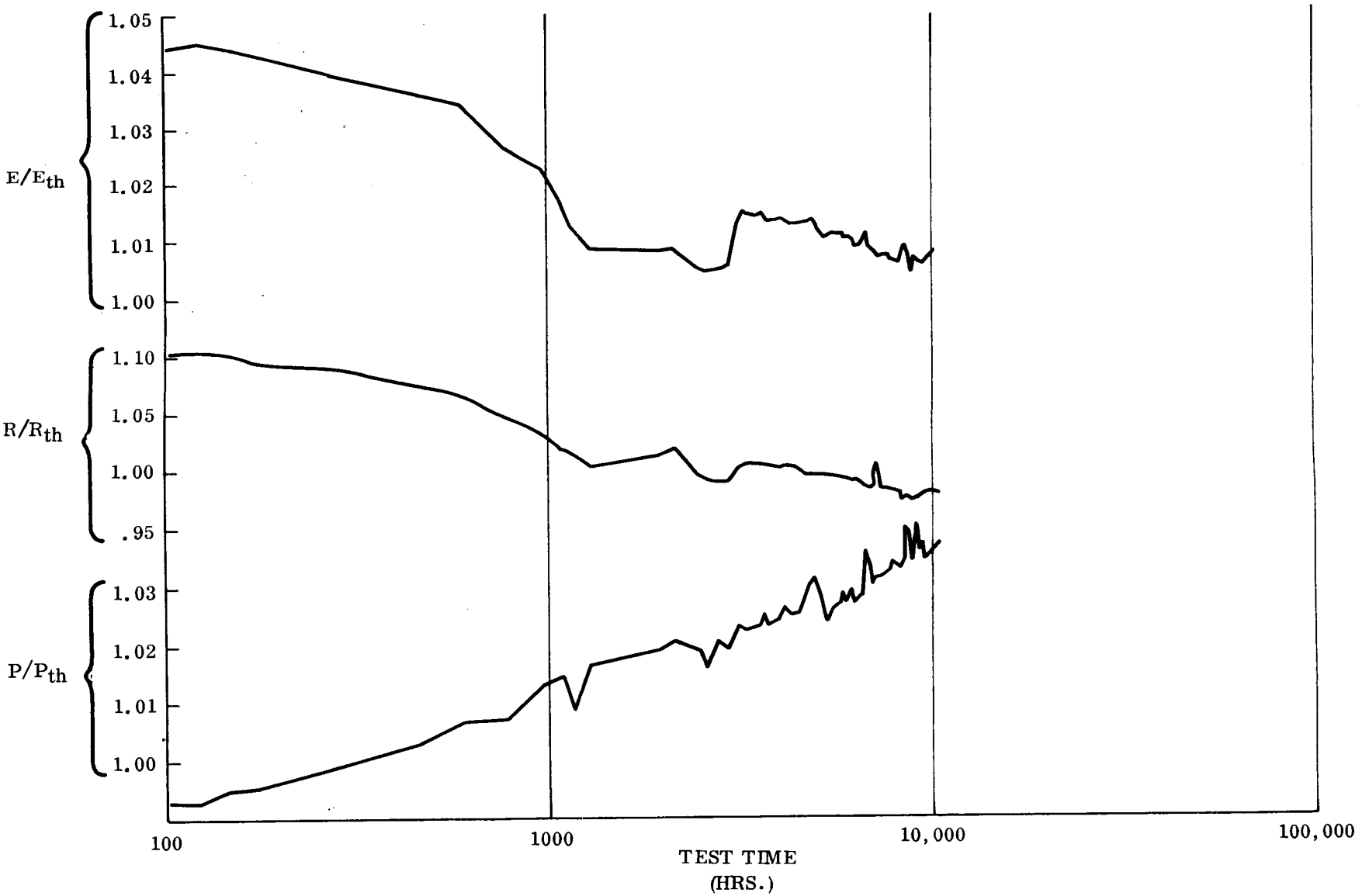

Figure 7.4-10. SN-5 1085°C New Data, DR Factors

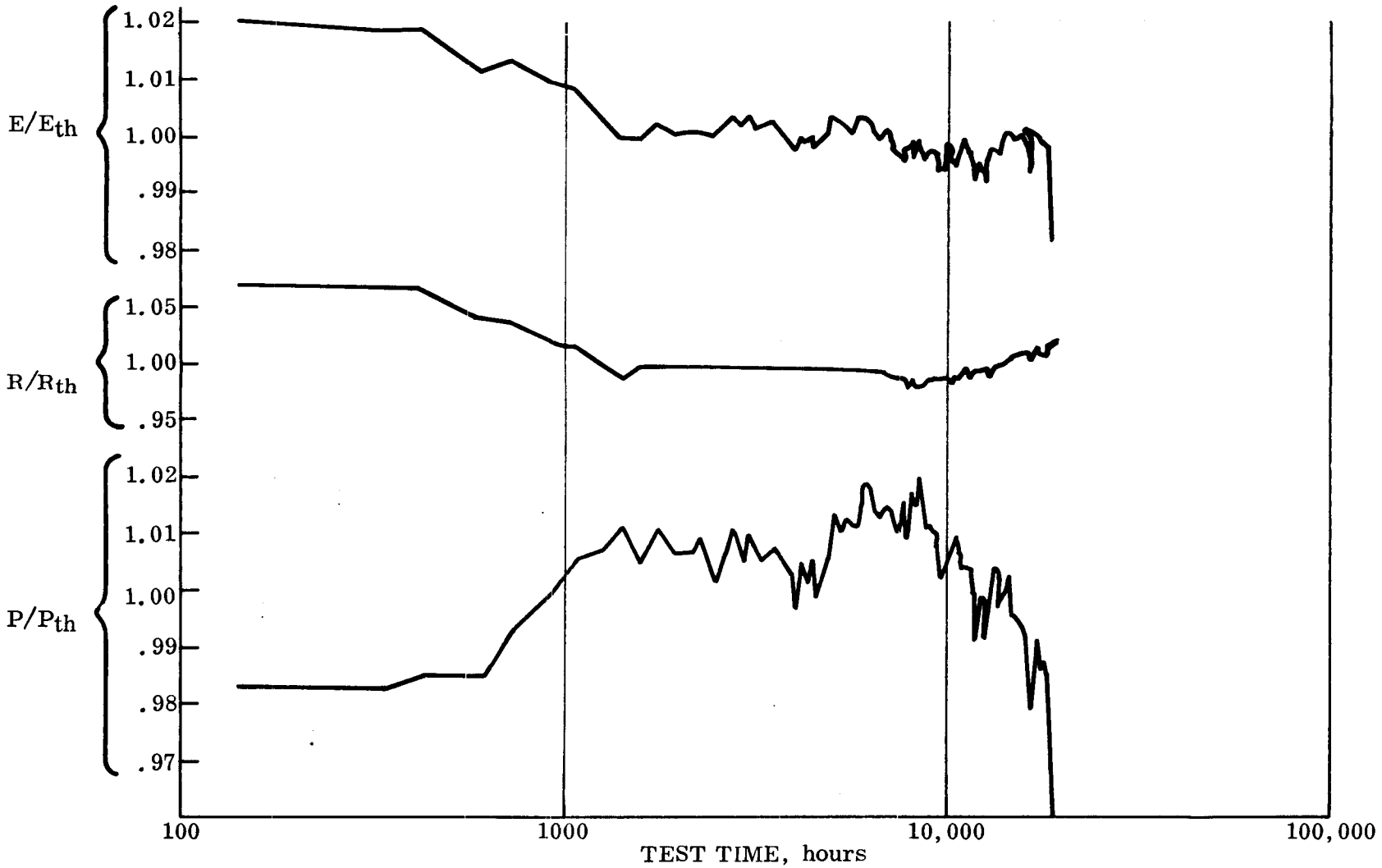

Figure 7.4-11. SN-1 1135°C New Data, DR Factors

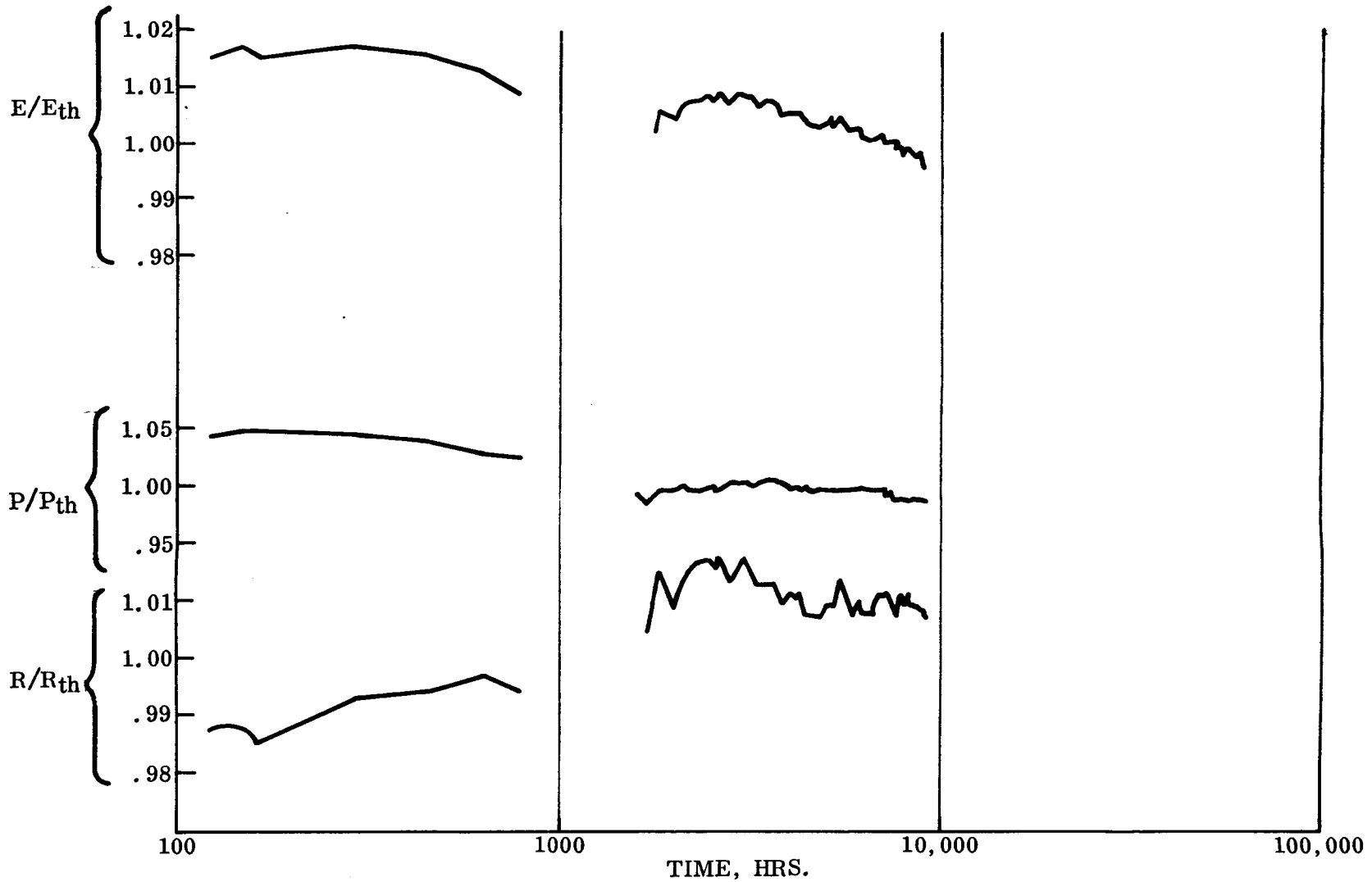

Figure 7.4-12. SN-4A 1135°C New Data, DR Factors

Figure 7.4-13 shows the updated ratio of the thermal conductance to its initial value for the uncoated and Si_3N_4 coated modules. The conductance change is clearly a function of temperature, related to the mass of silicon subliming from the T/E couples. The effect of the Si_3N_4 coating is seen by comparing the ratio for coated and uncoated couples operating at the same temperature. For example, 18D (uncoated) and SN-3 (coated), operating at the design initial hot shoe temperature of 1035°C, show changes of 9 percent and 30 percent, respectively, in thermal conductance at 18,000 hours, as shown in Figure 7.4-14.

The TEGS thermoelectric degradation program has been updated using the data from SN-3 to take into account the change in conductance of a full scale RTG with temperature and time. The correlation used is shown in Figure 7.4-15 where the conductance is a function of the cumulative amount of silicon sublimed. The program calculates the quantity of silicon sublimed as a function of time and temperature and incorporates the change in conductance into the overall heat balance in calculating the hot junction temperature in the time increment being considered.

For Si_3N_4 coated couples, the effect of insulation conductance change on end of mission power output is small, being less than 3 watts for a four year mission.

7.4.1.3 Electrical Insulation Degradation

Eighteen-couple modules were tested to determine the effect of temperature and the Si_3N_4 coating on the long-term resistance between the T/E circuit and the foil thermal insulation. The uncoated couple testing reached 30,000 hours while coated couple data reached 18,000 hours at 1035°C and 23,000 hours at 1135°C.

Figure 7.4-16 shows the updated performance of the uncoated 18-couple modules. The modules operated at an initial hot shoe temperature of 1035°C are shown in Figure 7.4-17. (The jumps in resistance shown were due to module shutdowns.) There is sufficient test time to reasonably extrapolate the data for four years. Table 7.4-1 shows the extrapolated resistance at four years and the calculated power loss that would occur in a full-scale converter.

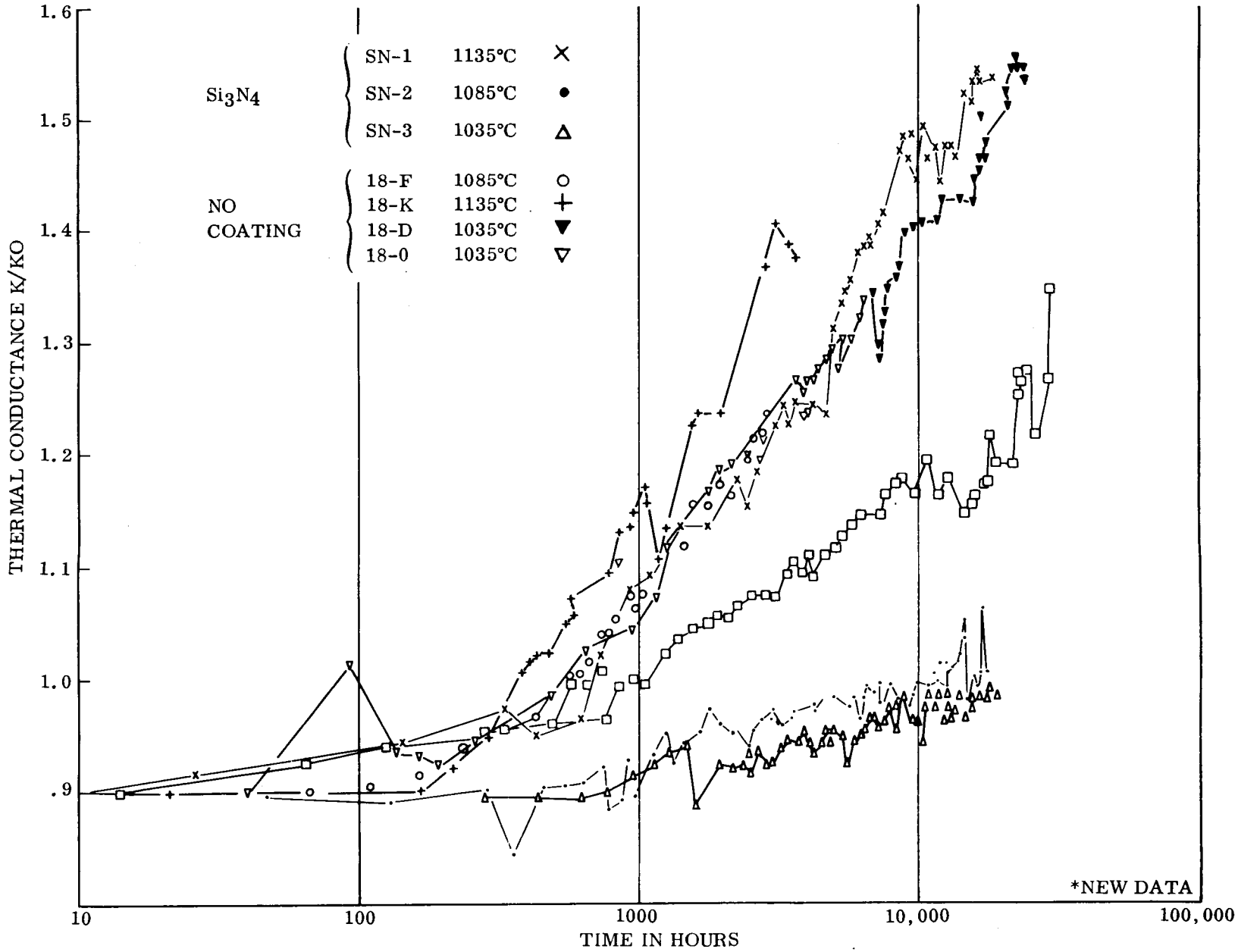

Figure 7.4-13. T/E Leg Conductivity Changes Taken into Account

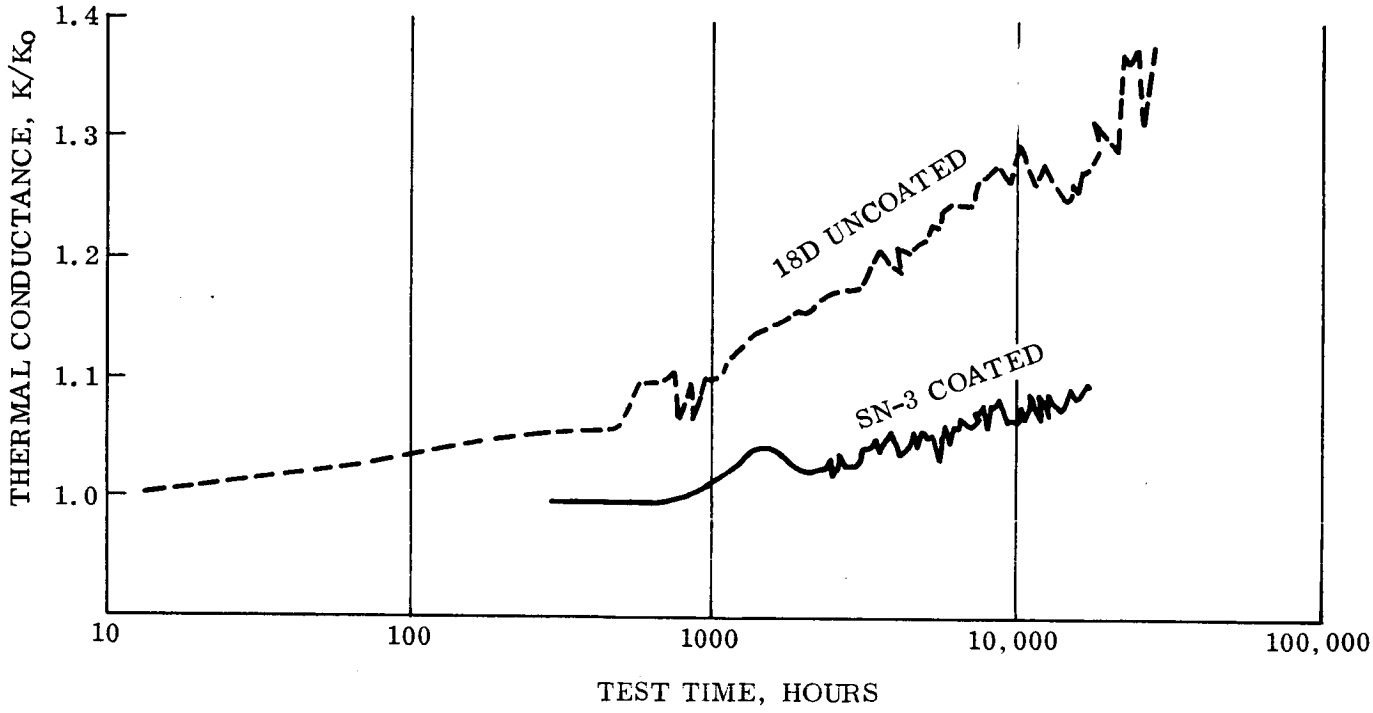

Figure 7.4-14. Insulation Thermal Conductance Ratio

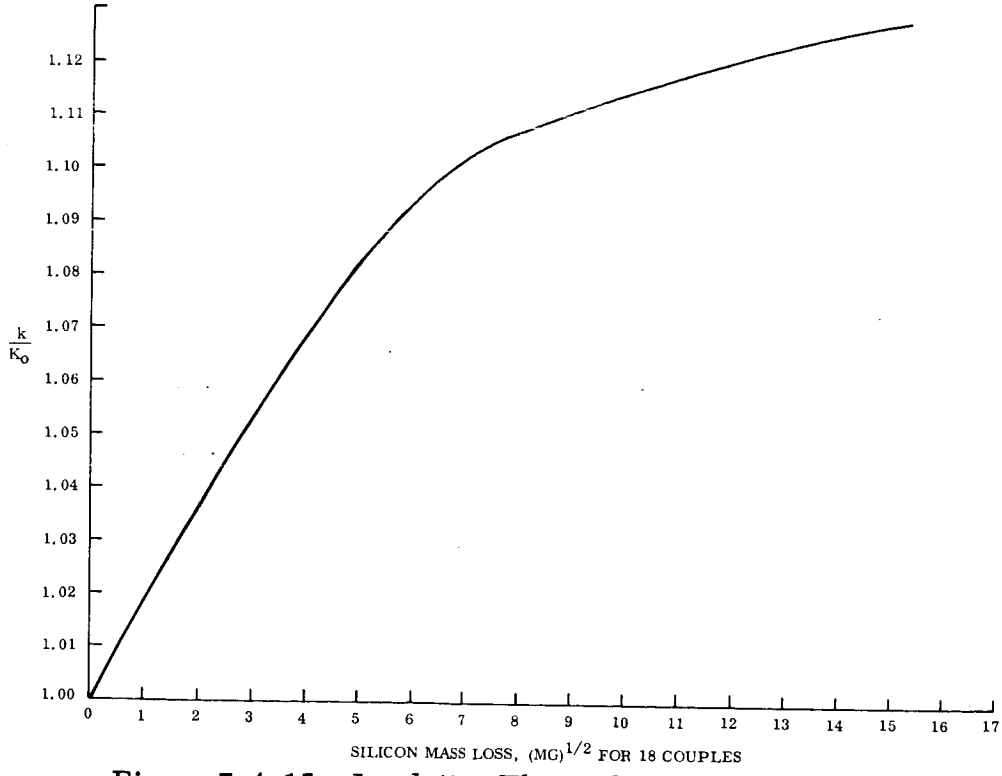

Figure 7.4-15. Insulation Thermal Conductance Change

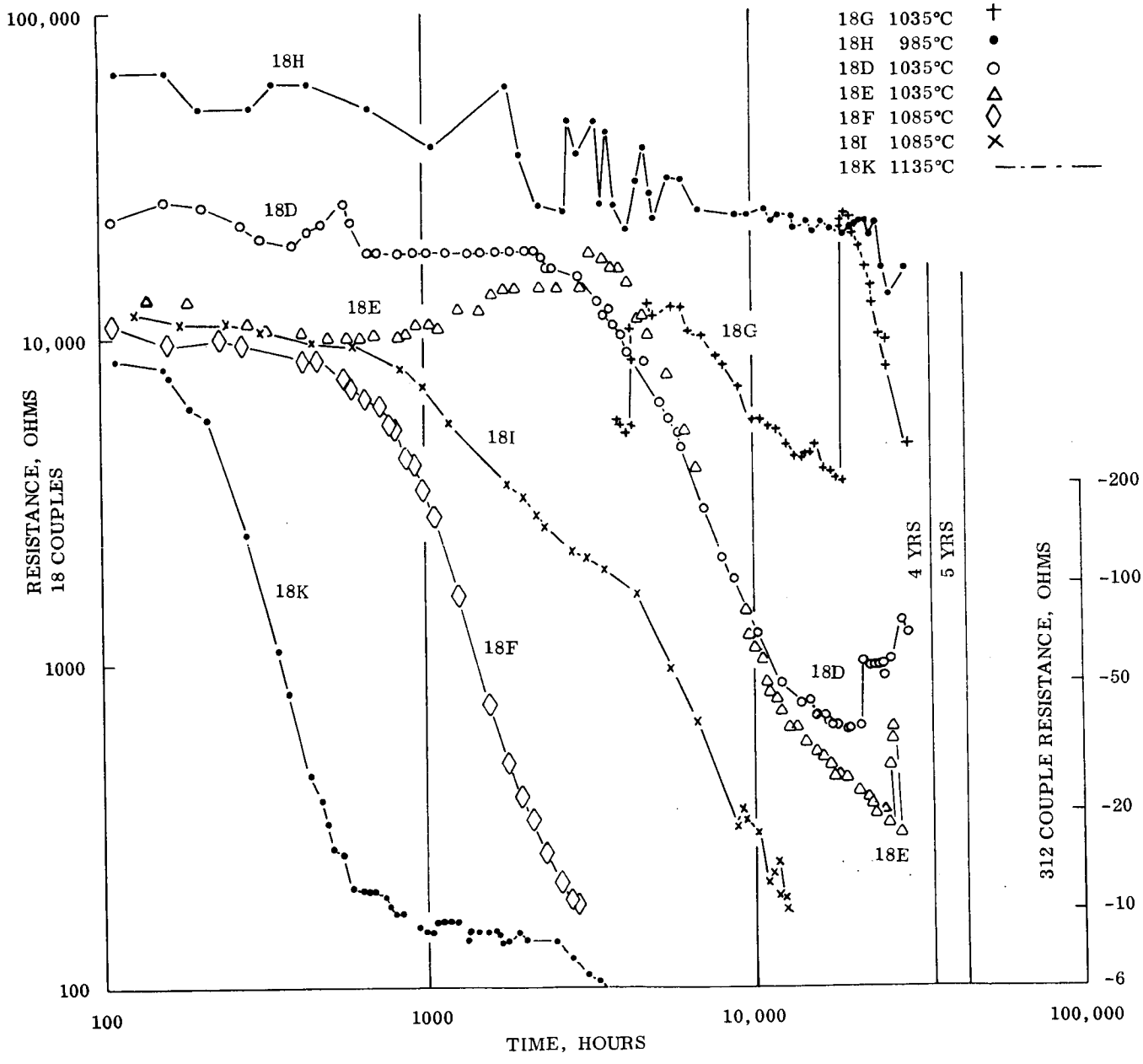

Figure 7.4-16. 18-Couple Modules Resistance to Foil

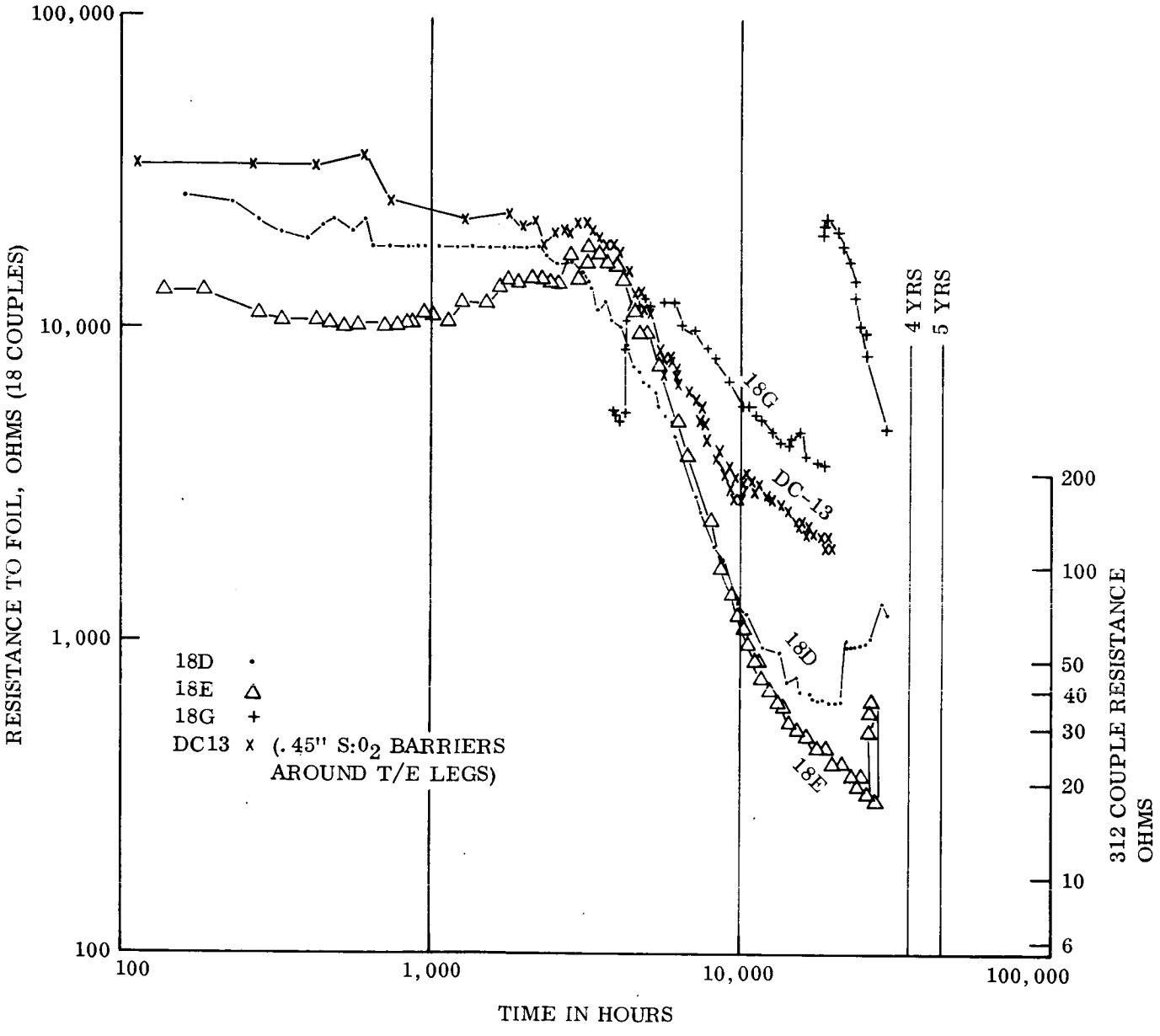

Figure 7.4-17. Modules 18D, E, G and DC-13 Uncoated Couples

Table 7.4-1. EXTRAPOLATED RESISTANCE TO FOIL AT FOUR YEARS UNCOATED COUPLES

Module	18-Couple Resistance, Ohm	Full Scale Converter Resistance, Ohms	Power Loss(2) Watts
18D	500	28.8	2.6
18E	250	14.4	5.2
18G	1000	57.8	1.3

(2) Power loss = $\frac{V_L^2}{12\ R_f}$ when V_L = load voltage

R_f = resistance to foil

Figure 7.4-18 shows the performance of the two Si_3N_4 coated modules operated at an initial nominal hot shoe temperature of 1035°C (Hot Junction - 1000°C) along with the uncoated module 18D. SN-3 (coated) showed the downward trend at 11,000 hours, while SN-6 was just reaching that test time when the modules were shut down. It is noted, from Figure 7.4-16, that all modules have a similar slope on the log-log plot (except 18I for a period and 18G which had a number of shutdowns and was not instrumented for resistance measurements until 3,900 hours). Applying this slope in the linear region to the SN-3 data results in a four year resistance of greater than 4,000 ohms, which is equivalent to over 230 ohms in a full-scale converter, or negligible power loss. Eighteen-couple modules operated at 1035°C have a CO pressure level lower than in the full-scale converter because of the openings in the outer case, compared with the PRD in the RTGs. Taking into account the maximum initial CO level calculated for the RTGs (see para. 7.4.1.4) of 4×10^{-5} Torr, the mass loss would be accelerated, shifting the resistance curve to the left by a factor of ~ 1.5, resulting in an extrapolated resistance to foil of ~ 100 ohms. This is a conservative extrapolation since SN-3 operated at a constant hot shoe temperature of 1040°C ± 3°C, whereas the flight units will experience a drop in temperature of 30°C over the four year mission.

Figure 7.4-19 shows the resistance to foil of all the Si_3N_4 coated modules operated at the design temperature of 1035°C, and the accelerated tests at 1085°C and 1185°C.

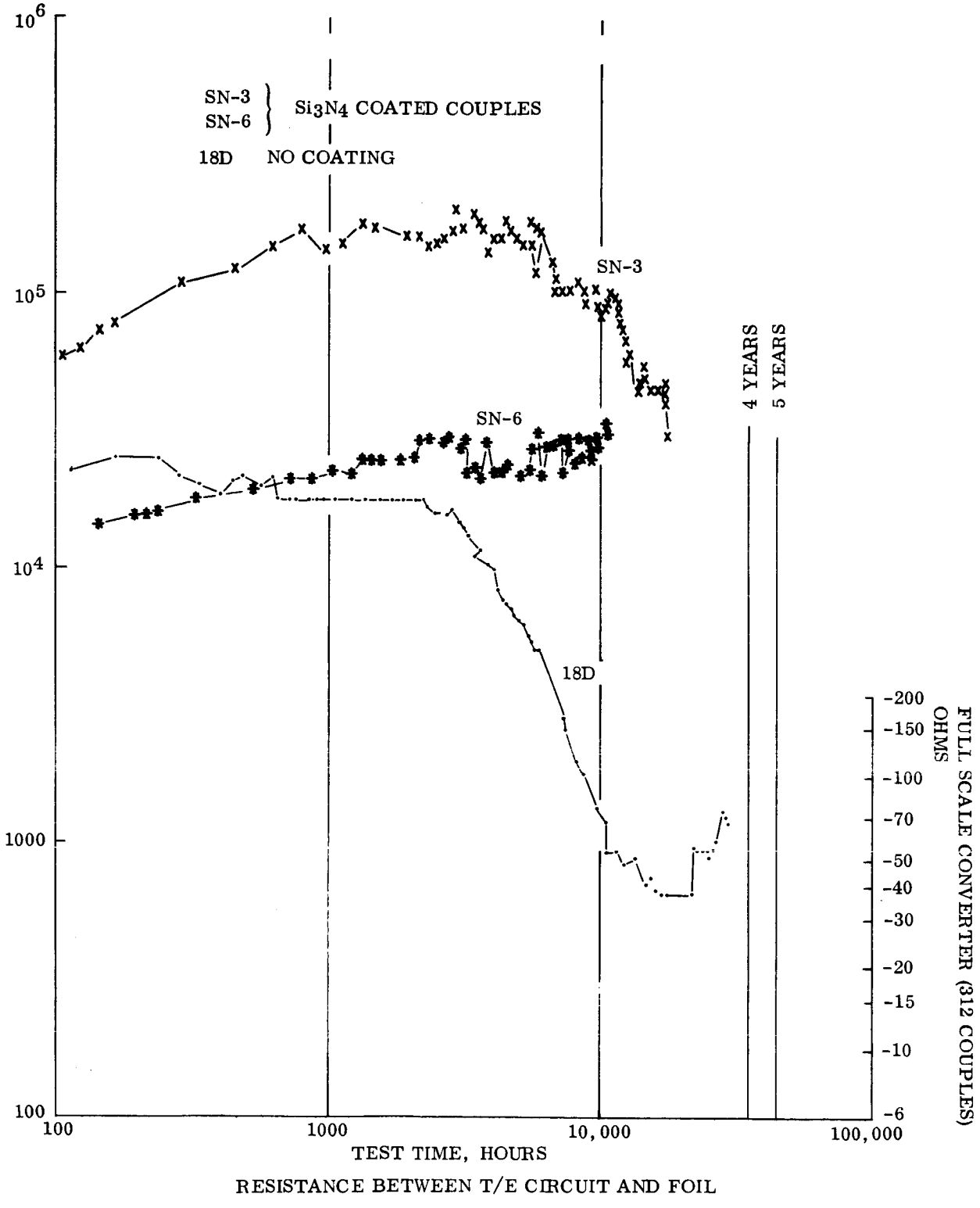

Figure 7.4-18. Modules Operated at 1000°C Hot Junction Design Temperature

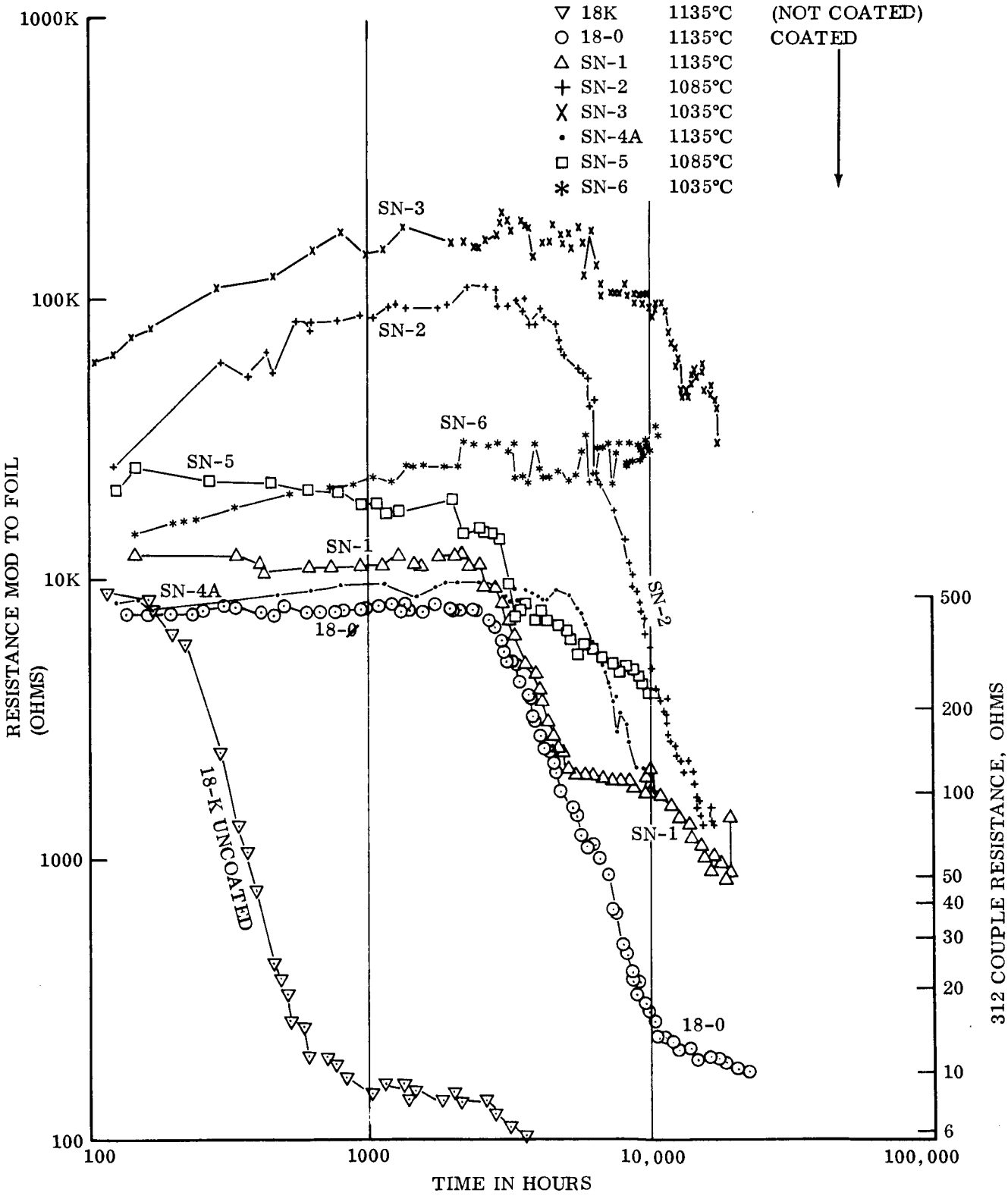

Figure 7.4-19. 18-Couple Modules, Resistance to Foil

A more accurate interpretation of the Si_3N_4 module data requires consideration of the actual hot junction temperature as a function of time and CO pressure level in the module.

Figure 7.4-20 shows the calculated mass of silicon that was evolved from the couples and affects the resistance. The mass was calculated from Figure 7.4-21, which is taken from JPL[1], and updated using data in their 19th Monthly Progress Report. This mass includes the loss from the legs and hot shoe in the hot junction region.

Two curves are shown for each module, the lower curve uses the vacuum loss rate curve of Figure 7.4-21. The upper curve uses a higher rate taking into account the estimated pressure of CO in the modules. For 1135°C, JPL[1] has estimated the CO pressure to be $\sim 5 \times 10^{-6}$ Torr. For 1085°C modules, $\sim 1.2 \times 10^{-6}$ Torr and for 1035°C modules, the estimate is 3×10^{-7} Torr.

Using Figure 7.4-27 of para. 7.4.1.4, to adjust the mass loss rate for CO pressure, results in a 10 percent increase in rate for 5×10^{-6} Torr for SN-1 and 18 O at 1135°C and a negligible correction for the 1035°C Module SN-3.

Also shown on Figure 7.4-27 is the calculated mass loss for an actual RTG, using the actual hot junction temperature history (see Figure 7.4-22 of para. 7.4.1.4). Again, the lower curve represents the rate for vacuum and the upper curve represents the rate for the maximum calculated CO pressure of 4×10^{-5} Torr (Table 7.4-6 of para. 7.4.1.4).

It is seen from Figure 7.4-20 that, at the end of mission 35,000 hours, the flight RTGs will have experienced a mass loss of 0.22 mg/couple with a CO pressure of 5×10^{-4} Torr. The 1135°C modules SN-1 and 18 O reached this mass loss in the range of 500 to 700 hours of testing. At 700 hours (Figure 7.4-18), the resistance of 18 O and SN-1 was still in the flat portion of the curve. Consequently, the power loss is negligible. The 1085°C modules reached the total flight unit mass loss in 3500 hours. From Figure 7.4-19 at 3500 hours, the lowest resistance is shown by SN-5, 7500 ohms, or 432 ohms minimum in a full-scale converter.

[1] Degradation Model for an RTG with a SiGe Thermopile, JPL 900-755, Sept. 1976

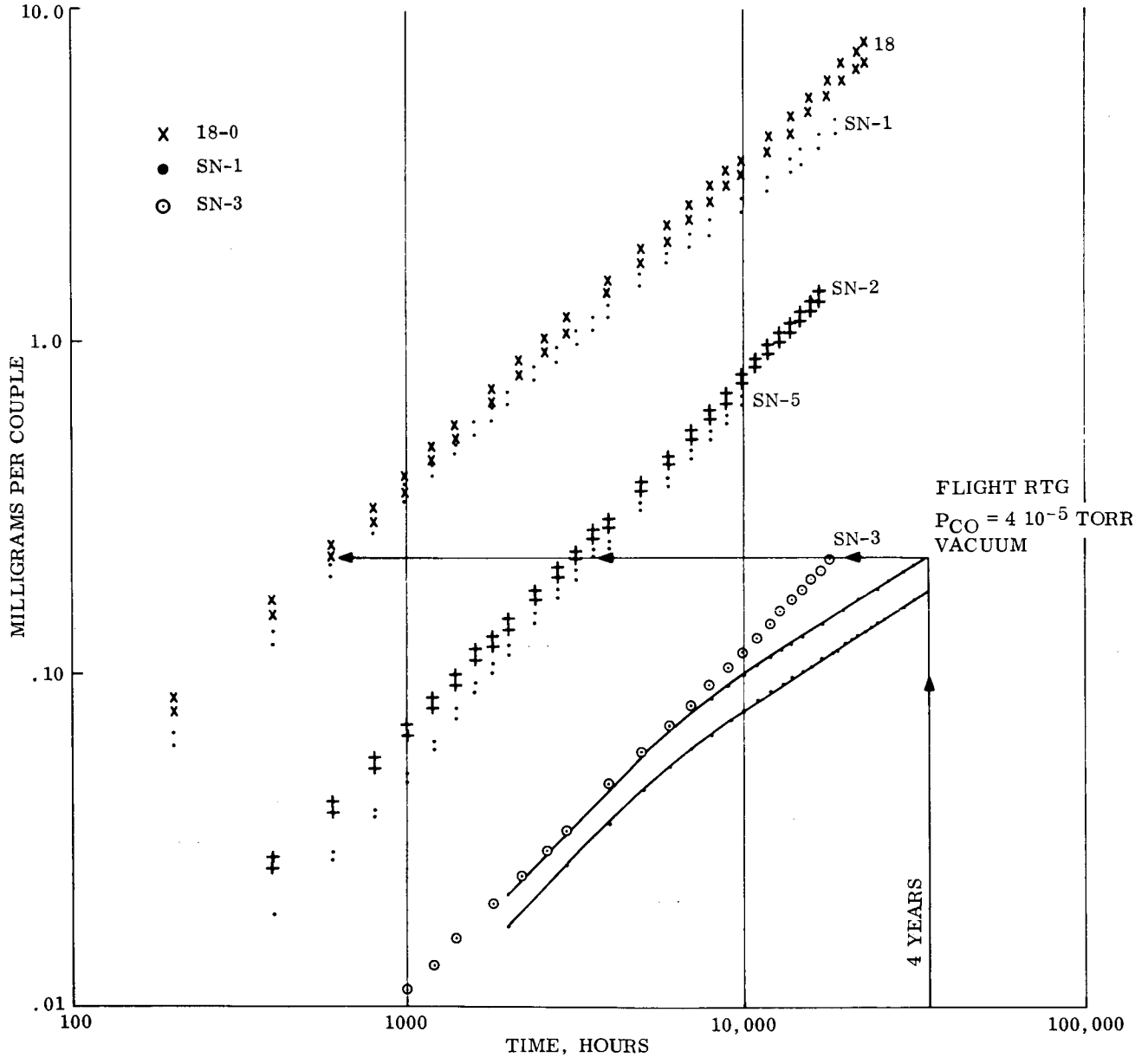

Figure 7.4-20. Mass Loss Per Couple as a Function of Time

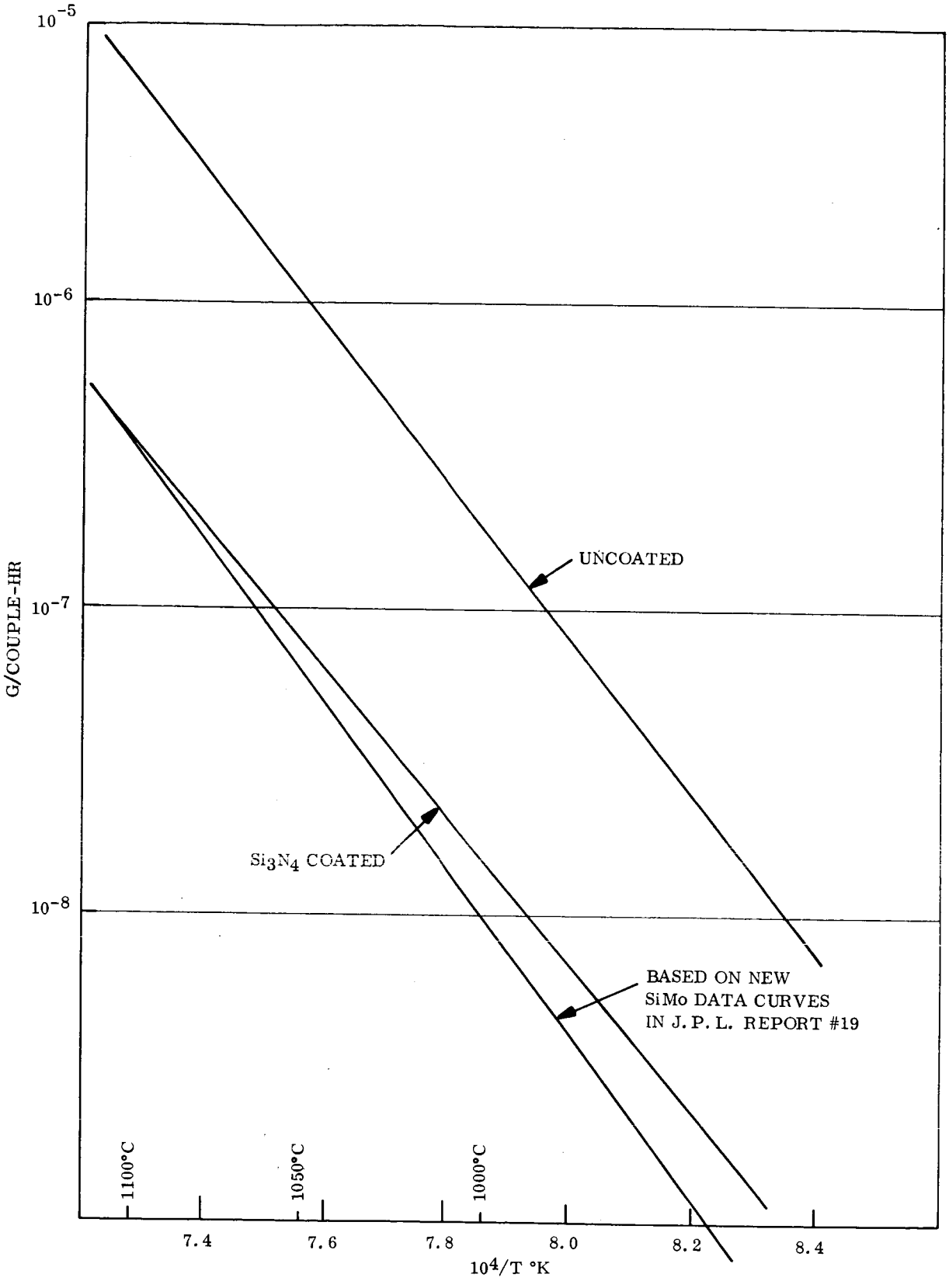

Figure 7.4-21. Silicon Loss Per Unicouple Which Contributes to Shunt Resistance and Insulation Degradation as a Function of Hot Junction Temperature

SN-3, because of its constant hot junction temperature (~ hot shoe 1040°C, hot junction 1005°C) throughout the test, has lost 0.22 mg/couple at 18,000 hours of testing. The resistance from Figure 7.4-18 is 30,000 ohms for 18 couples or 1,730 ohms in a full-scale converter. Again, the power loss is negligible.

These calculations were made based on the mass loss rates for coated couples. It is shown in para. 7.4.1.4 that the expected coating life for the flight RTGs is in excess of 50,000 hours.

7.4.1.4 Effects of Carbon Monoxide

The presence of CO in the RTG has been of concern since it reacts with the Si_3N_4 coating and with the Si substrate by diffusing through the coating. Based on the knowledge from JPL tests that a weight loss equivalent to two times the weight of the coating is lost before the weight loss curves take on the characteristic of uncoated SiMo, the reaction with the substrate is the most significant. The reaction is:

$$CO(g) + 2\ Si(s) \rightarrow SiO(g)\uparrow + SiC(s) \qquad (1)$$

The source of CO is two-fold. There is chemisorbed oxygen in the graphitic materials of the heat source which reacts with the carbon at high temperature and forms CO. This source of oxygen has been removed by establishing high temperature bakeout and handling procedures as determined by tests performed by Battelle (Columbus) and has been discussed in previous reports.

The second source of CO is from the reactions:

$$Si(g) + SiO_2(s) \rightarrow 2\ SiO(g)\uparrow \qquad (2)$$

$$SiO(g) + 2C(s) \rightarrow SiC(s) + CO(g)\uparrow \qquad (3)$$

$$CO(g) + 2\ Si(s) \rightarrow SiO(g)\uparrow + SiC(s) \qquad (4)$$

Si from the hot shoes sublimes and the major portion of it reacts with the graphite heat source surface. A smaller fraction reacts with the SiO_2 insulation to form SiO, this SiO then reacts

with the heat source surface to form CO + SiC. Some CO then reacts with the Si in the couple to form more SiO. Consequently, a cyclic reaction is set up whereby carbon, transported to the hot shoe to form SiC + Si, is transported to the heat source surface forming SiC.

To determine the Si_3N_4 coating lifetime in an RTG the following information is needed:

1. Hot junction temperature profile vs time and position
2. The CO pressure vs time
3. The mass loss rate as a function of temperature and CO pressure
4. A criteria for coating life as a function of temperature and pressure.

7.4.1.4.1 Hot Junction Temperature Profile

The hot and cold junction temperatures as a function of time are shown in Figure 7.4-22. The profile was obtained from the TEGS digital computer program which takes into account the fuel decay, the transport mechanisms which affect the hot junction temperature and the varying external heat flux impinging on the RTG surface. The axial temperature distribution is such that the maximum hot junction temperature is $12^{o}C$ above the average (to correlate cold junction temperature with flight RTG readings, use is made of the fact that during thermal vacuum testing, the MJS RTDs read $\sim 260^{o}C$, with an average cold junction of $\sim 300^{o}C$ and with a uniform $100^{o}F$ sink temperature).

7.4.1.4.2 CO Pressure Level in RTG

For the cyclic CO reaction, the CO pressure in the RTG is established by the generation rate and the rate at which the CO can escape through the thermopile and out through the outer case PRD into space.

$$P_{CO} = \frac{\dot{N}RT_1}{F_{PRD}} + \frac{\dot{N}RT_2}{F_{FB}} \qquad (5)$$

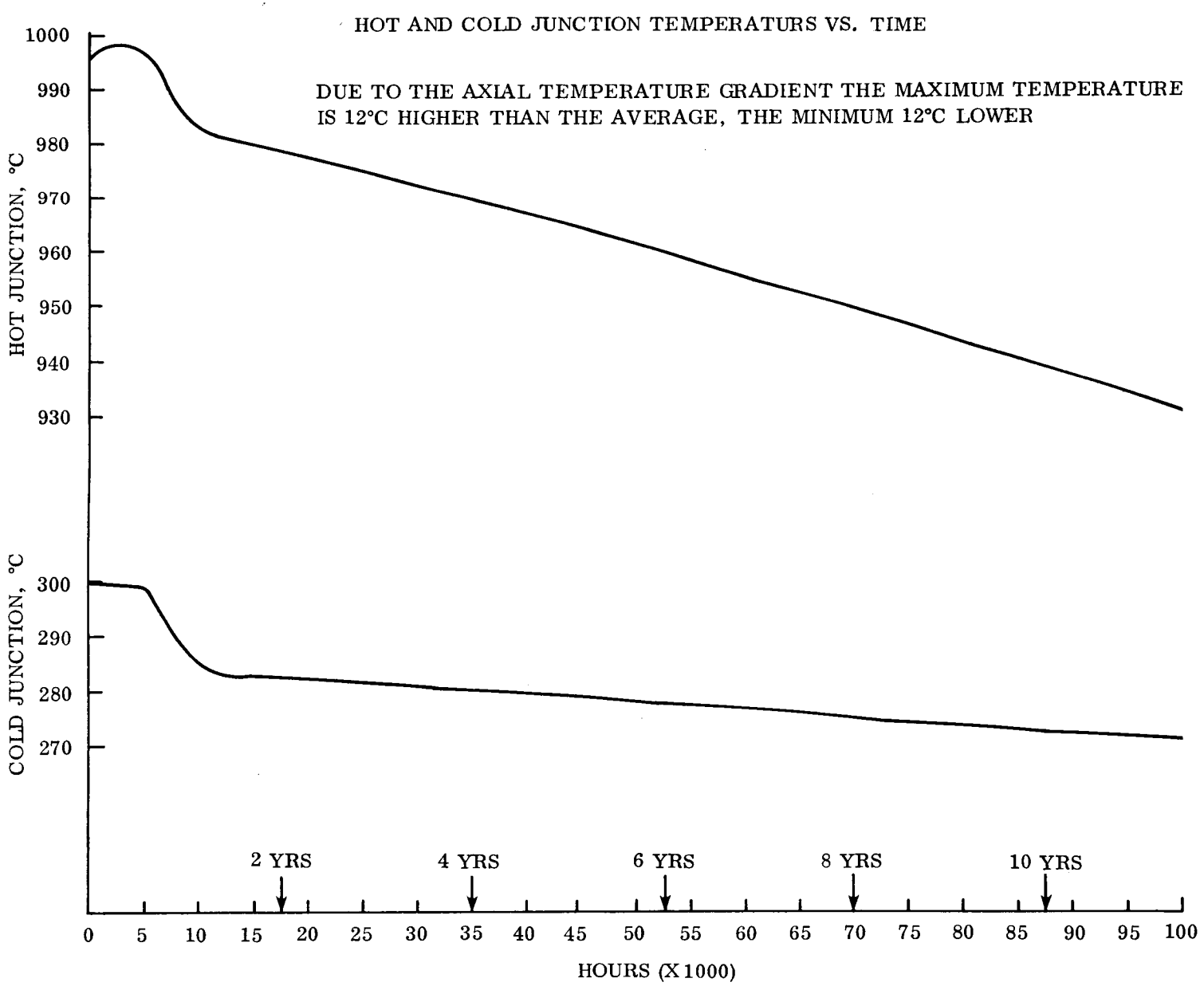

Figure 7.4-22. Hot and Cold Junction Temperature vs. Time

where $\dot{N}$ = CO generation rate, moles/sec

F_{PRD} = PRD conductance, cm^3/sec

F_{FB} = Conductance of the foil insulation system, cm^3/sec

R = Gas constant, 62,360 cm^3-Torr/^oK-gm-mole

T_1 = CO temperature at the PRD = 543^oK

T_2 = CO temperature at the foil hot side = 1108^oK

7.4.1.4.3 Conductances

The conductance of the PRD is known from tests to be 2000 cm^3/sec (270^oC). Approximate values for the conductance of the foil basket are available from two sources. Tests were run on the Q1A converter at room temperature with nitrogen gas introduced inside the foil cavity and pressures measured on both sides of the foil basket.

Tests were run with one hole open in the foil basket and with the hole plugged. Corrected to 1308^oK, the conductances calculated were:

One hole open	4,538 cm^3/sec
Hole plugged	2,895 cm^3/sec

Therefore, the conductance of the hole alone is 1,643 cm^3/sec. The Q1A converter was not the same as a flight unit in that it had a 10 mil solid Al_2O_3 barrier around the 4 sides of the T/E couple and two layers of Astroquartz wrap instead of the normal three layers of wrap. The presence of the solid Al_2O_3 on the one hand tends to decrease the conductance, however, on the other hand, gaps are formed at the Al_2O_3 - leg corners which tends to increase the conductance. In addition, the test was at room temperature and the foil-to-foil and foil-to-leg gaps change at operating temperature in an indeterminate way. Consequently, the use of the conductance of the single hole of 1,643 cm^3/sec is a conservatively low-value estimate of the conductance of the foil basket.

Tests were run by JPL on a single couple at room temperature to determine the conductance of the path down along the legs through the 3 layers of Astroquartz. These tests indicate a conductance of 16,850 cm^3/sec in the converter for the leg paths alone. CO pressures are shown later for both these conductance values.

7.4.1.4.4 CO Generation Rate

Two sources are available for the estimation of the CO generation rate.

18-Couple Modules

The hot shoes from five, 18-couple modules have been analyzed for carbon in the form of SiC. Table 7.4-2 lists the modules and their characteristics.

TABLE 7.4-2. MODULE CHARACTERISTICS

Module	Design Features	Hot Shoe Temp °C	Time Hours	Average Depth of SiC in Hot Shoe, Inches
18 I	TBC-4 types	1085	12,658	0.0154
DC-9	0.5" SiO_2 leg barrier 0.2" SiO_2 block in gap 0.018" SiO_2 wrap	1135	4,768	0.0154
DC-10	0.45" SiO_2 leg barrier	1135	1,645	0.0051
DC-11	Same as DC-9	1135	5,336	0.0216
DC-12A	Same as DC-9 and 0.012" SiO_2 wrap 0.018" SiO_2 wrap 0.028" SiO_2 wrap Isothermal bakeout	1135	7,326	0.0138

Figure 7.4-23 shows the SiC formation on a hot shoe from DC-9. (These modules did not contain the Si_3N_4 coating, since all modules with the Si_3N_4 coating were still operating.)

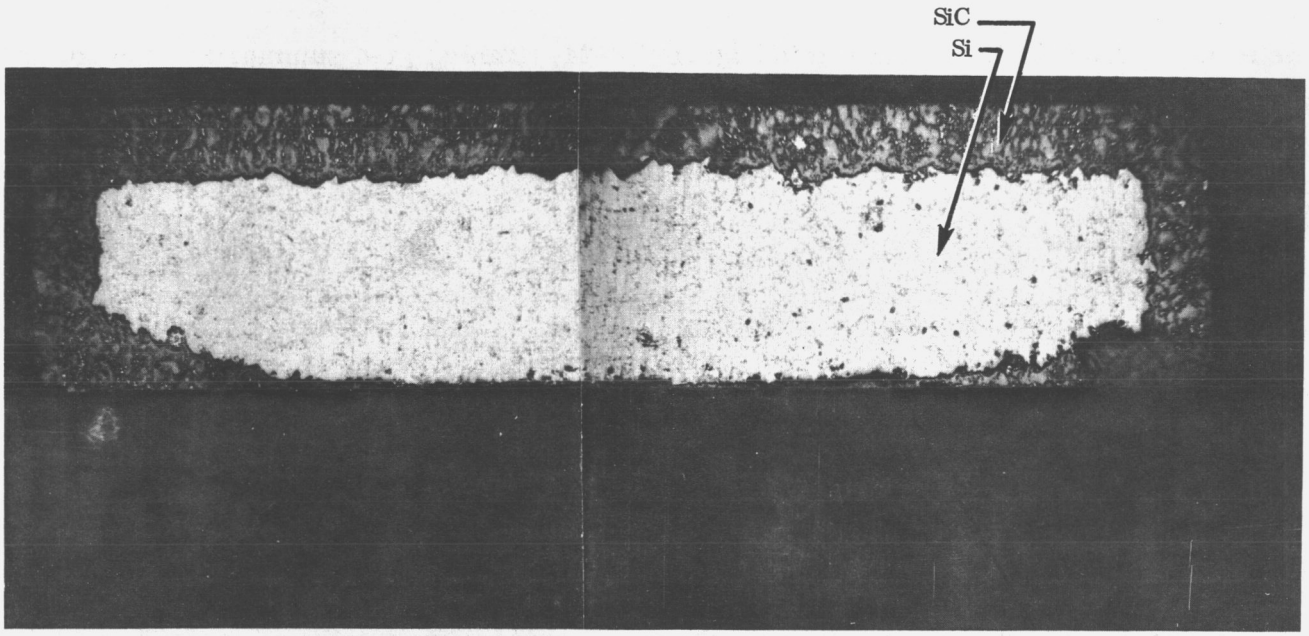

Figure 7.4-23. DC-9, Couple 7, SiC Formation on Hot Shoe (22X)

Table 7.4-3 shows the quantity of CO that would have had to react with the hot shoe to form the amount of SiC found and the average generation rate over the test time.

TABLE 7.4-3. QUANTITY OF REACTED CO

Weight of CO Reacted (3), gms		Av. CO Generation Rate gms/hr	
Module	Per Couple	Per Couple	Per RTG
18 I	0.302	$2.39 \cdot 10^{-5}$	$7.46 \cdot 10^{-3}$
DC-9	0.3024	$6.35 \cdot 10^{-5}$	$1.98 \cdot 10^{-2}$
DC-10	0.1038	$6.31 \cdot 10^{-5}$	$1.97 \cdot 10^{-2}$
DC-11	0.416	$7.79 \cdot 10^{-5}$	$2.43 \cdot 10^{-2}$
DC-12A	0.2733	$3.72 \cdot 10^{-5}$	$1.16 \cdot 10^{-2}$

(1) $Si(g) + SiO_2(s) \rightarrow 2\,SiO(g)\uparrow$

(2) $SiO(g) + 2C(s) \rightarrow SiC(s) + CO(g)\uparrow$

(3) $CO(g) + 2\,Si(s) \rightarrow SiO(g)\uparrow + SiC(s)$

To translate these data for uncoated couples at high temperature to coated couples at 1035°C, (the nominal initial hot shoe average temperature), use is made of the mass loss rate data

determined from JPL tests shown in Figure 7.4-24. Table 7.4-4 summarizes the hot shoe mass loss rates for selected temperatures. Using these data, a reduction in temperature from 1135°C to 1035°C results in a mass loss rate reduction by a factor of 21, the effect of the Si_3N_4 coating is to reduce the rate by an additional factor of 29.1.

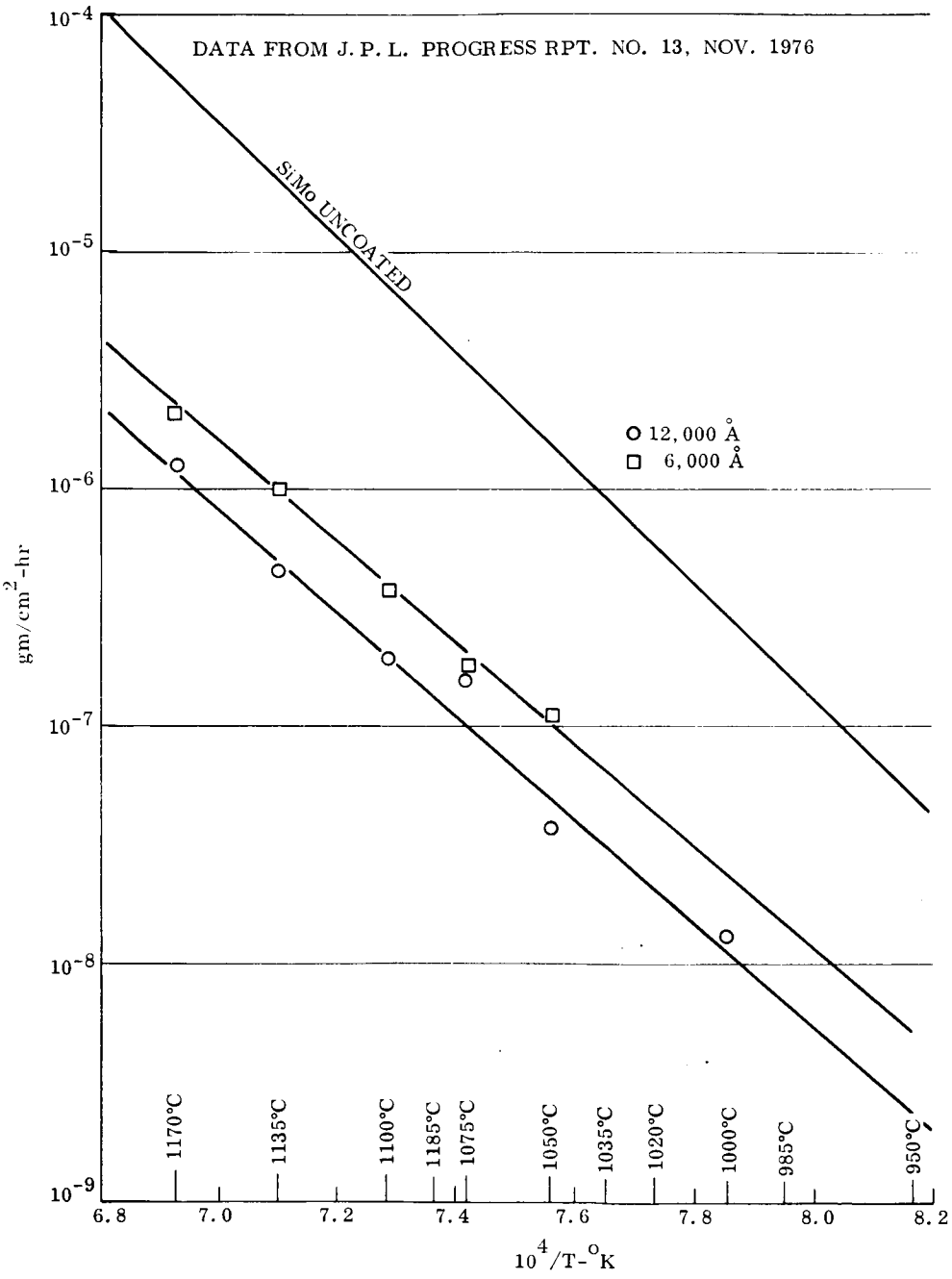

Figure 7.4-24. Weighed Loss Rate of Si_3N_4 Coated Hot Shoes in Vacuum

TABLE 7.4-4. MASS LOSS RATES FROM HOT SHOE, GM/CM^2 HR
(JPL DATA)

Temp. °C	Loss Rates gm/cm^2-hr		Ratio Uncoated/Coated
	Uncoated	Coated	
1000	2.9×10^{-7}	1.1×10^{-8}	26.4
1035	9.3×10^{-7}	3.2×10^{-8}	26.4
1085	4.52×10^{-6}	1.32×10^{-7}	34.2
1135	1.95×10^{-5}	4.95×10^{-7}	39.4

Consequently, if the 18-couple modules had been coated and operated at 1035°C, the mass loss rate and CO generation rate would have been reduced by a factor of 21 x 29.1 = 611. Table 7.4-5 summarizes the CO generation rates for an RTG with coated couples operating at 1035°C hot shoe temperature based on the module data.

TABLE 7.4-5. CALCULATED CO GENERATION RATE IN AN RTG AT 1035°C
FROM 18-COUPLE MODULE TESTS

	gms/hr
18 I	5.42×10^{-5}
DC-9	3.24×10^{-5}
DC-10	3.22×10^{-5}
DC-11	3.98×10^{-5}
DC-12A	1.9×10^{-5}

Using these generation rates in equation (5) results in the following initial CO pressures (Table 7.4-6) in an RTG at the beginning of the mission.

TABLE 7.4-6. CALCULATED INITIAL CO PRESSURE AT 1035°C HOT SHOE

Module No.	Foil Basket Conductance	
	GE	JPL
	1600 cm^3/sec	16,850 cm^3/sec
18 I	3.6×10^{-5} Torr	1.2×10^{-5} Torr
DC-9	2.2×10^{-5} Torr	7.2×10^{-6} Torr
DC-10	2.2×10^{-5} Torr	7.2×10^{-6} Torr
DC-11	2.7×10^{-5} Torr	8.8×10^{-6} Torr
DC-12A	1.3×10^{-5} Torr	4.2×10^{-6} Torr

The second source for the CO generation rate is from the analytical approach described by JPL in reference (1). Based on geometric considerations of the fraction of Si that leaves the hot shoe and reacts with the SiO_2 insulation, JPL calculated the CO generation rate in an RTG to be 8.32×10^{-9} gm/sec (2.99×10^{-5} gms/hr), which is in good agreement with the rates calculated from the module tests shown in Table 7.4-5. Using their foil basket conductance, their calculated initial CO pressure is 8.3×10^{-6} Torr.

Taking into account the change in hot shoe temperature with time, as given in Figure 7.4-22, the CO pressure as a function of mission time in an RTG was calculated from each module for both the high and low foil basket conductance and shown in Figure 7.4-25. The maximum initial CO pressure is calculated to be 3.6×10^{-5} Torr; this drops off to 1.6×10^{-5} Torr at 35,000 hours (4 years) and to 4.6×10^{-6} Torr at 100,000 hours. The minimum initial pressure is calculated to be 4.2×10^{-6} Torr, which drops off at 2×10^{-6} Torr at 35,000 hours and 5×10^{-7} Torr at 100,000 hours.

7.4.1.4.5 CO Generation Rate as a Function of Temperature and Pressure

JPL has determined the mass loss rate for Si_3N_4 coated hot shoes in vacuum, as previously shown in Figure 7.4-24, and for a CO pressure of 10^{-4} Torr, as shown in Figure 7.4-26. (For the vacuum tests, the CO pressure can be considered to be 10^{-7} Torr or lower with no significant difference in the results that follow.)

(1) Degradation model for an RTG with a Silicon Germanium thermopile 900-755 September 1976

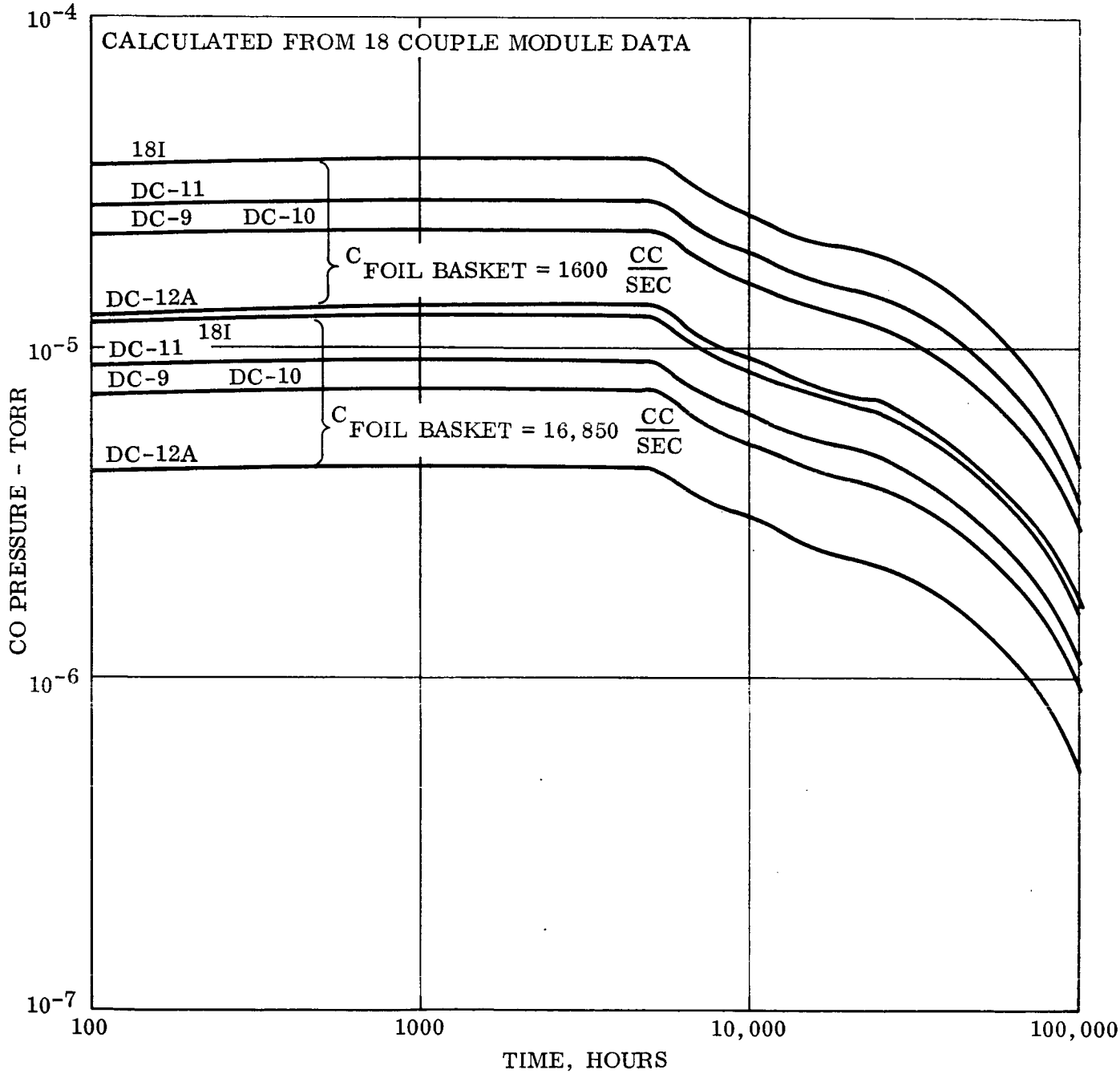

Figure 7.4-25. CO Pressure in RTG as a Function of Time and Calculated for Coated Couples

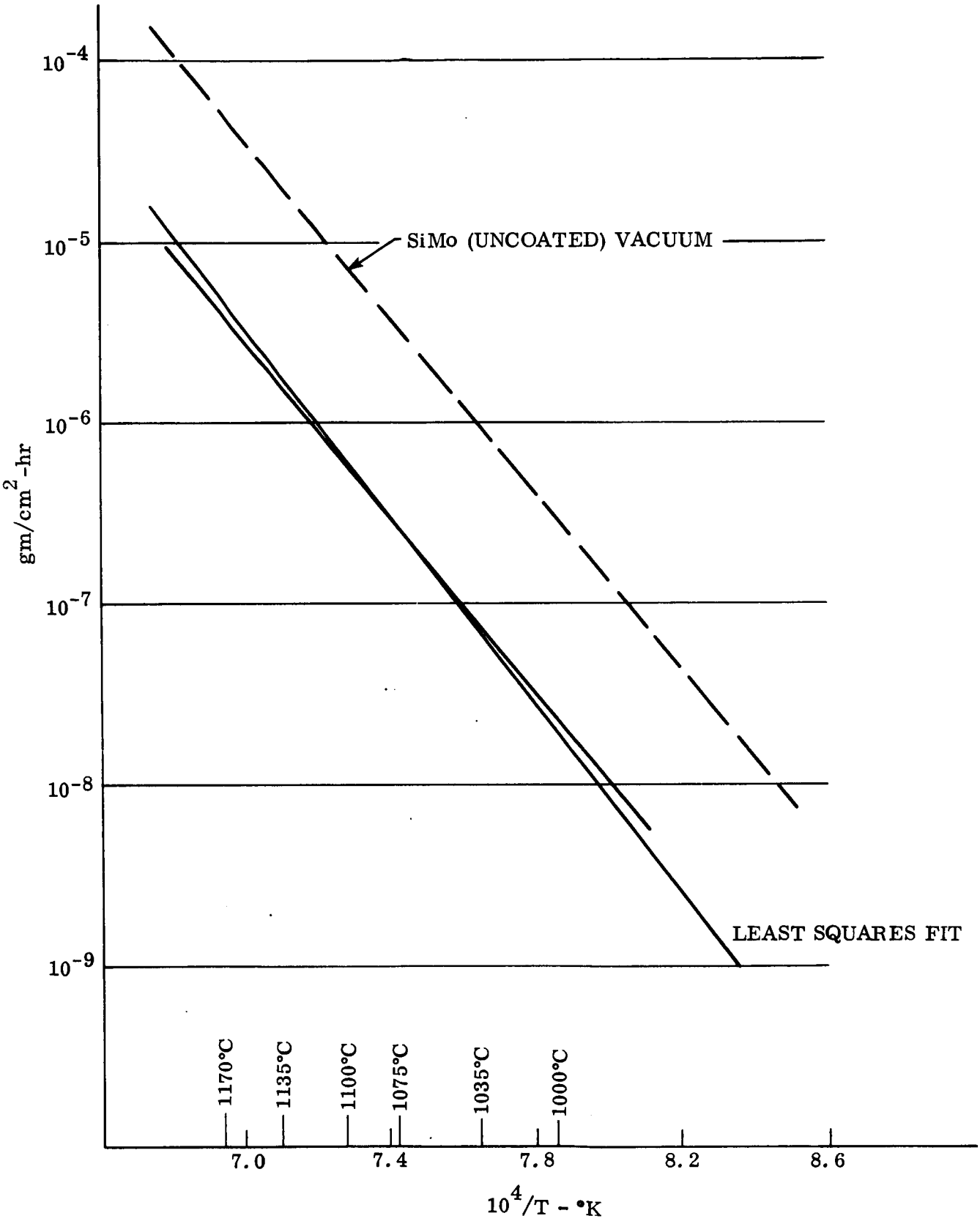

Figure 7.4-26. Weight Loss Rate of Si_3N_4 Coated SiMo Hot Shoes Operating in 1 x 10^{-4} Torr CO (JPL Data)

To determine the mass loss rate as a function of pressure we postulate that the pressure dependence is of the form

$$\dot{m} = \dot{m}_o + \frac{b P_{co}}{1 + bP_{co}}$$

where

$\dot{m}_o$ is the loss rate in vacuum (taken as 10^{-7} Torr CO)

b is a constant

P_{co} is the CO pressure

This form of pressure dependence is characteristic of a reaction in which absorption of the gas phase molecules is a preliminary step before reaction takes place.

Using the vacuum at 10^{-4} Torr, mass loss rate data for selected temperatures result in the rates as a function of temperature and pressure as shown in Figures 7.4-27 and 7.4-28.

7.4.1.4.6 Coating Life

The next relationship required is the criteria for definition of loss of coating. JPL has shown* from their vacuum tests as a function of temperature, that at the time the mass loss rates accelerate, indicating coating loss, there is a critical mass loss which is nearly the same for all temperatures. This is found to be mass loss of 1.1 mg/cm^2 for the 12,000 Å coating. The correlation is shown in Figure 7.4-29 where the straight lines represent the life calculated from the critical mass loss and the rates from Figure 7.4-24.

A similar approach for the 10^{-4} data results in a critical mass loss of 0.33 gm. The lower critical mass loss for the CO data can be understood in terms of the more disruptive undermining of the coating caused by the SiO produced under the coating. The critical mass loss is then a function of pressure and the pressure dependence can reasonably be assumed to be of the form

* JPL Progress Report 19 Nov. 1976.

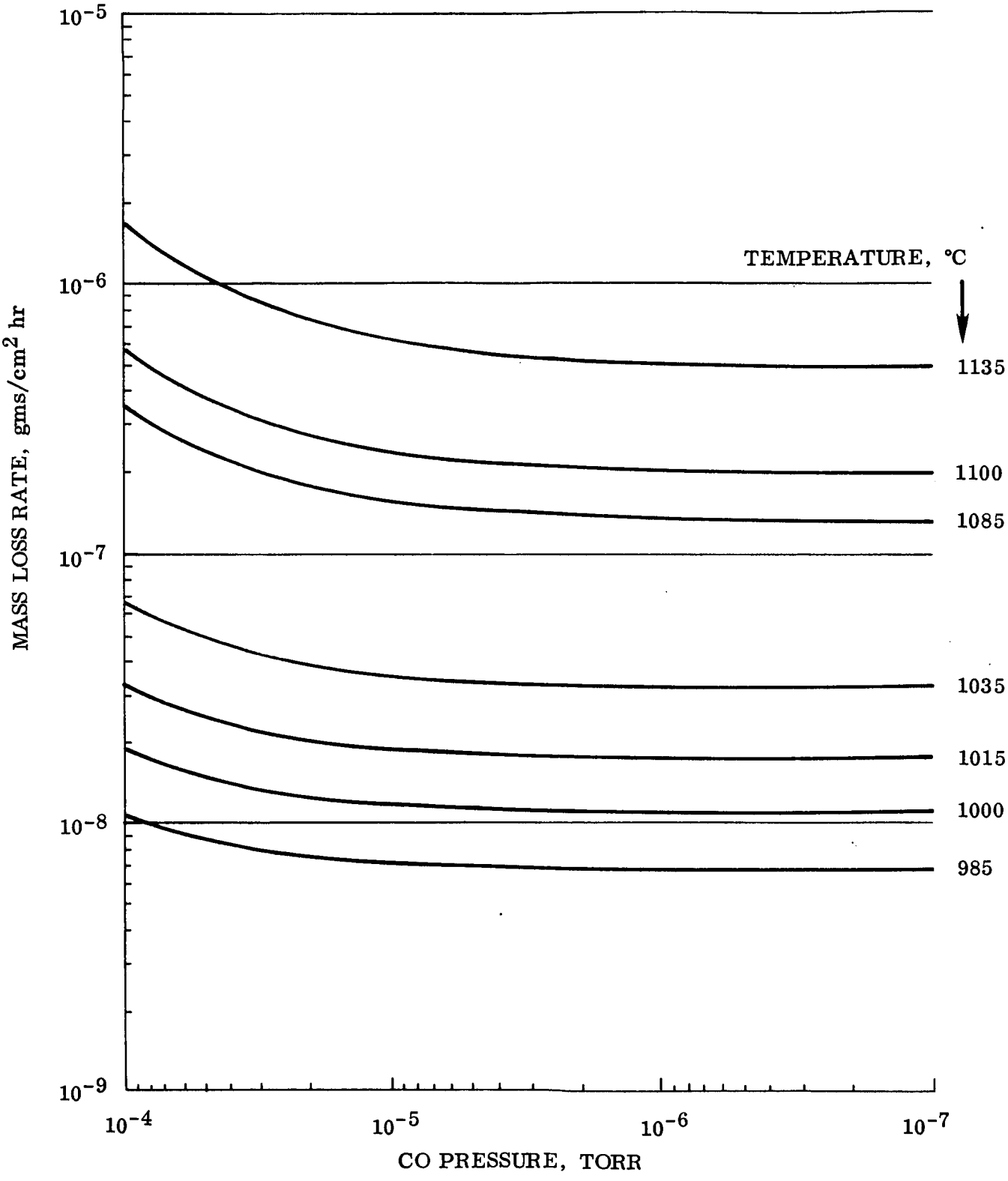

Figure 7.4-27. Mass Loss Rates as a Function of CO Pressure and Temperature

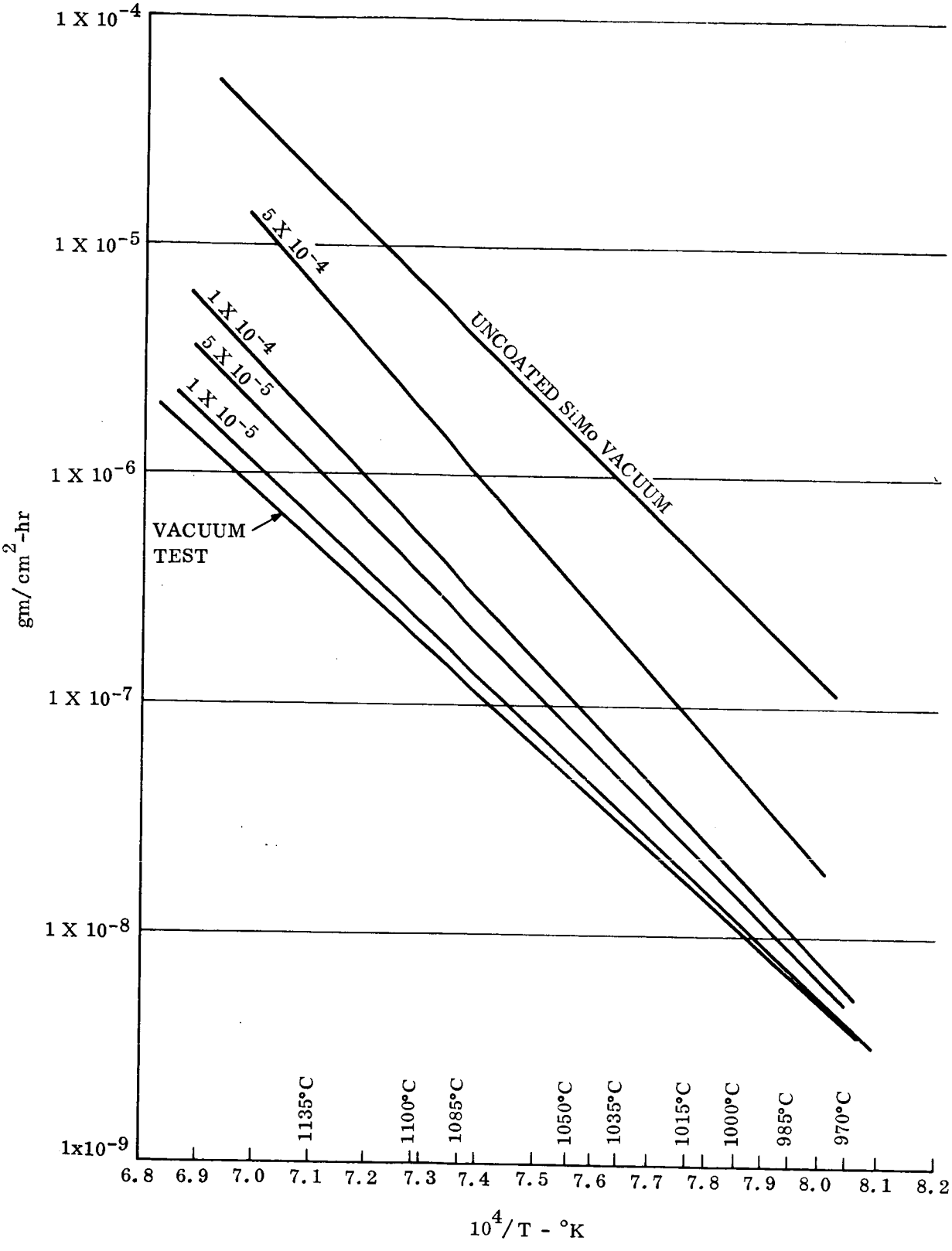

Figure 7.4-28. Mass Loss Rates as a Function of CO Pressure and Temperature

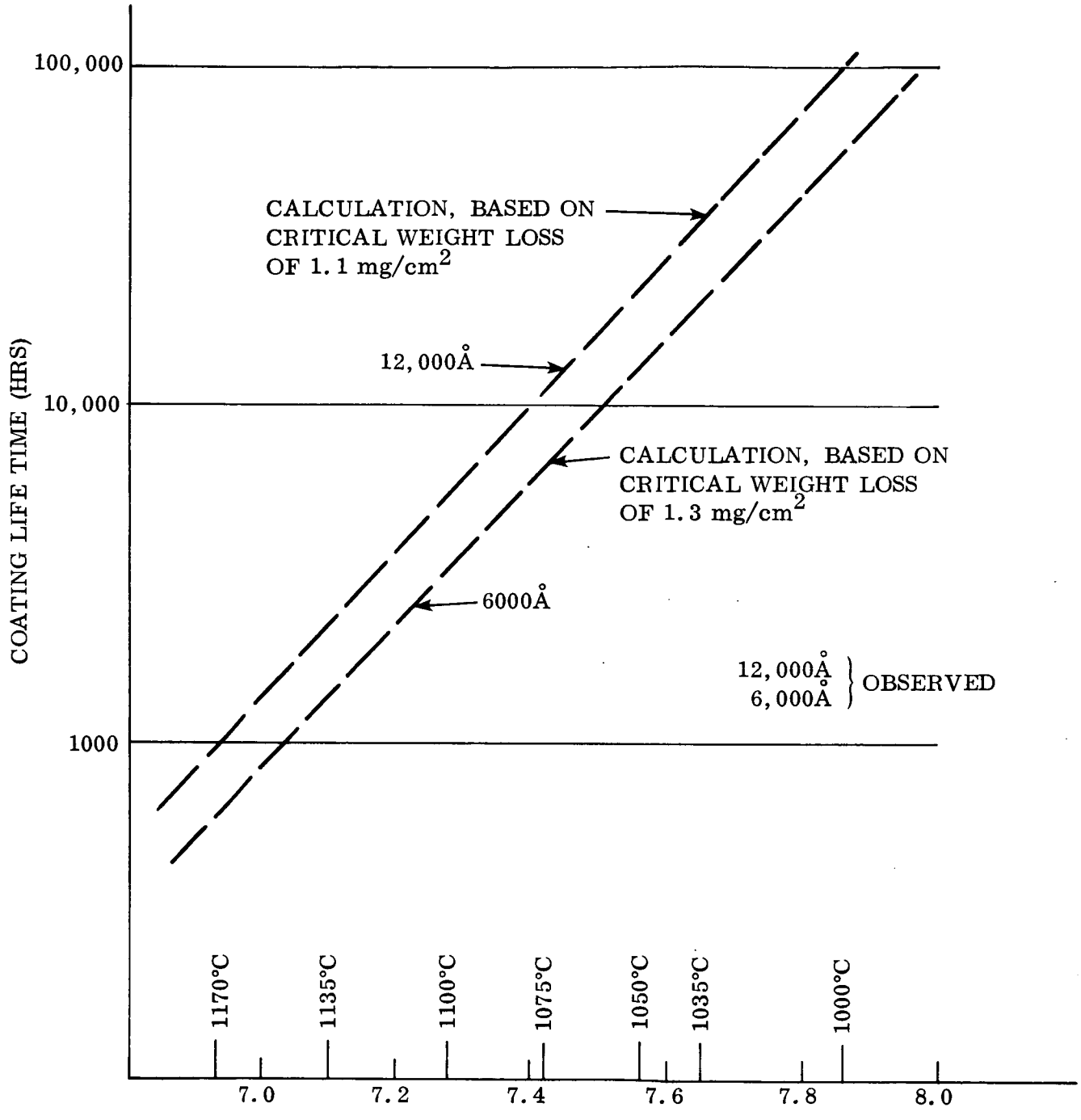

Figure 7.4-29. Coating Lifetime for Hot Shoes Operating in Vacuum

$$Mc = M_c^o \left(\frac{KP}{1 + KP}\right)$$

where

M_c^o is the critical mass loss for vacuum conditions

K - constant

From this relationship the critical mass loss as a function of CO pressure is found as shown in Figure 7.4-30.

Using the critical mass loss as a function of pressure and the mass loss rates as a function of temperature and pressure from Figures 7.4-24 and 7.4-26, the coating life as a function of temperature and CO pressure is shown in Figure 7.4-31.

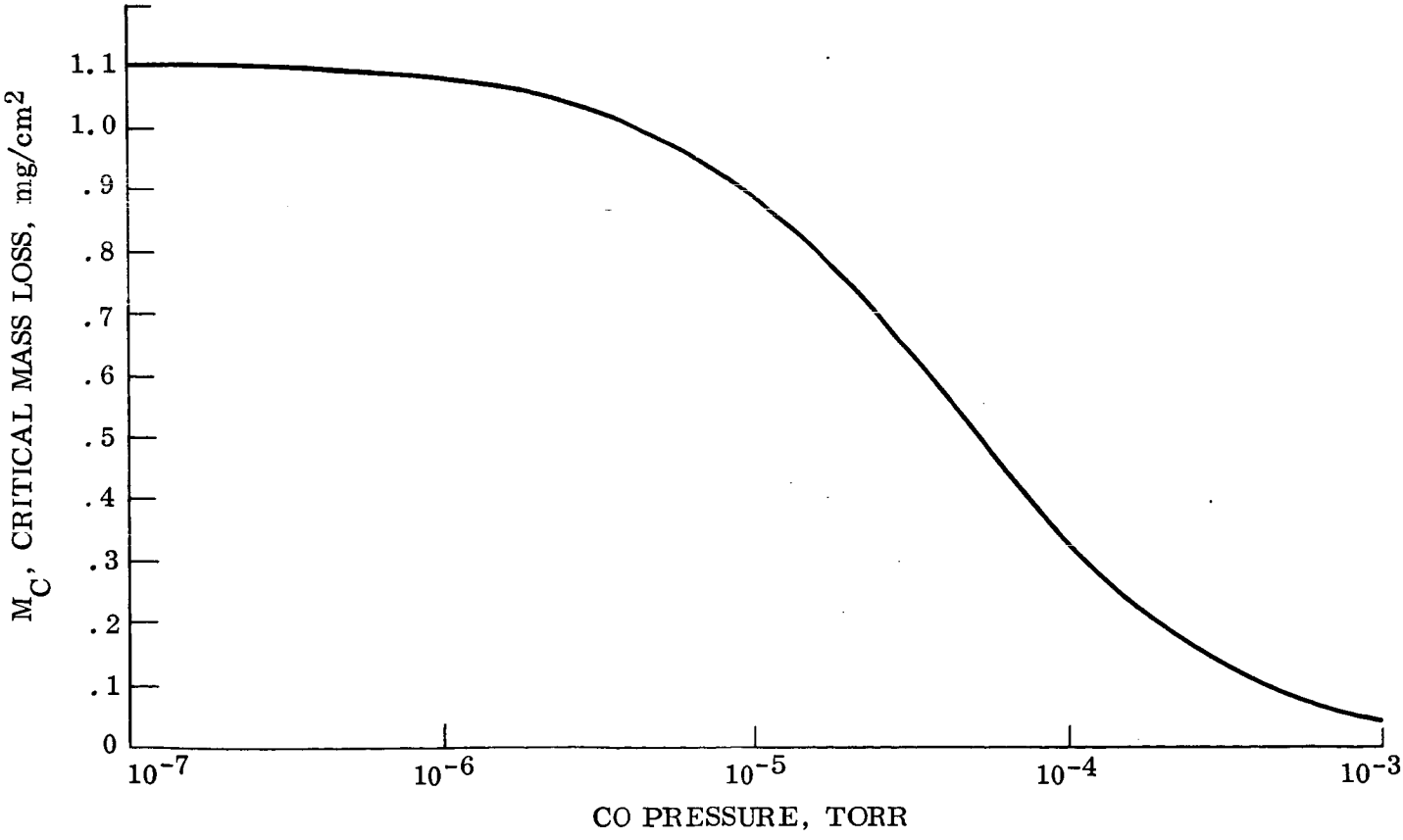

Figure 7.4-30. Critical Mass Loss as a Function of CO Pressure

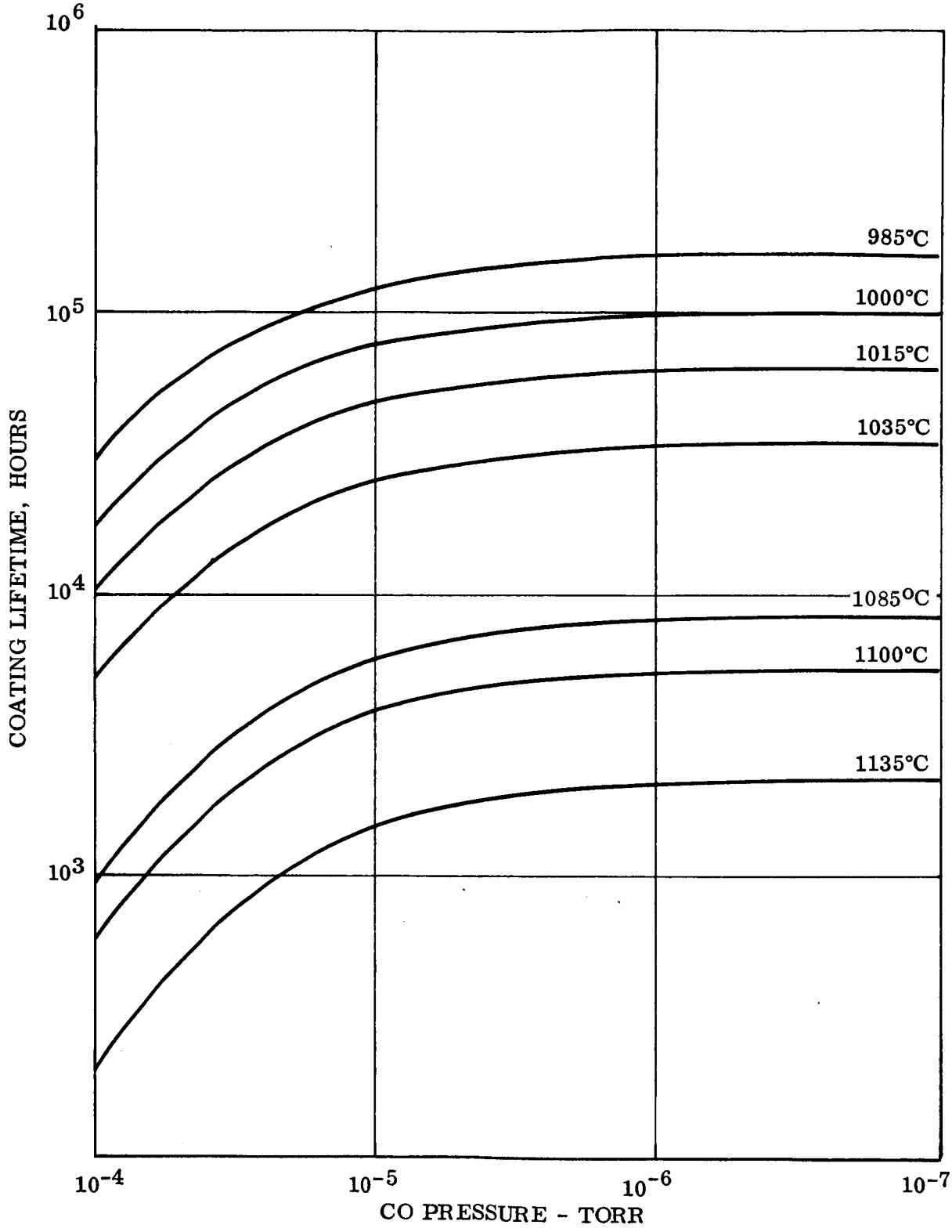

Figure 7.4-31. Coating Life as a Function of Temperature and CO Pressure

Since the CO pressure and hot junction temperature vary with time, the coating life can be found by calculating the accumulated mass loss as a function of time; and since the pressure changes by a factor of only 2 over the 35,000 hour mission, a conservative result will be obtained by calculating the mass loss at the initial RTG pressure.

This has been done by breaking the mission into 1000 hour increments and using the maximum and average hot junction temperature with the results shown in Figures 7.4-32 and 7.4-33.

It should be noted that the CO pressure is calculated from the hot shoe temperature, which is 35°C hotter at its outer edge than the hot junction temperature, whereas, in evaluating the coating life, we use the hot junction temperature because it is the coating in the region of the hot junction which predominately controls the Si loss that controls the rate of shorting between the T/E circuit and foil. Table 7.4-7 summarizes the results of three pressure levels.

It is seen for the maximum pressure of 3.6×10^{-5} Torr calculated from the 18 I module data and the conservative foil basket conductance, the coating life is in excess of 100,000 hours at the average hot junction temperature and 50,000 hours at the maximum hot junction temperature. For the minimum calculated pressure of 4.2×10^{-6}, the coating life is in excess of 100,000 hours at both the average and maximum temperatures.

7.4.2 PERFORMANCE PREDICTIONS

7.4.2.1 Launch Pad Power

Following the acceptance testing, the RTGs are placed in storage on short circuit with an argon gas fill. Prior to launch, the argon will be removed and replaced with xenon and the power output of each RTG will be checked.

The initial power output that would be obtained with a xenon gas fill at the start of storage is based on the test results from the F-13 RTG. A xenon fill test on this unit produced 118 watts following a thermal vacuum power output of 156.3 watts. This ratio of xenon to vacuum power of 75.5 percent was used for all the Voyager RTGs and is judged to be conservative. Table 7.4-8 summarizes the power that would be achieved at the start of storage for each RTG.

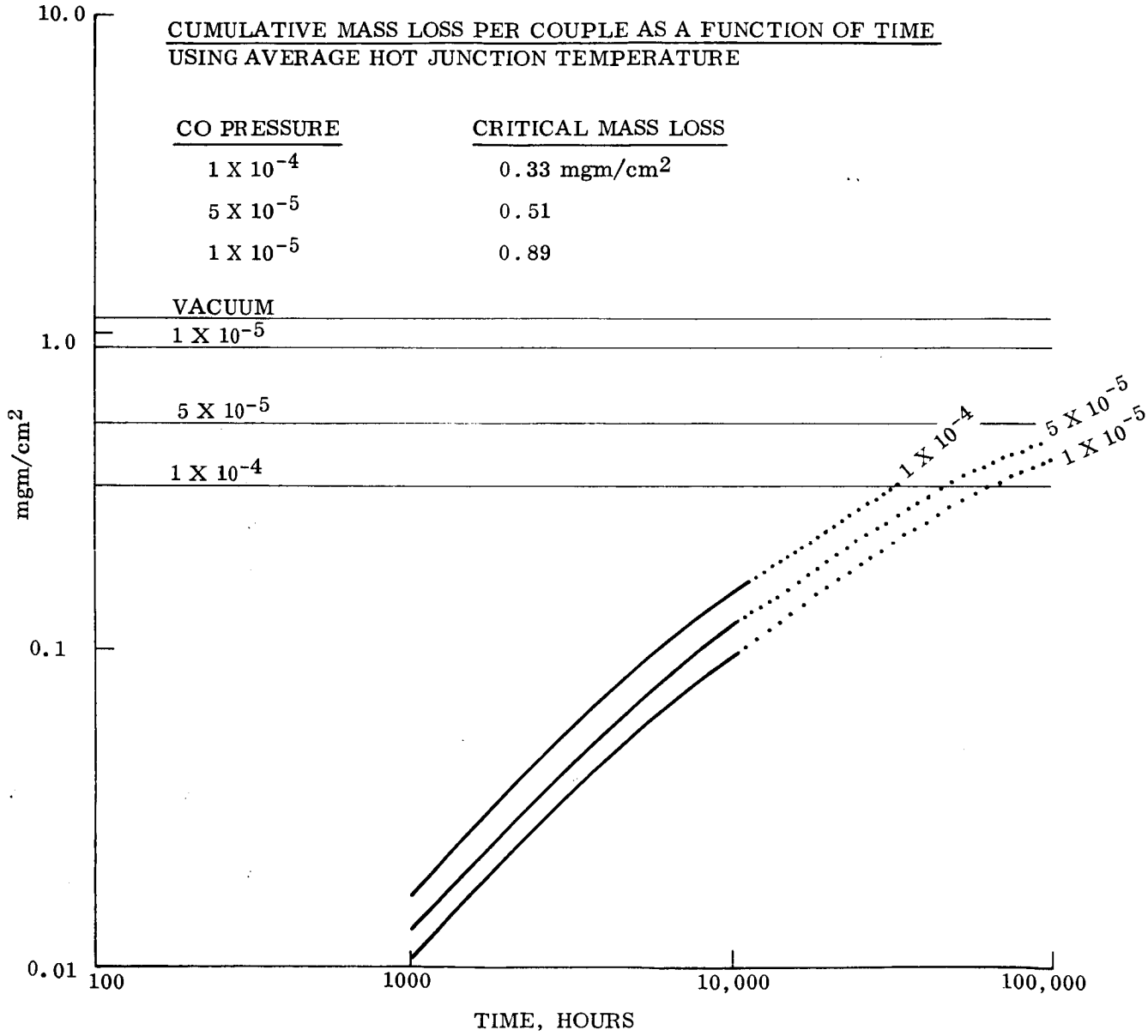

Figure 7.4-32. Cumulative Mass Loss Per Couple as a Function of Time Using Average Hot Junction Temperature

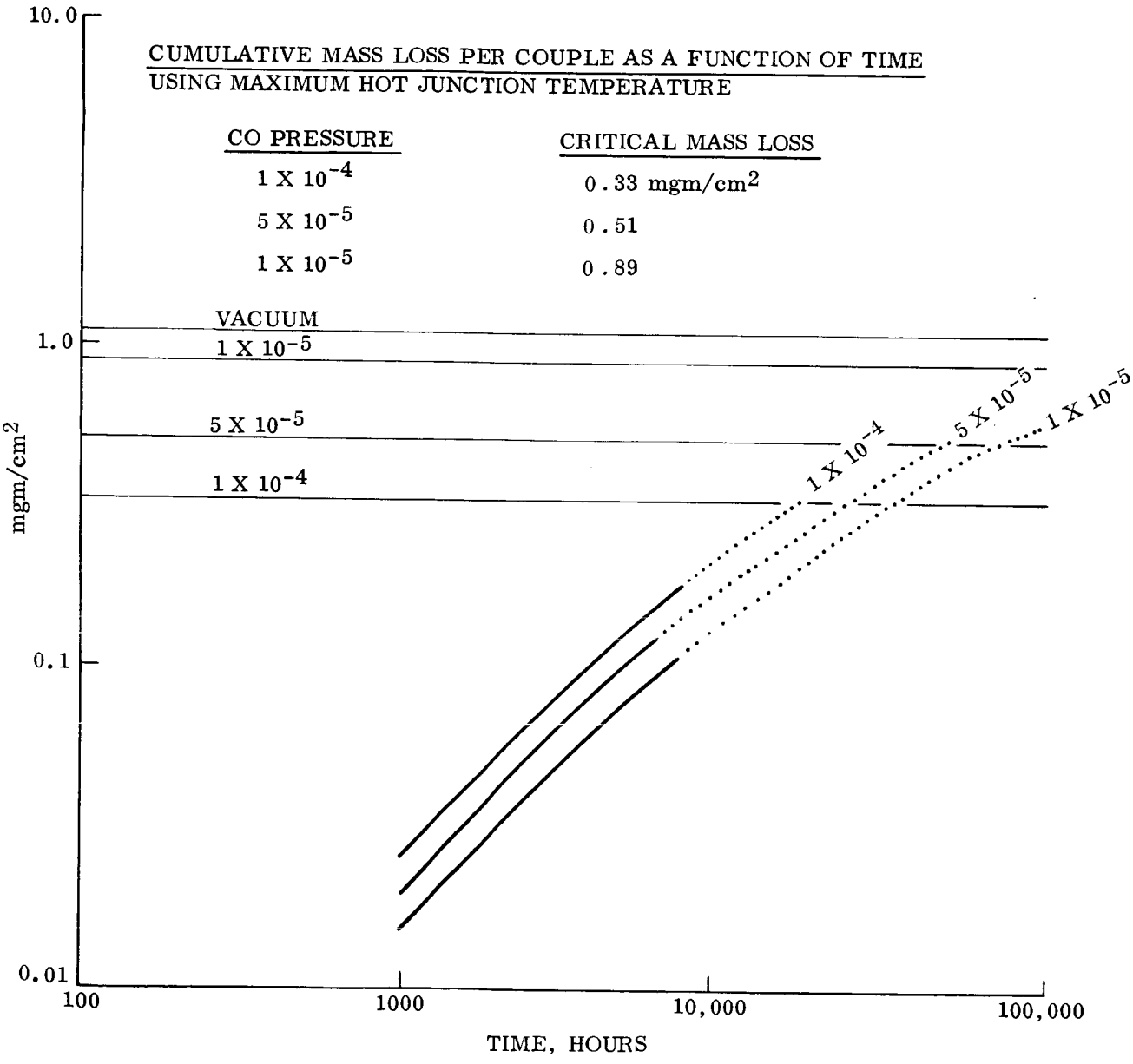

Figure 7.4-33. Cumulative Mass Loss Per Couple as a Function of Time Using Average Hot Junction Temperature

TABLE 7.4-7. PERCENTAGE OF CRITICAL MASS LOSS AS A FUNCTION OF CO PRESSURE AND TIME

CO Pressure Torr	Time Hours	Percent of Critical Mass Loss	
		Average Temp.	Maximum Temp.
1×10^{-5}	17,000	16	23
	35,000	26	38
	70,000	38	56
	100,000	44	65
5×10^{-5}	17,000	33	51
	35,000	54	82
	50,000	66	100
1×10^{-4}	17,000	65	100
	35,000	100	

TABLE 7.4-8. CALCULATED XENON POWER AT START OF STORAGE

RTG No.	Vacuum Power (1)	Calculated Xenon Power (75.5 % of Vacuum Power)
F-6	160.5	121.2
F-7	160.2	121.0
F-8	160.0	120.8
F-9	160.4	121.1
F-10	162.3	122.5
F-11	161.5	121.9
F-12	159.5	120.4

(1) corrected for He in RTG during thermal vacuum test.

During storage, the power degradation mechanisms are fuel decay and dopant precipitation effects since the temperatures are too low for any sublimation effects and there should be no significant change in the leg thermal conductivity. Table 7.4-9 shows the average hot and cold junction temperatures (RTD temperature readings are approximately 30°C lower than average cold junction tempe rature) that pertain to the various environments that the RTG experiences. Figure 7.4-34 shows the temperature distribution through the T/E elements from hot to cold junction for these conditions. It is seen that the storage and checkout conditions do not have identical temperature profiles.

TABLE 7.4-9. AVERAGE HOT AND COLD JUNCTION TEMPERATURE FOR VARIOUS ENVIRONMENTS

	Vibration Testing	Storage Condition	Checkout & Launch Pad	Flight Operation
RTG Internal	Argon	Argon	Xenon	Vacuum
External	Air (Natural Convection)	Shipping Container	Air Natural Convection	Vacuum
Voltage	30V	Short Circuit	30V	30V
Average Hot Junction	775°C	763	856	1000°C
Cold Junction	217	272	212	300

In addition, the buildup of helium during storage will cause the hot junction temperature to drop to an extent depending on the storage time and the amount of helium that is retained within the RTG.

Consequently, there will be some changes in the charge carrier concentraction and mobility throughout the legs. However, these changes are expected to be small, so that the actual pad power will not deviate by more than 1 to 2 percent from that predicted by assuming that the temperatures in storage correspond to those of the xenon filled checkout condition.

Consequently, the RTG degradation program was run to include fuel decay and dopant precipitation effects, using the 212°C cold junction temperature and an 856°C initial hot junction temperature. The results are shown in Figure 7.4-35 through 7.4-41, with effective age time at the start of storage as a parameter.

The effective age time for each RTG at the beginning of storage was estimated as follows. From the 18-couple module tests, a good fit for the slopes of the internal resistance and open circuit voltage was found by using 800 hours as the effective age time at the start of testing; i.e., after module outgassing processing was complete. This same age was used for the RTGs after processing at RCA and to this was added the age time over 700°C, accumulated up to the time of

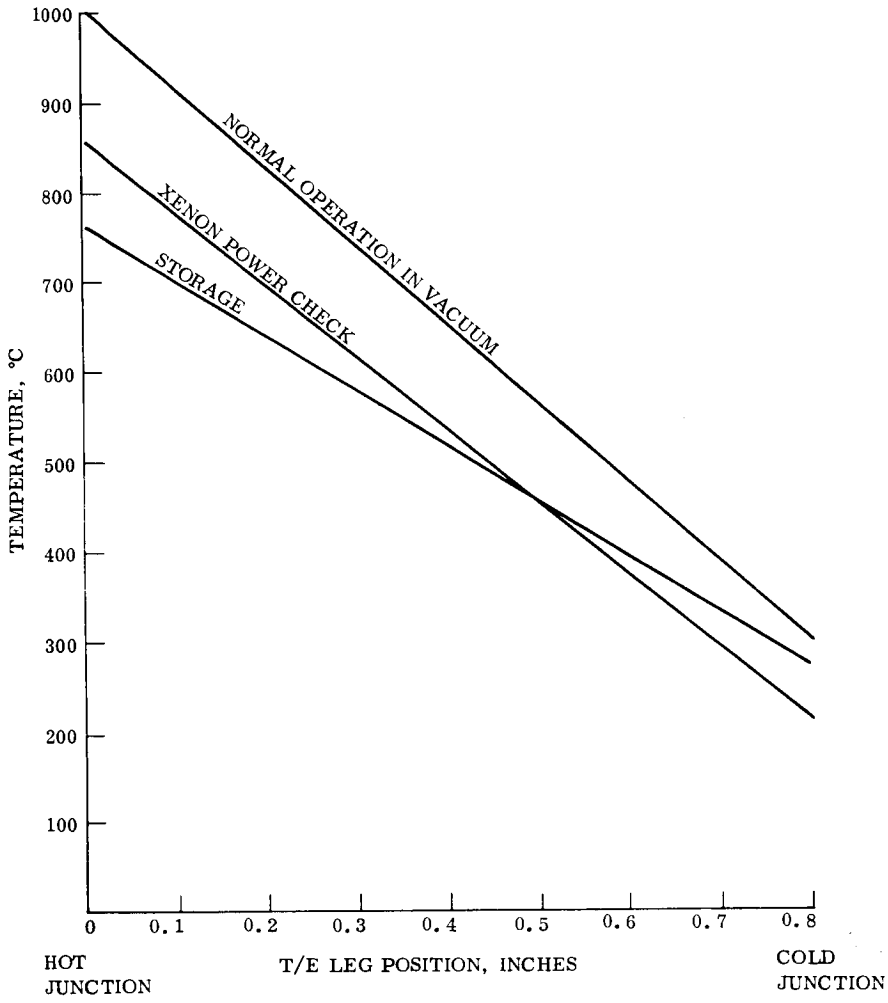

Figure 7.4-34. T/E Leg Temperature Profiles

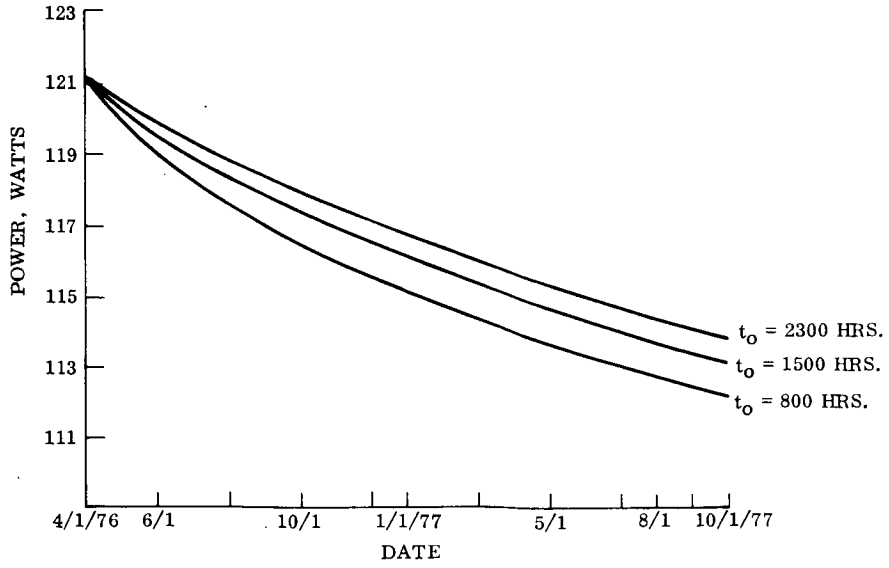

Figure 7.4-35. F-6 Xenon Power

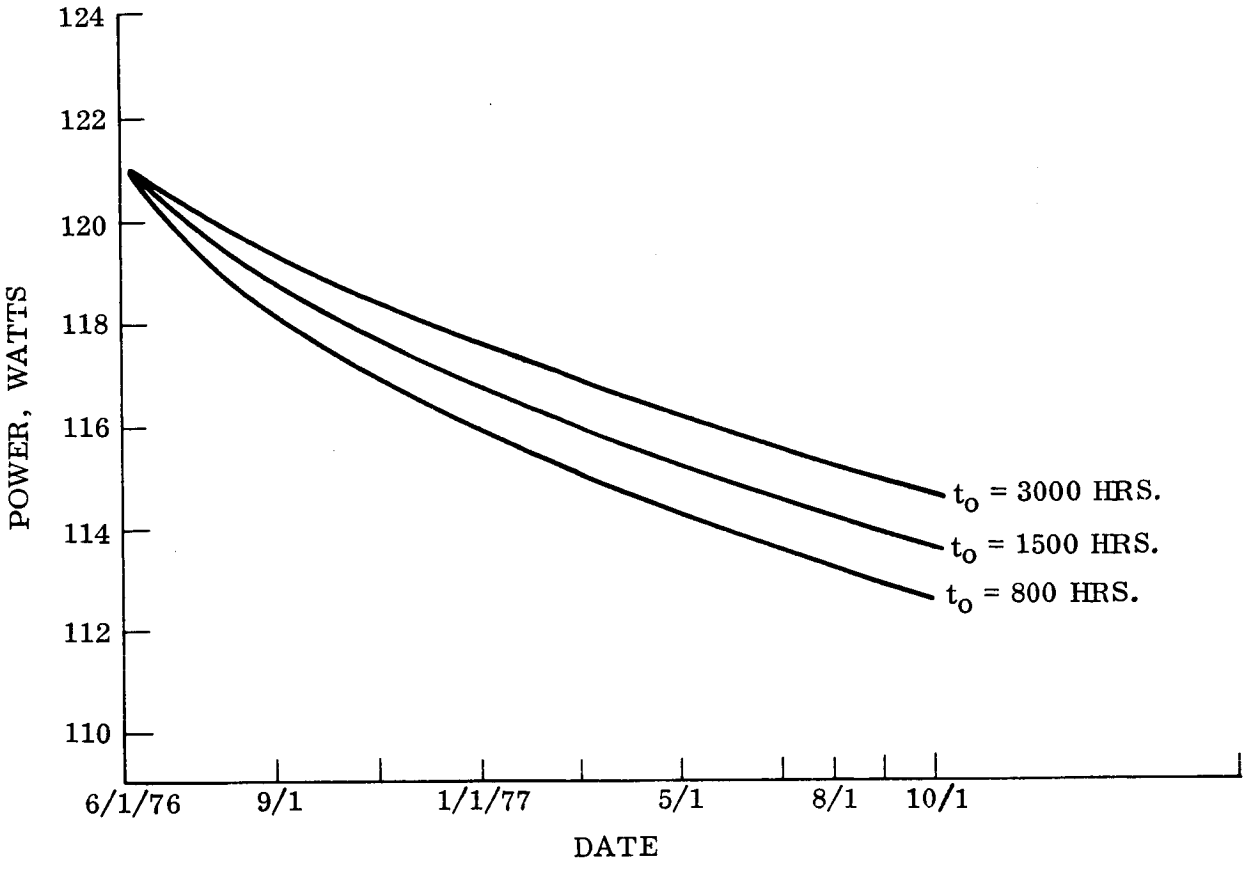

Figure 7.4-36. F-7 Xenon Power

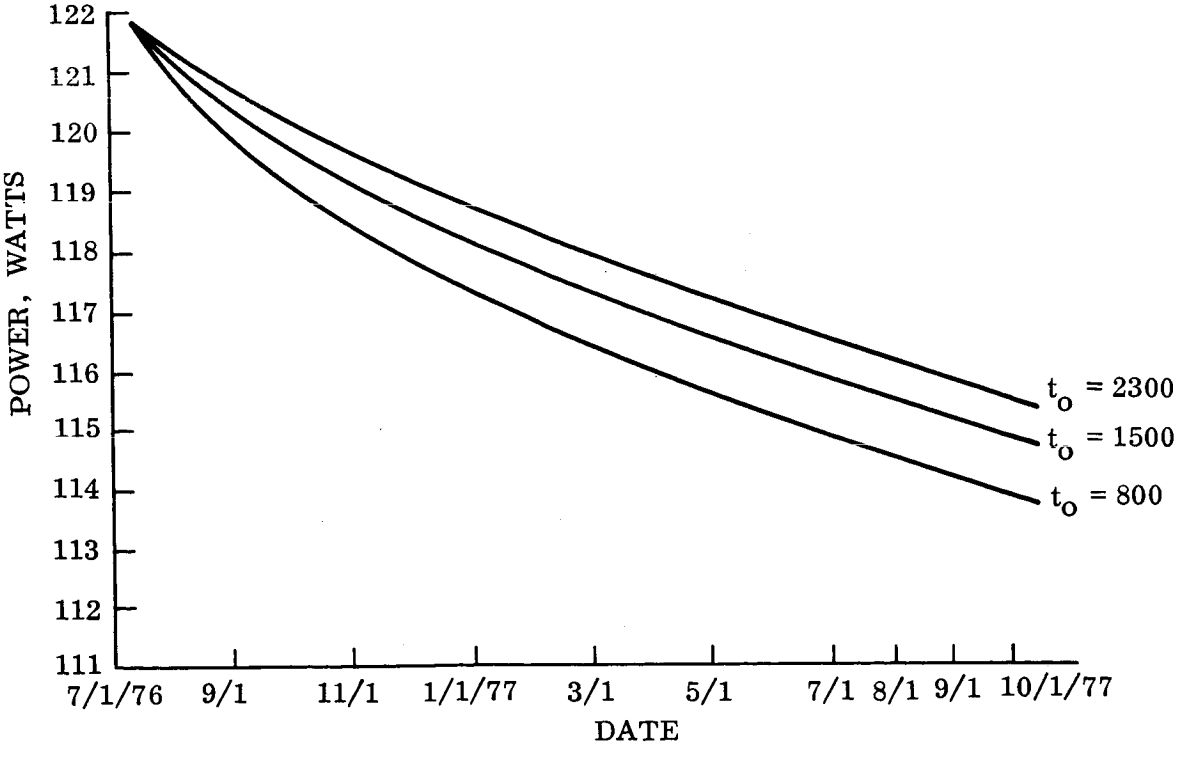

Figure 7.4-37. F-8 Xenon Power

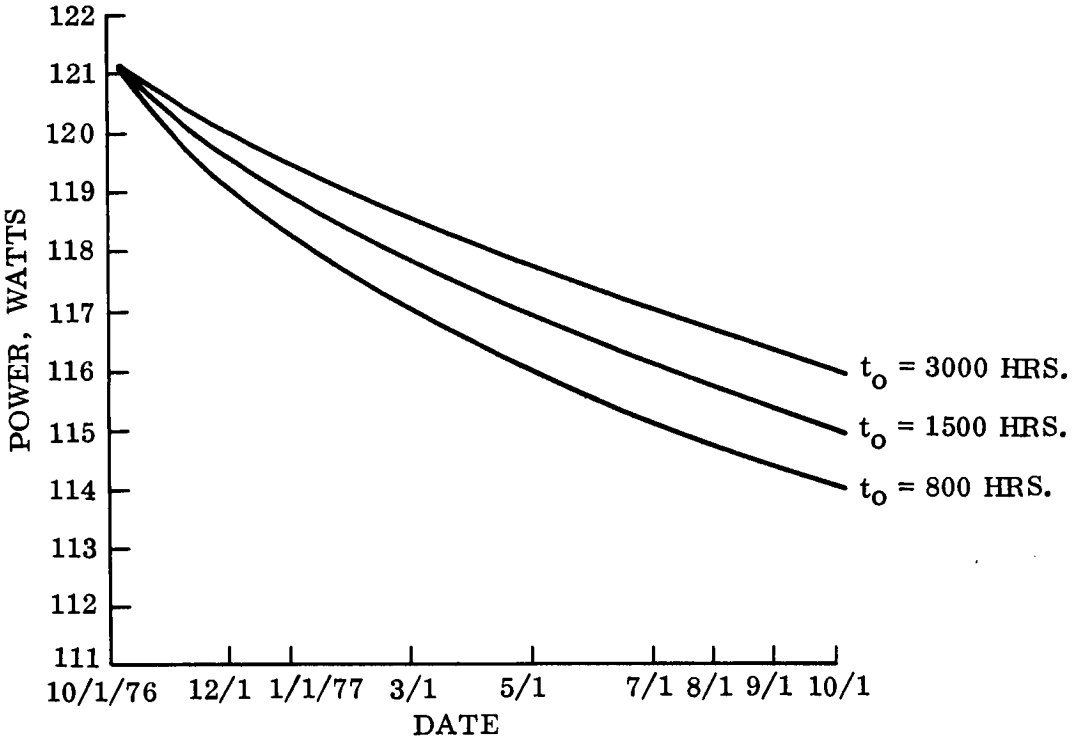

Figure 7.4-38. F-9 Xenon Power

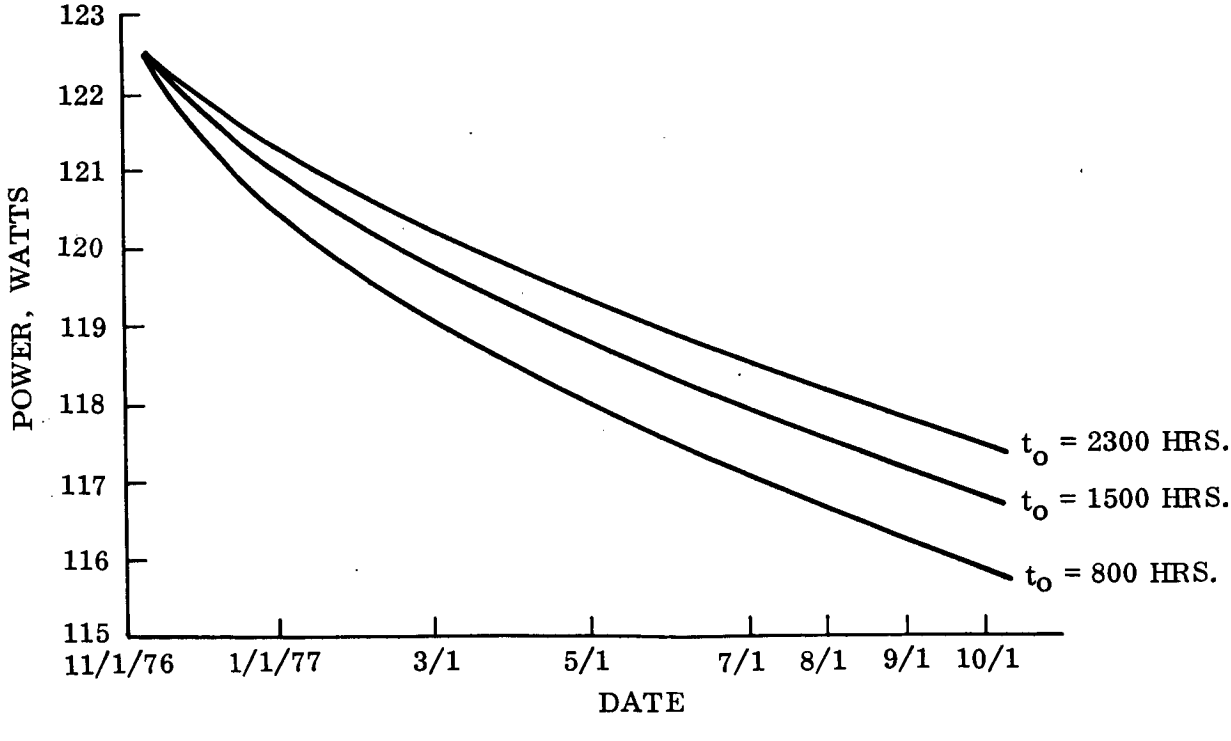

Figure 7.4-39. F-10 Xenon Power

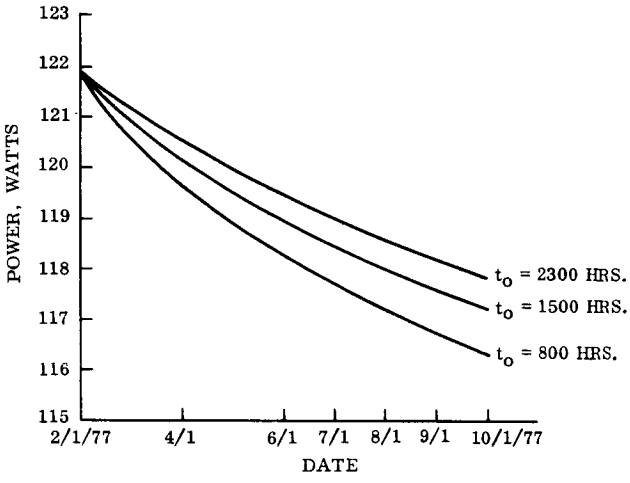

Figure 7.4-40. F-11 Xenon Power

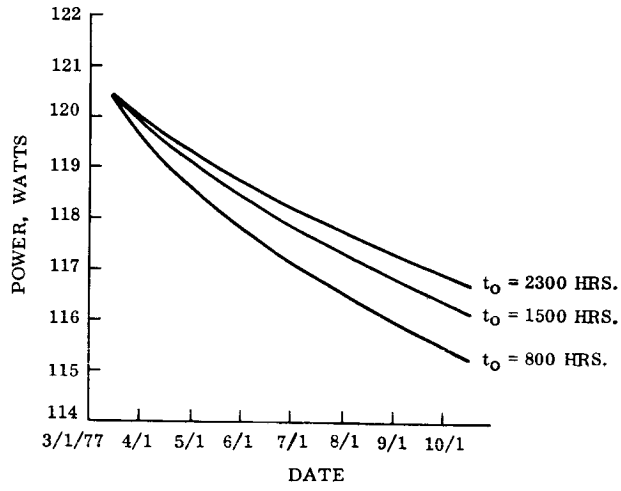

Figure 7.4-41. F-12 Xenon Power

the thermal vacuum test, immediately before initiation of storage. This resulted in the following effective age times for the RTGs shown in Table 7.4-10.

TABLE 7.4-10. CALCULATED EFFECTIVE AGE FOR START OF STORAGE HOURS

RTG No.	Hours				
F-6	800	+	1310	=	2110
F-7	800	+	2082	=	2882
F-8	800	+	971	=	1777
F-9	800	+	2459	=	3259
F-10	800	+	873	=	1673
F-11	800	+	968	=	1768
F-12	800	+	802	=	1602

It has been observed from acceptance testing that if an RTG is operated in air with an argon fill, then subjected to thermal vacuum conditions, then returned to the air/argon condition, the internal resistance and Seebeck coefficient are lower in the second argon test. However,

the power is insignificantly different, and the α and ρ rapidly approach the pre-vacuum values. Consequently, the method of evaluating the effective age for start of storage should be valid.

Using these effective age times, the initial powers given in Table 7.4-10 and the degradation characteristics shown in Figures 7.4-35 through 7.4-41 results in the xenon power versus time characteristics shown in Figures 7.4-42 through 7.4-48, for 30V and 31 volt operation. This is the expected power at any time with a Xenon fill and no helium buildup.

The soft limit on power is based on the evaluation of the combined uncertainties of measurement accuracy during acceptance testing and the uncertainties in the degradation model, and is 1.5 watts below the expected power.

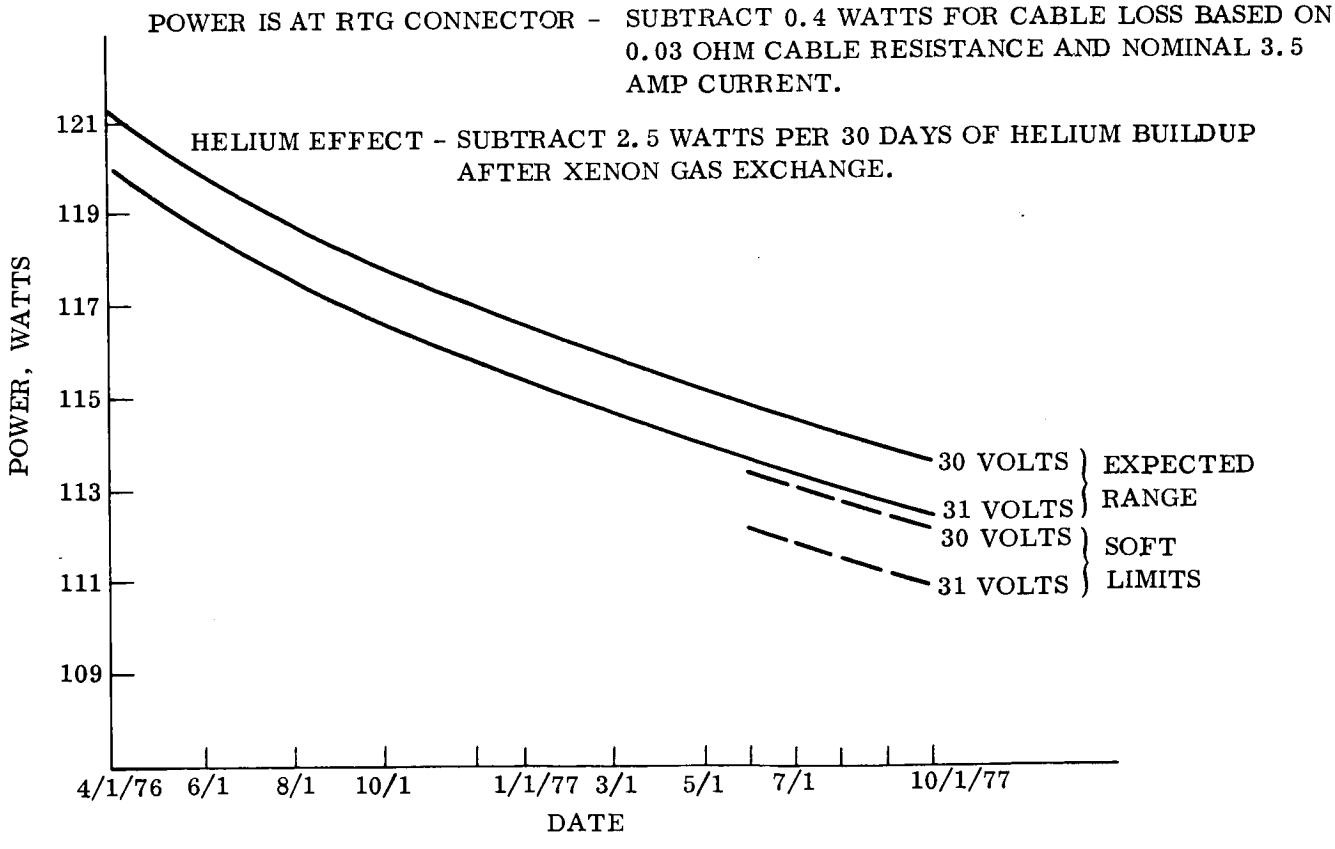

Figure 7.4-42. F-6 RTG Expected Power with Xenon Gas Fill

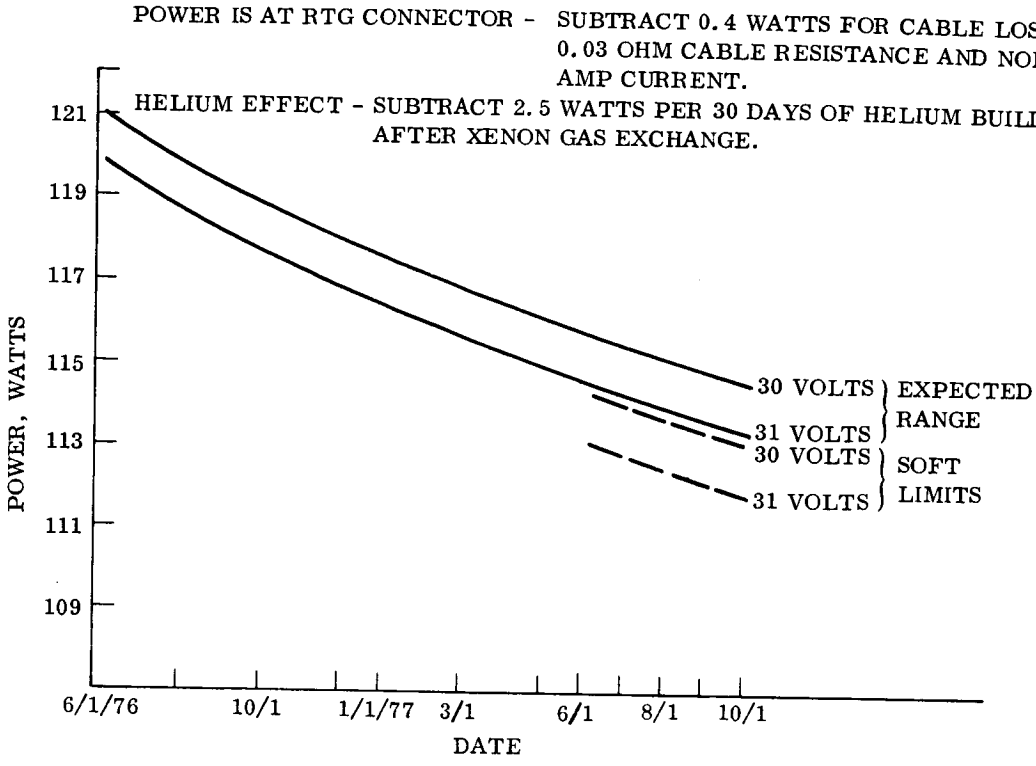

Figure 7.4-43. F-7 RTG Expected Power with Xenon Gas Fill

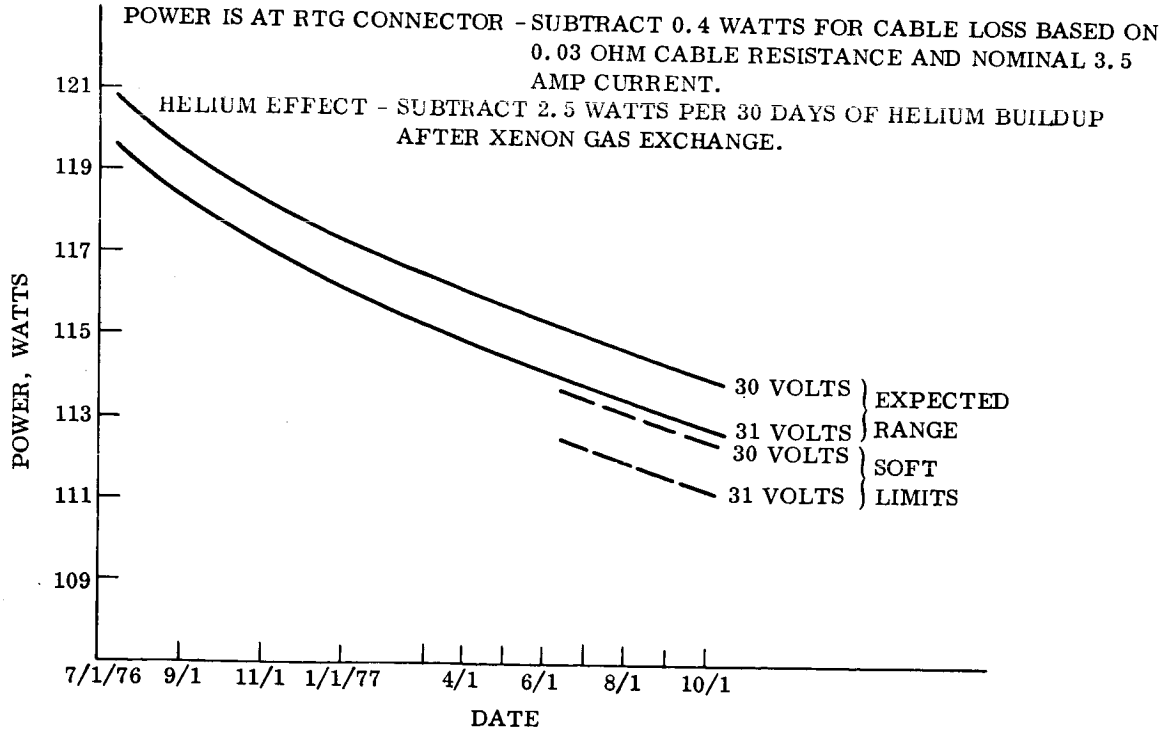

Figure 7.4-44. F-8 RTG Expected Power with Xenon Gas Fill

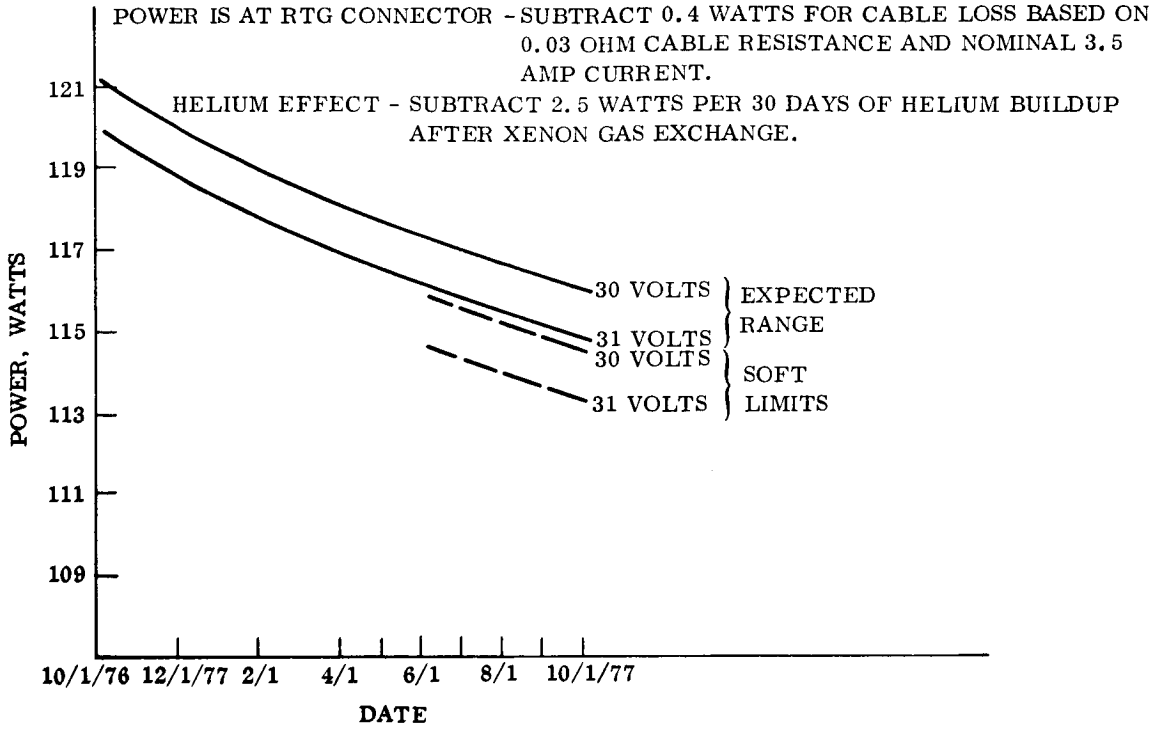

Figure 7.4-45. F-9 RTG Expected Power with Xenon Gas Fill

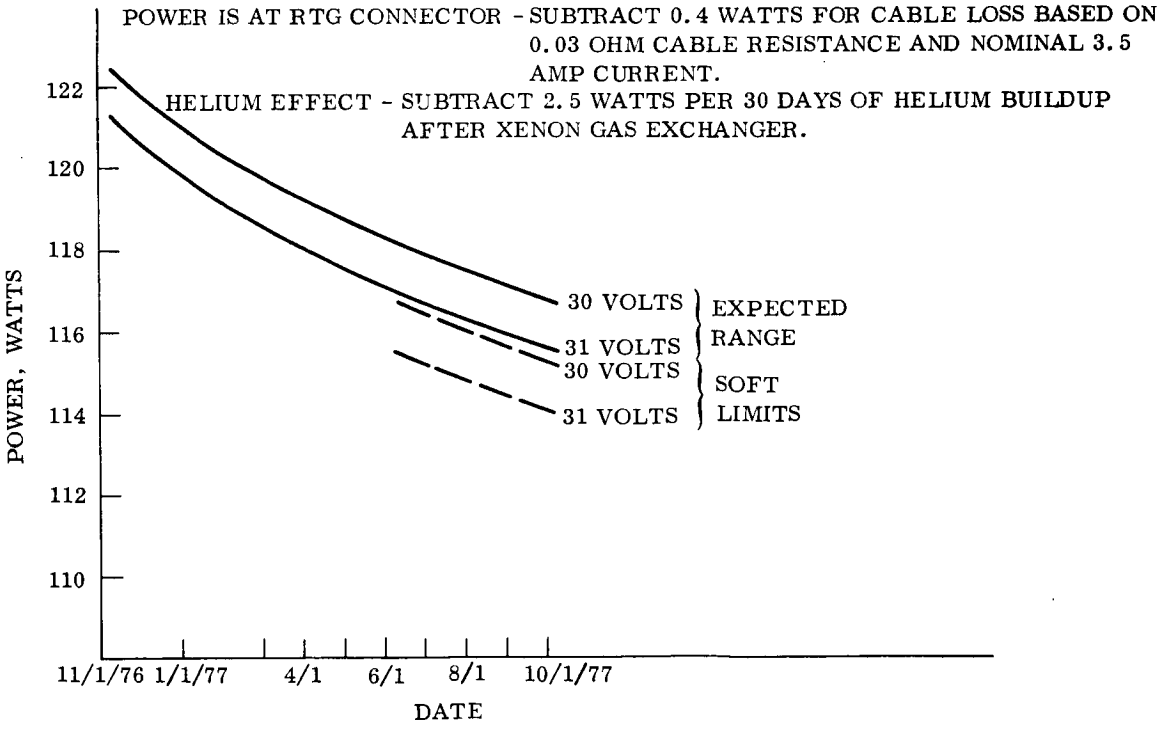

Figure 7.4-46. F-10 RTG Expected Power with Xenon Gas Fill

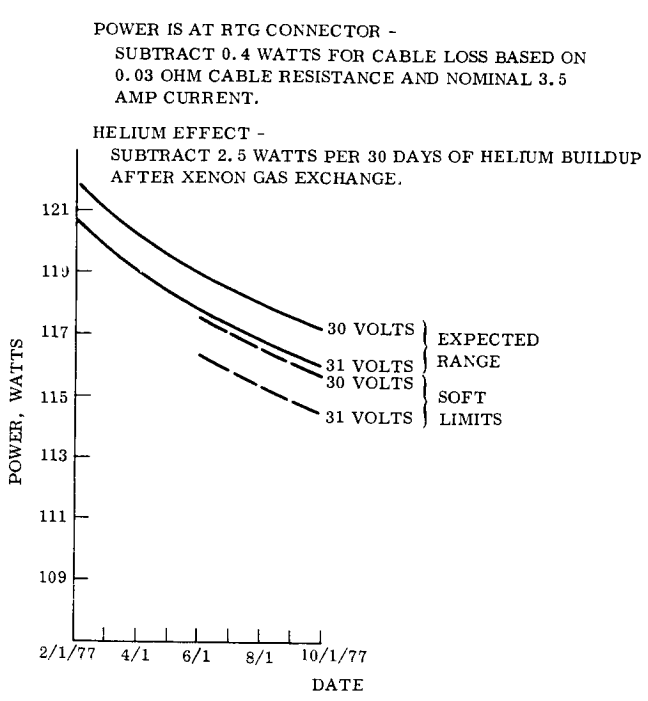

Figure 7.4-47. F-11 RTG Expected Power with Xenon Gas Fill

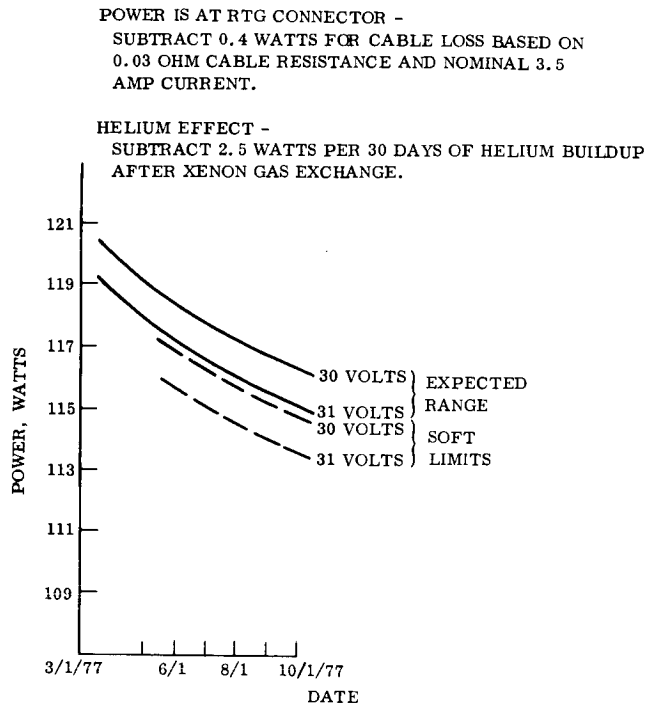

Figure 7.4-48. F-12 RTG Expected Power with Xenon Gas Fill

Voyager II RTGs F-10, 11 and 12

Power Checkout. There was a power check of these RTGs on 6/27 and 6/28/77. The xenon gas exchanges were made on 6/20 to 6/22. There will be about 6 days of helium buildup due to normal generation. The effect of helium on the power level is at most 2.5 watts per 30 days of helium generation. (This is based on test on the Q1A converter and assumes all helium generated stays within the RTG.) Table 7.4-11 shows the expected power at checkout. Included is a 0.4 W(e) correction for cable losses based on a nominal resistance of 0.030 ohms in the JPL cabling.

Launch Pad Power. Voyager II launch is scheduled for 8/20/77. At this time the RTGs will have about 60 days of helium generation. Table 7.4-12 shows the expected power range.

TABLE 7.4-11. POWER AT ELECTRICAL PERFORMANCE CHECKS
(F-10, F-11, F-12) VOYAGER II

Days of Helium Buildup(2)	Power, Watts(1)					
	F-10		F-11		F-12	
	30V	31V	30V	31V	30V	31V
0	117.5	116.3	118.1	116.9	117.4	116.2
6	117.0	115.8	117.6	116.4	116.9	115.7

Soft Limit - 1.5 watts below values shown

Hard Limit - 4.2 watts below values shown

(1) Electrical performance check scheduled for 6/27 and 6/28/77.
Power shown includes -0.4 watts correction for cable loss.

(2) Xenon gas exchange scheduled for 6/20 through 6/22/77.

TABLE 7.4-12. POWER AT LAUNCH
(F-10, F-11, F-12) VOYAGER II

Days of Helium Buildup(2)	Power, Watts(1)					
	F-10		F-11		F-12	
	30V	31V	30V	31V	30V	31V
0	116.7	115.5	117.2	116.0	116.4	115.2
60	111.2	110.5	112.2	111.0	111.4	110.2

Soft Limit - 1.5 watts below values shown

Hard Limit - 4.2 watts below values shown

(1) Launch scheduled for 8/20/77
Power shown includes -0.4 watts correction for cable loss

(2) Xenon gas exchange scheduled for 6/20 through 6/22/77.

Voyager I RTGs F-6, 8 and 9

Power Checkout. There will be a power check of these RTGs on 7/18 and 7/19/77, with 6 days of helium buildup. Table 7.4-13 shows the expected power.

TABLE 7.4-13. POWER AT ELECTRICAL PERFORMANCE CHECKS
(F-6, F-8, F-9) VOYAGER I

Days of Helium Buildup[2]	Power, Watts[1]					
	F-6		F-8		F-9	
	30V	31V	30V	31V	30V	31V
0	113.9	112.7	114.4	113.2	116.4	115.2
6	113.4	112.2	113.9	112.7	115.9	114.7

Soft Limit - 1.5 watts below values shown

Hard Limit - 4.2 watts below values shown

(1) Electrical performance check scheduled for 7/18 and 7/19/77

Power shown includes -0.4 watts correction for cable loss

(2) Xenon gas exchange scheduled for 7/11 through 7/13/77

Launch Pad Power. Voyager I launch is scheduled for 9/1/99. The expected power range is shown in Table 7.4-14. The hard limits shown in Figures 7.4-37 through 7.4-40 are based on the potential release of helium, stored in the fuel matrix during the low temperature storage, and evolved some time after the fuel reaches higher temperatures at the xenon gas exchange.

TABLE 7.4-14. POWER AT LAUNCH
(F-6, F-8, F-9) VOYAGER I

Days of Helium Buildup[2]	Power, Watts[1]					
	F-6		F-8		F-9	
	30V	31V	30V	31V	30V	31V
0	113.6	112.4	114.0	112.8	116.0	114.8
50	109.4	108.2	109.8	108.6	111.8	110.6

Soft Limit - 1.5 watts below values shown

Hard Limit - 4.2 watts below values shown

(1) Launch scheduled for 9/1/

Power shown includes -0.4 watts correction for cable loss

(2) Xenon gas exchange scheduled for 7/11 through 7/13/77

7.4.2.1.1 Launch Transient Power

After liftoff, there will be a drop in RTG power output below the pad power level, then a rise in power as the gas is vented and steady state temperatures are approached. There is a rapid rise in the cold junction temperature, primarily due to the loss of convective cooling of the radiator. The hot junction lags, and the result is a decrease in the temperature drop from hot to cold junction, with a subsequent drop in power. As the gas is vented, the insulation thermal conductance decreases, providing the driving force for an increase in ΔT from hot and cold junction. A computer model of the launch mode has been developed which takes into account these changes in environment and uses the PRD venting characteristics. The results are shown in Figure 7.4-49 for a nominal generator which has a pad power of 113.6 watts and a steady state vacuum power of 152.5 watts. The depth of the minimum power drop is a function of the outer case temperature on the pad and the degree of blockage (reduction in view factor from the RTG surface to space environment caused by proximity to the spacecraft before boom deployment). The launch pad outer case temperature is expected to be in the range of 300°F (149°C) to 400°F (204°C) and the maximum blockage is ~ 20 percent. Table 7.4-15 summarizes the predicted drop in power from the pad power value.

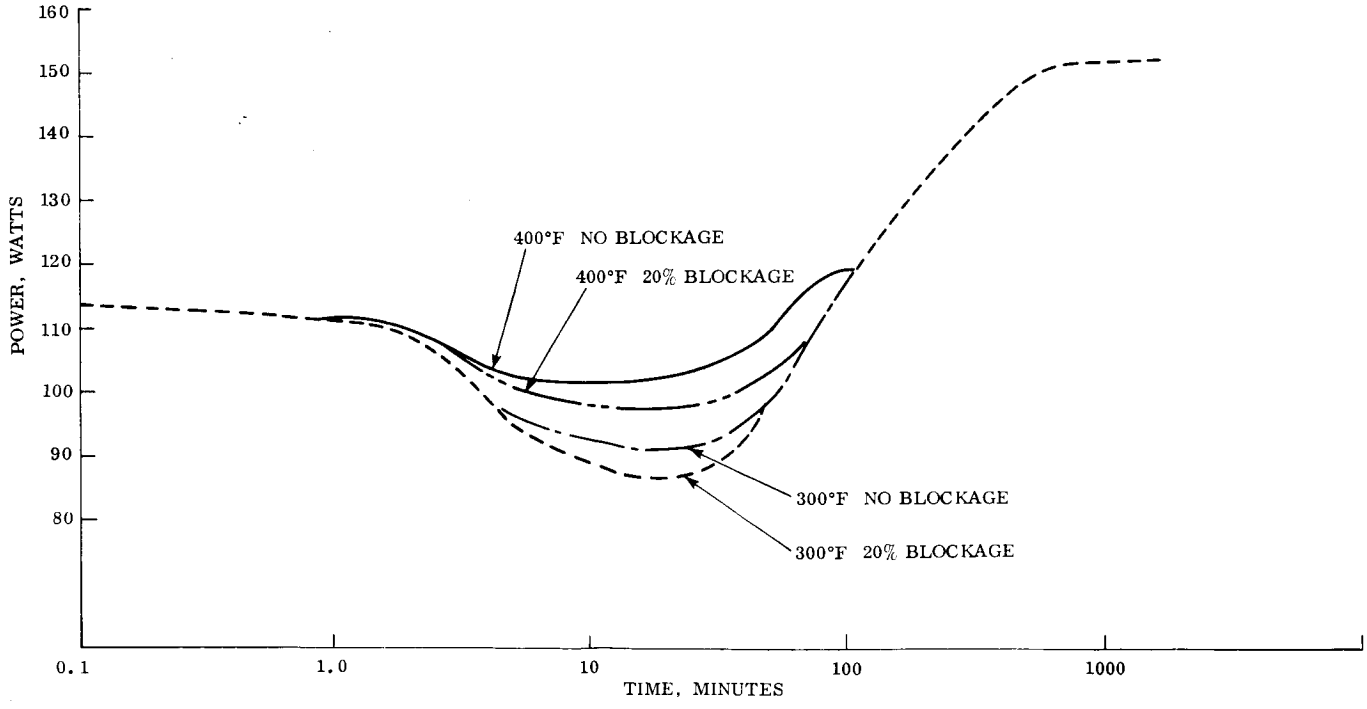

Figure 7.4-49. Launch Transient Power

TABLE 7.4-15. POWER DROP DURING LAUNCH

Launch Pad Case Temp.	Blockage	Power Drop, Watts
300°F	0	21.6
	20%	26.6
400°F	0	11.6
	20%	15.6

Six hours after launch the power output is predicted to be 95 percent of the steady state BOM vacuum power. Table 7.4-16 summarizes the predicted power six hours after launch for each RTG.

TABLE 7.4-16. PREDICTED POWER SIX HOURS AFTER LAUNCH

RTG	Power, Watts
F-6	145.4
F-8	146.6
F-9	147.9
F-10	149.3
F-11	150.7
F-12	149.3

7.4.2.2 Beginning of Mission Power

The beginning of mission (BOM) power (i.e., the stabilized initial flight power) was calculated from the thermal vacuum power at the end of acceptance testing shown in Table 7.4-17. The power at BOM was calculated by taking into account the power loss due to fuel decay and dopant precipitation effects. Table 7.4-18 lists the storage time from the thermal vacuum test till launch and the fuel loading at launch (using a nominal September 1, 1977 launch date).

TABLE 7.4-17. VOYAGER RTGs - THERMAL VACUUM POWER AT THE END OF ACCEPTANCE TESTING

RTG No. (Date)	Fuel Load -Watts(t)	Measured Power	Cable Loss	Power at RTG Connector at 30 Volts	Power Correction for He in RTG	Corrected Power At RTG Connector at 30 Volts
F-6 (3/23/76	2417.1	156.5	2.4	158.9	1.5	160.4
F-7 (6/8/76)	2409	156.5	2.2	158.7	1.5	160.2
F-8 (7/13/76)	2406.2	156.3	2.2	158.5	1.5	160.0
F-9 (10/7/76)	2408.6	156.2	2.7	158.9	1.5	160.4
F-10 (11/9/76)	2408.7	158.4	2.9	161.3	1.0	162.3
F-11 (2/1/77)	2401.5	158.4	2.1	160.5	1.0	161.5
F-12 (3/15/77)	2395.4	156.4	2.1	158.5	1.0	159.5

TABLE 7.4-18. STORAGE TIME FROM THERMAL VACUUM TEST TO LAUNCH AND FUEL LOADING AT LAUNCH

RTG	Storage Time Hours	Fuel Load at Launch Watts
F-6	12,624	2390
F-7	10,776	2385
F-8	9,855	2384
F-9	7,848	2391
F-10	7,118	2393
F-11	5,112	2390
F-12	4,056	2385

It is known from Ragg's work[1] that because of the temperature dependence of the electrical resistivity and Seebeck coefficient, due to changes in carrier concentration and mobility, the lower temperature MHW storage time is equivalent to some lesser effective aging at normal vacuum operating temperature. Raag's work showed that two years (17,520 hours) storage was equivalent to 1.2 months (876 hours) of vacuum operation. Raag considered only two years storage whereas the Voyager RTG storage time varied from 5.6 to 17.5 months. Using a linear scaling relationship, results in the equivalent effective vacuum age times, shown in Table 7.4-19.

TABLE 7.4-19. EFFECTIVE VACUUM AGING DUE TO STORAGE

RTG	Hours
F-6	630
F-7	540
F-8	493
F-9	392
F-10	356
F-11	256
F-12	203

(1) "Effects of low temperature storage on the performance characteristics of the MHW Converter," December 14, 1974, Syncal Corporation

To use this effective vacuum time due to storage, the TBC-4 vacuum life testing data is used coupled with the fact that the typical power loss for RTGs during the first two hundred hours of vacuum testing varied from 1.0 to 1.5 watts. Using these data results in the expected power loss band due to aging shown in Figure 7.4-50.

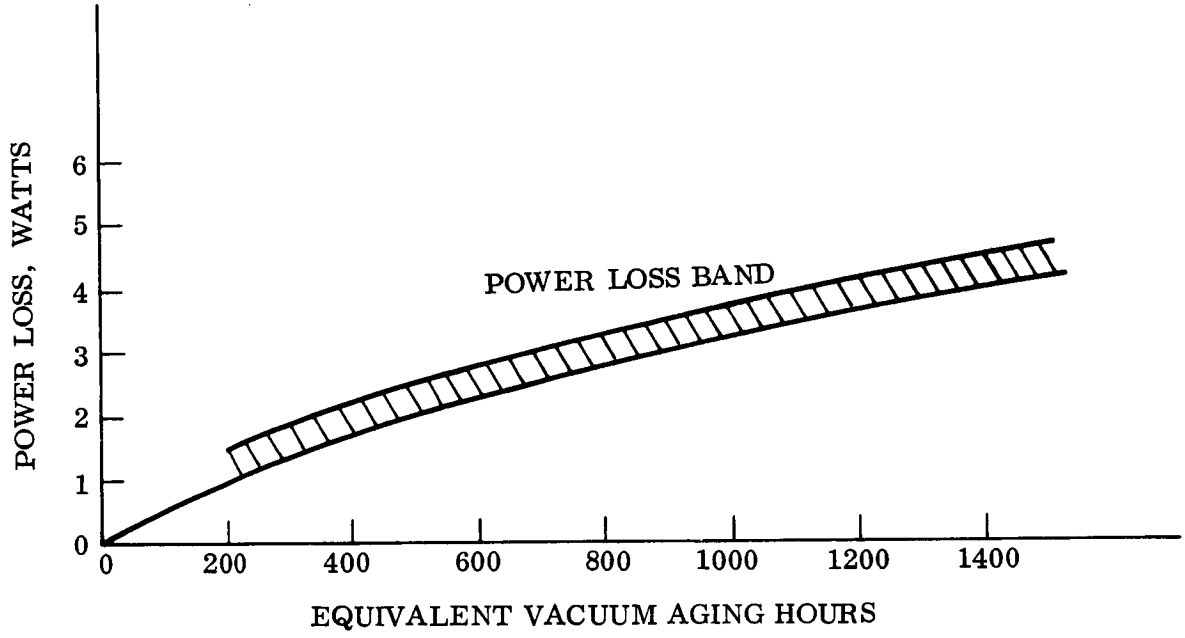

Figure 7.4-50. Power Loss as a Function of Equivalent Vacuum Aging Hours

A second approach is to make use of the data from the LES units F-2 and F-3. These units were subject to a thermal vacuum test at GE, shipped to Lincoln Labs for integration tests and returned to GE where a thermal vacuum acceptance test was run. Using the power loss between thermal vacuum tests, 1.2 watts (corrected for fuel decay), and 3,500 hours (4.8 months) between tests, results in a vacuum power loss rate due to dopant precipitation effects of 0.343 watts/1000 hours of non-vacuum aging. As a conservative approach, this rate was used as a constant. The results using both approaches and the power loss due to fuel decay are summarized in Table 7.4-20. The conservative powers using the linearized rates from F-2 and F-3 were used as the BOM powers for the flight power projections presented in the next section.

TABLE 7.4-20. CALCULATED BOM POWER RANGE

RTG	Power Loss Due to Fuel Decay	Power Loss Due To Dopant Effects		BOM Power Range	
		(1)	(2)	(1)	(2)
F-6	2.8	2.9	4.5	154.7	153.1
F-7	2.4	2.6	3.8	155.2	154.1
F-8	2.2	2.5	3.5	155.3	154.3
F-9	1.9	2.2	2.8	156.3	155.7
F-10	1.6	2.0	2.5	158.7	158.2
F-11	1.1	1.7	1.8	158.7	158.6
F-12	0.9	1.5	1.4	157.1	157.2

(1) Using TBC-4 data

(2) Using F-2 and F-3 data

7.4.2.3 Predicted Mission Performance

The TEGS RTG degradation program and the initial 8,000 hours of flight data from the LES 8 & 9 mission were used to make the final performance predictions for the Voyager missions.

The TEGS computer program is capable of taking into account the following effects:

- Seebeck voltage changes in N&P legs
- Resistivity changes in N&P legs
- Thermal conductivity changes in N&P legs
- Junction contact resistivities
- Hot and cold shoe resistances
- Insulation thermal conductance change with time
- Heat source support losses
- Radiator surface emissivity

- Heat sink temperature variation
- Fuel decay
- Sublimation effects on geometry of T/E legs and hot shoe
- Power loss due to electrical shorting.

Figure 7.4-51 shows the power ratio predicted for the LES 8&9 mission along with the measured data for the four RTGs. The predicted curve used an 800 hour effective age, for dopant precipitation effects for the T/E elements, at the beginning of mission. The measured power ratio is seen to be 1 to 2 percent higher than predicted after 8,000 hours. At the time that the LES predictions were made, the change in the thermal conductivity of the T/E legs was not incorporated into the model since testing was still underway at the Syncal Corporation.

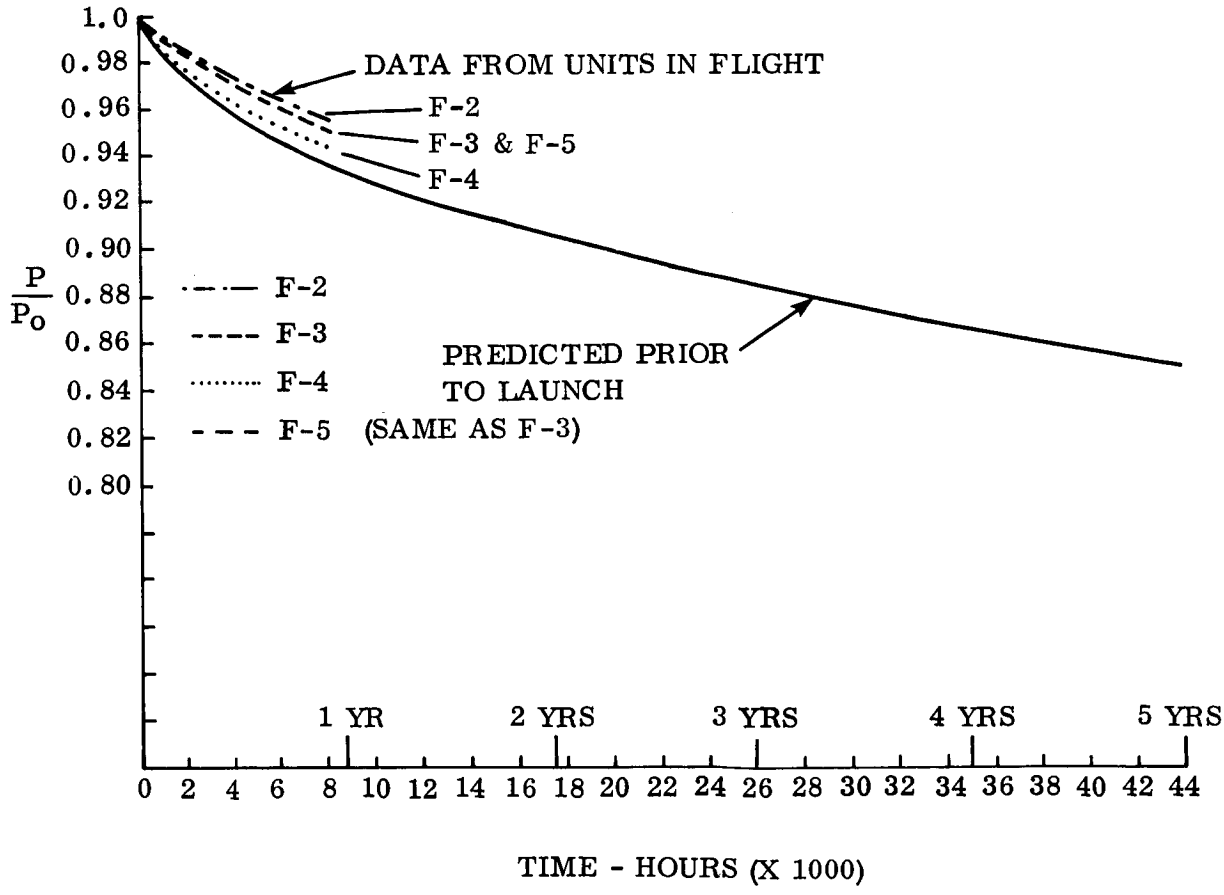

Figure 7.4-51. LES 8 & 9 Flight Power Ratio Measured vs Predicted

The incorporation of the leg conductivity changes shown in Figures 7.4-52 and 7.4-53 into the model and a recalculation of the insulation thermal conductance based on the 17,341 hours of test data from 18-couple module SN-3 (Si_3N_4 coated; T_{HS} = 1035°C), resulted in the data shown in Figure 7.4-54, for effective dopant precipitation (D.P.) ages of 400, 800 and 1500 hours. In all three TEGS runs the effective age for leg thermal conductivity effects was set at 400 hours at the beginning of mission. This value was based on the time prior to launch, during which the couples would be subject to temperature levels where the leg conductivity changes occur.

It is seen that the 400 to 1,500 hour D.P. effective age times bracket the LES flight data. The F-4 flight unit falls closest to the 400 hour curve, while the other three units follow the 800 hour curve to about 5,000 hours, then fall between the 800 and 1,500 hour curves. Beyond 8,000 hours all three effective dopant precipitation ages have essentially the same slope. Consequently, the Voyager performance predictions were made based on the observed spread in the LES data at 8,000 hours (1 percent) and the calculated slop beyond 8,000

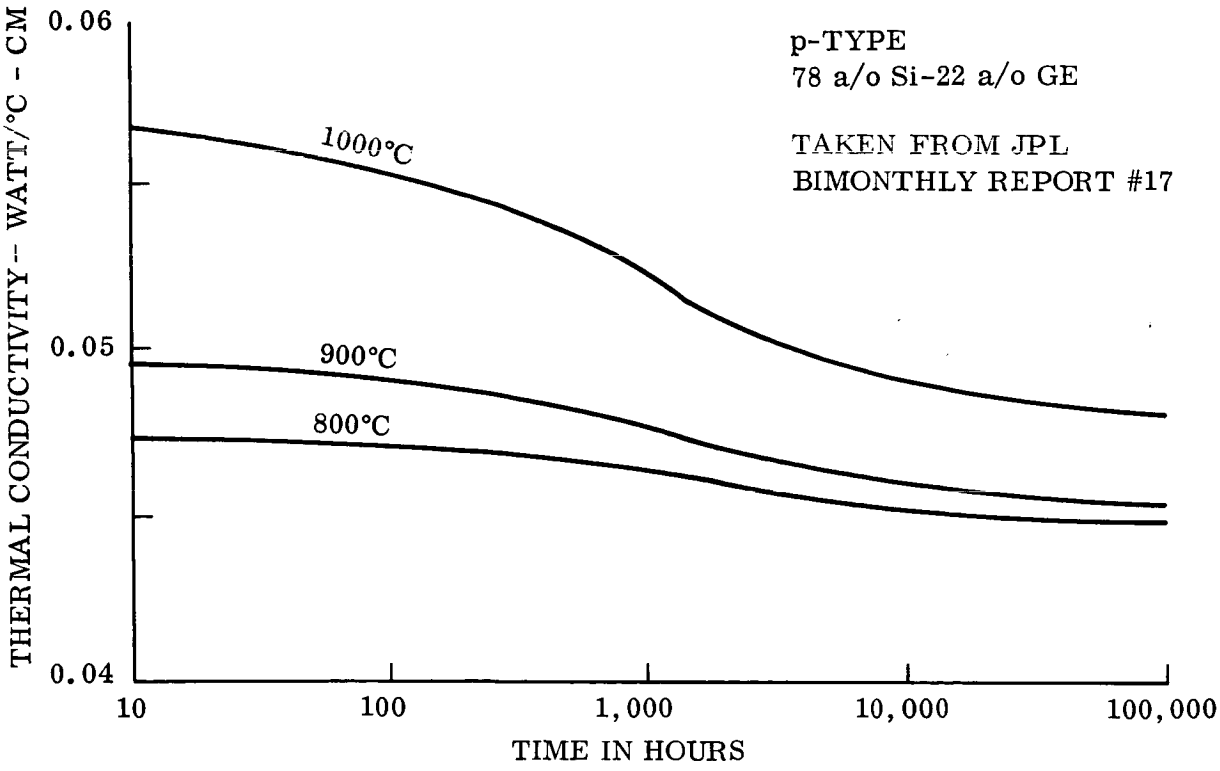

Figure 7.4-52. Leg Conductivity Changes

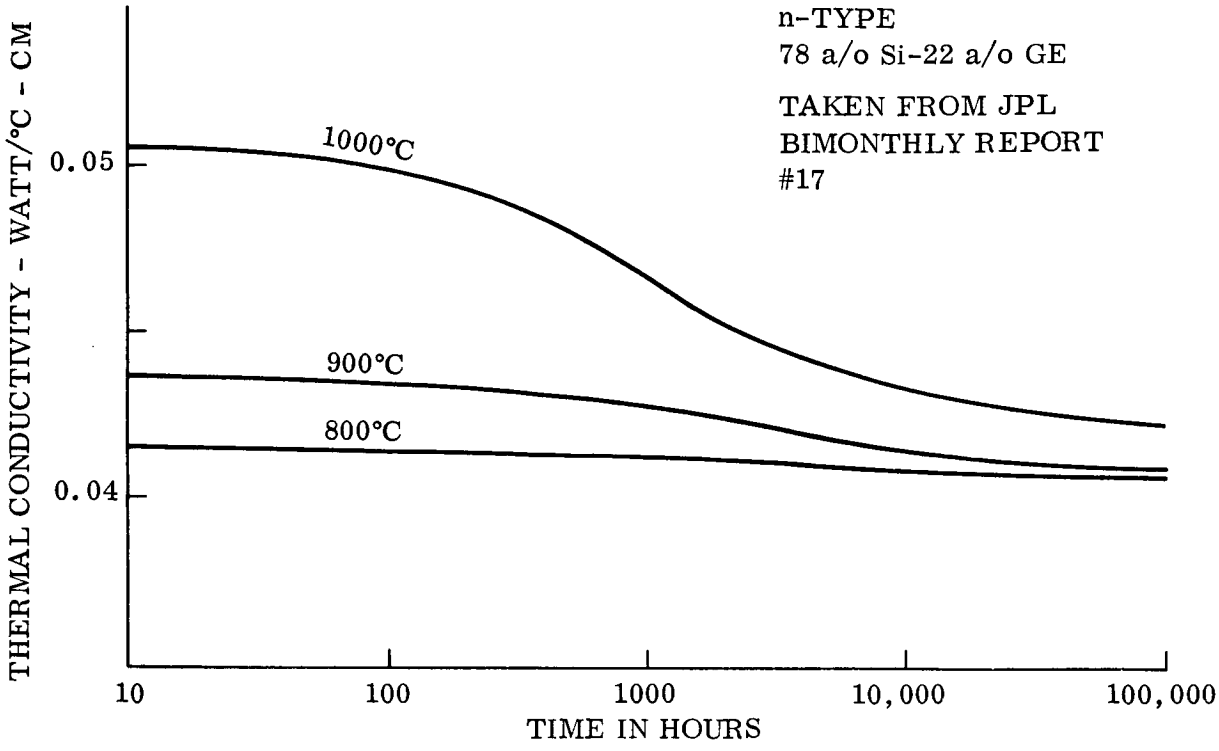

Figure 7.4-53. Leg Conductivity Change

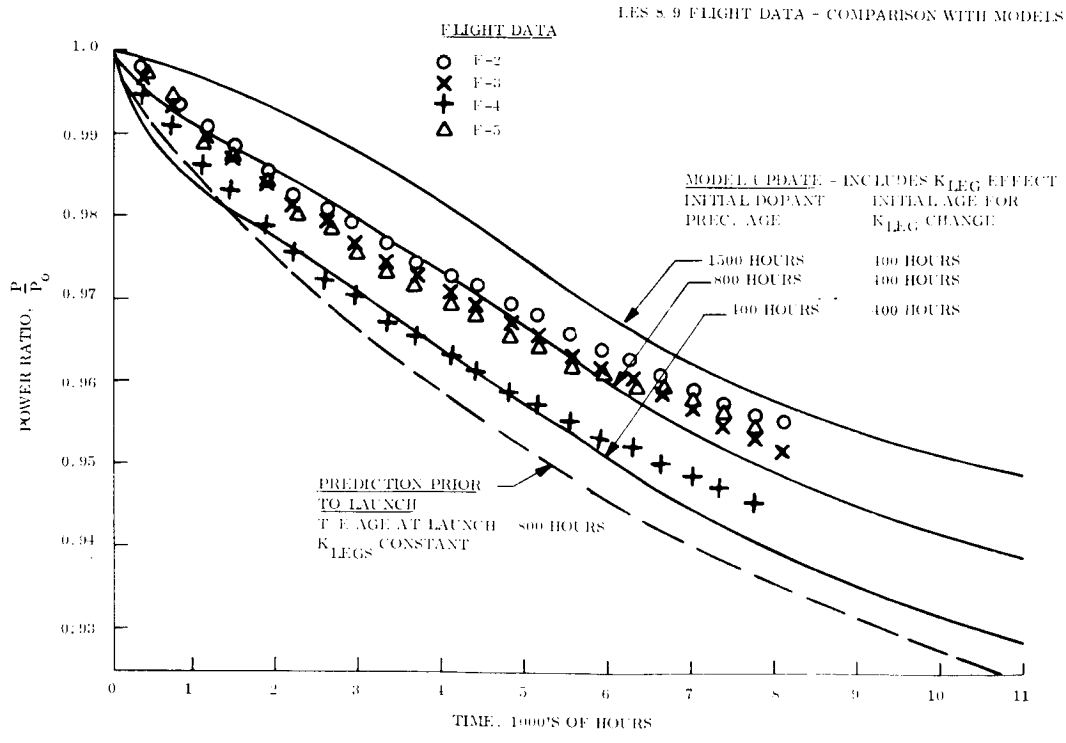

Figure 7.4-54. LES 8 & 9 Flight Power Ratio Measured vs Predicted

hours. These projections are shown in Figures 7.4-55 through 7.4-61. As previously discussed, the Si_3N_4 coating is expected to remain for the four year mission life and, consequently, there is no power drain, due to shorts to the foil or case, shown in these projections.

Table 7.4-21 lists the power predicted at one year intervals throughout the mission.

Table 7.4-22 shows the projected margin of each RTG, over the design requirement at four years of 128 watts.

Table 7.4-23 summarizes the predicted power for each RTG, from the launch pad to the end of mission.

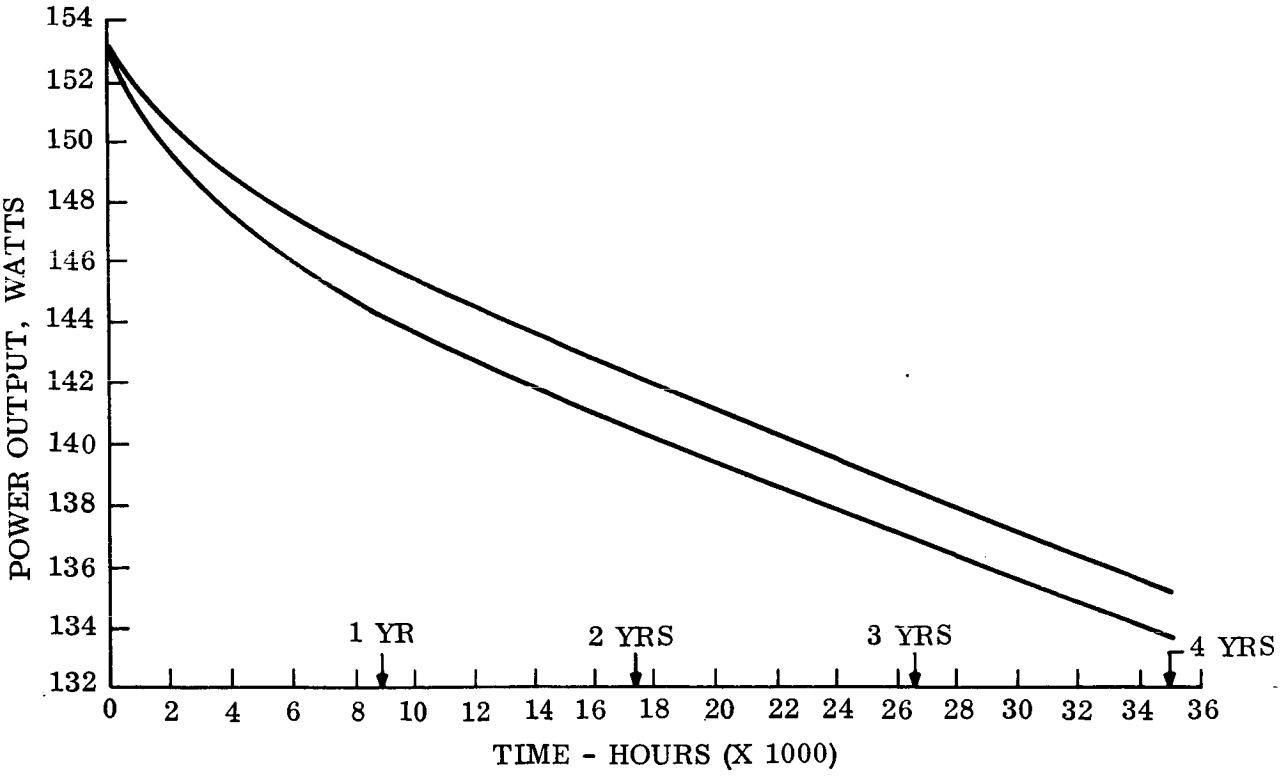

Figure 7.4-55. F-6 Predicted Performance Power at RTG Connector

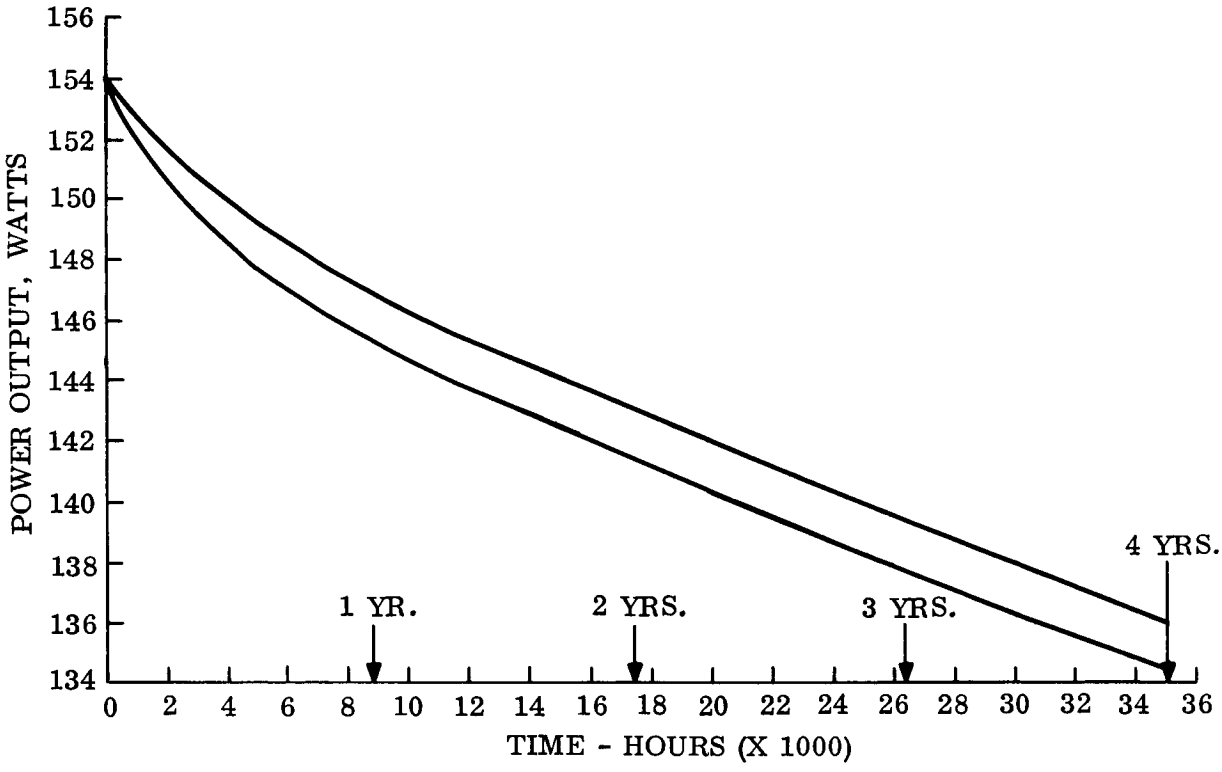

Figure 7.4-56. F-7 Predicted Performance Power at RTG Connector

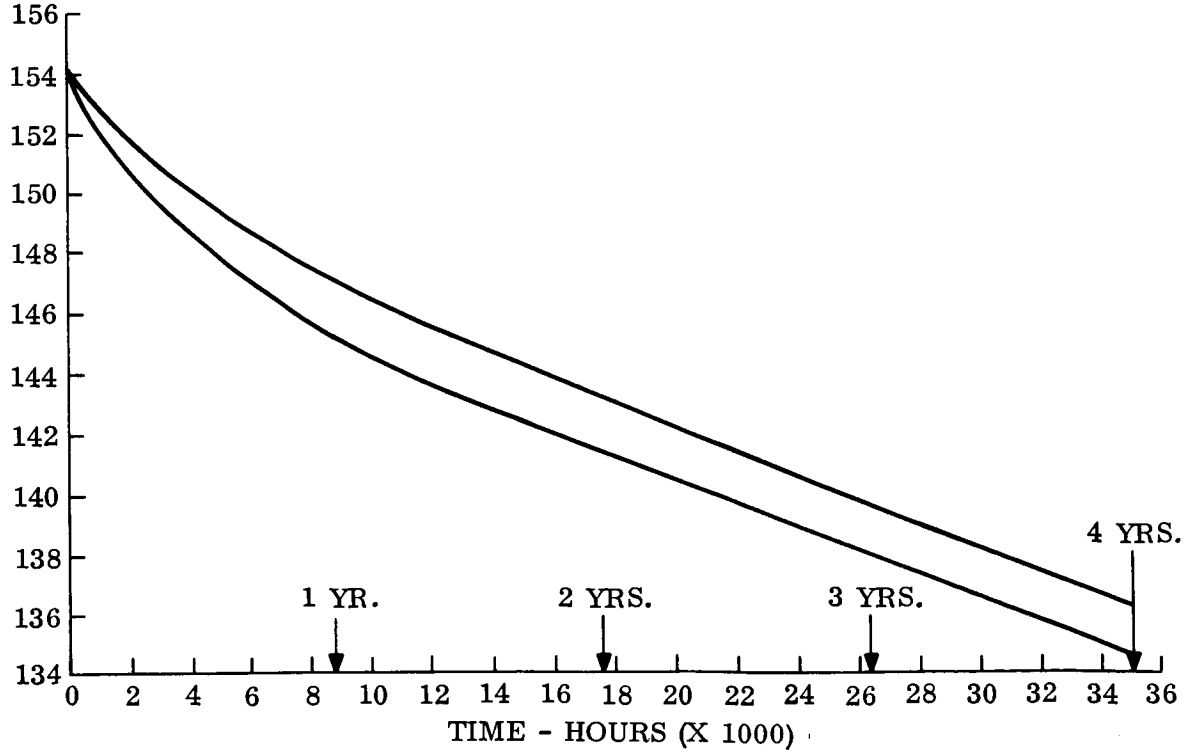

Figure 7.4-57. F-8 Predicted Performance Power at RTG Connector

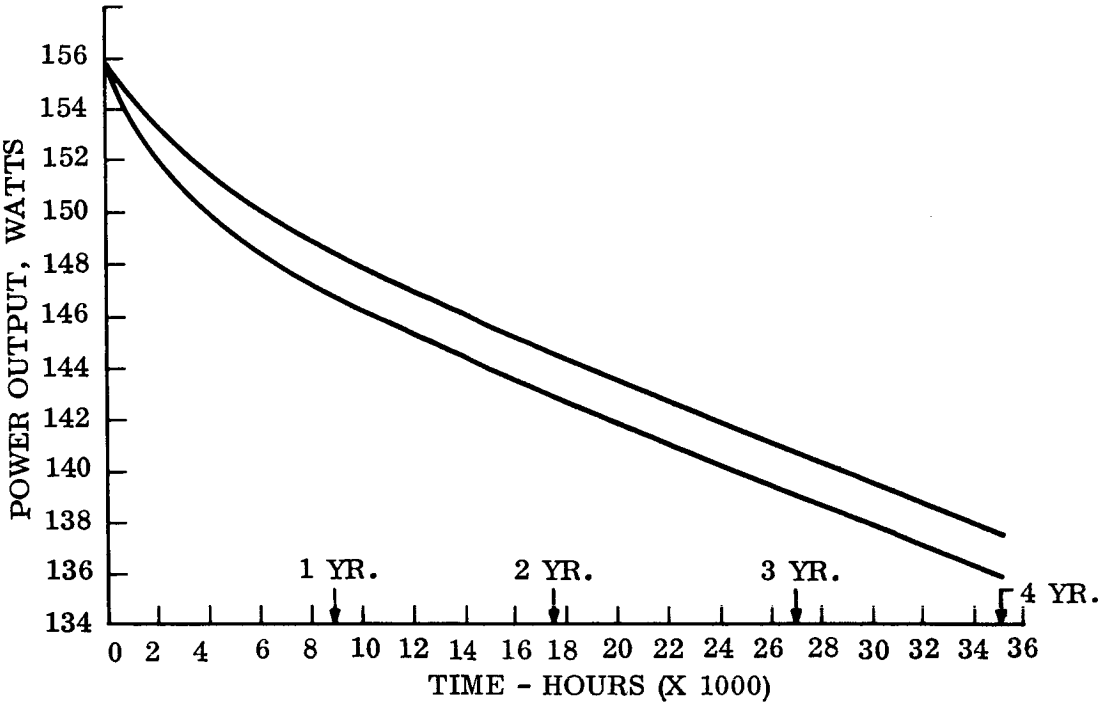

Figure 7.4-58. F-9 Predicted Performance Power at RTG Connector

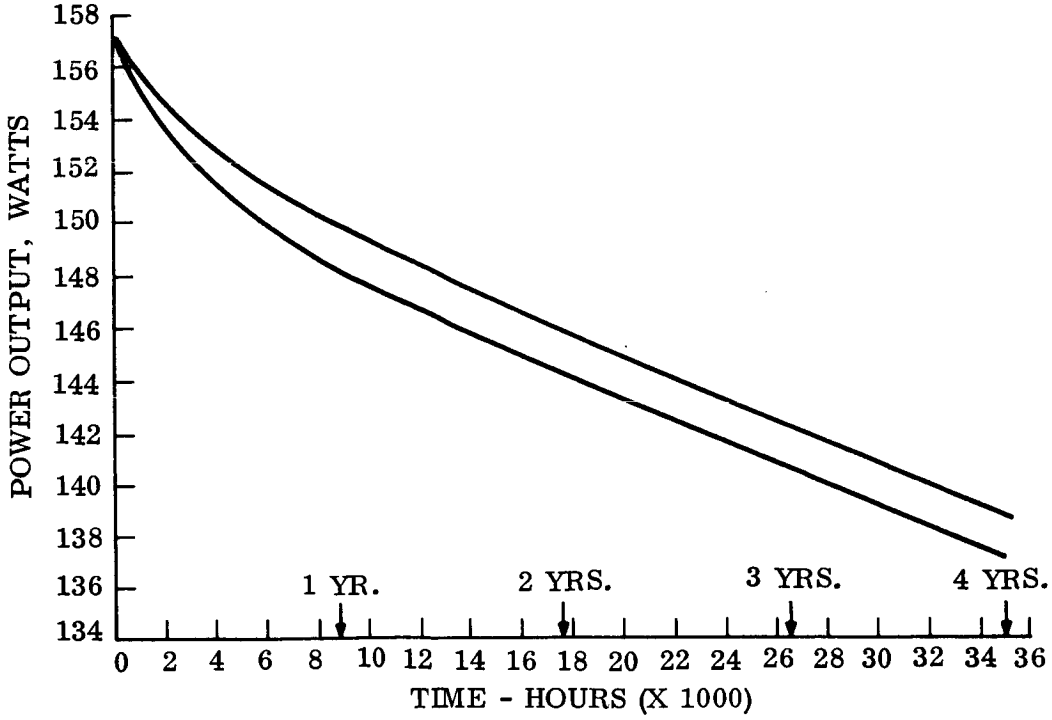

Figure 7.4-59. F-10 Predicted Performance Power at RTG Connector

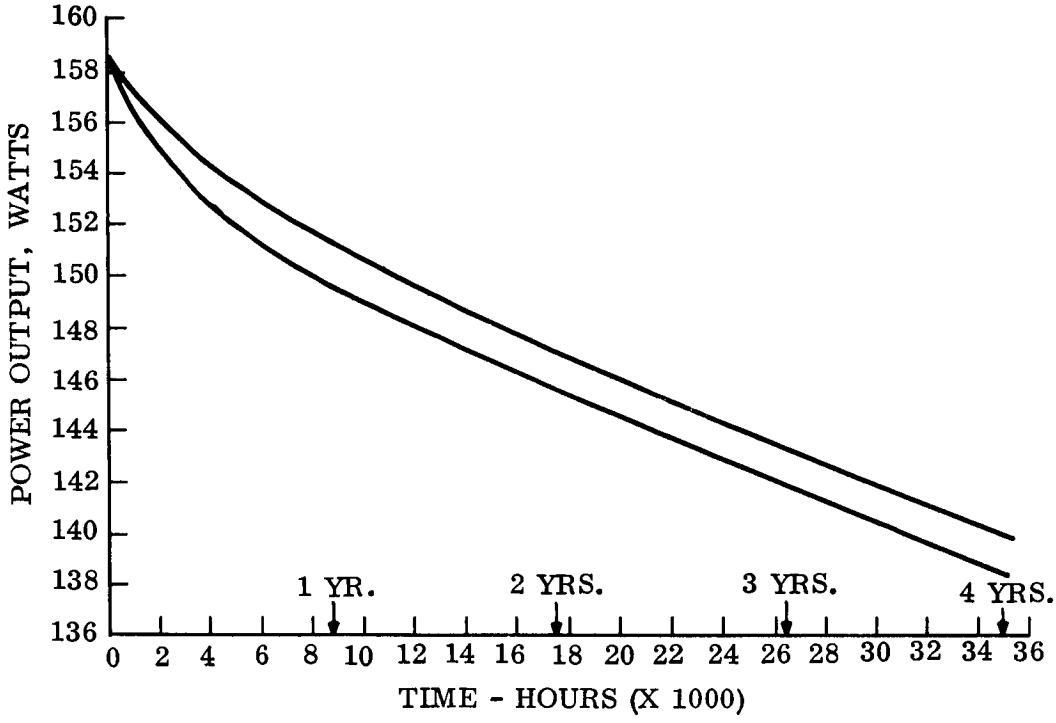

Figure 7.4-60. F-11 Predicted Performance Power at RTG Connector

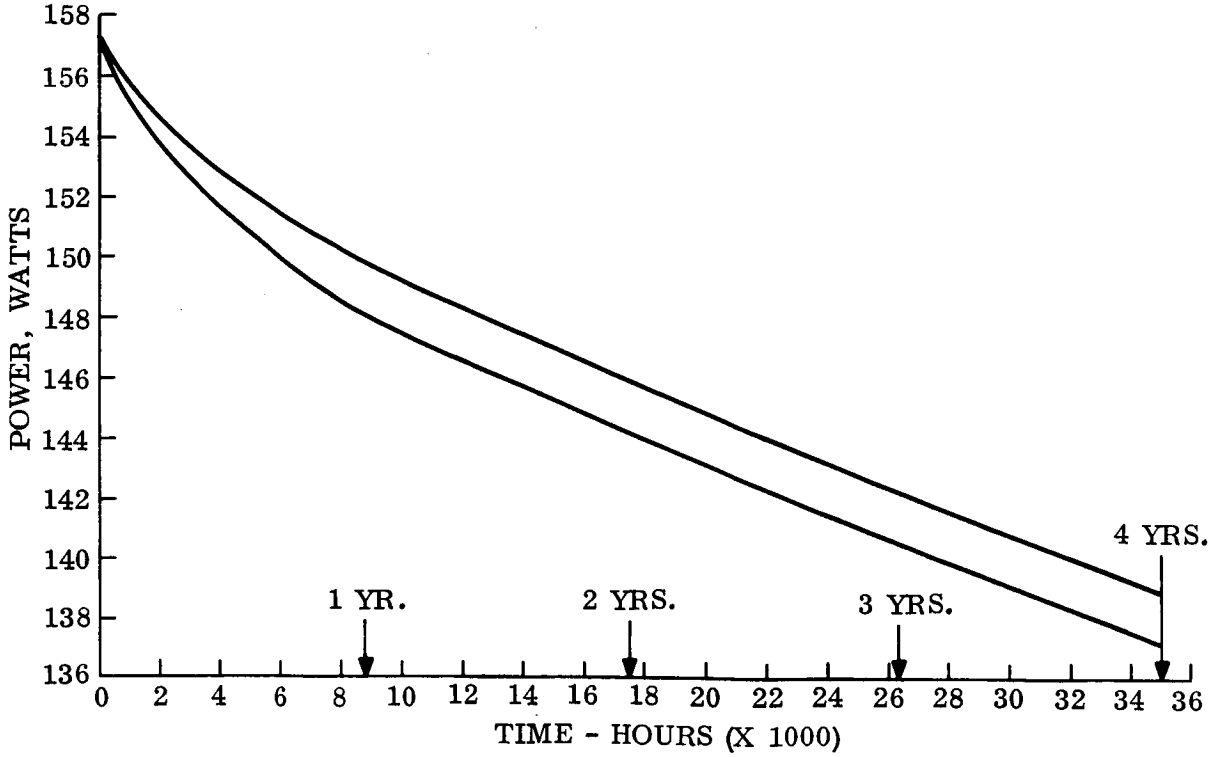

Figure 7.4-61. F-12 Predicted Performance Power at RTG Connector

TABLE 7.4-21. RTG POWER OUTPUT PREDICTIONS
(30 VOLT OPERATION)

Time	Power Output[1] Watts(e)						
	F-6	F-7	F-8	F-9	F-10	F-11	F-12
B.O.M. Sept. '77	153.1	154.1	154.3	155.7	158.2	158.6	157.2
1 yr.	144.3 to 146.0	145.2 to 146.8	145.4 to 147.1	146.8 to 148.4	149.1 to 150.9	149.5 to 151.2	148.2 to 149.9
2 yrs.	140.4 to 142.1	141.3 to 143.0	141.6 to 143.2	142.9 to 144.6	145.2 to 146.9	145.5 to 147.0	144.1 to 145.8
3 yrs.	136.9 to 138.6	137.8 to 139.4	138.0 to 139.6	139.3 to 131.0	141.6 to 143.2	141.9 to 143.3	140.6 to 142.2
4 yrs.	133.6 to 135.3	134.5 to 136.0	134.6 to 136.2	135.9 to 137.5	138.2 to 139.8	138.4 to 140.0	137.2 to 138.9

(1) Power available at RTG connector; all cable losses must be subtracted to obtain net power.

TABLE 7.4-22. PROJECTED MARGIN OVER DESIGN REQUIREMENT

RTG	Watts
F-6	5.6
F-7	6.5
F-8	6.6
F-9	7.9
F-10	9.7
F-11	10.4
F-12	9.2

TABLE 7.4-23. SUMMARY OF PROJECTED PERFORMANCE (1)

Event On Pad(2)	Requirement 105 watts	F-6	F-7	F-8	F-9	F-10	F-11	F-12
Days of Helium	0	114.0	114.9	114.4	116.4	117.1	117.6	116.8
	30	111.5	112.4	111.9	113.9	114.6	115.1	114.3
	50	109.8	110.7	110.2	112.2			
	60		109.9			112.1	112.6	111.8
T + 6 Hours	138.7 watts	145.4	146.4	146.6	147.9	149.3	150.7	149.3
Flight Operation (BOM)	146 watts	153.1	154.1	154.3	155.7	158.2	158.6	157.2
BOM + 4 Years (EOM)	128 watts	134.4	135.2	135.4	136.7	138.0	139.2	138

(1) At 30 volts, power at RTG connector

(2) Xenon gas

SECTION 8

CONVERTER FABRICATION

Fabrication of all converters for MJS was completed during 1976 and all units were delivered to GE-NP-SD by December 1976.

Seven complete, flight-qualified RTGs, six for flight plus one spare, were delivered to KSC in May and June 1977.

SECTION 9

CONVERTER DESIGN ANALYSIS, FABRICATION AND TESTING AT RCA

All the MHW-MJS flight converters (F-7, F-8, F-10, F-11 and F-12) were completed, processed and performance tested by RCA during 1976. All units were delivered to GE-SD by December 1976.

Converter anomalies involving RCA materials and fabrication problems as they pertained to converter development are discussed in Section 7 of this report.

SECTION 10

ACCEPTANCE TESTING

10.1 ETG ACCEPTANCE TESTING

The systems test schedule for MHW-MJS is shown in Figure 10-1.

10.1.1 Q-1A ETG - MJS COLD TEST UNIT

After mass properties testing, the Q-1A ETG had been placed into storage in Bldg. 800. On 5 January 1976, it was removed from its CSC for a repeat of the CG measurements, there having been an X-axis CG offset indicated from the results of the previous test. The CG measurements yielded acceptable values. The Q-1A was re-installed into its CSC, and transferred to Bldg. 100 for shipment to JPL.

10.1.2 Q-2 ETG - MJS QUALIFICATION UNIT

On 7 January 1976, the unit was transferred from the Bldg. 800 storage area to the test area, removed from its CSC and set-up on the slide tray assembly. After pneumatic flexible hose and electrical cable installation were completed, the ETG was installed into LAS #1. Remaining LAS preparations were completed, the chamber was secured and the chamber pump-down began. After an acceptable vacuum level was attained, argon backfilling and scrubbing operations were completed and ETG disassembly was initiated.

The forward dome was removed and the EHS was hoisted out of the converter. A visual examination of the cavity showed that the aft zirconia bearing discs were chipped at two places. The cavity appeared clean and there was no evidence of the chips being inside the converter. Bakeout can operations were completed with the installation of the aft graphite end cap into the converter and removal of the EHS from the chamber. See Section 10.2.1 for the Q-2 RTG operations.

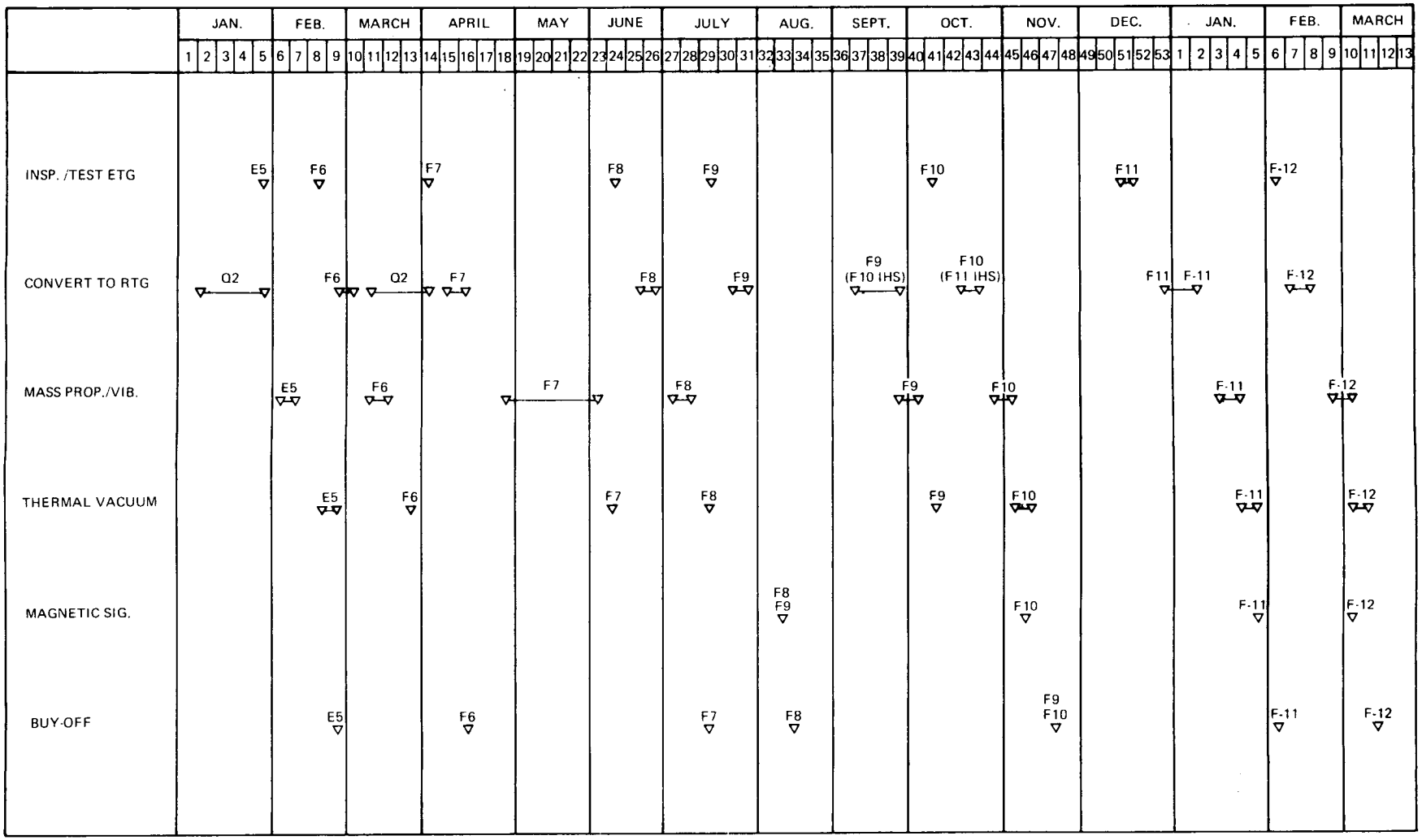

Figure 10-1. MHW-MJS System Test Schedule 1976

10.1.3 E-5 ETG

After receipt of the E-5 ETG from RCA, the receiving inspection operations were begun on 27 January 1976. Circuit resistance and isolation measurements were completed, and the G6 flex hose was then installed. This flex hose showed an unacceptable leak at the connection to the GMV. After unsuccessful attempts at effecting a proper seal, the original hose was replaced with the flex hose from the Q-2 ETG and the "cold" pressure decay test then yielded an acceptable leak rate of 0.0 psi/6-hours.

Six strain gages were mounted to the three converter fins, two gages at each, as additional diagnostic instrumentation to be used during vibration testing. RTD cable installation was completed and the unit was installed into its CSC and sent to Bldg. 400.

The E-5 ETG was removed from its CSC and set up on the vibration slip table in the forward end down orientation. ROC, PSC and gas cart interconnections with the ETG were completed and the EHS energization then began. The unit was allowed to stabilize for the start of the pre-vibration 48-hour air performance/pressure decay test.

The pressure decay test yielded an acceptable leak rate of 0.11 psi/48-hours. Generator output power over the 48-hour period averaged 74 watts. As this power was lower than anticipated, based on RCA vacuum performance power of 157 watts, trouble-shooting was initiated. The EHS power supply was de-energized and isolation measurments were performed between the EHS circuit and converter to ascertain if there was a path which might be shunting some of the EHS current. All measurements were greater than 2 megohms.

The EHS was again energized and purging cycles were initiated on the converter to see if a gas exchange would contribute to an increase in the output power. The ETG was bled to 18 psia, the re-pressurized to 25 psia with argon gas for a total of fifteen purge cycles. This operation removed the bulk of the helium gas which might have been present from the RCA operations. After the purging operations, the ETG output power was running at 76 watts (an increase of 2 watts) and authorization was given to start vibration testing.

The X-axis vibration cycle was performed with two 1/2-G sine sweeps, a 1/2 level MJS sinusoidal acceptance, a full-level sinusoidal acceptance, a 1/3-level random acceptance and a full-level random acceptance vibration being applied. The unit was rotated on the vibration slip table to the Z-axis orientation and the Z-axis vibration test cycle was performed. After positioning the ETG onto the exciter head, the Y-axis vibration test cycle was performed. There was no apparent structural degradation to the ETG due to the vibration exposures. A six-hour post-vibration air performance/pressure decay test yielded an ETG leak rate of 0.0 psi/6-hours and output power averaged 76.3 watts over this period. The EHS was then de-energized.

After the ETG had cooled to room ambient temperature, mass properties measurements were taken. The operations of installing the unit into its CSC were then completed and the ETG was transferred to the Bldg. 300 Long Life Lab.

Initial preparations were completed for thermal-vacuum testing in Chamber #1 and the ETG was installed onto the chamber's support fixture. Test readiness was completed, the chamber door secured and chamber evacuation was initiated. With the chamber pressure in the 10^{-6} torr range, the EHS energization cycle began and full input power of 2400 watts was achieved after 18 hours. After the ETG had thermally stabilized, a four-hour thermal-vacuum performance test yielded an average output power of 155.0 watts.

ETG backfilling with argon to 25 psia and chamber backfilling with nitrogen to one atmosphere were completed and the chamber door was opened and rolled out to allow the ETG to stabilize in ambient air. A visual examination of the ETG for superficial defects showed some separation of the RTV potting material at the RTD headers.

E-5 was thermally stabilized for the start of a 48-hour air performance/pressure decay test. Rate of pressure decay was 0.09 psi/48-hours and output power averaged 74.4 watts over the 48-hour period. The EHS was de-energized and the ETG was removed from the chamber support frame and installed into the lower half of the CSC. The separated RTV potting material was trimmed at the RTD headers at this time and the "H"-film tape was also removed from the RTD cable at the header areas. Installation of the ETG into the CSC was then completed and the unit was transferred to Bldg. 100 for shipment to JPL.

10.1.4 F-6 ETG - MJS FLIGHT UNIT (1)

The F-6 ETG was removed from its CSC in Bldg. B for pneumatic hose and electrical cable installations. The flex hose was installed onto the GMV and after converter pressure was measured as 20.7 psia, the unit was re-pressurized to 25 psia. The RTD cable and power out cables were installed and the unit was reinstalled into the CSC and transferred to Bldg. 800 on 19 February 1976.

Preparations were completed for the RTG assembly operations and the unit was installed into LAS #1. Test readiness was completed and chamber evacuation began. After attaining the 10^{-6} torr range, argon backfilling was initiated and acceptable purity levels were achieved. ETG disassembly operations were then completed. A visual examination of the converter cavity showed no anomalous indications. See Section 10.2.2 for the F-6 RTG operations.

10.1.5 F-7 ETG - MHW-MJS FLIGHT UNIT SPARE (1)

After its receipt from RCA on 16 March 1976, the F-7 ETG was placed into storage in Bldg. B. The unit was taken out of storage, removed from its CSC and a cold pressure decay test was completed which yielded an acceptable 0.02 psi/6-hour leak rate. Thermopile circuit resistance and isolation measurements were performed and these correlated properly with the pre-ship measurements taken at RCA.

RTD and power out cable installations were performed and the resistance and continuity measurements on these cable systems were completed. After flex hose installation onto the GMV, the unit was re-installed in its CSC and transferred to Bldg. 800.

On 5 April 1976, LAS #1 preparation was completed for the RTG assembly operations and F-7 was installed into the chamber onto the rotary table. Chamber evacuation was initiated and after attaining below 1×10^{-5} torr, argon backfilling was completed and acceptable purity levels were achieved. Bakeout can operations were also completed.

ETG disassembly began on 7 April. As had occurred also on Q-2, the fitting on the tube between the processing valve and spoolpiece port was seized to the port. Since the tube would be removed with the spoolpiece, there was no need to cut the fitting nut as had been done on Q-2. The forward dome, spoolpiece and EHS removals from the converter were completed. Visual examination of the converter cavity closed out the ETG disassembly and showed no anomalous conditions.

10.1.6 F-8 ETG - MHW-MJS FLIGHT UNIT (1)

After its receipt from RCA, on 4 May 1976, the F-8 ETG was placed in storage in Bldg. B. On 7 June 1976, the unit was taken out of storage and removed from its CSC. Measurements of thermopile circuit resistance and isolation from case and foil system were completed with favorable comparison to the RCA pre-ship measurements. A cold pressure decay test yielded a leak rate of zero psi/6-hours. The RTD cable and PRD bracket were then installed. The JPL power out cable, which was assigned to F-8, failed a pin retention test and was not installed. Pneumatic flex hose installation was completed and the 3500G3 adaptor cable to the RTD instrumentation cable was installed. RTD circuit measurements yielded acceptable resistance values and isolation measurements between the individual RTD circuits and converter case yielded greater than 200 megohms. The unit was installed in its CSC and transferred to Bldg. 800 in mid June.

On 14 June 1976, the F-8 ETG was removed from its shipping container and set up in the Bldg. 800 test area. A 2428G1 GSE-type power out cable was installed in place of the JPL cable and circuit resistance and isolation measurements were performed. The unit was installed into LAS #1 on the rotary table, electrical and pneumatic interconnections were completed, and the chamber was secured. Chamber evacuation was initiated shortly thereafter and the 10^{-6} torr range was attained. Argon backfilling and purification was completed. After completion of the bake-out can operations, ETG disassembly began with the forward dome disassembly. Subsequent examination of the converter cavity revealed no abnormalities.

10.1.7 F-9 ETG - MHW-MJS FLIGHT UNIT (1)

After its receipt from RCA on 7 July 1976, the F-9 ETG was removed from its converter shipping container and set up in a clean area in Bldg. B for ETG acceptance testing and electrical cable/pneumatic hose installation. Measurements of thermopile circuit resistance and isolation from case and foil system were performed. These showed a favorable comparison to the RCA pre-ship measurements. A cold pressure decay test yielded a leak rate of 0.0 psi/6-hours. A new JPL power cable had been recently received and this cable was installed per a new torque and safety wiring requirement by JPL personnel. The RTD instrumentation cable installation was completed along with that of the 3500G3 and 3500G4 adaptor cables which mate to the RTD and power out flight cables. After the pneumatic hose installation to the RTG gas management valve was completed the ETG was re-installed in its CSC.

After transfer of F-9 to Bldg. 800 20 July 1976, the unit was installed in LAS #1 on the rotary table. Electrical and pneumatic connections to the chamber penetrations were completed and the chamber was secured. LAS evacuation began and after attaining the 10^{-6} torr range, argon backfilling/purification was performed.

The Segment Readiness Review held prior to beginning ETG disassembly had questioned the suitability of the new potting compound used on the JPL power cable connector plug. Investigation showed that the material had an unacceptably low thermal limit and a decision was made to replace the JPL cable with a GE test cable. The LAS was opened and the flight cable was exchanged for a 2428 G1 GSE power cable.

After again securing the chamber, evacuation was attempted but an acceptable vacuum level could not be attained. Since the ETG was still in a safe pressurized mode, trouble-shooting was initiated and it was found that there was leakage into the chamber via the facility gas management system's inlet and outlet valves. The valves were cleaned and chamber pump-down and argon backfilling/purification completed. On completion of the bakeout can operations, ETG disassembly began with the forward dome removal. The EHS and spoolpiece were removed from the converter to complete the ETG disassembly operations. Visual examination

of the converter cavity revealed no discrepancy other than a burnishing of the innermost layer of astroquartz on the aft moly-foil end cap. Further inspection and discussion with Engineering, determined that there was no degradation to the astroquartz layer.

Installation of the aft graphite end cap assembly was completed and final preparations made for the heat source effort.

10.1.8 F-10 ETG - MHW-MJS FLIGHT UNIT (2)

The F-10 ETG was received from RCA on 27 August 1976, and placed into storage in Bldg. B. On 4 October 1976 the CSC was opened to allow ETG acceptance testing and installation of the peripheral converter components. Thermopile circuit resistance and isolation from the case and foil system were measured and indicated a favorable comparison to the RCA pre-ship measurements. Cold pressure decay rate indicated 0.0 psi/6-hours. The PRD housing, the pneumatic flex hose to the RTG GMV, the RTD cable and a 2428 GSE-type power cable (JPL flight power cable was unavailable at that time) were installed and the ETG was re-installed in its CSC.

After transfer of the unit to Bldg. 800, it was installed in LAS #1, on 12 October 1976. Electrical/pneumatic interconnections were completed, the chamber was secured and pump-down was initiated. After an acceptable vacuum level was attained, argon backfilling/purification operating were completed. The bakeout can operations were then performed. ETG disassembly began with the forward dome removal. The spoolpiece was disassembled from the case and the EHS was hoisted from the converter. Visual examination of the converter cavity revealed no obvious anomalies.

10.1.9 F-11 ETG - MHW-MJS FLIGHT UNIT (1)

The F-11 ETG was received from RCA on 22 October 1976 and placed in storage in Bldg. B. On 7 December 1976, the CSC was opened and the ETG set up in a clean area in Bldg. B for ETG Acceptance Testing and installation of the peripheral converter components. Visual examination of the unit revealed crazing and flaking of the emissive coating on the forward

stiffening ring and scratches near the GMV on both a fin and the converter shell. This was documented on NR-48419 and disposition was given to remove loose particles of the coating by brushing. Measurements of thermopile circuit resistance and isolation from case and foil systems were performed and showed a favorable comparison to the RCA pre-ship measurements.

Cold pressure decay rate indicated 0.0 psi/6-hours. The pneumatic flex hose to the RTG gas management valve, the RTD cable and the 2428 GSE-type power cable (JPL flight power cable was unavailable at that time) were installed.

The PRD housing was installed, final circuit resistance measurements obtained, and the flex hose integrity verified. The ETG was installed into its CSC and shipped to Bldg. 800 for storage. The converter was removed from its CSC and installed in LAS #1, on 30 December 1976. Electrical and pneumatic interconnections were completed, the bakeout can was installed, and the chamber was secured in preparation for chamber pumpdown.

On 4 January 1977, an acceptable chamber vacuum level was attained. During the attempt to bring the LAS GMS on-line, an abnormally high oxygen content of approximately 800 ppm was noted. Subsequent trouble-shooting revealed a slight crack in the Tygon tubing interconnecting the main GMS rack with the analyzer rack. After the tubing was repaired, the GMS was brought on-line and satisfactory gas purity levels were attained. The GMS was interconnected with the LAS and backfilling of the LAS proceeded without incident. Since the RTG had remained pressurized with 25 psia argon and the LAS had not been interconnected to the GMS during the purity level anomaly, the ETG had not been affected and Argon backfilling/purification was completed. ETG disassembly began with the forward dome removal. The EHS and spoolpiece were then removed from the converter to complete the ETG disassembly operations. Visual examination of the converter cavity revealed no discrepancies. The installation of the aft graphite end cap assembly was completed.

10.1.10 F-12 ETG - MHW-MJS FLIGHT UNIT (1)

The F-12 ETG was received from RCA on 10 December 1976, and placed in storage in Bldg. B. On 7 February 1977, the CSC was opened and the F-12 ETG set up in a clean area in Bldg. B

for ETG Acceptance Testing and installation of the peripheral converter components. Visual inspection revealed several scratches on the converter shell in the vicinity of the RTG gas management valve (GMV) and missing silver plating on the GMV fitting saver threads. These anomalies were photographed and documented on NR-48406. The RTD cable and the 3500G3 adaptor cable to the RTD instrumentation cable were installed. RTD circuit measurements yielded acceptable resistance values, and isolation measurements between the individual RTD circuits and converter case yielded greater than 200 megohms. Measurements of thermopile circuit resistance and isolation from case and foil system were performed and showed a favorable comparison to the RCA pre-ship measurements. Since the JPL power-out cable was not available, a 2428 GSE power-out cable was installed. A cold pressure decay test yielded a leak rate of 0.00 psi/6 hours. The pneumatic flex hose was mated to the RTG-GMV and the interconnection leak tested. NR-48474 was prepared to document various converter shell surface defects such as crazing of coating, scratches, scuff marks and chips in coating. The ETG was then re-installed in its CSC and stored in Bldg. B.

On 14 February 1977, F-12 ETG was transferred from Bldg. B to Bldg. 800 and installed in LAS #1. Electrical/pneumatic interconnections were completed, the chamber secured and pumpdown was initiated. Argon backfilling and purification was completed and bake-out container operations were performed.

ETG disassembly began with forward dome removal. Two problems occurred at this time:

1. The internal wrenching surfaces of the two Allen head screws securing the gas processing tube bracket rounded and these two screws had to be removed using additional tooling.
2. Difficulty in removing the gas processing tube at the spoolpiece penetration was experienced. This problem was resolved by allowing the gas tube to remain attached to the spoolpiece until it was removed from the LAS. The EHS was hoisted from the converter. Visual examination of the converter cavity revealed no discrepancies. The IHS aft end support was installed in the converter on 16 February.

After installation of the aft heat source support, the converter and prime hardware were secured for the weekend. The IHS forward end support was secured in the bakeout container which remained in the LAS. The forward end enclosure assembly was temporarily stored

within the converter. The converter was domed and pressurized to 25 psia. A cold 6-hour pressure decay test was performed. Leak rate was 0.11 psi/6-hours. The GMS was isolated from the chamber and the LAS secured and pressurized slightly to complete weekend shutdown operations.

With the resumption of operations in Bldg. 800 on 22 February 1977, the converter pressure was measured and the LAS prepared for evacuation. Following evacuation to the low 10^{-5} torr range, the chamber was backfilled with argon. Satisfactory purity levels were attained. The converter dome was removed and the forward end enclosure assembly which had been stored within the converter during the weekend shutdown was removed and stored. The IHS forward end support which had been stored in the bakeout container was removed and stored. The converter was temporarily domed using varglas spacers to assure converter evacuation during the IHS processing cycle.

10.2 RTG ACCEPTANCE TESTING

10.2.1 Q-2 RTG – MHW-MJS QUALIFICATION UNIT

On 15 January 1976, the SPC containing the Q-2 IHS in its EPC was installed in the LAS #1 load lock. The SPC dome was removed and an EPC gas sample obtained in an evacuated bottle. EPC lid removal was then completed. When the EPC lid was removed, it was observed that the forward aeroshell end cap was apparently cracked. Following additional visual inspection, the SPC was lowered into the load lock and the load lock cover was secured to provide a safe hold configuration while awaiting further MRB direction.

The load lock cover and EPC lid were removed and inspection operations revolving around the fractured IHS aeroshell end cap continued. As part of the investigation, the graphite pad from the underside of the EPC lid was dimensionally inspected. There was no evidence of an interference which would have damaged the aeroshell end cap. Direction was received to proceed with installation of the IHS into the SPC, for return to ML/MRC.

During operations to secure the IHS in the EPC/SPC, several problems occurred which resulted in inadequate sealing of the EPC. With the EPC not properly sealed, the SPC finally was satisfactorily sealed and an acceptable SPC leak rate of 0.06 psi for 6 hours was indicated.

The load lock was opened and the SPC was removed and installed in the IHS-SC. Installation operations were completed and the IHS-SC containing the Q-2 IHS placed into storage in Bldg. 800 while awaiting shipment to ML/MRC.

On 27 January 1976, the forward end enclosure assembly was stowed inside the Q-2 converter, the forward dome was installed, and the converter pressurized with argon. A pressure decay test yielded an acceptable 0.38 psi/6-hour leak rate (this was with a previously used P5 "C"-seal).

The converter was removed from LAS #1. While the unit was on the slide tray, the RTD cable was removed for rework and the flex hose was also removed for use on the E-5 ETG. Installation of the Q-2 converter into its CSC was completed and the unit was placed in storage in Bldg. 800.

Later, the CSC was opened and the power output cable and mounting bracket were removed from the Q-2 converter for installation on F-6. Q-2 was re-installed in its CSC and placed into storage.

On 9 March 1976, the Q-2 converter was removed from its CSC and set up in the Bldg. 800 test area. The power-out and RTD cables and the pneumatic flex hose were installed on the converter. Installation of the PRD bracket was completed and the converter was installed into LAS #1. Test readiness review for the RTG assembly operation was completed and the chamber was secured.

Chamber evacuation was initiated, and after achieving a vacuum below 1×10^{-5} torr, argon backfilling was completed and acceptable purity levels attained. After completion of the bakeout can operations, the forward dome was removed from the converter case. A layer of

astroquartz insulation material was placed on the innermost layer of the aft moly foil/ astroquartz end cap, to satisfy the disposition of NR-43638. At that time the inner layer of astro-quartz insulation had been torn during the removal of the aft graphite end support from the converter.

Following the Q-2 IHS re-work, the heat source now designated Q-2R/IHS, was received from from ML/MRC. Preparations were completed for the IHS operations and the IHS-SC containing the Q-2R heat source was removed from storage on 10 March 1976. The SPC was installed in the LAS #1 load lock, and the SPC dome was removed. After relieving EPC preload, the tripod assembly was removed and an EPC gas sample was obtained in an evacuated bottle. The EPC lid was removed and a visual examination showed no evidence of superficial damage to the upper area of the IHS. The heat source was hoisted from the EPC and lowered into the converter onto the aft graphite end support. Another visual examination at that time showed a mark in the surface of the forward aeroshell end cap. This was found to be a superficial scratch and was removed by rubbing the area with the fiberglass wipe sample material. The forward end enclosure assembly was installed and preliminary preload was established. With thermal stability achieved, a final preload of 28 mils dial indicator deflection was set. The lockwiring or the preload screw/bushing and the packing of the preload screw with microquartz was completed.

Chamber evacuation was initiated for the start of the RTG degassing processing. The vacuum degassing operation then ran for ~48 hours. After the argon backfilling and scrubbing operations were completed, forward dome installation began. Dome screw torquing sequences were repeated without achieving an acceptable gap at the dome/spoolpiece interface. An unsuccessful leak test was followed by replacement of the P-5 "C" seal and installation of a new set of screws. After additional leak tests failed, additional screws were replaced and finally helium was introduced into the Q-2 converter and preparations were made for performing leak detection using a helium mass spectrometer. A trace indication of helium was found at the "MS" fitting on the spoolpiece port. This fitting had been installed previously at 600 inch-pounds torque. A re-torquing to that level showed some movement of the fitting and another six-hour pressure decay test indicated an acceptable 0.05 psi/6-hour leak rate. The bulk of the helium gas was removed from the RTG by an iterative purging. After

bleeding-off pressure to 16 psia, the converter was backfilled with argon to 25 psia with a total of 10 purging cycles.

After removal of Q-2 from the LAS, installation in the RTG-SC was completed, the unit was transferred to Bldg. 400, and the RTG was secured in the MHW dynamic test cell.

See the Januuary-February and March-April Bi-monthly reports for additional Q-2 RTG test information. See Section 11.1 for the Q-2 RTG qualification testing.

10.2.2 F-6 RTG MHW-MJS FLIGHT UNIT

It was originally planned that the test cycle on the Q-2 RTG would be completed, before proceeding with testing of the flight units. The end cap failure in Q-2 IHS and schedule constraints, required that work be started on F-6 RTG as quickly as possible.

The F-6 IHS was received from ML/MRC and placed into storage in Bldg. 800. Preparations were made for the IHS operations and the IHS-SC containing the IHS was removed from storage on 26 February 1976. The SPC was installed in LAS #1 load lock and the SPC dome removed. After EPC pressure was measured as 16.5 psia and an EPC gas sample obtained, the tripod preloading was relieved and the EPC cover removed. Extensive visual examination of the top of the IHS was performed, along with visual comparison to photos taken of the IHS at Mound Lab. There was no evidence of physical damage to the aeroshell forward end cap or other areas on the upper end of the IHS.

The heat source was hoisted out of the SPC and dimensional inspection of the length of the IHS and visual examination of its exterior showed no abnormalities. The IHS was lowered into the F-6 converter and seated onto the aft graphite end support. Preliminary preload was established and the RTG was allowed to stabilize thermally. Later the heat source assembly preload was relieved to allow a slight re-positioning of the forward molyfoil end cap. The lockwiring in one of the ceramic plugs in the end cap was bearing against the end enclosure and the realignment corrected this. Preliminary preload was again set and after thermal stabilization, a final preload of 28.5 mils deflection was established.

The preload screw was packed with micro-quartz insulation and chamber evacuation for the start of a vacuum degassing process on the RTG was initiated. However, chamber evacuation was aborted twice; first, to replace a defective chamber ion gauge, and a second time to repair malfunctioning inlet and outlet valves which connect the facility GMS to the chamber. The forward dome was installed on the RTG and the unit was pressurized with argon to 25 psia. The valves were dismantled, cleaned and re-installed at their LAS penetrations. Chamber evacuation was initiated and after attaining 1×10^{-5} torr, argon backfilling and scrubbing operations were completed.

The RTG forward dome was removed to allow continuance of the degassing process. Chamber pumpdown was started and the mid 10^{-6} torr range was attained, indicating that chamber leakage had been corrected. The vacuum degassing on the F-6 RTG ran for ~60 hours. The chamber was then backfilled with argon. Output power averaged 159.4 watts over the period of vacuum operation.

The prime forward dome was passed into the chamber thru the load lock and installation began shortly thereafter. Dome screw torquing sequences continued until the required less-than-two mil gap at the dome/case interface was attained. The RTG was pressurized with argon to 25 psia and a subsequent six-hour pressure decay test yielded an acceptable leak rate of 0.03 psi/6-hours.

LAS #1 was opened and a visual inspection of the RTG showed that the potting material on the JPL power output cable connection to the RTG was separated. NR-43735 was written to document this condition.

The RTG was removed on the slide tray cart and the operations of installing the RTG into its RTG-SC began. Upon attempting installation of the handling sling's quick-set adaptors to the RTG forward mounting pads, an interference with the RTD cable was found. This was corrected by re-routing the RTD cable in that area.

For this handling sling use, the stacking brackets which were part of the original design sling were mounted to the RTG forward pads. Installation of the RTG into its SC was completed and the unit was transferred to Bldg. 400.

The RTG removal from the SC in Bldg. 400 was performed and weight and C.G. measurements were completed. The unit was set up on the vibration slip table in preparation for the pre-vibration air performance/pressure decay test. Test readiness review was completed and the RTG load was switched from short-circuit to the loaded mode. Thermal stability at the 30 volt load point was achieved for the start of the 48-hour test. Output power averaged 78.8 watts over the test period and rate of pressure decay was 0.0 psi/48-hours. After completion of the performance test, an RTG gas sample for mass spectrographic analysis was obtained in an evacuated bottle.

Preparations were made to start vibration testing, and the X-axis vibration cycle was performed, with no observed degradation to the hardware.

The RTG was rotated to the Z-axis orientation on the vibration slip table. When the unit had thermally stabilized, the Z-axis vibration cycle was performed. The RTG was hoisted off the slip table and set up on the exciter head for a Y-axis vibration exposure.

There was no evidence of structural degradation during any of the vibration testing. However, there was an electrical anomaly which repeatedly exhibited itself. This was an increase in circuit resistance by approximately 40 milliohms after a vibration application due to poor contact loosening of the JPL power output cable connector plug, from the RTG power-out receptacle by a few degrees rotation. With the tightening of this plug to the converter receptacle, there was always a subsequent decrease in circuit resistance by the approximate 40 milliohms to the pre-vibe level. There was no apparent explanation for the circuit resistance increase since there was still a full pin to socket contact mate even with the slight loosening of the connector plug.

A 6-hour post-vibration air performance/pressure decay test was performed. This test yielded a leak rate of 0.09 psi/6-hours and output power averaged 79.0 watts over this period. The load was switched to the short-circuit mode and after achieving a stable thermal condition, the CG measurement was obtained. This was a repeat of the earlier CG measurement, using a more refined method. This new method yielded a more accurate indication of the CG offsets. Prior to installing the RTG in its RTG-SC, the JPL power output cable, which had been giving anomalous indication of increased circuit resistance during the vibration cycle, was replaced. The unit was then placed in temporary storage in Bldg. 400.

Transfer of the RTG to Bldg. 300 was made and the RTG was installed on the chamber #4 support fixture. Test readiness was completed, the chamber door was secured, and evacuation was initiated. After the chamber reached a vacuum of 1×10^{-5} torr, F-6 was evacuated externally through the GSC to below 300 microns and was vented directly into the chamber. After the unit had thermally stabilized a four hour thermal-vacuum performance test yielded an average output power of 158.7 watts.

The only anomalous indication seen during the thermal-vacuum test, was a higher than normal converter internal pressure. This pressure, which is measured by a thermocouple gauge in the tubing leading to the converter and venting valve, usually indicates ~5 microns. At the F-6 test, converter internal pressure indicated 35-40 microns. This was proven to be erroneous. The thermocouple gauge and controller used for the measurement were re-calibrated after the test and it was found that filament current was off by a factor of ten for the gauge being used. The 35-40 micron indication for converter internal pressure was actually 3.5 to 4 microns.

RTG backfilling with argon to 25 psia and chamber backfilling with nitrogen to one atmosphere was completed. The chamber door was opened and rolled out to allow the RTG to stabilize in ambient air. It was observed that the RTG load current, as monitored on the DVM, was fluctuating between 2.1 to 2.6 volts (which is equivalent to the same value in amps). When monitored on the Data Logger, there was a stable 2.7 volts observed. The RTG load was switched over to the alternate load panel in the ROC. The load current data appeared to be consistent between the DVM and Data Logger after the load panel changeover.

While awaiting thermal stability, a step change in load voltage evidenced itself during the course of a routine data scan. This was a drop from the previously set load of 29.7 volts to a value of 29.6 volts, without being attributable to a resetting of the load adjust pot in the readout console. Upon checking the connection at the JPL power out cable, it was found that the plug connection to the converter power out receptacle was loose. The cable connector plug was re-tightened to the converter receptacle and the load adjust was then reset to 29.7 volts. This was a different circumstance than that seen during the vibration test cycle. At that time, with the initial JPL power out cable on F-6, the load current would decrease subsequent to a vibration application and then increase to the pre-vibe current level after the JPL connector plug was tightened. A special test was performed to ascertain if the JPL connector plug tightness/looseness would affect load current. There were no apparent anomalies associated with loosening the plug one full turn and pushing or pulling in the direction of pin/socket alignment. Electrical load was then removed from the RTG and the JPL connector plug was demated from the converter receptacle. The sockets in the plug and pins in the receptacle were visually examined; there was no indication that they were not interfacing properly when the plug/receptacle were mated. Load was re-established after the cable connector was mated to the converter and the RTG was allowed to stabilize for the post-thermal/vacuum air performance and pressure decay testing.

During the 48-hour performance test, output power averaged 79.4 watts and rate of pressure decay was 0.26 psi/48-hours. During this test, also there were several 50 to 100 millivolt step changes in load voltage, both increasing and decreasing from the 29.7 volt setting. These fluctuations were the same as those previously mentioned. The load panels in the readout console are designed for stable regulation at the 55 volt open-circuit voltage condition of vacuum mode testing. In air mode testing, with the generator open-circuit voltage running at 41-42 volts, voltage adjustments may be necessary to maintain a constant load during test.

The RTG load was switched to the short-circuit mode and the RTG was removed from the chamber support frame. Installation in the RTG-SC was completed and the unit transferred to the storage area in Bldg. 800 to await shipment to ML/MRC.

Periodic PTU checks of the F-6 RTG in its shipping container in storage at ML/MRC had indicated voltage fluctuations when short-circuited by the PTU. On 1 March 1977, GE personnel at ML/MRC performed tests to isolate and/or locate the cause of the voltage fluctuations. The RTG was removed from its SC and successive manipulations of the two shorting modules/cable train connections up to the RTG caused significant voltage changes primarily at the 3500G2 cable/JPL power output cable interface.

The cable train and shorting modules were replaced with the F-13 RTG LES 8/9 power cable and shorting modules. When the connections of the replacement cable train were manipulated, a maximum voltage fluctuation of only 0.001 volt was observed. The RTG was installed in its RTG-SC and returned to storage at ML/MRC. The cables and shorting modules removed from the F-6 were returned to GE, Bldg. B, for evaluation. Failure Analysis Report 1151-MHW-14 dated 22 March 1977 attributed the voltage fluctuation to a defective weld at pin D in the Gulton connector at the RTG end of the 3500G2 GSE power cable. See January-February '76 and March-April '76 Bi-monthly reports for additional test details of the F-6 RTG.

10.2.3 F-7 RTG – MHW-MJS FLIGHT UNIT

The F-7 IHS was received from ML/MRC and was placed in storage in Bldg. 800. On 8 April 1977, the IHS-SC was transferred to the Bldg. 800 test area. The SPC was removed from the SC; and was installed in the LAS #1 load lock. The SPC dome was removed and tripod preloading relieved from the EPC. After measuring EPC internal pressure as 15.7 psia, an IHS gas sample for spectrographic analysis was collected in an evacuated bottle. A visual examination of the upper area of the IHS was performed after the EPC cover was removed. No evidence of damage was found. The heat source was hoisted out of the EPC and routed to the converter station via the LAS gantry. Installation in the F-7 converter was completed.

The forward end enclosure assembly was installed on the IHS and engaged to the case brackets. Preliminary preloading was set and RTG load was switched from short-circuit to loaded mode. After thermal stabilization, a final preload of 28 mils deflection was established. Preload screw/bushing lock-wiring and screw packing with insulation was completed to allow the start of the vacuum degassing operation.

Evacuation was initiated and the LAS #1 chamber attained the 10^{-6} torr range. The RTG load was switched out of short-circuit after start of pumpdown. The vacuum degassing operation on F-7 requires 76.4 hours of vacuum time on the unit. Over the last four hours of vacuum operation, RTG power out averaged 159.09 watts. This power was not corrected for cable loss between the shorting module and converter receptacle.

Chamber backfilling with argon and "scrubbing" yielded acceptable purity levels. Dome installation began and screw torquing sequences were completed. The gap at the dome/case interface ranged up to 6 mils. The RTG was pressurized with argon to 25 psia and the subsequent pressure decay test, gave a leak rate of 0.0 psi/6-hours.

LAS #1 was opened and the F-7 RTG was removed. Installation of the unit in its SC was made and F-7 was then placed in storage in Bldg. 800, to await the completion of dynamic testing on the Q-2 RTG.

On 27 April 1976, F-7 was transferred to the Bldg. 400 dynamic test cell and the RTG was removed from the RTG-SC. Weight and C.G. measurements were completed and F-7 was mounted on the vibration slip table in the inverted (forward end down) attitude. The unit's pneumatic flex hose going to the gas management valve was replaced with a new hose, since the outer covering on the original hose had been abraded, during the assembly operations in the loading station.

It was also observed that there were small chips out of the edges of through holes in two of the forward mounting pads. NR-43816 documented this condition and its disposition was that the sharp edges of the damaged area were to be burnished smooth, prior to the start of vibration testing.

RTG load was switched out of the short-circuit condition to the loaded mode and thermal stability for the start of the pre-vibration, 48-hour air performance/pressure decay test was achieved. Output power was 80.95 watts at the converter power out receptacle. This was derived from a measured 80.34 watts, plus 0.61 watts added to correct for cable losses. Rate of pressure decay showed an increase of 0.11 psi/48-hours due to average case temperature increasing from 182°C to 186°C as indicated by the fin RTDs.

An RTG gas sample for mass spectrographic analysis was obtained. As previously reported, there had been chipped areas found at two of the forward mounting pads at their through holes. These areas, along with an additional damaged hole area found at the third mounting pad, were burnished to remove their sharp edges.

Another special operation performed at this time, was a measure of pin retention force at the sockets of the JPL power out cable, which mates to the converter power out pins. This was done to obtain a comparison to the pin retention forces which had been found at the Q-2 cable connector tests.

The JPL power out cable was demated from the RTG power out receptacle and a force gage was used to perform a pin retention test at the four sockets of the JPL cable connector. Forces required to start a pin moving out of socket ranged from 0.33 to 0.75 pounds for the four sockets. This was deemed acceptable and the JPL cable was again mated to the converter receptacle.

A similar test was performed on the 3500G3 RTD adapter cable. After demating the cable at the converter interface bracket, acceptable pin retention forces ranging from 0.40 to 0.70 pounds were indicated. The RTD adapter cable was again mated to the RTD receptacle at the converter interface bracket and preparations were made for vibration testing on the RTG.

The X-axis, inverted attitude, OA (operation acceptance) vibration cycle began with the 1/2 G sine sweep. There were no anomalies at that run. After the 1/2 acceptance level sinusoidal vibration was applied, the post-run performance data scan showed a decrease in output power of almost 3 watts and an increase in circuit resistance of 0.21 ohms. In addition, the shunt resistance between circuit and case fell from 2.7 megohms to 500K-ohms, apparently due to a loss of isolation between the case and foil system. There was strong suspicion that the 3 watt power loss was due to increased contact resistance at the JPL power out cable connector sockets, as had been exhibited during the F-6 and Q-2 dynamic tests. NR-43881 was written and direction was received to not disturb the cable connector until JPL representatives could witness the results.

While awaiting the arrival of the JPL personnel, a measurement of the current flow in each of the four RTG power leads (two positive and two return) was performed. The test cable at the ROC was demated and two current shunts were placed into the circuit, each at a pair of positive/negative leads. The current shunts themselves acted as an RTG short-circuit load and the millivolt drops across them were measured to obtain individual parameters for the four lines. After correcting for the current shunt resistance value, the current flows in the four lines were within +2%. Results were inconclusive as to which socket in the JPL cable connector was causing the high circuit resistance.

The JPL representatives arrived at Bldg. 400, the demonstration of the manipulation of their cable connector and associated return of the lost power was given to them. The JPL power out cable and 3500G4 adaptor cable were then replaced with a 2428G1 GSE-type power cable.

The full acceptance level sinusoidal input was applied, with some current fluctuations of up to 0.2 amp seen on the strip chart at 15 Hz during the run. The post-run performance data compared favorably with that of the pre-run scan. X-axis full acceptance level random vibration was completed and the pre-, post-run performance data comparison was favorable.

F-7 was rotated on the slip table to the Z-axis and the vibration cycle in that axis was completed with no anomalous indications, except that after the full level sinusoidal vibration, a separation was found in the potting of the RTD #3 header. NR-43883 was written against this condition. It could not be said for certain if the potting anomaly had occurred at that run or prior to it.

F-7 was transferred from the slip table to the exciter head for Y-axis (longitudinal) vibration testing. The 1/2 G sine sweep and 1/2 acceptance level sinusoidal run were completed with no anomalous indications.

During the full acceptance level sinusoidal run, on the sweep down from 2000 Hz to 5 Hz, there were load voltage and current transients of approximately 1 volt and 0.1 amp, indicated at the 75 Hz point. The post-run data scan showed a decrease in output power of 0.6 watts and decrease in open-circuit voltage of 0.08 volts, although circuit internal resistance was

normal. The major deviation was a drastic change in shunt resistance between circuit and case. The shunt resistance had been 400K-ohms prior to the vibration input, but indicated some very low value after the run. The common-mode voltage between thermopile and case showed a change from a pre-run 23.6 volts to 9.3 volts post-run. The voltage after the 10K-ohm resistor in the ROC was switched in parallel to the thermophile-to-case circuit showed no change, indicating that shunt resistance was something much smaller than 10K-ohms.

Vibration operations were suspended and a trouble-shooting mode was begun to determine the reality of the anomalous condition. As had been done on Q-2, a decade box was interconnected into the ROC measuring circuit, to allow smaller values of parallel resistance than 10K-ohms to be used. With a 650 ohm parallel resistance, a shunt resistance value of 72 ohms was calculated. The actual value of shunt resistance was somewhat lower, probably 50-60 ohms. A smaller than 650 ohm parallel resistor, would have allowed a more accurate calculation of shunt resistance, but the increased current flow would have most probably caused the low shunt resistance to return to its former high value, as had occurred during the trouble-shooting on Q-2. It was desirable at this time to maintain the low value on F-7 for the next stage of trouble-shooting.

To eliminate the ROC and associated power out cable string as contributing to the low shunt resistance, the RTG was open-circuited and that equipment was disconnected from the RTG. As had been done on Q-2, a breadboard resistive load was applied to the RTG and adjusted for a 30 volt load. Shunt resistance measurements were to be performed using the decade box as the parallel resistor between circuit and case. However, it was immediately evident that the shunt resistance had returned to a high value, since the common-mode voltage had changed from the approximate 9 volts to the original 21 volts. Measurement/calculation was completed using the breadboard and shunt resistance indicated 300K-ohms.

This test was performed as a means of isolating the ROC and power out cable string as the reason for anomalous shunt resistance and it would have been advantageous, if the short had still been present with the breadboard load. When the same test had been performed on Q-2, the low shunt resistance value had still been in evidence with the breadboard load. The F-7

RTG was again interconnected with the ROC and shunt resistance measurements using the ROC yielded the same 300K-ohms as the breadboard test. Verifying that case-to-circuit isolation had returned.

Load was switched into the short-circuit mode and test operations were suspended with the RTG on the shaker head. Later, direction was received to install F-7 in its RTG-SC and this operation was completed. The unit then remained in storage in Bldg. 400, for approximately three weeks.

On 1 June 1976, direction was received to continue the vibration test cycle on the unit. F-7 was removed from its RTG-SC and set up on the exciter head to complete the longitudinal axis vibration testing. All preparations for vibration testing were completed to allow the acceptance level random run in the Y-axis to be completed. For this run, the overall level was reduced from the previous MJS level of 6.6 G rms to an overall acceptance level of 5.9 G rms. No degradation was seen in the electrical performance parameters when comparing the pre- and post-run data scans. In addition, the shunt resistance voltage was monitored during the run on a strip chart recorder and no shorted conditions were observed. A short, post-vibration, air performance/pressure decay test was completed and yielded an average output power of 79.2 watts (corrected for cable loss) and leak rate of 0.01 psi/6-hours.

Installation of F-7 in its RTG-SC was completed and the unit remained in storage in Bldg. 400. After its transfer to the Bldg. 300 Long Life Lab, the RTG was set up on the chamber #4 support frame. Test readiness was completed, the chamber door was secured and evacuation was initiated. After the RTG had been evacuated externally to below 200 microns, it was vented directly to the chamber. Chamber pressure increased from the low 10^{-6} to the low 10^{-5} torr range at the time of RTG venting. Later, the system stabilized with chamber pressure in the low 10^{-6} torr vacuum performance test yielded an average RTG power out of 158.5 watts (corrected for cable power loss); shunt resistance in vacuum ran at 4.9K-ohms.

Prior to the termination of vacuum performance testing, a short test was run to determine the effects on RTG electrical performance from an increased converter internal pressure. The venting valve was closed to isolate the F-7 internal cavity from the chamber and performance parameters were monitored. RTG internal pressure increased from 6 microns (with RTG vented) to 103 microns after the vent valve was closed for a 30 minute period. Pressure had not stabilized at the end of that time, but was still increasing at a rate of 1 micron/minute. The RTG electrical performance parameters (load voltage, current and open-circuit voltage) remained essentially constant over the 30 minute period that the vent valve was closed. It is possible that there would have been an effect on electrical performance if RTG venting had been suspended for a longer duration.

The F-7 RTG was backfilled with argon to terminate the vacuum performance test. Chamber backfilling with dry nitrogen was completed and, after receiving Health Physic's approval, the chamber was opened. The RTG was then allowed to stabilize in ambient air for the post-T/V air performance/pressure decay test. Thermal stability was achieved, and the 48-hour test began. Power output averaged a corrected 80.0 watts over the time period and leak rate was 0.06 psi/48-hours.

Prior to removing F-7 from the chamber door support frame, the 2428G1 GSE-type power cable, which had been installed onto the unit was replaced with a new JPL power out cable and a 3500G4 adapter cable.

The RTG was removed from the chamber fixture and installed in its RTG-SC. F-7 was then transferred to Bldg. 800 where it was placed in secure storage, for shipment to ML/MRC.

10.2.4 F-8 RTG – MHW-MJS FLIGHT UNIT

After completion of the F-8 ETG disassembly, but prior to the F-8 RTG assembly, it was found that the loading station IHS lifting fixture was not operating properly. To allow for fixture repair, the forward and aft end supports were placed back in the bakeout can and the F-8 converter was domed and pressurized with argon. The LAS chamber was opened and the repair, which was a rework of the power leads to the drive mechanism, was performed. The

chamber was again secured and the evacuation/backfill/purification cycle was completed. Bakeout can operations were repeated and, after removal of the forward dome, the aft end support assembly was installed in the converter.

The F-8 heat source had been received from ML/MRC and placed in storage in Bldg. 800. On 21 June 1976, the IHS-SC was transferred to the test area and the SPC was removed from the IHS-SC and installed in the LAS #1 load lock. SPC dome removal and tripod preload relief from the EPC was accomplished. After measuring EPC internal pressure at 19.3 psia, an IHS gas sample for mass spectrographic analysis was obtained. The EPC cover was removed and a visual inspection of the upper end of the IHS indicated a possible defect on the forward aeroshell end cap. As it was uncertain whether this was a fracture or a superficial scratch, a considerable effort was expended in determining its exact nature. After determining that the defect was superficial, the mark was burnished out using varglass sleeving as the polishing material to prove that the marks were slight scratches.

The lifting fixture was used to hoist the heat source from the EPC. After visual examination showed no discrepancies, the IHS was routed to the converter station and was installed in F-8. After installation of the forward graphite heat source support on the IHS, the forward end enclosure assembly was positioned and engaged with the case brackets. Thermal equilibrium was achieved and a final preload of 29.5 mils deflection was established. The operations of lockwiring the preload screw/bushing assembly and packing the screw with micro-quartz were completed,to close out the first stage of RTG assembly.

Prior to the above installation of the forward end enclosure assembly, it was found that the edges of the assembly's moly-foil end cap were folded over at several of the foil layers and generally wavy in appearance. Since this condition was at the interface of the thermopile foil basket, there was some concern that there would be a loss of thermal efficiency. The condition most probably had occurred when the forward end enclosure assembly was stowed within the converter, prior to the converter doming to allow the LAS opening for repair of the lifting fixture wiring. NR-43884 was written against the discrepancy and initial MRB disposition was to straighten the edges of the end cap foils prior to installing the end enclosure onto the heat source and that was accomplished. The final disposition regarding this condition was based upon the performance of the RTG during its vacuum degassing operation in the LAS.

Preparations were made for the start of vacuum degassing operation, chamber evacuation was initiated and the RTG was switched out of the short-circuit condition to the loaded mode. The 10^{-6} torr range was attained and the vacuum degassing process on F-8 ran 48 hours, after satisfactory mass spectrometer (monopole) readings were obtained.

RTG output power for the last four hours of vacuum operation averaged 159.6 watts, corrected for cable losses up to the converter receptacle. This power level indicated that there had been no detrimental effect on thermopile efficiency due to the waviness of the forward moly-foil end cap mating edges and NR-43884 was closed out.

After the start of the vacuum operation, the RTD #3 instrumentation circuit indicated a loss of output voltage. This condition remained through the period of vacuum performance. Upon backfilling the chamber with argon, the RTD #3 voltage indication returned to normal. Investigation regarding this anomaly was subsequently performed, prior to the vibration testing in Bldg. 400.

Forward dome installation was begun and screw torquing sequences were completed. The less-then-two-mil gap requirement was met except for two small perimeter sections where it ranged 1/2 mil above specification. After pressurization with argon gas, a pressure decay test yielded an acceptable 0.02 psi/6-hour leak rate. LAS #1 was opened and the F-8 RTG was removed on the slide tray cart. Installation into the RTG-SC was completed and F-8 was transferred to Bldg. 400.

After removal of the RTG from the shipping container in Bldg. 400, a pin retention test was performed on the 3500G3 adaptor cable at the sockets which interface with the RTD instrumentation cable. This was to satisfy an MRB instruction regarding NR-43886, for the RTD No. 3 anomaly. Acceptable pin retention forces were measured at this interface. Subsequent MRB disposition regarding this RTD cable was to replace it. This cable exchange was completed.

Weight and C.G. measurements were performed and after the RTD cable exchange, F-8 was mounted on the vibration slip table in the inverted position (mono-balls up) in preparation for the pre-vibration air performance/pressure decay test. The RTG load was switched from the short-circuit mode to the loaded condition and thermal stability for the start of test was achieved. Output power to the end of test averaged 80.2 watts, corrected for cable loss, and rate of pressure decay was 0.0 psi/48-hours.

An RTG gas sample was obtained for mass spectrographic analysis. Preparations were completed for start of the vibration test cycle. Because of a recent change in the test specification requirements, there was no sinusoidal acceptance vibration on this unit as there had been on the previous MJS RTGs. Also, the overall level for random acceptance vibration was changed from 6.1 G rms to the overall level of 9.54 G rms, which had been used for the LES 8/9 RTG.

The X-axis vibration testing began with the 1/2 G sine survey and ended with the 9.54 G rms acceptance random vibration. A comparison of the pre-vibration and post-vibration performance data showed no degradation due to the environment.

The only anomaly exhibited during the X-axis testing was the appearance of load voltage and current transients on the strip chart record taken during the random equalization and random acceptance runs. These transients had previously been observed during MJS RTG vibration testing and there has been an on-going investigation into their cause. Of specific interest to the F-8 vibration testing was that the RTG load current, one of the parameters which was monitored in real time on the strip chart recorder, was also FM magnetic tape recorded in parallel. A playback of the mag tape record did not indicate the presence of the transient excursions that were exhibited on the strip chart record. This important piece of information suggested that the transients may have been due to some ground loop problem within the strip chart recorder.

Investigation following the F-8 vibration testing revealed that the strip chart recorder amplifiers had all been improperly tied together at their shielded input returns, thereby having no common mode rejection capability. This problem was corrected on vibration tests of

subsequent units. The RTG was rotated on the slip table to the Z-axis and the vibration test cycle in that axis was completed. There were no load voltage or current transients exhibited on the strip chart record and the pre- and post-run data scans showed favorable performance comparisons.

F-8 was transferred to the exciter head for Y-axis (longitudinal) vibration testing. The 1/2 G sine survey began the Y-axis test cycle and random acceptance run completed it. As with the Z-axis vibration, no transients were observed on the chart records made during the Y-axis runs. Electrical performance showed no degradation after a comparison of the pre- and post-vibration data scans.

A short post-vibration air performance/pressure decay test was performed and yielded an average output power of 80.3 watts (corrected for cable loss) and leak rate of 0.03 psi/ 6-hours. F-8 was removed from the shaker head and installation into the shipping container was completed.

Transfer of the F-8 RTG to the Bldg. 300 Long Life Lab was completed. The unit was removed from its shipping container and was installed on the chamber #4 support fixture. Test readiness was completed and the chamber door was secured. Chamber evacuation was initiated and after attaining a chamber vacuum in the 10^{-6} torr range, RTG evacuation began. After the RTG internal pressure was reduced to below 300 microns, using the gas service cart, the RTG was vented directly into the chamber. The venting solenoid remained open with RTG internal pressure indicating 16 microns and chamber pressure in the low 10^{-5} torr range at that time. RTG pressure/thermal conditions continued to stabilize and were acceptable for the start of the four hour vacuum performance test. With chamber pressure in the low 10^{-6} torr range and RTG internal pressure at 5 microns, output power over the four hour period averaged 158.1 watts, corrected for cable losses up to the converter receptacle, and shunt resistance between circuit and case ran at 6.4 K-ohms.

A short test was run on the F-8 RTG at the end of its thermal-vacuum testing, to measure the residual gas load pressure within the F-8 RTG. The venting solenoid valve was closed for a thirty minute period to isolate the RTG internal cavity from the chamber vacuum. RTG

internal pressure increased from 5 microns to 95 microns over the 30 minute test period, with pressure still increasing at a rate of 1 micron/minute at the end of that time. This correlated closely with F-7's pressure build-up which was 103 microns after 30 minutes. There was no change in the F-8 RTG electrical parameters with the vent valve closed for that time.

Argon backfilling of the RTG to terminate the vacuum testing was completed. Chamber backfilling with dry nitrogen was completed and after Health Physics approval, chamber #4 was opened. The RTG was allowed to stabilize in ambient air for the post-thermal/vacuum test. Thermal stability was achieved and the 48-hour test began. Output power averaged a corrected 79.9 watts over the time period and rate of pressure decay was 0.0 psi/48-hours.

RTG load was switched to the short-circuit mode and F-8 was removed from the chamber fixture. Installation in the RTG-SC was completed and the F-8 RTG was transferred to the Bldg. 800 secure storage area, for shipment to ML/MRC.

10.2.5 F-9 RTG – MHW-MJS FLIGHT UNIT

The F-9 heat source was received from ML/MRC and placed in storage in Building 800. On 26 July 1976, the IHS-SC was transferred to the test area and the SPC was removed from the SC. The SPC was installed in the LAS #1 load lock and SPC dome removal and tripod preload relief from the EPC were completed. After measuring EPC internal pressure as 16.4 psia, an IHS gas sample for mass spectrographic analysis was obtained. Removal of the EPC cover was completed and, after no obvious abnormalities were found, the heat source was hoisted out of the EPC and routed to the converter station. Installation of the IHS into the F-9 converter was completed, followed by the installation of the forward graphite end support and forward end enclosure assembly. After attaining thermal equilibrium, a preload of 28 mils of end enclosure deflection was established. Lockwiring of the preload screw/bushing and packing of the preload screw with microquartz insulation closed out the first stage of RTG assembly operations.

Chamber evacuation for the start of the vacuum degassing process was initiated and the 10^{-6} torr range was attained. The vacuum processing on the F-9 RTG was completed 48 hours later and the chamber was backfilled with argon. Generated output power for the last four hours of the vacuum operation averaged 160.7 watts. This power is corrected for cable losses up to the converter receptacle.

The forward dome installation began and dome screw torquing operations continued until an acceptable less-than-two-mil gap at the dome/case interface was indicated around the entire perimeter. The F-9 was pressurized to 25 psia with argon and a pressure decay test was initiated. This test yielded a leak rate of 0.01 psi/6-hours.

During the dome installation in the previous week, there had been an intermittent electrical shorting between ground and the GSE power cable within the chamber. The anomaly was positively identified as being in the test cabling and not within the RTG since it was dependent upon cable movement with a corresponding change in performance data. When the LAS #1 door was opened, examination disclosed that the unused voltage tap leads on the 2428G1 GSE cable were the cause of the fault. The terminal insulation wrap was frayed on these leads and and it was evident that they had been intermittently shorting to the LAS fixturing, showing that shorting was not within the RTG.

The unit was removed from LAS #1 on the slide tray cart and placed in temporary storage. F-9 RTG was transferred from the storage area to the test floor where it was installed in the test fixture in preparation for the magnetic signature mapping. The initial mapping operations were performed. These runs were made with the RTG open-circuited so as to have zero current flow through the thermopile. After completion of the zero current mapping, the RTG load was set up to obtain approximately 4 amps through the thermopile circuit. The second phase of mapping then was performed. There were no significant difficulties associated with performing the magnetic mappling operations.

The RTG was installed in its RTG-SC and transferred to the Building 800 storage area.

On 30 August 1976, a reappraisal of the F-9 heat source's preship radiographs taken at ML/MRC disclosed that there was an apparent damage to the aft tie-bolt head prior to the IHS transfer to GE and installation into the F-9 converter. See Section 5, Para. 5.2. This led to a programmatic decision to remove the F-9 IHS from the F-9 converter and replace it with the F-10 IHS, which did not show a pre-ship damage to its internal components.

The F-9 RTG was routed out of the Bldg. 800 storage area to the test floor area, removed from the RTG-SC and installed into LAS #1 on the rotary table fixture. Pneumatic and electrical interconnections to the chamber penetrations were completed, the chamber was secured and evacuation began. After the chamber attained the 10^{-6} torr range, backfilling with argon and gas purification was completed to allow the start of RTG disassembly.

Preload was relieved from the heat source and the only discrepancy noted after the removal of the forward end enclosure assembly was damage to the zirconia discs. Two of the three segments were fractured and one had a large chip out of it. Subsequent MRB disposition was to replace the three segments prior to the re-assembly of the RTG with the F-10 IHS.

The F-9 IHS was hoisted out of the converter. Visual examination of the heat source and converter cavity revealed no abnormalities. The heat source was then routed to the load lock station and lowered into the EPC/SPC. Although one of the cover bolts was sheared off in the EPC during the cover installation, there was no evidence that the leak-tight integrity of the EPC had been compormised. The EPC pressure decay test was completed, with an acceptable leak rate of 0.0 psi/6-hours being indicated. After EPC/SPC preload was established, it was observed that there was a discrepant dimensional relationship between the tripod and its preloading nut. This led to a relieving of preload and disassembly of the tripod which revealed that the graphite bearing disc was not in place beneath the preload nut. The disc was then installed and EPC/SPC preload was properly set.

After the SPC dome was installed, an unsuccessful attempt was made at evacuating and pressurizing the SPC. It became evident that the leakage was not external, with the EPC apparently allowing an in-leakage to the SPC. The dome was removed to allow access to the EPC and it was verified that the EPC leakage integrity had degraded since the time it had

passed its pressure decay test the previous day. The tripod preloading of the EPC was again relieved and the EPC cover was removed. The spare EPC cover with new gasket was then installed and the subsequent EPC pressure decay test yielded an acceptable 0.09 psi/6-hour leak rate. The original EPC cover was subsequently passed out of the chamber and visual examination revealed a small scoremark across the sealing knife-edge. There was no rationale as to why the first EPC pressure decay test did not yield an unacceptable leak rate other than that the increased thermal condition with the SPC dome installed had changed the sealing characteristic.

The tripod assembly was re-positioned onto the refurbished EPC. An unsuccessful attempt was then made at applying preload. Prior to full preload being established, there was a severe binding between the preloading nut and tripod. During the process of backing out the preload nut to remove it from the tripod for cleaning and re-aquadaging, the nut totally seized.

Since the EPC pressure was still holding, at the required level, a method was conceived for removing the seized tripod/nut from the SPC/EPC. A force was applied to the tripod using a screw jack between the top of the loadlock door opening and the tripod and then to rotate the tripod slightly, to disengage its three feet from the SPC lugs and to free the tripod/nut. The loadlock door was opened and the SPC was installed onto the slide tray cart and partially withdrawn from the loadlock to place the SPC beneath the door opening. The jacking mechanism was then introduced and the tripod/nut assembly was freed. The SPC was again installed into the loadlock and an EPC pressure measurement was performed, which indicated that the EPC was still maintaining proper pressure.

The seized tripod/nut was transferred to Bldg. B where, with an estimated 600-800 ft.-lbs. of torque, the preload nut was loosened from the tripod and removed. Visual examination showed an obvious galling of the ringnut and transfer of material between the parts at their mating threads.

With the receipt of a replacement tripod assembly, operations resumed. The SPC was routed out of the chamber loadlock on the slide tray, the tripod was installed and a proper preloading of the EPC/SPC was then established external to the chamber loadlock. After evacuating the

SPC, it was pressurized with helium to 31 psia and a pressure decay test then yielded a leak rate of 0.18 psi/6-hours. After SPC installation into the IHS-SC, that container was evacuated and pressurized with helium to 25 psia. The F-9 heat source was then placed into secure storage in Bldg. 800, for shipment to ML/MRC.

The damaged zirconia bearing discs in the forward heat source support assembly were replaced with a new set.

On 20 September 1976, preparations for the task of installing the F-10 IHS into the F-9 converter were completed and the IHS-SC containing the F-10 heat source was transferred out of storage to the test floor. The SPC was prepared and installed into the LAS #1 loadlock. Tripod preloading of the EPC/SPC was relieved and an attempt was then made to make the pneumatic connection to the EPC to measure EPC pressure and obtain an IHS gas sample. The pneumatic adapter fitting galled the EPC's vent fitting at the attempted connection, but minimal time was lost. The EPC vent fitting threads were re-chased with a die and a new adapter was successfully installed. EPC internal pressure was measured as 17.0 psia and the IHS gas sample was then obtained.

The EPC cover removal was completed and a visual inspection given to the forward end of the heat source. It had been previously reported by ML/MRC that the F-10 IHS had two chips out of the edge of the forward aeroshell end cap. One of the chips had previously been "blended-out" at ML/MRC and the second one had to be closely examined at this time to determine if it too should be reworked. GE engineering examined the damaged areas on the aeroshell end cap and, since there were no sharp edges evident, it was decided to accept as received.

The heat source was hoisted from the EPC and overall visual examination revealed no additional discrepancies. After positioning concentric with the converter, the heat source was successfully installed heat source support and forward end enclosure assembly were installed and the RTG was thermally stabilized to allow heat source preloading. An end enclosure deflection of 28 mils was then established to preload the assembly. Lockwiring of the preload screw/bushing and packing of the preload screw with microquartz then closed out the first stage of the RTG assembly operations.

Preparations were completed for the start of the vacuum operation to outgas residual CO from the F-10 heat source. Chamber evacuation began and the low 10^{-5} torr range was attained. The vacuum degassing process on the F-9 converter/F-10 IHS then ran for 48 hours when the chamber was backfilled with argon. Satisfactory monopole mass spectrometer readings were obtained prior to the termination of the vacuum operation.

Early in the vacuum operation, it was observed that there was an improper seating of the forward moly-foil end cap with the thermopile moly-foil basket. This was evidenced by an illumination from the heat source at a two inch section of their mating edges. A decision was made to continue through the vacuum operation and then attempt seating of the moly-foil sections working through the glove ports after argon backfilling. The RTG power for the last four hours of vacuum mode operation averaged 159.6 watts (corrected for cable losses up to the converter receptacle) as compared to the corrected 160.7 watts which was obtained at the F-9 converter/F-9 IHS vacuum operation in LAS #1 earlier. After normalizing for the differences in the thermal (fuel) inventories between the F-10 and F-9 heat sources, there was an apparent loss of 1.4 watts which was attributed to thermal shunting through the gap at the moly-foil sections. Later, the moly-foil end cap was manually seated to the foil basket. Visual examination showed no light appearing through a gap in the foil. The vacuum mode performance data,taken after vibration testing,verified that the foil seating operation had been successful.

Forward dome installation began and dome screw torquing sequences then continued until the required less-than-two-mil gap at the dome/case interface was obtained. Pressurization of the RTG with argon to 25 psia was completed and a pressure decay test then yielded an acceptable 0.02 psi/6-hour leak rate. The RTG was removed from LAS #1 on the slide tray cart and installed into the RTG-SC.

Transfer of the F-9 RTG to Bldg. 400 for mass properties and dynamic testing was completed and the unit was removed from its SC. Center of gravity and weight measurements were then obtained. During the set up for C.G. measurement, it was observed that there was a deposit of material, approximately 1/4" x 1-1/4" in size, on the center area of the forward dome. This residue was later found to be due to an inadvertant touching of the dome surface with the

Health Physicist's neutron counter's polyethylene ball which is used as a neutron moderator. Appropriate corrective action was taken. Following the thermal-vacuum mode testing of the unit later, the spot was still visible. Subsequent MRB disposition was to accept it as is. This was based upon analysis which showed that, after the exposure to vacuum at/below 10^{-6} torr and temperature in the range of 250° C, the high density polyethylene had decomposed completely to residual carbon.

The F-9 RTG was mounted to the vibration system's slip table in preparation for pre-vibration air performance/pressure decay testing. RTG load was switched from the short-circuit to the loaded condition and thermal stability for the start of test was achieved. Output power to the end of test averaged 80.8 watts, corrected for cable losses; rate of pressure decay was 0.01 psi/48-hours.

During the performance test period, stability was perturbed for a short period to allow the installation of the JPL flight configuration power cable. Load was switched to open-circuit, the 2428 GSE power cable was removed and the JPL cable and 3500G4 adapter cable were then installed to the converter receptacle prior to re-applying RTG load. The actual connection of the JPL cable plug to the converter receptacle, as well as the subsequent torquing/lockwiring operation, was performed by JPL personnel. Thermal stability was then re-attained. Since the pressure decay measurement points were taken pre- and post- the unstable period and the power out measurements during that time are excluded from the overall average, there are no effects on the reported performance test results due to the power cable exchange.

During the exercise of changing power cables, it was found that the shorting module being used for test was giving an anomalously high and varying resistance reading on one of its lines. Measurements on other available shorting modules also exhibited abnormal readings. It was decided to remove the shorting module from the power out cable string to preclude possible introduction of transients into the performance data during vibration testing. After an RTG gas sample had been obtained for mass spectrographic analysis, the RTG load was again switched open for a brief period and the shorting module was removed from the cable system.

X-axis vibration testing began with the 1/2 G sine survey and concluded with the 9.54 G-rms random acceptance vibration. After rotation on the slip table to the Z-axis, the vibration cycle in that axis was completed. With transfer of the RTG to the exciter head the Y-axis (longitudinal) vibration testing was completed.

A comparison of all pre-run and post-run performance data scans showed no degradation due to any vibration application. A 0.6 watt degradation in power was attributed to a 2° C RTD temperature rise. During the 9.54 G-rms X-axis run, there were some very minor disturbances on the strip chart recorder channel which was monitoring the R_{shunt} voltage. They were also seen on the magnetic tape record which was made in parallel to the strip chart record. These disturbances were attributed to fluctuations in case-to-foil isolation as it appeared that the shunt resistance was changing between 800 K-ohms to 300 K-ohms during the run. At the start and end of that run, the shunt resistance value was measured at 800 K-ohms, still indicating isolation between thermopile circuit, foil system and case ground. Of significance is that on the previous F-8 RTG vibration testing, the disturbances on the R_{shunt} voltage were also coincident on the load voltage and load current strip chart signals. It had been found after the F-8 testing that the strip chart recorder amplifiers had all been improperly tied together at their shielded input returns, thereby having no common mode rejection capability. This situation was corrected for the F-9 vibration testing and "cross-talk" between the R_{shunt} channel and the load voltage and load current channels was not indicated.

The F-9 RTG was transferred to the Long Life Lab vacuum testing facility in Bldg. 300. After the RTG had been installed on the chamber #4 support fixture, there was a failure of the primary facility power system,with a subsequent failure of the emergency generator power system,to switch onto the facility load. Maintenance personnel switched the facility load onto a back-up transformer. The RTG was in a completely safe mode during this period and there was no degradation in any manner.

The repair to the primary transformer was completed and the facility load was placed back onto that transformer. Since replacement switching components for the emergency generator system were not available, a maintenance electrician remained on duty to manually switch over in the event emergency power was needed.

Final preparations for thermal-vacuum testing were completed and evacuation was initiated. After attaining a chamber vacuum in the low 10^{-5} torr range, the bulk of the RTG fill gas was evacuated external to the chamber through the gas service cart. Pulse venting of the RTG directly into the chamber then began and shortly thereafter the venting solenoid valve remained open. RTG internal pressure and thermal conditions continued to stabilize and were acceptable for the start of the four hour vacuum performance test. With chamber pressure in the mid 10^{-6} torr range and RTG internal pressure at 5 microns, output power over the four hour period averaged 158.9 watts, corrected for cable losses up to the converter receptacle; shunt resistance between thermopile and case indicated 65 K-ohms at this vacuum operation.

A short test was performed after the above thermal-vacuum performance test period to measure the residual gas load pressure within the F-9 RTG. The venting solenoid valve was closed for a thirty minute period to isolate the RTG internal cavity from the chamber's vacuum. RTG internal pressure increased from 5 microns to 70 microns over that time. This correlated closely with F-7 and F-8 pressure build-ups, which were respectively 103 microns and 95 microns.

At the previous vacuum mode operation of F-9, which was the degassing process in LAS #1 output power had been measured as 159.6 watts. It had been estimated that power during that period was down by 1.4 watts due to thermal shunting through a gap at the mating edges of the forward foil end cap and thermopile foil basket. Seating of the foil system was subsequently performed, and although the gap appeared to be closed at that time, the vacuum measurement in the Long Life Lab chamber was to be the success criteria for the foil seating operation. A comparison of the output power in chamber #4 of 158.9 watts to that in LAS #1 of 159.6 watts indicated that foil seating was successful. There has historically been a disparity of almost 2 watts between performance in the loading station with the forward dome

removed and performance intthe Long Life chamber where venting conductance is greatly reduced, being restricted by the gas management valve on the RTG and small diameter tubing. The delta on F-9 of only 0.7 watts leads to the conclusion that an acceptable mating at the foil system edges had been attained.

Vacuum mode operation was terminated with the backfilling of the RTG with argon. After the chamber was backfilled with N_2, the Health Physicist gave his authorization to open the chamber. While still suspended from the chamber door support frame, the RTG was stationed in ambient air and allowed to stabilize for the post-thermal/vacuum performance test.

Visual examination shortly after opening the chamber disclosed a defect in the JPL power cable. The potting at the connector plug at the end of the cable opposite from the RTG receptacle was cracked radially outward from the cable and the potting was also separated circumferentially from the cable. Disposition on NR-48338 was subsequently given to replace that cable prior to flight.

Thermal stability for the start of the post-vacuum air performance test was achieved. Output power during the 48 hour test averaged 80.6 watts, corrected for cable losses, and rate of pressure decay measured 0.03 psi/48-hours.

Following the above performance test, the RTG was removed from the chamber door support fixture and was being transferred to the platform outside of the Long Life Lab for installation into the SC, when visual examination disclosed that there were deposits of foreign material on the unit. There was a "splotch" of residue of a blackish/brownish glazed appearance on the forward dome flange, the forward stiffener ring and another on the PRD housing. Numerous small spots of like appearance were in evidence on at least four of the six case fins. The deposit at the forward dome flange/stiffener ring appeared to be a single spattered globule which ran through the adjacent lightening hole in the stiffener ring and dropped onto the PRD housing directly beneath that hole. The deposits on the case fins were different in that, by virtue of their multitude and small size, they appeared to have been deposited by a "spray" of material.

An emergency MRB convened and a decision was made to clean the residue from the RTG where possible. The deposit on the PRD housing was readily removed with a wooden spatula, leaving no visual trace of residue. Much of the foreign material was also removed from the forward dome flange and forward stiffener ring. Due to better adhesion to these surfaces, all of the residue could not be removed as it had been on the smoother-finished PRD housing. The residue had a tan-colored powdery consistancy after being removed from those areas. To avoid potential degradation of the Radifrax coating on the case fins, no attempt was made to clean those spots except for a light wiping with a clean, lint-free cloth.

Investigation into the cause of contamination began. Comprehensionsive reporting of the actions/results stemming from this investigation is provided in the Drenker memos dated 10/11, 10/15 and 11/1/76, entitled F-9 RTG/F-10 IHS EXTERIOR RESIDUE ANOMALY.

A careful review of the actual events leading up to the initial opening of the vacuum chamber provided a circumstance which almost certainly produced the anomalous residue. After the Genesolv-D was blown out of the shroud lines as prescribed, there was a longer-than-normal period with the RTG still in the chamber while awaiting authorization from the Health Physicist to open the door. The RTG, mounted to the chamber door support fixture, was then withdrawn from the chamber. The uncapped coolant line on the chamber ejected drops and a spray of Genesolv-D in a single "burp", as described by the operator. This was attributed to a partial vaporization of the remaining coolant (35° C boiling point) when the RTG remained within the chamber for the extended period, with the bulk of the Genesolv-D having been removed from the shroud. Although the coolant was not seen to fall on the F-9 RTG, this is apparently what actually did occur. Corrective action has been taken to cap all of the coolant lines prior to opening the chamber.

After cleaning the residue from the converter, the unit was installed into the RTG-SC. During that operation, there was an erratic indication on the RTD #1 circuit which first evidenced itself as the RTG was being lowered into the SC. The case fin temperature was passing

through approximately 220° C (0.55 volts) at that time and after attaining a fin temperature of approximately 235° C (as indicated on RTD #2 and RTD #3), the RTD #1 circuit returned to normal. That reading remained normal after the F-9 RTG had been transferred to storage in Bldg. 800. Monitoring throughout the next two days continued to show a normal storage reading on the RTD #1 circuit of 0.57 volts or 240° C.

Later that day, the RTG-SC was opened and the F-9 RTG removed to allow investigation on the anomalous RTD #1 circuit. There were erratic readings on that circuit during the initial operation of removing the RTG from the SC, which was the venting of the SC argon cover gas to ambient pressure. These were erratic fluctuations of 0.6 to 1.38 volts, where the normal reading would have been approximately 0.57 volts. These fluctuations were similar to those indicated earlier during the RTG installation into the SC. After the RTG had been removed from the SC and case temperature had dropped to below 220° C (0.55 volts), the circuit indicated a proper reading. Manipulation of the cables and demating/mating of the connectors in the cable string between the PTU and the RTD cable could not reporduce the anomaly. A pin retention test on the 3500G3 cable, which is the adaptor test cable to the flight RTD cable, indicated proper retention forces. This closed out the first phase of investigation. The unit was re-installed into the SC. At this installation the erratic RTD #1 indications again appeared at the 220° C range and returned to normal at approximately 235° C.

The second phase of investigation into this anomaly was conducted a day later. There was positive elimination of the 3500G3 cable and the feedthrough cable at the underside of the SC lid as the fault in the RTD #1 circuit. Special test leads were provided to connect directly to the RTD #1 circuit pins on the flight cable connector and, after bypassing the usual test cabling with the test leads, the circuit was monitored during removal and installation operations of the RTG into the SC. The erratic RTD #1 circuit readings were again in evidence, pointing conclusively that the circuit fault was within the flight cable. After the test cabling was placed into the normal configuration, the RTG was reinstalled into the SC and placed into the secure storage area in Bldg. 800. A decision was made to replace the flight RTD cable.

On 15 November 1976, the F-9 RTG was removed from the RTG-SC. The purpose of this removal was to inspect the RTG outer case for the condition of previous contamination, to replace the RTD cable and to set the RTG conditions for shipment. The condition of the RTG outer case was accepted "as is", for no further cleanup was judged to be necessary. The RTD cable was replaced and its operational performance verified by standard procedures conducted when the RTG was reinstalled into the shipping container. The RTG shipment conditions were established and the RTG secured in the RTG-SC in preparation for shipment to ML/MRC.

Two additional items appeared when the RTG was removed from the SC which were not associated with the RTD #1 anomaly. The first was that the quantity of residue on the surfaces of the case fins had greatly diminished from the time that the contamination was originally seen two days earlier. The "spots" on the fins had, for the most part, become barely perceptible stains; whereas, initially, they were very apparent and had a thickness of several mils. Over the period of storage in the SC with the case fin temperature at 240° C, as compared to 195° C outside of the SC, there had been a definite change in the residue.

The other item which evidenced itself after the SC was opened was an oily appearing contamination at the bottom of the SC cavity. A specimen was obtained, analyzed, and positively identified as lubricating oil/grease. After examination of the overhead crane in the Bldg. 300 high-bay area, it was concluded that the lubricant had dropped into the SC after the lid had been removed two days previously. The RTG, protected by being attached to the underside of the lid, was not contaminated by oil/grease from the overhead crane. To preclude recurrence, corrective action was taken to add a catch tray beneath the crane motor housing. A plate has also been provided to cover the SC cavity at all times that the lid is not in place. Alghough there had not been evidence of lubricant falling from the overhead cranes in Bldgs. 400 and 800, those also had catch trays added as a preventive measure. More detailed F-9 RTG test information may be found in the Sept.-Oct. '76 Bi-monthly Report.

10.2.6 F-10 RTG - MHW-MJS FLIGHT UNIT

After installation of the aft heat source support, preparations were made for the task of installing the F-11 IHS into the F-10 converter. The F-11 heat source was received from ML/MRC and placed in storage in Bldg. 800. On 18 October 1976, the IHS-SC was transferred to the test area where the SPC was removed and routed into the LAS #1 loadlock. With the SPC dome removed and the tripod preload on the EPC/SPC relieved, the EPC internal pressure was measured as 15.2 psia and an IHS gas sample was obtained for mass spectrographic analysis. The EPC cover was then removed and a visual examination was given to the forward end of the heat source. No visual discrepancies were observed other than the minor abrasions which had previously been noted by ML/MRC.

Hoisting of the heat source from the EPC was completed and an overall visual examination revealed no anomalies. The IHS was then positioned and installed into the converter. Installation of the forward heat source support and engagement of the forward end enclosure to the case brackets was completed. The RTG assembly was thermally stabilized to allow preloading of the heat source support system. An end enclosure deflection of 28.5 mils was then established to preload the assembly. Lockwiring of the preload screw position in the preload bushing and packing of the preload screw with microquartz were completed and preparations were then made for the vacuum degassing operation. Chamber evacuation was initiated and the 10^{-6} torr range was attained. Acceptably low levels of CO was indicated, by monopole mass spectrometer scanning of the chamber partial pressures 48 hours later, and the chamber was backfilled at that time to terminate the vacuum processing of the F-10 converter/F-11 IHS. RTG output power for the last four hours of vacuum operation averaged 161.9 watts, corrected for cable losses up to the converter receptacle.

Installation of the forward dome to the converter case began and screw torquing continued until the required less-than-two-mil gap at the dome/case interface was achieved. The RTG was then pressurized with argon to 25 psia and a short pressure decay test indicated a leak rate of 0.00 psi/6-hours. LAS #1 was opened and the RTG was removed on the slide tray cart and installed into its shipping container. Visual examination of the unit prior to its removal from the LAS had indicated that one of the thermo-electric attachment screws had

been inadvertantly touched by the Health Physicist's neutron counter sphere. This was documented on NR-48378 and disposition was given to remove as much of the carbon impregnated polyethylene as possible with a lint-free cloth. Since remaining residue would be dissociated during the subsequent thermal-vacuum testing, the condition was acceptable.

Two additional superficial anomalies were noted at this time. During the operations of installing the RTG into the shipping container, the unit is rotated in the handling sling to the mono-balls up position. At that time it was observed that there was a burnish mark in the emissive coating on the aft dome. The mark had the appearance of a scratch but, after being examined under 10 power magnification, it was established that the beryllium material of the dome had not been penetrated and the condition was accepted "as is". The other anomaly was the appearance of what were initially thought to be burns on two of the RTG's mono-balls. After removing the material with a lint-free cloth, examination showed absolutely no mar in the surfaces of the mono-balls. Subsequent analysis identified the material as aluminum alloy, most probably from the clevises in the converter shipping container.

Transfer of the F-10 RTG to Bldg. 400 for mass properties measurement and vibration testing was completed and the RTG was removed from its SC. Mass properties measurement was completed and the RTG was then set up on the vibration slip table in the inverted attitude (mono-balls up) in preparation for the pre-vibration air performance /pressure decay test. RTG load was switched out of the short-circuit condition and thermal stability at the 29.7 volt operating point was achieved for the start of test. After the initial data point, the load was switched to open-circuit for a short period to allow the removal of the 2428 GSE power cable for replacement with the JPL flight cable and 3500G4 adaptor cable. Output power to the end of test averaged 83.5 watts, corrected for cable losses up to the converter receptacle; rate of pressure decay indicated 0.00 psi/48-hours. An RTG gas sample for mass spectrographic analysis was obtained.

The RTG load was briefly switched to the open-circuit condition and the shorting module was removed from the power cable string. This removal was made to preclude possible introduction of transients into the performance data from faulty switch contacts in the shorting module. Preparations were then completed for the vibration test cycle.

X-axis vibration began with the 0.5 G sine survey and concluded with the 9.54 G-rms random acceptance vibration. After rotation on the slip table to the Z-axis orientation, the vibration cycle in that axis was completed. After transfer of the RTG to the exciter head the Y-axis (longitudinal) vibration testing was completed. A comparison of all of the pre-run and post-run performance data scans showed no degradation due to any vibration application. Examination of the strip chart record, which recorded the generator load voltage, the voltage equivalent to load current and the R_{shunt} voltage during each vibration application, showed only minor perturbations on the R_{shunt} fluctuation occurred during the Z-axis random equalization run; pre-run isolation between the thermopile circuit and case indicated 4.4 megohms, whereas the post-run isolation measured 2.2 megohms, returning to 4.2 megohms one hour later. A shift in the R_{shunt} voltage occurred during the Y-axis random acceptance run; pre-run isolation between circuit and case measured 4.4 megohms and post-run isolation showed a decrease to 600 K-ohms. Isolation between circuit and case remained at 600 K-ohms after the completion of the vibration test cycle, indicating that there was a reduction of isolation resistance between the case and foil system. There were no indications of anomalies on the load voltage or current traces during any of the vibration applications. A six hour post-vibration performance test was completed and yielded an average output power of 83.7 watts (corrected for cable losses) and rate of pressure decay of 0.01 psi/6-hours. The shorting module, removed prior to the vibration test cycle, was re-installed and installation of the F-10 RTG into its SC was completed.

Transfer to the Bldg. 300 Long Life Lab vacuum testing facility was completed and the F-10 RTG was removed from its SC and installed onto the chamber #4 support fixture. After the completion of electrical and pneumatic interconnections, the Segment Readiness Review to allow the start of vacuum testing was conducted.

The chamber was secured and evacuation was initiated. After attaining a chamber pressure in the mid 10^{-5} torr range, the bulk of the RTG fill gas was evacuated external to the chamber through the gas service cart. The remainder of the argon in the RTG was pulse vented to the chamber until the solenoid venting valve could remain open. RTG internal pressure and thermal conditions continued to stabilize and were acceptable for the start of the four hour vacuum performance test. With chamber pressure in the mid 10^{-6} torr range and RTG internal pressure

at 4 microns, output power over the four hour period averaged 161.26 watts, corrected for cable losses; shunt resistance between thermopile and case indicated 110 K-ohms at this vacuum operation. After the four hour vacuum performance test, the solenoid venting valve was closed for a thirty minute period while the RTG internal pressure was monitored. With the RTG internal cavity isolated from chamber vacuum, pressure increased from 4 microns to 69 microns over thirty minutes, proving,as it also had on the previous RTGs, that there was still a residual gas load within the RTG from the heat source helium generation.

Argon backfilling of the RTG to terminate vacuum testing was completed. Backfilling of the chamber with dry nitrogen was completed, the Health Physicist gave his approval and the chamber was opened. While still stationed on the chamber door support fixture, the RTG was allowed to stabilize in ambient air for the post-vacuum performance test. A visual examination performed at this time disclosed no obvious anomalies. Thermal stability for the start of the 48-hour test was achieved. Output power averaged 83.7 watts, corrected for cable losses, and rate of pressure decay measured 0.09 psi/48-hours. During the thermal vacuum test, isolation between the foil and case returned. Data during the post-T/V air performance indicated a shunt value of 4 to 5 megohms, a value comparable to the pre-Y-axis acceptance vibration data. Preparations for a magnetic signature mapping of the unit in the Long Life Lab were completed and the RTG was removed fromthe chamber support fixture and set up in the magnetic test fixture.

After being placed into the magnetic fixture, the RTG was placed into a nominal 4 amp load condition and allowed to stabilize. The magnetic signature map of the RTG was then completed. Specific magnetic characteristics of the RTG will be determined by JPL and NASA, who will reduce and interpret the raw data. The magnetic test was run with the RTD GSE cable attached, a condition acceptable to JPL and NASA personnel, because of a tightness of the connector mating. Subsequent to the magnetic test,the connector was removed from the RTG bracket and the demating successfully accomplished. Reassembly of the RTD GSE cable was accomplished and the RTG prepared for installation into the RTG-SC. Following final inspection, the RTG was installed into the RTG-SC and all necessary RTG pre-shipment conditions set. The RTG was transferred to Bldg. 800 for storage prior to shipment to ML/MRC.

10.2.7 F-11 RTG - MHW-MJS FLIGHT UNIT

Preparations were made for the task of installing the F-12 IHS into the F-11 converter. The F-12 heat source was received from ML/MRC and placed into storage in Bldg. 800. On 6 January 1977, the IHS-SC was transferred to the test area, where the SPC was removed and placed into the LAS #1 loadlock. SPC internal pressure was 22.95 psia although the average SPC dome bolt torque was only 20 ft-lbs. compared to the specified value of 40 ft-lbs. The anomalous torque value was documented on NR-48382, and in this case was acceptable. Difficulty was experienced in removing the SPC tripod assembly due to hex heads of the EPC cover bolts extending beyond the edge of the EPC cover and binding against the tripod legs.

After measuring EPC internal pressure as 16.05 psia, an IHS gas sample for mass spectrographic analysis was obtained. Removal of the EPC cover was completed and a visual examination of the IHS showed the locking screw in the forward aeroshell end cap protruding approximately 0.015" above the surrounding surface. The locking screw is required to be at, or within 0.005" below the surrounding surface. Reference NR-48381.

The IHS was hoisted out of the EPC. Visual examination revealed no further abnormalities and the heat source was installed into the converter. The top of the locking screw was abraded flush with the top surface of the IHS end cap. Residue produced by the abrasion process was vacuumed from the top of the heat source.

The forward graphite end support and forward end enclosure assembly were installed and preload of the IHS was completed. Tamping of the forward moly-foil end cap effected proper mating of the end cap to the foil basket. Lockwiring of the preload screw/bushing and packing of the preload screw with microquartz insulation completed the first segment of RTG assembly operations. Chamber evacuation for the start of the vacuum degassing process was initiated and a vacuum level of 1×10^{-5} torr was attained. Vacuum power operation averaged 161.8 watts. This power is corrected for cable losses up to the connector receptacle.

The forward dome installation began and dome screw torquing operations continued until an acceptable less-than-two-mil-gap at the dome/case interface was indicated around the entire perimeter. The F-11 RTG was pressurized to 25 psia with argon and a pressure decay test was initiated. This test yielded a leak rate of 0.00 psi/6-hours.

The unit was removed from LAS #1 on the slide tray cart and visually examined. Separation of potting material on RTD #3 was noted; there were no other anomalies. The RTG was installed into the RTG-SC and transferred to the Building 800 storage area.

Movement of the F-11 RTG from Bldg. 800 to Bldg. 400 was accomplished. The unit was removed from its SC and center of gravity and weight measurements were obtained. The F-11 RTG was mounted to the vibration system slip table in preparation for the pre-vibration air performance/pressure decay testing. The RTG load was switched from the short-circuit to the loaded condition and thermal stability for the start of test was achieved. Output power to the end of test averaged 83.1 watts, corrected for cable losses. The rate of pressure decay was 0.00 psi/48-hours. An RTG gas sample for mass spectrographic analysis was obtained.

Vague spotting of an undertermined nature was observed on the F-11 converter shell at this time. Testing continued while further evaluation of the anomaly was made.

RTG thermal stability for the start of vibration testing was achieved. Due to mechanical interference of the restraining wrench and deformation of the torque wrench strap, the 2428 GSE power cable could not be tightened to the prescribed 140-150 inch-lbs. torque. With Engineering approval, the cable connector was tightened and lockwired.

X-axis vibration testing began with the 0.5 G sine survey and concluded with the 9.54 G-rms random acceptance vibration. The RTG was rotated on the slip table to the Z-axis and the vibration cycle in that axis was performed.

Transfer of the RTG to the exciter head was made and the Y-axis (longitudinal) vibration testing was completed. A comparison of all of the pre-run and post-run performance data scans showed no degradation due to any vibration applications. Examination of the strip chart

record, which recorded the generator load voltage, the voltage equivalent to load current and the R_{shunt} voltage during each vibration application, showed only very minor fluctuations. Thermopile circuit to case isolation measured greater than 3.0 megohms throughout the vibration test cycle.

A six-hour post-vibration performance test was completed and yielded an average output power of 85.2 watts (corrected for cable losses) and rate of pressure decay of 0.00 psi/6-hours. Installation of the F-11 RTG into its SC was completed. Visual inspection of the RTG while the converter was attached to the SC lid did not reveal any new anomalies. Spots on the converter shell and fins, originally observed earlier remained unchanged. The crazing and flaking areas of the emissive coating on the forward stiffening ring, originally observed during ETG acceptance testing and documented on NR-48419, may have increased slightly in size.

The F-11 RTG was transferred to the Long Life Lab vacuum testing facility in Bldg. 300. The RTG was removed from its SC and installed onto the chamber #4 support fixture. After the completion of electrical and pneumatic interconnections the Segment Readiness Review to allow the start of vacuum testing was conducted.

Final preparations for thermal vacuum testing were completed and evacuation was initiated. After attaining a chamber vacuum in the low 10^{-5} torr range, the bulk of the RTG fill gas was evacuated external to the chamber through the gas service cart. Later, the venting solenoid valve was opened. RTG internal pressure and thermal conditions continued to stabilize and were acceptable for the start of the four hour vacuum performance test. With chamber pressure in the mid 10^{-6} torr range and RTG internal pressure at 6 microns, output power over the four hour period averaged 160.3 watts, corrected for cable losses up to the converter receptacle; shunt resistance between thermopile and case indicated 117 K-ohms at this vacuum operation.

A short test was performed after the above thermal vacuum performance test period to measure the residual gas load pressure within the F-11 RTG. The venting solenoid was closed for a thirty minute period to isolate the RTG internal cavity from the chamber vacuum.

RTG internal pressure increased from 6 microns to 94 microns over that time. This correlated closely with the data obtained during similar tests performed on the F-7 through F-10 RTGs.

Vacuum mode operations terminated with the backfilling of the RTG with argon. Backfilling of the chamber was completed, the Health Physicist gave his authorization and the chamber. was opened. While still suspended from the chamber door support frame, the RTG was stationed in ambient air and allowed to stabilize for the post-thermal vacuum performance test. Thermal stability for the start of the post-vacuum air performance test was then achieved.

An FRB meeting convened to evaluate the crazing and flaking of the emissive coating on the forward stiffening ring, observed earlier and documented on NR-48419. It was decided that further rework was required. Average RTG power during the 48-hour pressure decay test was 83.4 watts, corrected for cable losses. Rate of pressure decay measured 0.00 psi/48-hours. Data during the post-T/V air performance indicated a shunt value of 4 to 5 megohms.

Preparations for a magnetic signature mapping of the F-11 RTG in the Long Life Lab were completed and the RTG was removed from the chamber support fixture and set up in the magnetic test fixture. The RTG was placed in a nominal 4 amp load condition and allowed to stabilize. The magnetic signature map of the RTG was then completed. Specific magnetic characteristics of the RTG will be provided by JPL and NASA who will reduce and interpret the raw data. As directed by MRC, photographs of the affected area on the forward stiffening ring were obtained and losse particles were removed.

Later, the F-11 RTG was inspected by representatives from JPL, ERDA, Sandia and GE. The MJS Project Manager then instituted an Investigative Task Force Team to investigate and resolve the emissivity coating problem. Task Force Reports were issued on 14 March, 20 April, and a final report on 26 May 1977, see Reports 1E40-GD-251A, 1E40-GD-267A, and 1E40-CWW-277A (Reference NR-48419). Following re-work and final inspection, the RTG was installed into the RTG-SC and necessary RTG pre-shipment conditions set. Since the JPL power cable was not available, the 2428 GSE power cable was accepted for storage conditions and will

be replaced with the JPL power cable prior to launch. (Reference NR-48473.) The RTG was transferred to Bldg. 800 for storage prior to shipment to ML/MRC.

10.2.8 F-12 RTG - MHW-MJS FLIGHT UNIT

On 22 February 1977, the IHS-SC containing the F-9R IHS was transferred from the storage area to the test area. The SPC was prepared and installed into LAS #1 loadlock. Tripod preloading of the EPC/SPC was relieved. During an attempt to mate the internal LAS pneumatic flex line to the EPC cover valve port, the threads on the valve port became galled. The anomaly was documented on NR-48452 and direction was to re-chase the valve port threads with a die. The rethreading operation was completed and, using the 2931 gas tap adapter, the LAS flex line was successfully mated to the valve port. EPC internal pressure was measured as 15.60 psia and the IHS gas sample for mass spectrographic analysis was then obtained.

The EPC cover removal was completed and a visual inspection of the forward end of the heat source revealed the end cap locking screw protruded approximately 2 mils above the surrounding surface. NR-48453 was prepared to document this anomaly. Disposition was to polish the screw flush with the surrounding surface. This operation was completed and all surfaces were vacuumed. The heat source was hoisted from the EPC and overall examination revealed the locking screw in the aft end cap also protruded above the surrounding surface, approximately 5 to 7 mils. There were no other new discrepancies noted.

In preparation for the F-9R IHS processing cycle, required as the result of an anomaly which occurred during F-9 IHS assembly at ML/MRC (reference NR-48456), the IHS was seated onto a graphite base fixture within the LAS. See Section 5, para. 5.2. All thermal gloves were removed from the chamber and a preparations were completed for the start of the vacuum operations to outgas residual CO from the F-9R heat source. Chamber evacuation began and several hours later, the low 10^{-5} torr range had been attained. After data from the monopole scan indicated the CO level was an acceptable 2.8×10^{-8} torr, IHS processing was terminated. Chamber backfill with argon was completed and gas purity levels attained.

The IHS was raised into the lifting fixture and the lower locking screw was torqued to 20 inch-ounces in an attempt to seat the screw. No change in level was noted. The raised screw was abraded flush with the aft end cap. The converter was prepared to receive the IHS and the IHS was installed into the converter. The forward heat source support and forward end enclosure assembly were installed. After the RTG had thermally stabilized to allow heat source preloading, an end enclosure deflection of 28.5 mils was established to preload the assembly. Lockwiring of the preload screw/bushing and packing of the preload screw with microquartz then completed the first stage of the RTG assembly operations.

Chamber evacuation for the start of the vacuum degassing process was initiated, and the 10^{-6} torr range was attained. The vacuum processing on the F-12 RTG continued for 48-hours. Generated output power for the last four hours of the vacuum operation averaged 159.0 watts, corrected for cable losses up to the converter receptacle. The chamber was then backfilled with argon.

The forward dome installation began and dome screw torquing operations continued until an acceptable less-than-two-mil gap at the dome/case interface was indicated around the entire perimeter. The F-12 RTG was pressurized to 25 psia with argon and a pressure decay test was initiated. The test yielded a leak rate of 0.00 psi/6-hours.

The F-12 RTG was removed from LAS #1 on the slide tray cart and visually examined. There were no new anomalies. The RTG was installed into the RTG-SC.

Movement of the F-12 RTG from Bldg. 800 to Bldg. 400 was accomplished. The unit was removed from its SC and center of gravity and weight measurements were obtained. The RTG was mounted to the vibration system slip table in preparation for the pre-vibration air performance/pressure decay testing. The RTG load was switched from the short-circuit to the loaded condition and thermal stability for the start of the test was achieved. Output power to the end of the test averaged 82.7 watts, corrected for cable losses. The rate of pressure decay was 0.00 psi/48-hours.

The maximum attainable torque of 80 inch pounds was applied to the RTG power cable connector and 125 inch pounds to the RTD instrumentation cable connector. The prescribed torque value of 140-150 inch-pounds was unattainable due to slippage of the strap torque wrench. NR-48461 was prepared to document the lower torque values which are acceptable for ground test and storage conditions.

An RTG gas sample for mass spectrographic analysis was obtained. Thermal stability for the start of vibration testing was then achieved. X-axis vibration testing began with the 0.5 G sine survey and concluded with the 9.54 G-rms random acceptance vibration. Thermopile to case resistance had been approximately 800K ohms prior to X-axis vibration. When the thermopile to case circuit was interconnected to the circuitry of the magnetic tape and pen chart recorders for calibration prior to the vibration run, the shunt resistance value increased to 2.4 megohms.

The thermopile to case shunt resistance remained at the higher value thru the completion of X-axis sine sweep vibration. During the X-axis random equalization, 3.2 G-rms for 30 seconds duration, the shunt resistance decreased to 180K ohms. Following completion of the X-axis 9.54 G-rms random vibration, the shunt value increased to 3.3 megohms and remained at approximately this value throughout the remaining vibration tests.

The RTG was rotated on the slip table to the Z-axis and the vibration cycle in that axis was completed. The RTG was transferred to the exciter head and Y-axis (longitudinal) vibration testing was completed. Due to a blown fuse in the magnetic tape recorder system, no vibration data was obtained during the Y-axis vibration. A comparison of all of the pre-run and post-run performance data scans showed no degradation due to the vibration application. Examination of the strip chart record which recorded the generator load voltage, the voltage equivalent to load current and the R_{shunt} voltage during each vibration application, showed no fluctuations.

A six-hour post-vibration performance test was completed and yielded an average output power of 83.6 watts (corrected for cable losses) and rate of pressure decay of 0.05 psi/6-hours.

Installation of the F-12 RTG into its SC was completed. Visual inspection of the RTG while the converter was attached to the SC lid did not reveal any new anomalies.

The F-12 RTG was transferred to the Long Life Lab vacuum testing facility in Bldg. 300. The RTG was removed from its SC and installed onto the chamber #4 support fixture. After the completion of electrical and pneumatic inter-connections, the Segment Readiness Review to allow the start of vacuum testing was conducted.

Final preparations for thermal vacuum testing were completed and evacuation was initiated. After attaining a chamber vacuum in the low 10^{-5} torr range, the bulk of the RTG fill gas was evacuated external to the chamber through the gas service cart. Later, the venting solenoid valve was opened. After RTG internal pressure and thermal stabilization had been achieved, the 4 hour vacuum performance test was started.

With chamber pressure in the mid 10^{-6} torr range and RTG internal pressure at 6 microns, output power over the 4 hour period averaged 159.2 watts, corrected for cable losses up to the converter receptacle. Shunt resistance between thermopile and case was 14K ohms during vacuum operations.

A short test was performed after the above thermal vacuum performance test period to measure the residual gas load pressure within the F-12 RTG. The venting solenoid was closed for a 30 minute period to isolate the RTG internal cavity from the chamber's vacuum. RTG internal pressure increased from 5.2 microns to 94 microns over that time.

Vacuum mode operations terminated with the backfilling of the RTG with argon. Backfilling of the chamber was completed and, after approval of the Health Physicist, the chamber door was opened. While still suspended from the chamber door support frame, the RTG was positioned in ambient air and allowed to stabilize for the start of the post-vacuum air performance test. Thermal stability for the start of the 48 hour test was achieved. The 48 hour pressure decay test was completed. Average RTG power was 81.8 watts, corrected for cable losses.

Rate of pressure decay measured 0.07 psi/48 hours. Data during the post-TV air performance indicated a shunt value of approximately 3 megohms comparable to the shunt resistance following vibration tests.

While the RTG remained suspended from the chamber door support fixture, a fit check of a pre-heated JPL interstitial structure, Dwg. 10073891, to the three RTG spherical bearings was successfully performed. The RTG was removed from the support fixture, and while secured on the platform lift truck, the room ambient temperature intersitial structure was mated to the forward RTG attachment points. The assembly was thermally stabilized and the six six mounting bolts securing the interstitial structure assembly to the RTG were torqued to 100 inch-lbs. After verification of the adequacy of the mounting, the structure was removed and preparations for a magnetic signature mapping of the unit in the Long Life Lab were completed.

Visual examination of the RTG during preparation for the magnetic test, revealed one broken strand at the thermal lug on the RTD cable ground wire. NR-48462 was prepared to document this anomaly. Disposition was to accept "as is".

After being placed into the magnetic fixture, the RTG was switched into a nominal 4 amp load condition and allowed to stabilize. The magnetic signature map of the F-12 RTG was then completed. Specific magnetic characteristics of the RTG will be provided by JPL and NASA, who will reduce and interpret the raw data. The RTG was then prepared for installation into the RTG-SC. Following final inspection, the RTG was installed into the RTG-SC and all necessary pre-shipment conditions were completed. The RTG was transferred to Bldg. 800 for storage prior to shipment, to ML/MRC

10.2.9 RTG ACCEPTANCE TESTING PERFORMANCE SUMMARIES

This section summarizes the RTG performance measured during the acceptance testing of each flight RTG. The performance is summarized in tables which were extracted from the Engineering Report that was issued for each RTG. For more detailed information see the individual Engineering Report. Tables 10-1 through 10-7 show the performance for each RTG for the following conditions:

1. Performance in the LAS (Loading and Assembly Station) argon and vacuum performance.
2. The partial pressure of the gases in the LAS during vacuum processing - monitored to assess CO removal.
3. The performance with an argon fill in air before and after vibration and thermal vacuum acceptance testing.
4. The changes in internal resistance, open circuit voltage and power before and after each individual vibration test.
5. The vacuum performance, RCA and GE.
6. The RTG weight and center of gravity.

Fuel Loading and Vacuum Performance Summary

Figure 10-2 shows the fuel loading as a function of time for each IHS during the MHW program. Table 10-8 summarizes the vacuum performance in the LAS and Table 10-9 summarizes the post vibration thermal vacuum acceptance test data.

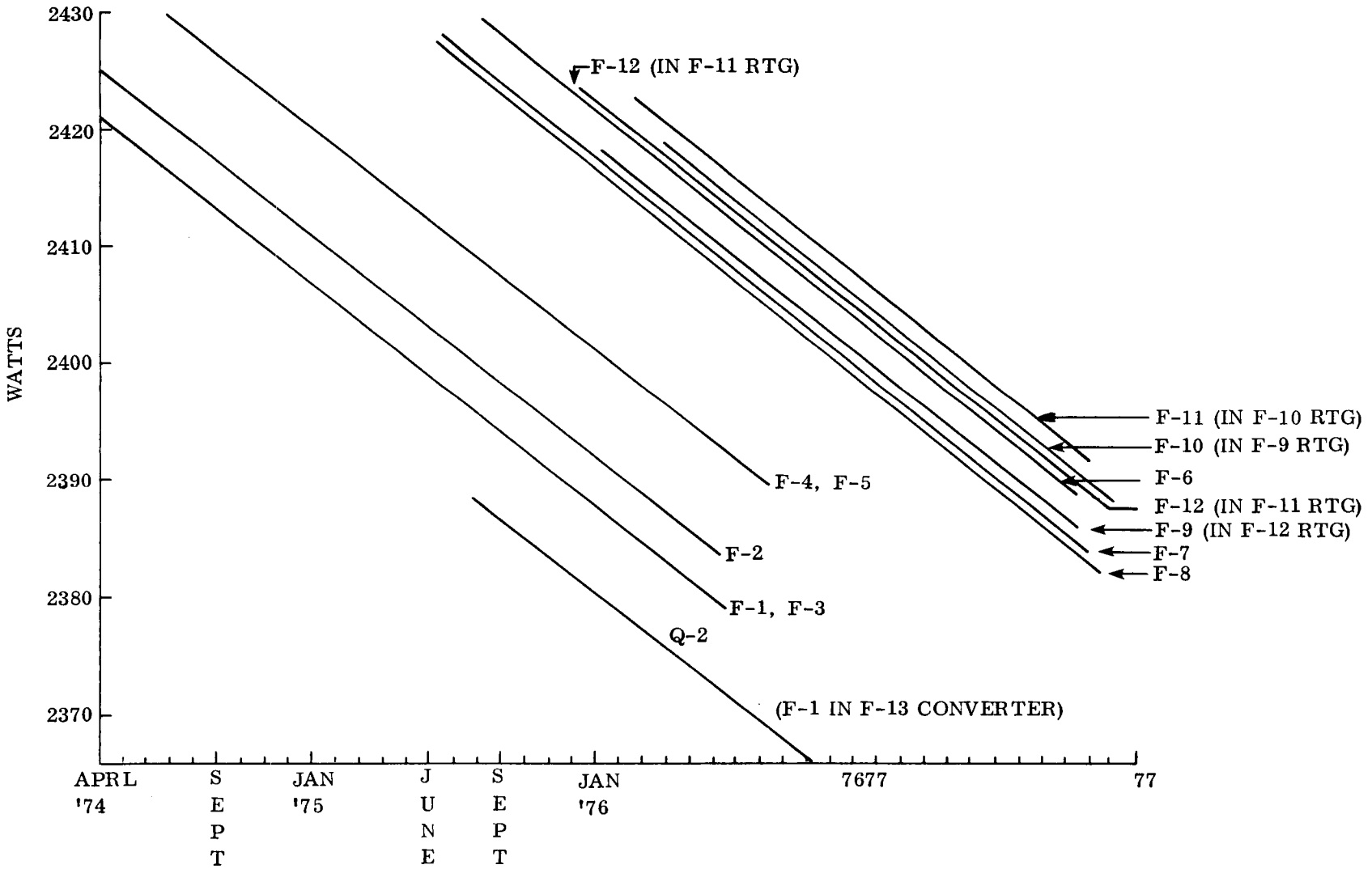

Figure 10-2. Heat Source Loadings vs. Time

F-6 RTG PERFORMANCE IN LAS

EVENTS		$P_{MEASURED}$ WATTS (e)	WATTS (t)	R_I (3) (Ω)	E_{OC} (VOLTS)
ETG PROCESSING AT RCA		156.7 (2)	2401	4.773	55.01
LAS PRE-PROCESSING (DOME REMOVED)		79.5 (2)	2418	4.379	41.52
LAS PROCESSING (END VACUUM PROCESSING)		161.7 (2)	2418	4.967	56.39
LAS POST-PROCESSING (DOME REMOVED)		80.7 (2)	2418	4.352	41.63
LAS POST-PROCESSING (DOME INSTALLED)	15 PSIA	82.8 (2)	2418	4.409	42.07
	25 PSIA	80.0 (2)	2418	4.440	41.75

(1) MEASURED AT END OF THERMOPILE
(2) CORRECTED TO RTG CONNECTOR
(3) INCLUDES 0.086 OHMS IN CABLE FOR GE TESTING

F-6 LAS MONOPOLE DATA PARTIAL PRESSURE (TORR)

SPECIES	3/3/76 t+5.5 HRS	3/3/76 t+20.5 HRS	3/4/76 t+37 HRS	3/4/76 t+44.5 HRS	3/5/76 t+61 HRS	3/5/76 t+65 HRS
He	1.5×10^{-8}	9.6×10^{-9}	6.6×10^{-9}	6.5×10^{-9}	3.5×10^{-9}	4.4×10^{-9}
H_2O	3.9×10^{-6}	2.4×10^{-6}	1.1×10^{-6}	1.0×10^{-6}	8.0×10^{-7}	8.1×10^{-7}
N_2	7.5×10^{-7}	6.8×10^{-7}	9.3×10^{-7}	9.6×10^{-7}	8.7×10^{-7}	7.7×10^{-7}
CO	2.0×10^{-7}	1.2×10^{-7}	8.1×10^{-8}	6.5×10^{-8}	5.8×10^{-8}	5.9×10^{-8}
O_2	2.0×10^{-7}	2.0×10^{-7}	2.2×10^{-7}	1.9×10^{-7}	1.5×10^{-7}	1.6×10^{-7}
Ar	1.3×10^{-6}	3.1×10^{-7}	2.3×10^{-7}	2.6×10^{-7}	2.0×10^{-7}	1.6×10^{-7}
CO_2	1.3×10^{-8}	1.8×10^{-8}	1.1×10^{-8}	1.0×10^{-8}	8.3×10^{-9}	7.4×10^{-9}
HYDROCARBONS & H_2	1.7×10^{-7}	2.8×10^{-7}	1.7×10^{-7}	1.7×10^{-7}	1.2×10^{-7}	1.2×10^{-7}
LAS CHAMBER	6.5×10^{-6}	4.0×10^{-6}	2.8×10^{-6}	2.7×10^{-6}	2.2×10^{-6}	2.1×10^{-6}

F-6 AIR PERFORMANCE

	PRE-VIB.	POST VIB.	START POST T. VAC.	END POST T. VAC.
POWER	79.80	79.02	78.42	79.03
CORRECTED TO CONN.	79.49	79.63	79.01	79.63
CORRECTED TO 30V	80.2	79.4	79.16	79.78
VOLTAGE	30.07	29.70	29.84	29.83
CONNECTOR	30.30	29.93	30.07	30.06
CURRENT	2.614	2.650	2.566	2.587
OPEN CIRCUIT	41.93	42.00	41.618	41.893
INTERNAL RESISTANCE	4.520	4.622	4.481	4.553
CORRECTED	4.434	4.536	4.395	4.467
RTD AV., °C	179	177	191	191
RESISTANCE TO CASE, OHMS	2.9M 2.9M	424K 424K	491K 491K	372K 372K
DATE	3/11/76 (1930)	3/16/76 (2100)	3/26/76 (1400)	3/27/76 (1400)

F-6 VACUUM PERFORMANCE
POWER NORMALIZED TO 2400 WATT HEAT INPUT AND TO RTG CONNECTOR

	RCA	LAS	POST VIBRATION THERMAL VACUUM
DATE:	11/11/75	3/5/76	3/23/76
POWER OUTPUT, WATTS:	157.8	159.6	157.2
INTERNAL RESISTANCE, OHMS:	4.773	4.967	5.014
E_{OC}	55.01	56.39	56.11
RESISTANCE TO FOIL:	18K	----	----
RESISTANCE TO CASE:	29.5K	61.5K	5.5K
RTD AVERAGE, °C:	----	269°C	261°C
CONVERTER PRESSURE:	----	----	3.3μ

VIBRATION TEST

X-AXIS	R_I	ΔR_I MΩ	E_{oc}	ΔE_{oc} V	P	ΔP W
3/12 0930	4.501	+ 23	41.93	- .03	79.22	- .57
3/12 1030 Pre-1/2 Level Sine	4.524	- 18	41.90	+ .14	78.65	+1.17
3/12 1100 Post	4.506	+ 5	42.04	- .15	79.82	-1.06
3/12 1400 Pre-Full Level Sine	4.511	+ 1	41.89	- .07	78.76	- .52
3/12 1430 Post	4.512	+ 3	41.82	- .01	78.24	- .08
3/12 1500 Pre-2.2G Random	4.515	+ 31	41.81	+ .04	78.16	- .28
3/12 1530 Post	4.546		41.85		77.88	
Z-AXIS						
3/15 1100 Pre-Sine	4.592	+ 7	41.95	- .01	79.11	- .14
3/15 1128 Post	4.599	- 1	41.94	- .02	78.97	- .19
3/15 1300 Pre-1/2 Level Sine	4.598	+ 1	41.92	0	78.78	- .21
3/15 1330 Post	4.599	+ 7	41.92	- .03	78.57	- .12
3/15 1400 Pre-Full Level Sine	4.606	0	41.89	0	78.45	0
3/15 1410 Post	4.606	- 3	41.89	- .04	78.45	- .20
3/15 1500 Pre-Random	4.603	+ 38	41.85	+ .03	78.25	- .45
3/15 1530 Post	4.641		41.88		77.8	
Y-AXIS						
3/16 0800	4.640	- 46	41.94	0	78.31	+ .7
3/16 0820 Tightened Connector	4.594	+ 1	41.94	0	79.02	- .03
3/16 1000 Pre-Sine	4.595	- 10	41.94	0	78.99	+ .18
3/16 1015 Post	4.585	+ 2	41.94	0	79.17	- .03
3/16 1100 Pre-1/2 Level Sine	4.587	+ 27	41.94	0	79.14	- .44
3/16 1140 Post	4.614	- 25	41.94	+ .01	78.70	+ .50
3/16 1210 Tightened Connector	4.589	+ 1	41.95	- .04	79.20	- .23
3/16 1400 Pre-Full Level Sine	4.590	+ 31	41.91	- .11	78.97	-1.25
3/16 1412 Post	4.621	- 39	41.80	0	77.72	+ .62
3/16 1418 Tightened Connector	4.582	+ 4	41.80	+ .06	78.34	+ .3
3/16 1445 Pre-Random	4.586	+122	41.86	+ .05	78.64	-1.73
3/16 1520 Post	4.708	-113	41.91	+ .03	76.91	+2.08
Tightened Connector	4.595		41.94		78.99	

TABLE 10-1. F-6 PERFORMANCE SUMMARY

F-6 RTG WEIGHT AND BALANCE

Table I

MEASURED UNBALANCED MOMENTS IN THE RTG COORDINATE SYSTEM

AXIS	MOMENT (IN.-LBS)	CORRECTION (IN.-LBS)	CORRECTED MOMENT (IN.-LBS)
X	- 21.0	- .9	- 21.9
Y	+ 29.5	0	+ 29.5
Z	- 23.0	0	- 23.0

Table II

RTG WEIGHT

TOTAL WEIGHT (RTG, FIXTURE & EQUIPMENT)		124.24 LBS.
FIXTURE	37.37 LBS	
RTD EXTENSION CABLE	.66 LBS.	
POWER OUTPUT EXTENSION CABLE	.77 LBS.	
SHORTING MODULE	1.32 LBS.	
RTG GMV FLEX LINE	.58 LBS.	
	40.70 LBS.	(40.70) LBS.
		83.54 LBS.

[1]WEIGHT SHOWN INCLUDES:

JPL POWER CABLE	.52 LBS.
CLAMPS, NUTS & SCREWS	.15 LBS.
ARGON GAS	.10 LBS.
SHIPPING BRACKET	.67 LBS.
	1.44 LBS.

NET WEIGHT = 82.10 LBS.

Table III

RTG CENTER OF GRAVITY COORDINATES

X	= - .20
Y	= -9.49
Z	= - .28

[1]CENTER OF GRAVITY CALCULATED FOR RTG WEIGHT OF 83.45 LBS. THIS WEIGHT INCLUDES JPL POWER CABLE, CLAMPS, NUTS AND SCREWS, ARGON GAS AND SHIPPING BRACKET.

10-59/60

F-7 RTG PERFORMANCE IN LAS

EVENT	$P_{measured}$ Watts (e)	Watts (t)	R_I(3) (Ω)	E_{OC} (Volts)
RTG PROCESSING AT RCA	157.66(1) 157.3 (2)	2401.8	4.718	54.80
LAS PRE-PROCESSING (DOME REMOVED)	82.76(2)	2412	4.340	41.71
LAS PROCESSING (END VACUUM PROCESSING)	161.5 (2)	2412	4.936	56.11
LAS POST-PROCESSING (DOME REMOVED)	84.1 (2)	2412	4.282	41.76
LAS POST-PROCESSING (DOME INSTALLED) 15 PSIA	84.2 (2)	2412	4.403	42.10
25 PSIA	81.4	2412	4.431	41.76

(1) MEASURED AT END OF THERMOPILE
(2) CORRECTED TO RTG CONNECTOR
(3) INCLUDES 0.084 OHMS IN CABLE FOR GE TESTING

F-7 AIR PERFORMANCE SUMMARY

	MAY				JUNE			
	PRE-VIB.			POST VIB.	PRE-VIB.	POST VIB.	START POST T. VAC.	END POST T. VAC.
	①	②	③					
POWER, MEASURED	80.0	80.3	80.3	79.9	78.3	78.5	79.57	79.45
VOLTAGE, MEASURED	29.71	29.71	29.72	29.78	29.71	29.70	29.70	29.71
CURRENT, MEASURED	2.693	2.704	2.703	2.683	2.636	2.644	2.679	2.674
POWER CORRECTED TO 30 VOLTS AT CONNECTOR	80.6	80.9	80.9	80.5	78.9	79.1	80.2	80.0
OPEN CIRCUIT VOLT	42.094	42.189	42.194	42.20	42.194	42.24	41.58	41.80
INTERNAL RESISTANCE MEASURED	4.600	4.164	4.616	4.631	4.737	4.737	4.434	4.521
(CORRECTED TO CONNECTOR)	4.516	4.530	4.532	4.553	4.659	4.666	4.124	4.211
RTD AVERAGE, °C	182	186	177	184	180	180	190	189
RESISTANCE TO CASE	2.1M	2.1M	2.3M	Not Read	445K	420K	540K	501K
V_{OC} TO CASE	13.2V	13.3V	12.3V	Not Read	3.32*	4.56*	10.8	17.8
DATE:	4/29/76 (0100)	5/1/76 (0100)	5/4/76 (0930)	5/7/76 (1105)	6/1/76 (0900)	6/1/76 (1000)	6/9/76 (1700)	6/11/76 (1700)

① START 48 HR.
② END 48 HR.
③ PRE 1ST VIB.

JPL CABLE REPLACED 5/4/76 (2000 HRS).
CABLE CORRECTION TO CONNECTOR = .0837 Ω FOR JPL AND 3500 CABLE.
CABLE CORRECTION TO CONNECTOR = .0779 Ω FOR 2428 GE CABLE.

*BRUSH RECORDER INFLUENCED VALUE OF V_{OC}.

F-7 LAS MONOPOLE DATA PARTIAL PRESSURE (TORR)

SPECIES	4/10/76 t + 8 HRS	4/11/76 t + 27 HRS	4/12/76 t + 50.5 HRS	4/13/76 t + 73 HRS
He	1.3×10^{-7}	1.6×10^{-8}	8.2×10^{-9}	6.1×10^{-9}
H_2O	2.7×10^{-6}	2.2×10^{-6}	1.5×10^{-6}	1.2×10^{-6}
N_2	6.6×10^{-7}	4.2×10^{-7}	5.7×10^{-7}	8.1×10^{-7}
CO	1.6×10^{-7}	2.0×10^{-7}	1.6×10^{-7}	1.2×10^{-7}
O_2	2.5×10^{-7}	1.1×10^{-7}	1.1×10^{-7}	1.2×10^{-7}
Ar	4.2×10^{-5}	3.7×10^{-6}	4.5×10^{-6}	5.4×10^{-6}
CO_2	3.1×10^{-8}	2.0×10^{-8}	1.5×10^{-8}	1.0×10^{-8}
HYDROCARBONS & H_2	1.0×10^{-6}	8.0×10^{-7}	6.6×10^{-7}	5.1×10^{-7}
LAS CHAMBER	9.2×10^{-6}	7.5×10^{-6}	7.5×10^{-6}	8.2×10^{-6}

F-7 VACUUM PERFORMANCE

POWER NORMALIZED TO 2400 WATT HEAT INPUT AND TO RTG CONNECTOR

DATE:	RCA 3/3/76	LAS 4/13/76	POST VIBRATION THERMAL VACUUM 6/8/76
POWER OUTPUT, WATTS:	158.4	160.2	157.8
INTERNAL RESISTANCE, OHMS:	4.718	4.852	4.936
E_{OC}	54.80	56.11	56.12
RESISTANCE TO FOIL:	8K	-----	-----
RESISTANCE TO CASE:	14K	43.3K	5K
RTD AVERAGE, °C:	-----	271°C	265°C
CONVERTER PRESSURE:	-----	-----	6μ

VIBRATION TEST F-7

X-AXIS	R_I	ΔR_I MΩ	E_{OC}	ΔE_{OC} V	P	ΔP W
5/4/76 0930 PRE-1/2G SINE SWEEP	4.616	----	42.19	----	80.33	----
0955 POST	4.617	+1	42.18	-.01	80.40	+ .07
1045 PRE-1/2 LEVEL SINE	4.606	-11	42.17	-.01	80.46	+ .06
1100 POST	4.817	+211	42.26	+.09	77.59	-2.87
5/4/76 2000 REPLACED JPL POWER CABLE WITH GE GSE CABLE						
5/5/76 0900 PRE-FULL LEVEL SINE	4.604	----	42.15	----	80.26	----
0925 POST	4.597	-7	42.16	+.01	80.47	+ .21
1000 PRE-1/3 LEVEL RANDOM	4.606	+9	42.09	-.07	79.87	- .60
1020 POST	4.610	+4	42.09	0	79.68	- .19
5/5/76 1040 POST-FULL LEVEL RANDOM	4.601	-9	42.10	+.01	79.89	+ .21
Z-AXIS						
5/6/76 0900 PRE-1/2G SINE SWEEP	4.629	----	42.23	----	80.19	----
0905 POST	4.628	-1	42.22	-.01	80.18	- .01
0950 PRE-1/2 LEVEL SINE	4.634	+6	42.23	+.01	80.07	- .11
1005 POST	4.633	-1	42.24	+.01	80.14	+ .07
1045 PRE-FULL LEVEL SINE	4.645	+12	42.20	-.04	79.56	- .58
1100 POST	4.638	-7	42.22	+.02	79.87	+ .31
1300 PRE-1/3 LEVEL RANDOM	4.628	-10	42.20	-.02	79.86	- .01
1330 POST	4.645	+17	42.20	0	79.66	- .20
5/6/76 1355 POST-FULL LEVEL RANDOM	4.644	-1	42.22	+.02	79.78	+ .12
Y-AXIS						
5/7/76 0900 PRE-1/2G SINE SWEEP	4.632	----	42.27	----	80.40	----
0913 POST	4.645	+13	42.27	0	80.22	- .18
1000 PRE-1/2 LEVEL SINE	4.629	-16	42.28	+.01	80.43	+ .21
1010 POST	4.645	+16	42.28	0	80.18	- .25
1055 PRE-FULL LEVEL SINE	4.623	-12	42.28	0	80.48	+ .30
5/7/76 1105 POST	4.631	+8	42.20	-.08	79.89	- .59
6/2/76 0900 PRE-1/3 LEVEL RANDOM	4.737	----	42.19	----	78.31	----
6/2/76 0933 POST	4.736	-1	42.23	+.04	78.57	+ .26
6/2/76 1000 POST-FULL LEVEL RANDOM	4.744	+8	42.24	+.01	78.52	- .05

F7 RTG WEIGHT AND BALANCE

MEASURED UNBALANCED MOMENTS IN THE RTG COORDINATE SYSTEM

AXIS	MOMENT (IN-LBS)	CORRECTION (IN-LBS)	CORRECTED MOMENT (IN-LBS)
X	-20.5	+.8	-19.7
Y	+37.3	0	+37.3
Z	-22.8	0	-22.8

RTG WEIGHT

TOTAL WEIGHT (RTG, FIXTURE & EQUIPMENT)		125.00 LBS.
FIXTURE	37.38 LBS.	
RTD EXTENSION CABLE	.65 LBS.	
POWER OUTPUT EXTENSION CABLE	.77 LBS.	
SHORTING MODULE	1.27 LBS.	
RTG GMV FLEX LINE	.62 LBS.	
	40.69 LBS.	40.69 LBS.
		84.31 LBS. [1]

[1] IN ADDITION TO .52 LBS. JPL POWER CABLE, WEIGHT SHOWN INCLUDES:

[2] CLAMPS, NUTS, SCREWS & MISC.	.13 LBS.	
[3] ARGON GAS	.10 LBS.	
[2] SHIPPING BRACKET	.67 LBS.	
	.90 LBS.	- .90 LBS.
[3] XENON GAS	.22 LBS.	+ .22 LBS.
FLIGHT WEIGHT:		83.63 LBS.

F7 RTG WEIGHT AND BALANCE (CONT'D)

RTG CENTER OF GRAVITY COORDINATES*

X = -0.17
Y = -9.52
Z = -0.27

[1] CENTER OF GRAVITY CALCULATED FOR RTG WEIGHT OF 84.31 LBS. THIS WEIGHT INCLUDES JPL POWER CABLE, CLAMPS, NUTS AND SCREWS, ARGON GAS AND SHIPPING BRACKET.

[2] SHIPPING BRACKET (0.67 LBS.) AND MISCELLANEOUS HARDWARE (0.13 LBS.) COORDINATES ARE:

X = - 4.51
Y = -14.86
Z = - 7.81

[3] WEIGHT OF XENON GAS (AT LAUNCH) IS 0.22 POUNDS.

*THE Y-AXIS IS THE LONGITUDINAL AXIS WITH +Y BEING TOWARD THE UNIBALL END, THE Z-AXIS IS NORMAL TO THE Y-AXIS AND IS CONTAINED IN THE LONGITUDINAL PLANE DEFINED BY THE Y-AXIS AND THE CENTERLINE OF THE RTG ELECTRICAL OUTPUT CONNECTOR. Z IS NEGATIVE IN THE DIRECTION OF THE CONNECTOR. THE X-AXIS IS NORMAL TO THE Y AND Z AXES. THE X-Z PLANE IS DEFINED BY THE CENTERLINE OF THE SELF-ALIGNING BEARINGS.

THE SPECIFICATION WEIGHT OF 83.50 POUNDS FOR THE MJS RTG'S WAS DERIVED AS A BEST ESTIMATE BASED ON THE WEIGHTS OF THE LES 8/9 RTG'S WITH THE IRIDIUM CLAD REMOVED. SPECIFICATIONS FOR GRAPHITE REQUIRE A MINIMUM DENSITY. ANALYSIS OF THE GRAPHITE PARTS FOR THE F7 RTG SHOWS THAT THE FORWARD END CAP, THE AEROSHELL AND ABLATIVE SLEEVE ARE THE HEAVIES ACCEPTED FOR THE PROGRAM. BASED ON WEIGHTS OBTAINED DURING FIT CHECKS THROUGH F10 PARTS, THE PREDICTED WEIGHT OF THE REMAINING RTG SHOULD BE APPROXIMATELY 9.2 POUNDS LIGHTER THAN THE F7.

F-8 RTG PERFORMANCE IN LAS

EVENTS	$P_{MEASURED}$ WATTS (e)	Q WATTS (t)	R_I (3) OHMS	E_{oc} VOLTS
ETG PROCESSING	157.6 (1) 157.2 (2)	2404	4.794	55.2
LAS PRE-PROCESSING (DOME REMOVED)	81.3 (2)	2407	4.378	41.61
LAS PROCESSING (END VACUUM PROCESSING)	159.7 (2)	2407	4.952	55.94
LAS POST-PROCESSING (DOME REMOVED)	81.1 (2)	2407	4.370	41.55
LAS POST-PROCESSING (DOME INSTALLED)				
ARGON 15 PSIA	83.0 (2)	2407	4.492	42.13
ARGON 25 PSIA	80.2	2407	4.498	41.75

(1) MEASURED AT END OF THERMOPILE

(2) CORRECTED TO RTG CONNECTOR

(3) INCLUDES .077 OHMS IN CABLE

F-8 VACUUM POWER SUMMARY

POWER NORMALIZED TO 2400 WATTS HEAT INPUT AND TO RTG CONNECTOR

	RCA	LAS	POST VIBRATION THERMAL VACUUM
DATE:	4/25/76	6/25/76	7/13/76
POWER OUTPUT, WATTS:	158.3	159.0	157.9
INTERNAL RESISTANCE, OHMS:	4.813	4.875	4.894
OPEN CIRCUIT VOLTAGE, VOLTS:	55.20	55.94	55.85
RESISTANCE TO FOIL:	18.5K	-------	-------
RESISTANCE TO CASE:	31K	60.4K	7.7K
RTD AVERAGE, °C:	-------	268°C	262°C
CONVERTER PRESSURE:	-------	-------	4.7μ

F-8 LAS PROCESSING MONOPOLE DATA
PARTIAL PRESSURE (TORR)

SPECIES	0900 6/24/76 t + 18 HOURS	0840 6/25/76 t + 41.5 HOURS
He	2.2×10^{-8}	8.4×10^{-9}
H_2O	2.8×10^{-6}	1.0×10^{-6}
N_2	6.0×10^{-8}	5.6×10^{-8}
CO	4.4×10^{-8}	4.4×10^{-8}
O_2	1.3×10^{-8}	1.1×10^{-8}
Ar	5.7×10^{-6}	7.2×10^{-6}
CO_2	2.0×10^{-9}	2.1×10^{-9}
H_2 & HYDROCARBONS	3.3×10^{-7}	2.1×10^{-7}
CHAMBER	8.5×10^{-6}	8.5×10^{-6}

VIBRATION TEST F-8

X-AXIS	R_I	ΔR_I MΩ	E_{OC}	ΔE_{OC} V	P	ΔP W
7/6/76						
(1000) PRE SINE SWEEP	4.559	----	41.873	----	79.22	----
(1030) POST SINE SWEEP	4.554	- 5	41.903	+.030	79.56	+.34
(1130) PRE "X" 3.18G RMS RANDOM	4.554	0	41.912	+.009	79.60	+.43
(1140) POST "X" 3.18G RMS RANDOM	4.546	- 8	91.879	-.033	79.52	-.08
(1140) PRE ACCEPTANCE RANDOM	4.546	0	41.879	0	79.52	0
(1200) POST "X" ACCEPTANCE LEVEL	4.548	+ 2	41.887	+.008	79.56	+.04
Z-AXIS						
7/7/76						
(0900) PRE SINE SWEEP	4.560	----	41.909	-----	79.50	----
(0925) POST SINE SWEEP	5.569	+ 9	41.922	+.013	79.38	-.12
(1045) PRE 3.18G RMS RANDOM	4.558	-11	41.919	-.003	79.54	+.16
(1055) POST 3.18G RMS RANDOM	4.570	+12	41.936	+.017	79.43	-.11
(1055) PRE FULL LEVEL RANDOM	4.570	0	41.936	0	79.43	0
(1105) POST FULL LEVEL RANDOM	4.568	- 2	41.950	+.014	79.55	+.12
Y-AXIS						
7/8/76						
(0930) PRE "Y" AXIS SINE SWEEP	4.568	----	41.971	----	79.69	----
(0945) POST "Y" AXIS SINE SWEEP	4.570	+ 2	41.957	-.014	79.61	-.08
(1015) PRE "Y" 3.18G RMS RANDOM	4.998	-72	41.768	-.189	79.69	+.08
(1025) POST 3.18G RMS RANDOM	4.569	+71	41.983	+.216	79.84	+.15
(1040) PRE "Y" AXIS FULL LEVEL	4.567	- 2	41.965	-.021	79.72	-.12
(1050) POST "Y" AXIS FULL LEVEL	4.567	0	41.979	+.014	79.79	+.07

F8 RTG WEIGHT AND BALANCE

MEASURED UNBALANCED MOMENTS IN THE RTG COORDINATE SYSTEM

AXIS	MOMENT (IN-LBS)	CORRECTION (IN-LBS)	CORRECTED MOMENT (IN-LBS)
X	-17.8	0	-17.8
Y	+50.0	0	+50.0
Z	-23.8	0	-23.8

RTG WEIGHT

TOTAL WEIGHT (RTG, FIXTURE & EQUIPMENT)		124.82 LBS.
FIXTURE	37.36[1] LBS.	
RTD EXTENSION CABLE	.63 LBS.	
POWER OUTPUT CABLE	1.22 LBS.	
SHORTING MODULE	1.51 LBS.	
RTG GMV FLEX LINE	.64 LBS.	
	41.16 LBS.	- 41.16 LBS.
		83.66 LBS.

[1] AVERAGE OF THREE WEIGHING OF FIXTURE.

[2] WEIGHT SHOWN INCLUDES:

[3] CLAMPS, NUTS, SCREWS & MISC.	.14 LBS.	
ARGON GAS	.10 LBS.	
[3] SHIPPING BRACKET	.67 LBS.	
PRD PROTECTIVE PLATE	.61 LBS.	
THREAD SAVER	.07 LBS.	
	1.59 LBS.	- 1.59 LBS.
[4] XENON GAS	.22 LBS.	
[5] JPL POWER CABLE	.52 LBS.	
PRD	.69 LBS.	
	1.43 LBS.	+ 1.43 LBS.
	FLIGHT WEIGHT:	83.50 LBS.

F8 RTG WEIGHT AND BALANCE (CONT'D)

RTG CENTER OF GRAVITY COORDINATES*

X = -0.18
Y = -9.54
Z = -0.27

[2] CENTER OF GRAVITY CALCULATED FOR RTG WEIGHT OF 83.66 LBS. THIS WEIGHT INCLUDES CLAMPS, NUTS AND SCREWS, ARGON GAS, SHIPPING BRACKET, PRD PROTECTIVE PLATE AND THREAD SAVER.

[3] SHIPPING BRACKET (0.67 LBS.) AND MISCELLANEOUS HARDWARE (0.13 LBS.) COORDINATES ARE:

X = - 4.51
Y = -14.86
Z = - 7.81

[4] WEIGHT OF XENON GAS (AT LAUNCH) IS 0.22 POUNDS.

[5] JPL POWER CABLE NOT AVAILABLE FOR F-8 MEASUREMENTS.

*THE Y-AXIS IS THE LONGITUDINAL AXIS WITH +Y BEING TOWARD THE UNIBALL END. THE Z-AXIS IS NORMAL TO THE Y-AXIS AND IS CONTAINED IN THE LONGITUDINAL PLANE DEFINED BY THE Y-AXIS AND THE CENTERLINE OF THE RTG ELECTRICAL OUTPUT CONNECTOR. Z IS NEGATIVE IN THE DIRECTION OF THE CONNECTOR. THE X-AXIS IS NORMAL TO THE Y AND Z AXES. THE X-Z PLANE IS DEFINED BY THE CENTERLINES OF THE SELF-ALIGNING BEARINGS.

F8 RTG WEIGHT AND BALANCE (CONT'D)

RTG CENTER OF GRAVITY COORDINATES*

X = - .54
Y = - 9.54
Z = - .27

[2] Center of Gravity calculated for RTG weight of 83.66 lbs. This weight includes Clamps, Nuts and Screws, Argon Gas, Shipping Bracket, PRD Protective Plate and Thread Saver.

[3] Shipping Bracket (.67 lbs.) and miscellaneous hardware (.13 lbs.) coordinates are:

X = - 4.51
Y = - 14.86
Z = - 7.81

[4] Weight of Xenon Gas (at launch) is .22 pounds.

[5] JPL Power Cable not available for F-8 measurements.

*The Y-axis is the longitudinal axis with +Y being toward the uniball end. The Z-axis is normal to the Y-axis and is contained in the longitudinal plane defined by the Y-axis and the centerline of the RTG electrical output connector. Z is negative in the direction of the connector. The X-axis is normal to the Y and Z axes. The X-Z plane is defined by the centerlines of the self-aligning bearings.

F-8 AIR PERFORMANCE SUMMARY

	PRESSURE DECAY TEST START	PRESSURE DECAY TEST END	PRE VIB.	POST VIB.	PRESSURE DECAY TEST START	PRESSURE DECAY TEST END
POWER, MEASURED	79.5	79.1	79.2	79.8	79.6	79.4
VOLTAGE, MEASURED	29.70	29.70	29.72	29.71	29.69	29.70
CURRENT, MEASURED	2.6772	2.663	2.666	2.686	2.682	2.675
POWER CORRECTED TO 30V AT CONNECTOR	80.0	79.6	79.7	80.4	80.2	80.0
OPEN CIRCUIT VOLTAGE	41.61	41.63	41.87	41.98	41.41	41.67
INTERNAL RESISTANCE MEASURED	4.448	4.480	4.559	4.567	4.372	4.476
CORRECTED TO CONNECTOR*	4.371	4.430	4.482	4.490	4.195	4.399
RTD AVERAGE, °C	174	178	183	184	188	190
RESISTANCE TO CASE	785K	791K	781K	257K	470K	462K
V_{OC} TO CASE	26.2	26.3	26.2	26.2	19.2	19.6
DATE/TIME:	6/30/76 (2200)	7/2/76 (2200)	7/6/76 (1000)	7/8/76 (1030)	7/14/76 (2100)	7/16/76 (2100)

*CABLE CORRECTION TO RTG CONNECTOR = 0.077 OHMS.

F-9 RTG PERFORMANCE IN LAS WITH F-9 IHS

EVENT	$P_{MEASURED}$ (WATTS (e))	Q (WATTS (t))	R_1 (OHMS)	E_{OC} (VOLTS)
ETG PROCESSING AT RCA	156.95 [1] 156.55 [2]	2394	4.754 [1]	55.12
LAS PRE-PROCESSING (DOME REMOVED) (7/27/76 @ 1400)	81.4 [2]	2407.6	4.378 [3]	41.708
LAS PROCESSING (END VACUUM PROCESSING) (7/29/76 @ 1500)	160.8 [2]	2407.5	4.968 [3]	56.2
LAS POST-PROCESSING (DOME INSTALLED)				
ARGON 15 PSIA (8/2/76 @ 0100)	84.0 [2]	2407.4	4.534 [3]	42.43
ARGON 25 PSIA (8/2/76 @ 1300)	81.4 [2]	2407.4	4.531 [3]	42.05

[1] MEASURED AT END OF THERMOPILE
[2] CORRECTED TO RTG CONNECTOR
[3] INCLUDES .075 OHMS IN CABLE

LAS VACUUM POWER NORMALIZED TO 2400W = 160 WATTS

F-9 RTG PERFORMANCE IN LAS WITH F-10 IHS

EVENT	$P_{MEASURED}$ (WATTS (e))	Q (WATTS (t))	R_1 (OHMS)	E_{OC} (VOLTS)
LAS PRE-PROCESSING (DOME REMOVED) (9/22/76 @ 1700)	83.5	2409.3	4.811	43.13
LAS PROCESSING (END VACUUM PROCESSING) (9/24/76 @ 1730)	159.5	2409.2	5.027	56.32
LAS POST-PROCESSING (DOME INSTALLED)				
ARGON 15 PSIA (9/25/76 @ 0945)	83.9	2409.2	4.437	42.16
ARGON 25 PSIA (9/25/76 @ 2100)	81.2		4.469	41.84

LAS VACUUM POWER NORMALIZED TO 2400W = 158.6 WATTS.

F-9 LAS REWORK PROCESSING MONOPOLE DATA
PARTIAL PRESSURE (TORR) (WITH F-10 IHS)

SPECIES	0920-1000 9/22/76 t + 16 HOURS	0845-0920 9/24/76 t + 40 HOURS
CHAMBER	1.2×10^{-5}	1.1×10^{-5}
He	5.0×10^{-8}	9.0×10^{-9}
H_2O	2.8×10^{-6}	1.4×10^{-6}
N_2	2.1×10^{-7}	1.4×10^{-7}
CO	4.0×10^{-8}	1.8×10^{-8}
O_2	3.7×10^{-8}	2.9×10^{-8}
Ar	8.5×10^{-6}	9.2×10^{-6}
CO_2	4.6×10^{-9}	3.9×10^{-9}
H_2 & HYDROCARBONS	3.6×10^{-7}	1.6×10^{-7}

STARTED CHAMBER PUMPDOWN 9/22/76 @ 1720.

F-9 LAS PROCESSING MONOPOLE DATA
PARTIAL PRESSURE (TORR)

SPECIES	1005-1100 7/28/76 t + 19 HOURS	0845-0935 7/29/76 t + 42 HOURS
CHAMBER	2.3×10^{-6}	1.0×10^{-6}
He	3.3×10^{-8}	7.3×10^{-9}
H_2O	1.8×10^{-6}	7.9×10^{-7}
N_2	8.6×10^{-8}	6.0×10^{-8}
CO	1.8×10^{-8}	6.9×10^{-9}
O_2	1.6×10^{-8}	1.1×10^{-8}
Ar	1.6×10^{-7}	5.8×10^{-8}
CO_2	4.0×10^{-9}	2.2×10^{-9}
H_2 & HYDROCARBONS	1.6×10^{-7}	7.0×10^{-8}

STARTED CHAMBER PUMPDOWN 7/27/76 @ 1450.

F-9 VACUUM POWER SUMMARY

POWER NORMALIZED TO 2400 WATTS HEAT INPUT
AND TO RTG CONNECTOR

	RCA	LAS [1]	LAS [2]	POST VIBRATION THERMAL VACUUM
DATE:	6/29/76	7/29/76	9/24/76	10/7/76
POWER OUTPUT, WATTS	158.3	160.0	158.6	158.0
INTERNAL RESISTANCE, OHMS:	4.808	4.891	4.952	4.961
OPEN CIRCUIT VOLTAGE, VOLTS:	55.12	56.20	56.32	56.31
RESISTANCE TO FOIL:	22K	-----	-----	-----
RESISTANCE TO CASE:	158K	86.9K	106K	66.5K
RTD AVERAGE, ^{o}C:	-----	266	265	259
CONVERTER PRESSURE:	-----	-----	-----	4.3μ

[1] F-9 IHS
[2] F-10 IHS

F-9 AIR PERFORMANCE SUMMARY

	48 HOUR PRESSURE DECAY TEST START	48 HOUR PRESSURE DECAY TEST END	PRE VIB.	POST VIB.	48 HOUR PRESSURE DECAY TEST START	48 HOUR PRESSURE DECAY TEST END
POWER, MEASURED	79.98	80.2	80.5	79.9	79.5	79.9
VOLTAGE, MEASURED	29.71	29.70	29.74	29.75	29.70	29.70
CURRENT, MEASURED	2.692	2.701	2.708	2.687	2.676	2.692
POWER CORRECTED TO 30V AT CONNECTOR	80.53	80.9	81.2	80.6	80.2	80.6
OPEN CIRCUIT VOLTAGE	41.79	42.01	42.04	42.10	41.65	42.0
INTERNAL RESISTANCE MEASURED	4.486	4.561	4.544	4.596	4.467	4.569
INTERNAL RESISTANCE CORRECTED TO CONNECTOR*	4.411 (1)	4.466 (2)	4.459 (2)	4.511 (1)	4.369 (4)	4.471 (4)
RTD AVERAGE, ^{o}C	182	186	179	181	188	187
RESISTANCE TO CASE	774K	765K	769K	753K	3.1M	3.1M
V_{OC} TO CASE, VOLTS	26.1	26.1	26.2	26.2	11.9	12.3
DATE/TIME:	9/27/76 (2100)	9/29/76 (2100)	9/30/76 (0530)	10/1/76 (0506)	10/8/76 (0900)	10/10/76 (0900)

*CABLE CORRECTION TO RTG CONNECTOR = (1) .075 OHMS 24ZS CABLE WITH SHORTING MODULE
(2) .095 OHMS 3500 CABLE WITH SHORTING MODULE
(3) .085 OHMS 3500 CABLE WITHOUT SHORTING MODULE
(4) .098 OHMS 3500 CABLE WITH SHORTING MODULE

F9 RTG WEIGHT AND BALANCE

MEASURED UNBALANCED MOMENTS
IN THE RTG COORDINATE SYSTEM

AXIS	MOMENT (IN-LBS)	CORRECTION (IN-LBS)	CORRECTED MOMENT (IN-LBS)
X	- 20.0	.5	- 19.5
Y	+ 47.0	0	+ 47.0
Z	- 18.0	0	- 18.0

RTG WEIGHT

TOTAL WEIGHT (RTG, FIXTURE AND EQUIPMENT)		124.63 LBS.
FIXTURE	37.34 LBS.	
RTD EXTENSION CABLE	.63 LBS.	
POWER OUTPUT CABLE	1.22 LBS.	
SHORTING MODULE	1.33 LBS.	
RTG GMV FLEX LINE	.61 LBS.	
	41.13 LBS.	- 41.13 LBS.
		83.50 LBS.

[1] WEIGHT SHOWN INCLUDES:

[2] CLAMPS, NUTS, SCREWS AND MISC.	.12 LBS.	
ARGON GAS	.10 LBS.	
[2] SHIPPING BRACKET	.68 LBS.	
PRD PROTECTIVE PLATE	.61 LBS.	
THREAD SAVER	.07 LBS.	
	1.58 LBS.	- 1.58 LBS.
[3] XENON GAS	.22 LBS.	
JPL POWER CABLE	.55 LBS.	
PRD	.69 LBS.	
	1.46 LBS.	+ 1.46 LBS.

FLIGHT WEIGHT: 83.38 LBS.

F9 RTG WEIGHT AND BALANCE (CONTINUED)

RTG CENTER OF GRAVITY COORDINATES*

X = - .20
Y = - 9.97
Z = - .20

[1] CENTER OF GRAVITY CALCULATED FOR RTG WEIGHT OF 83.50 LBS. THIS WEIGHT INCLUDES CLAMPS, NUTS AND SCREWS, ARGON GAS, SHIPPING BRACKET/ PRD PROTECTIVE PLATE AND THREAD SAVER.

[2] SHIPPING BRACKET (.68 LBS.) AND MISCELLANEOUS HARDWARD (.12 LBS.) COORDINATES ARE:

X = - 4.51
Y = -14.86
Z = - 7.81

[3] WEIGHT OF XENON GAS (AT LAUNCH) IS .22 POUNDS.

* THE Y-AXIS IS THE LONGITUDINAL AXIS WITH +Y BEING TOWARD THE UNIBALL END. THE Z-AXIS IS NORMAL TO THE Y-AXIS AND IS CONTAINED IN THE LONGITUDINAL PLANE DEFINED BY THE Y-AXIS AND THE CENTERLINE OF THE RTG ELECTRICAL OUTPUT CONNECTOR. Z IS NEGATIVE IN THE DIRECTION OF THE CONNECTOR. THE X-AXIS IS NORMAL TO THE Y AND Z AXES. THE X-Z PLANE IS DEFINED BY THE CENTERLINES OF THE SELF-ALIGNING BEARINGS.

VIBRATION TEST F-9

DATE/TIME		R_1 OHMS	R_1 MΩ	E_{OC} VOLTS	E_{OC} MV	RTD ^{o}C	P WATTS	P WATTS	R_{CASE} K OHMS
9/30/76	X-AXIS								
0530	PRE SINE SWEEP	4.544		42.044		179	81.18		769
0545	POST SINE SWEEP	4.539	- 5	42.056	+12	179	81.28	+.1	740
	PRE 3.1SG RANDOM								
0636	POST 3.1SG RANDOM	4.537	- 2	42.025	-31	179	81.13	-.15	709
0900	PRE ACCEPTANCE RANDOM	4.539	+ 2	42.001	-24	179	80.99	-.14	771
9/30/76	Z-AXIS								
1500	PRE SINE SWEEP	4.550	+ 4	41.993	-19	177	81.03	+.13	828
1532	POST SINE SWEEP	4.552	+ 2	41.995	+ 2	177	81.05	+.02	792
1730	PRE 3.1SG RANDOM	4.554	+ 2	41.989	- 6	177	80.78	-.27	822
	POST 3.1SG RANDOM								
	PRE ACCEPTANCE RANDOM								
1745	POST ACCEPTANCE RANDOM	4.565	+11	42.002	+13	177	80.71	-.07	820
10/1/76	Y-AXIS								
0400	PRE SINE SWEEP	4.581	+16	42.088	-14	182	80.77	+.06	824
0412	POST SINE SWEEP	4.581	0	42.089	+ 1	182	80.84	+.07	798
0453	PRE 3.1SG RANDOM	4.588	+ 7	42.094	+ 5	182	80.68	-.16	---
	POST 3.1SG RANDOM								
	PRE ACCEPTANCE RANDOM								
0506	POST ACCEPTANCE RANDOM	4.596	+ 8	42.102	+ 8	181	80.56	-.12	753

F-10 RTG PERFORMANCE IN THE LAS

	POWER MEASURED (WATTS)	HEAT INPUT (WATTS)	INTERNAL RESISTANCE (OHMS)	OPEN CIRCUIT VOLTAGE (VOLTS)
ETG PROCESSING AT RCA	157.1(1) 156.7(3)	2402.4	4.798	55.12
LAS PRE-PROCESSING (DOME REMOVED) 10/20/76 (1000)	83.8(2) 84.4(3)	2409.6	4.397	41.98
LAS PROCESSING (END OF VACUUM PROCESSING 10/22/76 (10o0)	159.69(2) 161.93(3)	2409.5	4.948	56.29
LAS POST-PROCESSING (DOME REMOVED) 10/22/76 (2200)	84.4(2) 85.0(3)	2409.5	4.338	42.03
LAS POST-PROCESSING (DOME INSTALLED)				
ARGON 15 PSIA (10/25/76) (0600)	86.20(2) 86.85(3)	2409.4	4.527	42.85
ARGON 25 PSIA (10/25/76) (2100)	83.63(2) 84.24(3)	2409.4	4.536	42.48

(1) MEASURED AT END OF THERMOPILE.

(2) MEASURED AT CABLE VOLTAGE TAP LOCATION.

(3) CORRECTED TO RTG CONNECTOR.

F-10 LAS PROCESSING MONOPOLE DATA
PARTIAL PRESSURE (TORR)

SPECIES	1530-1620 10/20/76 T + 6 HOURS	1240-1410 10/21/76 T + 28 HOURS	0730-0800 10/22/76 T + 46 HOURS
CHAMBER	7.5×10^{-6}	4.0×10^{-6}	3.2×10^{-6}
He	3.3×10^{-7}	3.9×10^{-8}	2.1×10^{-8}
H_2O	5.2×10^{-6}	2.8×10^{-6}	1.8×10^{-6}
N_2	3.2×10^{-7}	4.2×10^{-7}	5.4×10^{-7}
CO	5.7×10^{-8}	2.1×10^{-8}	1.6×10^{-8}
O_2	6.3×10^{-8}	7.6×10^{-8}	8.5×10^{-8}
Ar	9.5×10^{-7}	4.6×10^{-7}	5.1×10^{-7}
CO_2	2.6×10^{-8}	1.2×10^{-8}	7.7×10^{-9}
H_2 AND HYDROCARBONS	5.8×10^{-7}	3.4×10^{-7}	2.4×10^{-7}

STARTED CHAMBER PUMPDOWN ON 10/20/76 AT 1000 HOURS.

F-10 VACUUM POWER SUMMARY

POWER NORMALIZED TO 2400W HEAT
INPUT AND TO RTG CONNECTOR

DATE	RCA	LAS	POST VIBRATION THERMAL VACUUM
POWER OUTPUT, WATTS	157.7	160.9	160.4
INTERNAL RESISTANCE, OHMS	4.812	4.872	4.884
OPEN CIRCUIT VOLTAGE, VOLTS	55.12	56.29	56.26
RESISTANCE TO FOIL	22K	-----	-----
RESISTANCE TO CASE	130K	155K	107K
RTD AVERAGE, °C	-----	267	260
CONVERTER PRESSURE	-----	-----	4μ

VIBRATION TEST F-10

		R_I OHMS	ΔR_I MΩ	E_{OC} VOLTS	E_{OC} MV	P(1) WATTS	ΔP WATTS	RTD °C	R_{CASE} KΩ
11-1-76	X-AXIS								
1100	PRE SINE SWEEP	4.559		42.52		84.04		173	3M
1128	POST SINE SWEEP	4.556		42.50	-20	83.86	-.18	173	4.5M
1330	PRE 3.18G RANDOM	4.559	+3	42.45	-50	83.62	-.24	174	3.1M
1406	POST 3.18G RANDOM	4.569	+10	42.43	-20	83.26	-.36	175	5.1M
1428	POST ACCEPTANCE RANDOM	4.557	-12	----	---	83.44	+.18	175	5.8M
11-2-76	Z-AXIS								
0900	PRE SINE SWEEP	4.555		42.44	+10	83.76	+.32	173	4.2M
0940	POST SINE SWEEP	4.560	+5	42.45	+10	83.76	0	173	4.6M
1010	PRE 3.18G RANDOM	4.558	-2	42.45	0	83.79	+.03	173	4.4M
1032	POST 3.18G RANDOM	4.559	+1	42.44	+1	83.67	-.12	173	2.4M
1120	PRE ACCEPTANCE RANDOM	4.562	+3	42.43	+3	83.58	-.09	174	2.2M
1130	POST ACCEPTANCE RANDOM	4.559	-3	42.44	-3	83.66	+.08	174	2.4M
11-3-76	Y-AXIS								
0945	PRE SINE SWEEP	4.576		42.54	+10	83.89	+.23	176	3.9M
1005	POST SINE SWEEP	4.587	+11	42.54	0	83.71	-.18	176	4.0M
1100	PRE 3.18G RANDOM	4.583	-4	42.54	0	83.79	+.08	176	4.3M
1125	POST 3.18G RANDOM	4.577	-6	42.53	-10	83.80	+.01	176	4.4M
1140	POST ACCEPTANCE	4.585	+8	42.53	0	83.64	-.16	176	1.7M

(1) POWER CORRECTED TO RTG CONNECTOR.

F-10 AIR PERFORMANCE SUMMARY

	48 HOUR PRESSURE DECAY TEST START	48 HOUR PRESSURE DECAY TEST END	PRE VIB.	POST VIB.	48 HOUR PRESSURE DECAY TEST START	48 HOUR PRESSURE DECAY TEST END
POWER, MEASURED	82.74	82.56	83.36	82.96	82.94	83.02
VOLTAGE, MEASURED	29.73	29.69	29.75	29.73	29.70	29.70
CURRENT, MEASURED	2.783	2.781	2.802	2.790	2.793	2.795
POWER CORRECTED TO 30V AT CONNECTOR	83.51	83.23	84.04	83.64	83.72	83.80
OPEN CIRCUIT VOLTAGE	42.18	42.28	42.50	42.53	42.02	42.29
INTERNAL RESISTANCE MEASURED	4.471	4.528	4.559	4.585	4.411	4.503
CORRECTED TO CONNECTOR*	4.371(1)	4.441(2)	4.472(2)	4.496(2)	4.311(1)	4.403(1)
RTD AVERAGE, °C	174	175	173	176	189	186
RESISTANCE TO CASE	826K	3MEG	3MEG	1.1MEG	3.9MEG	4.2MEG
V_{OC} TO CASE, VOLTS	26.4	13.5	13.5	13.95	10.1	9.8
DATE/TIME:	10/27/76 (1200)	10/29/76 (1200)	11/1/76 (1100)	11/3/76 (1140)	11/9/76 (2400)	11/11/76 (2400)

* CABLE CORRECTION TO RTG CONNECTOR = (1) .100 OHMS J. P. L. + 3500 CABLE WITH SHORTING MODULE
(2) .087 OHMS J. P. L. + 3500 CABLE WITHOUT SHORTING MODULE

F10 RTG WEIGHT AND BALANCE

MEASURED UNBALANCED MOMENTS
IN THE RTG COORDINATE SYSTEM

AXIS	MOMENT (IN-LBS)	CORRECTION (IN-LBS)	CORRECTED MOMENT (IN-LBS)
X	-17.3	0	-17.3
Y	+46.9	0	+46.9
Z	-18.6	0	-18.6

RTG WEIGHT

TOTAL WEIGHT (RTG, FIXTURE & EQUIPMENT)		124.53 LBS.
FIXTURE	37.39 LBS.	
RTD EXTENSION CABLE	.63 LBS.	
POWER OUTPUT CABLE	1.26 LBS.	
SHORTING MODULE	1.32 LBS.	
RTG GMV FLEX LINE	.61 LBS.	
	41.21 LBS.	-41.21 LBS.
		83.32 LBS.

[1]WEIGHT SHOWN INCLUDES:

[2]CLAMPS, NUTS, SCREWS & MISC.	.09 LBS.	
ARGON GAS	.10 LBS.	
[2]SHIPPING BRACKET	.68 LBS.	
PRD PROTECTIVE PLATE	.61 LBS.	
THREAD SAVER	.06 LBS.	
	1.54 LBS.	- 1.54 LBS.
[3]XENON GAS	.22 LBS.	
JPL POWER CABLE	.55 LBS.	
PRD	.69 LBS.	
	1.46 LBS.	+ 1.46 LBS.
FLIGHT WEIGHT:		83.24 LBS.

F10 RTG WEIGHT AND BALANCE (CONT'D)

RTG CENTER OF GRAVITY COORDINATES*

X = -0.18
Y = -9.58
Z = -0.21

[1]CENTER OF GRAVITY CALCULATED FOR RTG WEIGHT OF 83.32 LBS. THIS WEIGHT INCLUDES CLAMPS, NUTS AND SCREWS, ARGON GAS, SHIPPING BRACKET, PRD PROTECTIVE PLATE AND THREAD SAVER.

[2]SHIPPING BRACKET (0.68 LBS.) AND MISCELLANEOUS HARDWARE (0.09 LBS.) COORDINATES ARE:

X = - 4.51
Y = -14.86
Z = - 7.81

[3]WEIGHT OF XENON GAS (AT LAUNCH) IS 0.22 POUNDS.

*THE Y-AXIS IS THE LONGITUDINAL AXIS WITH +Y BEING TOWARD THE UNIBALL END. THE Z-AXIS IS NORMAL TO THE Y-AXIS AND IS CONTAINED IN THE LONGITUDINAL PLANE DEFINED BY THE Y-AXIS AND THE CENTERLINE OF THE RTG ELECTRICAL OUTPUT CONNECTOR. Z IS NEGATIVE IN THE DIRECTION OF THE CONNECTOR. THE X-AXIS IS NORMAL TO THE Y AND Z AXES. THE X-Z PLANE IS DEFINED BY THE CENTERLINES OF THE SELF-ALIGNING BEARINGS.

F-11 RTG PERFORMANCE IN THE LAS

	POWER MEASURED (WATTS)	HEAT INPUT (WATTS)	INTERNAL RESISTANCE (OHMS)	OPEN CIRCUIT VOLTAGE (VOLTS)
ETG PROCESSING	158.1 (1)	2403.8	4.801 (1)	55.32
AT RCA	157.7 (3)		4.817 (3)	
LAS PRE-PROCESSING*	85.3 (2)	2402.5	4.483 (2)	42.58
(DOME REMOVED) 1/10/77 (1100)	85.9 (3)		4.410 (3)	
LAS PROCESSING	159.69 (2)	2402.4	4.957 (2)	56.32
(END OF VACUUM PROCESSING) 1/12/77 (1200)	161.76 (3)		4.884 (3)	
LAS POST-PROCESSING*	84.5 (2)	2402.4	4.342 (2)	42.11
(DOME REMOVED) 1/12/77 (2100)	85.4 (3)		4.269 (3)	
LAS POST-PROCESSING (DOME INSTALLED)				
ARGON 15 PSIA (1/13/77) (0100)	85.58 (2) 86.19 (3)	2402.4	4.378 (2) 4.305 (3)	42.30
ARGON 25 PSIA (1/13/77) (1600)	82.93 (2) 83.5 (3)	2402.4	4.422 (2) 4.349 (3)	42.04

*RTG NOT COMPLETELY STABILIZED.

(1) MEASURED AT END OF THERMOPILE.

(2) MEASURED AT CABLE VOLTAGE TAP LOCATION.

(3) CORRECTED TO RTG CONNECTOR.

F-11 LAS PROCESSING MONOPOLE DATA PARTIAL PRESSURE (TORR)

SPECIES	1525-1600 1/10/77 T + 4 HOURS	0845-0930 1/11/77 T + 22 HOURS	0845-0925 1/12/77 T + 46 HOURS
CHAMBER	8.0×10^{-6}	3.0×10^{-6}	2.1×10^{-6}
He	1.6×10^{-7}	5.1×10^{-8}	1.6×10^{-8}
H_2O	5.1×10^{-6}	1.9×10^{-6}	1.2×10^{-6}
N_2	2.1×10^{-7}	2.1×10^{-7}	2.3×10^{-7}
CO	1.2×10^{-7}	2.1×10^{-8}	1.4×10^{-8}
O_2	4.5×10^{-8}	4.7×10^{-8}	4.9×10^{-8}
Ar	1.4×10^{-6}	4.2×10^{-7}	2.8×10^{-7}
CO_2	8.0×10^{-9}	1.7×10^{-9}	9.9×10^{-10}
Hc & HYDROCARBONS	9.5×10^{-7}	4.0×10^{-7}	2.8×10^{-7}

STARTED CHAMBER PUMPDOWN ON 1/10/77 @ 1130 HOURS.

F-11 VACUUM POWER SUMMARY

POWER NORMALIZED TO 2400W HEAT INPUT AND TO RTG CONNECTOR

	RCA	LAS	POST VIBRATION THERMAL VACUUM
DATE	10/15/76	1/12/77	2/01/77
POWER OUTPUT, WATTS	158.6	161.5	160.4
INTERNAL RESISTANCE, OHMS	4.817	4.884	4.915
OPEN CIRCUIT VOLTAGE, VOLTS	55.32	56.32	56.28
RESISTANCE TO FOIL	23K	-------	-------
RESISTANCE TO CASE	49K	59.8K	129K
RTD AVERAGE, °C	------	265	257
CONVERTER PRESSURE	------	------	6μ

F11 RTG WEIGHT AND BALANCE

MEASURED UNBALANCED MOMENTS IN THE RTG COORDINATE SYSTEM

AXIS	MOMENT (IN.-LBS)	CORRECTION (IN.-LBS)	CORRECTED MOMENT (IN.-LBS)
X	-16.9	0	-16.9
Y	+46.2	0	+46.2
Z	-25.0	0	-25.0

RTG WEIGHT

TOTAL WEIGHT (RTG, FIXTURE & EQUIPMENT)		124.67 LBS.
FIXTURE	37.43 LBS.	
RTD EXTENSION CABLE	0.78 LBS.	
POWER OUTPUT CABLE	1.22 LBS.	
SHORTING MODULE	1.29 LBS.	
RTG GMV FLEX LINE	0.63 LBS.	
	41.35 LBS.	-41.35 LBS.
		83.32 LBS.

WEIGHT INCLUDES:

[2] CLAMPS, NUTS, SCREWS & MISC.	0.13 LBS.	
ARGON GAS	0.10 LBS.	
[2] SHIPPING BRACKET	0.68 LBS.	
PRD PROTECTIVE PLATE	0.61 LBS.	
THREAD SAVER	0.06 LBS.	
	1.58 LBS.	-1.58 LBS.
[3] XENON GAS	0.22 LBS.	
[4] JPL POWER CABLE	0.55 LBS.	
PRD	0.69 LBS.	
	1.46 LBS.	+1.46 LBS.
	FLIGHT WEIGHT:	83.24 LBS.

F11 RTG WEIGHT AND BALANCE (CONT'D)

RTG CENTER OF GRAVITY COORDINATES*

X = -0.17
Y = -9.60
Z = -0.28

[1] CENTER OF GRAVITY CALCULATED FOR RTG WEIGHT OF 83.32 LBS. THIS WEIGHT INCLUDES CLAMPS, NUTS AND SCREWS, ARGON GAS, SHIPPING BRACKET, PRD PROTECTIVE PLATE AND THREAD SAVER.

[2] SHIPPING BRACKET (0.68 LBS.) AND MISCELLANEOUS HARDWARE (0.13 LBS.) CO-ORDINATES ARE:

X = - 4.51
Y = -14.86
Z = - 7.81

[3] WEIGHT OF XENON GAS (AT LAUNCH) IS 0.22 POUNDS.

[4] WEIGHT OF JPL POWER CABLE NOT AVAILABLE. WEIGHT SHOWN IS ASSUMED BASED ON F-10 CABLE WEIGHT.

*THE Y-AXIS IS THE LONGITUDINAL AXIS WITH +Y BEING TOWARD THE UNIBALL END. THE Z-AXIS IS NORMAL TO THE Y-AXIS AND IS CONTAINED IN THE LONGITUDINAL PLANE DEFINED BY THE Y-AXIS AND THE CENTERLINE OF THE RTG ELECTRICAL OUTPUT CONNECTOR. Z IS NEGATIVE IN THE DIRECTION OF THE CONNECTOR. THE X-AXIS IS NORMAL TO THE Y AND Z AXES. THE X-Z PLANE IS DEFINED BY THE CENTERLINES OF THE SELF-ALIGNING BEARINGS.

VIBRATION TEST F-11

1-24-77	X-AXIS	R_I OHMS	ΔR_I MΩ	E_{OC} VOLTS	ΔE_{OC} MV	P (1) WATTS	ΔP WATTS	RTD °C	R_{case} KΩ
1130	PRE SINE SWEEP	4.522		42.48		83.86		175	3M
1135	POST SINE SWEEP	4.404	-17	42.49	+10	84.28	+0.42	175	4.6M
1400	PRE 3.18G RANDOM	4.508	+ 3	42.47	-20	84.07	-0.21	176	3.5M
1400	POST 3.18G RANDOM	4.511	+ 3	42.48	+10	84.08	+0.01	176	3.7M
1425	POST ACCEPTANCE RANDOM	4.506	- 5	42.51	+30	84.33	+0.25	176	4.3M
1-24-77	Z-AXIS								
0850	PRE SINE SWEEP	4.496	-10	42.50	-10	84.52	+0.19	176	3.3M
0915	POST SINE SWEEP	4.510	+14	42.53	+30	84.45	-0.07	175	4.1M
0950	PRE 3.18G RANDOM	4.505	- 5	42.50	-30	84.33	-0.12	175	3.3M
1000	POST 3.18G RANDOM	4.503	- 2	42.50	00	84.41	+0.08	176	4.1M
1010	POST ACCEPTANCE RANDOM	4.503	0	42.49	-10	84.32	-0.09	176	4.4M
1-26-77	Y-AXIS								
0830	PRE SINE SWEEP	4.538	+35	42.64	+150	84.64	+0.32	179	3.8M
0845	POST SINE SWEEP	4.536	- 2	42.63	-10	84.67	+0.03	179	4.1M
0925	PRE 3.18G RANDOM	4.533	- 3	42.63	0	84.66	-0.01	179	3.9M
0930	POST 3.18G RANDOM	4.531	- 2	42.66	+20	84.85	+0.19	179	4.1M
0945	POST ACCEPTANCE	4.529	- 2	42.63	-30	84.71	-0.14	179	4.3M

(1) POWER MEASURED AT CABLE.

F-11 AIR PERFORMANCE SUMMARY

	48 HOUR PRESSURE DECAY TEST START	48 HOUR PRESSURE DECAY TEST END	PRE-VIB.	POST VIB.	48 HOUR PRESSURE DECAY TEST START	48 HOUR PRESSURE DECAY TEST END
POWER, MEASURED	82.42	83.2	83.86	84.71	82.81	83.1
VOLTAGE, MEASURE	29.7	29.67	29.72	29.72	29.70	29.7
CURRENT, MEASURED	2.775	2.804	2.822	2.850	2.788	2.798
POWER CORRECTED TO 30V AT CONNECTOR	83.0	83.8	84.5	85.3	83.4	83.7
INTERNAL RESISTANCE MEASURED	4.498	4.527	4.522	4.529	4.386	4.492
CORRECTED TO CONNECTOR*	4.425	4.454	4.449	4.456	4.313	4.419
RTD AVERAGE, °C	171	172	175	179	180	184
RESISTANCE TO CASE	3.6 MEG	3.6 MEG	3.0 MEG	4.3 MEG	4.1 MEG	4.3 MEG
V_{OC} TO CASE, VOLTS	11.85	11.7	11.96	10.6	9.49	9.8
DATE/TIME:	1/19/77 (1300)	1/21/77 (1300)	1/24/77 (1130)	1/26/77 (0945)	2/2/77 (0100)	2/4/77 (0100)

*CABLE CORRECTION TO RTG CONNECTOR

F-12 RTG PERFORMANCE IN THE LAS

	POWER MEASURED (WATTS)	HEAT INPUT (WATTS)	INTERNAL RESISTANCE (OHMS)	OPEN CIRCUIT VOLTAGE (VOLTS)
ETG PROCESSING AT RCA:	157.6(1) 157.2(3)	2401.5	4.832(1) 4.847(2)	55.39
LAS PRE-PROCESSING* (DOME REMOVED) 2/26/77 @ 0200	81.2(2) 81.8(3)	2396.4	4.476(2) 4.400(3)	41.95
LAS PROCESSING (END OF VACUUM PROCESSING) 2/28/77 @ 0300	156.8(2) 159.0(3)	2396.2	5.030(2) 4.954(3)	56.24
LAS POST-PROCESSING* (DOME REMOVED) 2/28/77 @ 1800	81.5(2) 82.1(3)	2396.2	4.495(2) 4.379(3)	41.93
LAS POST-PROCESSING (DOME INSTALLED)				
ARGON 15 PSIA 3/01/77 @ 0400	83.0(2) 83.6(3)	2396.0	4.598(2) 4.422(3)	42.31
ARGON 25 PSIA 3/01/77 @ 1500	80.4(2) 81.0	2396.0	4.536(2) 4.460(3)	42.00

*RTG NOT COMPLETELY STABILIZED.

(1)MEASURED AT END OF THERMOPILE.

(2)MEASURED AT CABLE VOLTAGE TAP LOCATION.

(3)CORRECTED TO RTG CONNECTOR.

F-12 LAS PROCESSING MONOPOLE DATA
PARTIAL PRESSURE (TORR)

SPECIES	0955-1030 2/26/77 t+6 HOURS	0845-0915 2/27/77 t+29 HOURS	2135-2205 2/27/77 t+42 HOURS
CHAMBER	8.5×10^{-6}	3.7×10^{-6}	3.6×10^{-6}
He	1.6×10^{-7}	1.4×10^{-8}	1.1×10^{-8}
H_2O	4.6×10^{-6}	1.4×10^{-6}	1.2×10^{-6}
N_2	3.0×10^{-7}	2.6×10^{-7}	2.7×10^{-7}
CO	3.1×10^{-8}	8.9×10^{-9}	8.3×10^{-9}
O_2	9.8×10^{-8}	6.9×10^{-8}	6.4×10^{-8}
Ar	2.7×10^{-6}	1.8×10^{-6}	1.9×10^{-6}
CO_2	1.4×10^{-8}	5.1×10^{-9}	3.7×10^{-9}
H_2 & HYDROCARBONS	6.3×10^{-7}	2.2×10^{-7}	1.8×10^{-7}

STARTED CHAMBER PUMPDOWN ON 2/26/77 AT 0315 HOURS.

F-12 VACUUM POWER SUMMARY
POWER NORMALIZED TO 2400W HEAT INPUT AND TO RTG CONNECTOR

	RCA	LAS	POST VIBRATION THERMAL VACUUM
DATE:	12/3/76	2/28/77	3/15/77
POWER OUTPUT, WATTS:	158.4	159.4*	159.0
INTERNAL RESISTANCE, OHMS:	4.847	4.954	4.955
OPEN CIRCUIT VOLTAGE, VOLTS:	55.39	56.24	56.18
RESISTANCE TO FOIL:	9.8	-----	-----
RESISTANCE TO CASE:	18K	40K	11.3K
RTD AVERAGE, °C:	-----	270	261
CONVERTER PRESSURE:	-----	-----	5.5μ

*POSSIBLE INSTRUMENTATION ERROR; POWER COULD BE AS MUCH AS 1.4 WATTS HIGHER.

F-12 AIR PERFORMANCE SUMMARY

	48-HOUR PRESSURE DECAY TEST		PRE-VIB.	POST VIB.	48-HOUR PRESSURE DECAY TEST	
	START	END			START	END
POWER, MEASURED:	81.8	82.3	82.8	83.0	80.97	81.7
VOLTAGE, MEASURED:	29.70	29.69	29.70	29.69	29.74	29.7
CURRENT, MEASURED:	2.753	2.772	2.787	2.795	2.723	2.750
POWER CORRECTED TO 30V AT CONNECTOR	82.3	82.9	83.4	83.6	81.53	82.2
OPEN CIRCUIT VOLTAGE:	41.82	42.09	42.27	42.33	41.70	42.08
INTERNAL RESISTANCE MEASURED:	4.402	4.473	4.508	4.520	4.395	4.501
CORRECTED TO CONNECTOR*:	4.326	4.396	4.432	4.444	4.319	4.425
RTD AVERAGE, °C:	175	180	178	183	190	186
RESISTANCE TO CASE:	821K	815K	2.5MEG	3.6MEG	4.1MEG	4.1MEG
V_{OC} TO CASE, VOLTS:	26.2	26.2	14.9	11.4	11.6	12.1
DATE/TIME:	3/3/77 (0400)	3/5/77 (0400)	3/7/77 (1830)	3/9/77 (1830)	3/16/77 (0300)	3/18/77 (0300)

*CABLE CORRECTION TO RTG CONNECTOR.

VIBRATION TEST - F-12

3/7/77 X-AXIS	R_1 OHMS	ΔR_1 MΩ	E_{OC} VOLTS	ΔE_{OC} MV	$P^{(1)}$ WATTS	ΔP WATTS	RTD °C	R_{CASE} KΩ
1830 PRE SINE SWEEP	4.508		42.27		83.37		178	2.5M
1845 POST SINE SWEEP	4.507	- 1	42.27	0	83.45	+.08	179	2.7M
2050 PRE 3.18G RANDOM	4.503	- 4	42.24	-30	83.33	-.12	177	2.6M
2105 POST 3.18G RANDOM	4.493	-10	42.22	-10	83.44	+.11	177	179K
2130 POST ACCEPTANCE RANDOM	4.506	+13	42.23	+10	83.21	-.23	177	185K
3/8/77 Z-AXIS								
1700 PRE SINE SWEEP	4.517	+11	42.23	0	82.84	-.37	179	3.4M
1730 POST SINE SWEEP	4.508	- 9	42.21	-20	82.90	+.06	179	4.0M
1800 PRE 3.18G RANDOM	4.501	- 7	42.23	+20	83.18	+.28	179	3.1M
1820 POST 3.18G RANDOM	4.511	+10	42.26	+30	83.20	+.02	179	3.3M
1840 POST ACCEPTANCE RANDOM	4.511	0	42.26	0	83.28	+.08	179	3.7M
3/9/77 Y-AXIS								
1700 PRE SINE SWEEP	4.527	+16	42.32	+60	83.38	+.10	183	3.3M
1715 POST SINE SWEEP	4.526	- 1	42.31	-10	83.45	+.07	183	4.0M
1755 PRE 3.18G RANDOM	4.527	+ 1	42.34	+30	83.57	+.12	183	3.3M
1810 POST 3.18G RANDOM	4.524	- 3	42.34	0	83.56	-.01	183	3.9M
1830 POST ACCEPTANCE RANDOM	4.520	- 4	42.33	-10	83.58	+.02	183	3.6M

F-12 RTG WEIGHT AND BALANCE

AXIS	MOMENT (IN-LBS)	CORRECTION (IN-LBS)	CORRECTED MOMENT (IN-LBS)
X	-18.0	0	-18.0
Y	+46.5	0	+46.5
Z	-25.0	0	-25.0

RTG WEIGHT

TOTAL WEIGHT (RTG, FIXTURE AND EQUIPMENT)		124.55 LBS.
FIXTURE	37.40 LBS.	
RTD EXTENSION CABLE	.76 LBS.	
POWER OUTPUT CABLE	1.27 LBS.	
SHORTING MODULE	1.26 LBS.	
RTG GMV FLEX LINE	.60 LBS.	
	41.29 LBS.	-41.29 LBS.
		83.26 LBS.

WEIGHT SHOWN INCLUDES:

[2]CLAMPS, NUTS, SCREWS AND MISCELLANEOUS	.04 LBS.	
[3]ARGON GAS	.10 LBS.	
[4]SHIPPING BRACKET	.67 LBS.	
PRD PROTECTIVE PLATE	.61 LBS.	
THREAD SAVER	.06 LBS.	
	1.48 LBS.	- 1.48 LBS.
[3]XENON GAS	.22 LBS.	
[4]JPL POWER CABLE	.55 LBS.	
PRD	.69 LBS.	
	1.46 LBS.	+ 1.46 LBS.
	FLIGHT WEIGHT:	83.24 LBS.

F-12 RTG WEIGHT AND BALANCE (CONTINUED)

RTG CENTER OF GRAVITY COORDINATES*

X = - .19
Y = -9.59
Z = - .28

[1]CENTER OF GRAVITY CALCULATED FOR RTG WEIGHT OF 83.26 LBS. THIS WEIGHT INCLUDES CLAMPS, NUTS AND SCREWS, ARGON GAS, SHIPPING BRACKET, PRD PROTECTIVE PLATE AND THREAD SAVER.

[2]SHIPPING BRACKET (.67 LBS.) AND MISCELLANEOUS HARDWARE (.04 LBS.) COORDINATES ARE:

X = - 4.51
Y = -14.86
Z = - 7.81

[3]WEIGHT OF XENON GAS (AT LAUNCH) IS .22 POUNDS.

[4]WEIGHT OF JPL POWER CABLE NOT AVAILABLE. WEIGHT SHOWN IS ASSUMED BASED ON F-10 CABLE WEIGHT.

*THE Y-AXIS IS THE LONGITUDINAL AXIS WITH +Y BEING TOWARD THE UNI-BALL END. THE Z-AXIS IS NORMAL TO THE Y-AXIS AND IS CONTAINED IN THE LONGITUDINAL PLANE DEFINED BY THE Y-AXIS AND THE CENTERLINE OF THE RTG ELECTRICAL OUTPUT CONNECTOR. Z IS NEGATIVE IN THE DIRECTION OF THE CONNECTOR. THE X-AXIS IS NORMAL TO THE Y AND Z AXES. THE X-Z PLANE IS DEFINED BY THE CENTERLINE S OF THE SELF-ALIGNING BEARINGS.

COMPARISON WITH PREVIOUS UNITS

UNIT	CENTER OF GRAVITY (IN.) X	Y	Z	WEIGHT (LBS)
F-6	-.20	-9.49	-.28	82.84
F-7	-.17	-9.52	-.27	83.63
F-8	-.18	-9.54	-.27	83.50
F-9	-.20	-9.57	-.20	83.38
F-10	-.18	-9.58	-.21	83.24
F-11	-.17	-9.60	-.28	83.20
F-12	-.19	-9.59	-.28	83.24

TABLE 10-8. COMPARISON OF LAS PERFORMANCE

	F - 6	F - 7	F - 8	(F-9 IHS) F - 9	(F-10 IHS) F - 9	(F-11 IHS) F - 10	(F-12 IHS) F - 11	(F-9R* IHS) F - 12
$P_{MEASURED}$	159.3	159.1	157.5	158.6	157.4	159.7	159.62	156.8
R_{CABLE}	0.086	0.084	0.077	0.075	0.075	0.076	0.073	0.076
ΔP	2.4	2.4	2.2	2.2	2.1	2.2	2.14	2.15
$P_{CORRECTED}$ TO CONNECTOR	161.7	161.5	159.7	160.8	159.5	161.9	161.8	159.0
Q	2418	2412	2407.2	2407.5	2409.2	2409.5	2402.4	2396.2
$P_{NORM\ (2400)}$ 30V CONNECTOR	159.6	160.3	159.0	160.0	158.6	160.9	161.5	159.4
I	5.296	5.400	5.335	5.375	5.333	5.410	5.408	5.317
V_L	30.08	29.46	29.52	29.50	29.51	29.52	29.52	29.5
E_{OC}	56.39	56.11	55.941	56.20	56.32	56.29	56.32	56.24
R_I MEASURED	4.967	4.936	4.952	4.966	5.027	4.948	4.957	5.030
R_I AT CONNECTOR	4.881	4.852	4.875	4.891	4.952	4.872	4.884	4.954
RTD	269	271	268	266	265	267	265	270
V_{OC}	12.2	10.3	11.1	10.4	10.3	8.75	8.5	11.1
R_{CASE} (2 SEC)	61.5K	43.3K	60.4K	86.9K	106K	155K	89.8K	40K
(2 MIN)	71.3K	77.5K	61.9K	88.6K	109K	162K	95.3K	63K
CHAMBER PRESSURE	1.9×10^{-6}	7.5×10^{-6}	8.5×10^{-6}	8×10^{-7}	8.3×10^{-6}	3×10^{-6}	2×10^{-6}	3.6×10^{-6}
DATE TIME	3/5/76 (1500)	4/13/76 (0700)	6/25/76 (1500)	7/29/76 (1500)	9/24/76 (1730)	10/22/76 (1000)	1/12/77 (1300)	2/28/77 (0300)

*F-9R/IHS REBUILT TO REPLACE AFT SPRING ASSEMBLY BOLT WITH POCO NUT

TABLE 10-9. COMPARISON OF POST VIBRATION VACUUM PERFORMANCE

	F - 6	F - 7	F - 8	F - 9	F - 10	F - 11	F - 12
$P_{MEASURED}$	156.5	156.5	156.3	156.2	158.4	158.4	156.4
R_{CABLE}	.086	.078	.077	.098	.100	.073	.076
ΔP	2.4	2.2	2.2	2.7	2.9	2.1	2.1
$P_{CORRECTED}$ TO CONNECTOR	158.9	158.8	158.5	158.9	161.3	160.5	158.5
Q	2417.1	2409	2406.2	2408.6	2408.7	2401.5	2395.4
$P_{NORM\ (2400)}$ 30V CONNECTOR	157.2	157.8	157.9	158.0	160.4	160.4	159.0
I	5.282	5.297	5.293	5.295	5.410	5.371	5.329
V_L	29.63	29.54	29.54	29.49	29.48	29.49	29.55
E_{OC}	56.11	56.12	55.85	56.31	56.26	56.28	56.18
R_I MEASURED	5.014	5,020	4.971	5.065	4.984	4.988	5.031
R_I AT CONNECTOR	4.928	4.942	4.894	4.967	4.884	4.915	4.955
RTD	261	263	262	259	260	257	261
V_{OC}	13.7	11.3	12.6	12.2	11.6	12.1	12.2
R_{CASE} (2 SEC) (2 MIN)	5.5K 7.5K	4.9K 6.8K	6.4K 8.5K	66.5K 85.9K	107K 127K	129K 145K	11.3K 14.2K
RTG PRESSURE	3.3μ	5.3μ	4.7μ	4.3μ	4μ	6.1μ	5.5μ
CHAMBER PRESSURE	2.8×10^{-6}	1.2×10^{-6}	2.4×10^{-6}	4.3×10^{-6}	3.5×10^{-6}	4.2×10^{-6}	3.4×10^{-6}
DATE TIME	3/23/76 (2400)	6/8/76 (1800)	7/13/76 (2200)	10/7/76 (1600)	11/9/76 (0500)	2/1/77 (0300)	3/15/77 (1000)

SECTION 11

QUALIFICATION TESTING - Q-2 RTG

11.1 RTG QUALIFICATION TESTING

The Q2 ETG operations were started in January 1976 and the conversion to an RTG was completed at the end of March. See Section 10.2.1 for details of the RTG assembly and acceptance testing operations. The schedule for the Qualification Test Program is shown in Figure 11-1.

11.2 Q2 RTG DYNAMIC TESTING

The RTG Qualification Test sequence performed in Building 400 is outlined below:

- Transfer RTG to Building 400
- Facility preparation and RTG removal from RTG-SC
- Pre-vibration Air Performance and Pressure Decay Test

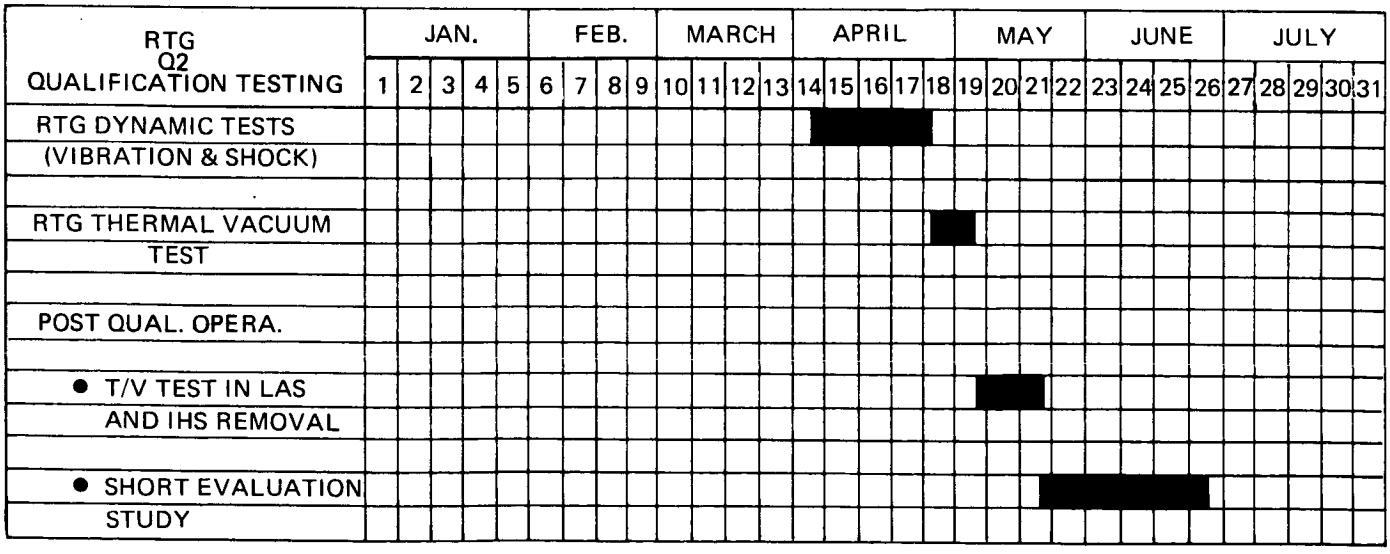

Figure 11-1. MJS RTG Qualification Test Program

- PRD Bellows installation
- RTG Gas Tap
- RTG Acceptance Level Vibration
  (RTG Inverted) X - Axis
  Z - Axis
  Y - Axis
- RTG Qual Level Vibration
  (RTG Inverted) Y - Axis
  Z - Axis
  X - Axis
- RTG Qual Level Vibration and Shock
  (RTG Upright) X - Axis
  Z - Axis
  Y - Axis
- Post-Vibration Air Performance and Pressure Decay Test
- RTG Weight Measurement
- PDR Bellows removal
- RTG Installation into RTG-SC

The Q2 RTG was delivered to Building 400 for Dynamic Testing on 2 April 1976.

On 5 April 1976, the Q-2 RTG was removed from the SC and set-up on the vibration slip table in the forward-end-down orientation. Test readiness was completed, and the RTG load was switched from short-circuit to the loaded mode. After stability had been achieved, the pre-vibration 48-hour air performance/pressure decay test was conducted. This test showed a leak rate of 0.22 psi/48-hours and an average output power of 76.0 watts.

The PRD bellows (without lance) and arming pin were then installed onto the PRD bracket. The arming pin remained in place through the acceptance level vibration cycle and then was removed for the qualification level dynamic testing. An RTG gas sample was collected in an evacuated bottle, and final preparations were completed for vibration testing.

The shock and vibration test input levels for the Q-2/RTG in each axis are given in Table 11-1 for acceptance levels and in Tables 11-2 and 11-3 for qualification levels.

TABLE 11-1. Q-2/RTG SHOCK AND VIBRATION - ACCEPTANCE LEVELS

A C C E P T A N C E T E S T		
Mounted on end opposite uniballs (inverted).		
X-AXIS		
1/2 g (O-P) Sine Survey	2 Oct/Min	20-2000 HZ
1/2 Level Accept. Sine	2 Oct/Min	5-2000 HZ
Full Level Accept. Sine	7 Oct/Min Log.	5-2000-5 HZ
1/3 Level Accept. Random (EQ)	$\leq$ 20 Sec.	
	1.0 Min	
Z-AXIS		
1/2g (O-P) Sine Survey	2 Oct/Min	20-2000 HZ
1/2 Level Accept. Sine	2 Oct/Min	5-2000 HZ
Full Level Accept. Sine	6 Oct/Min Log.	5-2000-5 HZ
1/3 Level Accept. Random (EQ)	$\leq$ 20 Sec.	
Full Level Accept. Random	1.0 Min	
Y-AXIS		
1/2g (O-P) Sine Survey	2 Oct/Min	20-2000 HZ
1/2 Level Accept. Sine	2 Oct/Min	5-2000 HZ
Full Level Accept. Sine	6 Oct/Min	5-2000-5HZ
1/3 Level Accept. Random (EQ)	$\leq$ 20 Sec.	
Full Level Accept. Random	1.0 Min	

Figure 11-2 shows these level and frequencies graphically. The total vibration exposure time for this qualification test unit, was ~73 minutes.

On 8 April 1976, the X-axis acceptance level vibration cycle with the RTG inverted began with the 1/2 G sine sweep, and ended with the full level random vibration. There were several anaomalous indications during the course of the X-axis cycle.

TABLE 11-2. Q-2/RTG SHOCK AND VIBRATION - QUALIFICATION LEVELS

Q U A L I F I C A T I O N T E S T		
Mounted on end opposite uniballs (inverted).		
Y-AXIS		
Full Level Qual. Sine	2 Oct/Min	5-2000 HZ
1/3 Level Accept. Random (EQ)	≦ 20 Sec.	
Full Level Qual. Random	1.5 Min	
12g (O-P) Sine	30 Sec Dwell @ 25 HZ	
Z-AXIS		
1/2g (O-P) Sine Survey	2 Oct/Min	20-2000 HZ
Full Level Qual. Sine	2 Oct/Min	5-2000 HZ
1/3 Level Accept. Random (EQ)	≦ 20 Sec.	
Full Level Qual. Random		
X- AXIS		
1/2g)O-P) Sine Survey	2 Oct/Min	20-2000 HZ
Full Level Qual. Sine	2 Oct/Min	5-2000 HZ
1/3 Level Accept. Random (EQ)	≦ 20 Sec.	
Full Level Qual. Random	1.5 Min	

During the full level sinusoidal acceptance and full level random acceptance runs, there were load current fluctuations, as seen on the strip chart record, of up to 0.5 amp. In addition, output power dropped by 0.8 watt after the full level sinusoidal run, continued to decrease by another 0.5 watt one hour later, and then recovered 0.3 watt, two hours later, ending 0.95 watt lower than the output prior to the full level sinusoidal input. There was no appreciable change in thermopile internal resistance over this period.

After the full level random vibration run, the output power dropped 3.3 watts from the pre-run power level. At that time, it was found that the connector plug on the JPL power cable had loosened from the converter's receptacle. With the tightening of that connector, the 3.3 watts was recovered. Along with the power loss, there was an increase in the calculated internal

TABLE 11-3. Q-2 RTG SHOCK AND VIBRATION - QUALIFICATION LEVELS

Q U A L I F I C A T I O N T E S T		
Mounted on uniballs (upright).		
X-AXIS		
1/2g (O-P) Sine Survey	2 Oct/Min	20-2000 HZ
1/2 Level Accept. Sine	2 Oct/Min	2000-5 HZ
Full Level Qual. Sine	2 Oct/Min	2000-5 HZ
1/3 Level Accept. Random (EQ)	$\leq$ 20 Sec.	
Full Level Qual. Random	1.5 Min.	
Qual. Shock	3 Shocks	
Z-AXIS		
1/2g (O-P) Sine Survey	2 Oct/MIN	20-2000 HZ
1/2 Level Accept. Sine	2 Oct/Min	2000-5 HZ
Full Level Qual. Sine	2 Oct/Min	2000-5 HZ
1/3 Level Accept. Random (EQ)	$\leq$ 20 Sec.	
Full Level Qual. Random	1.5 Min.	
Qual. Shock	3 Shocks	
Y-AXIS		
1/2g (O-P) Sine Survey	2 Oct/Min	20-2000 HZ
1/2 Level Accept. Sine	2 Oct/Min	2000-5 HZ
Full Level Qual. Sine	2 Oct/Min	2000-5 HZ
1/3 Level Accept. Random (EQ)	$\leq$ 20 Sec.	
Full Level Qual. Random	1.5 Min	
Qual. Shock	3 Shocks	
1/2g (O-P) Sine Survey	2 Oct/Min	20-2000 HZ

resistance of 0.22 ohms, but this also returned to normal after the connector plug tightening. Q-2 was then rotated on the slip table to the Z axis orientation.

On 9 April 1976, the Z-axis cycle with the RTG still inverted began with the 1/2 G sine sweep. After completing the full level sinusoidal acceptance sweep, there was a drop of 0.46 watt from the pre-run power level and an increase in the internal resistance of 0.05 ohm as compared to the pre-run value. The connector plug on the JPL power-out cable was tightened

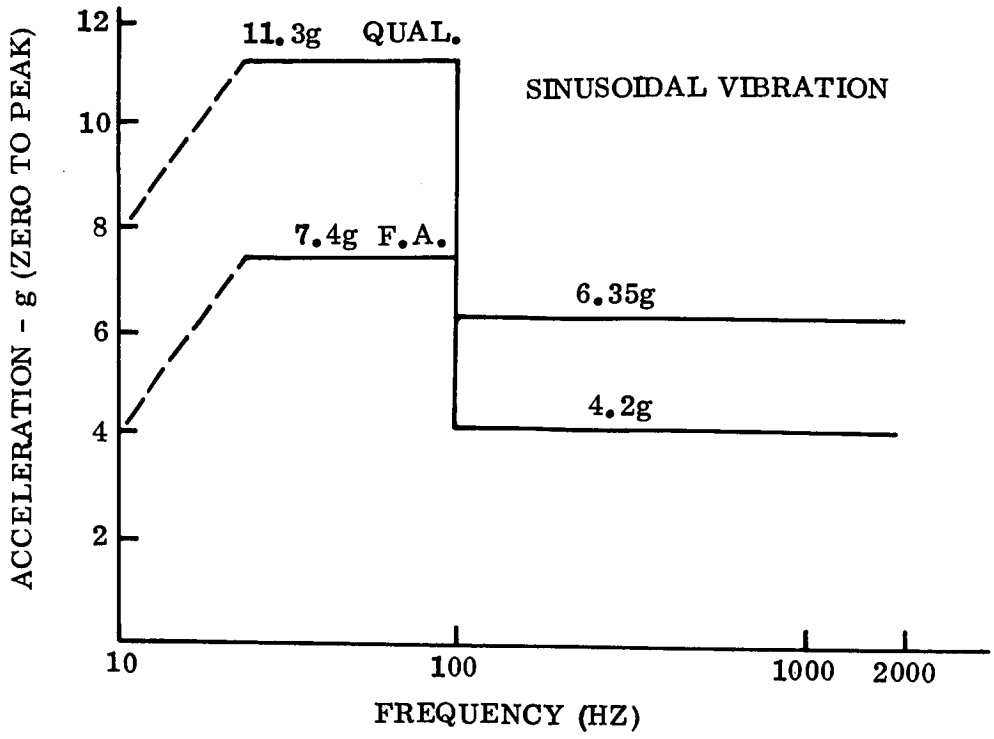

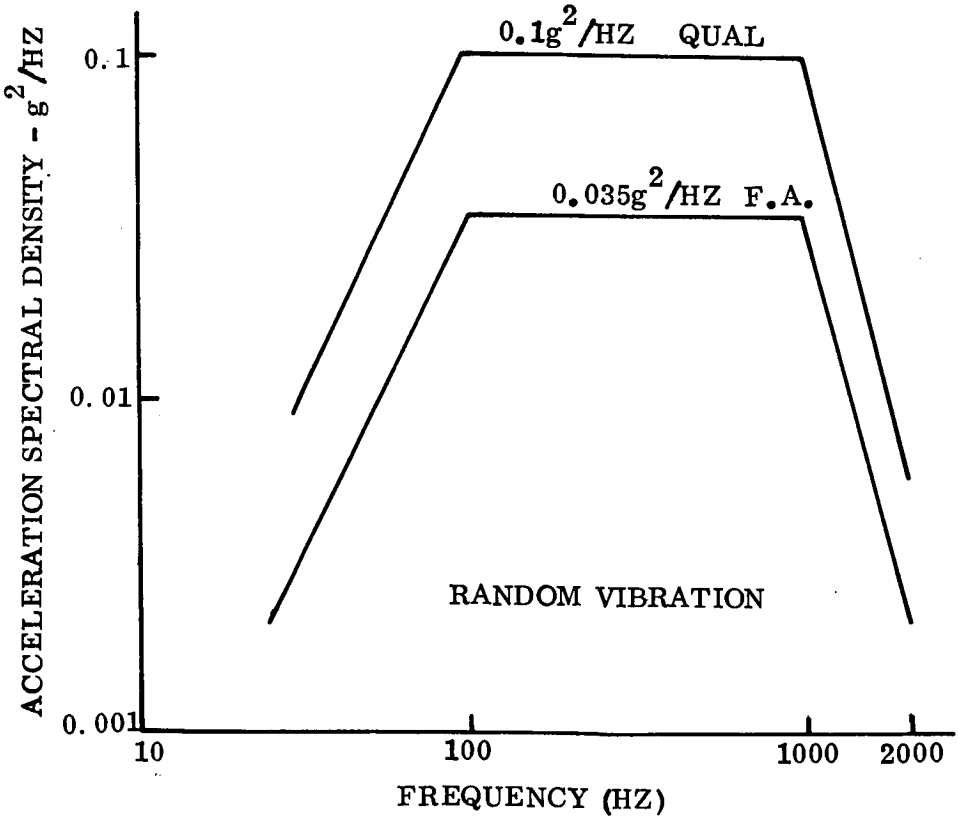

Figure 11-2. MJS RTG Vibration Test

and, although there was no visible rotational movement of that connector, there was an effect on the data. Power and internal resistance returned to the pre-vibration run values.

The full level random vibration test was then performed. Following the Z-axis acceptance level random vibration run, the data scan showed that output power had decreased by 2.14 watts from that prior to the run, and circuit internal resistance had increased by 0.13 ohm. Both power and internal resistance returned to their pre-run values after tightening of the JPL power-out cable connector. Some movement was observed at this tightening, whereas earlier there was no visible movement of the connector plug.

The RTG was hoisted from the vibration slip table and set up on the exciter head for Y-axis testing. A decision was made to exchange the JPL power-out cable with a 2428G1 GSE-type cable. The 3500G2 power-out adapter cable was also eliminated from the cabling configuration with the use of the 2428G1 GSE power cable. The RTG load was then changed to the short-circuit mode and operations were suspended for the weekend.

On 11 April 1976, after the weekend suspension of operations, the RTG load was switched from short-circuit to the loaded mode. The RTG was thermally stabilized at the 29.7 volt load and the Y-axis vibration cycle began with the 1/2 G sine sweep. During the course of the acceptance level sinusoidal vibration, there were current fluctuations of up to 0.3 amp, and voltage fluctuations of up to 1.0 volt between 30 and 50 Hz. These occurred in this frequency range at both the sweep up to 2000 Hz and the sweep down to 5 Hz. However, there were no anomalous indications at the post-run data scan as compared to the pre-run scan.

The acceptance level random vibration run was completed with no fluctuations showing on the strip chart, and no anomalous power or internal resistance indications at the pre and post-run data comparison. There was an anomaly on the RTD #3 reading at the post-run scan. This was an increase in voltage from 0.503 to 0.510 volt (corresponding to a change from 176°C to 182°C). The reading returned to the normal 0.503 volt after the RTD connector at the converter interface bracket was tightened.

On 13 April 1976, the arming pin for the PRD bellows was removed for the qualification level testing.

The qualification level sinusoidal vibration in the Y-axis, with the RTG inverted, was completed. As with the acceptance level sinusoidal run, there were current fluctuations of 0.5 amp, and load voltage fluctuations of up to 1.0 volt during the sweep between 20 to 60 Hz. The pre-run and post-run performance data scans compared favorably.

Qualification level random vibration (11.1 G-rms) was then completed. The strip chart data taken during the run showed some current fluctuations of up to 0.1 ampere, but no load voltage changes. There were no deviations between the pre- and post-run data scans, except that the RTD #3 circuit was again erratic. Its voltage changed from 0.500 volt level after the converter interface connector was tightened. This had also been seen after the Y-axis acceptance level random burst. The "tightening" of the connector plug was not an actual rotational movement of the plug, but an application of torque to it.

The Y-axis 12 G (zero-peak) dwell, at 25 Hz for 30 seconds, was then completed. There were load current spikes of up to 0.3 amp seen during this vibration input. The data scan taken immediately after the run compared favorably with the pre-run data, but the data taken twenty minutes later were anomolous. Open circuit voltage dropped by 0.4 volt and power decreased 2.47 watts within 2 hours. These readings later recovered to the normal values.

Q-2 was transferred from the exciter head to the slip table for Z-axis, inverted orientation, dynamic testing. On 14 April 1976 the 1/2 G sine sweep was performed. There were some load current fluctuations of 0.1 amp seen during the sweep at frequencies of 75 Hz and 750 Hz. Pre- and post-run data compared favorably.

The Z-axis qualification level sinusoidal application was completed. There were no anomalous load voltage or current indications during the run, but there was an anomoly on the RTD #3 circuit. The voltage on that circuit was monitored during the vibration input, and showed an increase from 0.50 volt to 0.84 volt. With a tightening of the RTG interface connector, the circuit voltage returned to the normal 0.50 volt indication. The performance data scan taken

after the run showed that output power had fallen from the pre-run level by 2.1 watts and open-circuit voltage had decreased by 0.34 volt. Internal resistance did not change. Output power and open-circuit voltage then gradually returned to their pre-run levels over the next two hours.

Qualification level random vibration in the Z-axis was then completed. Performance parameters were normal after this run. The 2428G1 GSE power-out cable was then removed from the converter power out receptacle, and replaced with the JPL power-out cable and 3500G4 adapter cable which had been removed from the RTG earlier.

On 15 April 1976, rotation on the slip table to the X-axis position was completed, and the 1/2 G sine sweep and qualification level sinusoidal run was completed on the inverted RTG. There were some load voltage and current perturbations seen on the strip chart during the run. The post-run performance scan parameters were normal as compared to the pre-run scan.

The X-axis qualification level random vibration was applied and during the run, the reaction of the PRD bellows was photographed by a high-speed camera. The lamps used during the photography caused an extreme shifting of all performance parameters during the run. When compared to the pre-run data, the post-test scan showed a drop in load current of 0.25 ampere, with a corresponding power loss of 7.6 watts, an increase in converter case temperature of 5° C, and an increase in circuit internal resistance of 0.52 ohm. The performance scan (taken 2.7 hours after the initial post-run scan) indicated that power had returned to normal, but internal resistance was still 0.15 ohm higher than the pre-run level. After a demonstration to JPL personnel showed that a physical movement of the JPL power-out cable connector plug would yield swings of RTG load current from 2.398 to 2.567 amperes, a decision was made to again remove the JPL power cable and to re-install the 2428G1 test cable.

On 15 April 1976, the RTG load was switched to short-circuit mode. The RTG was then rotaged and set up in the normal (forward-end-up) orientation along the X-axis on the slip table. Load was switched back to 29.7 volts, and thermal stability achieved.

On 16 April 1976, the 1/2 G sine sweep was run and the only anomaly seen was an increase in the RTD #3 circuit voltage, equivalent to a 6° C change. This changed slightly after the run, but still indicated a 4° C change. Without any external action, the RTD #3 circuit voltage gradually increased over the next hour, ending with an equivalent 12° C increase from the pre-run level. The RTD cable interface connector was tightened and the circuit voltage immediately decreased to the pre-sine sweep level.

Qualification level sinusoidal X-axis vibration with the RTG in the upright configuration was completed and again there were no anomalous load voltage or current indications. The RTG load was switched to short-circuit and the unit secured for the weekend.

On 19 April 1976, the RTG load was switched out of short-circuit to the loaded mode, and thermal stability achieved. The 1/3 level (2.2 G rms) random equalization run was then performed. The post-run data scan indicated that the shunt resistance between the thermopile and case, which had been at 340K-ohms, was some very low value. Output power and internal resistance were normal. Shunt resistance returned to a normal value (350K-ohms) in $\approx$6 hours with no apparent external stimulus.

The 1/3 level random equalization run was then repeated with no anomalous indications. Qualification level random vibration was then performed. As seen on the strip chart record taken during the run, there were positive and negative load voltage fluctuations of up to 0.5 volt, negative-going current spikes of up to 0.6 amp and positive-going current spikes of up to 0.3 ampere. Although the post-run data scan showed that output power and internal resistance were normal, the low shunt resistance value had returned.

Trouble shooting was initiated to resolve the abnormal shunt resistance problem. The ROC was verified to be functioning properly and FRB directed tests found no conclusive cause.

On 21 April 1976, direction was given to proceed with the dynamic test cycle and the Ling SS6 shock spectrum synthesizer/analyzer was coupled into the MB-C150 shaker system's amplifier in preparation for the upright shock applications. The low shunt resistance between thermopile and case returned with the application of the 1/4-level shock, and then increased to the normal value after the 1/2-level shock application. Three qualification level shocks along the X-axis were applied, with the shunt resistance still at a high value (620K ohms). Pre- and post-qualification shock application data scans showed no anomalous performance parameters.

On 22 April 1976, Q-2 was rotated to align its Z-axis along the slip table and the 1/2G sine sweep was completed. Other than there being a load voltage fluctuation of 0.5 volt at 175 Hz during the run, performance was normal. After the 1/2-level sinusoidal vibration was applied, there was a drop in load current of 28 milliamps (which equaled a power loss of 0.8 watt) and a decrease in open-circuit voltage of 0.5 volt. The RTD #3 circuit voltage changed from an equivalent 177° C to 204° C. There was no return to the nominal 177° C value after the RTD cable connector was "tightened". Previous experience with the anomaly showed a return to normal after a manipulation of the RTD connector at the converter interface bracket. Load current and open-circuit voltage continued to decrease over the next hour, and then recovered within 1-1/2 hours to the levels seen just after the 1/2-level sinusoidal run. The 2428G1 GSE power out cable connector was "tightened" but this did not influence a change in load current.

During the qualification level sinusoidal application, there was a positive-going load current spike of 0.5 ampere seen on the strip chart record at 125 Hz. The voltage from the thermopile-to-case was being monitored on the DVM and, concurrent with the current spike at 125 Hz, there was a change in voltage which indicated that the shunt resistance had decreased from the 627-ohm value seen prior to the run. The data scan obtained post-run verified that the shunt resistance had fallen to some very low value. The RTD #3 circuit had been indicating an anomalously high value since the 1/2 level sinusoidal run earlier. This circuit returned to normal with the application of the qualification level sinusoidal vibration.

The performance data scan taken after the qual sinusoidal run showed an increase in load current of 0.12 amp, corresponding to an output power increase of 3.58 watts; open-circuit voltage increased to 0.54 volts and average case temperature decreased by 2° C. The temperature in the vibration cell remained at 70° F over this period, and should not have influenced the decrease in case temperature. Except for the shunt resistance still being low, performance parameters returned to normal within an hour.

The qualification level (11.1 G-rms) random input along the Z-axis, with the converter upright mounted at its uniballs or "normal" attitude, was run. During the run, there were several load voltage and load current perturbations of up to 1.5 volts and 0.4 ampere. Coincident with the initial spike, which was approximately five seconds into the run and prior to full force being applied, there was a change in the voltage from thermopile-to-case which was being monitored on the DVM. This indicated that the previously low shunt resistance had increased to the high normal value. The post-run data scan verified this occurrence, and also showed a favorable comparison between the pre-run and post-run performance parameters.

The shock equipment was interconnected with the shaker system, and after applying the 1/4-level shock, the shunt resistance dropped off to a low value coincident with a 0.4 ampere negative-going fluctuation of load current. The 1/2-level shock was completed with no anomalies other than the shunt resistance still being low. The three qualification level shock applications in the Z-axis were completed, with load voltage and/or load current spikes occurring at the time of each application. In addition, at the third qualification level shock, the shunt resistance changed to the high isolation value.

The RTG was then hoisted off the slip table and set-up with the uniballs mounted to the clevis blocks on the exciter head for the Y-axis (longitudinal) testing. This was the last series of dynamic tests to be run on Q-2. Prior to performing the 1/2 G sine survey, an RTG gas sample was collected in an evacuated bottle for mass spectrographic analysis. This was to be compared for helium concentration with a sample to be taken after the qualification sinusoidal run.

On 23 April 1976, the qualification level sinusoidal vibration was completed. During the sweep up, the shunt resistance isolation changed to the anomalous low value at approximately 1100 Hz. The post-run data scan confirmed this large decrease in thermopile-to-case isolation. Load current increased by 0.09 amp, with a corresponding increase in output power of 2.85 watts; open-circuit voltage increased by 0.46 volt, and case temperature decreases slightly by a 2° C average as seen at the RTD's. Part of the above increase in power could be due to a post-run decrease in the ambient temperature of the vibration cell by 2° F. Within an hour, the performance parameters had almost returned to their pre-run values. The second RTG gas sample (to be compared to the pre-qual sinusoidal sample) was then obtained.

Qualification level random vibration in the Y-axis, upright attitude, was completed. Pre-run and post-run performance parameters compared favorably, except that the RTD #3 circuit voltage had increased by an equivalent 37° C (from 185° C to 227° C).

The shock equipment was coupled into the vibration exciter's amplifier, and preparations were made for shock testing. The three qualification level shock applications in the Y-axis were completed. The RTD #3 circuit returned to normal some time during the shock sequences, and the shunt resistance isolation returned at the application of the third qualification level shock. Pre-shock and post-shock performance showed a favorable comparison.

A final 1/2 G sine survey completed the Y-axis testing with all performance parameters normal. This last sine sweep completed all of the planned dynamic testing on Q-2.

A short pressure decay test on the RTG was completed. Leak rate for this test was 0.08 psi/6-hours. After setting the RTG load to the short-circuit mode and stabilizing the RTG internal pressure, the RTG was secured for a weekend suspension of operations early 24 April 1976.

Operations resumed in Building 400 early 4/26, with the weight measurement on Q-2. C.G. measurements were not performed (not planned) since the converter with a spoolpiece would not fit into the C.G. fixture. The PRD bellows was removed from its bracket on the converter case, and the RTG was then installed into the shipping container.

11.3 Q-2 RTG THERMAL-VACUUM TESTING

The Q-2 RTG Qualification Test sequence performed in Building 300 is shown below:

- Transfer RTG to Building 300
- Facility preparation and RTG removal from RTG-SC
- Special tests to evaluate vibration anomalies
- Thermal Vacuum performance test (RTG vented)
- RTG Xenon Backfill Operations
- Transient Venting Test
- RTG Argon Backfill Operations
- Post T/V Air Performance and 48 hour Pressure Decay Test
- RTG installation into RTG-SC

Transfer of the Q-2 RTG to the Building 300 Long Life Lab was completed on 26 April 1976 and the unit was removed from the RTG-SC and installed onto the chamber #4 support frame.

Prior to thermal vacuum testing, some special tests were started. These were a part of the investigation to determine the cause of the anomalies seen during the dynamic test sequence. The first special test was a monitoring of the three RTD circuit voltages, while the 3500G3 adaptor cable was flexed at the area where it mates to the converter interface bracket. No anomalous voltages were indicated during this test. Next, the 3500G3 adaptor cables' connector plug was loosened one full turn from the RTD interface receptacle, and the connector plug was manipulated. Again, there were no anomalous RTD voltages.

The 3500G3 adaptor cable connector plug was then demated from the RTD receptacle at the converter interface bracket, and a force gage was used to perform a pin retention test at each of the connector plug sockets. Low force readings were seen at one of the RTD #3 sockets. (RTD #3 circuit had been anomalous during the dynamic testing.)

A "NO-GO" type gage was then used at the pins of the RTD connector at the converter interface bracket. This gage was a socket machined to an I.D. just smaller than the minimum specified connector pin O.D. The gage did not fit onto any of the connector pins, indicating that they were all larger than minimum specified O.D.

Another 3500G3 adaptor cable was to be used in place of the one which had the low pin retention at one of the RTD #3 circuit's sockets. However, the new cable's pin retention was poor at one socket and the original cable was allowed to remain.

Although there had not been an anomaly on the power circuit due to 2428G1 GSE-type power-out cable, as there had been with the JPL power-out cable, special tests were also performed at the converter's power-out interface. The 2428G1 cable was demated from the converter power receptacle, and was given the same type of pin retention test as had been performed on the RTD's 3500G3 adaptor cable. The force required to extract a pin from each of the 2428G1 connector's sockets was measured. All pin-to-socket retention forces indicated acceptable values.

A "NO-GO" gage was then applied to each of the pins in the converter's power-out receptacle. The gage did not go onto any of the four pins, indicating an acceptable minimum O.D. of these pins. The 2428G1 cable was mated to the converter power-out receptacle and final preparations for thermal-vacuum testing were completed.

On 29 April 1976, the chamber door was secured and evacuation was initiated. After the chamber had attained the low 10^{-5} torr range, converter evacuation through the gas service cart was begun. After the bulk of the converter's argon fill gas was evacuated external to

the chamber, pulse venting directly into the chamber began. After the venting solenoid valve remained open, the RTG internal pressure indicated 80 microns and chamber pressure 6×10^{-5} torr.

Chamber pressure and RTG internal pressure continued to decrease, and RTG output power increased until the power peaked at 149.06 watts. Chamber pressure was 8.8×10^{-6} torr and RTG internal pressure was 14 microns at that time. RTG output power then gradually decreased to a low of 147.44 watts and then recovered to 148.03 watts by the termination of the thermal-vacuum test on 2 May 1976. At the time of the 147.44 watts power, chamber pressure had increased to 1.2×10^{-5} torr and converter internal pressure was indicating 22 microns. These pressures also recovered slightly and at the end of test were 9.2×10^{-6} torr and 14 microns.

During this thermal-vacuum test period, two independent checks were made to determine if the venting solenoid valve was open. After temporarily de-energizing the vent valve, RTG internal pressure increased to approximately 400 microns over a 5-minute period, and chamber pressure decreased into the low 10^{-7} torr range (a two-decade drop). There was no doubt that the vent valve was operating. In addition to the check on the vent valve, the argon pressure head up to the automatic backfill valves was eliminated as a contribution to higher-than-normal converter internal pressure. The argon backfill gas was evacuated from the chamber external lines up to the backfill valves. There was no subsequent decrease in chamber or converter pressures after this gas was removed; this indicated that there had been no leakage past the backfill valves into the converter's venting line.

With a correction factor of 0.8 watts added for cable loss, output power at the end of test was 148.83 watts. NR-43818 was then written against power being below 156 watts and depositioned to continue on to the xenon transient vent test.

On 2 May 1976 the Q-2 RTG was backfilled with xenon gas in preparation for the transient vent test. Chamber backfilling with dry nitrogen was completed and the chamber door was opened.

Due to the anomalous performance during the vacuum testing, there was a suspicion that the RTG's gas management valve was not fully open. The amount of opening was measured at this time as 3/4 of a turn on the valve stem, whereas, the fully open position was two full turns. The valve stem was set to the fully open position and the chamber door was again secured. An extra pumpdown/backfill cycle was necessary since the chamber had been opened to check the condition of the gas management valve. With the transient vent to occur when chamber pressure would be at 50 mmHg during its evacuation cycle, there had to be an assurance that the partial chamber atmosphere was not air.

On 3 May 1976 this chamber evacuation was initiated and after attaining a vacuum in the 10^{-5} torr range, the chamber was backfilled with argon to one atmosphere.

On 4 May 1976, thermal conditions were stabilized for the start of the transient venting test. With the RTG pressurized to 24.2 psia xenon and the chamber at one atmosphere of argon, the output power had stabilized at 116.7 watts. Chamber evaucation began and when a chamber pressure of 50 mmHg was attained (4 minutes after start of pumpdown), the venting solenoid valve was energized to allow the RTG's xenon gas load to be vented to the chamber. Output power gradually decreased for the first 30 minutes after the start of chamber evacuation from the initial 116.7 watts to 96.1 watts. Power then recovered to 121.4 watts at the 2-hour mark and to 144.8 watts at 6 hours after the start of chamber evacuation. The RTG then stabilized at 148.3 watts at the 13-hour mark into the transient test. Chamber pressure at the end of the transient test was 1×10^{-5} torr and RTG internal pressure was 17 microns.

The RTG remained under thermal-vacuum conditions for an additional 9-1/2 hours (22-1/2 hour mark). At that time, output power was still at 148.3 watts, chamber pressure was 8.4×10^{-6} torr and converter internal pressure was 17 microns. As it was apparent that the output power had peaked out, with essentially no difference, between the RTG gas management valve being fully open (2 turns) as compared to the initial vacuum test where the valve had been opened 3/4 of a turn, a decision was made to terminate thermal-vacuum testing on the unit.

On 6 May 1976, RTG backfilling with argon to 25 psia and chamber backfilling with dry nitrogen to one atmosphere were completed, and the chamber door was opened and rolled out to allow the RTG to stabilize in ambient air for the post-T/V air performance/pressure decay test. A 48 hour air performance and pressure decay test was conducted. Output power averaged 75.6 watts over this period and the rate of pressure decay was 0.24 spi/48-hours.

On 8 May 1976, the RTG load was switched to the short-circuit mode and the unit removed from the chamber support frame. On 9 May, installation of the RTG into its shipping container was completed and the unit was transferred to the storage area in Bldg. 800.

11.4 Q-2 RTG POST-QUALIFICATION OPERATIONS

Q-2 remained in storage in Bldg. 800 while awaiting direction as to how the anomaly investigation was to be conducted. Late on 13 May 1976, the unit was removed from storage and transferred to the Bldg. 800 test area. After removal from the shipping container, the RTG's pneumatic flex hose was demated from the gas management valve for inspection; there was no visible evidence of internal blockage in the hose. It was then sent to Bldg. B for a flow conduction test to be performed by the Engineering lab.

A new flex hose was received and its installation onto the RTG gas management valve was completed. Q-2 was then installed into LAS #1 in preparation for the forthcoming thermal-vacuum test in the LAS chamber. This test would yield a performance comparison with the previous LAS vacuum testing in March, with the recently completed test in Bldg. 300 vacuum chamber. With Q-2 installed, the LAS chamber was secured and operations were suspended for the weekend.

Prior to vacuum performance testing, an initial chamber evacuation/argon backfill cycle was necessary in order to remove the air from the chamber and allow the opening of the converter's gas management valve. At the second chamber evacuation, the RTG, being vented to the chamber, would then be evacuated.

On 17 May 1976, pumpdown was initiated, the chamber backfilled with argon and acceptable purity levels established. The RTG remained pressurized with argon to 25 psia through those operations. After bleeding RTG pressure to 16 psia, the pneumatic line inside the LAS interconnected with the RTG flex hose was demated and a filter housing with a silver membrane filter was installed onto the flex hose, to retain any particulates. With the opening of the RTG gas management valve, the unit was vented to the chamber argon atmosphere through the membrane filter.

On 18 May 1976, chamber evacuation for the RTG vacuum performance test began and a high 10^{-6} torr range was attained. RTG output power at that time, had stabilized at 146.3 watts with the RTG vented to the chamber; there was no capability of measuring RTG internal pressure during this test. Shunt resistance between thermopile circuit and case ranged from 210 to 280 ohms over the above test period.

As the RTG output power was still indicating an anomalous value, preparations were made for the next stage of vacuum performance testing, with the RTG forward dome removed to duplicate the condition of the Q-2 vacuum degassing operation in LAS #1 late in March. RTG output power at the end of that 200-hour vacuum degassing in March was 155.8 watts. LAS backfilling with argon was completed and after radiological measurements and chamber gas purity levels were acceptable, the forward dome was removed from the spoolpiece.

Prior to evacuating the chamber for the "dome-off" test, a visual examination was given to the upper cavity of the open RTG. There was nothing found that could be definitely causing the short between thermopile and case. However, there was a coating of white fibrous material over most of the upper cavity of the converter and spoolpiece, especially on the surfaces which were "traps", i.e., the cutouts in the end enclosure legs and the flat area on the spoolpiece just inside of the sealing surface. This material was apparently from the outer layer of astroquartz pad on the moly-foil end cap where it had been abraded away by the six end enclosure spring clips, the purpose of which was to retain the pad. They had actually worn through the astroquartz during the previous dynamic testing and were bearing on the outer moly-foil layer, causing a loss of electrical isolation between converter case and foil system.

In addition to the areas under the end enclosure pad retainer clips, there were abraded areas around the three ceramic plugs in the moly-foil end cap. These plugs were in the feed-through holes in the cap used for the EHS thermocouples and power leads when Q-2 was an ETG. The lock wiring in the ceramic plugs had abraded the material during the dynamic tests. At first, there was conjecture that the feed-through holes in the foil were enlarged, but this was proven to be illusory and it was only the outer layer of astroquartz that was damaged.

On 19 May 1976, direction was given to prepare for the vacuum performance test with the forward dome removed.and chamber/converter evacuation began. The RTG stabilized at 153.6 watts with the chamber in the high 10^{-6} torr range. This showed a performance improvement of 7.3 watts over the previous vacuum testing of 5/18 in the LAS with the dome on and the converter venting only through the gas management valve. This gave evidence that the valve or tube between the valve and case was blocked and not allowing a proper venting conduction.

When the 153.6 watts obtained at this "dome-off" test as compared to Q-2's performance of 155.8 watts at the end of the vacuum degassing on 3/25, there is a difference of 2.2 watts. Part of this can be accounted for as a 0.3 watt loss due to fuel decay and 0.5 watt loss due to thermo-electric aging over the 56-day time differential.

On 20 April 1976, argon backfilling to terminate the vacuum testing was initiated, and late that day probing operations began on suspected areas in the RTG which might be causing the low thermopile-to-case shunt resistance. While the voltage across the shunt resistance was being monitored, the strain gage leads were probed with no change in the voltage across the thermopile-to-case.

After the spoolpiece was removed from the converter case, there was an abrupt change in the voltage from thermopile-to-case. After completion of the measurement/calculation, the shunt resistance indicated an increase from 290 ohms to an isolation value of 550 K-ohms.

The stimulus at the time that the change occurred, was the RTG being turned on the rotary table. Some effort was then spent in rotating the RTG, "tugging" on the power leads and mildly shaking the converter case to create the shorted condition. None of that manipulation caused a change; however, it later returned to a low value, apparently without any external stimulus.

Operations began leading to the removal of the IHS from the converter. Heat source assembly preload was relieved and a loading equivalent to 32 mils deflection of the forward end enclosure was indicated. This compared favorably to the 28 mils which was established at the IHS installation on 17 March. After the forward end enclosure assembly was removed from the converter, visual examination showed some small chips out of the zirconia bearing discs but otherwise the three segments were intact.

The threaded plug in the forward end cap of the IHS was removed to permit the IHS handling tool to be installed. A small quantity of black dust adhered to the bottom of the plug. This dust was dislodged when the plug was placed in the LAS storage tray. A contamination check on this dust, gave approximately 1000 DPM which was shown to be from ^{238}Pu. The forward heat source support was also found to be slightly contaminated, ≤ 300 DPM, on the surface mating with the forward end cap. No significant additional contamination was found in the LAS.

On 21 May 1976, after preparation of the EPC/SPC for receiving the heat source, the IHS handling tool was installed and the IHS was hoisted out of the converter. (The shorted thermopile-to-case condition existed at this time.) A visual examination of the IHS showed only some burnish marks and minor discolorations of the graphite aeroshell. The IHS was then lowered into the EPC.

Upon reinstallation of the graphite plug into the lifting hole in the forward aeroshell end cap, it was found that the plug would not seat flush with the top of the aeroshell but actually could be run in at least 1/4 inch below that surface. The plug was removed and depth measurements into the hole to the top of the upper tie-bolt were performed. This showed that there

was probably some deformation of the laminated end crushup material. Contact was made with the crushup assembly at $\sim$0.8 inch below the normal location as shown in the sketch of Figure 11-3. See Section 5.0 for further discussion of the post-test conditions in the Q-2R/IHS.

On 22 May 1976, the EPC lid was installed and the EPC/IHS evacuated to below 0.1 psia and pressurized with helium to 19 psia. The EPC then passed a pressure decay test with a rate of 0.01 psi/4-hours. After opening the LAS load lock and removing the SPC, the tripod assembly was installed and an EPC preload of 131 mils deflection was established. The SPC was then evacuated to below 100 microns and backfilled with argon to 30.8 psia. Installation of the SPC into the IHS-Shipping Container was completed and the Q-2R/IHS was transferred to the Bldg. 800 storage area.

On 24 May 1976, after Health Physics approval, the LAS was opened and inspection operations on the Q-2 converter began. The forward moly-foil end cap/end enclosure assembly showed particles of metallic material at the underside of the moly-foil end cap and the edges of the end cap which intersect with the ends of the thermopile's moly-foil basket showed a ragged condition.

Resistance between the thermopile-to-case circuit was directly measured at 1.4 ohms using an ohmmeter. This was the first time that the "cold" isolation measurement had been performed since the unit was an ETG and verified that the shorted condition still existed.

The results of diagnostic evaluations conducted on Q-2 were unable to reveal the cause of the shorts. Therefore, a decision was made to disassemble the Q-2 converter, down to the thermopile level if necessary, to establish the specific cause of the short(s).

The Q-2 disassembly was performed in two phases; in the LAS and in the clean room in Bldg. "B", both under the direction of RCA personnel. Reference the "MHW RTG Short Evaluation Study", dated 1 September 1976, for details of this investigation which found the Q-2 shorts caused by metallic chips from the foil insulation shorting out the Al_2O_3 insulator between the unicouple electrical connector and heat shunt and by the degaussing loop insulation wearing and shorting to the foil basket (see Section 7, Para. 7.4).

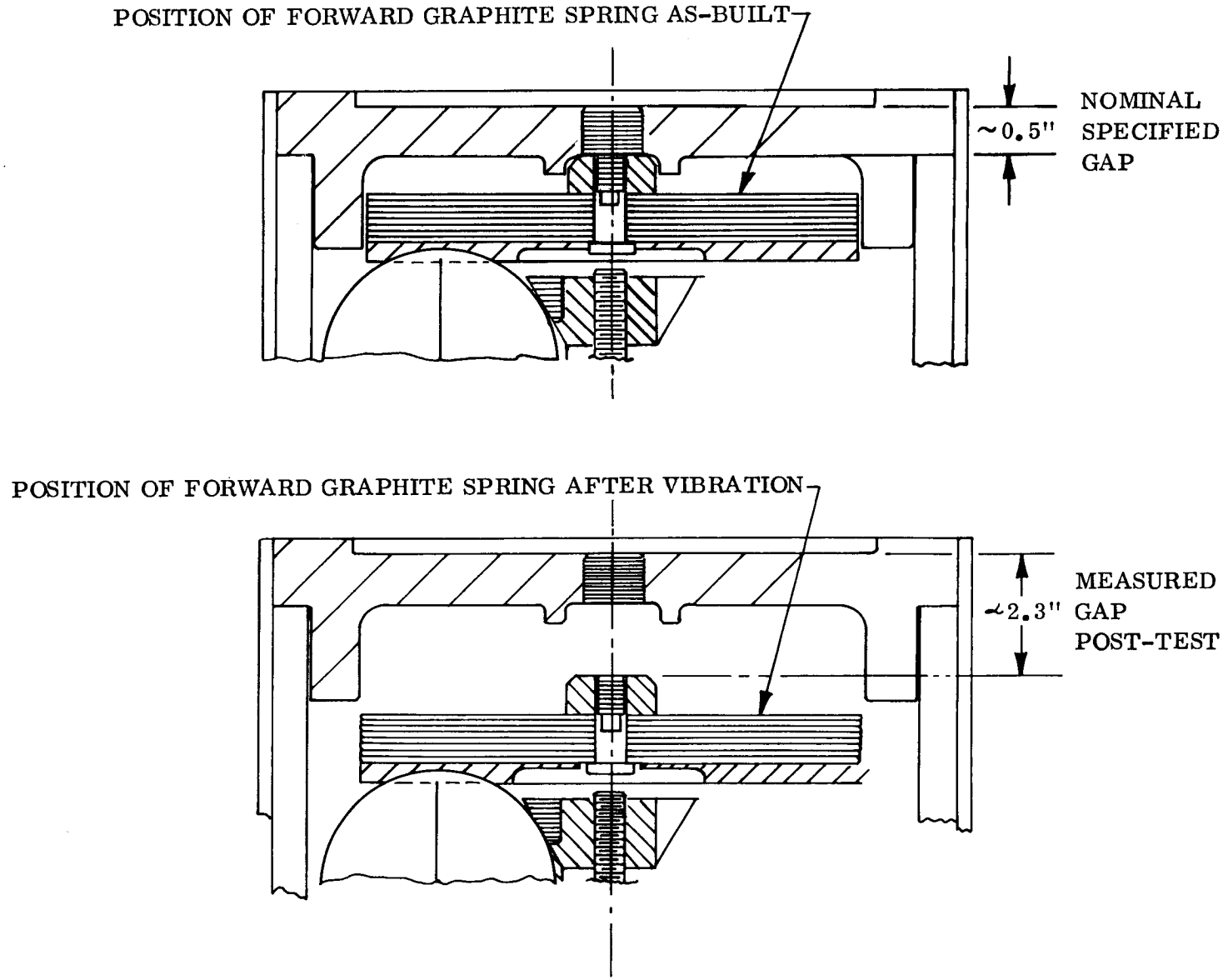

Figure 11-3. Q-2R 1HS Before and After Qualification Vibration Tests